

**Stable Functionalized Unsaturated Siliconoids:
From a Tetrylene/Siliconoid Hybrid to Application
in Homogeneous Catalysis**

Dissertation

zur Erlangung des Grades
des Doktors der Naturwissenschaften
der Naturwissenschaftlich-Technischen Fakultät
der Universität des Saarlandes

von

M.Sc. Nadine Elisabeth Poitiers

Saarbrücken

2020

Tag des Kolloquiums:	09.06.2021
Dekan:	Prof. Dr. Jörn Walter
Berichterstatter:	Prof. Dr. David Scheschkewitz Prof. Dr. Gregor Jung Prof. Dr. Thomas Müller
Vorsitz:	Prof. Dr. Andreas Speicher
Akademischer Mitarbeiter:	Dr. Bernd Morgenstern

Meiner Familie gewidmet

The present dissertation was prepared in the time between June 2016 and September 2020 at Saarland University at the institute for General and Inorganic Chemistry of the Faculty of Natural Science and Engineering at the Saarland University in the group of Prof. Dr. David Scheschkewitz.

Die vorliegende Arbeit entstand in der Zeit von Juni 2016 bis September 2020 an der Universität des Saarlandes am Institut für Allgemeine und Anorganische Chemie der Naturwissenschaftlich-Technischen Fakultät im Arbeitskreis von Prof. Dr. David Scheschkewitz.

Literarum radices amarae, fructus dulces!

Cicero, 106–43 v. Chr.

Abstract

Siliconoids have received tremendous attention due to the prominent role of silicon in technologies of the modern society. The presence of the partially unsubstituted cluster scaffold resembles silicon surface materials at molecular regimes. While siliconoids play important roles as presumed intermediates during chemical vapor deposition processes or in heterogeneous catalysis, the possibility to graft functional groups to the Si_6 benzpolarene scaffold is a prerequisite for their incorporation as building blocks into extended systems. Main attention of this thesis is the introduction and transformation of functionalities in the periphery of Si_6 siliconoids.

Dichlorinated metallocenes of Group 4 are shown to be suitable reagents for the transfer of metals to the Si_6 siliconoid. The electrophilic transfer of a chlorinated amidinato tetrylene to the Si_6 siliconoid facilitates the coordination to transition metal fragments. As will be shown, depending on the nature of the substituents of the transition metal fragments, different and unprecedented structural motifs can be obtained.

In context of the application of siliconoids in homogeneous catalysis, the reactivity of a silylene/siliconoid hybrid towards chalcogens and carbon monoxide was investigated resulting in unprecedented and unsaturated chalcogen-expanded heterosiliconoids as well as in the full cleavage of the $\text{C}\equiv\text{O}$ triple bond under formation of an $\text{Si}=\text{C}$ Enol ether bridge in the periphery of the cluster scaffold.

Zusammenfassung

Silicoide erregten aufgrund der herausragenden Rolle von Silicium in den Technologien der modernen Gesellschaft eine enorme Aufmerksamkeit. Das Vorhandensein des teilweise unsubstituierten Clustergerüsts ähnelt Silicioberflächenmaterialien im molekularen Bereich. Während Silicoide als vermutete Zwischenprodukte bei chemischen Gasphasenabscheidungsprozessen oder bei der heterogenen Katalyse eine wichtige Rolle spielen, ist die Möglichkeit, funktionelle Gruppen auf das Si_6 Benzpolarengerüst zu übertragen eine Voraussetzung für deren Einbau als Bausteine in erweiterte Systeme. Das Hauptaugenmerk dieser Arbeit liegt auf der Einführung und Transformation von Funktionalitäten in der Peripherie von Si_6 Silicoiden.

Es wurde gezeigt, dass dichlorierte Metallocene der Gruppe 4 geeignete Reagenzien für die Übertragung von Metallen auf das Si_6 Siliciumgerüst sind. Der elektrophile Transfer eines chlorierten Amidinatotetrylens auf ein Si_6 Silicoid erleichtert die Koordination an Übergangsmetallfragmente. Wie gezeigt werden wird, können unabhängig von der Art der Substituenten der Übergangsmetallfragmente unterschiedliche und beispiellose Struktur motive erhalten werden.

Im Zusammenhang mit der Anwendung von Silicoiden in der homogenen Katalyse wurde die Reaktivität eines Silylen/Silicoid Hybrids gegenüber Chalkogenen und Kohlenmonoxid untersucht, was zu beispiellosen, ungesättigten Chalkogen-expandeden Heterosilicoiden, sowie zur vollständigen Spaltung der $\text{C}\equiv\text{O}$ Dreifachbindung unter Bildung einer $\text{Si}=\text{C}$ Enoletherbrücke in der Peripherie des Clustergerüsts führte.

List of Publications

This thesis has been published in parts in:

- Yannic Heider*, Nadine E. Poitiers*, Philipp Willmes, Kinga I. Leszczyńska, Volker Huch, David Scheschkewitz, Site-selective functionalization of Si₆R₆ siliconoids, *Chem. Sci.*, **2019**, 10, 4523-4530.

<https://doi.org/10.1039/C8SC05591B>

* These authors contributed equally.

- Nadine E. Poitiers, Luisa Giarrana, Kinga I. Leszczyńska, Volker Huch, Michael Zimmer, David Scheschkewitz, Indirect and Direct Grafting of Transition Metals to Siliconoids. *Angew. Chem. Int. Ed.* **2020**, 59, 8532-8536; *Angew. Chem.* **2020**, 132, 8610-8614.

English Version: <https://doi.org/10.1002/anie.202001178>

German Version: <https://doi.org/10.1002/ange.202001178>

- Nadine E. Poitiers, Luisa Giarrana, Volker Huch, Michael Zimmer, David Scheschkewitz, Exohedral functionalization vs. core expansion of siliconoids with Group 9 metals: catalytic activity in alkene isomerization, *Chem. Sci.*, **2020**, 11, 7782-7788.

<https://doi.org/10.1039/D0SC02861D>

- Nadine E. Poitiers, Volker Huch, Michael Zimmer, David Scheschkewitz, Chalcogen-expanded unsaturated silicon clusters: thia-, seleno- and tellurasiliconoids, *Chem. Eur. J.* **2020**, published as early view.

<https://doi.org/10.1002/chem.202003180>

- Nadine E. Poitiers, Volker Huch, Michael Zimmer, David Scheschkewitz, Nickel-Assisted Complete Cleavage of CO by a Silylene/Siliconoid Hybrid under Formation of an Si=C Enol Ether bridge, *Chem. Comm.* **2020**, 56, 10898-10901.

<https://doi.org/10.1039/D0CC04922K>

Acknowledgements/Danksagung

„Vergiss den Anfang nicht, den Dank!“

Albert Schweitzer (1875 - 1965)

Als Erstes möchte ich **Prof. Dr. David Scheschkewitz** ganz herzlich für die Möglichkeit danken dieses spannende Projekt im Zuge meiner Doktorarbeit zu bearbeiten. Weiterhin möchte ich mich für das fortwährende Interesse an meiner Arbeit bedanken und für die Freiheit, die er mir bei der Durchführung und Planung der experimentellen Arbeit gewährt hat. Mein Dank gilt zudem seiner vorbehaltlosen Unterstützung beim Schreiben der Publikationen und der Ermöglichung zahlreicher Konferenzbesuche während meiner Zeit als Doktorandin.

Herrn **Prof. Dr. Gregor Jung** möchte ich ganz herzlich danken, dass er das Zweitgutachten übernimmt und für die Betreuung als wissenschaftlicher Begleiter während meiner Promotion.

Herrn **Prof. Dr. Thomas Müller** danke ich ganz herzlich für das Übernehmen des Drittgutachtens.

Ein besonderer Dank gilt der weltbesten Sekretärin, **Bianca Iannuzzi**, die durch ihre ruhige und sachliche Art in jeder Situation hilfreich zur Seite stand. Auch für die oft recht lustigen, zwingend notwendigen Kaffeepausen möchte ich mich bedanken, die so manch einen Tag definitiv gerettet haben.

Ein spezieller Dank gilt zudem **Dr. Diego Andrada**, der mir bei Fragen bezüglich DFT-Rechnungen immer beratend zur Seite stand.

Meiner sehr talentierten Bachelorstudentin, **Luisa Giarrana**, möchte ich von Herzen für die schöne, angenehme und freundschaftliche Atmosphäre danken. Mit ihrem Enthusiasmus, Fleiß und ihrer freundlichen Art war sie stets eine große Hilfe und machte die gemeinsamen Wochen im Labor unvergesslich.

Herzlichen Dank an **Dr. Michael Zimmer** für die Durchführung zahlreicher Festkörper NMR-Studien und VT-Experimente sowie die Hilfe bei NMR-spektroskopischen Fragestellungen.

Bei **Dr. Volker Huch** möchte ich mich für die Kristallstrukturanalytik bedanken sowie für die ausdauernden Bemühungen, bei Problemen zahlreiche Versuche des Messens zu unternehmen.

Für die Messung der Elementaranalysen möchte ich mich bei **Susanne Harling** bedanken.

Ein großes Danke auch an die anderen Mitarbeiter **Hui Zhao, Naim M. Obeid, Isabell Omlor, Andreas Kell, Lukas Klemmer, Yvonne Kaiser, Yannic Heider, Marc Hunsicker, Thomas Büttner, Dr. Carsten Präsang, Dr. Kinga Leszczyńska, Dr. Paresh K. Mahji, Dr. Cem. B. Yildiz, Dr. Andreas Rammo, Evelyne Altmeyer, Andreas Adolf, Günther Berlin** und **Britta Schreiber** für die Unterstützung und die gute Arbeitsatmosphäre.

Ein besonderer Dank geht an **Marcel Lambert**, der mir als Kollege und guter Freund während Studium und Promotion in jeder Situation beratend zur Seite stand.

Bei meiner Familie möchte ich mich für die bedingungslose Unterstützung während nun inzwischen bereits 30 Jahren bedanken, besonders bei: **Oma Klara, Oma Gertrud, Opa Jean**, meiner Patentante **Barbara Darsch** und meinen Eltern **Elisabeth Poitiers** und **Bernd Poitiers**.

Meiner Schwiegermutter in Spe, **Anne Lorenz**, möchte ich für die Unterstützung und Fürsorge während der letzten anstrengenden Jahre während des Umbaus danken.

Meinem Verlobten, **Patric Lorenz**, danke ich von Herzen für seine stetige Unterstützung, Aufmerksamkeit und Liebe. Danke, dass ich mich immer auf deinen Rückhalt verlassen konnte und dass wir ein so gutes Team sind!

Content

List of Abbreviations	1
List of Schemes	3
Foreword	8
Preface	10
1. Introduction	11
1.1. Stable N-heterocyclic Silylenes.....	11
1.1.1. Transition metal complexes of monodentate N-heterocyclic silylenes	11
1.1.2. Bidentate N-heterocyclic silylenes and transition metal complexes	15
1.1.3. Application of NHSi complexes in homogeneous catalysis	17
1.1.4. Reactivity of silylenes towards chalcogens	18
1.2. Small molecule activation by low-valent silicon compounds	20
1.3. Stable silicon cluster compounds.....	23
1.3.1. Zintl Phases, Cage Compounds and Metalloid Clusters of Group 14	23
1.3.2. Zintl Silicide Transition Metal complexes	28
1.3.3. Stable unsaturated Silicon Clusters (Siliconoids)	30
2. Aims and Scope	43
3. Results and Discussion.....	46
3.1. Site-selective functionalization of Si_6R_6 siliconoids	46
3.2. Indirect and Direct Grafting of Transition Metals to Siliconoids.....	55
3.3. Exohedral functionalization vs. core expansion of siliconoids with Group 9 metals: catalytic activity in alkene isomerization.....	61
3.4. Chalcogen-expanded unsaturated silicon clusters: thia-, seleno- and tellurasiliconoids	70
3.5. Nickel-Assisted Complete Cleavage of CO by a Silylene/Siliconoid Hybrid under Formation of an Si=C Enol Ether bridge.....	75
4. Summary, Conclusion and Outlook.....	80
5. References.....	88

6. Supporting Information	105
6.1. Site-selective functionalization of Si_6R_6 siliconoids	105
6.2. Indirect and Direct Grafting of Transition Metals to Siliconoids	148
6.3. Exohedral functionalization vs. core expansion of siliconoids with Group 9 metals: catalytic activity in alkene isomerization.....	225
6.4. Chalcogen-expanded unsaturated silicon clusters: thia-, seleno- and tellurasiliconoids	279
6.5. Nickel-Assisted Complete Cleavage of CO by a Silylene/Siliconoid Hybrid under Formation of an Si=C Enol Ether bridge.....	328
7. Permission of Redistribution/Licensing	369
8. Curriculum Vitae	375

List of Abbreviations

222-crypt	4,7,13,16,21,24-hexaoxa-1,10-diaza-bicyclo[8.8.8]hexacosane
Å	Angström
Ar	2,6-Mes-C ₆ H ₃
C	Celsius
cal	calories
Cp	Cyclopentadienyl, C ₅ H ₅ ⁻
Cp*	Pentamethylcyclopentadienyl (C ₅ Me ₅ ⁻)
CP/MAS	Cross-Polarization Magic Angle Spinning
CVD	Chemical Vapor Deposition
Cod	1,5-cyclooctadiene
DFT	Density Functional Theory
Dip	2,6-Diisopropylphenyl (2,6- <i>i</i> -Pr ₂ C ₆ H ₃)
DPPE	1,2-bis(diphenylphosphino)ethane
Et	Ethyl, -C ₂ H ₅
en	ethylenediamine
h	hour
HBPin	Pinacolborane
HOMO	Highest Occupied Molecular Orbital
<i>i</i> -Pr	<i>iso</i> -Propyl, -C ₃ H ₇
IR	Infrared
K	Kelvin
kJ	Kilojoule
LUMO	Lowest Occupied Molecular Orbital

List of Abbreviations

M	Molar
Me	Methyl, -CH ₃
Mes	Mesityl = 2,4,6-Trimethylphenyl (2,4,6-Me ₃ C ₆ H ₂)
NHC	N-heterocyclic carbene
NHSi	N-heterocyclic silylene
nm	nanometer
NMR	Nuclear Magnetic Resonance Spectroscopy
Np	Neopentyl, -CH ₂ ^t Bu
O ^t Bu	<i>tert</i> -Butylester
PCy ₃	Tricyclohexylphosphine
Ph	Phenyl
ppm	parts per million
<i>p</i> Tol	<i>p</i> -Toluenesulfonic acid
rt	room temperature
^t Bu	<i>tert</i> -Butyl, -C ₄ H ₉
thf	tetrahydrofuran
TMS	Trimethylsilyl
TOF	Turnover number
TON	Turnover frequency
Tip	2,4,6-Triisopropylphenyl
UV	Ultraviolet
vis	visible
VT	variable temperature

List of Schemes

Scheme 1. Selected examples of monodentate N-heterocyclic silylenes. ⁵⁸⁻⁶³	11
Scheme 2. Synthesis of the first N-heterocyclic silylene complex 9 by Welz and Schmid in 1977. ⁶⁴	12
Scheme 3. Classification of four distinct silylene transition metal complexes I-IV....	12
Scheme 4. Selected examples of monodentate silylene transition metal complexes of Group 5 (10), ⁷¹ Group 6 (11), ⁷² Group 8 (12), ⁷³ Group 9 (13) ⁷⁴ , Group 10 (14) ⁷⁵ and Group 11 (15). ⁷⁶	13
Scheme 5. Synthesis of Co-complexes 16 and 17 by Roesky and Stalke <i>et al.</i> ⁷¹	14
Scheme 6. The only existing examples of N-heterocyclic bis(silylene) complexes of Group 4 (18a-c , R = Cl, CH ₃ , H), ⁷⁹ Group 7 (19,20) ⁸⁰ and Group 12 (21-24).	14
Scheme 7. The first spacer-separated bis(silylene) 25 by Lappert <i>et al.</i> ⁸⁹ and the first interconnected bis(silylenes) 26,27 by Robinson <i>et al.</i> ⁸⁴ (with L = C[N(2,6- <i>i</i> Pr ₂ -C ₆ H ₃)CH] ₂).....	15
Scheme 8. Reaction of a disilyne 28 with phenylacetylene led to 1,2-disilabenzene 29a,b (top, R = Si ^{<i>i</i>} pr-[CH(SiMe ₃) ₂] ₂) ⁹³ ; 1,4-disilabenzene 31 obtained from reaction with interconnected bis(silylene) 30 and two equivalents of diphenylalkyne ⁹⁴ (bottom).	16
Scheme 9. Selected examples of chelating NHSi transition metal complexes.....	17
Scheme 10. Selected examples of N-heterocyclic silylenes (NHSi) used as ligands in homogeneous catalysis.	18
Scheme 11. Oxidation of amidinato silylene 39 with one equivalent of chalcogen (E = S, Se, Te) led to the silicon-chalcogen double bond compound 40a-c (with 39a : E = S, 39b : E = Se, 39c : E = Te). ¹²⁹	19
Scheme 12. Synthesis of the bridged sulfur-silicon compound 43 and the Si=E double bond compounds 42a,b (with 42a : E = Se, 42b : E = Te) from four-membered cyclic silylene 41 . ¹²⁸	19
Scheme 13. Reductive coupling of carbon monoxide by disilenide 44 . ⁴⁵	20

Scheme 14. Reaction of the acyclic silylene 46 with CO and CO ₂ led to the reductive coupling of CO in 47 and the Brook-type migration of the Me ₃ Si unit from nitrogen to oxygen in 48 . ¹⁷⁰	21
Scheme 15. Reaction of bidentate silylene ligands 49a,b with carbon monoxide CO. ⁴⁶	22
Scheme 16. Synthesis of the silylene carbonyl complex 53 . ¹⁷⁰	22
Scheme 17. Structures of Group 14 Zintl Anions E ₉ ⁴⁻ 54a-d (a : E = Si, b : E = Ge, c : E = Sn, d : E = Pb).	24
Scheme 18. Synthesis of the first silicon Zintl Anions Si ₅ ²⁻ 55 and Si ₉ ³⁻ 56 from Zintl phases K ₁₂ Si ₁₇ and Rb ₁₂ Si ₁₇ by Sevov and Goicoechea in 2004. ¹⁷⁹	24
Scheme 19. Structures of selected Group 14 Zintl Anions. E ₄ ⁴⁻ 57a-d (a : E = Si, b : E = Ge, c : E = Sn, d : E = Pb).	25
Scheme 20. The first protonated Zintl Anions [HSi ₉] ³⁻ 58 , [H ₂ {Si/Ge} ₉] ²⁻ 59 and [HSi ₄] ³⁻ 60 isolated from liquid ammonia by the groups of Korber ^{183,185} and Fässler ¹⁸⁴ .	25
Scheme 21. Selected examples of mixed Zintl Anions 61 ¹⁸⁷ and 62 ¹⁸⁴ of the Group 14.	26
Scheme 22. Synthesis of Group 14 E ₄ -tetrahedrons 63a-c (a : E = Si, X = Br, R = SitBu ₃ ; b : E = Ge X = Cl, R = SitBu ₃ ; c : E = Si, X = Br, R = CH(SiMe ₃) ₂ MeSi) of Wiberg <i>et al.</i> ^{194,195} followed by reductive cleavage to obtain the corresponding tetrahydride 65c . ¹⁹⁶	26
Scheme 23. Schematic representation of hemispheroidal and (distorted) tetrahedral environments using the parameter ϕ to quantify the hemispheroidality. ²⁰³	27
Scheme 24. The formal biradical 66' and ionic 66'' character of [1.1.1]propellane.	28
Scheme 25. Synthesis of the first metalloids Sn ₈ R ₆ 68 by Wiberg <i>et al.</i> (left, R = Si ^t Bu ₃) ²⁰⁶ and Sn ₈ Ar ₄ 70 by Power <i>et al.</i> ²⁰⁷ (right, Ar = 2,6-Mes-H ₃ C ₆ , Mes = 2,6-Me-H ₃ C ₆).	28
Scheme 26. Synthesis of the first silicide transition metal complex 72 by Korber <i>et al.</i> in 2009. ²²¹	29

- Scheme 27.** Synthesis of the intermetalloid clusters $[\text{Sn}_9\text{Ir}(\text{C}_8\text{H}_{12})]^{3-}$ **73** and $[\text{Ir}@\text{Sn}_{12}]^{3-}$ **74** by Fässler *et al.*²³⁴ 30
- Scheme 28.** Synthesis of spiropentadiene **76** after reduction of the halogenated precursor $\text{R}_3\text{Si-SiBr}_2\text{Cl}$ **75** with potassium graphite by Kira *et al.*²³⁸ and a cyclotrisilene **77** as side product with $\text{R} = t\text{BuMe}_2\text{Si}$ 31
- Scheme 29.** Synthesis of the first siliconoid Si_5Tip_6 **78** by Scheschkewitz in 2005 (with $\text{R} = \text{Tip} = 2,4,6\text{-}i\text{Pr}_3\text{-H}_2\text{C}_6$).²³⁹ 32
- Scheme 30.** Synthesis of Wiberg's eight-membered siliconoid Si_8R_6 **81** ($\text{R} = \text{Si}^i\text{Bu}_3$).²⁴¹ 32
- Scheme 31.** Synthesis of Breher's pentasilapropellane **84** ($\text{R} = \text{Mes} = 2,4,6\text{-Me}_3\text{-H}_2\text{C}_6$).²⁴² 33
- Scheme 32.** Reactivity studies of **84**: closed shell reactivity led to addition of $\text{R}' =$ **85a**: OH, **85b**: OPh, **85c**: SPh, **85d**: SnMe_3 over the bridgehead atoms in **85a-d**; biradical-type reactivity was observed in case of treatment with 9,10-dihydroanthracene resulting in **86** ($\text{R} = \text{Mes} = 2,4,6\text{-Me}_3\text{-H}_2\text{C}_6$).²⁴² 33
- Scheme 33.** Synthesis of 1,1,2-cyclotrisilane **87** followed by reduction with three equivalents of $\text{Li}/\text{C}_{10}\text{H}_8$ to obtain the dismutational hexasilabenzene isomer **88**.²⁴⁴ . 34
- Scheme 34.** Resonance structures of dismutational hexasilabenzene isomer **88** (**88'**: $\text{R} = \text{Tip} = 2,4,6\text{-triisopropylphenyl}$; **88''**: $\text{R} = \text{Dip} = 2,6\text{-diisopropylphenyl}$; **88'''**: $\text{R} = \text{Dip} = 2,6\text{-diisopropylphenyl}$).²⁴⁴ 35
- Scheme 35.** Synthesis of dismutational hexasilabenzene isomer **88** by reaction of disilenide **44** with Cp^*Si^+ cation **89**.^{248,249} 35
- Scheme 36.** Isomerization of the Si_6 -scaffold of the dismutational hexasilabenzene isomer **88** to the global minimum isomer **91**.²⁵⁰ 36
- Scheme 37.** Dihalogenation **92a,b** of the bridgehead silicon atoms of the global minimum isomer.²⁵⁰ 36
- Scheme 38.** Synthesis of tetraaryl-substituted cyclopentasilane **93** (left) and the thermally or photolytically induced Si_{11} cluster **94** isolated as byproduct in the thermal rearrangement of **88** to the bridged propellane **91** (right) with $\text{R} = \text{Tip} = 2,4,6\text{-triisopropylphenyl}$.²⁰² 37

Scheme 39. Reaction of dismutational hexasilabenzene 88 with BiCl ₃ leading to Si ₆ chlorinated derivatives 95 , 96 , 92c (R = Tip = 2,4,6-triisopropylphenyl). ²⁰²	38
Scheme 40. Synthesis of partially germanium- and tin substituted siliconoids 98a , 99a,b reported by Scheschkewitz <i>et al.</i> in 2014. ¹⁹⁸	38
Scheme 41. Synthesis of the first anionic siliconoid Si ₆ Tip ₅ ⁻ 100 . Reduction of 88 with 2 equivalents of lithium/naphthalene (left). Reduction of a cyclotrisilene 87 with 8 equivalents of lithium/naphthalene (right). ⁵³	39
Scheme 42. Synthesis of functionalized siliconoids 101a-e with substituents: a = BH ₃ , b = C(O) ^t Bu, c = SiCl ₃ , d = P(NMe ₂) ₂ . ⁵³	39
Scheme 43. Atomically precise cluster expansion of an anionic Si ₆ Tip ₅ ⁻ siliconoid 100 with decamethylsilicocene SiCp* and further reduction with lithium/naphthalene leads to cluster-core expanded siliconoids 102 , 103 and 105 . ²⁵⁹	40
Scheme 44. Synthesis of dianionic siliconoid 106 via reduction of global minimum isomer 91 with 4 equivalents of lithium/naphthalene. ²⁶⁴	41
Scheme 45. Synthesis of bis(trimethylsilyl)-substituted Si ₅ siliconoid 107 and boron- and phosphorous doped siliconoids 108 and 109 (R = Tip = 2,4,6-triisopropylphenyl). ²⁶⁴	41
Scheme 46. Synthesis of anionic heterosiliconoid Si ₄ Ge ₂ Li 110 (Tip = 2,4,6-triisopropylphenyl). ⁵⁴	42
Scheme 47. Synthesis of the dianionic siliconoid 106 and the proposed reaction of 91 with two equivalents of Li/C ₁₀ H ₈ and its further proposed functionalization with various electrophiles.	43
Scheme 48. Schematic representation of the silicon vertices in the propellane bridged Si ₆ cluster.	44
Scheme 49. Proposed reactivity of anionic siliconoid 98 towards dichlorinated metallocenes (M = Zr, Hf; R = Tip = 2,4,6-triisopropylphenyl).	44
Scheme 50. Proposed reactivity of anionic siliconoid 100 towards chlorinated amidinato tetrylenes (E = Si, Ge, Sn).	45
Scheme 51. Proposed reaction of a silylene/siliconoid hybrid with chalcogens.	45

Scheme 52. Schematic representation of the proposed prefixes for Si ₆ benzpolarenes.	80
Scheme 53. Synthesis of benzoyl- and trimethylsilyl-substituted siliconoids 101e,f and recently functionalized siliconoids 101a-d . ⁵³ Reagents: (a) SiCl ₄ , (b) BH ₃ ·SMe ₂ , (c) ^t BuCOCl, (d) ClP(NMe ₂) ₂ , (e) Me ₃ SiCl, (f) PhCOCl. 101a : E = SiCl ₃ , 101b : E = BH ₃ ⁻ , 101c : E = ^t BuCO, 101d : E = P(NMe ₂) ₂ , 101e : E = Me ₃ Si, 101f : E = CPh. ...	80
Scheme 54. Synthesis of <i>privo</i> -lithiated siliconoid 111 by reduction with 2 equivalents of Li/C ₁₀ H ₈ and its further functionalization with suitable electrophiles. Reagents: (a) SiCl ₄ , (b) BH ₃ ·SMe ₂ , (c) ^t BuCOCl, (d) ClP(NMe ₂) ₂ , (e) Me ₃ SiCl, (f) PhCOCl. 112a : E = SiCl ₃ , 112b : E = BH ₃ ⁻ , 112c : E = ^t BuCO, 112d : E = P(NMe ₂) ₂ , 112e : E = Me ₃ Si, 112f : E = CPh.	81
Scheme 55. Synthesis of the first transition-metal-substituted neutral siliconoids 113a,b (a: M = Zr, b: M = Hf).	82
Scheme 56. Synthesis of the tetrylene-functionalized Si ₆ siliconoids 114a-c and their corresponding Fe(CO) ₄ complexes 115a-c (a: E = Si, b: E = Ge, c: E = Sn).	83
Scheme 57. Synthesis of tetrylene-Si ₆ iridium complexes 116a-c from the tetrylene functionalized Si ₆ siliconoids 114a-c with [Ir(cod)Cl] ₂ (a: E = Si, b: E = Ge, c: E = Sn).	84
Scheme 58. Synthesis of Si ₇ rhodium complexes 117 and 118 from silylene-functionalized Si ₆ siliconoid 114a	85
Scheme 59. Synthesis of chalcogen-expanded Si ₇ heterosiliconoids 119a-c (119a : E = S, 119b : E = Se, 119c : E = Te).	86
Scheme 60. Synthesis of the <i>privo-ligato</i> silanolether-bridged siliconoid 120	87

Foreword

After oxygen with 46.6% by weight, silicon, carbon's heavier congener, is the second most prevalent element in the earth's crust with 27.7% by mass.¹ Silicon mostly appears in the form of silicates or oxides in a wide variety of rocks such as quartz, feldspar or mica but in nature it is rarely found in its elemental form. In fact, silicon has been an essential element for humans since ancient times – a long time before the pure elemental form has been discovered by Lavoisier in 1787 which was later on characterized as silicon by Berzelius in 1824.² Silicon-based materials have been used e. g. in form of obsidian as a cutting tool or simply as clay for pottery/ceramics³ and concrete/cement⁴ for construction of houses, respectively. One popular extracted rock in local chalk areas such as Denmark or Belgium is flint, which as a representative silicon-containing mineral served namesake for the element. The latin word for flint/pebble ("silex") was fused with the ending -on by Thomas Thomson in 1817 in order to highlight the chemical relationship to carbon and boron resulting in the now well-known element name "silicon".⁵

In addition to its role in naturally occurring silicon dioxide and silicates, which dominate the construction industry, elemental silicon is an important raw material for the polysiloxanes materials, colloquially known as "silicones". Silicones are find widespread application in daily-life products such as adhesives, sealants and lubricants.⁶ Elemental, high-purity silicon moved into focus due to its excellent semiconductor properties leading to its abundant role in modern electronics and the solar industries.⁷ The first silicon-based semiconductor device, a transistor, was patented in 1905 by Greenleaf Whitthier Pickard⁸ but germanium remained the dominant material in this area for several decades. Even the discovery in 1940 of the photovoltaic effects and the pn barrier (today known as p-n junction) in silicon could not replace germanium as the main component in the semiconducting device industry. The situation changed with the development of efficient purification of metallurgical silicon in the 1950s. The Siemens process converts metallurgical silicon of about 99% purity (obtained by electrothermal reduction of quartzite, SiO_2) into semiconductor-grade (99.9999% purity) by its conversion into liquid trichlorosilane, HSiCl_3 , subsequent purification by fractionate distillation and finally decomposition to elemental silicon. The production of ultrahigh-purity silicon in the floating zone process in 1954 and prompted the stepwise replacement of germanium by silicon in

the semiconductor industry.⁹ The selective control of silicon's electronic properties became possible by the incorporation of small quantities of either electron donors as e. g. phosphorous^{10,11} (n-type doping¹²) or electron acceptors as e. g. boron¹³ (p-type doping¹⁴).

The omnipresence of silicon in semiconducting devices such as integrated circuits, solar cells and light emitting diodes led to the suggestion that the second half of the 20th century should be referred to as the “silicon age”.¹⁵⁻¹⁷ The down-scaling of devices well below the sub-100-nm regime¹⁸ has led to revolutionary changes in economy, technology culture and thinking.¹⁹ With the anticipated further shrinkage of device dimensions, the control of the properties of materials in the subnano-regime necessarily entails a more profound understanding of the behavior of silicon at the molecular level.²⁰ The growth of metal and semi-metal clusters are by now established as key process of the deposition of zero- to two-dimensional nanostructures as well as bulk-materials.²¹ Cluster expansion methods provide a popular computational tool for the simulation of nanoparticle growth,²² which have to be accompanied by experimental data. The chemistry of stable unsaturated silicon clusters is the central topic of this PhD thesis.

Preface

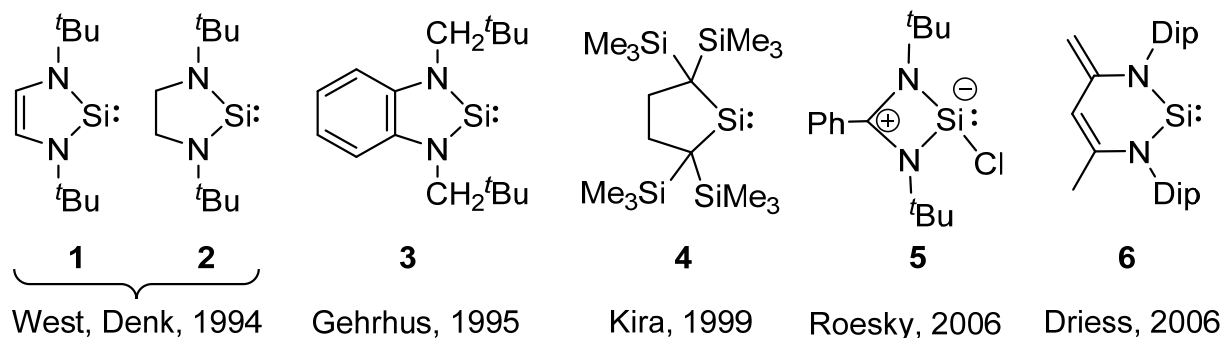
The virtually endless synthetic possibilities of carbon with its ability to form multiple bonds are fundamental in organic chemistry and of course in biological life forms. Silicon, the next heavier element in the Group 14, has not yet been investigated as intensely as carbon. The reason is undoubtedly the longlasting absence of stable compounds with Si=Si double bonds.^{23,24} In general, for the better part of the 20th century, any attempt to isolate compounds with double bonds between two heavier main group elements, leading to oligomers with single bonds exclusively.²⁴⁻²⁹ This led to the assumption that compounds with heavier multiple bonds were nonexistent.²⁵ In 1948, Pitzer disclosed on the basis of theoretical calculations that multiple bonds between heavier main group elements are weakened by the repulsive interactions of the inner electron shells.³⁰ Mulliken amended Pitzer's theory by the realization that these weak double bonds are less a consequence of weakened π -bonds rather than strengthened σ -bonds.^{31,32} Later in 1975, Jutzi brought forward the idea that bulky substituents as protecting groups could kinetically stabilize heavier unsaturated main group species and thus allow for the isolation of structures containing E=E π -bonds as well as their incorporation into extended π -systems.³³

Milestones of the chemistry of unsaturated main group species were published in rapid succession in 1981 with the first silene (Si=C) by Brook,³⁴ the first disilene (Si=Si) by West³⁵ and the first diphosphene (P=P) by Yoshifuji.³⁶ On this basis, low-valent main group chemistry in general³⁷ and particular that of silicon³⁸ flourished. These developments are manifest in the synthesis of numerous further examples, for instance, stable disilynes,^{39,40} the silicon analogues of alkynes. In contrast to carbon, low-valent main group compounds feature entirely different chemical and physical properties. Low-valent and unsaturated silicon compounds move increasingly into focus due to their potential as precursors in catalytic applications⁴¹⁻⁴⁴ or in the activation of small molecules such as carbon monoxide⁴⁵⁻⁴⁷ as well as intermediates in deposition processes.⁴⁸⁻⁵² The presence of functional groups is a prerequisite for the incorporation of the unsaturated moieties into extended systems such as polymers.⁵³ Taking advantage of the reactivity of low-valent centers with substituted functional groups, novel and unprecedented structural motifs of heavier Group 14 compounds can be targeted in a systematic and deliberate manner and thus fully awaken the potential of Group 14 chemistry in various applications.⁵⁴

1 Introduction

1.1 Stable N-heterocyclic Silylenes

Disilenes^{55,38e} and silylenes⁵⁶ constitute the two most important classes of unsaturated silicon compounds. With their inherent surplus of electrons (due to the lower electronegativity of silicon) they show stronger σ -donating properties than the carbon analogues. After the report on the first stable silicon(II) species in 1986 by Jutzi *et al.*⁵⁷ with the decamethylsilicocene, several stable silylenes have been developed.⁵⁶ While West and Denk were able to isolate the first stable two-coordinate, mainly donor-stabilized N-heterocyclic silylenes **1** and **2** in 1994,⁵⁸ Kira's silylene **4** represents the first two-coordinate silylene free of obvious electron donors and thus mainly stabilized by steric crowding.⁵⁹ N-heterocyclic silylenes (NHSi) are the heavier analogues of N-heterocyclic carbenes (NHC) with nitrogen atoms and varying substituents in the backbone. The overlap of the nitrogen lone pairs with the vacant orbital of the silylene center allows the delocalization of the electrons across the N-heterocyclic ring. The chlorosilylene **5**, reported in 2006 by Roesky *et al.*,^{60,61} receives additional stabilization by the intramolecular coordination of a second nitrogen donor (Scheme 1).

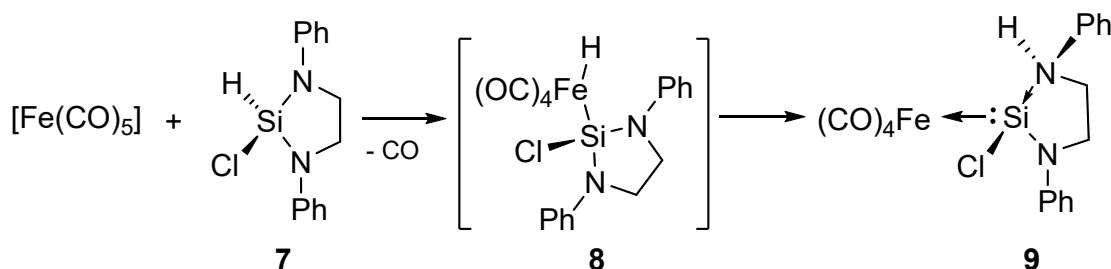


Scheme 1. Selected examples of monodentate N-heterocyclic silylenes.⁵⁸⁻⁶³

1.1.1 Transition metal complexes of monodentate N-heterocyclic silylenes

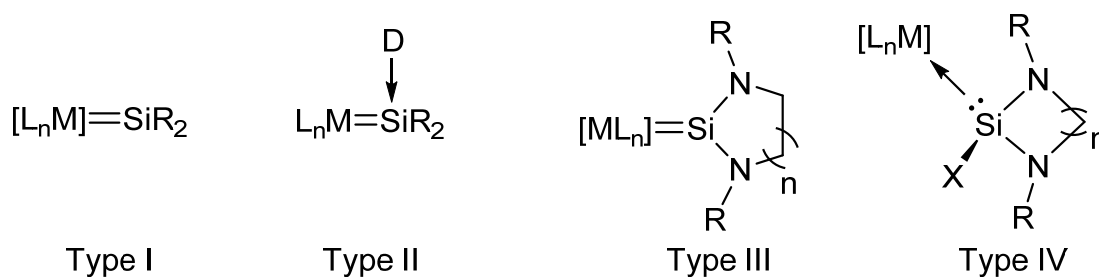
The excellent σ -donating properties of silylenes allow for their coordination to transition metal centers. In 1977, the first N-heterocyclic silylene metal complex **9** was reported by Welz and Schmid.⁶⁴ Treatment of 1,3-diaza-2-silacyclopentane **7**

with $\text{Fe}(\text{CO})_5$ led to the thermolabile silylene-iron complex **9** through insertion of the iron center into the Si-H bond (Scheme 2).



Scheme 2. Synthesis of the first N-heterocyclic silylene complex **9** by Welz and Schmid in 1977.⁶⁴

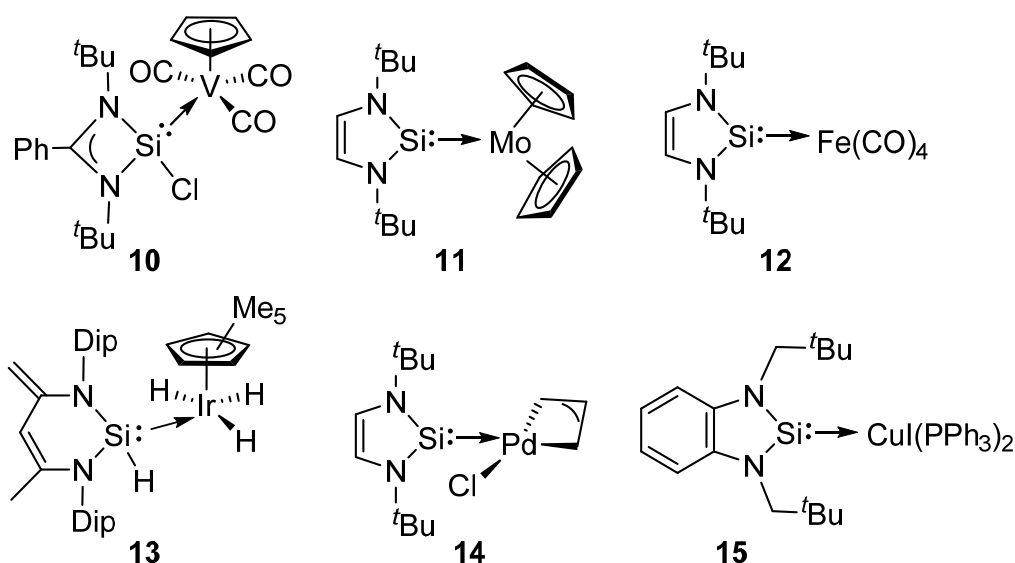
Subsequently, numerous other silylenes⁵⁶ as well as their corresponding transition metal complexes have been reported.^{65,66} These complexes can be seen as an interface between main group chemistry and the classical organometallic chemistry of transition metals. They are classified in four distinct types I-IV (Scheme 3). Silylenes of type I are the analogues of the classical Fischer or Schrock carbene transition metal complexes and are not stabilized by the coordination of an external base to the vacant p orbital at silicon. Examples for type I include $[\text{PtH}(\text{PCy}_3)_2=\text{Si}(\text{SEt})_2][\text{BPh}_4]^-$ or $[(\text{CO})_4\text{Os}=\text{Si}\{\text{S}^p\text{Tol}\}\{\text{Ru}(\eta^5\text{-C}_5\text{Me}_5)\}]$ as reported by Tilley *et al.*⁶⁷⁻⁶⁹



Scheme 3. Classification of four distinct silylene transition metal complexes I-IV.

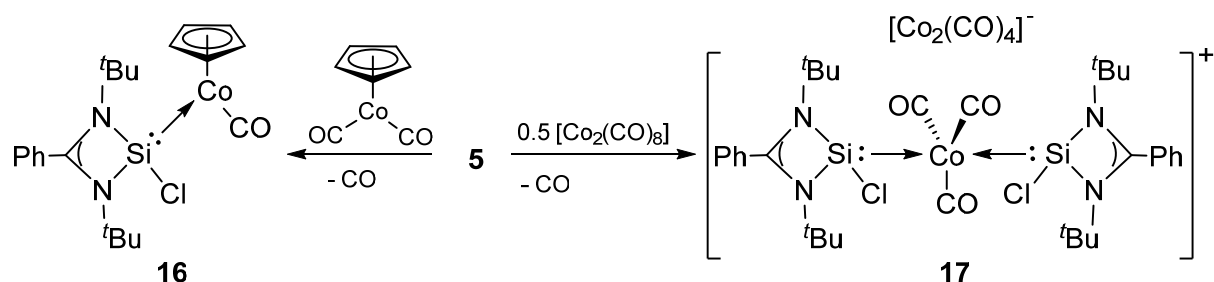
In contrast, type II represents the base-stabilized silylenes coordinated to transition metal fragments, e. g. $[(\text{CO})_4\text{Fe}=\{\text{Si}(\text{OtBu})_2\leftarrow\text{D}\}]$ (with $\text{D} = \text{THF}$ or HMPA) reported by Zybail *et al.*⁷⁰ in 1987. While type III with $n = 1$ or 2 represent N-heterocyclic silylenes with bulky aromatic or aliphatic substituents (also including derivatives with unsaturated backbone), type IV describes N-heterocyclic halide or hydride complexes with $n = 1, 2$ or 3 . Complexes of type III and IV are more recent from the historical perspective as they became accessible after the first isolated N-heterocyclic silylenes

(NHSi) **1** and **2** in 1994 by West and Denk.⁵⁸ Several transition metal silylene complexes of type III and IV from Group 4 to Group 12 have been reported. Selected examples of monodentate silylene transition metal complexes **10-15** are depicted in Scheme 4.⁷¹⁻⁷⁶ Notably, the tetrahedral Cu-complex **15** was prepared by Lappert *et al.*⁷⁶ and represents the first example of an isolated and characterized Group 11 NHSi transition metal complex. After more than a decade has passed, a few NHSi transition metal complexes Group 11 have been reported by Driess *et al.* with the first existing examples of heteroleptic amidinato stabilized Cu-complex⁷⁷ and Stalke *et al.* with a pseudocubane Cu-complex using amidinato ligands.⁷⁸



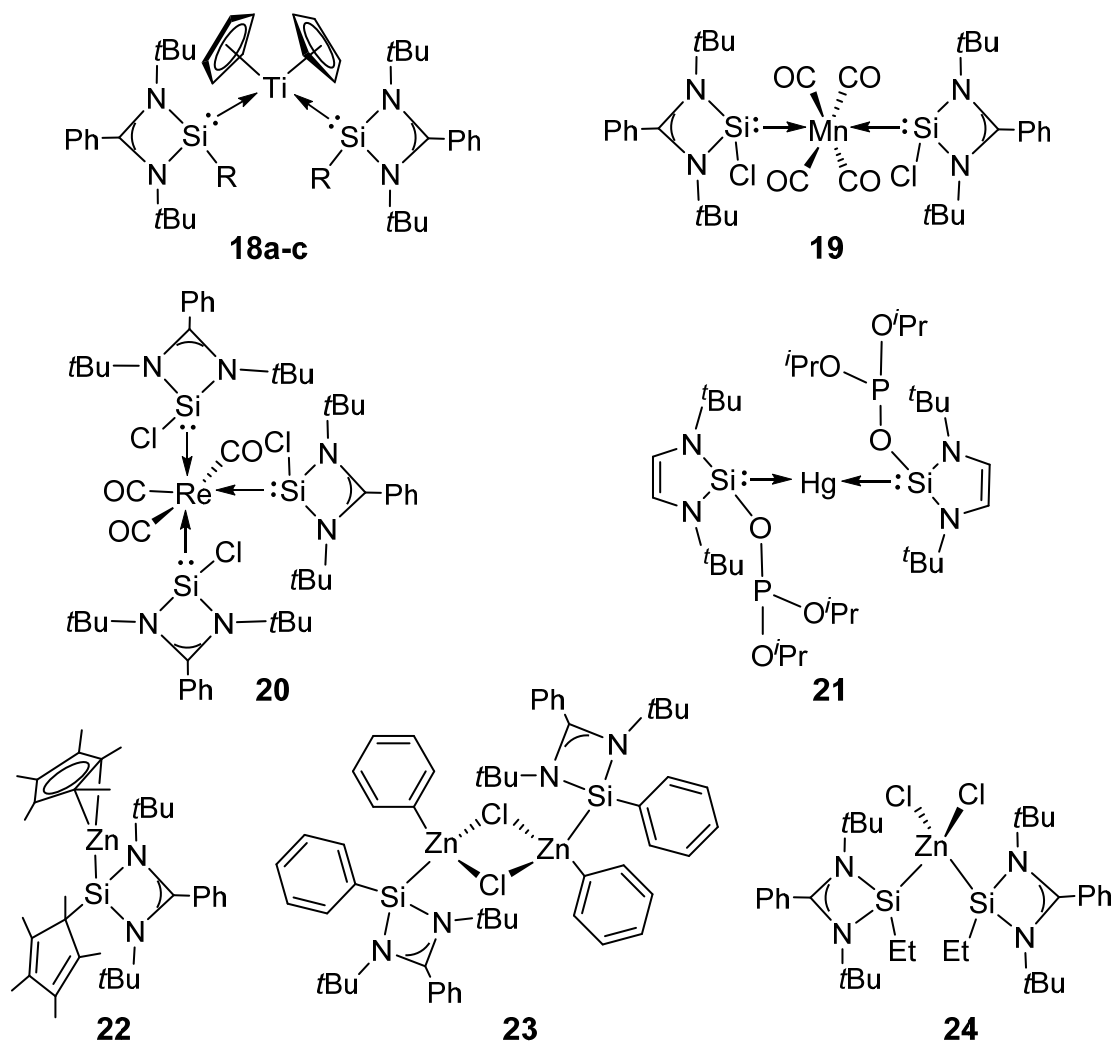
Scheme 4. Selected examples of monodentate silylene transition metal complexes of Group 5 (**10**),⁷¹ Group 6 (**11**),⁷² Group 8 (**12**),⁷³ Group 9 (**13**)⁷⁴, Group 10 (**14**)⁷⁵ and Group 11 (**15**).⁷⁶

Depending on the pattern of residual ligands, silylene transition metal complexes of type L_nM ($n = 1-4$) can be observed. Roesky and Stalke *et al.* reported on the synthesis of silylene-cobalt complexes **16** and **17** following a decarbonylation strategy in both cases.⁷¹ Treatment of the chlorinated amidinato silylene **5** with dicarbonylcyclopentadienyl cobalt(I) $[\text{CpCo}(\text{CO})_2]$ resulted in complex **16**. In a similar reaction, the reactivity of **5** was studied towards dicobalt octacarbonyl $\text{Co}_2(\text{CO})_8$ and led to a bis(silylene) complex **17** which could be isolated as the salt *trans*- $[\text{Co}(\mathbf{5})_2(\text{CO})_3]^+[\text{Co}(\text{CO})_4]^-$ (Scheme 5).



Scheme 5. Synthesis of Co-complexes **16** and **17** by Roesky and Stalke *et al.*⁷¹

Silylene transition metal complexes of Group 4, 7 and 12 are rare and only reported for bis(silylene)-coordinated derivatives of type L_2M (Scheme 6). The group of Driess reported the Ti^{II} complexes **18a-c** as the only existing examples of Group 4 N-heterocyclic silylene transition metal complexes.⁷⁹

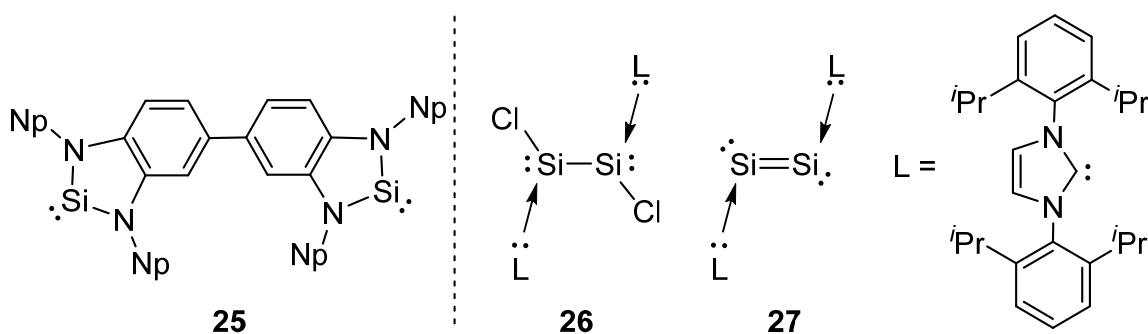


Scheme 6. The only existing examples of N-heterocyclic bis(silylene) complexes of Group 4 (**18a-c**, R = Cl, CH₃, H),⁷⁹ Group 7 (**19,20**)⁸⁰ and Group 12 (**21-24**).

With Mn and Re complexes **19** and **20**, Roesky *et al.* prepared the so far sole examples of Group 7 NHSi complexes⁸⁰ employing a decarbonylation procedure similar to that used for the preparation of NHSi vanadium complex **10**. In 1998, Frenking and Boehme reported a theoretical study on the stability of Cu-, Ag- and Au-NHSi complexes.⁸¹ While four examples of isolated Group 11 and 12 NHSi complexes have been reported, the Cu-complex **15** of Lappert *et al.*⁷⁶ was the first crystallographically characterized complex followed by three amidinato Zn-complexes **22-24** of Roesky *et al.* in 2014.⁸² The NHSi Hg-complex **21** of Apeloig *et al.*⁸³ was found to be thermolabile and unstable at room temperature and could not be characterized by x-ray crystallography.

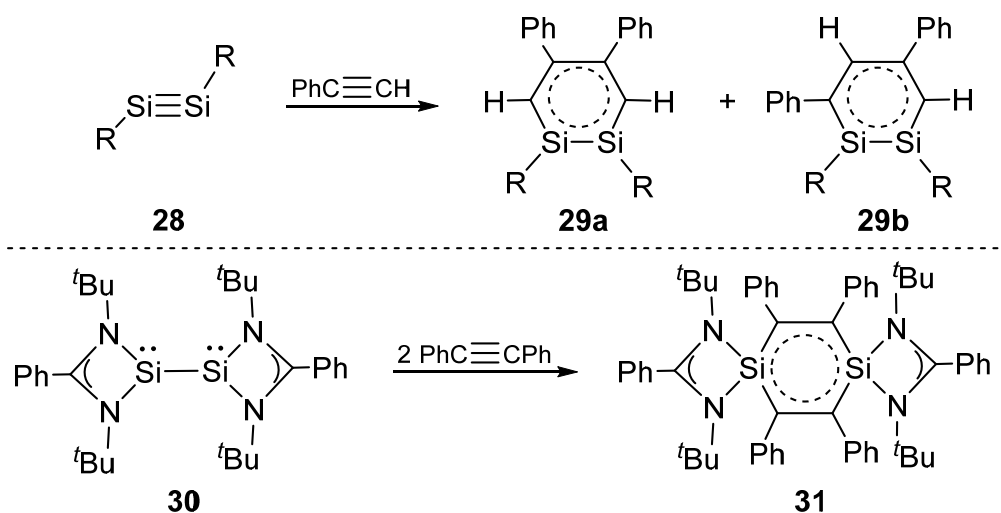
1.1.2 Bidentate N-heterocyclic silylenes and transition metal complexes

The electrophilic nature of the chlorosilylene **5** allows for the facile interconnection of two such entities. In this manner, bidentate N-heterocyclic silylenes, are readily accessible and can be classified in two categories: interconnected⁸⁴⁻⁸⁸ and spacer-separated⁸⁹⁻⁹² bis(silylenes). The interconnected bis(silylenes) contain two directly adjacent low-valent silicon atoms and are accessible by reductive coupling approaches. The spacer-separated bis(silylenes) consist of two low-valent silicon atoms separated by a polyatomic spacer, which is introduced by simple reaction of chlorosilylene precursors with appropriate dinucleophiles. In 2008, Robinson *et al.*⁸⁴ reported the synthesis and isolation of the first interconnected bis(silylenes) **26** and **27** (Scheme 7). The first spacer-separated bis(silylene) **25** was reported by Lappert *et al.*⁸⁹ in 2005.



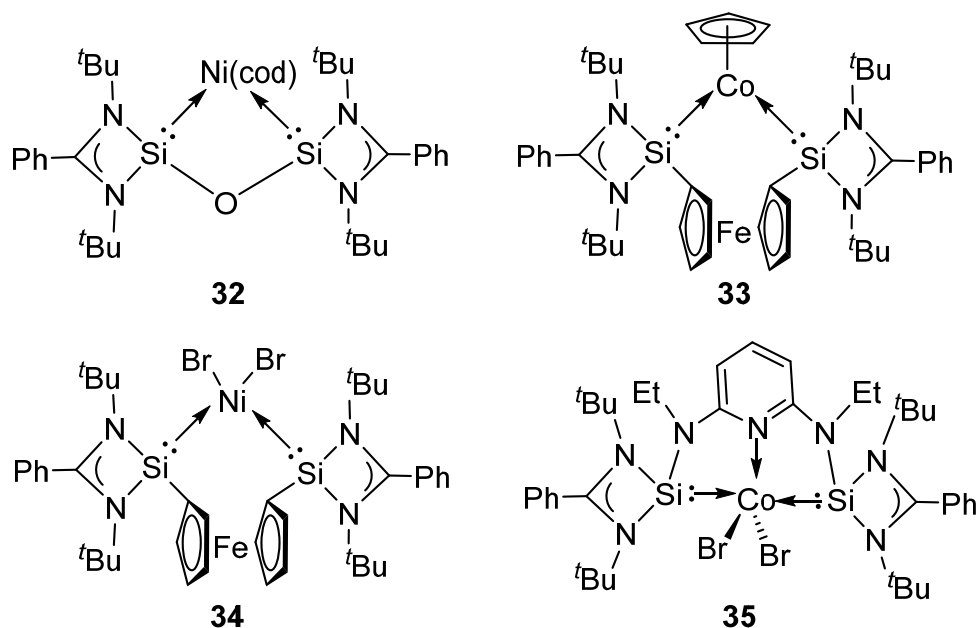
Scheme 7. The first spacer-separated bis(silylene) **25** by Lappert *et al.*⁸⁹ and the first interconnected bis(silylenes) **26,27** by Robinson *et al.*⁸⁴ (with $L = C[N(2,6\text{-}i\text{Pr}_2\text{-C}_6\text{H}_3)\text{CH}]_2$).

The interconnected N-heterocyclic silylenes show a distinctly different reactivity from that of the isoelectronic disilynes: treatment of the first stable disilyne **28** of Sekiguchi *et al.*⁴⁰ with two equivalents of phenylacetylene, for instance, resulted in the first stable 1,2-disilabenzene as a mixture of regioisomers **29a,b**. The formation of the 1,2-disilabenzene was supported by theoretical calculations: the formation of a 1,2-disilacyclobutadiene-like intermediate as initial product was suggested which then undergoes a [2+4] cycloaddition with the second phenylacetylene molecule to form the final compound **29a,b** preserving the Si–Si single bond.⁹³ In contrast, reaction of interconnected bis(silylene) **30** with two equivalents of diphenylalkyne led to the cleavage of the Si(I)–Si(I) bond and the formation of a 1,4-disilabenzene **31** (Scheme 8).⁹⁴



Scheme 8. Reaction of a disilyne **28** with phenylacetylene led to 1,2-disilabenzenes **29a,b** (top, R = Siⁱpr-[CH(SiMe₃)₂]₂)⁹³; 1,4-disilabenzene **31** obtained from reaction with interconnected bis(silylene) **30** and two equivalents of diphenylalkyne⁹⁴ (bottom).

More recently, the groups of Driess and Hartwig isolated the first NHSi-based SiCSi pincer ligand in a collaborative effort.⁹⁵ Based on these bidentate ligands, numerous complexes have been reported in addition to several examples with more than one unbridged monosilylene ligand of the type L_nM ($n = 1-4$). The bis(N-heterocyclic silylene) Ni complex **32**⁹⁰ was followed by further examples with bidentate chelating silylenes such as **33**⁹¹, **34**⁹⁶ and **35**⁹⁷ (Scheme 9).



Scheme 9. Selected examples of chelating NHSi transition metal complexes.

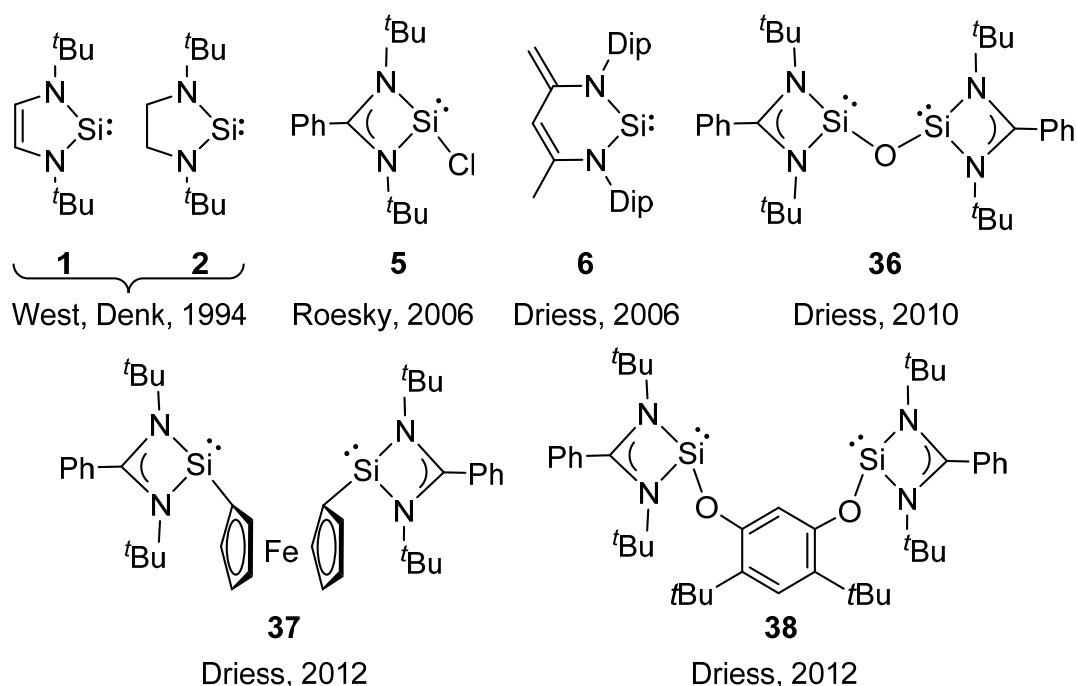
N-heterocyclic silylene metal complexes have been reported for a large variety of transition metals and with different substitution patterns at the N-heterocyclic backbone. While N-heterocyclic carbenes (NHCs) metal complexes are ubiquitously occurring as ligands in homogeneous catalysis,⁹⁸⁻¹⁰⁵ the related NHSi complexes have only recently been considered in this regard.¹⁰⁶

1.1.3 Application of NHSi complexes in homogeneous catalysis

As the control of reactivity is of fundamental interest in all synthetic fields, the design of new catalysts is a pivotal aspect in organometallic chemistry. Silylenes are promising ligands for the construction of new catalysts and have already been shown to be as competitive ligands in homogenous catalysis¹⁰⁶ (Scheme 10). In 2001, the first application of a simple N-heterocyclic silylene palladium complex in a homogenous metal-mediated Suzuki reaction of aryl boronic acids with bromoarenes was reported by Fürstner *et al.*¹⁰⁷ followed by numerous novel and exciting synthetic transformations with silylene transition metal complexes as catalyst.

An iridium pincer type NHSi complex of **38** of Driess *et al.* was successfully used in C–H borylation^{108,109} of arenes with pinacolborane (HBPin) and a related nickel pincer complex found application in Sonogashira¹¹⁰ cross coupling. Roesky and coworkers

found a palladium NHSi complex of **5** with good catalytic performance in the Heck⁷⁵ cross-coupling reactions of styrene and bromoacetophenone. Silylene transition metal complexes also showed competitive selectivity in numerous further reactions such as hydrosilylation of ketones¹¹¹ and alkenes,¹¹²⁻¹¹⁴ reduction of organic amides,¹¹⁵ formation of C=C double bonds,¹¹⁵ hydrogenation of alkynes,¹¹⁷ hydrogenation of olefins,¹¹⁸ Suzuki coupling reaction of aryl boronic acids¹⁰⁷ and [2+2+2] cyclotrimerization of phenylacetylene.⁹¹

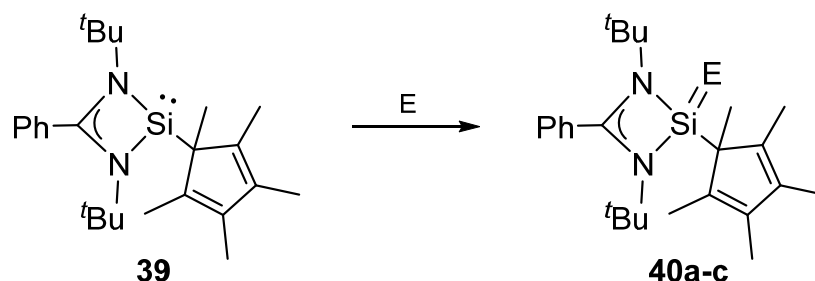


Scheme 10. Selected examples of N-heterocyclic silylenes (NHSi) used as ligands in homogeneous catalysis.

1.1.4 Reactivity of silylenes towards chalcogens

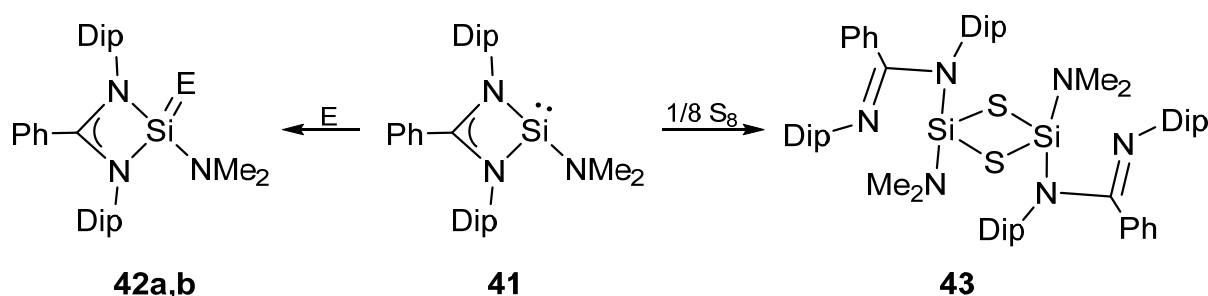
Throughout the history of humankind, chalcogen-containing silicon materials have always been tremendously important in particular those based on silicon dioxide and silicates.¹¹⁹⁻¹²² Only in relatively recent times sub-valent materials such as the “silicon monoxide”¹²³ have moved into focus. Silylenes provide the unique opportunity to stabilize low-valent or low-coordinate molecular chalcogenides. Oxidation of silylenes with chalcogens leads to various structural motifs predominantly depending on the steric shielding of the Si(II) center.¹²⁴⁻¹²⁸ Stable monomeric heavier silaketones with formal Si=E double bonds (E = chalcogen) require severe electronic stabilization or

extremely bulky substituents.^{126,129} In the absence of such measures, dimeric species with two chalcogen bridges between the silicon atoms are obtained.^{124,127,128} The group of P. W. Roesky investigated e. g. the oxidation of the amidinato silylene **39** with heavier chalcogens resulting in the oxidized derivatives **40a-c** (Scheme 11).¹²⁹



Scheme 11. Oxidation of amidinato silylene **39** with one equivalent of chalcogen (E = S, Se, Te) led to the silicon-chalcogen double bond compound **40a-c** (with **39a**: E = S, **39b**: E = Se, **39c**: E = Te).¹²⁹

The oxidation of the silicon atom in **40a-c** resulted in a distorted tetrahedral coordination environment at the silicon centre. The upfield-shifted ²⁹Si NMR signals in **40a-c** compared to **39** confirmed the oxidation of the divalent Si(II) to a Si(IV) species. The bond length of Si–E in **40a-c** is significantly shorter than Si–E single bonds suggesting a certain double bond character between the positively polarized silicon atom and the chalcogen atom with its partial negative charge. Bridging structural motifs were mostly observed for five-membered silylenes¹²⁵ and only in one case for a four-membered¹²⁸ NHSi. Tacke *et al.* reported the treatment a four-membered amidinato silylene **41** with an equimolar amount of sulfur to result in the sulfur-bridged dimer **43** instead of the expected monomeric Si=S species as in the case of **40a**. In contrast, reaction of **41** with one equivalent of the heavier chalcogens selenium and tellurium led to the formation of Si=Se and Si=Te species **42a,b** as expected for four-membered cyclic silylenes (Scheme 12).¹²⁸

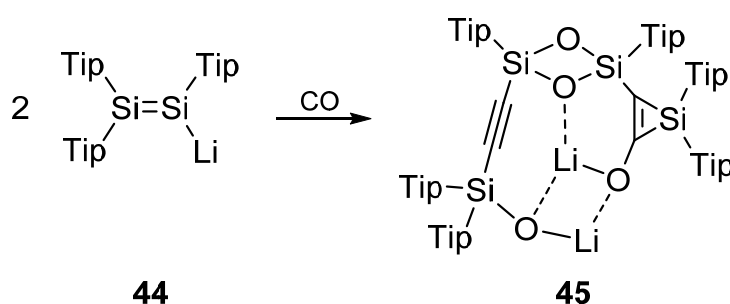


Scheme 12. Synthesis of the bridged sulfur-silicon compound **43** and the Si=E double bond compounds **42a,b** (with **42a**: E = Se, **42b**: E = Te) from four-membered cyclic silylene **41**.¹²⁸

1.2 Small molecule activation by low-valent silicon compounds

The demand for new low-valent silicon compounds increased in the last decade due to their importance as precursors in chemical vapor deposition processes as well as increasing evidence for their potential in homogeneous catalysis.¹³³⁻¹³⁷ The activation of small molecules constitutes the first logical step towards a catalytic cycle although reversibility of key steps as well as sufficiently low kinetic barriers often constitute more formidable challenges. Especially the reduction of carbon monoxide is of fundamental interest due to the CO containing combustion products in large scale industrial processes. A prominent example is the Fischer-Tropsch process, which usually employs heterogeneous transition metal catalysts at elevated temperatures.¹³⁸⁻¹⁴¹ Substantial investigations have thus been carried out to the cleavage of the extremely strong C≡O bond ($1077.1 \text{ kJ mol}^{-1}$)¹⁴² under milder and homogeneous conditions. While d- and f-block elements reductively couple CO,¹⁴³ the subsequent reduction step is almost unexplored. Early transition metal complexes that provide a highly reducing nature were also found to cleave the strong C≡O bond.¹⁴⁴⁻¹⁴⁷

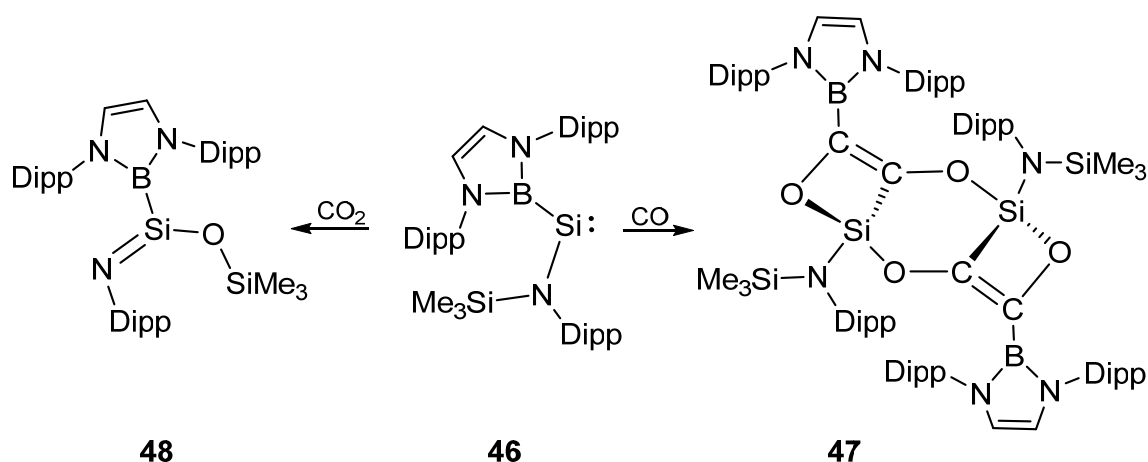
Low-valent main group^{45,145-155} compounds are an increasingly plausible alternative for transition-metal catalysts.¹⁵⁶⁻¹⁶³ Early attempts, however, resulted in the reductive coupling of CO but did not lead to cleavage of the C≡O bond as seen, for instance, in the reaction with potassium that results in various C–C coupling products.¹⁶⁴ More recently, Braunschweig *et al.* reported the coupling of CO to a bis(boralactone) by an NHC stabilized B≡B bond under preservation of the CO linkages as single bonds.¹⁶⁵ In a similar manner, the reaction of a stable diarylgermylene with two equivalents of carbon monoxide as reported by Power *et al.* results in the formation of a C–C bond, but not in the complete cleavage of CO.¹⁴⁸



Scheme 13. Reductive coupling of carbon monoxide by disilenide **44**.⁴⁵

In 2015, Scheschkewitz *et al.* finally reported the complete reductive cleavage via reductive coupling of two CO fragments in a complex reaction with disilenide **44** to afford compound **45** featuring a bis(silyl) alkyne motif (Scheme 13).⁴⁵

While transient CO adducts have been characterized in the gas phase and cold matrices early on,¹⁶⁶⁻¹⁶⁹ the reaction of various silylenes with carbon monoxide was recently reported in independent contribution by the groups of Driess,⁴⁶ Aldridge/Jones⁴⁷ and Schulz¹⁷⁰. In 2019, the groups of Jones and Aldridge reported on the reductive coupling of carbon monoxide by an acyclic silylene in a collaborative work (Scheme 14).⁴⁷

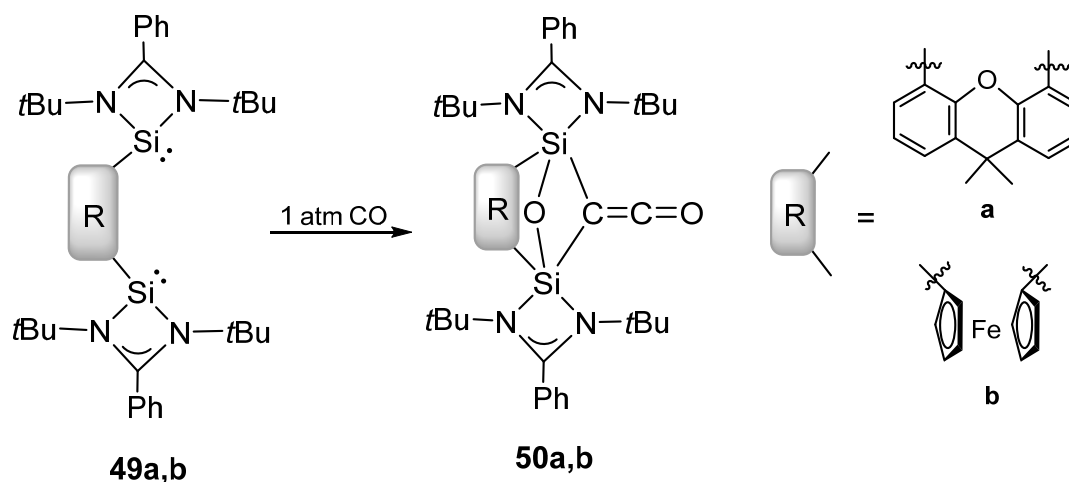


Scheme 14. Reaction of the acyclic silylene **46** with CO and CO₂ led to the reductive coupling of CO in **47** and the Brook-type migration of the Me₃Si unit from nitrogen to oxygen in **48**.¹⁷⁰

Treatment of **46** with excess of carbon monoxide CO resulted in the reductive coupling of CO, the tricyclic dimer **47** with completely cleaved Si-B bonds. The structural motif of **47** resembles that of a donor-stabilized bis(silene) reported by Scheschkewitz *et al.* which is readily accessible from the reaction of carbon monoxide with cyclotrisilene.¹⁴⁷ In contrast, reaction of **46** with carbon dioxide CO₂ led to the formation of silimine **48**. While the Si-B bond was retained in **48**, one oxygen atom was abstracted from CO₂ followed by a Brook-type migration¹⁷¹ of the Me₃Si unit from nitrogen to oxygen.¹⁷⁰

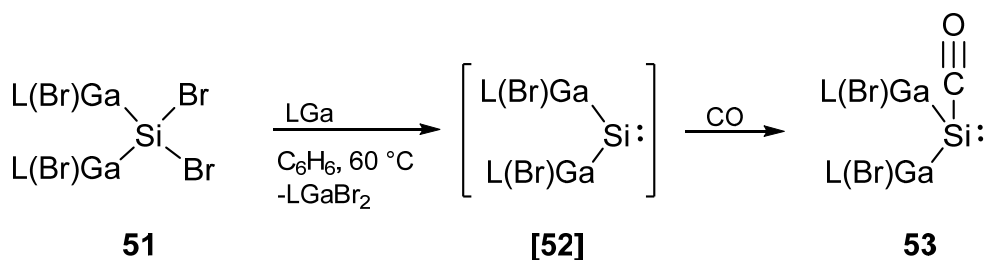
The same year, the group of Driess reported the transition metal-free hetero- and homocoupling of carbon monoxide by bidentate silylene ligands. Treatment of the N-heterocyclic silylenes **49a,b** at room temperature with one equivalent of CO led to the observation of a C=O vibration band in the IR at $\nu = 2069\text{ cm}^{-1}$, which was attributed

to the C=C=O ketene moiety of the final compounds **50a,b** (Scheme 15). This structural motif was observed in case of all employed silylene ligands.⁴⁶



Scheme 15. Reaction of bidentate silylene ligands **49a,b** with carbon monoxide CO.⁴⁶

The generation of a silylene intermediate and its in-situ reaction with small molecules such as carbon monoxide was described in 2020 by Schulz *et al.*¹⁷⁰ The digallyl-substituted dibromosilane **51** obtained by insertion of the β -diketiminato-stabilized gallium(I) species LGa ($\text{L} = \text{HC}[\text{C}(\text{Me})\text{N}(2,6\text{-}i\text{Pr}_2\text{-C}_6\text{H}_3)]_2$) undergoes reduction by one additional equivalent of LGa to the transient silylene **[52]**, which was trapped as adduct **53** if generated under 1 atm of CO (Scheme 16). Kato and Baceiredo *et al.* had previously reported on the selective reduction of CO₂ to CO by a disilyne bisphosphine adduct.⁸⁶



Scheme 16. Synthesis of the silylene carbonyl complex **53**.¹⁷⁰

The activation of small molecules such as carbon monoxide by low-valent main group compounds is still less developed and only a few examples of low-valent silicon compounds are reported to date.^{45-47,145,147,161,166-170}

1.3 Stable silicon cluster compounds

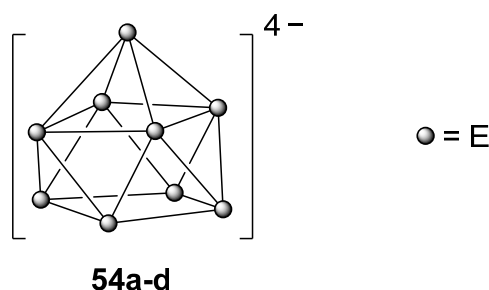
Due to its semiconducting properties, silicon is the key component of electronic applications such as solar cells and microprocessors. In the light of still ongoing miniaturization of integrated circuits, the generation of thin silicon films remains a pivotal task. They are typically prepared by gas phase processes of silane precursors such as chemical vapor deposition (CVD). Although the structures of the amorphous bulk and surfaces are experimentally inaccessible, theoretical calculations by Zhang *et al.*¹⁷² provide hints to the formation of cluster-like structures by residual hydrogen, which give rise to defects in the crystal lattice. A direct correlation exists between the hydrogen content of amorphous silicon (a-Si) and thus the presence of small to medium-sized silicon clusters. A long-term goal of the systematic synthesis of stable silicon clusters is therefore the establishment of structure-property relationships. While the reduction of small, halogenated, low-valent precursors of heavier Group 14 precursors led to the corresponding unsaturated Group 14 clusters in the case of elements heavier than silicon, similar precursors in case of silicon have only recently emerged.⁵³ Although to date, numerous stable molecular silicon clusters have been reported, the targeted synthesis of unsaturated derivatives is still in its infancy. The available general approaches often rely on non-systematic or unselective methods thus leading to difficulties in terms of reproducibility and selectivity. The involved formation mechanisms remain obscure in most cases, but would be of tremendous use for the prediction of reactions and the improvement of synthetic routes.

A large variety of synthetic protocols to prepare silicon cluster compounds emerged during the last 30 years. In general, silicon cluster compounds include saturated cage compounds, completely unsubstituted and negatively charged Zintl ions as well as neutral, partial unsubstituted clusters.

1.3.1 Zintl Phases, Cage Compounds and Metalloid Clusters of Group 14

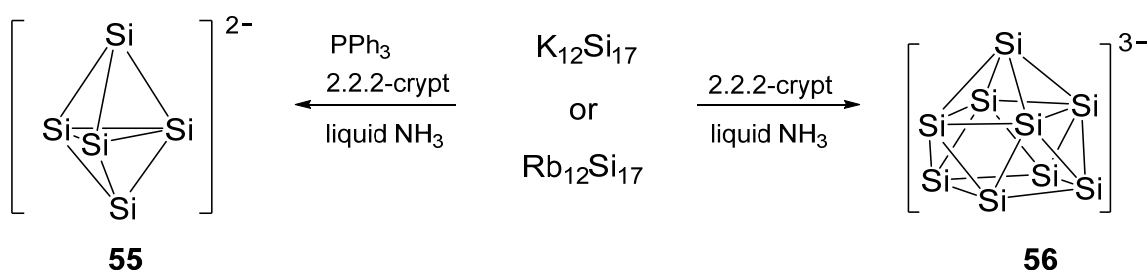
Zintl Anions are polyanionic, deltahedral cluster compounds without any substituent and known since the first observation of an anionic Pb_9 species **51d** by Joannis¹⁷³ more than a century ago in 1891 (Scheme 17). The pioneering work of the namesake Eduard Zintl who employed potentiometric titration to determine the composition of these anionic species in solution,¹⁷⁴⁻¹⁷⁸ enlarged the emerging field giving first

systematic insights into the chemistry of these compounds. To date, Zintl clusters are still under investigation; in particular their extraction from solid state phases into polar solvents such as liquid ammonia has been a main goal in order to enable their derivatization in solution.



Scheme 17. Structures of Group 14 Zintl Anions E_9^{4-} **54a-d** (**a**: E = Si, **b**: E = Ge, **c**: E = Sn, **d**: E = Pb).

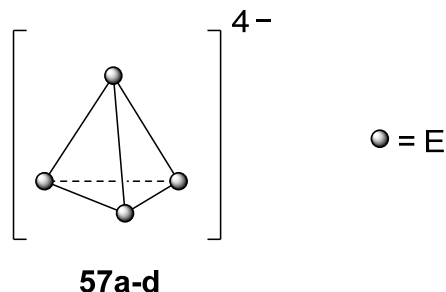
While soluble deltahedral Zintl Ions of the Group 14 of elements heavier than silicon have already been known as E_9^{n-} and E_5^{n-} (E = Ge, Sn, Pb), the isolation of the first silicon derivatives was reported by Sevov and Goicoechea as late as 2004.¹⁷⁹ Solutions of $K_{12}Si_{17}$ and $Rb_{12}Si_{17}$ in liquid ammonia resulted in crystallization of silicon Zintl ions as $[Rb(\text{crypt-2.2.2})]_2Si_5 \cdot 4NH_3$ **55** and $[K(\text{crypt-2.2.2})]_3Si_9 \cdot 8NH_3$ **56** as well as $[Rb(\text{crypt-2.2.2})]_6Si_9Si_9 \cdot 6.3NH_3$ **56** upon addition of 2.2.2-crypt (Scheme 18). Notably, in 2005 Sevov and Goicoechea reported the isolation of a ligand-free deltahedral Si_9^{2-} Zintl Anion.¹⁸⁰



Scheme 18. Synthesis of the first silicon Zintl Anions Si_5^{2-} **55** and Si_9^{3-} **56** from Zintl phases $K_{12}Si_{17}$ and $Rb_{12}Si_{17}$ by Sevov and Goicoechea in 2004.¹⁷⁹

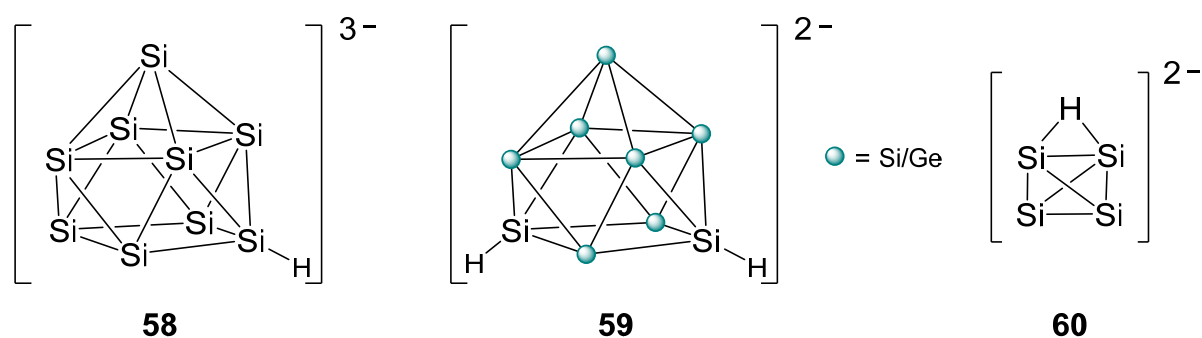
The multiple negative charges of Zintl Anions can be approximately equated with nucleophilic functionalities. According to a suggestion by Wiberg, the formal addition of substituents of type R^+ to Zintl Anions could in principle compensate the negative charges to give straightforward access to completely neutral cluster compounds. In a

so-called “top-down” approach, the addition of substituents to the smallest Zintl Anions E_4^{4-} **57a-d** (Scheme 19) would plausibly result in anionic ($n = 1-3$) or neutral ($n = 4$) cage compounds.



Scheme 19. Structures of selected Group 14 Zintl Anions. E_4^{4-} **57a-d** (a: E = Si, b: E = Ge, c: E = Sn, d: E = Pb).

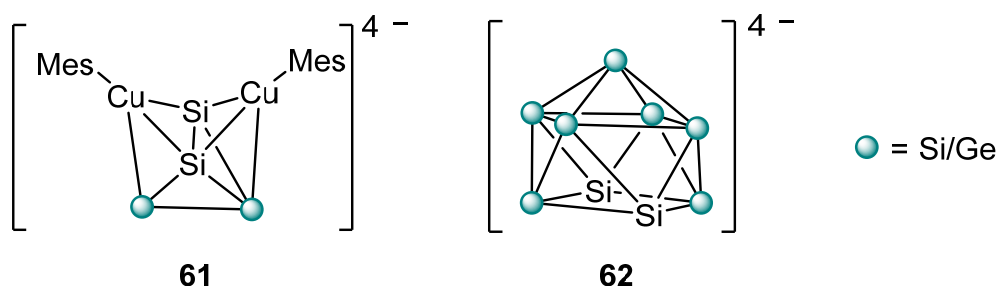
For elements of Group 14 heavier than silicon, the “top-down” approach to obtain the corresponding substituted clusters has already been reported^{181,182} in low yields and with a poor selectivity due to competing radical reactions. Nevertheless, the report on the partial compensation of the multiple negatively charged Zintl Anions serves as a proof-of-concept for chemical transformations to yield the corresponding anionic cluster compounds. The “top-down” approach in case of silicon remained elusive due to the strong reducing properties of the multiply charged Zintl Anions until the groups of Korber¹⁸³ and Fässler¹⁸⁴ independently reported on the protonation of $[HSi_9]^{3-}$ **58** and $[H_2Si/Ge]_9^{2-}$ **59** in 2018.



Scheme 20. The first protonated Zintl Anions $[HSi_9]^{3-}$ **58**, $[H_2Si/Ge]_9^{2-}$ **59** and $[HSi_4]^{3-}$ **60** isolated from liquid ammonia by the groups of Korber^{183,185} and Fässler¹⁸⁴.

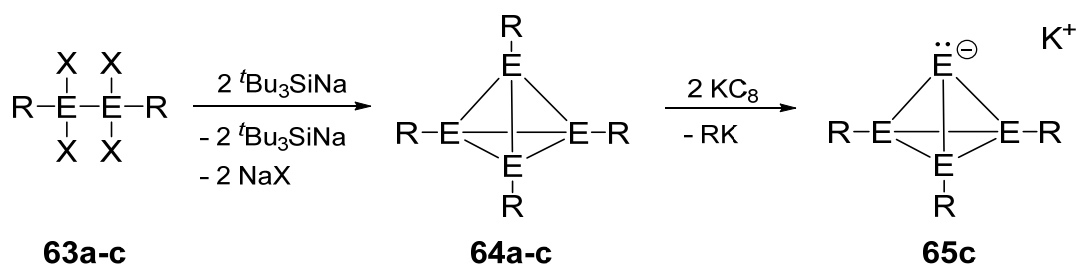
In addition, the group of Korber reported on the protonation of $[HSi_4]^{3-}$ **60**¹⁸⁵ (Scheme 20) and Fässler *et al.* succeeded in the transfer of silyl substituents to Si_9^{4-} .¹⁸⁶

Doping with heavier Group 14 elements such as germanium and tin is expected to increase the photoluminescence quantum efficiencies of nanostructured materials of silicon. On a molecular scale, binary Zintl anions and metalloids containing germanium and tin are well established.^{185,187-190} In contrast, the isolation of the first binary Si–Ge cluster was reported by Fässler *et al.*¹⁸⁹ only in 2011 followed by further examples of mixed Si–Ge Zintl clusters. The mixed Si–Ge clusters **61** and **62** of Fässler *et al.*^{184,187} show pronounced disorder of the germanium or silicon positions (Scheme 21).



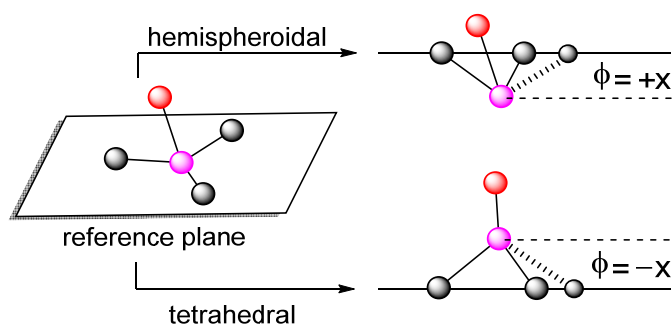
Scheme 21. Selected examples of mixed Zintl Anions **61**¹⁸⁷ and **62**¹⁸⁴ of the Group 14.

Molecules with unusual structures are ideal benchmarks for the further development of existing and novel concepts of chemical bonding. Since Nagase *et al.* predicted the octasilacubane would be less strained than the corresponding carbon compound,¹⁹¹ its experimental realization gathered attention in the organosilicon chemistry community. In 1988, Matsumoto and Nagai¹⁹² reported the first successful so-called “bottom-up” approach of the neutral silicon cage compound $\text{Si}_8(\text{Si}^t\text{BuMe}_2)_8$ and the development of this new field enlarged rapidly.¹⁹³ In a bottom-up approach, Wiberg *et al.* demonstrated the reduction of **63a-c** to obtain the corresponding Group 14 E_4 -tetrahedrons **64a-c**.^{194,195} The reductive cleavage of one silyl substituent from the neutral tetrahedrane Si_4R_4 **64c** by Sekiguchi *et al.*¹⁹⁶ finally led to the tetrahdranide Si_4R_3^- **65c** as shown in Scheme 22.



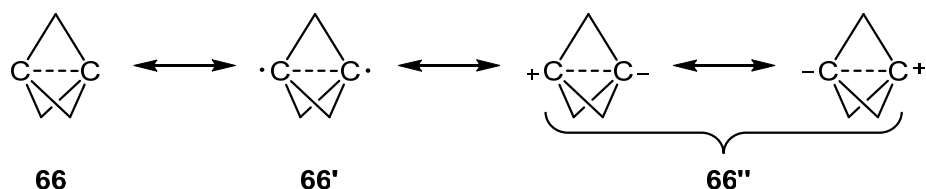
Scheme 22. Synthesis of Group 14 E_4 -tetrahedrons **63a-c** (a: E = Si, X = Br, R = Si^tBu_3 ; b: E = Ge X = Cl, R = Si^tBu_3 ; c: E = Si, X = Br, R = $\text{CH}(\text{SiMe}_3)_2\text{MeSi}$) of Wiberg *et al.*^{194,195} followed by reductive cleavage to obtain the corresponding tetrahdranide **65c**.¹⁹⁶

Charge-neutral unsaturated clusters of Group 14 constitute a third essential class of cluster compounds,^{56,190-199} which are referred to as metalloid clusters according to the definition introduced by Schnöckel *et al.* for unsaturated Group 13 clusters.¹⁹⁹ According to Schnepf, metalloid clusters of Group 14 adhere to the general formula E_nR_m ($n > m$) resulting in average oxidation states between 0 and 1.^{200,201} In contrast, Scheschkewitz *et al.* proposed a slightly different definition where the presence of a three dimensionally silicon backbone with at least one unsubstituted silicon vertex in the formal oxidation state zero is sufficient to fulfill the definition of metalloid character.²⁰² In addition, the corresponding silicon atom must exhibit a hemispheroidal environment²⁰³ in which all bonds point into one half of the coordination sphere (Scheme 23).



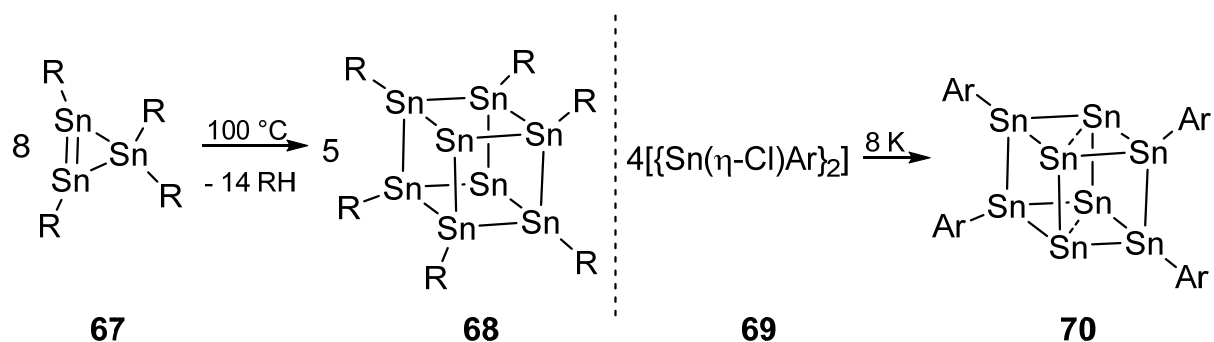
Scheme 23. Schematic representation of hemispheroidal and (distorted) tetrahedral environments using the parameter ϕ to quantify the hemispheroidality.²⁰³

Such a situation is encountered, for instance, in the propellane motif, which has intrigued theorists and experimentalists alike since 1972. The investigation of [1.1.1]propellane shows a non-classical structure with the bridgehead silicon atoms arranged in an umbrella-type hemispheroidal coordination environment. As the inverted σ -bond between the bridgehead atoms of [1.1.1]propellane **66** shows a considerable reactivity, biradical (**66'**) or ionic contributions (**66''**) to the electronic ground state were proposed (Scheme 24). In this context, Shaik *et al.* introduced the concept of the “charge-shift bond”^{204,205} to describe the electronic structure of **66''**. This bonding situation is indistinguishable from cluster bonding and the hemispheroidal geometry of the unsubstituted atoms is as such indispensable for metalloid structures and therefore a prerequisite for unsaturated cluster derivatives.



Scheme 24. The formal biradical **66'** and ionic **66''** character of [1.1.1]propellane.

The "bottom-up" synthesis of a metalloid cluster of the Group 14 was first reported by Wiberg *et al.* with the Sn_8R_6 cluster **68** which was prepared by a thermal induced isomerization of the corresponding cyclotristannene **67**.²⁰⁶ The more unsaturated eight-vertex metalloid cluster Sn_8R_4 **70** was obtained by Power *et al.* by reduction of $[\{\text{Sn}(\eta\text{-Cl})(2,6\text{-Mes-H}_3\text{C}_6)\}_2]$ **69** with elemental potassium (Scheme 25).²⁰⁷



Scheme 25. Synthesis of the first metalloids Sn_8R_6 **68** by Wiberg *et al.* (left, $\text{R} = \text{Si}^t\text{Bu}_3$)²⁰⁶ and Sn_8Ar_4 **70** by Power *et al.*²⁰⁷ (right, $\text{Ar} = 2,6\text{-Mes-H}_3\text{C}_6$, $\text{Mes} = 2,6\text{-Me-H}_3\text{C}_6$).

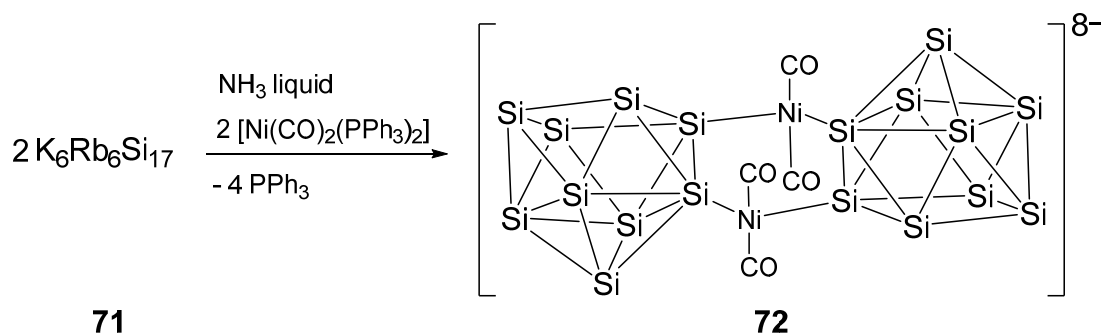
This pioneering work led to numerous metalloid cluster compounds of Group 14 elements heavier than silicon^{201,208-215} and the work of Fässler¹⁸⁴ and Korber^{184,185} can be regarded as a breakthrough top-down assembly of silicon-based metalloids build up from soluble Zintl phases.

1.3.2 Zintl Silicide Transition Metal complexes

Since the pioneering work of Haushalter and Pennington *et al.*²¹⁷ regarding the isolation and characterization of a *closo*- $\text{Sn}_9\text{Cr}(\text{CO})_3^{4-}$ cluster in 1988, the new class of polyhedral clusters connected to transition metals has evolved considerably. Numerous further examples have been reported for Group 14 elements heavier than silicon.²¹⁷⁻²²⁰ While transition metal complexes of the heavier Group 14 elements were already well established, the poor solubility of the $\text{M}^{12}\text{Si}_{17}$ phases limited the

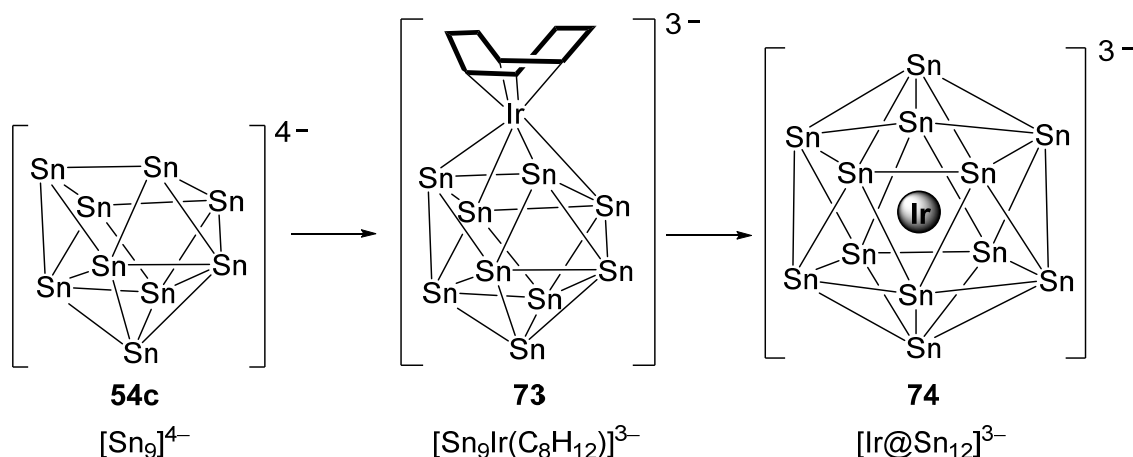
application of Zintl silicides as precursors for the corresponding transition metal complexes. Almost two decades later, Korber *et al.* finally succeeded in the isolation of the first transition metal complex of a silicide ion. Treatment of $\text{K}_6\text{Rb}_6\text{Si}_{17}$ **71** with $[\text{Ni}(\text{CO})_2(\text{PPh}_3)_2]$ in liquid ammonia in the presence of 18-crown-6 results in two $[\text{Si}_9]^{4-}$ clusters bridged by two $\text{Ni}(\text{CO})_2$ moieties, the endohedral $[\{\text{Ni}(\text{CO})_2\}_2(\mu\text{-Si}_9)_2]^{8-}$ complex **72** (Scheme 26).²²¹

As concerns the endohedral incorporation of transition metal centers into Zintl anions, so far only Group 14 elements heavier than silicon have been successfully employed to yield metal-centered derivatives of type $\text{M}@\text{E}_n^{x-}$.²²² These ligand free heteroatomic clusters are defined as intermetaloids, a combination of metalloids and elementoids with cluster compounds of at least two different (semi)metals at low oxidation states with structural similarities to intermetallic compounds. Intermetaloid clusters can occur as spherical cluster compounds with an encapsulated (late) transition-metal atom such as $[\text{Ni}@\text{Ge}_9]^{3-}$,^{223,224} $[\text{Cu}@\text{E}_9]^{3-}$ ($\text{E} = \text{Sn}, \text{Pb}$),²²⁵ $[\text{M}@\text{Pb}_{12}]^{2-}$ ($\text{M} = \text{Ni}, \text{Pd}, \text{Pt}$) or as nonspherical,²²⁶⁻²²⁸ larger endohedral clusters with more than one transition metal atom such as $[\text{Ni}_2@\text{Sn}_{17}]^{4-}$,²²⁹ $[\text{Pt}_2@\text{Sn}_{17}]^{4-}$,²³⁰ $[\text{Pd}_2@\text{E}_{18}]^{4-}$ ($\text{E} = \text{Ge}, \text{Sn}$)²³¹⁻²³³ and $[\text{Ni}_3@\text{Ge}_{18}]^{4-}$.²²³



Scheme 26. Synthesis of the first silicide transition metal complex **72** by Korber *et al.* in 2009.²²¹

In 2009, Fässler *et al.* reported the intriguing icosahedral Sn_{12} cluster anion with an encapsulated iridium center (Scheme 27).²³⁴ Accordingly, the reaction of $[\text{Sn}_9]^{4-}$ **54c** with $[\text{Ir}(\text{cod})\text{Cl}]_2$ in ethylenediamine in the presence of 18-crown-6 or (2.2.2)-cryptand afforded the iridium-capped cluster $[\text{Sn}_9\text{Ir}(\text{cod})]^{3-}$ **73** as the intermediate product (Scheme 27). Subsequent addition of triphenylphosphine (PPh_3) or 1,2-bis(diphenylphosphino)ethane (DPPE) to the ethylenediamine solution of $[\text{Sn}_9\text{Ir}(\text{cod})]^{3-}$ **73** and heating to 80 °C led to the formation of the $[\text{Ir}@\text{Sn}_{12}]^{3-}$ anion **74**, isolated as the $[\text{K}(2,2,2\text{-crypt})]_3[\text{Ir}@\text{Sn}_{12}]$ salt.²³⁴



Scheme 27. Synthesis of the intermetalloid clusters $[\text{Sn}_9\text{Ir}(\text{C}_8\text{H}_{12})]^{3-}$ **73** and $[\text{Ir}@\text{Sn}_{12}]^{3-}$ **74** by Fässler *et al.*²³⁴

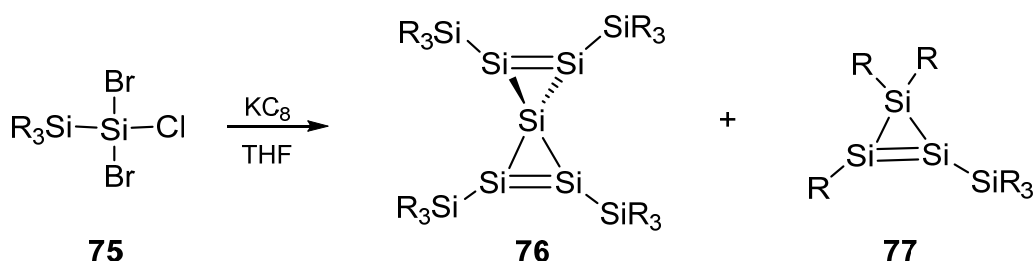
Although silicide transition metal complexes have been employed as extraordinarily electron-rich ligands towards transition metals, the residual negative charges in the transition metal derivatives of Zintl ions and the resulting poor solubility limited their application, e.g. in homogeneous catalysis. As the presence of organic substituents in siliconoids and their charge-neutrality ensure higher solubility, siliconoids may turn out to be the logical next step in the chemistry of intermetalloid clusters as they fulfill both conditions. With the possibility to graft functional groups to the Si_6 scaffold, the introduction of silylenes in the periphery of the cluster scaffold could be useful to facilitate the coordination of transition metals to the siliconoid scaffold.

1.3.3 Stable unsaturated Silicon Clusters (Siliconoids)

The general understanding and the possibility to manipulate silicon surfaces moved elemental silicon into focus to improve the capabilities of silicon-based technologies. The pronounced chemical activity of the silicon surfaces is based on the unsaturated silicon vertices, which formally are radical sites, but are referred to as “dangling bonds” by surface scientists.²³⁵ The decrease of the particles size entails the increase of the surface-to-volume ratio as a comparatively large number of atoms in small particles are surface atoms. The contribution of the surface to the bulk properties thus becomes continuously more significant as the size decreases. In addition, the decreasing size leads to a situation progressively approaching the molecular state with discrete energy terms instead of electronic band structures, a phenomenon called “quantum confinement”.^{236,237} The bonding electrons of surface

atoms of spherical particles point into one half of a sphere constituting a hemispheroidal coordination environment.²⁰³ The lack of suitable analytical techniques and the low stability of the native surfaces towards air is still challenging the characterization of nanoparticles. The synthesis of stable unsaturated silicon clusters has therefore attracted considerable interest not only due to the presumed intermediacy in gas phase deposition processes but also as suitable model systems for the unsubstituted vertices of silicon surfaces and silicon nanoparticles.

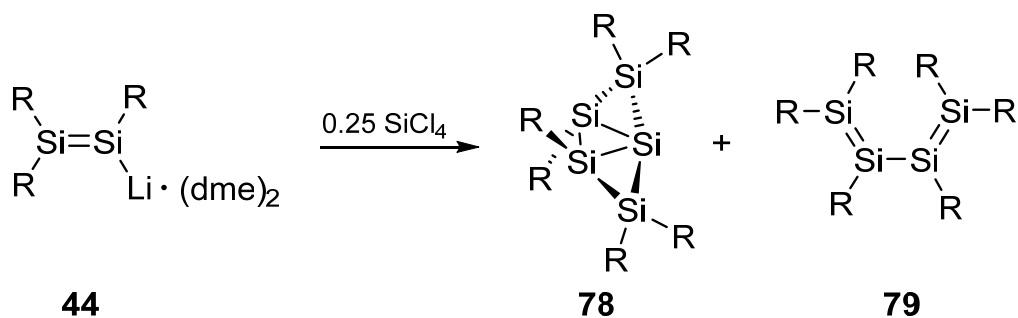
According to Schnepf's definition of the term metalloid,²⁰⁰ the first metalloid silicon cluster was reported by Kira in 2000.²³⁸ The reduction of $R_3Si-SiBr_2Cl$ **75** by potassium graphite led to the spiropentadiene **76** in only 3.5 % yield and a cyclotrisilene **77** as side product (Scheme 28).



Scheme 28. Synthesis of spiropentadiene **76** after reduction of the halogenated precursor $R_3Si-SiBr_2Cl$ **75** with potassium graphite by Kira *et al.*²³⁸ and a cyclotrisilene **77** as side product with $R = tBuMe_2Si$.

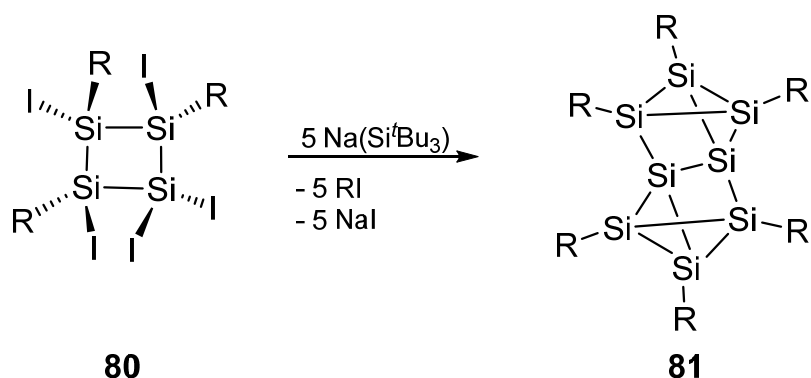
The bonding in spiropentadiene **76** is electron-precise and the *spiro*-silicon atom exhibits a distorted tetrahedron coordination instead of the hemispheroidal coordination environment found at bulk and nano surfaces of silicon. In order to account for this deficiency in Schnöckel's definition,¹⁹⁸ the term siliconoid was introduced by Scheschkewitz *et al.* for neutral metalloid silicon clusters containing one or more unsubstituted silicon vertices in a hemispheroidal coordination environment and hence featuring a "dangling bond".²⁰¹

The first siliconoid was reported in 2005 by Scheschkewitz.²³⁹ Treatment of disilenide **44** with 0.25 equivalents tetrachlorosilane $SiCl_4$ led to the formation of a five-membered siliconoid **78** with one "naked" silicon atom in the vertex with a hemispheroidality parameter $\phi = +0.1915 \text{ \AA}$ and Weidenbruch's tetrasilabutadiene²⁴⁰ **79** as a side product, systematically formed by oxidation of **44** (Scheme 29). The formation of tetrasilabutadiene **79** in this reaction suggests that **44** acts both as a nucleophile and reducing agent.



Scheme 29. Synthesis of the first siliconoid Si_5Tip_6 **78** by Scheschkewitz in 2005 (with $\text{R} = \text{Tip} = 2,4,6\text{-}^i\text{Pr}_3\text{-H}_2\text{C}_6$).²³⁹

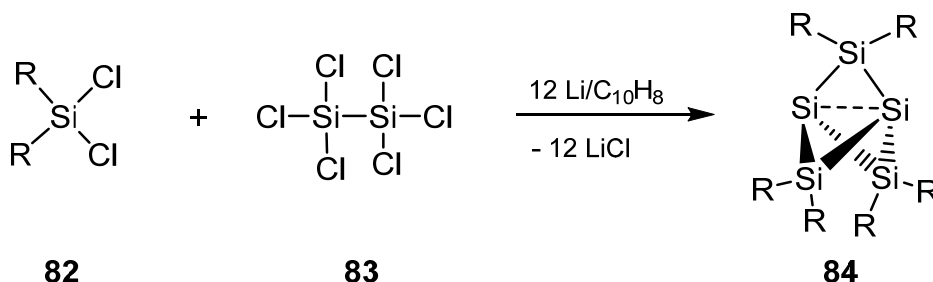
In the same year, a second siliconoid was published by Veith and Wiberg *et al.*²⁴¹ With the complete reductive dehalogenation of a pentaiodotetrasilabutane derivative **80** with NaSi^iBu_3 , an eight-membered siliconoid **81** of the type Si_8R_6 with two naked silicon atoms was isolated and characterized (Scheme 30). While the bond length between the unsubstituted vertices was determined to be remarkably short with 2.29 Å, the hemispheroidal environment of the unsubstituted vertices results in ϕ values of 0.0984 Å and +0.1233 Å.



Scheme 30. Synthesis of Wiberg's eight-membered siliconoid Si_8R_6 **81** ($\text{R} = \text{Si}^i\text{Bu}_3$).²⁴¹

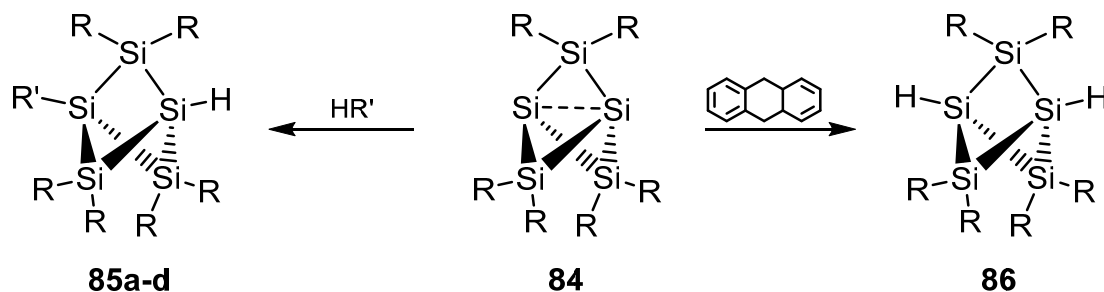
Reduction of dimesityldichlorosilane **82** (mesityl = 2,4,6- $\text{Me}_3\text{C}_6\text{H}_2$) and hexachlorodisilane **83** in a ratio of 3:1 with 12 equivalents of Li/naphthalene (Scheme 31) led to a persilapropellane **84**, which was reported by Breher in 2010.²⁴² While the presence of organic substituents in siliconoids ensures higher solubility, the electronic properties of silicon-based Zintl ions are retained in the wide dispersion of ^{29}Si NMR chemical shifts. The ^{29}Si NMR of persilapropellane **84** shows the signal of the naked silicon vertices at unusual high field ($\delta = -273.2$ ppm) while the other signals are found in the typical range of tetracoordinate silicon atoms ($\delta = 25.5$ ppm).

In addition, hemispheroidal environments were observed for the naked bridgehead silicon atoms with two distinct ϕ values of +1.3227 Å and +1.3134 Å. Due to the long distance between the bridgehead silicon atoms and based on theoretical calculations, a diradicalic character was suggested as in case of [1.1.1]propellane **66'** (Scheme 24).



Scheme 31. Synthesis of Breher's pentasilapropellane **84** (R = Mes = 2,4,6-Me₃-H₂C₆).²⁴²

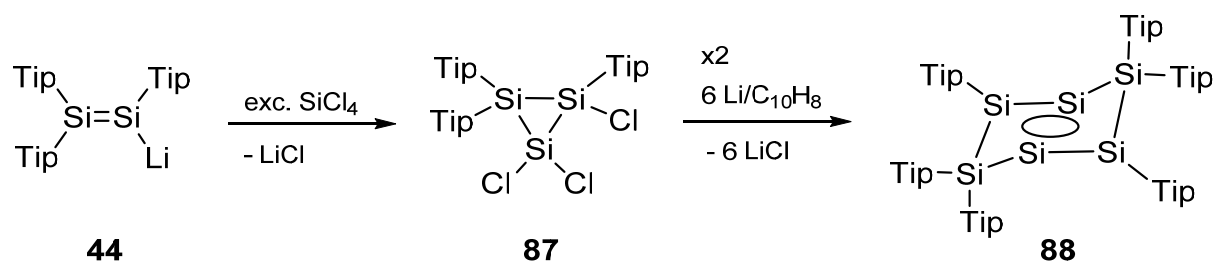
With the calculated bond strengths of ~ 174 kJ mol⁻¹ the bond between the bridgehead silicon atoms was found to be considerably weaker than Si-Si single bonds (306-332 kJ mol⁻¹).²⁴² The question of whether the path between the bridgehead atoms of propellane-like structures constitutes a direct chemical bond, however, remains an open question and has been the topic of theoretical and experimental investigations (*vide infra*, Scheme 33). Reactivity studies of the bridged propellane **84** were performed to shed some light on the nature of the bonding situation between the bridgehead silicon atoms. While the pentasilapropellane **84** was treated with H₂O, PhOH, PhSH and Me₃SNH, closed-shell reactivity was observed with the addition over the bridgehead silicon atoms in **85**.



Scheme 32. Reactivity studies of **84**: closed shell reactivity led to addition of R' = **85a**: OH, **85b**: OPh, **85c**: SPh, **85d**: SnMe₃ over the bridgehead atoms in **85a-d**; biradical-type reactivity was observed in case of treatment with 9,10-dihydroanthracene resulting in **86** (R = Mes = 2,4,6-Me₃-H₂C₆).²⁴²

In contrast, treatment of **84** with 9,10-dihydroanthracene led to the dehydrogenated adduct, a prototypical example of biradical-type reactivity (Scheme 32).²⁴² These experimental studies supports the electronic ambiguous character of the bridgehead atoms in propellane-like structures.

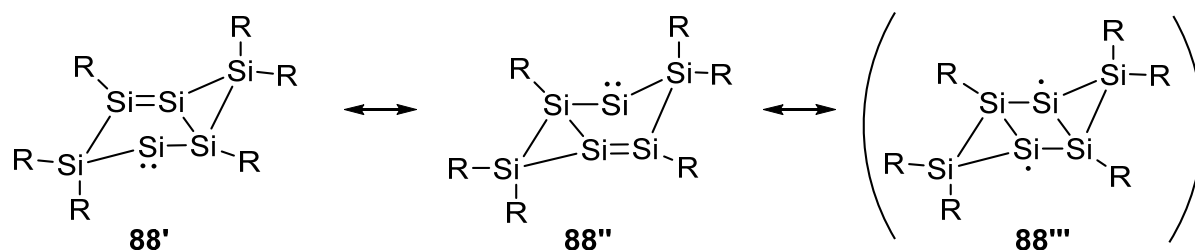
As Scheschkewitz showed already with the report on the first stable siliconoid **78**,²³⁹ disilenes can be used as a building block for unsaturated stable silicon clusters. Following reports on stable sila- and 1,2-disilabenzenes with planar Hückel-aromatic structures,^{93,243} Scheschkewitz *et al.* reported a tricyclic isomer of hexasilabenzene **88** in 2010 (Scheme 33).²⁴⁴ Treatment of disilenide **44** with an excess of tetrachlorosilane led to 1,1,2-trichlorocyclotrisilane **87**. The reductive dehalogenation of **87** with three equivalents of lithium/naphthalene resulted in dimerization and thus in the formation of the six-membered siliconoid **88** with two hemispheroidally coordinated vertices as shown by the ϕ value of +1.1151 Å (Scheme 33).²⁴⁴ The intensely green crystals as well as the wide distribution of signals in the ²⁹Si NMR spectrum (SiTip: δ = 124.6, SiTip₂: δ = -84.8, Si: δ = -89.3 ppm) are not in line with an electron precise, saturated system. The structure was thus discussed as a sila-aromatic compound with six delocalized electrons across a central rhomboid Si₄-ring with two SiR₂ vertices pointing up and downwards with respect to the Si₄-plane.



Scheme 33. Synthesis of 1,1,2-cyclotrisilane **87** followed by reduction with three equivalents of Li/C₁₀H₈ to obtain the dismutational hexasilabenzene isomer **88**.²⁴⁴

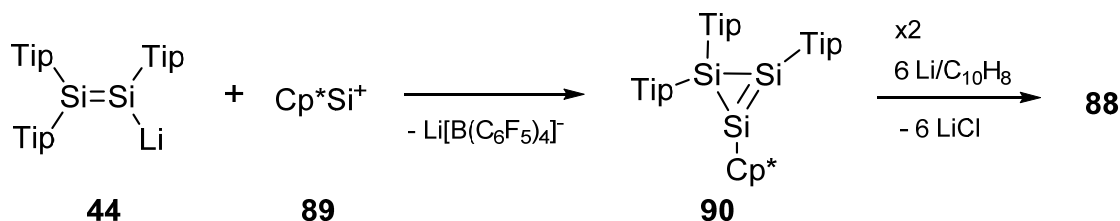
Since experimental charge density investigations as well as nucleus-independent chemical shift calculations indicate an important degree of aromaticity in **88**,²⁴⁵ the term “dismutational” was introduced by Scheschkewitz and Rzepa for the novel type of aromaticity in siliconoid **88**.²⁴⁴ In contrast to conventional Hückel aromatic systems, the electronic structure of the dismutational hexasilabenzene isomer **88** can be described by the cyclic delocalization of two π , two σ and two non-bonding electrons as represented by the two degenerate resonance structures **88'** and **88''** (Scheme

34). A hybrid resonance structure between **88'** and **88''** is considered as the best description of the electronic structure. The triplet state **88'''** was found to be by 24.1 kcal⁻¹mol⁻¹ higher in Gibbs energy than the singlet. The resonance structure **88'''** of the dismutational hexasilabenzene **88** shows topological similarities to the singlet diradicals of the Niecke-type.²⁴⁶ In contrast to the uniform oxidation state of +1 in hexasilabenzenes, the dismutational hexasilabenzene isomer **88** shows formal oxidation states of +2 (SiTip₂), +1 (SiTip) and 0 (naked Si). The long distance (2.7287 Å) between the unsubstituted silicon atoms indicated the absence of direct bonding, which was further supported by experimental and computational electron density studies resulting in a (pseudo)-tricoordination sphere and thus in the strong hemispheroidality of the unsubstituted vertices.²⁴⁵



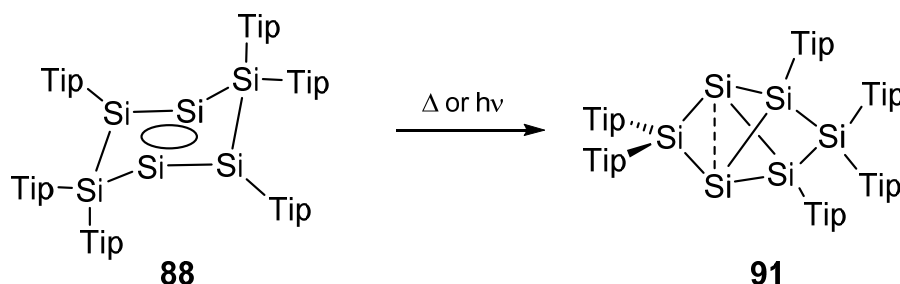
Scheme 34. Resonance structures of dismutational hexasilabenzene isomer **88** (**88'**: R = Tip = 2,4,6-triisopropylphenyl; **88''**: R = Dip = 2,6-diisopropylphenyl; **88'''**: R = Dip = 2,6-diisopropylphenyl).²⁴⁴

In a collaborative work, Scheschkewitz and Jutzi *et al.* investigated an alternative synthetic route to obtain the dismutational hexasilabenzene isomer: treatment of disilenide **44** with Jutzi's Cp^{*}Si⁺ cation **89** as a silicon source²⁴⁷ initially afforded the cyclotrisilene **90**. Cleavage of the Cp^{*} ligand in a one electron reduction led to dimerization of the presumably occurring transient cyclotrisilenyl radical resulting in the dismutational hexasilabenzene isomer **88** (Scheme 35).^{248,249}



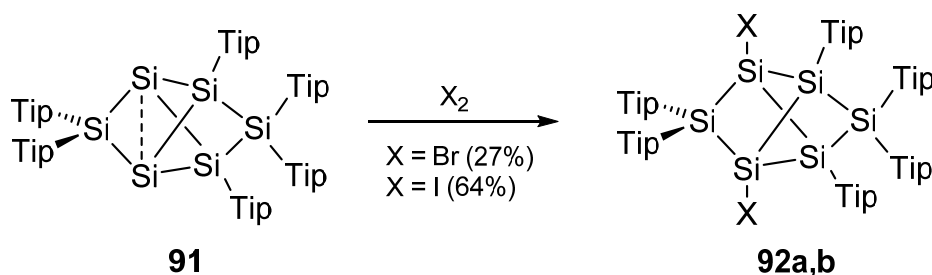
Scheme 35. Synthesis of dismutational hexasilabenzene isomer **88** by reaction of disilenide **44** with Cp^{*}Si⁺ cation **89**.^{248,249}

While the dismutational hexasilabenzene isomer **88** exhibits a high, unusual thermal stability, Scheschkewitz *et al.* reported its rearrangement to a bridged propellane structure **91** (Scheme 36) at temperatures above 250 °C or by irradiation.²⁵⁰ According to theoretical calculations the bridged propellane structure **91** represents the first stable derivative of the presumed global minimum on the Si₆H₆ potential energy surface. Thus, the global minimum isomer **91** constitutes the energetic analogue of benzene in case of silicon. Notably, the wide distribution in ²⁹Si NMR chemical shifts is still retained in the bridged propellane **91** (SiTip₂: δ = 174.6, SiTip₂: δ = 14.8, SiTip₂: δ = -7.5 SiTip, Si: δ = -274.2 ppm). Both isomers **88** and **91** therefore carry all the hallmarks of siliconoids and accordingly were classified as such later on.²⁰²



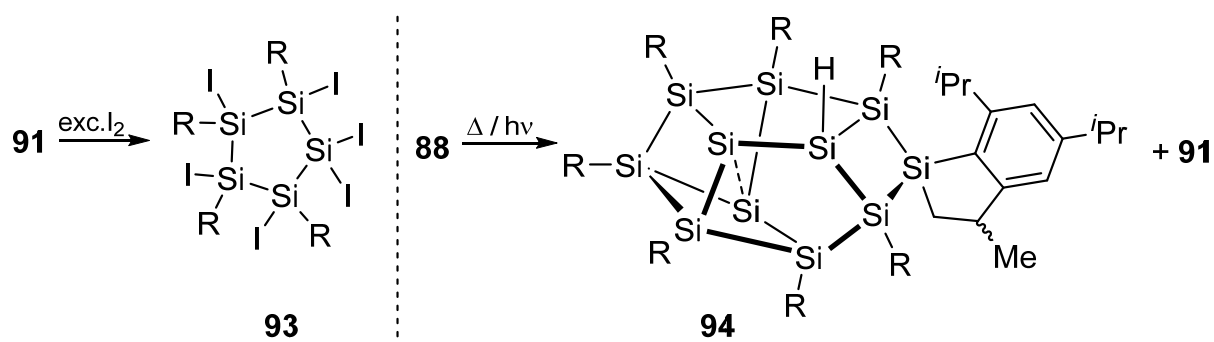
Scheme 36. Isomerization of the Si₆-scaffold of the dismutational hexasilabenzene isomer **88** to the global minimum isomer **91**.²⁵⁰

The distance between the unsubstituted bridgehead silicon atoms is elongated (2.7076 Å) as already observed in the bridged propellane **84** and the dismutational hexasilabenzene isomer **88**. The bridgehead silicon atoms feature a hemispheroidal environment with a ϕ value of +1.3535 Å.²⁵⁰ Reactivity studies showed the unsubstituted bridgehead silicon atoms to be highly reactive: simple treatment of **91** with bromine or iodine resulted in the dihalogenated derivatives **92a,b** (Scheme 37).



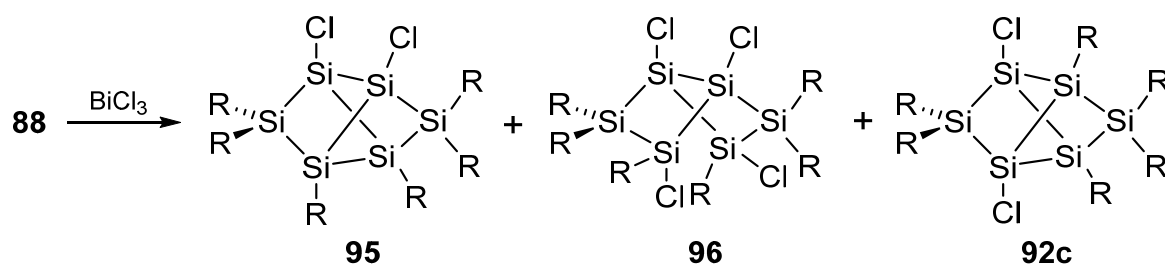
Scheme 37. Dihalogenation **92a,b** of the bridgehead silicon atoms of the global minimum isomer.²⁵⁰

Compared to the global minimum isomer, the longest wavelength absorption bands of **92a,b** in the UV-vis show only a slight shift. Unexpectedly, the distance between the now substituted bridgehead silicon atoms in **92a,b** atoms undergoes a merely slight shortening compared to that in the global minimum isomer **91**.²⁵⁰ In contrast, an excess of iodine to the global minimum isomer **91** led to the contraction of the cluster scaffold resulting in the highly functionalized 1,2,3,4-tetraaryl-substituted cyclopentasilane **93**.²⁰² Furthermore, a core-expanded siliconoid Si_{11} **94** was observed as a side product during the thermal isomerization of the dismutational hexasilabenzene isomer **88** to the global minimum isomer **91** (Scheme 38).²⁰² With the Si_{11} cluster **94**, the first example of a siliconoid cluster core expansion in the condensed phase was reported together with the highest number of silicon atoms in the cluster scaffold of a siliconoid. In contrast to the situation in the propellane motif **91**, the two unsubstituted silicon atoms in **94** are staggered.



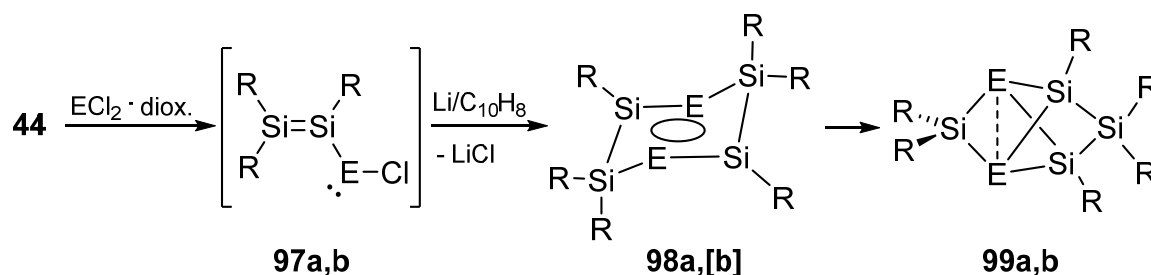
Scheme 38. Synthesis of tetraaryl-substituted cyclopentasilane **93** (left) and the thermally or photolytically induced Si_{11} cluster **94** isolated as byproduct in the thermal rearrangement of **88** to the bridged propellane **91** (right) with $\text{R} = \text{Tip} = 2,4,6\text{-triisopropylphenyl}$.²⁰²

Exploring the reactivity of the dismutational hexasilabenzene **88** towards BiCl_3 resulted in the 1,2-dichloro isomer **95** as main product, which resembles the structural motif of the global minimum isomer albeit with the formerly unsubstituted vertices being adjacent to one another. The twofold chlorinated species **96** and the dichlorinated product across the unsubstituted silicon atoms **92c** were isolated as side products (Scheme 39).²⁰²



Scheme 39. Reaction of dismutational hexasilabenzene **88** with BiCl_3 leading to Si_6 chlorinated derivatives **95**, **96**, **92c** ($\text{R} = \text{Tip} = 2,4,6\text{-triisopropylphenyl}$).²⁰²

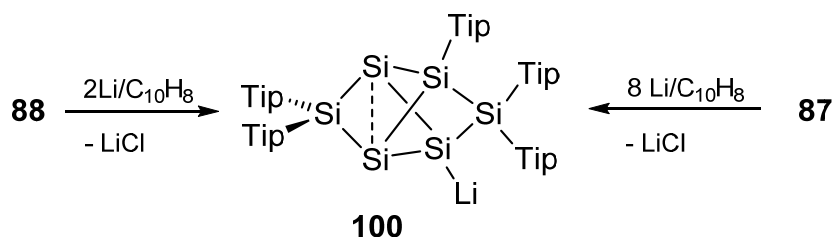
Inspired by the dismutational hexasilabenzene isomer **88**, Scheschkewitz *et al.* investigated the synthesis of mixed Group 14 siliconoids in 2014.¹⁹⁸ The formal replacement of silicon atoms in the dismutational isomer **88** by germanium and tin atoms was realized by reduction of the corresponding suitable precursors. The reaction of disilenide **44** with $\text{GeCl}_2\cdot\text{dioxane}$ or $\text{SnCl}_2\cdot\text{dioxane}$ resulted in the plausible, yet unobserved intermediates disilenyl chloro tetrylenes **97a,b**. Further reduction with lithium/naphthalene led in case of germanium to the dismutational digermatetrasilabenzene **98a** which unlike **88** rearranges already at ambient temperature to the corresponding bridged propellane structure **99a**. In contrast, the dismutational distannatetrasilabenzene isomer **98[b]** could not be observed after the reduction of **97b** with lithium/naphthalene and was only suggested as transient intermediate. The bridged propellane structure of $\text{Sn}_2\text{Si}_4\text{R}_6$ **99b** was isolated as a stable compound continuing the stability trend observed in case of germanium (Scheme 40).¹⁹⁸



Scheme 40. Synthesis of partially germanium- and tin substituted siliconoids **98a**, **99a,b** reported by Scheschkewitz *et al.* in 2014.¹⁹⁸

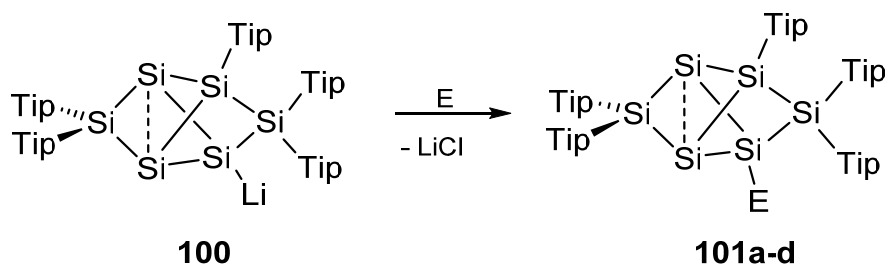
The pivotal role of unsaturated silicon cluster compounds in silicon-based materials led to a rapid growth in the field of siliconoids and a variety of examples have been prepared in the meantime by the groups of Fässler,¹⁸⁶ Iwamoto,²⁵¹ Kyushin^{252,253} and Lips^{254,255}. Further development in the field of unsaturated silicon clusters, however,

were strongly limited by the absence of possibilities to graft functional groups to siliconoids. As the cleavage of aryl^{256,257} or silyl^{196,258} groups from electron-precise unsaturated silicon species via reduction was already known, a logical step after the isolation of the dismutational hexasilabenzene isomer **88** was the reduction of **88** with three equivalents of lithium/naphthalene. Indeed an anionic Si₆Tip₅⁻ siliconoid **100** was isolated in good yields (Scheme 41).



Scheme 41. Synthesis of the first anionic siliconoid Si₆Tip₅⁻ **100**. Reduction of **88** with 2 equivalents of lithium/naphthalene (left). Reduction of a cyclotrisilene **87** with 8 equivalents of lithium/naphthalene (right).⁵³

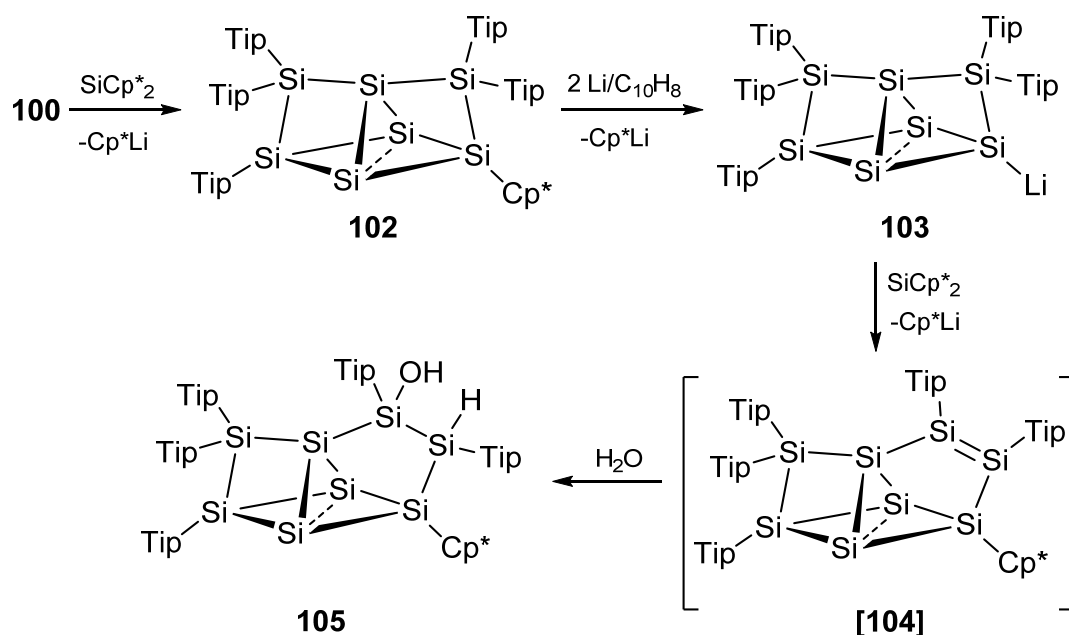
The two unsubstituted silicon atoms are retained as confirmed by the characteristic ²⁹Si NMR shifts.⁵³ The synthesis of **100** and its further functionalization with suitable electrophiles (Scheme 42) closed the gap between neutral unsaturated silicon clusters the completely unsubstituted silicon-based Zintl Anions. Reaction of the anionic siliconoid **100** with electrophiles such as borane dimethyl sulfide complex, pivaloyl chloride, silicon tetrachloride and bis(dimethylamino)chlorophosphane indeed led to the corresponding borate-, carbonyl-, silyl- and phosphanyl-functionalized siliconoids **101a-d**. Without exception, these functionalizations leave the unsubstituted bridgehead silicon atoms untouched.⁵³



Scheme 42. Synthesis of functionalized siliconoids **101a-e** with substituents: a = BH₃, b = C(O)^tBu, c = SiCl₃, d = P(NMe₂)₂.⁵³

More recently, Scheschkewitz *et al.* investigated the atomically precise cluster expansion of siliconoids.²⁵⁹ Treatment of the anionic siliconoid **100** with Jutzi's decamethylsilicocene⁵⁷ Cp*₂Si as electrophilic silicon source led to the core-

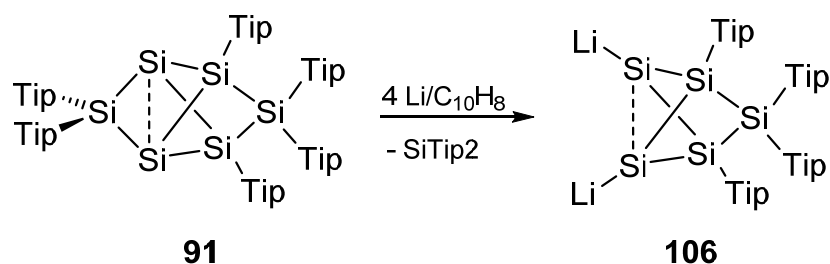
expanded $\text{Si}_7\text{Tip}_5\text{Cp}^*$ siliconoid **102**. Reduction of the Si_7 siliconoid with lithium/naphthalene resulted in the cleavage of the Cp^* group and thus the formation of an anionic Si_7 siliconoid **103**. Further addition of Jutzi's Cp^*Si to the novel anionic Si_7 siliconoid **103** again expands the cluster core to an eight-membered siliconoid $\text{Si}_8\text{Tip}_5\text{Cp}^*$, which was characterized as the hydrolyzed adduct **105** (Scheme 43).



Scheme 43. Atomically precise cluster expansion of an anionic $\text{Si}_6\text{Tip}_5^-$ siliconoid **100** with decamethylsilicocene SiCp^* and further reduction with lithium/naphthalene leads to cluster-core expanded siliconoids **102**, **103** and **105**.²⁵⁹

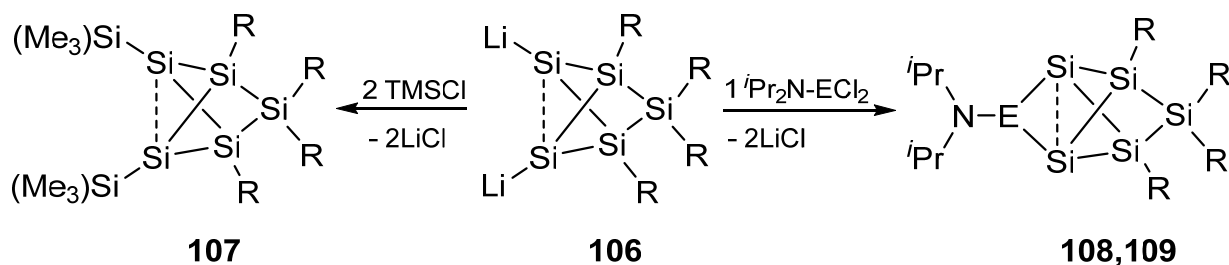
The systematic transformation and stepwise expansion of the silicon scaffold offers with the possibility of a stepwise increase of the unsubstituted silicon atoms in the scaffold. As the synthetic procedure allows the regeneration of the anionic functionality by alternating addition of decamethylsilicocene and the reducing reagent, a “living nanoparticle” synthesis might be possible in the future. The “living” nanoparticle synthesis may be expected in a one-pot reaction with alternating addition of decamethylsilicocene and lithium/naphthalene as reducing reagent leading to siliconoids of the type Si_nR_5 with an ever-growing number of unsubstituted silicon atoms while maintaining the number of organic substituents. The incorporation of hetero atoms such as boron and phosphorous is likewise conceivable with the exchange of SiCp^* as silicon source to a hetero atom source.

According to theoretical studies, the doping of silicon clusters with phosphorous has a significant effect on the optoelectronic properties.²⁶⁰⁻²⁶³ In this light, Scheschkewitz *et al.* investigated the synthesis of p- and n-doped molecular siliconoids. In contrast to the aforementioned synthesis with the anionic Si_6Li **100** as starting point, a highly reactive dianionic siliconoid **106** was employed, which was obtained by reductive cleavage of the SiTip_2 bridge adjacent to the unsubstituted vertices of the global minimum isomer **91** with four equivalents lithium/naphthalene (Scheme 44).²⁶⁴



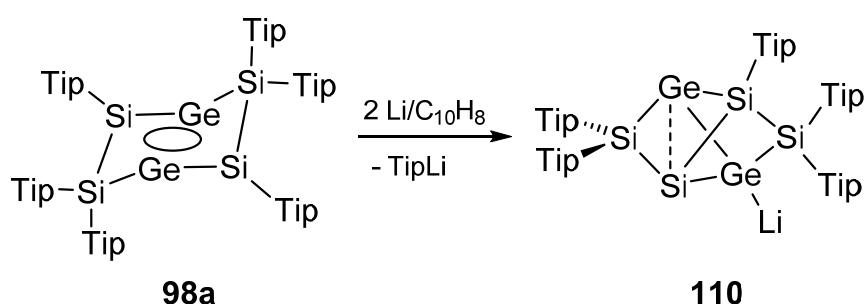
Scheme 44. Synthesis of dianionic siliconoid **106** via reduction of global minimum isomer **91** with 4 equivalents of lithium/naphthalene.²⁶⁴

The crystal structure of **106** could be resolved as the dimeric structure in the solid state. Treatment of dianionic siliconoid **106** with two equivalents of Me_3SiCl led to the expected neutral Si_5 cluster **107** with two trimethylsilyl substituents. More interestingly, the reactions of dianionic siliconoid **106** with one equivalent of dichloro-N,N-diisopropylaminoborane or -phosphane resulted in restoring of a six-atomic scaffold with the incorporation of a heteroatom instead of the SiR_2 bridge and thus leading to the first boron- and phosphorous-doped siliconoids **108** and **109** (Scheme 45).²⁶⁴



Scheme 45. Synthesis of bis(trimethylsilyl)-substituted Si_5 siliconoid **107** and boron- and phosphorous doped siliconoids **108** and **109** ($\text{R} = \text{Tip} = 2,4,6\text{-triisopropylphenyl}$).²⁶⁴

Doping of siliconoids with heteroatoms also offers new opportunities regarding the formation mechanism of siliconoid structures. The atomically precise cluster expansion of Scheschkewitz *et al.*,²⁵⁹ for instance, can be considered as a model pathway for reductive elimination – oxidative addition pathways in the gas phase. As another example, the rearrangement of a Si₄Ge₂ scaffold to the dismutational isomer of 1,4-digermatetrasilabenzene **98a** (Scheme 40) shows the occupation of both unsubstituted positions by germanium.¹⁹⁸ In contrast, in the corresponding lithiated species Si₄Ge₂Li **110** one germanium atom is located at either unsubstituted vertex and the second one exclusively at the anionic position (Scheme 46).⁵⁴



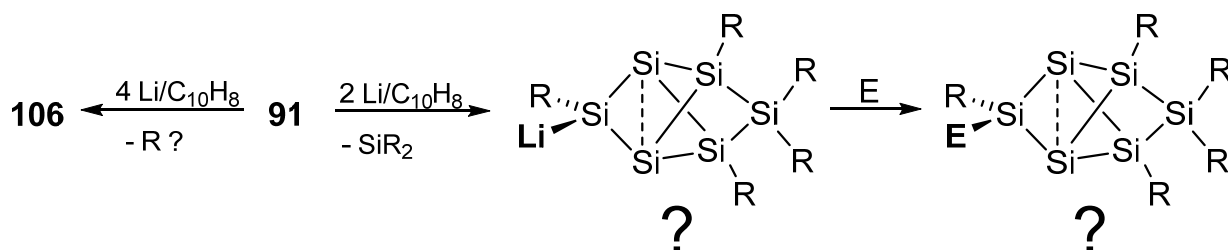
Scheme 46. Synthesis of anionic heterosiliconoid Si₄Ge₂Li **110** (Tip = 2,4,6-triisopropylphenyl).⁵⁴

The formation of the germanium-doped anionic heterosiliconoid **110** gives some insight to the complex multi-step rearrangement properties of the cluster backbone. In general, the synthetic strategies to access unsaturated siliconoids can be summarized in three categories: application of heavier vinyl anions analogues such as the disilene precursors, the reductive coupling of halogenated precursors in different ratios and the recently disclosed approach of the partial substitution of Zintl silicide anions.

2 Aims and Scope

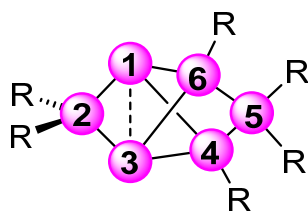
The central focus of this thesis is the synthesis of functionalized unsaturated silicon clusters and the examination of their reactivity towards small molecules and transition metals. Residual functionalities at the cluster core played a major role in these endeavors.

Recently, the Scheschkewitz group reported the synthesis of an anionic siliconoid **100** by reduction of **88** with an excess of lithium/naphthalene.⁵³ According to preliminary studies, the anionic site allowed for the functionalization of the cluster scaffold with suitable electrophiles. Consequently, one task of this PhD project was the functionalization of anionic siliconoid **100** with further functional groups. In terms of the further elaboration of synthetic protocols, an efficient and progressively substitution of all aryl substituents might be conceivable to control the reactivity and to realize embedding of siliconoids into extended systems. Therefore, reduction of the global minimum isomer **91** is going to be studied. In order to explore the nucleophilic transfer of the new anionic siliconoid, its reaction with several electrophiles was going to be investigated in this project (Scheme 47).



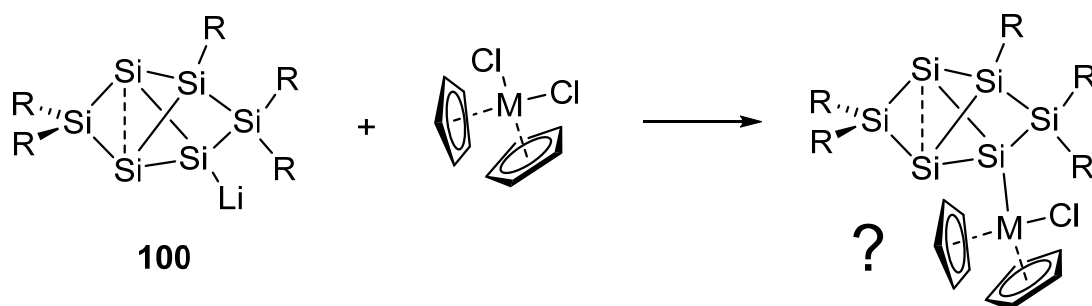
Scheme 47. Synthesis of the dianionic siliconoid **106** and the proposed reaction of **91** with two equivalents of Li/C₁₀H₈ and its further proposed functionalization with various electrophiles.

The rapidly increasing number of functionalized Si₆ benzpolarenes required the distinction of the different vertices which was accounted for by the introduction of a novel nomenclature. The characteristic bonding situation of each silicon vertex of the benzpolarene scaffold is thus reflected in the selection of the prefixes for the bridgehead silicon atoms 1 and 3, the mono-substituted vertices 4 and 6, the characteristically deshielded SiTip₂ bridge in 2-position and SiTp₂ in position 5 (Scheme 48).



Scheme 48. Schematic representation of the silicon vertices in the propellane bridged Si_6 cluster.

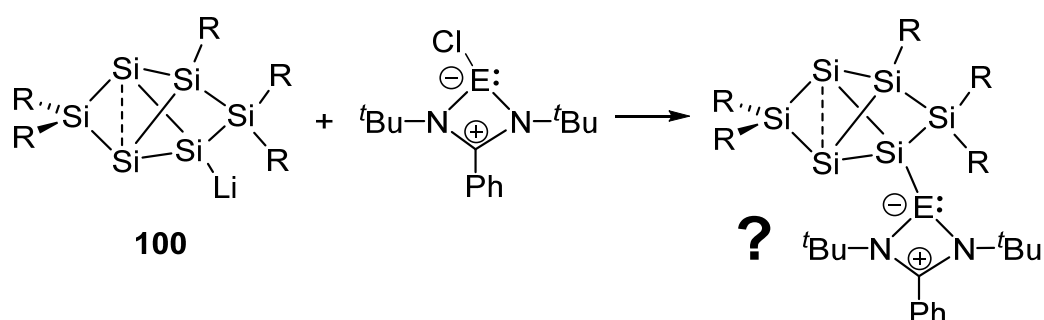
Furthermore, functionalization of siliconoids with transition metals is of particular interest as the electron-rich siliconoids are expected to be powerful σ -donating ligands for application in homogeneous catalysis. While the coordination behavior of siliconoids is virtually unexplored, Zintl Anions of Group 14 elements have already been applied as transition metal ligands. Their application in homogeneous catalysis, however, is limited due to the poor solubility of the multiple negatively charged anions. As the anionic siliconoid **100** is a useful reagent to transfer functionalities to the Si_6 benzpolarene scaffold,⁵³ one major target of this work was the investigation of its suitability for the grafting of the Si_6 framework to transition metals. Therefore, the reaction of **100** with dichlorinated metallocenes was going to be investigated in order to achieve the isolation of novel metallocene substituted siliconoids (Scheme 49).



Scheme 49. Proposed reactivity of anionic siliconoid **100** towards dichlorinated metallocenes ($M = \text{Zr}, \text{Hf}$; $R = \text{Tip} = 2,4,6\text{-triisopropylphenyl}$).

As described in the introduction in chapter 1.1.1 and 1.1.2, N-heterocyclic silylenes are useful ligands in the coordination to transition metals. Dative coordination of charge-neutral siliconoids to metals is to date unknown, but should in principle be possible with the help of a pending auxiliary silylene ligand. As the recently reported reaction of anionic siliconoids with Jutzi's silicocene led to cluster-core expansion,²⁶⁰ the synthesis of a siliconoid/silylene hybrid with intact silylene functionality would be an attractive goal.

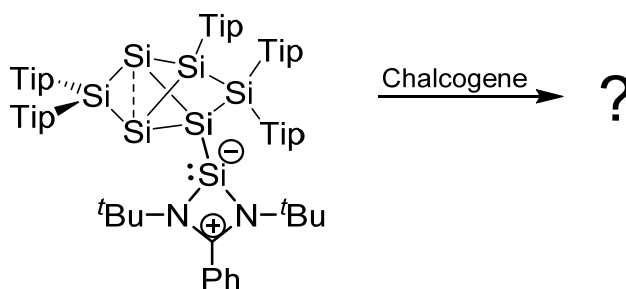
In this work the chlorinated amidinato silylene **5** was going to be employed as a precursor under the assumption that the electron deficiency of the Si(II) center is sufficiently tamed by the adjacent nitrogen donors to introduce the silylene functionality in a simple salt elimination reaction to the Si₆ benzpolarene scaffold. Subsequently, the coordination behavior of the envisaged tetrylene functionalized siliconoids towards transition metals should be investigated in order to evaluate the donor properties of the tetrylene/siliconoid hybrids (Scheme 50).



Scheme 50. Proposed reactivity of anionic siliconoid **100** towards chlorinated amidinato tetrylenes (E = Si, Ge, Sn).

Catalytic benchmark reactions were finally going to be included to demonstrate the suitability as ligands in a homogeneous catalytic setting.

Although Si–Si single bonds are well-known to oxidatively add chalcogens under mild conditions,²⁶⁵⁻²⁷⁰ those hetero silicon clusters are rare²⁷⁰⁻²⁷⁵ and exclusively reported for saturated silicon clusters. As treatment of saturated silicon clusters with chalcogens resulted in cluster core expansions,^{254,266,273-276} a similar strategy could be envisaged for the unsaturated siliconoids. Therefore, the reactivity of chalcogens towards a silylene/siliconoid hybrid was going to be studied in this project in order to achieve the isolation of the first chalcogen-doped heterosiliconoids (Scheme 51).



Scheme 51. Proposed reaction of a silylene/siliconoid hybrid with chalcogens.

3 Results and Discussion

3.1 Site-selective functionalization of Si₆R₆ siliconoids

Yannic Heider*, Nadine E. Poitiers*, Philipp Willmes, Kinga I. Leszczyńska, Volker Huch, David Scheschkewitz, *Chem. Sci.*, **2019**, *10*, 4523-4530.

[DOI: 10.1039/C8SC05591B](https://doi.org/10.1039/C8SC05591B)

* These authors contributed equally.

The article has been published by the Royal Society of Chemistry (RSC) as an “Open Access” Article and is licensed under a “Creative Commons Attribution-NonCommercial 3.0 Unported (CC BY-NC 3.0)” Licence (<https://creativecommons.org/licenses/by-nc/3.0/>).

The article is reproduced by permission of The Royal Society of Chemistry and all authors. The results are additionally concluded and put into context in Chapter 4.

Contributions of the Authors:

Yannic Heider: Lead: Synthesis, and characterization of *privo*-functionalized Si₆ siliconoids (R = CPh, CO^tBu, P(NMe₂)₂, SiCl₃, BH₃⁻); Equal (N.P.): Conceptualization, Visualization, Investigation, Methodology, Data Curation, Formal Analysis, Writing — review and editing of the Supporting Information; Equal (P.W.): Synthesis and characterization of *privo*-anionic Si₆ siliconoid; Supporting: Writing — Review and Editing of the manuscript.

Nadine E. Poitiers: Lead: Writing — Review and Editing of the manuscript, Synthesis and characterization of *ligato*-functionalized Si₆ siliconoids (R = TMS, CPh); Equal (Y.H.): Conceptualization, Visualization, Investigation, Methodology, Data Curation, Formal Analysis, Writing — review and editing of the Supporting Information.

Philipp Willmes: Equal (Y.H.): Synthesis and characterization of *privo*-anionic Si₆ siliconoid; Lead: Synthesis and characterization of *privo*-TMS substituted Si₆ siliconoid; Supporting: Investigation, Methodology.

Kinga I. Leszczyńska: Supporting: Supervision.

Volker Huch: Lead: X-ray analysis.

David Scheschkewitz: Lead: Project administration, Supervision, Acquisition of funding and resources; Supporting: Writing — review and editing.

Cite this: *Chem. Sci.*, 2019, 10, 4523

All publication charges for this article have been paid for by the Royal Society of Chemistry

Received 14th December 2018

Accepted 7th March 2019

DOI: 10.1039/c8sc05591b

rsc.li/chemical-science

Site-selective functionalization of Si₆R₆ siliconoids†Yannic Heider,[‡] Nadine E. Poitiers,[§] Philipp Willmes, Kinga I. Leszczyńska, Volker Huch and David Scheschkewitz^{§*}

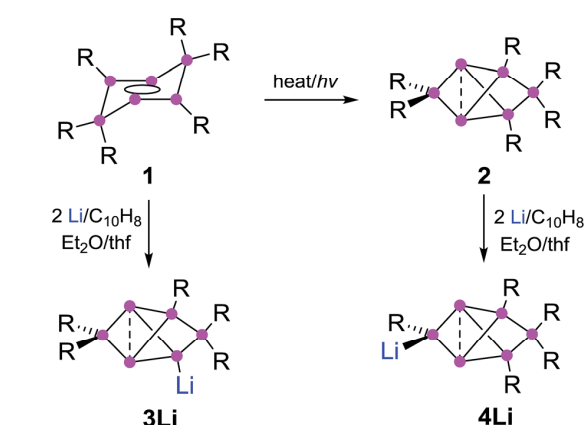
The recent progress in the synthesis of partially substituted neutral silicon clusters (siliconoids) revealed unique structures and electronic anisotropies that are reminiscent of bulk and nano surfaces of silicon. Here, we report the selective 2-lithiation of the global minimum Si₆R₆ siliconoid at a different vertex than in the previously reported isomeric 4-lithiated derivative (R = 2,4,6-*t*-Pr₃C₆H₂). In order to enable an intuitive distinction of the vertices of the global minimum Si₆R₆ scaffold (which can be considered the silicon analogue of benzene in terms of thermodynamic stability), we introduce a novel nomenclature in analogy to the *ortho*–*meta*–*para* nomenclature of disubstituted benzenes. By treatment of the 2-lithiated Si₆ cluster with Me₃SiCl, SiCl₄, H₃B·SMe₂, (Me₂N)₂PCl as well as with carboxylic acid chlorides RCOCl (R = *t*-Bu, Ph) various 2-functionalized Si₆ clusters were obtained and characterized in solution and – in most cases – the solid state. The structural and spectroscopic effect of the position of the newly introduced functional group is discussed by comparison to the corresponding 4-functionalized derivatives.

Introduction

Partially substituted neutral silicon clusters (siliconoids)^{1–4} are fleeting intermediates during the production of silicon from molecular precursors and can typically only be detected in the gas phase.^{5–9} The synthesis of stable derivatives has attracted considerable interest as the unsubstituted vertices of siliconoids are reminiscent of the free valences at bulk and nano surfaces of silicon, the so-called “dangling bonds”.^{10–13} Since the report on the first stable siliconoid Si₅R₆ with one “naked” vertex in a hemispheroidal coordination environment by one of us,¹⁴ numerous examples have been prepared by the groups of Wiberg,¹⁵ Breher,¹⁶ Kyushin,^{17,18} Iwamoto,¹⁹ Fässler²⁰ and ourselves.^{14,21–23} The Si₆R₆ isomers **1** (ref. 22) and **2** (ref. 23) are lower energy isomers of the hypothetical hexasilabenzene and as such prime examples of the often drastic differences between carbon and silicon (Scheme 1). While of the known C₆H₆ isomers, benzene is by far the lowest in energy, the tricyclic **2** corresponds to the global minimum isomer of Si₆H₆ and can therefore be considered as the silicon analogue of benzene on grounds of thermodynamic stability.^{23,24}

The functionalization of such clusters is a prerequisite for the further development of their chemistry and ultimately the

application of their fascinating electronic properties in extended materials. Compared to the related Zintl anions of the heavier group 14 elements,^{25–31} which are (poly)anionic, completely unsubstituted deltahedral clusters, siliconoids are partially substituted yet exhibit a similarly wide dispersion of ²⁹Si NMR shifts.^{14,16–18,22,24} Very recently, the protonation of silicon Zintl anions to partially H-substituted anionic siliconoids was reported independently by the groups of Fässler and Gschwind/Korber.^{30,31} We had previously described the reductive functionalization of the dismutational Si₆R₆ isomer **1** to the

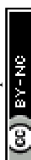


Scheme 1 Synthesis of **3Li** (ref. 32) and **4Li** (this work) from dismutational hexasilabenzene isomer **1** and from the global minimum isomer **2** (Tip = 2,4,6-triisopropylphenyl).

Krupp-Chair of General and Inorganic Chemistry, Saarland University, 66123 Saarbrücken, Germany. E-mail: scheschkewitz@mx.uni-saarland.de

† Electronic supplementary information (ESI) available: CCDC 1877380 (**5a**), 1877381 (**5b**), 1877378 (**4Li**), 1877379 (**6a**), 1877382 (**6c**), 1877383 (**6f**). For ESI and crystallographic data in CIF or other electronic format see DOI: 10.1039/c8sc05591b

‡ These authors contributed equally.



anionic siliconoid **3Li** as well as its reactivity with several representative electrophiles of groups 13 to 15.^{32,33}

Herein, we show that reduction of the global minimum isomer **2** under similar conditions selectively affords the regiomeric anionic Si₆ siliconoid **4Li** instead of **3Li** by cleavage of an aryl substituent in the 2-position of the bridged propellane scaffold (Scheme 1). In order to account for the rapidly increasing number of species with the thermodynamically favored bridged-propellane scaffold and unequivocally distinguish between the different vertices, we propose a novel terminology for this structural motif, inspired by the well-established *ortho-meta-para* nomenclature for disubstituted benzenes.^{34–37} The functionalization of **3Li** and **4Li** with selected electrophiles is shown to result in several sets of regiomeric derivatives allowing for the systematic comparison of the structural and spectroscopic consequences of the functional group's position.

Results and discussion

Nomenclature of Si₆ siliconoids

Structures with [1.1.1]propellane motif have intrigued experimentalists and theorists alike ever since the early 1970s,^{38,39} because of their non-classical structure containing bridgehead atoms in an umbrella-type hemispheroidal coordination environment. The bonding situation between the bridgehead atoms of [1.1.1]propellanes can be described by biradical or ionic contributions to the electronic ground state^{40–43} and was discussed by Shaik *et al.* as a “charge-shift-bond”.^{44,45} The Si₆ siliconoids **2** and **3Li** show a closely related structure having two propeller blades bridged by one SiTip₂ moiety. Strongly deshielded ²⁹Si NMR signals had been explained by a cluster-like delocalization of the two electrons in question.²³ Electron density determinations of the Si₆ siliconoid **2** confirmed the absence of direct bonding between the bridgehead silicon vertices.⁴⁶ For nomenclature purposes,^{47,48} the Si₆ scaffold is nonetheless formally considered as tetracyclic system with a direct connection between the hemispheroidally coordinated vertices that are depicted in the schemes as a dashed line.

The high thermodynamic stability of Si₆ siliconoid **2** as the alleged global minimum of the Si₆H₆ potential energy surface^{23,24} suggests a considerable prevalence of this structural motif. This received first corroboration by the successful synthesis of mixed group 14 systems⁴⁹ and a Sn₆ derivative recently.⁵⁰ Saturated variations of the six-atom scaffold occur in numerous other species throughout main group chemistry.^{51–54} In the past, the tetracyclic core structure has been variously referred to as “edge-capped trigonal bipyramid”⁵⁵ “doubly edge-bridged tetrahedron”⁵⁶ or “bridged propellane”.²³ As these terminologies do not seem to do justice to the ubiquity of the structural motif, we propose a novel term that echoes the relationship to the iconic benzene molecule and – at the same time – takes into account the extraordinary polarization of **2** and related species.^{39,57–64} We thus suggest the term “benzpolarene” – in analogy to benzvalene – for the tetracyclic arrangement of vertices in the cluster core of **2** and **3Li**. In addition, we feel that the availability of the first Si₆ siliconoid regiomers described

herein requires a descriptive nomenclature not unlike the well-established *ortho*, *meta* and *para* prefixes used for disubstituted benzenes. The prefixes thus proposed in the following reflect the characteristic bonding situation of each vertex (Chart 1).

The latin words for “naked” (lat. nudus), “bonded” (lat. ligatus), “remote” (lat. remotus) and “deprived” (lat. privus) served as inspirations. The *nudo* prefix is assigned to the unsubstituted (“naked”) bridgehead silicon atoms in 1,3-position, the *ligato* prefix to the mono-substituted vertices (4,6-position) bonded to one substituent each, the *remoto* prefix to the remote bridge in 5-position and the *privo* prefix to the characteristically deshielded (“deprived” of electrons) atom in 2-position.

Functionalization in *ligato* position

In addition to the previously reported persilabenzpolarenes,^{32,33} we investigated two further reactions of siliconoid **3Li** with electrophiles. The novel *ligato* functionalized siliconoids **5a,b** were thus obtained by treatment of **3Li** in benzene at room temperature with Me₃SiCl and benzoyl chloride, respectively (Scheme 2). The reactions proceed quantitatively according to ²⁹Si NMR spectroscopy. The siliconoids **5a,b** were isolated as single crystals and fully characterized by X-ray analysis, NMR spectroscopy, UV/Vis (Table 1) and by IR spectroscopy in case of the CO containing species.

The ²⁹Si NMR spectra of **5a,b** show the typical distribution of chemical shifts for *ligato* functionalized persilabenzpolarenes as recently reported by our group for **5c–f**.^{32,33} The two unsubstituted bridgehead silicon atoms give rise to two ²⁹Si signals in a range of –257 to –280 ppm (Table 1). The C_{2v} symmetry of the benzpolarene scaffold of **2** is lowered to C_s in the substituted cases. As we had shown by VT NMR studies for some of the *ligato*-functionalized species,³² hindered rotation further reduces the symmetry so that the two seemingly identical *nudo* atoms become diastereotopic. The resonances of the SiTip₂ groups in *privo* position are strongly deshielded with signals at 169.9 (**5a**) and 174.7 ppm (**5b**). The surprisingly downfield shifted signals (for tetracoordinate silicon atoms) had been rationalized by invoking magnetically induced cluster currents or – in a complementary manner – by the strong LUMO contribution at this atom.^{49,65,66} The ²⁹Si NMR chemical shifts of the remaining cluster vertices are located in the typical range for saturated silicon atoms and vary only slightly with the introduced functionality. The longest wavelength absorption bands in the UV/Vis are observed at λ_{max} = 459 nm (**5a**) and 477 nm (**5b**). The characteristic CO stretching mode in the IR of **5b** at ν = 1605 cm^{–1} compares well with that of **5c**.^{32,33} Single crystals

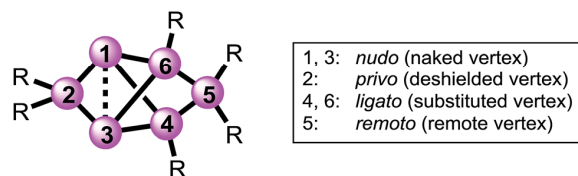
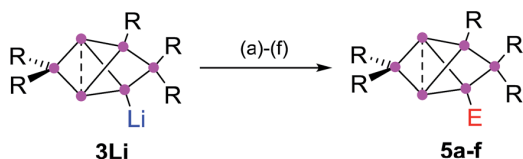


Chart 1 Proposed prefixes for unique assignment of vertices in bridged propellane-type (“benzpolarene”) siliconoids.





Scheme 2 Synthesis of *ligato*-functionalized siliconoids **5a–f**. Reagents: (a) Me₃SiCl, (b) PhCOCl, (c) ^tBuCOCl, (d) ClP(NMe₂)₂, (e) SiCl₄, (f) BH₃·SMe₂. **5a**: E = Me₃Si, **5b**: E = CPh and the previously reported³² **5c**: E = CO^tBu, **5d**: E = P(NMe₂)₂, **5e**: E = SiCl₃, **5f**: E = BH₃[–].

were obtained in 45% (**5a**) and 66% (**5b**) yield and the structures confirmed by X-ray diffraction studies (Fig. 1).⁶⁷ The distances between the unsubstituted bridgehead silicon atoms Si1 and Si3 are slightly shorter than in the global minimum isomer,²³ in line with the observations for the previously reported *ligato* functionalized persilabenzpolarenes **3Li** and **5c–f**.^{32,33} The distance between the *ligato* positions Si4 and Si6 of **5a–f** increases with decreasing distance between the *nudo* positions Si1 and Si3, presumably in order to minimize strain (Table 1). Apparently, the variation of the *ligato* functionality of the benzpolarene structures **5a–f** directly influences the bonding between the unsubstituted silicon atoms Si1 and Si3.

Synthesis of *privo* lithiated siliconoid **4Li**

The reduction of the dismutational isomer of hexasilabenzene **1** had yielded the lithiated siliconoid with a benzpolarene scaffold **3Li** and thus a functionalized derivative of the Si₆H₆ global minimum isomer **2**.^{32,33} In order to probe the possible intermediacy of **2**, its reduction with lithium/naphthalene was investigated (Scheme 3).

Treatment of **2** with 2.2 equivalents of Li/C₁₀H₈ in Et₂O and thf indeed results in the complete and uniform conversion into

a novel anionic Si₆ species as confirmed by ²⁹Si NMR spectroscopy. The six resonances show a similar chemical shift distribution as in **3Li**, but with distinctly different values suggesting the functionalization had taken place in another position of the benzpolarene scaffold (Table 1). The reduction product **4Li** was fully characterized by X-ray diffraction on single crystals, NMR spectroscopy and UV/Vis spectroscopy.

A strongly deshielded ²⁹Si NMR signal at 267.9 ppm is significantly broadened (presumably due to coupling to the quadrupolar ⁷Li-nucleus) and only shows a cross-peak to the aromatic H atoms of a single Tip ligand in the 2D ¹H/²⁹Si correlation spectrum. These observations led us to conclude that the anionic functionality of **4Li** is located at the tetra-coordinate silicon atom in the *privo* position Si2. The ²⁹Si chemical shift of 267.9 ppm is particularly remarkable as saturated silyl anions typically show resonances at much higher field often deep in the negative ppm region.⁶⁹ According to our previous calculations,⁶⁶ the magnetically induced cluster currents circumvent the *privo* position and thus cause its pronounced deshielding even in case of the peraryl-substituted benzpolarene **2**. On the basis of a complementary explanation referring to the topology of the LUMO,⁴⁹ this phenomenon is probably due to the pronounced silylene character of the *privo* atom. The presence of a directly attached electron-releasing substituent could lead to an increased localization of the vacant p orbital in the *privo* position and thus to the observed even more pronounced deshielding. The signals for the *remoto* SiTip₂ and the two *ligato* SiTip units appear at δ = 15.3 and 100.2/–43.8 ppm, respectively. The reason for the large difference between the chemical shifts is unclear although the electronic environments of the *ligato* atoms are certainly dominated by their relative position to the anionic functionality and the lithium counter cation in *privo* position. The unsubstituted bridgehead silicon atoms in the *nudo* positions are apparently

Table 1 Comparison of NMR spectroscopic and structure data of *ligato* functionalized siliconoids **5a–f** and *privo* functionalized siliconoids **6a–f**

Position of E	Comp.	Functional group (E)	Si1, Si3 [ppm]	Si2 [ppm]	Si4 [ppm]	λ _{max} [nm]	ΔSi1–Si3 [Å]	ΔSi4–Si6 [Å]	σ _m ^{a,67}	Hemisphericity ^b φ [Å]
—	2	Tip ²³	–274.2	174.6	–7.5	473	2.7076(8)	2.9037	0.08	1.3535
<i>ligato</i>	3Li	Li ³²	–230.9, –232.6	152.2	–66.8	364	2.5506(9)	3.2243	—	1.2805
<i>privo</i>	4Li	Li	–222.2, –231.4	267.9	–43.8	468	2.5562(10)	2.9171(11)	—	1.3078
<i>ligato</i>	5a	TMS	–257.8, –266.6	169.9	–3.7	459	2.6176(5)	2.9643(8)	–0.04	1.3283
<i>ligato</i>	5b	COPh	–263.0, –279.0	174.7	–26.5	477	2.6598(9)	2.8854(8)	0.34	1.3333
<i>ligato</i>	5c	CO ^t Bu ³²	–264.7, –271.1	171.8	–27.4	475	2.6430(6)	2.9095	0.27	1.3458
<i>ligato</i>	5d	P(NMe ₂) ₂ (ref. 32)	–256.0, –261.4	168.7	–33.8	475	2.6231(5)	2.9508	0.18	1.3498
<i>ligato</i>	5e	SiCl ₃ (ref. 32)	–252.3, –264.2	175.4	12.9	460	2.635(1)	2.8920	0.48	1.3409
<i>ligato</i>	5f	BH ₃ (ref. 32)	–257.3, –265.0	161.2	–4.8	475	2.620(1)	2.9988	–0.48	1.3153
<i>privo</i>	6a	TMS	–242.0, –253.3	193.6	–15.9	469	2.6118(6)	2.9482(6)	–0.04	1.3308
<i>privo</i>	6b	COPh	–268.5, –271.1	166.2	–16.2	—	—	—	0.34	—
<i>privo</i>	6c	CO ^t Bu	–263.1, –265.8	173.1	–14.5	473	2.6350(5)	2.9641(7)	0.27	1.3439
<i>privo</i>	6d	P(NMe ₂) ₂	–246.0, –256.1	186.5	–16.9	—	—	—	0.18	—
<i>privo</i>	6e	SiCl ₃	–251.6, –258.9	161.7	–6.4	—	—	—	0.48	—
<i>privo</i>	6f	BH ₃ [–]	–243.3, –255.6	237.3	–28.8	454	2.6024(8)	2.9431(7)	–0.48	1.3155

^a For substituents BH₃[–] and Tip no Hammett parameters are available. The Hammett parameters of similar compounds were used for the correlation plots in Fig. 4: B(OH)₃[–] for BH₃[–] and (C₆H₅-4-CHMe₂) for the Tip substituent (see ref. 68). ^b The hemisphericity φ is the distance of a naked cluster vertex from the plane spanned by its three substituents. Its value is taken as a measure for the degree of hemisphericity of the vertex. For a detailed explanation see ref. 4.

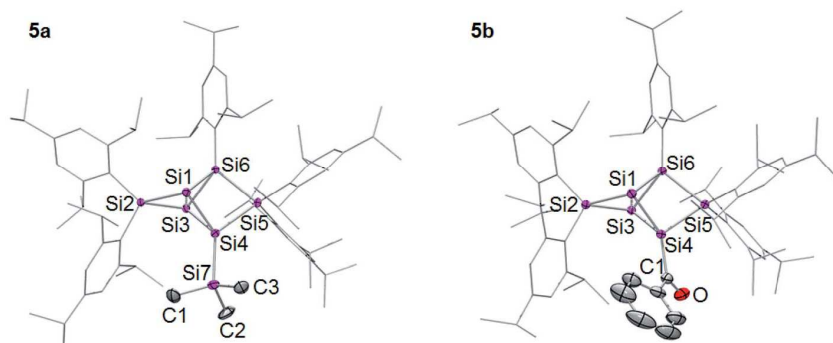
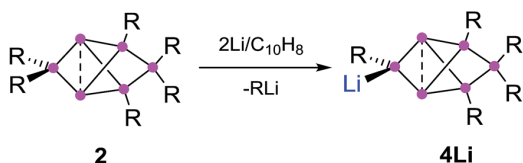


Fig. 1 Structures of **5a,b** in the solid state (thermal ellipsoids at 50% probability). Hydrogen atoms and co-crystallized pentane omitted. a: E = SiMe₃, b: E = COPh.



Scheme 3 Synthesis of *primo*-lithiohexasilabenzpolarene **4Li** by reduction with 2 equivalents of Li/C₁₀H₈.

not compromised by the reduction and give rise to two signals at the usual high field at $\delta = -222.2$ and -231.4 ppm, comparable to the corresponding signals of the *ligato* lithiated **3Li**. The constitution of the reduction product of benzpolarene **2** was finally proven as the *primo* functionalized **4Li** by X-ray diffraction on single crystals (Fig. 2).⁶⁷

The distance between the bridgehead silicon atoms (Si1–Si3 2.5562(10) Å) is similar to that in **3Li**, but shorter than in the fully Tip-substituted siliconoid **2** and the *ligato* functionalized siliconoids **5a–b**. This shortening is tentatively attributed to delocalization of the lone-pair of the anionic silicon vertex into cluster bonding orbitals. The formation of the two regioisomeric derivatives is predominantly a consequence of the

different topologies of the LUMOs of both the dismutational Si₆R₆ isomer **1** and the benzpolarene isomer **2**. The initial reduction plausibly occurs at the unsubstituted vertices of the starting materials (A, D), which provide dominant contributions to the respective LUMOs.^{22,23} Other important LUMO contributions are located precisely at the silicon vertices to which the preferentially eliminated aryl groups are bonded. The subsequent isomerizations are likely driven by the very low energy of the benzpolarene scaffold (Scheme 4). The lithiated regioisomer **3Li** is formed due to a *syn* TipLi elimination (B) followed by a cyclobutene–bicyclobutane rearrangement (C). In case of the reduction of the benzpolarene isomer **2**, we suggest an orbital- and strain-controlled TipLi elimination followed by a 1,2-migration of the lithium counteraction (F) to yield **4Li**.

Functionalization in *primo* position

In order to evaluate the suitability of *primo* lithiated siliconoid **4Li** as nucleophilic transfer reagent for the intact unsaturated Si₆ scaffold, we treated it with several electrophiles (Me₃SiCl, PhCOCl, ^tBuCOCl, ClP(NMe₂)₂, SiCl₄, BH₃·SMe₂). Indeed, the corresponding *primo* substituted siliconoids **6a–f** are obtained by straightforward combination of the reagents in toluene at room temperature (Scheme 5).

According to ²⁹Si NMR spectra, the reactions lead to full conversion of **4Li** to the *primo* functionalized siliconoids **6a–f**. Crystallization of **6a,c,f** from concentrated hexane solutions affords single crystals in moderate to good yields (**6a**: 66%; **6c**: 27%; **6f**: 78%), which were fully characterized by multinuclear NMR spectroscopy, UV/Vis spectroscopy and X-ray diffraction (Fig. 3).⁶⁷ In case of **6b,d,e**, the reactions were only performed on the NMR scale and characterized by multinuclear NMR spectroscopy. The ²⁹Si NMR data of the *primo* substituted species display a similarly wide dispersion in chemical shifts as the corresponding *ligato* isomers. The ²⁹Si NMR spectra of **6a–f** thus show two signals in the high-field region for the *nudo* positions and a strongly deshielded signal for the *primo* silicon atom, which carries one Tip substituent and the functional group E in this case.

The UV/Vis spectra of the isolated products **6a,c,f** and **4Li** show the position of the longest wavelength absorption

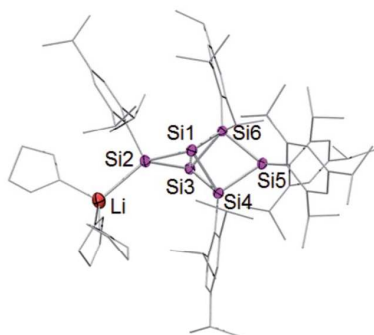
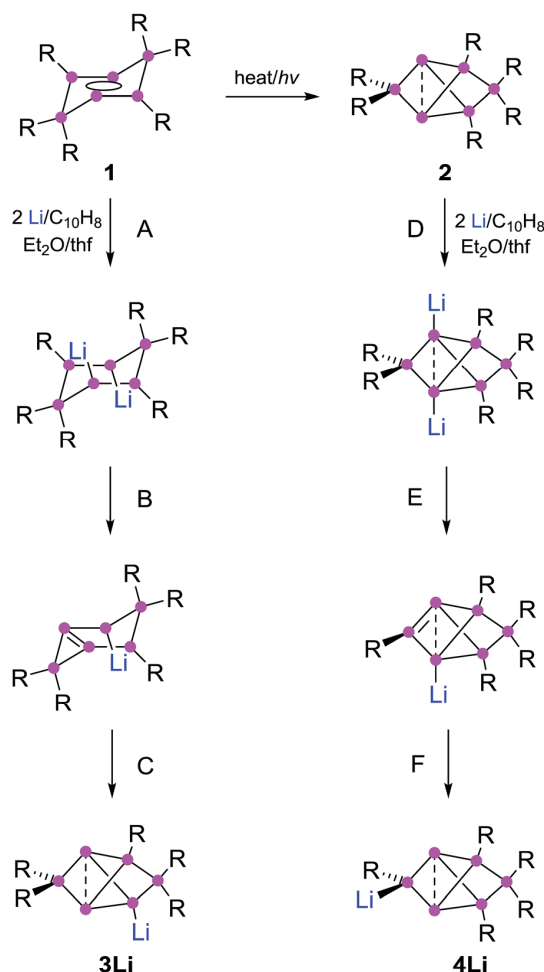
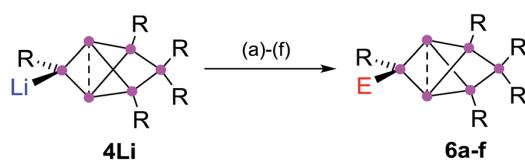


Fig. 2 Structure of **4Li** in the solid state (thermal ellipsoids at 50% probability). Hydrogen atoms and co-crystallized solvent molecules omitted.





Scheme 4 Mechanistic explanation of the regioselective formation of 3Li and 4Li.



Scheme 5 Synthesis of *privo*-functionalized siliconoids **6a–d**. Reagents: (a) Me₃SiCl, (b) PhCOCl, (c) ^tBuCOCl, (d) ClP(NMe₂)₂, (e) SiCl₄, (f) BH₃·SMe₂. **6a**: E = Me₃Si, **6b**: E = COPh, **6c**: E = CO^tBu, **6d**: E = P(NMe₂)₂, **6e**: E = SiCl₃, **6f**: E = BH₃[–].

maximum to strongly depend on the substituents of the Si₆ scaffold (λ_{max} : **6a** 469 nm; **6c** 473 nm; **6f** 454 nm; **4Li** 468 nm). As in case of the *ligato* functionalized species, it can presumably be assigned to the vertical HOMO–LUMO singlet excitation.

The distances between the bridgehead silicon atoms Si1–Si3 in the crystal structure of **6a,c,f** (**6a** 2.6118(6), **6c** 2.6350(5), **6f** 2.6024(6) Å) are longer than in the *ligato* lithiated siliconoid **3Li**^{32,33} and *privo* lithiated siliconoid **4Li**, but slightly shorter than

in the *ligato* functionalized siliconoids **5a,c,f**. This is in line with a more effective σ donation in the *privo* position. While for siliconoids **5a–f**, a reciprocal interdependency between the distances of Si1–Si3 and Si4–Si6 is observed, no such relationship is present in case of the *privo* functionalized siliconoids **6a–f**.

The ²⁹Si NMR resonances of the *privo* silicon atom are strongly influenced by the nature of the pending functionality. The signal is shifted to higher field with increasing electron-withdrawing power of the substituent: Li > BH₃ > TMS > P(NMe₂)₂ > Tip > CO^tBu > COPh > SiCl₃. This sequence correlates nicely with the Hammett parameter σ_m ,^{70–73} which is based on the relative reaction kinetics of a second substitution in the *meta* position of benzene relative to the functionality in question.

Correlation with Hammett parameters σ

Fig. 4 shows the two correlations between the ²⁹Si NMR chemical shift at the *privo* position of compounds **2**, **5a–f** and **6a–f** and the Hammett parameter σ_m drawn separately for the two synthetically accessible positions of the functional group. The correlations with the σ_p Hammett parameter are similar, but slightly less satisfactory (see ESI†).

The plot for the *ligato* functionalized compounds **5a–f** (Fig. 3, top) shows a linear relationship ($R^2 = 0.912$). The response of the ²⁹Si chemical shift, however, is moderate as indicated in its range (160 to 180 ppm) and the resulting slope ($m = 14.346$ ppm). Electron-withdrawing substituents in *ligato* position result in a stronger deshielding of the *privo* atom in the ²⁹Si NMR (**5b,c,d,e**) while electron-donating groups exert the opposite effect (**5a,f**). The σ_m value for the Tip substituent (red triangle in Fig. 4) had to be approximated by that of C₆H₅-4-CHMe₂ (ref. 68) and was therefore disregarded for the linear fit. Surprisingly, there is no apparent correlation of the Hammett parameters with the ²⁹Si chemical shifts of the *nudo* silicon atoms Si1 and Si3 (Table 1).

In case of the *privo* functionalized benzopolarenes (**6a–f**), the correlation of the Hammett parameters σ_m is even better with a very good linear dependency ($R^2 = 0.978$). This is due to a markedly stronger response than in case of *ligato* functionalization with a slope of $m = -79.76$ ppm and a consequently larger chemical shift range (160 to 240 ppm). The stronger influence of the functional group is readily explained by its direct attachment to the silicon atom in question (Si2) vs. an additional distance of two Si–Si bonds in case of *ligato* functionalization. Remarkably, the slope of the linear fit is negative proving a reciprocal relationship between the electron-withdrawing strength of the substituent and its deshielding effect in the *privo* position. We had shown previously that the formal substitution of the *nudo* silicon atoms by germanium or tin results in a pronounced deshielding of the *privo* positions as well, which we tentatively rationalized by the strong influence of the LUMO shape on the paramagnetic contribution to the chemical shift.⁴⁹

In contrast to our findings, in the case of mono-substituted carbon-based benzenes, the correlation of the Hammett parameter σ_p with the chemical shift of the *para*-carbon atom is known,⁷⁴ i.e. the ring atom opposite to the one carrying the functional group.

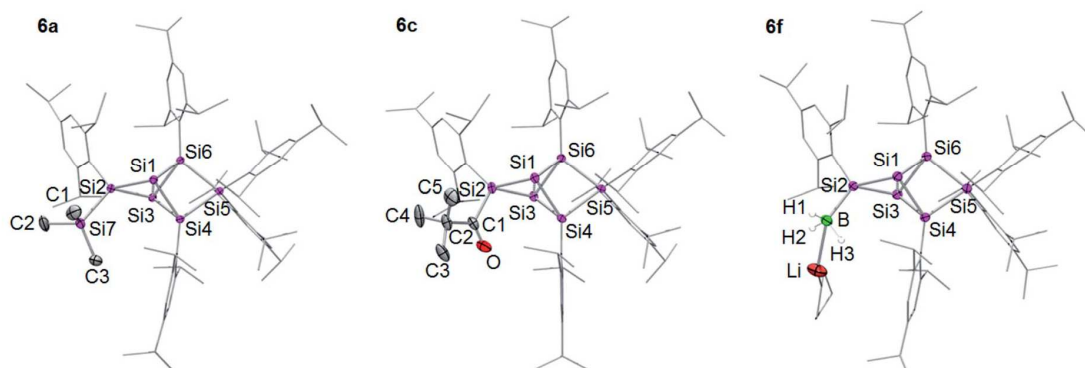


Fig. 3 Structures of **6a**, **6c** and **6f** in the solid state (thermal ellipsoids at 50% probability). Hydrogen atoms and co-crystallized solvent molecules omitted. a: E = TMS, c: E = CO²Bu, f: E = BH₃[−].

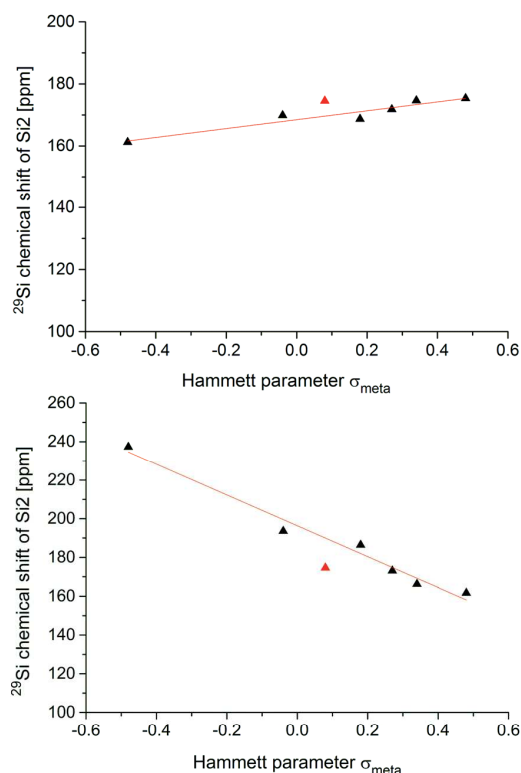


Fig. 4 Plots of the Hammett parameters σ_m vs. ^{29}Si chemical shifts of the *privo* silicon vertices of *ligato* (**5a–f**; top) and *privo* functionalized hexasilabenzpolarenes (**6a–f**; bottom). The data pair marked with red triangles corresponds to the unfunctionalized hexaaryl derivative **2**.

Conclusion

Si₆ siliconoids **1** and **2** can be selectively reduced to yield derivatives of the global minimum isomer of the Si₆H₆ potential energy surface with an anionic functionality at distinct vertices. In order to distinguish between the different positions of the

tricyclic Si₆ scaffold, we propose a nomenclature that refers to the characteristic environment of the four conceivable symmetry-independent positions: *nudo*, *privo*, *ligato* and *remoto*. The anisotropic electronic structure of the global minimum Si₆H₆ scaffold is accounted for by the introduction of “benzopolarene” as unique name for this ever more frequently occurring structural motif. The *privo* lithiated hexasilabenzpolarene is accessible by reductive cleavage of one of the Tip groups of the perarylated derivative, while the *ligato* lithiated isomer had been obtained from the dismutational isomer previously. The *privo* derivative is shown to be an equally suitable nucleophilic reagent for the transfer of the uncompromised benzopolarene framework. The electronic influence of the functional groups in two distinct positions is rationalized on the basis of linear correlations with the Hammett parameter σ_m . With the possibility of functionalization in different positions of the Si₆ scaffold the construction of larger systems comprising Si₆ siliconoid motifs has become a viable option, which is currently being investigated in our laboratory.

Conflicts of interest

There are no conflicts to declare.

Acknowledgements

Funding by the Deutsche Forschungsgemeinschaft (DFG SCHE906/4-1 and 4-2) and COST Action CM1302 (Smart Inorganic Polymers) is gratefully acknowledged.

Notes and references

- 1 F. Breher, *Coord. Chem. Rev.*, 2007, **251**, 1007.
- 2 T. Iwamoto and S. Ishida, *Chem. Lett.*, 2014, **43**, 164.
- 3 S. Kyushin in *Organosilicon Compounds: Theory and Experiment (Synthesis)*, ed. V. Y. Lee, Academic Press, 2017, vol. 1, ch. 3.
- 4 Y. Heider and D. Scheschkewitz, *Dalton Trans.*, 2018, **47**, 7104.
- 5 T. M. I. Davidson, *J. Organomet. Chem.*, 1970, **24**, 97.



- 6 G. A. Rechtsteiner, O. Hampe and M. F. Jarrold, *J. Phys. Chem. B*, 2001, **105**, 4188.
- 7 H. Murakami and T. Kanayama, *Appl. Phys. Lett.*, 1995, **67**, 2341.
- 8 W. M. M. Kessels, M. C. M. Van De Sanden and D. C. Schram, *Appl. Phys. Lett.*, 1998, **72**, 2397.
- 9 M. Watanabe, H. Murakami, T. Miyazaki and T. Kanayama, *Appl. Phys. Lett.*, 1997, **71**, 1207.
- 10 Y. Ge and J. D. Head, *Int. J. Quantum Chem.*, 2003, **95**, 617.
- 11 G. Hadjisavvas, G. Kopidakis and P. Kelires, *Phys. Rev. B*, 2001, **64**, 125413.
- 12 M. F. Jarrold, *Science*, 1991, **252**, 1085.
- 13 H. Neergaard Waltenburg and J. T. Yates Jr, *Chem. Rev.*, 1995, **95**, 1589.
- 14 D. Scheschkeewitz, *Angew. Chem., Int. Ed.*, 2005, **44**, 2954.
- 15 G. Fischer, V. Huch, P. Payer, S. K. Vasisht, M. Veith and N. Wiberg, *Angew. Chem., Int. Ed.*, 2005, **44**, 7884.
- 16 D. Nied, R. Köppe, W. Kloppe, H. Schnöckel and F. J. Breher, *Am. Chem. Soc.*, 2010, **132**, 10264.
- 17 A. Tsurusaki, C. Iizuka, K. Otsuka and S. Kyushin, *J. Am. Chem. Soc.*, 2013, **135**, 16340.
- 18 S. Ishida, K. Otsuka, Y. Toma and S. Kyushin, *Angew. Chem., Int. Ed.*, 2013, **52**, 2507.
- 19 T. Iwamoto, N. Akasaka and S. Ishida, *Nat. Commun.*, 2014, **5**, 5353.
- 20 L. J. Schiegerl, A. J. Karttunen, W. Klein and T. F. Fässler, *Chem. Eur. J.*, 2018, **24**, 19171.
- 21 K. Abersfelder, S. Russell, H. S. Rzepa, A. J. P. White, P. R. Haycock and D. Scheschkeewitz, *J. Am. Chem. Soc.*, 2012, **134**, 16008.
- 22 K. Abersfelder, A. J. P. White, H. S. Rzepa and D. Scheschkeewitz, *Science*, 2010, **327**, 564.
- 23 K. Abersfelder, A. J. P. White, R. J. F. Berger, H. S. Rzepa and D. Scheschkeewitz, *Angew. Chem., Int. Ed.*, 2011, **50**, 7936.
- 24 M. Moteki, S. Maeda and K. Ohno, *Organometallics*, 2009, **28**, 2218.
- 25 E. Zintl and A. Z. Harder, *Z. Phys. Chem. Abt. A*, 1931, **154**, 47.
- 26 F. T. Fässler, *Struct. Bond.*, 2011, **140**, 91.
- 27 S. Scharfe, F. Kraus, S. Stegmaier, S. Schier and T. F. Fässler, *Angew. Chem., Int. Ed.*, 2011, **50**, 3630.
- 28 J. M. Goicoechea and S. C. Sevov, *J. Am. Chem. Soc.*, 2004, **126**, 6860.
- 29 M. Waibel and T. F. Fässler, *Inorg. Chem.*, 2013, **52**, 5861.
- 30 T. Henneberger, W. Klein and T. F. Fässler, *Z. Anorg. Allg. Chem.*, 2018, **644**, 1018.
- 31 C. Lorenz, F. Hastreiter, K. Hioe, N. Lokesh, S. Gärtner, N. Korber and R. M. Gschwind, *Angew. Chem., Int. Ed.*, 2018, **57**, 12956.
- 32 P. Willmes, K. Leszczyńska, Y. Heider, K. Abersfelder, M. Zimmer, V. Huch and D. Scheschkeewitz, *Angew. Chem., Int. Ed.*, 2016, **55**, 2907.
- 33 K. I. Leszczyńska, V. Huch, C. Präsang, J. Schwabedissen, R. J. F. Berger and D. Scheschkeewitz, *Angew. Chem., Int. Ed.*, 2019, DOI: 10.1002/anie.201811331.
- 34 K. Lonsdale, *Nature*, 1928, **122**, 810.
- 35 E. D. Glending, R. Faust, A. Streitwieser, K. Peter, C. Vollhardt and F. Weinhold, *J. Am. Chem. Soc.*, 1993, **115**(23), 10952.
- 36 E. G. Cox, *Rev. Mod. Phys.*, 1958, **30**(1), 159–162.
- 37 T. C. Dinadayalane, U. D. Prixakumar and G. N. J. Sastry, *J. Phys. Chem. A*, 2004, **108**, 11433.
- 38 M. D. Newton and J. M. Schulman, *J. Am. Chem. Soc.*, 1972, **93**, 773.
- 39 A. M. Dilmac, E. Spuling, A. de Meijere and S. Bräse, *Angew. Chem., Int. Ed.*, 2017, **56**, 5684.
- 40 F. Breher, *Coord. Chem. Rev.*, 2007, **251**, 1007.
- 41 P. P. Power, *Chem. Rev.*, 2003, **103**, 789.
- 42 H. Grützmacher and F. Breher, *Angew. Chem., Int. Ed.*, 2002, **41**, 4006.
- 43 D. Nied and F. Breher, *Chem. Soc. Rev.*, 2011, **40**, 3455.
- 44 S. Shaik, P. Maitre, G. Sini and C. P. Hiberty, *J. Am. Chem. Soc.*, 1992, **114**, 7861.
- 45 W. Wu, J. Gu, J. Song, S. Shaik and P. C. Hiberty, *Angew. Chem., Int. Ed.*, 2009, **48**, 1407.
- 46 D. Kratzert, D. Leusser, J. J. Holstein, B. Dittrich, K. Abersfelder and D. S. D. Stalke, *Angew. Chem., Int. Ed.*, 2013, **52**, 4478.
- 47 IUPAC Nomenclature of Organic Chemistry 1957, *J. Am. Chem. Soc.*, 1960, **82**, 5545.
- 48 International Union of Pure and Applied Chemistry, *Nomenclature of Organic Chemistry, sections A, B, C, D, E, F, H*, Pergamon Press, 1979 edn, 1979.
- 49 A. Jana, V. Huch, M. Repisky, R. J. F. Berger and D. Scheschkeewitz, *Angew. Chem., Int. Ed.*, 2014, **53**, 3514.
- 50 C. P. Sindlinger and L. Wesemann, *Chem. Sci.*, 2014, **5**, 2739.
- 51 M. Veith, *Angew. Chem., Int. Ed.*, 1987, **26**, 1.
- 52 Y. Xiong, S. Yao, M. Brym and M. Driess, *Angew. Chem.*, 2017, **119**, 4595.
- 53 Y. Peng, H. Fan, H. Zhu, H. W. Roesky, J. Magull and C. E. Hughes, *Angew. Chem., Int. Ed.*, 2004, **43**, 3443.
- 54 T. Iwamoto, K. Uchiyama, K. Chizuko and M. Kira, *Chem. Lett.*, 2007, **36**, 368.
- 55 K. Raghavachari and V. Logovinsky, *Phys. Rev. Lett.*, 1985, **55**, 2853.
- 56 D. Nieder, C. B. Yildiz, A. Jana, M. Zimmer, V. Huch and D. Scheschkeewitz, *Chem. Commun.*, 2016, **52**, 2799.
- 57 L. R. Sita and R. D. Bickerstaff, *J. Am. Chem. Soc.*, 1989, **111**, 6454.
- 58 D. Nied, W. Kloppe and F. Breher, *Angew. Chem.*, 2009, **121**, 1439.
- 59 L. R. Sita and I. Kinoshita, *J. Am. Chem. Soc.*, 1990, **112**, 8839.
- 60 L. R. Sita and I. Kinoshita, *J. Am. Chem. Soc.*, 1991, **113**, 5070.
- 61 L. R. Sita and I. Kinoshita, *J. Am. Chem. Soc.*, 1992, **114**, 7024.
- 62 A. F. Richards, M. Brynda and P. P. Power, *Organometallics*, 2004, **23**, 4009.
- 63 A. F. Richards, M. Brynda, M. M. Olmstead and P. P. Power, *Organometallics*, 2004, **23**, 2841.
- 64 C. Drost, M. Hildebrand and P. Lönnecke, *Main Group Met. Chem.*, 2002, **25**, 93.
- 65 J. Juselius, D. Sundholm and J. Gauss, *Chem. Phys.*, 2004, **121**, 3952.



- 66 R. J. F. Berger, H. S. Rzepa and D. Scheschkewitz, *Angew. Chem., Int. Ed.*, 2010, **49**, 10006.
- 67 Details of crystal structure analyses are available in the ESI. CCDC 1877380 (**5a**), 1877381 (**5b**), 1877378 (**4Li**), 1877379 (**6a**), 1877382 (**6c**) and 1877383 (**6f**) contain the supplementary crystallographic data for this paper.†
- 68 C. Hansch, A. Leo and R. W. Taft, *Chem. Rev.*, 1991, **91**, 165.
- 69 H. W. Lerner, *Coord. Chem. Rev.*, 2005, **249**, 781.
- 70 L. P. Hammett, *Trans. Faraday Soc.*, 1938, **34**, 156.
- 71 L. P. Hammett, *Physical Organic Chemistry*, McGraw Hill, 1940, p. 184.
- 72 H. H. Jaffe, *Chem. Rev.*, 1953, **53**, 191.
- 73 L. P. Hammett, *Physical Organic Chemistry*, 2nd edn, McGraw-Hill, New York, 1970.
- 74 H. Spiesecke and W. G. Schneider, *J. Chem. Phys.*, 1961, **35**, 731.



3.2 Indirect and Direct Grafting of Transition Metals to Siliconoids

Reproduced with permission from Nadine E. Poitiers, Luisa Giarrana, Kinga I. Leszczyńska, Volker Huch, Michael Zimmer, David Scheschkewitz, *Angew. Chem.* **2020**, *132*, 8610-8614; *Angew. Chem. Int. Ed.* **2020**, *59*, 8532-8536.

Copyright © 2020 Wiley-VCH Verlag GmbH & Co. KGaA.

English Version: <https://doi.org/10.1002/anie.202001178>

German Version: <https://doi.org/10.1002/ange.202001178>

The Communication is reproduced in this thesis by permission of all authors and Wiley-VCH Verlag GmbH & Co. KGaA. The results are additionally concluded and put into context in Chapter 4.

Contributions of the Authors:

Nadine Poitiers: Equal (D.S.): Conceptualization; Lead: Data curation, Formal analysis, Investigation, Methodology, Validation, Visualization, Writing Review and Editing.

Luisa Giarrana: Supporting: Investigation, Data curation, Formal analysis of Si₆-Zr, Si₆NHSi→Fe(CO)₄ species (Bachelor-Thesis).

Kinga I. Leszczyńska: Supporting: Methodology, Conceptualization of Si₆-NHSi, Si₆-NHGe species.

Volker Huch: Lead: X-ray analysis.

Michael Zimmer: Lead: CP/MAS NMR and VT-NMR.

David Scheschkewitz: Lead: Conceptualization, Project administration, Supervision Funding acquisition and resources; Supporting: Methodology, Writing — review and editing.



Siliconoids Hot Paper

How to cite: *Angew. Chem. Int. Ed.* **2020**, 59, 8532–8536

International Edition: doi.org/10.1002/anie.202001178

German Edition: doi.org/10.1002/ange.202001178

Indirect and Direct Grafting of Transition Metals to Siliconoids

Nadine E. Poitiers, Luisa Giarrana, Kinga I. Leszczyńska, Volker Huch, Michael Zimmer, and David Scheschkewitz*

Dedicated to Professor Reinhold Tacke on the occasion of his 70th birthday

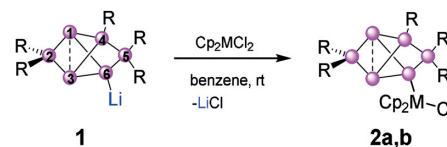
Abstract: Unsaturated charge-neutral silicon clusters (siliconoids) are important as gas-phase intermediates between molecules and the elemental bulk. With stable zirconocene- and hafnocene-substituted derivatives, we here report the first examples containing directly bonded transition-metal fragments that are readily accessible from the ligato-lithiated Si_6 siliconoid (**1Li**) and Cp_2MCl_2 ($\text{M} = \text{Zr}, \text{Hf}$). Charge-neutral siliconoid ligands with pending tetrylene functionality were prepared by the reaction of amidinato chloro tetrylenes $[\text{PhC}(\text{NtBu})_2]\text{ECl}$ ($\text{E} = \text{Si}, \text{Ge}, \text{Sn}$) with **1Li**, thus confirming the principal compatibility of such low-valent functionalities with the unsaturated Si_6 cluster scaffold. The pronounced donor properties of the tetrylene/siliconoid hybrids allow for their coordination to the $\text{Fe}(\text{CO})_4$ fragment.

The synthesis of stable unsaturated silicon clusters (siliconoids)^[1] has attracted considerable interest because of the presumed intermediacy of the parent species in gas-phase deposition processes^[2] as well as the fact that the unsubstituted vertices are reminiscent of the free valencies of bulk and nano silicon surfaces.^[3] Since the report of the first stable siliconoid,^[4] a variety of further examples have been prepared by the groups of Wiberg,^[5] Kyushin,^[6] Iwamoto,^[7] Breher,^[8] Fässler,^[9] Lips,^[10] and our group.^[11] The two recent syntheses of regioisomeric lithiated Si_6 siliconoids (benzpolarenes)^[11d,f] and their facile functionalization with suitable electrophiles considerably enlarged the scope of this emerging field towards the related Zintl anions (polyanionic, deltahedral clusters without any substituents). The presence of organic substituents in siliconoids confers higher solubility, while the electronic properties are retained as manifest in the wide dispersion of ^{29}Si NMR shifts.^[4,6,8,11,12] While Zintl anions of Group 14 elements heavier than silicon have been frequently

applied in the synthesis of partially substituted metalloidal clusters,^[13] the grafting of substituents to silicon-based Zintl anions has only been achieved very recently by the groups of Korber^[14] and Fässler,^[15] who independently reported the protonation of silicon Zintl anions to the partially H-substituted anionic clusters $[\text{HSi}_6]^{3-}$, $[\text{H}_2\text{Si}_6]^{2-}$, and $[\text{HSi}_4]^{3-}$.^[16] In addition, the Fässler group successfully transferred silyl substituents to Si_9^{4-} .^[9]

Zintl silicide anions have been employed as extraordinarily electron-rich ligands towards transition-metal centers.^[17] Conversely, the coordination of neutral siliconoids to metals has thus far remained elusive. Here, with zirconocene and hafnocene derivatives, we report the first examples of siliconoids bearing covalently attached transition-metal functionalities. As attempts to coordinate charge-neutral siliconoids to transition-metal fragments in a dative manner remained inconclusive, we resorted to the grafting of amidinato tetrylene residues $\text{PhC}(\text{NtBu})_2\text{E}$ ($\text{E} = \text{Si}, \text{Ge}, \text{Sn}$)^[18–20] to the Si_6 scaffold. Given that tetrel(II) species are well established as ligands in catalysis,^[21] it was conceivable that tetrylene functionalization would facilitate the coordination of electron-rich siliconoid moieties to transition-metal centers. As will be elaborated further on, the targeted tetrylene-siliconoid hybrids are stable and indeed readily transformed into the corresponding $\text{Fe}(\text{CO})_4$ complexes.

Treatment of Cp_2MCl_2 ($\text{M} = \text{Zr}, \text{Hf}$) with the ligato-lithiated siliconoid **1Li** results in rapid and uniform conversion into the corresponding Group 4 metalated siliconoids **2a** and **2b** (Scheme 1). In contrast, reaction with one equivalent of titanocene dichloride led to a complicated mixture of products, presumably because of competing redox reactions. The diagnostically wide dispersion of ^{29}Si signals confirmed the presence of uncompromised benzpolarene scaffolds.^[11d,f] The signals of the *privo*-silicon atoms appear at the usual low field at 162.6 (**2a**) and 162.8 ppm (**2b**), while the two unsubstituted *nudo*-vertices give rise to two individual signals



Scheme 1. Synthesis of ligato-metalloocene-substituted Si_6 siliconoids **2a** and **2b**. **2a**: $\text{M} = \text{Zr}$; **2b**: $\text{M} = \text{Hf}$. Tip = triisopropylphenyl. The “naked” positions 1 and 3 are referred to as *nudo*, the NMR-desielded position 2 as *privo*, the mono-substituted positions 4 and 6 as *ligato*, and the remote position 5 as *remoto*.^[11]

[*] N. E. Poitiers, L. Giarrana, Dr. K. I. Leszczyńska, Dr. V. Huch, Dr. M. Zimmer, Prof. Dr. D. Scheschkewitz
Krupp-Chair of Inorganic and General Chemistry
Saarland University
Campus Saarbrücken C4.1, 66123 Saarbrücken (Germany)
E-mail: scheschkewitz@mx.uni-saarland.de

Supporting information and the ORCID identification number(s) for the author(s) of this article can be found under:
https://doi.org/10.1002/anie.202001178.

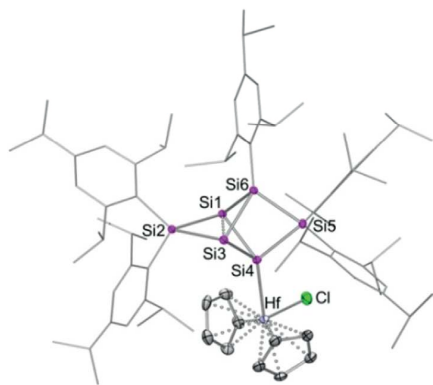
© 2020 The Authors. Published by Wiley-VCH Verlag GmbH & Co. KGaA. This is an open access article under the terms of the Creative Commons Attribution Non-Commercial NoDerivs License, which permits use and distribution in any medium, provided the original work is properly cited, the use is non-commercial, and no modifications or adaptations are made.

Table 1: Selected analytical data of metallocene-substituted siliconoids **2a** and **2b**.

	$\delta(^{29}\text{Si}2)$ [ppm]	$\delta(^{29}\text{Si}1/3)$ [ppm]	Si1–Si3 [Å]	Si4–M [Å], exp	Si4–M [Å], calc	λ_{max} [nm]
2a (M = Zr)	162.6	–233.5 –240.6	2.588(2)	2.782(1)	2.741	521
2b (M = Hf)	162.8	–232.1 –240.3	2.588(1)	2.770(1)	2.738	497

at characteristically high field at –233.5 and –240.6 ppm for **2a** and –232.1 and –240.3 ppm for **2b** (Table 1). The apparent symmetry reduction is typical for *ligato*-substituted benzpolarenes and has been attributed to hindered rotation of the pending functionality.^[11d] The other ^{29}Si NMR chemical shifts are located within the usual range for saturated silicon atoms and vary only slightly with the introduced ligand (see the Supporting Information).

The longest-wavelength absorptions in the UV/Vis spectra are at $\lambda_{\text{max}} = 521$ nm (**2a**) and 497 nm (**2b**), and therefore slightly red-shifted in comparison with previously reported *ligato*-substituted siliconoids ($\lambda_{\text{max}} = 364$ –477 nm).^[11d,f] Single crystals were obtained by crystallization from hexane/toluene in 53 % (**2a**) and 66 % (**2b**) yield, and their structures were confirmed by X-ray diffraction in the solid state (Figure 1).

**Figure 1.** Representative molecular structure of siliconoid **2b** in the solid state.^[30] Hydrogen atoms omitted for clarity. Thermal ellipsoids set at 50% probability. For the structure of **2a**, see the Supporting Information.

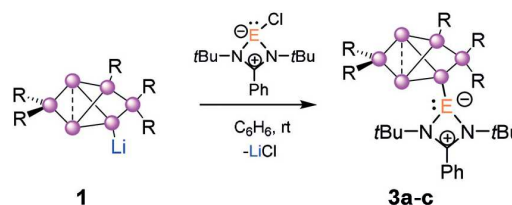
The distances between the unsubstituted bridgehead silicon atoms Si1 and Si3 (**2a**: 2.588(2) Å; **2b**: 2.588(1) Å) are significantly shorter than those of the peraryl-substituted global-minimum isomer^[11b] and in line with previously reported persilabenzpolarenes with electropositive groups in the *ligato*-position.^[11d,f] The electronic nature of the substituent apparently affects the electron density available for cluster bonding.

The Zr–Si bond length of 2.782(1) Å in **2a** is in between that reported for a disilanyl-substituted zirconocene chloride on the one hand (2.7611 Å)^[22c] and silyl-substituted zircono-

cene complexes on the other hand (2.813–2.8214 Å).^[22] Similarly, the Hf–Si bond of 2.7702(9) Å in **2b** is shorter than those reported for tetracoordinated hafnium compounds (2.835–2.888 Å).^[23] The experimental bond lengths were satisfyingly reproduced by DFT calculations for **2a** and **2b** at the BP86 + D3(BJ)/def2-SVP level of theory (Table 1).

In solution, even smallest traces of water lead to the progressive hydrolysis of *ligato*-zirconocene-functionalized siliconoid **2a** as indicated by the gradual appearance of a second set of signals, including a characteristic Si–H resonance at 4.103 ppm, in the ^1H NMR spectrum.^[22c] The Si–Hf bond of *ligato*-hafnocene-functionalized siliconoid **2b** exhibits a considerably higher stability towards hydrolysis (see the Supporting Information for details). In view of the instability of the covalent silicon–metal bond in **2a** and **2b**, it is unsurprising that attempts to directly graft later transition metals to siliconoids have failed thus far. In the same vein, the dative coordination of charge-neutral siliconoids to transition metals is also unknown. We therefore considered the functionalization of the Si_6 scaffold with an auxiliary tetrylene ligand in order to facilitate coordination.

Tetrylenes are known for their excellent σ -donating properties. As the reaction of *ligato*-lithiated benzpolarene **1Li** with Jutzi's silicocene affords the cluster-expanded Si_7 siliconoid^[11c] instead of the simple substitution product, we chose the N-heterocyclic chloro tetrylenes of the Roesky type in the expectation that the nitrogen donors adjacent to the Si^{II} center would tame its electron deficiency sufficiently to allow for the isolation of a silylene-functionalized Si_6 siliconoid. In fact, the tetrylenes $[\text{PhC}(\text{N}t\text{Bu})_2]\text{ECl}$ are known to readily undergo nucleophilic substitution of the chlorine substituent.^[19] Treatment of the *ligato*-lithiated benzpolarene **1Li** with 1.1 equivalents of $[\text{PhC}(\text{N}t\text{Bu})_2]\text{ECl}$ ^[19,20] indeed leads to rapid conversion into uniform products (E = Si, Ge, Sn; Scheme 2)

**Scheme 2.** Synthesis of the tetrylene-functionalized Si_6 siliconoids **3a–c**. **3a**: E = Si; **3b**: E = Ge; **3c**: E = Sn.

accompanied by precipitation of LiCl. ^{29}Si NMR analysis showed the diagnostic wide dispersion of chemical shifts (as discussed above for **2a** and **2b**), and thus confirmed the anticipated integrity of the benzpolarene scaffolds suggesting the formation of siliconoids **3a–c**. An additional signal in the ^{29}Si NMR spectrum of **3a** was assigned to the pending silylene center.^[20a,c]

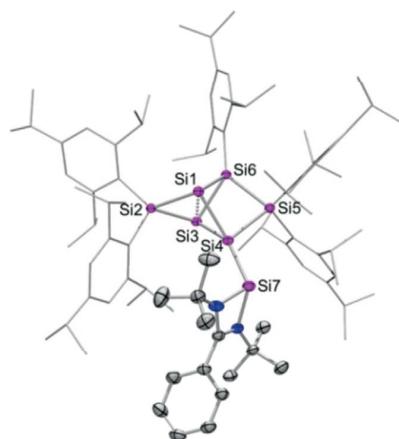
The occurrence of two sets of signals each in the ^{29}Si and ^{119}Sn NMR spectra of **3b** and **3c** suggested the presence of rotational isomers in solution. Indeed, ^{29}Si and ^{119}Sn solid-state NMR spectra of **3a–c** show just a single set of signals (Table 2 and the Supporting Information). A VT-NMR study

Table 2: Selected NMR shifts of the tetrylene-functionalized siliconoids **3a–c**.

	$\delta(^{29}\text{Si}2)$ [ppm]	$\delta(^{29}\text{Si}1/3)$ [ppm]	$\delta(^{29}\text{Si}2)$ solid [ppm]	$\delta(^{29}\text{Si}1/3)$ solid [ppm]	$\delta(^{119}\text{Sn})$ [ppm]	$\delta(^{119}\text{Sn})$ solid [ppm]
3a	166.7	–244.6 –260.7	160.0	–250.5 –262.6	–	–
3b major	167.3	–245.4 –261.1	163.4	–248.9 –261.2	–	–
3b minor	165.6	–233.9 –238.1	–	–	–	–
3c major	162.3	–232.6 –236.9	–	–	267.8	–
3c minor	168.8	–242.3 –259.3	162.9	–244.3 –259.9	336.5	332.0

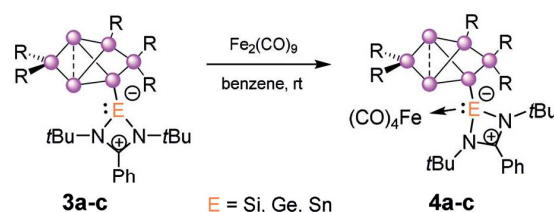
in toluene solution revealed the onset of coalescence at 343 K for germylene-substituted **3b** although the barrier proved to be too high to allow for accurate determination of the coalescence temperature ($> 70^\circ\text{C}$). The ^{29}Si and ^1H NMR spectra of stannylene-substituted **3c** show broad signals with poor signal-to-noise ratios at room temperature, suggesting that the coalescence temperature may be within reach. Accordingly, VT-NMR analysis of **3c** at low temperature (226 K) revealed sharpened signals in the ^1H NMR spectrum as well as a second set of less intense signals in the ^{29}Si NMR spectrum (Table 2).

The longest-wavelength absorption bands in the UV/Vis spectra are at $\lambda_{\text{max}} = 472\text{ nm}$ (**3a**), 436 nm (**3b**), and 436 nm (**3c**). Single crystals were obtained in 72 % (**3a**), 78 % (**3b**), and 74 % (**3c**) yield, and the structures were confirmed by X-ray diffraction studies (Figure 2). The structure of the Si_6 cluster core is hardly influenced by the nature of the tetrylene ligand. The distances between the unsubstituted bridgehead

**Figure 2.** Representative molecular structure of silylene-functionalized siliconoid **3a** in the solid state.^[30] Hydrogen atoms omitted for clarity. Thermal ellipsoids set at 50% probability. For the structures of **3b** and **3c**, see the Supporting Information.

silicon atoms Si1 and Si3 (**3a**: 2.6039(9) Å; **3b**: 2.612(2) Å; **3c**: 2.6149(8) Å) are slightly shorter than in the global-minimum isomer Si_6Tip_6 ^[11b] and in line with previously reported *ligato*-functionalized siliconoids with electropositive groups.^[11d,f] The bonds between Si4 and the pending tetrylene (**3a**: 2.4294(9) Å; **3b**: 2.493(2) Å; **3c**: 2.6753(6) Å) are longer than typical single bonds.^[24–27]

In order to probe the suitability of **3a–c** as neutral ligands towards transition metals, we attempted the coordination to $\text{Fe}(\text{CO})_4$ in a proof-of-principle study (Scheme 3). Complexes **4a–c** are obtained in a straightforward manner by stirring a benzene solution of **3a–c** with 4 (**4a**), 5 (**4b**), or 1.5 (**4c**) equivalents of $\text{Fe}_2(\text{CO})_9$ ^[18,19a,28] at room temperature. Complexes **4a–c** were fully characterized by X-ray diffraction on single crystals, elemental analysis, as well as multinuclear NMR, UV/Vis, and IR spectroscopy.

**Scheme 3.** Reaction of the tetrylene-functionalized Si_6 siliconoids **3a–c** with $\text{Fe}_2(\text{CO})_9$ to afford the corresponding $\text{Fe}(\text{CO})_4$ complexes **4a–c**.

The ^{29}Si NMR spectra of **4a–c** show a similarly wide distribution in chemical shifts as those of **3a–c**, albeit with distinctly different numerical values. In the ^{29}Si NMR spectrum, the additional signal of the silylene moiety of **4a** at 110.0 ppm is drastically downfield-shifted compared to that of **3a** (48.0 ppm). Similarly, the stannylene side arm of **4c** shows a ^{119}Sn NMR signal at 456.3 ppm (Table 3). A related $\text{LSnCl-Fe}(\text{CO})_4$ complex resonates at much higher field at 255 ppm.^[19a] ^1H and ^{13}C NMR analyses of **4a–c** in C_6D_6 confirmed the presence of two singlet resonances each assignable to the *tert*-butyl groups.

According to the UV/Vis spectra of **4a–c**, the longest-wavelength absorption bands are observed at $\lambda_{\text{max}} = 470\text{ nm}$ (**4a**), 469 nm (**4b**), 466 nm (**4c**) and thus slightly blue-shifted compared to those of **3a–c**. The $\text{Fe}(\text{CO})_4$ complexes **4a–c** exhibit IR characteristics of tetrylene- $\text{Fe}(\text{CO})_4$ complex-

Table 3: Selected NMR shifts of $\text{Fe}(\text{CO})_4$ complexes of tetrylene-substituted siliconoids **4a–c**.

	$\delta(^{29}\text{Si}2)$ [ppm]	$\delta(^{29}\text{Si}1/3)$ [ppm]	$\delta(^{29}\text{Si}2)$ solid [ppm]	$\delta(^{29}\text{Si}1/3)$ solid [ppm]	$\delta(^{119}\text{Sn})$ [ppm]	$\delta(^{119}\text{Sn}_{\text{CP/MAS}})$ [ppm]
4a	165.1	–198.2 –230.4	158.2	–195.9 –231.2	–	–
4b	163.7	–203.0 –231.4	156.7	–202.2 –232.8	–	–
4c	160.2	–201.7 –230.7	154.1	–200.3 –232.8	456.3	469.2

es,^[28a,29] with CO stretching modes at $\nu = 1899, 1913, 1948, 2022\text{ cm}^{-1}$ (**4a**), $1908, 1918, 1949, 2025\text{ cm}^{-1}$ (**3b**), and $1902, 1914, 1942, 2015\text{ cm}^{-1}$ (**4c**). The donor strength of **4a–c** can be classified by the asymmetric carbonyl absorptions at $\nu = 2022\text{ cm}^{-1}$ (**4a**), 2025 cm^{-1} (**4b**), and 2015 cm^{-1} (**4c**), which indicate a slightly lower ligand-to-metal σ -donation compared to other tetrylene $\text{Fe}(\text{CO})_4$ complexes such as $[\text{PhC}(\text{N}t\text{Bu})_2\text{Si}(\text{O}t\text{Bu})\text{Fe}(\text{CO})_4]$ ($\nu = 2026\text{ cm}^{-1}$)^[28a] and $[\text{PhC}(\text{N}t\text{Bu})_2\text{GeCl}\text{Fe}(\text{CO})_4]$ ($\nu = 2042\text{ cm}^{-1}$).^[28c] Single crystals of **4a–c** were obtained in 75 % (**4a**), 60 % (**4b**), and 70 % (**4c**) yield, and the structures were confirmed to be isosteric by X-ray diffraction studies (Figure 3). The distances between the bridgehead silicon atoms Si1–Si3 (**4a**: $2.560(1)\text{ \AA}$; **4b**: $2.566(1)\text{ \AA}$; **4c**: $2.5756(7)\text{ \AA}$) are slightly shorter than in **3a–c**. This is indicative of increased electron density within the cluster scaffold upon formation of the transition-metal complex. The bonds Si–E in **4a–c** (**4a**: $2.384(1)\text{ \AA}$; **4b**: $2.4422(8)\text{ \AA}$; **4c**: $2.5896(5)\text{ \AA}$) are equally shortened compared to **3a–c** and now in the typical range of Si–E single bonds ($\text{E} = \text{Si, Ge, Sn}$).^[24–27] The $\text{Fe}(\text{CO})_4$ complexes **4a–c** exhibit typical Fe–E distances (**4a**: $2.279(1)\text{ \AA}$; **4b**: $2.3496(5)\text{ \AA}$; **4c**: $2.4957(3)\text{ \AA}$).^[18,19a,28a–c]

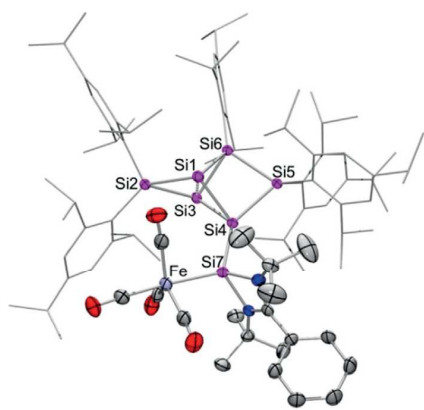


Figure 3. Representative molecular structure of the $\text{Fe}(\text{CO})_4$ complex of **4a** in the solid state.^[30] Hydrogen atoms omitted for clarity. Thermal ellipsoids set at 50% probability. For the structures of **4b** and **4c**, see the Supporting Information.

In conclusion, with **2a** and **2b**, we have reported the first transition-metal-substituted neutral siliconoids. The reaction of an anionic Si_6 siliconoid with $\text{PhC}(\text{N}t\text{Bu})_2\text{ECl}$ ($\text{E} = \text{Si, Ge, Sn}$) gave rise to siliconoids with pending Roesky-type silylene, germylene, and stannylene moieties, an unprecedented feature in silicon cluster chemistry. Unlike in the case of the previously attempted grafting of a Cp^* -substituted silylene fragment,^[11c] the electrophilicity of the tetrylenes of the Roesky type is sufficiently low, thereby avoiding the otherwise observed expansion of the cluster core. As proof of concept for the suitability of these novel ligands in the coordination to transition metals, we synthesized and characterized the corresponding $\text{Fe}(\text{CO})_4$ complexes **4a–c**.

Acknowledgements

Funding by the Deutsche Forschungsgemeinschaft (DFG SCHE 906/4-1 and 4-2) is gratefully acknowledged. We thank Dr. Diego Andrada for helpful discussions and DFT calculations.

Conflict of interest

The authors declare no conflict of interest.

Keywords: clusters · ligands · low-valent species · silicon · siliconoids

- [1] a) Y. Heider, D. Scheschkewitz, *Dalton Trans.* **2018**, 47, 7104–7112; b) S. Kyushin in *Organosilicon Compounds: Theory and Experiment (Synthesis)*, Vol. 1 (Ed.: V. Y. Lee), Academic Press, New York, **2017**, chap. 3; c) T. Iwamoto, S. Ishida, *Chem. Lett.* **2014**, 43, 164–170; d) F. Breher, *Coord. Chem. Rev.* **2007**, 251, 1007–1043.
- [2] a) T. M. I. Davidson, *J. Organomet. Chem.* **1970**, 24, 97–100; b) H. Murakami, T. Kanayama, *Appl. Phys. Lett.* **1995**, 67, 2341–2343; c) M. Watanabe, H. Murakami, T. Miyazaki, T. Kanayama, *Appl. Phys. Lett.* **1997**, 71, 1207–1209; d) W. M. M. Kessels, M. C. M. Van De Sanden, D. C. Schram, *Appl. Phys. Lett.* **1998**, 72, 2397–2399; e) G. A. Rechtsteiner, O. Hampe, M. F. Jarrold, *J. Phys. Chem. B* **2001**, 105, 4188–4194.
- [3] H. Neergaard Waltenburg, J. T. Yates, Jr., *Chem. Rev.* **1995**, 95, 1589–1673.
- [4] D. Scheschkewitz, *Angew. Chem. Int. Ed.* **2005**, 44, 2954–2956; *Angew. Chem.* **2005**, 117, 3014–3016.
- [5] G. Fischer, V. Huch, P. Mayer, S. K. Vasisht, M. Veith, N. Wiberg, *Angew. Chem. Int. Ed.* **2005**, 44, 7884–7887; *Angew. Chem.* **2005**, 117, 8096–8099.
- [6] a) A. Tsurusaki, C. Iizuka, K. Otsuka, S. Kyushin, *J. Am. Chem. Soc.* **2013**, 135, 16340–16343; b) A. Tsurusaki, J. Kamiyama, S. Kyushin, *J. Am. Chem. Soc.* **2014**, 136, 12896–12898.
- [7] T. Iwamoto, N. Akasaka, S. Ishida, *Nat. Commun.* **2014**, 5, 5353.
- [8] D. Nied, R. Köppe, W. Kloppe, H. Schnöckel, F. Breher, *J. Am. Chem. Soc.* **2010**, 132, 10264–10265.
- [9] L. J. Schiegerl, A. J. Karttunen, W. Klein, T. F. Fässler, *Chem. Eur. J.* **2018**, 24, 19171–19174.
- [10] J. Keuter, K. Schwedtmann, A. Hepp, K. Bergander, O. Janka, C. Doerenkamp, H. Eckert, C. Mück-Lichtenfeld, F. Lips, *Angew. Chem. Int. Ed.* **2017**, 56, 13866–13871; *Angew. Chem.* **2017**, 129, 14054–14059.
- [11] a) K. Abersfelder, A. J. P. White, H. S. Rzepa, D. Scheschkewitz, *Science* **2010**, 327, 564–566; b) K. Abersfelder, A. J. P. White, R. J. F. Berger, H. S. Rzepa, D. Scheschkewitz, *Angew. Chem. Int. Ed.* **2011**, 50, 7936–7939; *Angew. Chem.* **2011**, 123, 8082–8086; c) A. Jana, V. Huch, M. Repisky, R. J. F. Berger, D. Scheschkewitz, *Angew. Chem. Int. Ed.* **2014**, 53, 3514–3518; *Angew. Chem.* **2014**, 126, 3583–3588; d) P. Willmes, K. Leszczyńska, Y. Heider, K. Abersfelder, M. Zimmer, V. Huch, D. Scheschkewitz, *Angew. Chem. Int. Ed.* **2016**, 55, 2907–2910; *Angew. Chem.* **2016**, 128, 2959–2963; e) K. I. Leszczyńska, V. Huch, C. Präsang, J. Schwabedissen, R. J. F. Berger, D. Scheschkewitz, *Angew. Chem. Int. Ed.* **2019**, 58, 5124–5128; *Angew. Chem.* **2019**, 131, 5178–5182; f) Y. Heider, N. E. Poitiers, P. Willmes, K. I. Leszczyńska, V. Huch, D. Scheschkewitz, *Chem. Sci.* **2019**, 10, 4523–4530; g) L. Klemmer, V. Huch, A. Jana, D. Scheschkewitz, *Chem. Commun.* **2019**, 55, 10100–10103.

- [12] a) M. Moteki, S. Maeda, K. Ohno, *Organometallics* **2009**, *28*, 2218–2224; b) S. Ishida, K. Otsuka, Y. Toma, S. Kyushin, *Angew. Chem. Int. Ed.* **2013**, *52*, 2507–2510; *Angew. Chem.* **2013**, *125*, 2567–2570.
- [13] a) S. C. Sevov, J. M. Goicoechea, *Organometallics* **2006**, *25*, 5678–5692; b) S. Scharfe, F. Kraus, S. Stegmaier, A. Schier, T. F. Fässler, *Angew. Chem. Int. Ed.* **2011**, *50*, 3630–3670; *Angew. Chem.* **2011**, *123*, 3712–3754; c) F. Li, A. Muñoz-Castro, S. C. Sevov, *Angew. Chem. Int. Ed.* **2012**, *51*, 8581–8584; *Angew. Chem.* **2012**, *124*, 8709–8712; d) F. Li, S. C. Sevov, *J. Am. Chem. Soc.* **2014**, *136*, 12056–12063; e) O. Kysliak, C. Schrenk, A. Schnepf, *Inorg. Chem.* **2015**, *54*, 7083–7088; f) O. Kysliak, A. Schnepf, *Dalton Trans.* **2016**, *45*, 2404–2408; g) F. S. Geitner, J. V. Dums, T. F. Fässler, *J. Am. Chem. Soc.* **2017**, *139*, 11933–11940; h) F. S. Geitner, W. Klein, T. F. Fässler, *Angew. Chem. Int. Ed.* **2018**, *57*, 14509–14513; *Angew. Chem.* **2018**, *130*, 14717–14721; i) S. Frischhut, W. Klein, M. Drees, T. F. Fässler, *Chem. Eur. J.* **2018**, *24*, 9009–9014.
- [14] C. Lorenz, F. Hastreiter, K. Hioe, N. Lokesh, S. Gärtner, N. Korber, R. M. Gschwind, *Angew. Chem. Int. Ed.* **2018**, *57*, 12956–12960; *Angew. Chem.* **2018**, *130*, 13138–13142.
- [15] T. Henneberger, W. Klein, T. F. Fässler, *Z. Anorg. Allg. Chem.* **2018**, *644*, 1018–1027.
- [16] F. Hastreiter, C. Lorenz, J. Hioe, S. Gärtner, N. Lokesh, N. Korber, R. M. Gschwind, *Angew. Chem. Int. Ed.* **2019**, *58*, 3133–3137; *Angew. Chem.* **2019**, *131*, 3165–3169.
- [17] a) S. Joseph, M. Hamberger, F. Mutzbaurer, O. Härtl, M. Meier, N. Korber, *Angew. Chem. Int. Ed.* **2009**, *48*, 8770–8772; *Angew. Chem.* **2009**, *121*, 8926–8929; b) M. Waibel, F. Kraus, S. Scharfe, B. Wahl, T. F. Fässler, *Angew. Chem. Int. Ed.* **2010**, *49*, 6611–6615; *Angew. Chem.* **2010**, *122*, 6761–6765; c) F. S. Geitner, T. F. Fässler, *Chem. Commun.* **2017**, *53*, 12974–12977.
- [18] B. Blom, M. Stoelzel, M. Driess, *Chem. Eur. J.* **2013**, *19*, 40–62.
- [19] a) S. S. Sen, M. P. Kritzer-Kosch, S. Nagendran, H. W. Roesky, T. Beck, A. Pal, R. Herbst-Irmer, *Eur. J. Inorg. Chem.* **2010**, 5304–5311; b) S. S. Sen, S. Khan, P. P. Samuel, H. W. Roesky, *Chem. Sci.* **2012**, *3*, 659–682; c) B. Prashanth, S. Singh, *Dalton Trans.* **2016**, *45*, 6079–6087.
- [20] a) C.-W. So, H. W. Roesky, J. Magull, R. B. Oswald, *Angew. Chem. Int. Ed.* **2006**, *45*, 3948–3950; *Angew. Chem.* **2006**, *118*, 4052–4054; b) S. Nagendran, S. S. Sen, H. W. Roesky, D. Koley, H. Grubenmüller, A. Pal, R. Herbst-Irmer, *Organometallics* **2008**, *27*, 5459–5463; c) S. S. Sen, H. W. Roesky, D. Stern, J. Henn, D. Stalke, *J. Am. Chem. Soc.* **2010**, *132*, 1123–1126.
- [21] a) A. Brück, D. Gallego, W. Wang, E. Irran, M. Driess, J. F. Hartwig, *Angew. Chem. Int. Ed.* **2012**, *51*, 11478–11482; *Angew. Chem.* **2012**, *124*, 11645–11649; b) D. Gallego, A. Brück, E. Irran, F. Meier, M. Kaupp, M. Driess, J. F. Hartwig, *J. Am. Chem. Soc.* **2013**, *135*, 15617–15626; c) B. Blom, D. Gallego, M. Driess, *Inorg. Chem. Front.* **2014**, *1*, 134–148.
- [22] a) K. W. Muir, *J. Chem. Soc. A* **1971**, 2663–2666; b) T. D. Tilley, *Organometallics* **1985**, *4*, 1452–1457; c) T. Nguyen, D. Scheschkewitz, *J. Am. Chem. Soc.* **2005**, *127*, 10174–10175.
- [23] a) H. G. Woo, R. H. Heyn, T. D. Tilley, *J. Am. Chem. Soc.* **1992**, *114*, 5698–5707; b) A. D. Sadow, T. D. Tilley, *J. Am. Chem. Soc.* **2003**, *125*, 9462–9475; c) C. Kayser, D. Frank, J. Baumgartner, C. Marschner, *J. Organomet. Chem.* **2003**, *667*, 149–153; d) M. Aghazadeh Meshgi, R. Zitz, M. Walewska, J. Baumgartner, C. Marschner, *Organometallics* **2017**, *36*, 1365–1371.
- [24] J. Hlina, R. Zitz, H. Wagner, F. Stella, J. Baumgartner, C. Marschner, *Inorg. Chim. Acta* **2014**, *422*, 120–133.
- [25] S. Martens, S. Traut, O. Wunnicke, A. Torvisco, R. Fischer, M. Haas, A. Temmel, V. Christopoulos, H. Stueger, *Inorg. Chem.* **2016**, *55*, 4034–4038.
- [26] S. P. Mallela, R. A. Geanangel, *Inorg. Chem.* **1990**, *29*, 3525–3528.
- [27] J. Baumgartner, R. Fischer, J. Fischer, A. Wallner, C. Marschner, *Organometallics* **2005**, *24*, 6450–6457.
- [28] a) W. Yang, H. Fu, J. Wang, M. Chen, Y. Ding, H. W. Roesky, A. Jana, *Inorg. Chem.* **2009**, *48*, 5058–5060; b) B. Blom, S. Enthaler, S. Inoue, E. Irran, M. Driess, *J. Am. Chem. Soc.* **2013**, *135*, 6703–6713; c) M. El Ezzi, T.-G. Kocsor, F. D'Accrescio, D. Madec, S. Mallet-Ladeira, A. Castel, *Organometallics* **2015**, *34*, 571–576; d) J. A. Baus, F. M. Mück, H. Schneider, R. Tacke, *Chem. Eur. J.* **2017**, *23*, 296–303.
- [29] a) C. Zybill, G. Müller, *Organometallics* **1988**, *7*, 1368–1372; b) T. A. Schmedake, M. Haaf, B. J. Paradise, A. J. Millevolte, D. R. Powell, R. West, *J. Organomet. Chem.* **2001**, *636*, 17–25.
- [30] CCDC 1978002 (**2a**), 1978003 (**2b**), 1978004 (**3a**), 1978005 (**3b**), 1978006 (**3c**), 1978007 (**4a**), 1978008 (**4b**), and 1978009 (**4c**) contain the supplementary crystallographic data for this paper. These data are provided free of charge by The Cambridge Crystallographic Data Centre.

Manuscript received: January 23, 2020

Accepted manuscript online: February 24, 2020

Version of record online: March 20, 2020

3.3 Exohedral functionalization vs. core expansion of siliconoids with Group 9 metals: catalytic activity in alkene isomerization

Nadine E. Poitiers, Luisa Giarrana, Volker Huch, Michael Zimmer and David Scheschkewitz, *Chem. Sci.*, **2020**, *11*, 7782-7788.

<https://doi.org/10.1039/D0SC02861D>

The article has been published by the Royal Society of Chemistry (RSC) as an “Open Access” Article and is licensed under a “Creative Commons Attribution-NonCommercial 3.0 Unported (CC BY-NC 3.0)” Licence (<https://creativecommons.org/licenses/by-nc/3.0/>).

The article is reproduced in this thesis by permission of The Royal Society of Chemistry and all co-authors. The results are additionally concluded and put into context in Chapter 4.

Contributions of the Authors:

Nadine Poitiers: Equal (D.S.): Conceptualization; Lead: Data curation, Formal analysis, Investigation, Methodology, Validation, Visualization, Writing Review and Editing.

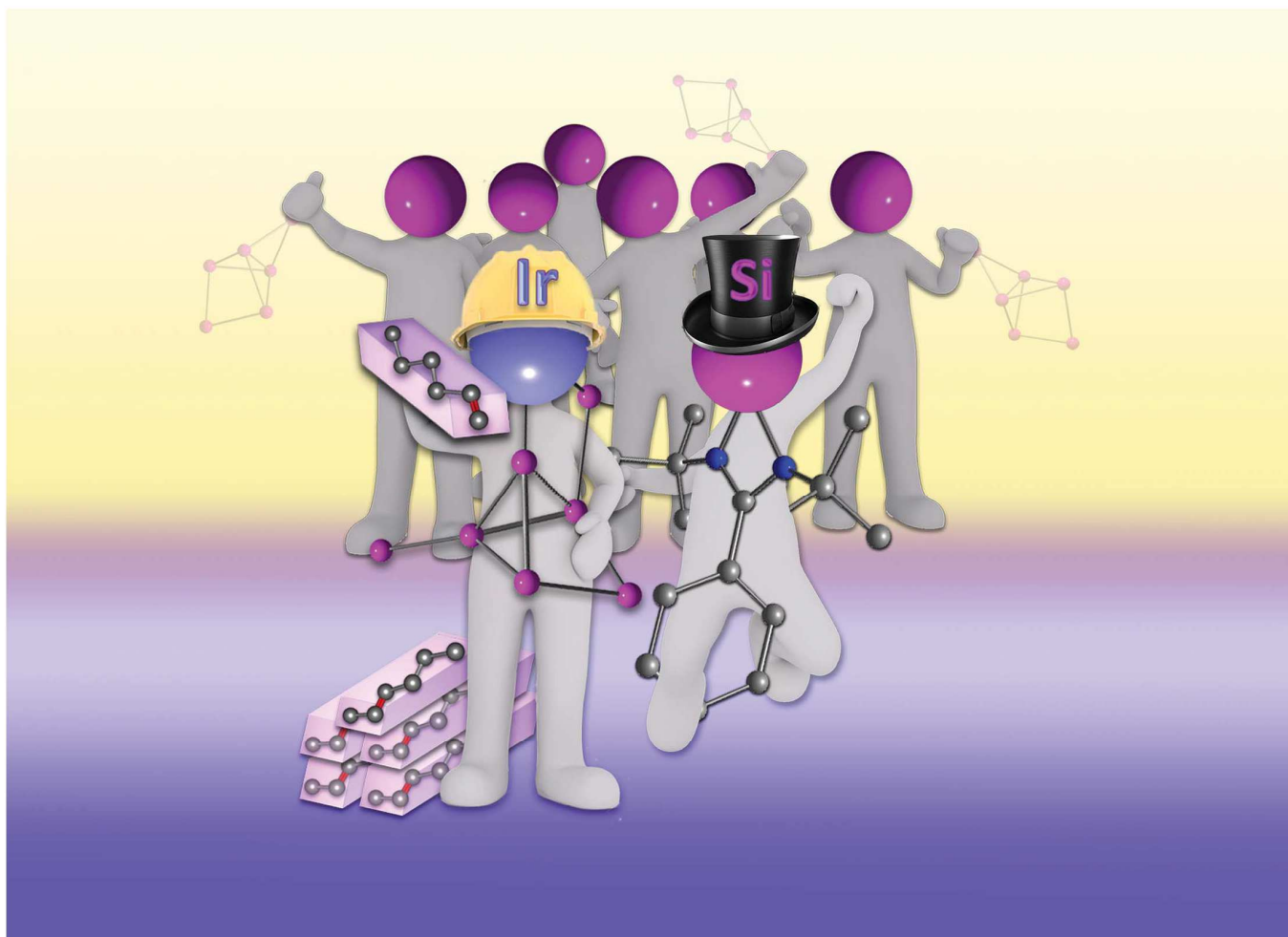
Luisa Giarrana: Supporting: Investigation, Data curation, Formal analysis of Si₆-NHSi-Ir(cod) and Si₆-NHSi-Rh(CO)₂ species (Bachelor-Thesis).

Volker Huch: Lead: X-ray analysis.

Michael Zimmer: Lead: CP/MAS NMR.

David Scheschkewitz: Lead: Conceptualization, Project administration, Supervision Funding acquisition and resources; Supporting: Methodology, Writing — review and editing.

3.3 Exohedral functionalization vs. core expansion of siliconoids with Group 9 metals: catalytic activity in alkene isomerization



Showcasing research from Professor Scheschkewitz's laboratory at Saarland University (Germany).

Exohedral functionalization vs. core expansion of siliconoids with Group 9 metals: catalytic activity in alkene isomerization

Unprecedented rhodium and iridium incorporated siliconoids are readily accessible from the silylene-substituted Si_6 siliconoid and Group 9 metal fragments. The pending N-heterocyclic silylene ligand acts as a handle enabling unique coordination environments with up to five silicon atoms. In particular, the iridium species shows competitive catalytic activity in the isomerization of terminal alkenes to 2-alkenes.

As featured in:





See David Scheschkewitz *et al.*, *Chem. Sci.*, 2020, 11, 7782.

Cite this: *Chem. Sci.*, 2020, 11, 7782

All publication charges for this article have been paid for by the Royal Society of Chemistry

Exohedral functionalization vs. core expansion of siliconoids with Group 9 metals: catalytic activity in alkene isomerization†

Nadine E. Poitiers,  Luisa Giarrana, Volker Huch, Michael Zimmer and David Scheschkewitz ^{*}

Taking advantage of pendant tetraylene side-arms, stable unsaturated Si₆ silicon clusters (siliconoids) with the benzpolarene motif (the energetic counterpart of benzene in silicon chemistry) are successfully employed as ligands towards Group 9 metals. The pronounced σ-donating properties of the tetraylene moieties allow for sequential oxidative addition and reductive elimination events without complete dissociation of the ligand at any stage. In this manner, either covalently linked or core-expanded metallasiliconoids are obtained. [Rh(CO)₂Cl]₂ inserts into an endohedral Si–Si bond of the silylene-functionalized hexasilabenzpolarene leading to an unprecedented coordination sphere of the Rh centre with five silicon atoms in the initial product, which is subsequently converted to a simpler derivative under reconstruction of the Si₆ benzpolarene motif. In the case of [Ir(cod)Cl]₂ (cod = 1,5-cyclooctadiene) a similar Si–Si insertion leads to the contraction of the Si₆ cluster core with concomitant transfer of a chlorine atom to a silicon vertex generating an exohedral chlorosilyl group. Metallasiliconoids are employed in the isomerization of terminal alkenes to 2-alkenes as a catalytic benchmark reaction, which proceeds with competitive selectivities and reaction rates in the case of iridium complexes.

Received 20th May 2020
Accepted 2nd July 2020

DOI: 10.1039/d0sc02861d

rsc.li/chemical-science

Introduction

The control of the reactivity of transition metal centres is a pivotal aspect of homogenous catalysis and therefore the development of novel ligands for transition metals is one of the priorities of organometallic chemistry. Unsaturated silicon compounds with the two major sub-categories of silylenes¹ and disilenes^{1a,2} are typically characterized by a surplus of electrons and are therefore inherently stronger σ-donors than the corresponding carbon species, while retaining π-acceptor properties in some cases due to their unsaturated nature.³ First applications in homogeneous catalysis include C–H borylation,⁴ reduction of organic amides,⁵ Sonogashira and Heck cross-coupling reactions⁶ and hydrosilylation of ketones.⁷

Recently, a third widely occurring sub-category was introduced into the class of stable unsaturated silicon species, the so-called siliconoids, partially unsubstituted neutral silicon clusters.⁸ Despite their unsaturated nature, applications of siliconoids as ligands towards transition metals are virtually unexplored. With our report on anionically functionalized Si₆

derivatives,⁹ however, a conceptual link towards (poly)anionic, completely unsubstituted deltahedral Zintl anions of silicon¹⁰ was established, which in fact exhibit a rich chemistry towards transition metals: silicides and their heavier congeners of germanium and tin have frequently been employed as extraordinarily electron-rich ligands towards transition metal centres,¹¹ and Zintl anions of Group 14 elements heavier than silicon can be converted to transition metal-centred derivatives M@E_n^{x−}.¹² In all reported cases, the negative charges of the polyanionic precursors are (at least partially) retained in the transition metal-containing products with often adverse consequences for their solubility and stability, limiting their application, *e.g.* in homogeneous catalysis. Siliconoids with their stabilizing shell of organic ligands and high solubility due to their charge-neutrality appear to be the logical choice to overcome both limitations.

The first transition metal-substituted siliconoids, *ligato*-hexasilabenzpolarenes Si₆–Zr(Cp)₂Cl and Si₆–Hf(Cp)₂Cl with the covalently attached metallocene moiety were disclosed just recently.¹³ In contrast, the application of siliconoids as direct charge-neutral ligands towards transition metals has remained unsuccessful so far although the introduction of a silylene side-arm allowed for the coordination to Fe(CO)₄ moieties in the periphery of the hexasilabenzpolarene motif.¹³ Now we show that by using the Group 9 metals rhodium and iridium a much larger variety of unprecedented coordination modes to

Krupp Chair of General and Inorganic Chemistry, Saarland University, D-66123 Saarbrücken, Germany. E-mail: scheschkewitz@mx.uni-saarland.de

† Electronic supplementary information (ESI) available. CCDC 2000911–2000916. For ESI and crystallographic data in CIF or other electronic format see DOI: 10.1039/d0sc02861d



siliconoids can be realized. We demonstrate that covalent bonding modes between the metal and the uncompromised hexasilabenzpolarene scaffold are related to the endohedral incorporation of the metal centre into the siliconoid cluster in a reversible manner. Finally, with the isomerization of alkenes we provide a first proof-of-principle for the application of the thus prepared soluble transition metal/silicon hybrid clusters as homogenous catalysts.

Results and discussion

Synthesis of iridium complexes

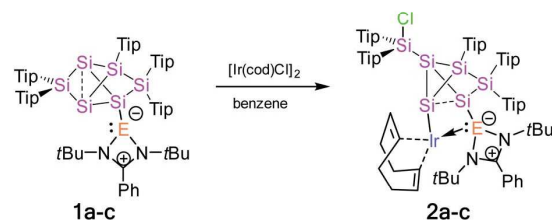
Treatment of tetrylene-functionalized siliconoids **1a–c** with 0.5 equivalents of bis[(1,5-cyclooctadiene)iridium(i) chloride] affords the tetrylene-Si₆ iridium complexes **2a–c** in an NMR spectroscopically quantitative manner (Scheme 1). Complexes **2a–c** were fully characterized by X-ray diffraction on single crystals, elemental analysis, and multinuclear NMR spectroscopy.

The ²⁹Si NMR spectrum of **2a–c** shows six sharp resonances in a much narrower range than usual for hexasilabenzpolarenes (+175.4 to −279.0 ppm),⁹ which provides a first hint at the rearrangement of the cluster scaffold and the ensuing loss of the spherical aromaticity and the associated magnetically induced cluster current. On the basis of the 2D ²⁹Si/¹H correlation NMR spectrum, the signals at 56.7 ppm (**2a**), 52.6 ppm (**2b**) and 50.2 ppm (**2c**) are assigned to the endohedral SiTip₂ moieties. The signals at 13.3 (**2a**), 12.8 (**2b**) and 12.2 ppm (**2c**) are very close in chemical shift to that of the exocyclic silicon atom in chlorosilyltricyclo[2.1.0.0^{2,5}]pentasilane (5.8 ppm)¹⁴ and were therefore tentatively attributed to the extrusion of one SiTip₂ unit from the cluster core of **2a–c**. The resonances at −38.4 (**2a**), −41.5 (**2b**) and −42.1 ppm (**2c**) are assigned to the SiTip vertices. Most remaining ²⁹Si signals are observed at

a higher field (see ESI†) with the exception of one distinct resonance of **2a** at 33.4 ppm, which is apparently due to the pendant silylene centre (Table 1).

Single crystals of **2a–c** were obtained by crystallization from hexane in 68% (**2a**), 61% (**2b**) and 63% (**2c**) yield and the tricyclic structures of the siliconoid–iridium complexes were confirmed by X-ray diffraction in the solid state (Fig. 1). As anticipated on the basis of NMR data, the *privo*-vertex has been extruded from the cluster core due to the additional bond to the chlorine atom transferred from the iridium centre, which in turn is not only coordinated by the pendant tetrylene moiety but also by the former *nudo*-vertex of the benzpolarene starting material. The structural model of **2c** could not be refined in a satisfactory manner; the following discussion thus focuses on **2a,b**. The Ir–E bond lengths (E = Si, Ge, Sn; **2a**: Si3–Ir: 2.320(1) Å and Si7–Ir: 2.334(1) Å; **2b**: Si3–Ir: 2.3517(7) Å and Ge–Ir: 2.4113(3) Å) are those of single bonds.¹⁶ The slightly longer distance between the pendant tetrylene and the iridium centre may be explained by the dative vs. covalent bonding situation. The endohedral bond distance between the iridium-bonded vertex and that bearing the tetrylene moiety (Si3–Si4 **2a**: 2.549(2) Å, **2b**: 2.565(1) Å) is considerably elongated in comparison to those in the aforementioned chlorosilyltricyclo[2.1.0.0^{2,5}]pentasilane (2.356 Å)¹⁴ and a dianionic Si₅ cluster with the same tricyclic scaffold (2.3822 Å).¹⁵

This is probably a consequence of the back and forth electron transfer between iridium and cluster orbitals, but may also indicate a propellane-like bonding situation as suggested by the hemispheroidality of Si4. On the other hand, Si3 does not fulfill the criterion of hemispheroidality,^{8a} but rather adopts a very near planar-tetracoordinate coordination environment instead (**2a**: $\phi(\text{Si3}) = -0.0154^\circ$, $\phi(\text{Si4}) = +0.7559^\circ$; **2b**: $\phi(\text{Si3}) = -0.0060^\circ$, $\phi(\text{Si4}) = +0.7276^\circ$). The bond lengths between the bridgehead silicon atoms Si1 and Si3 in **2a,b** (**2a**: 2.305(2) Å, **2b**: 2.2962(2) Å) are now at the short end of the usual range for silicon single bonds as also observed in the chlorosilyltricyclo[2.1.0.0^{2,5}]pentasilane (2.312 Å).¹⁴ The ²⁹Si CP/MAS spectra of **2a–c** show very similar signals to those in C₆D₆ solution thus confirming the integrity of the coordination modes upon solvation (the stannylene-Si₆ iridium complex **2c** shows a double set of signals due to two crystallographically independent molecules in the asymmetric unit; see ESI†). The longest wavelength absorption bands in the UV/vis spectra at $\lambda_{\text{max}} = 576$ nm (**2a**), 580 nm (**2b**), 592 nm (**2c**) are strongly red-shifted compared to previously reported *ligato*-substituted siliconoids ($\lambda_{\text{max}} = 364$ to 521 nm).^{9,13}



Scheme 1 Synthesis of tetrylene-Si₆ iridium complexes **2a–c** from tetrylene-functionalized Si₆ siliconoids **1a–c** (**2a**: E = Si, **2b**: E = Ge, and **2c**: E = Sn).

Table 1 Selected ²⁹Si NMR data of **2a–c**, **3**, **4**

Siliconoid	$\delta^{29}\text{Si2}$ [ppm]	$\delta^{29}\text{Si5}$ [ppm]	$\delta^{29}\text{Si6}$ [ppm]	$\delta^{29}\text{Si3}$ [ppm]	$\delta^{29}\text{Si4}$ [ppm]	$\delta^{29}\text{Si7}$ [ppm]	$\delta^{29}\text{Si2}$ solid [ppm]	$\delta^{29}\text{Si6}$ solid [ppm]	$\delta^{29}\text{Si7}$ solid [ppm]
2a	13.3	55.3	−38.4	−128.2	−126.8	32.9	11.5	−41.6	32.9
2b	12.8	52.6	−41.6	−90.8	−121.7	—	12.3	−41.5	—
2c	12.2	50.6	−42.1	−103.8	−120.2	—	10.2	−42.2	—
3	158.8	−58.3	58.3	165.7	—	108.7	157.3	54.1	107.7
4	162.6	17.6	21.8	—	−9.0	48.2	161.8	14.5	42.7



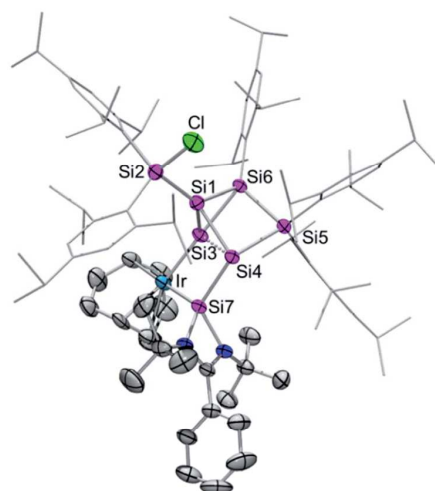
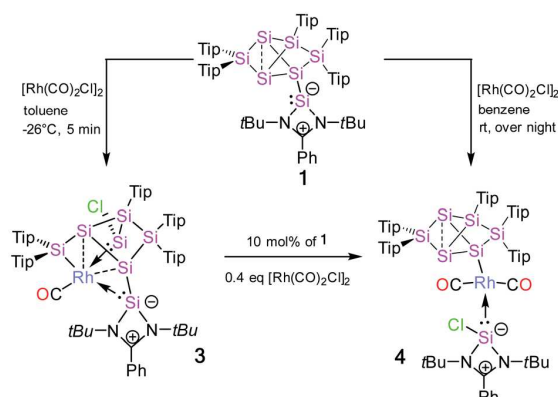


Fig. 1 Representative molecular structure of silylene-functionalized siliconoid iridium complex **2a** in the solid state. Hydrogen atoms are omitted for clarity. Thermal ellipsoids are set at 50% probability. For structures of **2b,c** see ESI†. Selected bond lengths [Å] and angles [°]: **2a**: Ir–Si7 2.320(1), Ir–Si3 2.334(1), Si1–Si3 2.305(2), Si1–Si4 2.313(2), Si1–Si6 2.364(2), Si1–Si2 2.369(2), Si3–Si6 2.353(1), Si3–Si4 2.548(2), Si3–Si7 2.764(2), Si4–Si5 2.391(2), Si4–Si7 2.402(2), Si7–N2 1.857(3), Si7–N1 1.884(3), Cl–Si2–Si1 99.03(6), Si1–Si3–Ir 124.02(5), Ir–Si3–Si6 174.93(6), Ir–Si3–Si4 105.99(5), Ir–Si3–Si7 53.33(3), and Si7–Si4–Si3 67.81(4); **2b**: Ir–Si3 2.3517(7), Ir–Ge 2.4113(3), Ge–Si4 2.4444(8), Ge–Si3 2.8481(8), Si1–Si3 2.296(1), Si1–Si4 2.302(1), Si1–Si2 2.356(1), Si1–Si6 2.375(1), Si3–Si6 2.339(1), Si3–Si4 2.565(1), Si4–Si5 2.389(1), Si5–Si6 2.368(1), Ge–N2 1.995(2), Ge–N1 2.005(2), Cl–Si2–Si1 100.91(4), Ir–Si3–Ge 54.243(17), Ir–Si3–Si4 106.90(3), Si6–Si3–Ir 173.61(4), Si1–Si3–Ir 124.75(4), Ir–Ge–Si3 52.322(16), Ir–Ge–Si4 108.95(2), Si3–Ir–Ge 73.436(19), and Ge–Si4–Si3 69.25(3).

Synthesis of rhodium complexes

The reaction of 1 equivalent of bis[(1,5-cyclooctadiene)rhodium(i) chloride] with **1a–c** led to a complicated mixture of products in all cases, presumably due to competing oxidative addition and reductive elimination reactions. In one crystallization attempt of the product mixture from **1b** (E = Ge) a few red-brownish crystals were collected and then investigated by X-ray diffraction showing the same motif as observed in **2a–c** (see ESI†). In the anticipation that it might react in a similar manner despite the differing ligand set, we considered the rhodium(i) dicarbonyl chloride dimer $[\text{Rh}(\text{CO})_2\text{Cl}]_2$ as an alternative. The reactions of **1a–c** with 1 equivalent of $[\text{Rh}(\text{CO})_2\text{Cl}]_2$, however, led to uniform conversion only in the case of **1a** and inseparable mixtures of products for **1b,c** according to NMR spectra. In addition, ^1H NMR monitoring of the reaction mixture revealed the rearrangement of the initial product overnight in the case of **1a** (Scheme 2).

Treatment of **1a** with 1 equivalent of $[\text{Rh}(\text{CO})_2\text{Cl}]_2$ in toluene followed by cooling to -26°C after three minutes of stirring at ambient temperature yields dark red crystals of the primary product **3** after storage for 2 to 3 h in 56% crystalline yield. Conversely, the secondary product **4** is obtained as red-brownish crystals in 63% yield by crystallization from hexane after stirring the reaction mixture overnight. Both **3** and **4** were



Scheme 2 Synthesis of Si_7 rhodium complexes **3** and **4** from silylene-functionalized Si_6 siliconoid **1**.

fully characterized by multinuclear NMR spectroscopy and X-ray diffraction on single crystals (Fig. 2 and 3).

In contrast to the iridium complexes **2a–c**, the rhodium centre of **3** is fully incorporated into the core structure under expansion to a 7-vertex motif. Only one of the CO ligands is retained in **3** completing the distorted trigonal-pyramidal coordination sphere at rhodium in an apical position (C16–

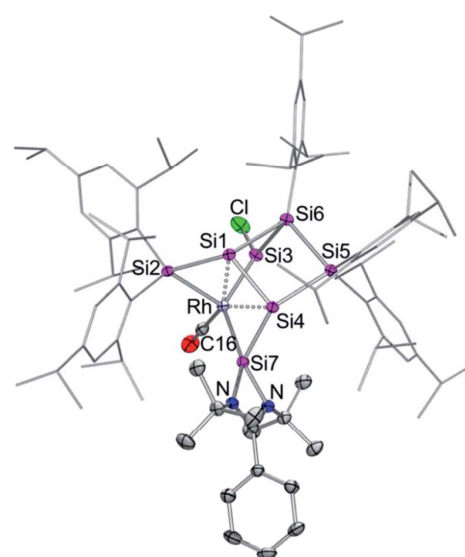


Fig. 2 Molecular structure of silylene-functionalized siliconoid rhodium complex **3** in the solid state. Hydrogen atoms are omitted for clarity. Thermal ellipsoids are set at 50% probability. Selected bond lengths [Å] and angles [°]: Rh–Si3 2.2455(7), Rh–Si7 2.3104(7), Rh–Si5 2.3872(8), Rh–Si2 2.5936(7), Rh–Si1 2.5965(7), Si3–Cl 2.102(1), Si1–Si2 2.279(1), Si1–Si5 2.373(1), Si1–Si4 2.499(1), Si2–Si7 2.254(1), Si2–Si6 2.333(1), Si3–Si4 2.308(1), Si4–Si6 2.401(1), Si7–N1 1.837(2), Si7–N2 1.822(2), Si3–Rh–Si7 132.05(3), Si3–Rh–Si5 97.85(3), Si7–Rh–Si5 116.30(3), Si3–Rh–Si2 87.62(2), Si7–Rh–Si2 54.36(2), Si5–Rh–Si2 102.19(2), Si3–Rh–Si1 72.23(2), Si7–Rh–Si1 98.48(2), Si5–Rh–Si1 56.69(2), Si4–Si1–Rh 94.98(3), Si7–Si2–Rh 56.40(2), Si1–Si2–Rh 64.02(3), and Si6–Si2–Rh 115.58(3).

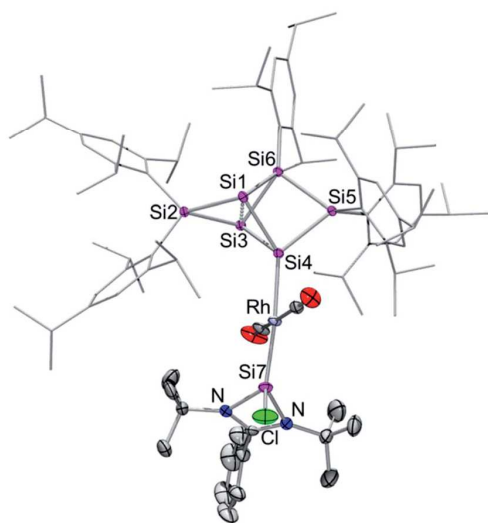


Fig. 3 Molecular structure of silylene-functionalized siliconoid rhodium complex **4** in the solid state. Hydrogen atoms are omitted for clarity. Thermal ellipsoids are set at 50% probability. Selected bond lengths [Å] and angles [°]: Rh–Si7 2.305(1), Rh–Si4 2.398(1), Si3–Si6 2.342(1), Si2–Si3 2.352(1), Si3–Si4 2.386(1), Si1–Si2 2.619(1), Si1–Si4 2.336(1), Si1–Si6 2.351(1), Si1–Si2 2.392(1), Si1–Si3 2.619(1), Si4–Si5 2.384(1), Si5–Si6 2.371(1), Si7–N1 1.826(3), Si7–N2 1.831(3), Si7–Cl 2.077(2), Si7–Rh–Si4 172.63(4), Si3–Si4–Rh 131.22(5), Si5–Si4–Rh 132.67(5), Si1–Si4–Rh 124.01(5), and Si4–Si1–Si2 97.15(5).

Rh–Si2 102.586(4)°, C16–Rh–Si3 104.881(5)°, C16–Rh–Si7 45.489(4)°, centre(Si1–Si4)–Rh–Si2 79.149(4)°, centre(Si1–Si4)–Rh–Si3 78.869(4)°, centre(Si1–Si4)–Rh–Si7 75.997(4)°, C16–Rh–centre(Si1–Si4) 175.493(6)°, and Si7–Rh–Si3 132.095(5)°. The geometric parameter $\tau = (\beta - \alpha)/60$ is commonly used for pentacoordinate complexes as an index of the degree of the trigonality in trigonal-bipyramidal and square-planar pyramidal structural motifs.¹⁷ With the two largest angles α and β of 3 (β : C16–Rh–centre(Si1–Si4) 175.493(6)°; α : Si7–Rh–Si3 132.095(5)°) the angular parameter is $\tau = 0.72$ in line with a distorted trigonal-bipyramidal coordination sphere of Rh. The chlorine atom is shifted to one of the former *nudo*-vertices so that the extrusion of the *privo*-SiTip₂ moiety as in **2a–c** is avoided in this case. Intriguingly, the chloro-substituted silicon vertex (Si3) is conferred a significant silylene character: the corresponding bond distance to rhodium (Si3–Rh 2.2455(7) Å) is considerably shorter than that of the amidinato silylene moiety, which binds to rhodium at a distance (Si7–Rh 2.3104(7) Å) similar to those reported for other complexes with this motif.^{5,16e} The former *privo*-vertex binds to the Rh centre at a distance (Si2–Rh 2.3872(8) Å) in line with the covalent radii of silicon and rhodium. Si2, Si3 and Si7 bind in equatorial positions and thus form the base of the trigonal-bipyramidal coordination environment at Rh.

The Si1–Si4 bond is unusually short (2.279(1) Å) and occupies the remaining apical positions at Rh at relatively long distances (Si4–Rh 2.5936(7) Å and Si1–Rh 2.5965(7) Å). Both Si1 and Si4 exhibit a hemispheroidal coordination environment

with hemispheroidalities of $\phi(\text{Si1}) = +0.8003$ Å and $\phi(\text{Si4}) = +0.4764$ Å.^{8a} The degree of the metallacyclopropane character of this coordinating interaction according to the Dewar–Chatt–Duncanson model¹⁸ is difficult to estimate due to the complexity of the bonding situation as Si1–Si4, albeit shorter than a usual single bond, is heavily involved in cluster bonding.

The ²⁹Si NMR spectrum in C₆D₆ is consistent with the bonding situation as discussed on the basis of the solid state structure. Four of the seven resonances are split into doublets by the coupling to the ¹⁰³Rh nucleus suggesting the coordination of rhodium being uncompromised by solvation. The signals are, however, not as broadly dispersed as typically observed for Si₆ siliconoids.^{9,13} The former *privo*-vertex Si2 gives rise to a low-field ²⁹Si NMR signal, albeit it splits into a doublet at 158.8 ppm with a coupling constant of $J^{29\text{Si}, 103\text{Rh}} = 41.0$ Hz. The silylene character of the former *nudo*-vertex Si3, now bearing the chloro substituent, results in the significant deshielding of the corresponding ²⁹Si NMR signal at 165.7 ppm. The interaction with the rhodium centre is reflected in the coupling constant of $J^{29\text{Si}, 103\text{Rh}} = 53.4$ Hz. The ¹⁰³Rh coupling of the two hemispheroidally coordinated vertices Si1 and Si4 is too small to resolve resulting in singlets at –140.2 and –122.1 ppm. Although a discussion of the magnitude of experimental coupling constants is next to impossible in polycyclic systems such as **3** the absence of detectable coupling is in line with a predominant π -character of the coordination to rhodium.^{3a} The assignment is backed by the absence of cross-peaks to Tip groups in the 2D ²⁹Si/¹H correlation. The doublet at 108.7 ppm ($J^{29\text{Si}, 103\text{Rh}} = 59.6$ Hz) is assigned to the N-heterocyclic silylene moiety (Si7) based on the observation of a cross-peak to the *t*-butyl groups. In notable contrast, the signal of the not directly Rh-bonded Si6 at 58.3 ppm (assigned on the basis of a cross-peak to one Tip substituent) is split into a doublet with $J^{29\text{Si}, 103\text{Rh}} = 14.3$ Hz.

Surprisingly, after the rearrangement of Rh(I) complex **3** to **4**, the diagnostic wide dispersion of ²⁹Si NMR shifts is again observed, which suggested the re-establishment of an uncompromised benzpolarene^{9,13} scaffold. Besides the characteristic highfield resonances for the *nudo*-vertices Si1 and Si3 at –256.1 and –258.3 ppm, the ²⁹Si NMR signal of the tetracoordinate *privo*-vertex Si2 appears at the typical low field at 162.6 ppm. The doublet in the ²⁹Si NMR at 48.2 ppm with $J^{29\text{Si}, 103\text{Rh}} = 84.5$ Hz is attributed to the N-heterocyclic silylene moiety on the basis of a cross-peak to the *t*-butyl groups in the 2D ²⁹Si/¹H correlation and the large coupling indicative of pronounced s-orbital contributions. In contrast, the doublet at –9.0 ppm with $J^{29\text{Si}, 103\text{Rh}} = 31.5$ Hz suggests a covalent bond to the ¹⁰³Rh nucleus. Due to the absence of a cross-peak to a Tip group in the 2D ²⁹Si/¹H correlation NMR spectrum, it can be attributed to the *ligato*-vertex Si4. The remaining ²⁹Si NMR chemical shifts are located in the usual range of saturated silicon atoms; only one of the signals showing a small coupling to the Rh centre (21.8 ppm; $J^{29\text{Si}, 103\text{Rh}} = 8.5$ Hz). The anticipated structure of **4** as an uncompromised benzpolarene scaffold covalently attached to rhodium was confirmed by X-ray diffraction in the solid state (Fig. 3).

The rhodium centre of **4** exhibits a typical square-planar coordination environment, with the hexasilabenzpolarene moiety indeed connected through the *ligato*-position Si4. Astonishingly, not only has the Si₆ moiety been reinstated during the isomerization from **3**, but the amidinato silylene – now disconnected from the siliconoid and coordinated to the rhodium centre in a *trans*-fashion – has reacquired its chloro-substituent as well. The coordination at the rhodium centre is completed by two CO ligands, which requires the “come-back” of the initially dissociated CO molecule. The Si7–Rh bond length of 2.305(1) Å is in line with the reported donor–acceptor bond length of Si–Rh complexes.^{5,16e} Interestingly, it is significantly shorter than the covalent Si4–Rh bond length of 2.398(1) Å in the same molecule. The distance between the bridgehead silicon atoms (Si1–Si3 2.6188(4) Å) is similar to that in previously reported *ligato*-substituted Si6 siliconoids.^{9,13} The longest wavelength absorption bands are observed at $\lambda_{\text{max}} = 461$ nm (**3**) and 466 nm (**4**) and thus are slightly blue-shifted compared to the *ligato*-metalated siliconoids Zr and Hf (Zr: 521 nm, Hf: 497 nm).¹³ The Rh complexes **3** and **4** exhibit IR characteristics of rhodium carbonyl complexes¹⁹ with CO stretching modes at $\nu = 1978$ cm^{−1} (**3**) and 1951, 1949 cm^{−1} (**4**).

Mechanistic considerations

Due to the flexibility of the coordination environments, reactions involving transition metals generally proceed through multiple steps and, consequently, the mechanisms are often complicated, especially when backbone structures are reconstructed such as in the present case through a sequence of cleavage and formation of Si–Si bonds. Although, a computational treatment of such mechanisms is well out of reach to us due to the anticipated complexity of the potential energy surfaces and the large size of the involved molecules, we propose a plausible mechanism for the Ir and Rh structures based on the structurally characterized products (Chart 1).

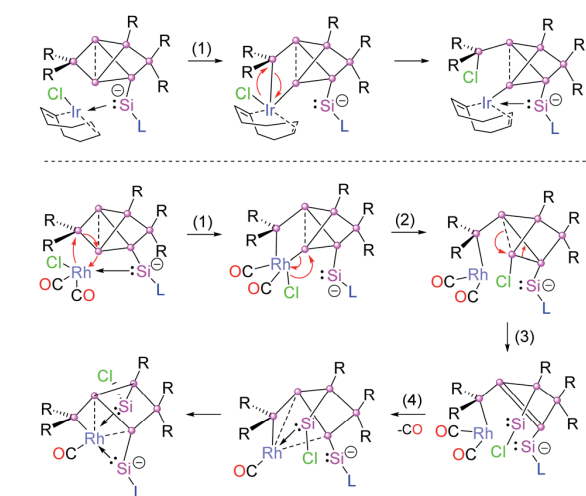


Chart 1 Proposed mechanism of the formation of **2a** (top) and **3** (bottom).

All reactions are likely initiated by the straightforward coordination of the pendant silylene ligand to the metal. For the subsequent rearrangements, we suggest the oxidative addition to the Si2–Si3 single bond as the common first step (step 1 in Chart 1). From the second step onwards, however, the isomerizations proceed through distinct pathways for the rhodium and iridium species. In the case of **2a**, the oxidative addition is directly followed by reductive elimination of the chloro group and the SiTip₂ moiety from the Ir centre resulting in the formation of the exohedral chlorosilyl group in the final product **2a** (and by extension **2b,c**). In contrast, in the case of the primary rhodium product **3** the chlorine migrates to Si3 (step 2). In step 3, the formation of the chlorosilylene Si3 is suggested, while a formal double bond between Si1–Si4 is formed as a consequence. In the last step, the final product **3** is formed by elimination of a CO unit enforced by the coordination of the Si1–Si4 bond and the silylenes (Si3 and Si7) to the Rh centre. The question of the re-establishment of the intact hexasilabenzpolarene scaffold from intermediate **3** to yield the final product **4** is even more daunting as it requires the return of the previously eliminated CO ligand into the coordination sphere of rhodium. Notably, a solution of crystallized **3** turned out to be inert towards exposure to CO atmosphere as well as the addition of excess [(CO)₂RhCl]₂. We therefore assumed that the formation of **4** can only be attained by a reactive species formed *in situ* during the reaction of **1a** with [(CO)₂RhCl]₂. Indeed, treatment of a solution of isolated crystals of **3** with 10 mol% of silylene-substituted siliconoid **1a** and 0.4 equivalents of additional [(CO)₂RhCl]₂ results in the uniform conversion of isolated **3** to **4** in the course of 24 h. We speculate that either an extremely short-lived intermediate of monomeric [(CO)₃RhCl]²⁰ or a heterodimer not unlike the one reported by Braunschweig *et al.*²¹ might be responsible for the CO delivery.

Alkene isomerization catalysis

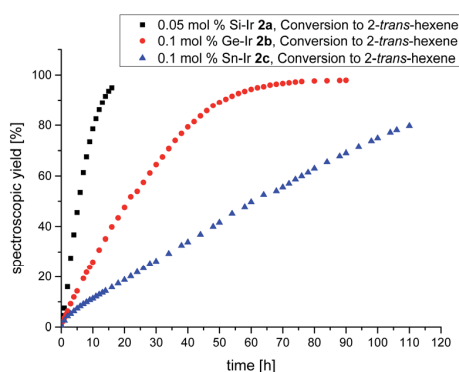
Despite the plethora of synthetic methods available for the introduction of C–C double bonds, the regioisomerization of an existing C–C double bond is a viable alternative.²² The so-called alkene isomerization, however, results in mixtures of (*E*) and (*Z*)-alkenes in many cases²³ or further migration along a saturated carbon chain. The selective transformation of terminal alkenes to 2-alkenes has thus attracted considerable interest.²⁴ We anticipated that electron-rich siliconoid ligands might fulfill two functions in a homogenous catalyst for alkene isomerization: (a) acting as an electron reservoir and thus facilitating oxidative addition reactions and (b) providing sufficient steric bulk to improve the selectivity regarding the number of positions the C–C double bond migrates. We therefore probed the isomerization of terminal alkenes to 2-alkenes in the presence of catalytic quantities of complexes **2a–c**, **3** and **4**.

As rapidly indicated by first preliminary tests, no solvent is required for the catalytic activity of **2a–c**, **3** and **4** and therefore all runs were carried out with the neat substrate, an attractive feature from both ecologic and economic perspectives. Allyltrimethylsilane and 1-hexene were used as neat substrates on an NMR scale using a C₆D₆ capillary as the locking signal; yields

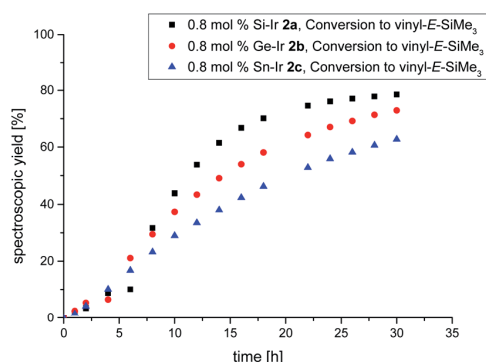


Table 2 Reaction conditions, conversion determined by ^1H NMR spectroscopy

Catalyst	Substrate	Cat. loading [mol%]	Time [h]	Temperature [$^{\circ}\text{C}$]	Σ conversion [%]	<i>E</i> -isomer [%]	<i>Z</i> -isomer [%]	TON	TOF [h^{-1}]
2a	1-Hexene	0.05	16	25	95	—	—	1902.7	118.9
2b	1-Hexene	0.1	72	25	97	—	—	968.8	13.5
2c	1-Hexene	0.1	100	25	75	—	—	748.4	7.5
2a	Allyl-SiMe ₃	0.8	26	60	94	77	17	117.4	4.5
2b	Allyl-SiMe ₃	0.8	30	60	89	73	16	111.6	3.7
2c	Allyl-SiMe ₃	0.8	30	60	78	63	15	97.4	3.2

Fig. 4 Plot of the spectroscopically determined conversion to 2-*trans*-hexene. Black = Si-Ir **2a** (0.05 mol%), red = Ge-Ir **2b** (0.1 mol%), and blue = Sn-Ir **2c** (0.1 mol%).

were calculated from ^1H NMR integrations (Table 2). Fig. 4 shows the spectroscopic conversion to 2-*trans*-hexene using 0.05 mol% (**2a**), 0.1 mol% (**2b**, **2c**) of the catalysts at room temperature as a function of time. The side chain migration to 3-*trans*-hexene is disregarded in the plots due to the overlap of the chemical shifts, and estimated to be <10% from the spectroscopic data. Blind tests without catalyst or in the presence of $[(\text{cod})\text{IrCl}]_2$ or $[(\text{CO})_2\text{-RhCl}]_2$ led to no detectable conversion under identical conditions. The reaction can therefore easily be quenched after the formation of 2-*trans*-hexene is complete by simple addition of

Fig. 5 Plot of the spectroscopically determined conversion to *E*-vinyltrimethylsilane 60 $^{\circ}\text{C}$ using the 0.8 mol% catalyst. Black = Si-Ir **2a**, red = Ge-Ir **2b**, blue = Sn-Ir **2c**.

water leading to the hydrolysis of the catalyst. The catalytic performance is best in the case of **2a** ($\text{E} = \text{Si}$, $\text{TOF} = 119 \text{ h}^{-1}$) with catalyst loadings as low as 0.05 mol% and strongly decreases from **2b** ($\text{E} = \text{Ge}$, $\text{TOF} = 13.5 \text{ h}^{-1}$) to **2c** ($\text{E} = \text{Sn}$, $\text{TOF} = 7.5 \text{ h}^{-1}$) both requiring double catalyst loads. Preliminary results show a much lower catalytic activity of the rhodium complexes **3** and **4** which was therefore not investigated in detail (see ESI†). The isomerization of allyltrimethylsilane to 2-*E/Z*-vinyltrimethylsilane proceeds significantly slower even with the more active **2a-c** and requires higher temperatures as well as one order of magnitude larger amounts of catalyst (0.8 mol%, 60 $^{\circ}\text{C}$, Fig. 5, ESI†).

It should be noted, however, that the reaction at room temperature is probably slowed down even further due to the moderate solubility of the crystalline samples of the catalysts **2a-c** in neat allyltrimethylsilane. This phenomenon is manifest in an extended induction period of approximately 5 h (Fig. 5) after which the spectroscopic yield increases much faster due to rapid dissolution in the mixture of allyltrimethylsilane and the isomerization products.

The driving force of the alkene isomerization is the higher thermodynamic stability of internal alkenes.²⁵ As suggested by the negative blind tests with the siliconoid-free precursors, the intramolecular hydrogen migration is supported through the extremely electron-rich hexasilabenzpolarene scaffold.

Conclusion

In conclusion, with the Group 9 metal complexes **2a-c** and **3** we reported the first siliconoids with endohedral incorporation of transition metals. As demonstrated by the isomerization of **3** to the **4** with complete reconstitution of the uncompromised benzpolarene scaffold, a temporary change in the coordination mode of these ligands is possible in principle. All isolated complexes show catalytic activity in the isomerization of alkenes with the best (**2a**) reaching competitive selectivity at satisfactory conversion rates in the case of 1-hexene.

Conflicts of interest

There are no conflicts to declare.

Acknowledgements

Funding by the Deutsche Forschungsgemeinschaft (DFG SCHE906/4-1 and 4-2) is gratefully acknowledged.



Notes and references

- Recent reviews: (a) E. Rivard, *Chem. Soc. Rev.*, 2016, **45**, 989–1003; (b) B. Blom and M. Driess, Functional Molecular Silicon Compounds II, in *Structure and Bonding*, ed. D. Scheschkewitz, 2013, vol. 156, pp. 85–123; (c) S. Mandal and H. W. Roesky, *Acc. Chem. Res.*, 2012, **45**, 298–307; (d) M. Asay, C. Jones and M. Driess, *Chem. Rev.*, 2011, **111**, 354–396; (e) Y. Mizuhata, T. Sasamori and N. Tokitoh, *Chem. Rev.*, 2009, **109**, 3479–3511.
- Recent reviews: (a) A. Rammo and D. Scheschkewitz, *Chem.-Eur. J.*, 2018, **24**, 6866–6885; (b) T. Matsuo and N. Hayakawa, *Sci. Technol. Adv. Mater.*, 2018, **19**, 108–129; (c) C. Präsang and D. Scheschkewitz, *Chem. Soc. Rev.*, 2016, **45**, 900–921; (d) T. Iwamoto and S. Ishida, Functional Molecular Silicon Compounds II, in *Structure and Bonding*, ed. D. Scheschkewitz, 2013, vol. 156, pp. 125–202.
- Recent reviews: (a) S. Ishida and T. Iwamoto, *Coord. Chem. Rev.*, 2016, **314**, 34–63; (b) S. Raoufmoghaddam, Y.-P. Zheng and M. Driess, *J. Organomet. Chem.*, 2017, **829**, 2–10; (c) B. Blom, M. Stoelzel and M. Driess, *Chem.-Eur. J.*, 2013, **19**, 40–62.
- (a) A. Brück, D. Gallego, W. Wang, E. Irran, M. Driess and J. F. Hartwig, *Angew. Chem., Int. Ed.*, 2012, **51**, 11478–11482; (b) B. Blom, D. Gallego and M. Driess, *Inorg. Chem. Front.*, 2014, **1**, 134–148.
- M. Stoelzel, C. Präsang, B. Blom and M. Driess, *Aust. J. Chem.*, 2013, **66**, 1163–1170.
- (a) D. Gallego, A. Brück, E. Irran, F. Meier, M. Kaupp, M. Driess and J. F. Hartwig, *J. Am. Chem. Soc.*, 2013, **135**, 15617–15626; (b) M. Zhang, X. Liu, C. Shi, C. Ren, Y. Ding and H. W. Roesky, *Z. Anorg. Allg. Chem.*, 2008, **634**, 1755–1758.
- B. Blom, S. Enthaler, S. Inoue, E. Irran and M. Driess, *J. Am. Chem. Soc.*, 2013, **135**, 6703–6713.
- Reviews: (a) Y. Heider and D. Scheschkewitz, *Dalton Trans.*, 2018, **47**, 7104–7112; (b) S. Ishida and T. Iwamoto, *Chem. Lett.*, 2014, **43**, 164–170.
- (a) P. Willmes, K. Leszczyńska, Y. Heider, K. Abersfelder, M. Zimmer, V. Huch and D. Scheschkewitz, *Angew. Chem., Int. Ed.*, 2016, **55**, 2907–2910; (b) Y. Heider, N. E. Poitiers, P. Willmes, K. I. Leszczyńska, V. Huch and D. Scheschkewitz, *Chem. Sci.*, 2019, **10**, 4523–4530.
- (a) S. Scharfe, F. Kraus, S. Stegmaier, A. Schier and T. F. Fässler, *Angew. Chem., Int. Ed.*, 2011, **50**, 3630–3670; (b) J. M. Goicoechea and S. C. Sevov, *Organometallics*, 2006, **25**, 5678–5692.
- Recent review: R. J. Wilson, B. Weinert and S. Dehnen, *Dalton Trans.*, 2018, **47**, 14861–14869.
- Recent review: (a) S. D. Hoffmann and T. F. Fässler, *Angew. Chem., Int. Ed.*, 2004, **43**, 6242–6247; (b) K. Mayer, J. Weßing, T. F. Fässler and R. A. Fischer, *Angew. Chem., Int. Ed.*, 2018, **57**, 14372–14393.
- N. E. Poitiers, L. Giarrana, K. I. Leszczyńska, V. Huch, M. Zimmer and D. Scheschkewitz, *Angew. Chem., Int. Ed.*, 2020, **59**, 8532–8536.
- K. Abersfelder, A. Russell, H. S. Rzepa, A. J. P. White, R. Haycock and D. Scheschkewitz, *J. Am. Chem. Soc.*, 2012, **134**, 16008–16016.
- Y. Heider, P. Willmes, V. Huch, M. Zimmer and D. Scheschkewitz, *J. Am. Chem. Soc.*, 2019, **141**(49), 19498–19504.
- (a) M. Kilian, H. Wadeppohl and L. H. Gade, *Organometallics*, 2008, **27**(4), 524–533; (b) A.-K. Jungton, A. Meltzer, C. Präsang, A. Penner, T. Braun and M. Driess, *Dalton Trans.*, 2010, **39**, 5436–5438; (c) D. O. Downing, P. Zavalij and B. W. Eichhorn, *Eur. J. Inorg. Chem.*, 2010, 890–894; (d) A. Wagenpfeil, C. Nickl, H. Schubert, K. Eichele, M. A. Fox and L. Wesemann, *Eur. J. Inorg. Chem.*, 2011, 3349–3356; (e) S. Kaufmann, S. Schäfer, M. T. Gamer and P. W. Roesky, *Dalton Trans.*, 2017, **46**, 8861–8867; (f) B. Su, K. Ota, Y. Li and R. Kinjo, *Dalton Trans.*, 2019, **48**, 3555–3559; (g) K. M. Krebs, S. Freitag, J.-J. Maudrich, P. Sirsch and L. Wesemann, *Dalton Trans.*, 2018, **47**, 83–95.
- A. W. Addison and T. N. Rao, *J. Chem. Soc., Dalton Trans.*, 1984, 1349–1356.
- (a) M. J. S. Dewar, *Bull. Soc. Chim. Fr.*, 1951, **18**, C71; (b) J. Chatt and L. A. Duncanson, *J. Chem. Soc.*, 1953, 2939–2947.
- D. K. Dutta and M. M. Singh, *Transition Met. Chem.*, 1979, **4**, 230–234.
- M. P. Keyes and K. L. Watters, *J. Catal.*, 1986, **100**, 477–481.
- K. Radacki, M. Forster and H. Braunschweig, *Angew. Chem., Int. Ed.*, 2006, **45**, 2132–2134.
- G.-J. Boons, A. Burton and S. Isles, *Chem. Commun.*, 1996, 141–142.
- G. Chahboun, C. E. Petrisor, E. Gómez-Bengoia, E. Royo and T. Cuenca, *Eur. J. Inorg. Chem.*, 2009, 1514–1520.
- (a) R. H. Grubbs, *Tetrahedron*, 2004, **60**, 7117–7140; (b) C. R. Larsen and D. B. Grotjahn, *J. Am. Chem. Soc.*, 2012, **134**, 10357–10360; (c) C. Chen, T. R. Dugan, W. W. Brennessel, D. J. Weix and P. L. Holland, *J. Am. Chem. Soc.*, 2014, **136**, 945–955; (d) J. Becica, O. D. Glaze, D. I. Wozniak and G. E. Dobereiner, *Organometallics*, 2018, **37**, 482–490.
- D. B. Dahl, C. Davies, R. Hyden, M. L. Kirova and W. G. Lloyd, *J. Mol. Catal. A: Chem.*, 1997, **123**, 91–101.



3.4 Chalcogen-expanded unsaturated silicon clusters: thia-, seleno- and tellurasiliconoids

Reproduced with permission from Nadine E. Poitiers, Volker Huch, Michael Zimmer, David Scheschkewitz, *Chem. Eur. J.* **2020**,

Copyright © 2020 WILEY-VCH Verlag GmbH & Co. KGaA, Weinheim.

<https://doi.org/10.1002/chem.202003180>

The article is reproduced in this thesis by permission of Wiley-VCH Verlag GmbH & Co. KGaA and all authors. The results are additionally concluded and put into context in Chapter 4.

Contributions of the Authors:

Nadine Poitiers: Equal (D.S.): Conceptualization; Lead: Data curation, Formal analysis, Investigation, Methodology, Validation, Visualization, Writing Review and Editing.

Volker Huch: Lead: X-ray analysis.

Michael Zimmer: Lead: CP/MAS NMR and VT-NMR.

David Scheschkewitz: Lead: Conceptualization, Project administration, Supervision Funding acquisition and resources; Supporting: Methodology, Writing — review and editing.

Cluster Compounds | Very Important Paper |

VIP Chalcogen-Expanded Unsaturated Silicon Clusters: Thia-, Seleno-, and Tellurasiliconoids
Nadine E. Poitiers, Volker Huch, Michael Zimmer, and David Scheschkewitz*^[a]

Abstract: Reactions of silylenes with heavier chalcogens (E) typically result in Si=E double bonds or their π -addition products. In contrast, the oxidation of a silylene-functionalized unsaturated silicon cluster (siliconoid) with Group 16 elements selectively yields cluster expanded siliconoids Si₇E (E=S, Se, Te) fully preserving the unsaturated nature of the cluster scaffold as evident from the NMR signatures of the products. Mechanistic considerations by DFT calculations suggest the intermediacy of a Si₆ siliconoid with exohedral Si=E functionality. The reaction thus may serve as model system for the oxidation of surface-bonded silylenes at Si(100) by chalcogens and their diffusion into the silicon bulk.

The synthesis of unsaturated silicon clusters (siliconoids)^[1] as well as the corresponding hetero derivatives^[2] draws increasing attention due to their role as presumed intermediates during chemical vapor deposition^[3] or heterogeneous catalysis.^[4] In addition, the unsubstituted vertices share important features of native silicon surfaces, in particular the presence of free valencies, the so-called “dangling bonds”.^[5]

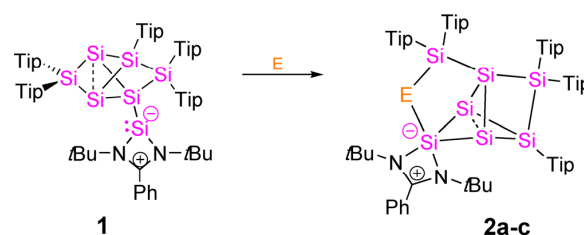
A variety of neutral and anionic stable siliconoids has been reported during the last decades.^[2,6,7–16] The manipulation of stable representatives under retention of the unsaturated character is mostly limited to the shell of stabilizing ligands. A notable exception is the deliberate core expansion from Si₆ via Si₇ and Si₈ using silicocene SiCp*₂ as a source of atomic silicon.^[13d] In general, reactions of siliconoids with oxidizing reagents result in the saturation of the free valencies and thus the loss of siliconoid character according to the definition.^[17] More particularly, while saturated silicon clusters are well-known to undergo cluster expansion with chalcogens^[12,18] the related chemistry of neutral siliconoids is completely unexplored, pre-

sumably due to the facile oxidation of the “naked” vertices. In view of the tremendous importance of chalcogen-containing silicon materials,^[19] including sub-valent varieties such as the famous “silicon monoxide”,^[20] we contemplated the possibility of the incorporation of Group 16 elements as heteroatoms into the cluster core without compromising the siliconoid characteristics. A large variety of molecular model systems for silicon subchalcogenides has been described in recent years, which are strictly electron-precise without exception and thus do not reflect the widely accepted assumption of nanoscale cluster domains in these composite materials.^[18a–c] N-heterocyclic silylenes, for instance, are well-known to readily undergo oxidation to the corresponding silanones and heavier versions thereof.^[21–24]

We therefore envisaged that chalcogens may initially attack the pending silylene center of our recently reported siliconoid/silylene hybrid species^[13g] instead of the unsubstituted vertices of the Si₆ scaffold. In the same communication we had shown that the Fe(CO)₄ fragment coordinates to the silylene moiety exclusively.^[13g] We now report that this strategy indeed leaves the “naked” vertices untouched in the reaction with chalcogens as well, while the pronounced electrophilicity of the plausibly formed Si=E moiety (E=S, Se, Te) expands the cluster core to incorporate two additional vertices: a pentacoordinate silicon and the heavier chalcogen.

Simple stirring of a benzene suspension of the silylene-functionalized siliconoid **1** with an excess of the chalcogen at room temperature (**2a**: E=S, 2.5 equiv, 4 h; **2b**: E=Se, 2.5 equiv, 16 h; **2c**: E=Te, 7 equiv, 72 h) results in the uniform conversion to the chalcogen-expanded siliconoids **2a–c** (Scheme 1).

The longest wavelength absorptions in the UV/Vis spectra are at $\lambda_{\text{max}}=394$ nm (**2a**), 396 nm (**2b**), 404 nm (**2c**) and thus within the range observed for previously reported siliconoids ($\lambda_{\text{max}}=364$ to 477 nm).^[13c,d] The chalcogen-expanded ESi₇ siliconoids **2a–c** exhibit a high thermal stability, showing almost no



Scheme 1. Synthesis of chalcogen-expanded Si₇ siliconoids **2a–c** (**2a**: E=S, **2b**: E=Se, **2c**: E=Te).

[a] N. E. Poitiers, Dr. V. Huch, Dr. M. Zimmer, Prof. Dr. D. Scheschkewitz
Krupp-Chair of Inorganic and General Chemistry
Saarland University
Campus Saarbrücken C4.1, 66123 Saarbrücken (Germany)
E-mail: scheschkewitz@mx.uni-saarland.de

Supporting information and the ORCID identification numbers for the authors of this article can be found under:
<https://doi.org/10.1002/chem.202003180>.

© 2020 The Authors. Published by Wiley-VCH GmbH. This is an open access article under the terms of Creative Commons Attribution NonCommercial-NoDerivs License, which permits use and distribution in any medium, provided the original work is properly cited, the use is non-commercial and no modifications or adaptations are made.

decomposition at their melting points up to 380 °C. In the solid state, crystals can be exposed to air for a few minutes without apparent decomposition. This is remarkably reminiscent of the stability of selenium and other heavier chalcogens bonded to silicon surfaces, which require temperatures of up to 1000 K for desorption.^[22]

The structures of siliconoids Si₇E **2a–c** in the solid state were determined by X-ray diffraction on bright yellow crystals obtained in 74% (**2a**), 70% (**2b**) and 75% (**2c**) yield, respectively (Figure 1). The cluster cores resemble that of the aforementioned Si₇Tip₅Cp* siliconoid and its expansion to Si₈Tip₅Cp*.^[13d] As in Si₇Tip₅Cp*, the Si1, Si2 and Si5 vertices are arranged as a central isosceles triangle, although only the two vertices of the base (Si1 and Si2) show hemispheroidal coordination environments^[1a] (**2a**: $\phi(\text{Si1}) = +1.3628^\circ$, $\phi(\text{Si2}) = 1.2919^\circ$, $\phi(\text{Si5}) = -0.2267^\circ$; **2b**: $\phi(\text{Si1}) = +1.3603^\circ$, $\phi(\text{Si2}) = +1.2850^\circ$, $\phi(\text{Si5}) = -0.2120^\circ$; **2c**: $\phi(\text{Si1}) = +1.3616^\circ$, $\phi(\text{Si2}) = +1.2758^\circ$, $\phi(\text{Si5}) = -0.2356^\circ$). The Si₇E cluster is formally derived from the Si₅ propellane motif distorted by the twofold interconnection of the “propeller blades”. This distortion results in a seesaw-type coordination environment at Si5 with a quasi-linear arrangement towards Si6 and Si5 (Si4–Si5–Si6 162.705(4)° (**2a**); 161.951(2)° (**2b**); 158.951(3)° (**2c**) vs. 173.77° for Si₇Tip₅Cp*^[13d]). The SiTip₂-bridge between Si5 and the former N-heterocyclic silylene moiety Si7 is extended by the insertion of the chalcogen atom. Together with the two nitrogen centers and the two adjacent “naked” silicon vertices pentacoordination of Si7 is attained. The distance between the unsubstituted silicon atoms in **2a–c** (Si1–Si2 **2a**: 2.6583(5) Å, **2b**: 2.6483(7) Å, **2c**: 2.611(7) Å, Table 1) are comparable with those of the Si₇Tip₅Cp* (2.648 Å).^[13d] The Si2–Si7 bonds are markedly longer (**2a**: 2.4967(5) Å, **2b**: 2.4904(7), **2c**: 2.5017(7) Å) than all remaining Si–Si bonds of the cluster core. The Si6–E bonds of

Table 1. Selected analytical data of Group 16 core-expanded siliconoids **2a–c**.

	$\delta^{29}\text{Si5}$ [ppm]	$\delta^{29}\text{Si1/2}$ [ppm]	Si1–Si2 [Å]	Si7–E [Å]	Si6–E [Å]	λ_{max} [nm]
2a (E = S)	–109.7	–251.1 –314.9	2.6583(5)	2.1438(5)	2.2044(5)	395
2b (E = Se)	–100.4	–251.5 –309.3	2.6483(7)	2.2923(6)	2.3474(6)	397
2c (E = Te)	–86.7	–250.2 –299.3	2.611(7)	2.5120(5)	2.5764(5)	405

2a–c (**2a**: 2.2044(5) Å, **2b**: 2.3474(6) Å, **2c**: 2.5764(5) Å) are significantly longer than Si7–E (**2a**: 2.1438(5) Å, **2b**: 2.2923(6) Å, **2c**: 2.5120(5) Å) and hence in the range of typical Si–E single bonds as, for example, in dichalcogenatrisilabicyclopentanes (Si–S: 2.198 Å; Si–Se: 2.339 Å; Si–Te: 2.561 Å).^[25] The difference in Si–E bond lengths may be interpreted as manifestation of some residual double bond character of Si7–E and consequently a somewhat weaker interaction Si6–E, possibly with a certain donor-acceptor character.

At first glance, the typical wide dispersion of ²⁹Si NMR signals of siliconoids is not retained in **2a–c**. While two of signals for the unsubstituted silicon atoms Si1 and Si2 are observed in the characteristic region between about –250 and –300 ppm, a third strongly shielded signal at –109.7 ppm (**2a**), –100.4 ppm (**2b**) and –86.7 ppm (**2c**) without a cross-peak in the 2D ²⁹Si/¹H correlation NMR spectra is indicative of the presence of the additional silicon vertex Si5 without substituent, similar to the observations in the hetero-atom-free Si₇ siliconoid.^[13d] The resonances at 33.5 (**2a**), 26.6 (**2b**) and 2.3 ppm (**2c**) are assigned to the silicon vertex of the former N-heterocyclic silylene moiety. While siliconoids Si₇Tip₅Cp* and Si₈Tip₅Cp*^[13d] still exhibit a similarly wide ²⁹Si NMR shift distribution as the Si₆ benzpolarenes,^[13c,e] the chemical shifts of **2a–c** for Si7 may seem quite ordinary at first, but are in fact extraordinarily deshielded considering the pentacoordination of Si7. Pentacoordinate silicon atoms containing the same amidinato ligand typically give rise to signals between –124.9 and –82.9 ppm.^[26] All other signals are observed at unremarkable chemical shifts and are assigned to either SiTip₂ or SiTip vertices on the basis of the number of cross-peaks to aryl hydrogens in the 2D ²⁹Si/¹H NMR correlation spectra (see Supporting Information). The occurrence of two sets of signals in the ¹H NMR of **2c** suggests the presence of rotational isomers. Indeed, a VT-NMR study in toluene solution revealed an increase in intensity of the second set of signals with temperature although the barrier proved to be too high to accurately determine the coalescence temperature (> 343 K). The low solubility of **2a–c** hindered the acquisition of ²⁹Si NMR with sufficient signal-to-noise ratio and thus prevented the detection of the second set of signals for **2c**. The ¹²⁵Te spectrum of **2c**, however, reveals a major signal at –93.72 ppm and a second less intense signal at –22.84 ppm. The ⁷⁷Se spectrum of **2b** shows one sharp signal at 53.9 ppm.

In the CP-MAS ²⁹Si NMR, very similar chemical shifts are observed proving the identity of the cluster in the solid state and

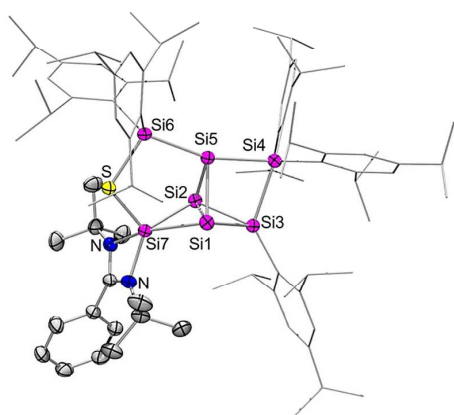


Figure 1. Representative molecular structure of siliconoid **2a** in the solid state. Hydrogen atoms omitted for clarity. Thermal ellipsoids at 50%. For structure of **2b,c** see Supporting Information. Selected bond length [Å] and angles [°]: **2a**: Si1–Si7 2.4967(5), Si1–Si2 2.6583(5), Si4–Si5 2.4067(5), Si6–S 2.2044(5), Si7–S 2.1438(5), Si7–N1 1.852(1), Si7–N2 1.909(1); **2b**: Si2–Si7 2.4904(7), Si1–Si2 2.6483(7), Si4–Si5 2.4101(8), Se–Si7 2.2923(6), Se–Si6 2.3474(6), Si7–N21.860(2), Si7–N1 1.924(2); **2c**: Si2–Si7 2.5017(7), Si1–Si2 2.6411(7), Si4–Si5 2.4249(7), Te–Si7 2.5120(5), Te–Si6 2.5764(5), Si7–N1 1.862(2), Si7–N2 1.928(2).

the major rotational isomer in solution. The CP/MAS NMR chemical shifts of the heavier chalcogen atoms in **2b** and **2c** depend slightly on the rotation frequency of the rotors, a commonly observed phenomenon due to the heating of the sample induced by fast spinning of the rotor.^[27] This effect is more pronounced in case of the ¹²⁵Te signals of **2c** with a downfield shift of $\Delta\delta = 9.1$ ppm upon increasing the frequency from 5 to 15 KHz. In comparison, the ⁷⁷Se signals of **2b** are only shifted by $\Delta\delta = 3.2$ ppm under identical conditions. The same phenomenon, albeit significantly less pronounced, is observed for the ²⁹Si CP/MAS NMR chemical shifts of **2b,c** (Supporting Information) with downfield-shifts $\Delta\delta$ between 0.2 and 0.9 ppm with increasing rotation frequency from 5 to 15 KHz.

The mechanism of chalcogen-expansion of the cluster is of particular relevance in view of the considerable interest in chalcogen and chalcogenide diffusion through silicon materials spurred by applications in micro- and optoelectronics as well as batteries.^[19d,28] The formation of heterosiliconoids **2a–c** is readily understood by an initial oxidation of the pending silylene center by the chalcogen leading to the formation of an intermediate siliconoid [1-Int] with Si=E functionality in *ligato*-position. Such a pathway may well correspond to the an initial step of the sorption of chalcogens to the deconstructed Si(100)(1×1) surface with its surface-bonded silylene centers. After rotation about the Si–Si bond between silylene and siliconoid core, the strongly polar Si=E moiety of [1-Int] would be predisposed to attack the *privo*-vertex (which typically hosts major contributions to the LUMO of functionalized benzopolarene siliconoids)^[13b] with its negatively polarized chalcogen end. In this scenario, the silicon end with its partial positive charge would accept electron density from one of the *nudo*-vertices in concert with the cleavage of the bond between the *nudo*- and the *privo*-silicon atoms (Scheme 2). We speculate that similar pathways may be active during the process of chalcogen diffusion from the silicon surface into the bulk.^[28b]

In order to support our mechanistic proposal, optimization of the electronic structures of the sulfur-expanded siliconoid **2a** and the proposed intermediates [1-Int] and [1-Int]' with E=S were carried out at the BP86-D3(BJ)/def2-SVP level of theory (Supporting Information). Compared to [1-Int], the final product **2a** is favored by $\Delta\Delta G = -9.26$ kcal mol⁻¹ in free en-

thalpy, which is in line with the fast and spontaneous formation of **2a** (see Supporting Information). According to the Hammond postulate,^[29] an approximate idea about the activation barrier for this process can be deduced from the free enthalpy of [1-Int]' as necessary intermediate, which is by $\Delta\Delta G = +4.71$ kcal mol⁻¹ higher in free enthalpy than [1-Int]. The shape of the frontier orbitals of [1-Int] adds further support for this scenario. The HOMO and HOMO-1 represent the lone pairs at the sulfur atom, while the LUMO exhibits a major contribution at the *privo*-vertex as commonly found for hexasilabenzopolarene structures (Figure 2). The intramolecular in phase-overlap of HOMO and LUMO upon rotation of the Si=E moiety towards the *privo*-vertex as in [1-Int]' would plausibly result in relaxation to **2a** with a small barrier (Scheme 2).

In conclusion, we reported the expansion of the core structure of neutral silylene-functionalized siliconoids with chalcogens in the backbone. The heterosiliconoids of type Si₇E (E=S, Se, Te) feature three unsubstituted vertices and are shown to be thermally extremely robust. The former silylene moiety is now pentacoordinate, yet shows a chemical shift at unusually low field presumably due to the characteristic deshielding effect of the cluster current. The mechanistic scenario for cluster expansion may serve as inspiration for the consideration of alternative pathways in surface and bulk interactions of chalcogens with silicon.

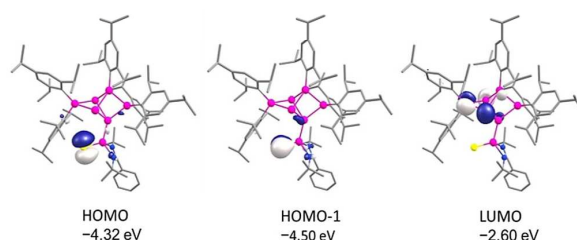


Figure 2. Selected Molecular orbitals of [1-Int]' at the BP86-D3(BJ)/def2-SVP level of theory (isocontour value at 0.051840).

Acknowledgements

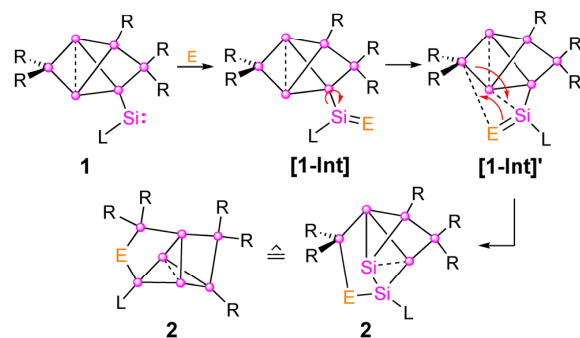
Funding by the Deutsche Forschungsgemeinschaft (DFG SCHE 906/4-1 and 4-2) is gratefully acknowledged. Open access funding enabled and organized by Projekt DEAL.

Conflict of interest

The authors declare no conflict of interest.

Keywords: chalcogens • cluster expansion • low-valent species • silicon • siliconoids

- [1] a) Y. Heider, D. Scheschke, Dalton Trans. **2018**, 47, 7104–7112; b) S. Kyushin in *Organosilicon Compounds: Theory and Experiment (Synthesis)*, Vol. 1 (Ed.: V. Y. Lee), Academic Press **2017**, pp. 69–144; c) T. Iwamoto, S. Ishida, Chem. Lett. **2014**, 43, 164–170; d) F. Breher, Coord. Chem. Rev. **2007**, 251, 1007–1043.



Scheme 2. Mechanistic considerations regarding the formation of chalcogen-expanded Si₇E siliconoids **2a–c**.

- [2] a) A. Jana, V. Huch, M. Repisky, R. J. F. Berger, D. Scheschke-witz, *Angew. Chem. Int. Ed.* **2014**, *53*, 3514–3518; *Angew. Chem.* **2014**, *126*, 3583–3588; b) L. Klemmer, V. Huch, A. Jana, D. Scheschke-witz, *Chem. Commun.* **2019**, *55*, 10100–10103.
- [3] a) T. M. I. Davidson, *J. Organomet. Chem.* **1970**, *24*, 97–100; b) H. Murakami, T. Kanayama, *Appl. Phys. Lett.* **1995**, *67*, 2341–2343; c) M. Watanabe, H. Murakami, T. Miyazaki, T. Kanayama, *Appl. Phys. Lett.* **1997**, *71*, 1207–1209; d) W. M. M. Kessels, M. C. M. Van De Sanden, D. C. Schram, *Appl. Phys. Lett.* **1998**, *72*, 2397–2399; e) G. A. Rechtsteiner, O. Hampe, M. F. Jarrold, *J. Phys. Chem. B* **2001**, *105*, 4188–4194.
- [4] N. E. Poitiers, L. Giarrana, V. Huch, M. Zimmer, D. Scheschke-witz, *Chem. Sci.* **2020**, *11*, 7782–7788.
- [5] H. Neergaard-Waltenburg, J. T. Yates, Jr., *Chem. Rev.* **1995**, *95*, 1589–1673.
- [6] D. Scheschke-witz, *Angew. Chem. Int. Ed.* **2005**, *44*, 2954–2956; *Angew. Chem.* **2005**, *117*, 3014–3016.
- [7] G. Fischer, V. Huch, P. Mayer, S. K. Vasisht, M. Veith, N. Wiberg, *Angew. Chem. Int. Ed.* **2005**, *44*, 7884–7887; *Angew. Chem.* **2005**, *117*, 8096–8099.
- [8] a) A. Tsurusaki, C. Iizuka, K. Otsuka, S. Kyushin, *J. Am. Chem. Soc.* **2013**, *135*, 16340–16343; b) A. Tsurusaki, J. Kamiyama, S. Kysushin, *J. Am. Chem. Soc.* **2014**, *136*, 12896–12898.
- [9] T. Iwamoto, N. Akasaka, S. Ishida, *Nat. Commun.* **2014**, *5*, 5353.
- [10] D. Nied, R. Köppe, W. Klopfer, H. Schnöckel, F. Breher, *J. Am. Chem. Soc.* **2010**, *132*, 10264–10265.
- [11] L. J. Schiegl, A. J. Karttunen, W. Klein, T. F. Fässler, *Chem. Eur. J.* **2018**, *24*, 19171–19174.
- [12] J. Keuter, K. Schwedtmann, A. Hepp, K. Bergander, O. Janka, C. Doerenkamp, H. Eckert, K. Mück-Lichtenfeld, F. Lips, *Angew. Chem. Int. Ed.* **2017**, *56*, 13866–13871; *Angew. Chem.* **2017**, *129*, 14054–14059.
- [13] a) K. Abersfelder, A. J. P. White, H. S. Rzepa, D. Scheschke-witz, *Science* **2010**, *327*, 564–566; b) K. Abersfelder, A. J. P. White, R. J. F. Berger, H. S. Rzepa, D. Scheschke-witz, *Angew. Chem. Int. Ed.* **2011**, *50*, 7936–7939; *Angew. Chem.* **2011**, *123*, 8082–8086; c) P. Willmes, K. Leszczyńska, Y. Heider, K. Abersfelder, M. Zimmer, V. Huch, D. Scheschke-witz, *Angew. Chem. Int. Ed.* **2016**, *55*, 2907–2910; *Angew. Chem.* **2016**, *128*, 2959–2963; d) K. I. Leszczyńska, V. Huch, C. Präsang, J. Schwabedissen, R. J. F. Berger, D. Scheschke-witz, *Angew. Chem. Int. Ed.* **2019**, *58*, 5124–5128; *Angew. Chem.* **2019**, *131*, 5178–5182; e) Y. Heider, P. Willmes, V. Huch, M. Zimmer, D. Scheschke-witz, *J. Am. Chem. Soc.* **2019**, *141*, 19498–19504; f) Y. Heider, N. E. Poitiers, P. Willmes, K. I. Leszczyńska, V. Huch, D. Scheschke-witz, *Chem. Sci.* **2019**, *10*, 4523–4530; g) N. E. Poitiers, L. Giarrana, K. I. Leszczyńska, V. Huch, M. Zimmer, D. Scheschke-witz, *Angew. Chem. Int. Ed.* **2020**, *59*, 8532–8536; *Angew. Chem.* **2020**, *132*, 8610–8614.
- [14] C. Lorenz, F. Hastreiter, K. Hioe, N. Lokesh, S. Gärtner, N. Korber, R. M. Gschwind, *Angew. Chem. Int. Ed.* **2018**, *57*, 12956–12960; *Angew. Chem.* **2018**, *130*, 13138–13142.
- [15] T. Henneberger, W. Klein, T. F. Fässler, *Z. Anorg. Allg. Chem.* **2018**, *644*, 1018–1027.
- [16] F. Hastreiter, C. Lorenz, J. Hioe, S. Gärtner, N. Lokesh, N. Korber, R. M. Gschwind, *Angew. Chem. Int. Ed.* **2019**, *58*, 3133–3137; *Angew. Chem.* **2019**, *131*, 3165–3169.
- [17] K. Abersfelder, A. Russell, H. S. Rzepa, A. J. P. White, R. Haycock, D. Scheschke-witz, *J. Am. Chem. Soc.* **2012**, *134*, 16008–16016.
- [18] a) C. W. Carlson, R. West, *Organometallics* **1983**, *2*, 1798–1801; b) W. Wojnowski, B. Dręzewski, A. Herman, K. Peters, E.-M. Peters, H. G. von Schnering, *Angew. Chem. Int. Ed. Engl.* **1985**, *24*, 992–993; *Angew. Chem.* **1985**, *97*, 978–979; c) M. Unno, N. Yamashita, H. Matsumoto, *Phosphorus Sulfur Silicon Relat. Elem.* **2011**, *186*, 1259–1262; d) L. C. Siemes, J. Keuter, A. Hepp, F. Lips, *Inorg. Chem.* **2019**, *58*, 13142–13149; e) K. Schwedtmann, A. Hepp, K. Schwedtmann, J. J. Weigand, F. Lips, *Eur. J. Inorg. Chem.* **2019**, 4719–4726.
- [19] a) J. E. Carey, C. H. Crouch, M. Shen, E. Mazur, *Opt. Lett.* **2005**, *30*, 1773–1775; b) Z. Huang, J. E. Carey, M. Liu, Y. Guo, E. Mazur, J. C. Campbell, *Appl. Phys. Lett.* **2006**, *89*, 033506; c) A. J. Said, D. Recht, J. T. Sullivan, J. M. Warrender, T. Buonassisi, P. D. Persans, M. J. Aziz, *Appl. Phys. Lett.* **2011**, *99*, 073503; d) K. Eom, J. Lee, M. Oschatz, F. Wu, S. Kaskel, G. Yushin, T. F. Fuller, *Nat. Commun.* **2017**, *8*, 13888.
- [20] Y. Wang, M. Chen, Y. Xie, P. Wie, H. F. Schaefer, P. von R. Schleyer, G. H. Robinson, *Nat. Chem.* **2015**, *7*, 509–513.
- [21] a) A. C. Filippou, B. Baars, O. Chernov, Y. N. Lebedev, G. Schnakenburg, *Angew. Chem. Int. Ed.* **2014**, *53*, 565–570; *Angew. Chem.* **2014**, *126*, 576–581; b) S. S. Sen, *Angew. Chem. Int. Ed.* **2014**, *53*, 8820–8822; *Angew. Chem.* **2014**, *126*, 8964–8966; c) S. U. Ahmad, T. Szilvási, E. Irran, S. Inoue, *J. Am. Chem. Soc.* **2015**, *137*, 5828–5836.
- [22] a) A. C. Papageorgopoulos, M. Kamaratos, *Surf. Sci.* **2000**, *466*, 173–182; b) M. Y. Ali, M. Tao, *J. Appl. Phys.* **2007**, *101*, 103708.
- [23] a) H. Suzuki, N. Tokitoh, S. Nagase, R. Okazaki, *J. Am. Chem. Soc.* **1994**, *116*, 11578–11579; b) T. Iwamoto, K. Sato, S. Ishida, C. Kabuto, M. Kira, *J. Am. Chem. Soc.* **2006**, *128*, 16914–16920; c) S. Yao, Y. Xiong, M. Driess, *Chem. Eur. J.* **2010**, *16*, 1281–1288; d) S.-H. Zhang, H.-Xian, C.-W. So, *Chem. Eur. J.* **2011**, *17*, 3490–3499; e) Y. Xiong, S. Yao, M. Driess, *Angew. Chem. Int. Ed.* **2013**, *52*, 4302–4311; *Angew. Chem.* **2013**, *125*, 4398–4407; f) R. Tacke, C. Kobelt, J. A. Baus, R. Bertemann, C. Burschka, *Dalton Trans.* **2015**, *44*, 14959–14974; g) N. Parvin, S. Pal, S. Khan, S. Das, S. K. Pati, H. W. Roesky, *Inorg. Chem.* **2017**, *56*, 1706–1712; h) M. K. Bisai, V. S. V. S. N. Swamy, T. Das, K. Vanka, R. G. Gonnade, S. S. Sen, *Inorg. Chem.* **2019**, *58*, 10536–10542; i) D. Sarkar, V. Nesterov, T. Szilvási, J. Altmann, S. Inoue, *Chem. Eur. J.* **2019**, *25*, 1198–1202; j) R. Kobayashi, S. Ishida, T. Iwamoto, *Angew. Chem. Int. Ed.* **2019**, *58*, 9425–9428; *Angew. Chem.* **2019**, *131*, 9525–9528; k) M.-P. Luecke, E. Pens, S. Yao, M. Driess, *Chem. Eur. J.* **2020**, *26*, 4500–4504.
- [24] Heavier analogues: a) N. Tokitoh, T. Matsumoto, R. Okazaki, *Tetrahedron Lett.* **1992**, *33*, 2531–2534; b) N. Tokitoh, T. Matsumoto, K. Manmaru, R. Okazaki, *J. Am. Chem. Soc.* **1993**, *115*, 8855–8856; c) T. Matsumoto, N. Tokitoh, R. Okazaki, *Angew. Chem. Int. Ed. Engl.* **1994**, *33*, 2316–2317; *Angew. Chem.* **1994**, *106*, 2418–2420; d) M. Saito, N. Tokitoh, R. Okazaki, *J. Am. Chem. Soc.* **1997**, *119*, 11124–11125; e) N. Tokitoh, *Phosphorus Sulfur Silicon Relat. Elem.* **1998**, *136*, 123–138; f) R. Okazaki, N. Tokitoh, *Acc. Chem. Res.* **2000**, *33*, 625–630; g) W.-P. Leung, W.-H. Kwok, Z.-Y. Zhou, T. C. Mak, *Organometallics* **2000**, *19*, 296–303.
- [25] H. Zhao, L. Klemmer, M. J. Cowley, V. Huch, M. Zimmer, D. Scheschke-witz, *Z. Anorg. Allg. Chem.* **2018**, *644*, 999–1005.
- [26] a) C.-W. So, H. W. Roesky, J. Magull, R. B. Oswald, *Angew. Chem. Int. Ed.* **2006**, *45*, 3948–3950; *Angew. Chem.* **2006**, *118*, 4052–4054; b) R. S. Ghadwal, S. S. Sen, H. W. Roesky, M. Granitzka, D. Kratzert, S. Merkel, D. Stalke, *Angew. Chem. Int. Ed.* **2010**, *49*, 3952–3955; *Angew. Chem.* **2010**, *122*, 4044–4047; c) R. S. Ghadwal, K. Pröpper, B. Dittrich, P. G. Hones, H. W. Roesky, *Inorg. Chem.* **2011**, *50*, 358–364; d) K. Junold, M. Nutz, J. A. Baus, C. Burschka, C. Fonseca Guerra, F. M. Bickelhaupt, R. Tacke, *Chem. Eur. J.* **2014**, *20*, 9319–9329; e) F. M. Mück, J. A. Baus, M. Nutz, C. Burschka, J. Poater, F. M. Bickelhaupt, R. Tacke, *Chem. Eur. J.* **2015**, *21*, 16665–16672.
- [27] J. Brus, *Solid State Nucl. Magn. Reson.* **2000**, *16*, 151–160.
- [28] a) L. Du, Z. Wu, F. Tang, R. Li, Y. Jiang, *Proc. SPIE* **2016**, *9686*, 96860Y; b) S. Hu, P. Han, Y. Mi, Y. Xing, P. Liang, Y. Fan, *Mater. Sci. Semicond. Process.* **2013**, *16*, 987–991.
- [29] G. S. Hammond, *J. Am. Chem. Soc.* **1955**, *77*, 334–338.

Manuscript received: July 5, 2020

Accepted manuscript online: July 23, 2020

Version of record online: ■■■ 0000

3.5 Nickel-Assisted Complete Cleavage of CO by a Silylene/Siliconoid Hybrid under Formation of an Si=C Enol Ether bridge

Nadine E. Poitiers, Volker Huch, Michael Zimmer, David Scheschkewitz, Chem. Commun. **2020**, **56**, 10898-10901.

<https://doi.org/10.1039/D0CC04922K>

The Communication has been published by the Royal Society of Chemistry (RSC). The Communication is reproduced by permission of The Royal Society of Chemistry and all authors and the results are additionally concluded and put into context in Chapter 4.

Contributions of the Authors:

Nadine Poitiers: Equal (D.S.): Conceptualization; Lead: Data curation, Formal analysis, Investigation, Methodology, Validation, Visualization, Writing Review and Editing.

Volker Huch: Lead: X-ray analysis.

Michael Zimmer: Lead: CP/MAS NMR and VT-NMR.

David Scheschkewitz: Lead: Conceptualization, Project administration, Supervision Funding acquisition and resources; Supporting: Methodology, Writing — review and editing.



Cite this: *Chem. Commun.*, 2020, 56, 10898

Received 17th July 2020,
Accepted 11th August 2020

DOI: 10.1039/d0cc04922k

rsc.li/chemcomm

Nickel-assisted complete cleavage of CO by a silylene/siliconoid hybrid under formation of an Si=C enol ether bridge†

Nadine E. Poitiers, , Volker Huch, Michael Zimmer and David Scheschkewitz *

Reaction of a silylene-functionalized Si₆ siliconoid with CO in the presence of catalytic quantities of a nickel(0) complex results in the complete cleavage of the CO triple bond, but preserves the Si₆ scaffold with an exohedrally incorporated Si=C enol ether bridge. The uncompromised cluster core emphasizes the role of the so-called benzpolarene motif as the energetic silicon pendants of benzene in carbon chemistry.

Low-valent silicon compounds are increasingly coming into focus not only due to their apparent role as intermediates in industrially important gas phase processes,¹ but also for their potential in the activation of small molecules such as carbon monoxide (CO)² and even in catalytic applications.³ With partially unsubstituted neutral silicon clusters (siliconoids),⁴ the class of stable unsaturated silicon compounds has recently been extended beyond the electron-precise silylenes⁵ and disilylenes^{5a,6}. After the report of the first stable siliconoid by one of us,⁷ numerous further examples followed by the groups of Wiberg,⁸ Breher,⁹ Kyushin,¹⁰ Iwamoto,¹¹ Fässler,¹² Lips¹³ and our group.¹⁴ With the introduction of the term “benzpolarene” for the Si₆ siliconoid that constitutes the global minimum of the Si₆H₆ potential energy surface,^{14b} we emphasized its isomeric relationship to the still unknown hexasilabenzene. The four distinct positions of the Si₆ benzpolarene scaffold are unambiguously identified with the prefixes *privo*, *nudo*, *ligato*, *remoto*,^{14f} in analogy to the established prefixes *ortho*, *meta*, *para* for benzenes. With the now available anionic Si₅,^{14h} Si₆^{14d,e,f} and Si₇ derivatives^{14e} the straightforward functionalization with suitable electrophiles is possible.^{14d,f,h} As the unusual persistence of the benzpolarene scaffold even in the presence of relatively reactive side chain functionalities becomes more and more apparent,^{14d,f} the involvement of this unique motif in catalytic

cycles is a realistic option. We recently isolated the first transition-metal substituted siliconoids¹⁴ⁱ as well as cluster-expanded derivatives with incorporated platinum group metals.¹⁵ In the latter case, a silylene/siliconoid hybrid species proved effective in facilitating complex formation allowing for the first applications of siliconoids as electron-rich ligands in homogeneous catalysis to emerge.¹⁵

The activation of carbon monoxide (CO) as a C₁ building block is of fundamental and economic interest. A prominent example of the value-added conversion of CO is the Fischer-Tropsch process,¹⁶ which usually employs heterogeneous transition-metal catalysts at elevated temperatures.¹⁷ Considerable efforts have thus been devoted to the cleavage of the extremely strong C≡O bond (1077.1 kJ mol⁻¹)¹⁸ under milder and homogeneous conditions.¹⁹ The interaction of CO with low-valent main group species has received significant attention in this context,^{2,20} culminating in the complete reductive cleavage of CO and the coupling of two CO fragments.^{2a,b,d}

Given that silylenes are particularly useful in the activation of small molecules,^{2b-d} we were curious whether the silylene/siliconoid hybrid **1** would prove reactive towards CO. We now report on the reaction of **1** with CO in the presence of catalytic quantities of Ni(cod)₂ (cod = 1,5-cyclooctadiene) and the full cleavage of the CO bond under the formation of a Si=C double bond in the periphery of the uncompromised benzpolarene scaffold (Scheme 1).

While treatment of silylene-substituted siliconoid **1** with 1 eq. of Ni(cod)₂ led to no reaction, upon exposure of the mixture to 1 atm of CO in order to generate more reactive Ni(CO)₄ *in situ*²¹ the colour of the reaction mixture gradually changed to intensely green. According to ¹H NMR monitoring, uniform conversion to a single product was achieved after 1 h (Scheme 1). The product was fully characterized by X-ray diffraction on single crystals, elemental analysis, as well as multinuclear NMR spectroscopy. The diagnostically wide dispersion of ²⁹Si signals suggested the presence of an uncompromised benzpolarene scaffold. The signal of the *privo*-silicon atom appears at the usual low field at 160.9 ppm, while the two unsubstituted *nudo*-vertices give rise to

Krupp Chair of General and Inorganic Chemistry, Saarland University, Campus C4.1, 66123 Saarbrücken, Germany. E-mail: scheschkewitz@mx.uni-saarland.de

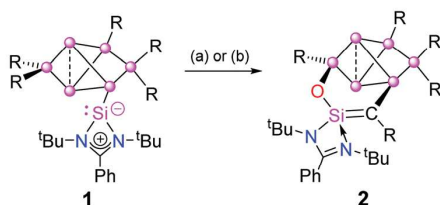
† Electronic supplementary information (ESI) available. CCDC 2016837. For ESI and crystallographic data in CIF or other electronic format see DOI: 10.1039/d0cc04922k

3.5 Nickel-Assisted Complete Cleavage of CO by a Silylene/Siliconoid Hybrid under Formation of an Si=C Enol Ether bridge

Communication

View Article Online

ChemComm



Scheme 1 Synthesis of the *privo-ligato* silaenol ether-bridged hexasilabenzpolarene **2**. (a) 1 eq. Ni(cod)₂, CO atmosphere, 25 °C; (b) 10 mol% Ni(cod)₂, CO atmosphere, 2 days at 45 °C (cod = 1,5-cyclooctadiene, \bullet = Si, R = Tip = 2,3,6-triisopropylphenyl).

two individual signals at characteristically high field (−268.2 and −300.5 ppm). This apparent symmetry reduction of the idealized *C_s* symmetric product is typical for *ligato*-substituted hexasilabenzpolarenes and has been attributed to hindered rotation of the pending functionality.^{14d,f} As the signal of the former silylene silicon atom was observed at the unusual high field of −33.6 ppm according to a 2D ²⁹Si/¹H correlation NMR spectrum (cross-peaks to *t*-butyl groups), we initially assumed that coordination to the nickel centre had occurred. The remaining ²⁹Si NMR chemical shifts are located within the usual range of saturated silicon atoms.

Green single crystals were obtained by crystallization from hexane in 66% yield and the constitution of the product revealed by X-ray diffraction in the solid state (Fig. 1). While the presence of an intact benzpolarene scaffold and the incorporation of one equivalent of CO are indeed confirmed, the product **2** surprisingly does not contain nickel. The CO bond is completely cleaved under migration of one of the Tip substituents from the *privo*-vertex to the CO carbon atom, which in turn is bonded to the *ligato*-vertex. The CO oxygen atom assumes the liberated position at the *privo*-vertex. The former silylene moiety is now situated between the carbon and the oxygen centre overall resulting in the formation of a silaenol ether bridge between the *privo*- and the *ligato*-positions of the hexasilabenzpolarene scaffold.

The distance between the *nudo*-vertices of **2** (Si1–Si3 2.6979(7) Å) is approximately the same as in the perarylated global minimum isomer Si₆Tip₆ (2.7076 Å)^{14b} and with that slightly longer compared to other *ligato*-functionalized benzpolarenes.^{14d,f} The newly formed Si–C bond (Si7–C1 1.759(2) Å) is of a length within the usual range for silicon–carbon double bonds despite the fact that the silicon atom is tetracoordinate and could thus be equally well described by an ylidic formulation. This observation is in line with previously reported doubly bonded silicon centres with amidinato ligands, e.g. the sila-analogue of carboxylic acid anhydrides reported by Driess *et al.*²² or Tacke's donor-stabilized Si=Se and Si=Te species.²³ In comparison, the bond between the *ligato*-vertex and the former CO carbon atom (Si4–C1 1.8386(1) Å) is significantly longer confirming its single bond nature. The Si–N bonds of the former silylene silicon centre differ significantly (Si7–N2 1.827(1) Å, Si7–N1 1.867(1) Å) suggesting a partial double bond character for Si7–N2 and thus a somewhat disturbed delocalization of the N1–Si7–N2 π system as frequently observed for amidinato stabilized silylene fragments.²⁴ In the CP-MAS ²⁹Si NMR, very

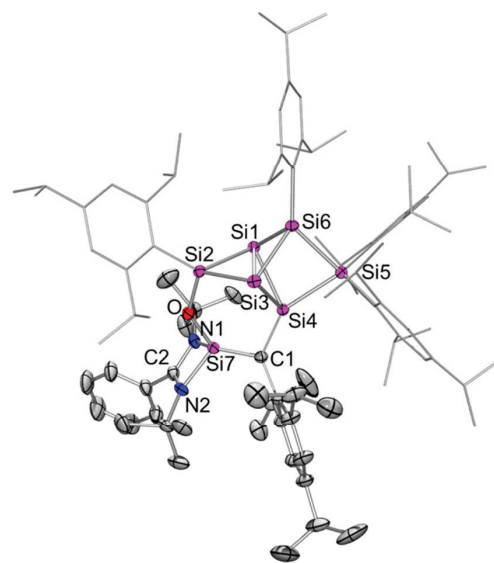


Fig. 1 Molecular structure of siliconoid **2** in the solid state. Hydrogen atoms omitted for clarity. Thermal ellipsoids at 50%. Selected bond length [Å] and angles [°]: Si6–Si3 2.3021(6), Si6–Si1 2.3260(6), Si6–Si5 2.3930(6), Si3–Si2 2.3333(6), Si3–Si4 2.3571(6), Si3–Si1 2.6967(6), Si1–Si2 2.3391(6), Si1–Si4 2.3475(5), Si7–O1 1.642(1), Si7–C1 1.756(2), Si7–N2 1.827(1), Si7–N1 1.867(1), Si5–Si4 2.3907(6), Si4–C1 1.8386(1), Si2–Si3–Si4 85.15(2), Si4–Si3–Si1 54.86(2), Si6–Si1–Si2 101.17(2), Si4–Si3–Si1 55.19(2), Si3–Si2–Si1 70.50(2), Si7–O1–Si2 134.83(7), Si7–C1–Si4 111.49(8), N2–Si7–N1 71.06(6), O1–Si7–N1 108.28(6).

similar chemical shifts are observed, which confirms that the solid state structure of siliconoid **2** is fully retained in solution. The longest wavelength UV/Vis absorption band of **2** is observed at $\lambda_{\text{max}} = 638$ nm ($\epsilon = 940$ M^{−1} cm^{−1}) and thus significantly red-shifted compared to previously reported *ligato*-functionalized Si₆ siliconoids (364 to 521 nm).^{14d,f,i} The experimental UV/Vis absorption bands are in satisfactory agreement with the TD-DFT calculations at the CAM-B3LYP-D3(BJ)/def2-SVP level of theory (see ESI†) for **2**. The longest wavelength absorption band is calculated at $\lambda_{\text{calc}} = 705$ nm with 91% contributions of HOMO → LUMO.

Just as in case of the recently reported reaction of **1** with Group 9 complexes¹⁵ the reaction mechanism is presumably rather complicated. As CO does not react with **1** in the absence of Ni(cod)₂, the involvement of the transition metal in a catalytic cycle leading to the formation of **2** is virtually guaranteed. On this basis, we can propose a reasonable course of reaction in line with the experimental findings as well as the well-established electrophilicity of the *privo*-vertex of hexasilabenzpolarenes.^{14f,25}

In order to support our mechanistic considerations, we optimized the *ligato*-silylene functionalized siliconoid **1**, the proposed intermediates [Int-a], [Int-b], [Int-c] and the final product **2** at the BP86-D3(BJ)/def2-SVP level of theory (see ESI†). Since the reaction of the silylene-functionalized Si₆ siliconoid **1** requires 10 mol% of Ni(cod)₂ during the exposition to carbon monoxide, we suggest the formation of a silylene–Ni(CO)₃ complex [Int-a] from *in situ* prepared Ni(CO)₄ as initial step (a).²¹ Indeed, the reaction of **1** with stoichiometric amounts of

3.5 Nickel-Assisted Complete Cleavage of CO by a Silylene/Siliconoid Hybrid under Formation of an Si=C Enol Ether bridge

View Article Online

Communication

ChemComm

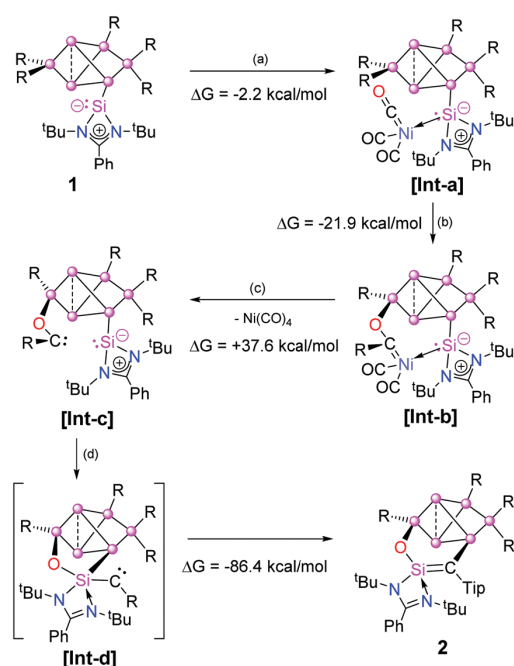


Chart 1 Proposed mechanism for the formation of the Si=C enol ether bridged hexasilabenzpolarene **2**.

freshly generated $\text{Ni}(\text{CO})_4$ also results in clean conversion to **2**. In step (b), the nucleophilic attack of the oxygen to the *privo*-silicon vertex likely occurs with the concomitant transfer of a Tip substituent²⁶ to the carbon atom of CO leading to **[Int-b]**. According to the optimized structures the rearrangement from **[Int-a]** to **[Int-b]** is exergonic by $\Delta G = -21.9 \text{ kcal mol}^{-1}$. Although the elimination of Ni likely occurs in metallic form (based on the observation of a grey solid in the reaction mixture, removable by amalgamation with Hg), we arbitrarily assume the elimination of $\text{Ni}(\text{CO})_4$ in step (c) for the sake of obtaining comparable energy values. The formal elimination of $\text{Ni}(\text{CO})_4$ in step (c) is thus endergonic by $\Delta G = +37.6 \text{ kcal mol}^{-1}$, a value likely to be reduced in reality due to formation of metallic nickel (Chart 1).

The insertion of the N-heterocyclic silylene centre into the C–O bond would result in the formation of **[Int-d]** with a five-membered bridge between the *ligato*- and *privo*-vertices thus satisfying the oxophilicity of the silicon atom of the silylene moiety at the penalty of the generation of an *a priori* highly reactive (aryl)(silyl)carbene functionality. As a consequence, the barrier, if any, to the formation of the final product is expected to be small. Indeed, all attempts to optimize the plausible intermediate **[Int-d]** resulted in the relaxation to the experimentally isolated product **2** by insertion of the carbene moiety into the Si–Si single bond between the *ligato*-vertex and the former silylene centre. The elimination of metallic nickel, while exceedingly difficult to model computationally, is probably the rate-determining step: compared to **[Int-c]**, the final product **2** is by $\Delta G = -86.4 \text{ kcal mol}^{-1}$ lower in free enthalpy. In conclusion, with the formation of a Si=C enol ether bridge

in the periphery of the uncompromised benzpolarene scaffold, we reported the nickel-assisted full cleavage of the triple bond of carbon monoxide by a neutral siliconoid. The persistence of the hexasilabenzpolarene scaffold during substantial reorganization in its periphery is testimony for the privileged role of this structural motif, which can thus be anticipated to be of particularly use as functional ligand in homogenous catalytic processes.

Funding by the Deutsche Forschungsgemeinschaft (DFG SCHE 906/4-1 and 4-2) is gratefully acknowledged. The authors thank Dr Diego Andradá for access to his computational clusters.

Conflicts of interest

There are no conflicts to declare.

Notes and references

- (a) T. M. I. Davidson, *J. Organomet. Chem.*, 1970, **24**, 97–100; (b) H. Murakami and T. Kanayama, *Appl. Phys. Lett.*, 1995, **67**, 2341–2343; (c) W. Watanabe, H. Murakami, T. Miyazaki and T. Kanayama, *Appl. Phys. Lett.*, 1997, **71**, 1207–1209; (d) W. M. M. Kessels, M. C. M. Van De Sanden and D. V. Schram, *Appl. Phys. Lett.*, 1998, **72**, 2397–2399; (e) G. A. Rechtsteiner, O. Hampe and M. F. Jarrold, *J. Phys. Chem. B*, 2001, **105**, 4188–4194.
- (a) M. Majumdar, I. Omlor, C. B. Yildiz, A. Azizoglu, V. Huch and D. Scheschkewitz, *Angew. Chem., Int. Ed.*, 2015, **54**, 8746–8750; (b) Y. Wang, A. Kostenko, T. J. Hadlington, M.-P. Luecke, S. Yao and M. Driess, *J. Am. Chem. Soc.*, 2019, **141**, 626–634; (c) A. V. Prochenko, P. Vasko, D. C. Huan Do, J. Hicks, M. Angeles Fuentes, C. Jones and S. Aldridge, *Angew. Chem., Int. Ed.*, 2019, **58**, 1808–1812; (d) Y. Wang, A. Kostenko, T. J. Hadlington, M.-P. Luecke, S. Yao and M. Driess, *J. Am. Chem. Soc.*, 2019, **141**, 626–634; (e) A. V. Prochenko, P. Vasko, D. C. H. Do, J. Hicks, M. A. Fuentes, C. Jones and S. Aldridge, *Angew. Chem., Int. Ed.*, 2019, **58**, 1808–1812.
- (a) E. Fritz-Langhals, P. Jutzi and R. Weidner, *WACKER Chemie A.G.*, EP3440088A1, 2017; (b) B.-X. Leong, J. Lee, M.-C. Yang, C.-K. Siu, M.-D. Su and C.-W. So, *J. Am. Chem. Soc.*, 2019, **141**(44), 17629–17636; (c) E. Fritz-Langhals, *Org. Process Res. Dev.*, 2019, **23**, 2369; (d) Y. Xiong, S. Yao, T. Szilvási, A. Ruzicka and M. Driess, *Chem. Commun.*, 2020, **56**, 747–750.
- A. K. Abersfelder, A. Russell, H. S. Rzepa, A. J. P. White, R. Haycock and D. Scheschkewitz, *J. Am. Chem. Soc.*, 2012, **134**, 16008–16016.
- Recent reviews: (a) E. Rivard, *Chem. Soc. Rev.*, 2016, **45**, 989–1003; (b) B. Blom and M. Driess in *Functional Molecular Silicon Compounds II*, ed. D. Scheschkewitz, Struct. Bonding, 2013, vol. 156, pp. 85–123; (c) S. Mandal and H. W. Roesky, *Acc. Chem. Res.*, 2012, **45**, 298–307; (d) M. Asay, C. Jones and M. Driess, *Chem. Rev.*, 2011, **111**, 354–396; (e) Y. Mizuhata, T. Sasamori and N. Tokito, *Chem. Rev.*, 2009, **109**, 3479–3511.
- Recent reviews: (a) A. Rammo and D. Scheschkewitz, *Chem. – Eur. J.*, 2018, **24**, 6866–6885; (b) T. Matsuo and N. Hayakawa, *Sci. Technol. Adv. Mater.*, 2018, **19**, 108–129; (c) C. Präsang and D. Scheschkewitz, *Chem. Soc. Rev.*, 2016, **45**, 900–921; (d) T. Iwamoto and S. Ishida, in *Functional Molecular Silicon Compounds II*, ed. D. Scheschkewitz, Struct. Bonding, 2013, vol. 156, pp. 125–202.
- D. Scheschkewitz, *Angew. Chem., Int. Ed.*, 2005, **44**, 2954–2956.
- G. Fischer, V. Huch, P. Mayer, S. K. Vasisht, M. Veith and N. Wiberg, *Angew. Chem., Int. Ed.*, 2005, **44**, 7884–7887.
- D. Nied, R. Köppe, W. Kloppe, H. Schnöckel and F. Breher, *J. Am. Chem. Soc.*, 2010, **132**(30), 10264–10265.
- (a) A. Tsurusaki, C. Iizuka, K. Otsuka and S. Kyushin, *J. Am. Chem. Soc.*, 2013, **135**, 16340–16343; (b) A. Tsurusaki, K. Kamiyama and S. Kyushin, *J. Am. Chem. Soc.*, 2014, **136**, 12896–12898.
- T. Iwamoto, N. Akasaka and S. Ishida, *Nat. Commun.*, 2014, **5**, 5353.
- L. J. Schiegl, A. J. Karttunen, W. Klein and T. F. Fässler, *Chem. – Eur. J.*, 2018, **24**, 19171–19174.
- J. Keuter, K. Schwedtmann, A. Hepp, K. Bergander, O. Janka, C. Doerenkamp, H. Eckert, C. Mück-Lichtenfeld and F. Lips, *Angew. Chem., Int. Ed.*, 2017, **56**, 13866–13871.

3.5 Nickel-Assisted Complete Cleavage of CO by a Silylene/Siliconoid Hybrid under Formation of an Si=C Enol Ether bridge

View Article Online

Communication

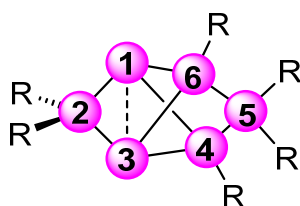
ChemComm

- 14 (a) K. Abersfelder, A. J. P. White, H. S. Rzepa and D. Scheschkewitz, *Science*, 2010, **327**, 564–566; (b) K. Abersfelder, A. J. P. White, R. J. F. Berger, H. S. Rzepa and D. Scheschkewitz, *Angew. Chem., Int. Ed.*, 2011, **50**, 7936–7939; (c) A. Jana, V. Huch, M. Repisky, R. J. F. Berger and D. Scheschkewitz, *Angew. Chem., Int. Ed.*, 2014, **53**, 3514–3518; (d) P. Willmes, K. Leszczyńska, Y. Heider, K. Abersfelder, M. Zimmer, V. Huch and D. Scheschkewitz, *Angew. Chem., Int. Ed.*, 2016, **55**, 2907–2910; (e) K. I. Leszczyńska, V. Huch, C. Präsang, J. Schwabedissen, R. J. F. Berger and D. Scheschkewitz, *Angew. Chem., Int. Ed.*, 2019, **58**, 5124–5128; (f) Y. Heider, N. E. Poitiers, P. Willmes, K. I. Leszczyńska, V. Huch and D. Scheschkewitz, *Chem. Sci.*, 2019, **10**, 4523–4530; (g) L. Klemmer, V. Huch, A. Jana and D. Scheschkewitz, *Chem. Commun.*, 2019, **55**, 10100–10103; (h) Y. Heider, P. Willmes, V. Huch, M. Zimmer and D. Scheschkewitz, *J. Am. Chem. Soc.*, 2019, **141**(49), 19498–19504; (i) N. E. Poitiers, L. Giarrana, K. I. Leszczyńska, V. Huch, M. Zimmer and D. Scheschkewitz, *Angew. Chem., Int. Ed.*, 2020, **59**, 8532–8536; (j) N. E. Poitiers, V. Huch, M. Zimmer and D. Scheschkewitz, *Chem. – Eur. J.*, 2020, DOI: 10.1002/chem.202003180.
- 15 N. E. Poitiers, L. Giarrana, V. Huch, M. Zimmer and D. Scheschkewitz, *Chem. Sci.*, 2020, **11**, 7782–7788.
- 16 (a) *Advances in Fischer – Tropsch Synthesis Catalysts and Catalysis* ed. B. H. Davis and M. L. Occelli, CRC, Boca Raton, FL, 2009; (b) A. Y. Khodakov, W. Chu and P. Fongarland, *Chem. Rev.*, 2007, **107**, 1692–1744; (c) C. K. Rofer-DePoorter, *Chem. Rev.*, 1981, **81**, 447–474; (d) C. Masters, *Adv. Organomet. Chem.*, 1979, **17**, 61–103.
- 17 (a) A. A. Adesina, *Appl. Catal., A*, 1996, **138**, 345–367; (b) H. Schulz, *Appl. Catal., A*, 1999, **186**, 3–12; (c) P. M. Maitlis, *J. Organomet. Chem.*, 2004, **689**, 4366–4374; (d) P. M. Maitlis and V. Zanolli, *Chem. Commun.*, 2009, 1619–1634.
- 18 A. F. Hollemann, E. Wiberg and N. Wiberg, *Lehrbuch der Anorganischen Chemie*, de Gruyter, Berlin, 102nd edn, 2007.
- 19 (a) G. Christian, R. Stranger, S. Petrie, B. F. Yates and C. C. Cummins, *Chem. – Eur. J.*, 2007, **13**, 4264–4272; (b) R. Whyman, A. P. Wright, J. A. Iggo and B. T. Heaton, *J. Chem. Soc., Dalton Trans.*, 2002, 771–777; (c) N. M. West, A. J. M. Miller, J. A. Labinger and J. E. Bercaw, *Coord. Chem. Rev.*, 2011, **255**, 881–898.
- 20 (a) M. A. Pearsall and R. West, *J. Am. Chem. Soc.*, 1988, **110**, 7228–7229; (b) M. Tacke, Ch. Klein, D. J. Stufkens, A. Oskam, A. Bunte and P. Jutzi, *Z. Anorg. Allg. Chem.*, 1993, **619**, 865–868; (c) H. Bornemann and W. Sander, *J. Organomet. Chem.*, 2002, **641**, 156–164; (d) X. Wang, Z. Zhu, Y. Peng, H. Lei, J. C. Fetting and P. P. Power, *J. Am. Chem. Soc.*, 2009, **131**, 6912–6913; (e) A. Fukazawa, J. L. Dutton, C. Fan, L. G. Mercier, A. Y. Houghton, Q. Wu, W. E. Piers and M. Parvez, *Chem. Sci.*, 2012, **3**, 1814–1818; (f) M. J. Cowley, Y. Ohmori, V. Huch, M. Ichinohe, A. Sekiguchi and D. Scheschkewitz, *Angew. Chem., Int. Ed.*, 2013, **52**, 13247–13250; (g) M. Sajid, L. M. Elmer, C. Rosorius, C. G. Daniliuc, S. Grimme, G. Kehr and G. Erker, *Angew. Chem., Int. Ed.*, 2013, **52**, 2243–2246; (h) R. Dobrovetsky and D. W. Stephan, *J. Am. Chem. Soc.*, 2013, **135**, 4974–4977; (i) J. Böhnke, H. Braunschweig, T. Dellermann, W. C. Ewing, K. Hammond, J. O. C. Jimenez-Halla, T. Kramer and J. Mies, *Angew. Chem., Int. Ed.*, 2015, **54**, 13801–13805; (j) H. Braunschweig, R. D. Dewhurst, F. Hupp, M. Nutz, K. Radacki, C. W. Tate, A. Vargas and Q. Ye, *Nature*, 2015, **522**, 237–330; (k) M. M. Hansmann, R. Jassar and G. Bertrand, *J. Am. Chem. Soc.*, 2016, **138**, 8356–8359; (l) W. Lu, H. Hu, Y. Li, R. Ganguly and R. Kinjo, *J. Am. Chem. Soc.*, 2016, **138**, 6650–6661; (m) M. Arrowsmith, J. Böhnke, M. A. Elik and H. Braunschweig, *Angew. Chem., Int. Ed.*, 2017, **56**, 14287–14292; (n) M. Devillard, B. de Bruin, M. A. Siegler and I. J. I. van der Vlugt, *Chem. – Eur. J.*, 2017, **23**, 13628–13632; (o) C. Ganesamoorthy, J. Schoening, C. Wölper, L. Song, P. R. Schreiner and S. Schulz, *Nat. Chem.*, 2020, **12**, 608–614.
- 21 M. Marín, J. J. Moreno, C. Navarro-Gilabert, E. Álvarez, C. Maya, R. Peloso, M. C. Nicasio and E. Carmona, *Chem. – Eur. J.*, 2019, **25**, 260–272.
- 22 Y. Xiong, S. Yao and M. Driess, *Angew. Chem., Int. Ed.*, 2013, **52**, 4302–4311.
- 23 C. Kobelt, J. A. Baus, R. Bertermann, C. Burschka and R. Tacke, *Dalton Trans.*, 2015, **44**, 14959–14974.
- 24 R. Azhakar, R. S. Ghadwal, H. W. Roesky, H. Wolf and D. Stalke, *Organometallics*, 2012, **31**(12), 4588–4592.
- 25 L. Klemmer, V. Huch, A. Jana and D. Scheschkewitz, *Chem. Commun.*, 2019, **55**, 10100–10103.
- 26 (a) D. Scheschkewitz, *Angew. Chem., Int. Ed.*, 2004, **43**, 2965–2967; (b) C. Strohmann, D. Schilbach and D. Auer, *J. Am. Chem. Soc.*, 2005, **127**, 7968–7971.

4 Summary, Conclusion and Outlook

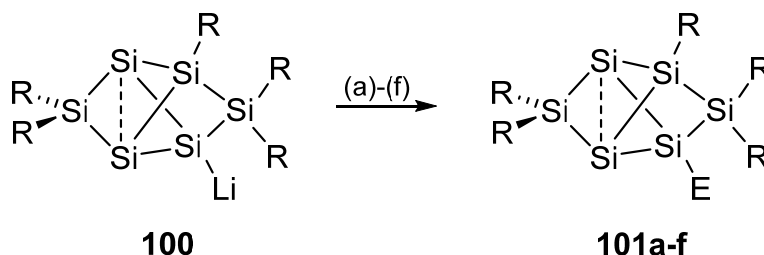
During the last decade, the study of unsaturated silicon clusters as well their functionalization with different functional groups has moved into focus. Especially functionalization of the cluster scaffold is of continuous interest with a view to the incorporation of such low-valent systems into extended systems.

The rapidly increasing number of functionalized Si₆ benzpolarenes required the distinction of the different vertices. Inspired by the *ortho*, *meta* and *para* nomenclature for disubstituted benzene, short prefixes for the characteristic bonding situation of each silicon vertex of the Si₆ benzpolarene scaffold have been introduced (Scheme 52). The corresponding latin words served as inspirations for the creation of the prefixes “*nudo*” (lat. nudus) for the unsubstituted silicon atoms 1 and 3, “*ligato*” (lat. ligatus) for the mono Tip-substituted vertices 4 and 6, “*remoto*” (lat. remotus) for the remote bridge in 5-position and “*privo*” (lat. privus) for the characteristically deshielded silicon atom in position 2.



Scheme 52. Schematic representation of the proposed prefixes for Si₆ benzpolarenes.

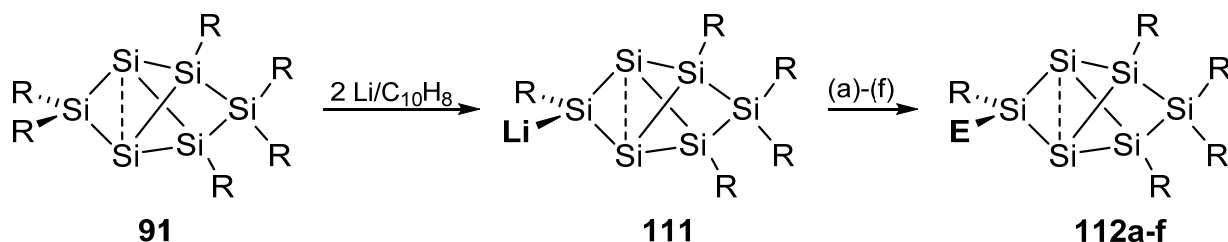
Reaction of the anionic Si₆ siliconoid **100** with electrophiles provides access to several new Si₆ siliconoids **101a-f**. In the first part of this thesis, the nucleophilic transfer of the *ligato*-anionic moiety to benzoylchloride (e) and trimethylchlorosilane (f) has been demonstrated (Scheme 53). The structures have been determined by x-ray crystallography and show the uncompromised Si₆ benzpolarene framework.



Scheme 53. Synthesis of benzoyl- and trimethylsilyl-substituted siliconoids **101e,f** and recently functionalized siliconoids **101a-d**.⁵³ Reagents: (a) SiCl₄, (b) BH₃·SMe₂, (c) ^tBuCOCl, (d) ClP(NMe₂)₂, (e) Me₃SiCl, (f) PhCOCl. **101a**: E = SiCl₃, **101b**: E = BH₃⁻, **101c**: E = ^tBuCO, **101d**: E = P(NMe₂)₂, **101e**: E = Me₃Si, **101f**: E = CPh.

As expected, the distance between the bridgehead silicon atoms are longer than a typical Si–Si single bond but comparable with those reported for functionalized *ligato*-siliconoids.⁵³ The characteristic wide distribution of NMR chemical shifts is retained in the ^{29}Si NMR spectra of **101e,f**.

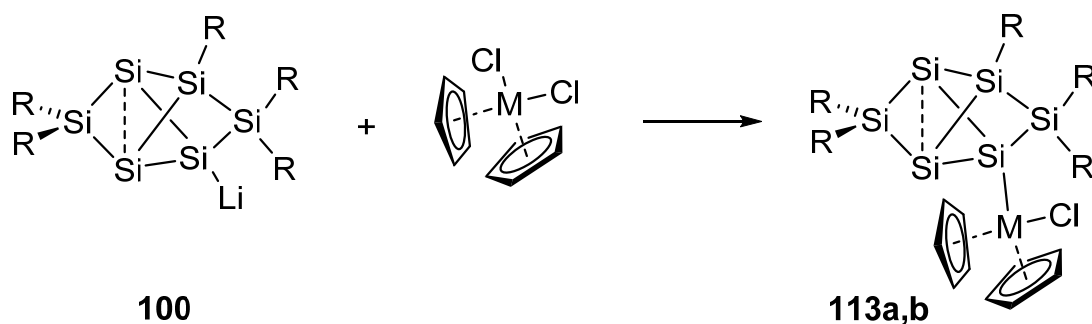
As reduction of hexasilabenzene **88** selectively yields the *ligato*-anionic moiety, the reduction of the global minimum isomer **91** was investigated by Yannic Heider from our group (equal contribution author in publication 3.1). While treatment of **91** with four equivalents of lithium/naphthalene led to the dianionic species **106**, reduction with two equivalents lithium/naphthalene results in the uniform conversion into the *privo*-lithiated siliconoid **11**. The ^{29}Si NMR reveals a similar chemical shift distribution as in *ligato*-lithiated siliconoid **100** but with distinctly different values leading to the suggestion that the lithiation had taken place in another position of the benzpolarene framework. The strongly deshielded signal at 267.9 ppm is significantly broadened due to the coupling to the quadrupolar ^7Li nucleus and shows coupling to one Tip unit in a 2D NMR spectrum. The structure of **111** has been finally confirmed by x-ray crystallography, showing the lithium functionality at the *privo*-position. In order to proof the nucleophilic transfer of **111**, treatment with several electrophiles such as Me_3SiCl , PhCOCl , $t\text{BuCOCl}$, $\text{ClP}(\text{NMe})_2$, SiCl_4 and $\text{BH}_3\cdot\text{SMe}_2$ was investigated. The corresponding *privo*-functionalized siliconoids **112a-f** were obtained and characterized by multi nuclear NMR spectroscopy (Scheme 54). The structures of **112b**, **112c** and **112e** were determined by x-ray crystallography and exhibit slightly longer distances between the bridgehead silicon atoms than the *ligato*-lithiated siliconoids **101e,f**.



Scheme 54. Synthesis of *privo*-lithiated siliconoid **111** by reduction with 2 equivalents of $\text{Li}/\text{C}_{10}\text{H}_8$ and its further functionalization with suitable electrophiles. Reagents: (a) SiCl_4 , (b) $\text{BH}_3\cdot\text{SMe}_2$, (c) $t\text{BuCOCl}$, (d) $\text{ClP}(\text{NMe}_2)_2$, (e) Me_3SiCl , (f) PhCOCl . **112a**: $\text{E} = \text{SiCl}_3$, **112b**: $\text{E} = \text{BH}_3^-$, **112c**: $\text{E} = t\text{BuCO}$, **112d**: $\text{E} = \text{P}(\text{NMe}_2)_2$, **112e**: $\text{E} = \text{Me}_3\text{Si}$, **112f**: $\text{E} = \text{COPh}$.

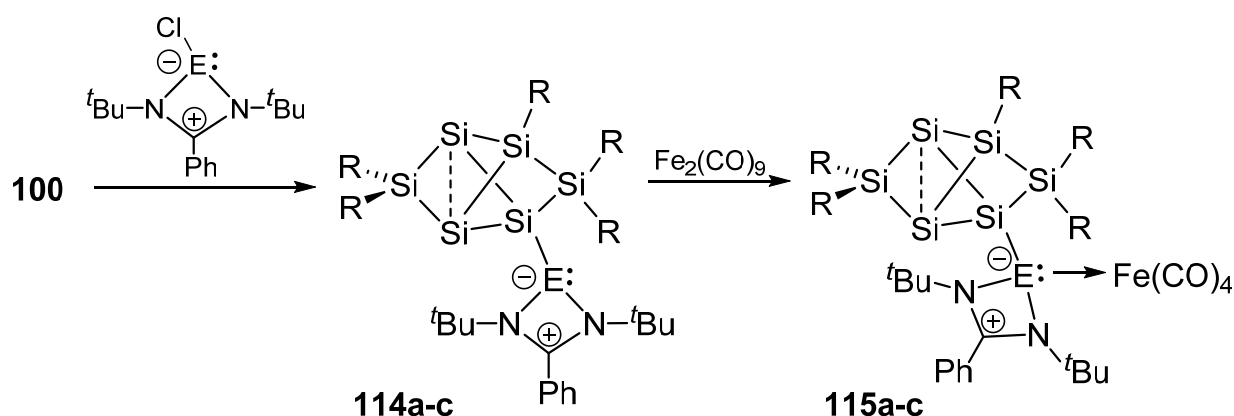
During these investigations, the relationship of the *privo* atom chemical shift and the Hammett parameter was drawn separately for *privo*- and *ligato*-functionalized siliconoids **101a-f** and **112a-f** showing linear relationships in both cases. While the stronger deshielding of the *privo* vertex in the ^{29}Si NMR is the result of electron withdrawing substituents, electron donating groups have exactly the opposite effect resulting in more shielded signals. In case of *privo*-substituted siliconoids **112a-f**, stronger linear dependency as in case of *ligato* **101a-f** was observed due to the stronger influence as the substituents are directly attached to the *privo* silicon atom. The ^{29}Si NMR shifts of the *nudo* silicon vertices show no apparent correlation to the Hammett parameters. With the present report, we shed some light on the fundamental understanding of siliconoids and provide synthetic approaches which might gain a more comprehensive insight on the complex multi-step construction of the cluster backbone.

Due to the lack of the covalent or dative coordination of neutral siliconoids to transition metals, the synthesis of the first examples of siliconoids bearing acovalently attached transition metal functionality has been investigated in this project. Nucleophilic transfer of the *ligato*-anionic Si_6 moiety to Cp_2MCl_2 ($\text{M} = \text{Zr}, \text{Hf}$) resulted in the isolation of the first transition-metal-substituted neutral siliconoids **113a,b** (Scheme 55). In contrast, reaction with the corresponding titanocene dichloride led to an inseparable mixture of products due to presumed competing redox reactions. The structures have been characterized by x-ray crystallography confirming the integrity of the benzpolarene scaffold. The ^{29}Si NMR spectrum revealed the diagnostic wide dispersion of NMR chemical shifts as discussed for the previous *ligato*-functionalized siliconoids **101a-f**.



Scheme 55. Synthesis of the first transition-metal-substituted neutral siliconoids **113a,b** (a: $\text{M} = \text{Zr}$, b: $\text{M} = \text{Hf}$).

The covalent silicon-metal bond in **113a,b** was found to be extremely unstable as even smallest traces of water lead to partial hydrolysis of **113a**, indicating the progressive appearance of a characteristic Si–H resonance at 4.103 ppm in the ^1H NMR spectrum. As grafting of later transition metals to siliconoids have remained elusive so far, we resorted to the dative coordination of charge-neutral siliconoids to transition metal centers. This was achieved by prior introduction of a tetrylene side arm, which have frequently been applied in the coordination to transition metals due to their excellent σ -donating properties. The chlorinated amidinato tetrylenes of type $\text{PhC}(\text{N}^t\text{Bu})_2\text{ECl}$ ($\text{E} = \text{Si}, \text{Ge}, \text{Sn}$) are known to react in a nucleophilic substitution reaction and thus have been treated with the *ligato*-lithiated siliconoid **100** resulting in uniform conversion to the tetrylene-substituted siliconoids **114a-c** (Scheme 56). The wide dispersion in the ^{29}Si NMR spectrum suggested to the preservation of the cluster framework which was finally confirmed by x-ray crystallography of **114a-c**. Notably, in the ^{29}Si and ^{119}Sn NMR spectra of **114b** and **114c**, the occurrence of two sets of signals were observed suggesting rotational isomers in solution which could be confirmed by VT-NMR studies and measurements of ^{29}Si and ^{119}Sn solid state NMR spectra.

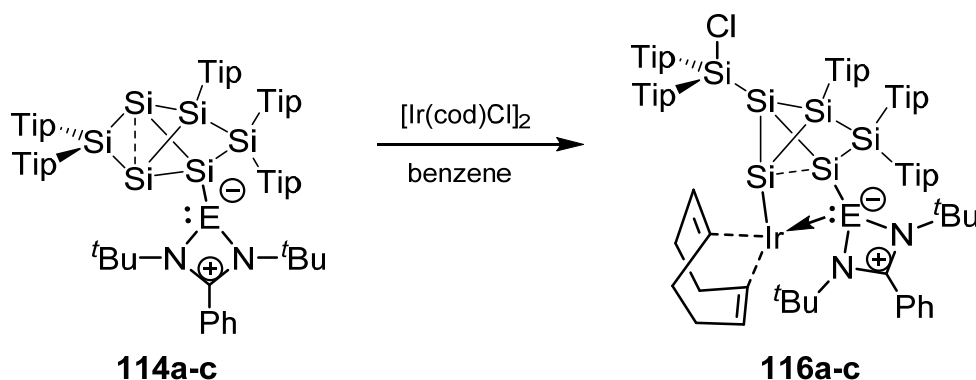


Scheme 56. Synthesis of the tetrylene-functionalized Si_6 siliconoids **114a-c** and their corresponding $\text{Fe}(\text{CO})_4$ complexes **115a-c** (**a**: $\text{E} = \text{Si}$, **b**: $\text{E} = \text{Ge}$, **c**: $\text{E} = \text{Sn}$).

The suitability of **114a-c** as neutral ligands in the coordination to transition metals was shown in the synthesis of the corresponding $\text{Fe}(\text{CO})_4$ complexes **115a-c** (Scheme 56). The constitution of the first siliconoid $\text{Fe}(\text{CO})_4$ complexes **115a-c** was confirmed by x-ray crystallography and ^{29}Si NMR spectroscopy. While the six signals of the Si_6 framework occur with the diagnostic wide dispersion, the additional signal

of the silylene side-arm in **115a** shows a drastically downfield-shifted signals at 110.0 ppm compared to that in **114a** (48.0 ppm). In addition, the ^{119}Sn NMR of **115c** at 456.3 ppm is also strongly downfield-shifted signal compared to that in **114c**. With the present work on the first transition metal-substituted siliconoids **113a,b** we disclosed a missing synthon in the emerging field of siliconoids. Furthermore, the stable siliconoid/tetrylene hybrids allow for the coordination to transition metals which was shown as proof-of-concept with the Fe-complexes **105a-c**. Cleavage of one carbonyl group of Fe-complexes **105a-c** might be considered as a logical next step in order to convert the Fe-complexes **105a-c** in more reactive species with regard to their application in a catalytic cycle.

Treatment of the tetrylene-functionalized siliconoids **114a-c** with $[\text{Ir}(\text{cod})\text{Cl}]_2$ resulted in the contraction of the Si_6 cluster framework accompanied by a transfer of a chlorine to the former *privo*-vertex and of its extrusion to an exohedral chlorosilyl group resembling the structural motif of chlorosilyltricyclo[2.1.0.0^{2,5}]pentasilane.¹⁹⁸ The obtained tetrylene- Si_6 iridium complexes **116a-c** were finally confirmed by x-ray crystallography. The ^{29}Si NMR spectra of **116a-c** show a much narrower distribution of the chemical shifts due to the loss of the spherical aromaticity and the concomitant magnetically induced cluster current.

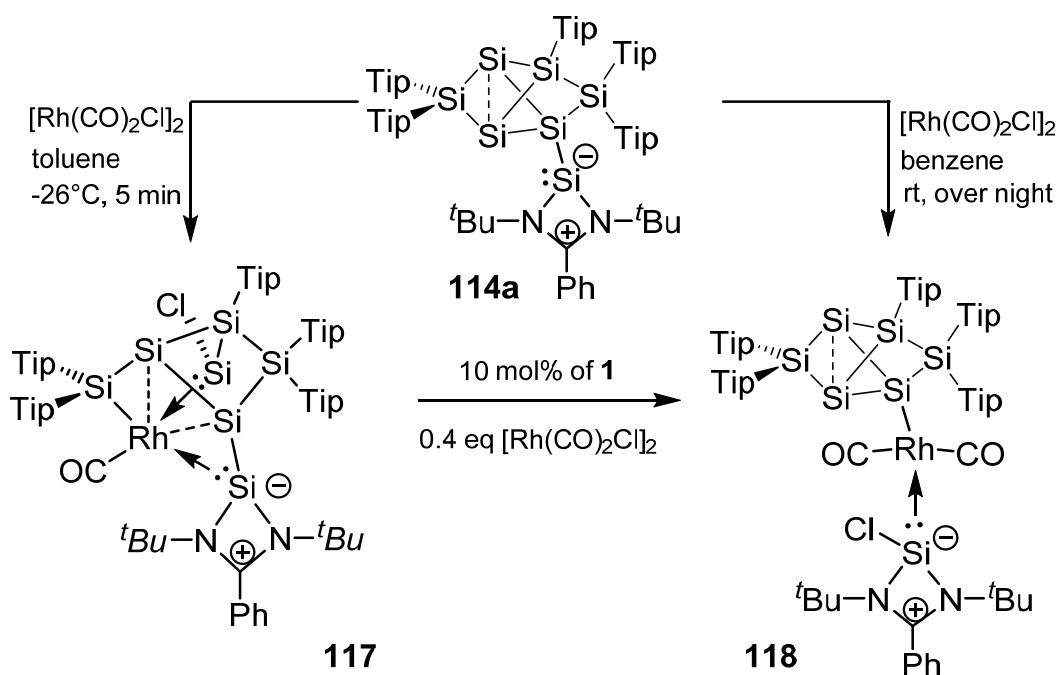


Scheme 57. Synthesis of tetrylene- Si_6 iridium complexes **116a-c** from the tetrylene functionalized Si_6 siliconoids **114a-c** with $[\text{Ir}(\text{cod})\text{Cl}]_2$ (**a**: E = Si, **b**: E = Ge, **c**: E = Sn).

Treatment of **114a-c** with the corresponding $[\text{Rh}(\text{cod})\text{Cl}]_2$ led in all cases to inseparable and complicated mixture of products due to a presumably complicated sequence of oxidative addition and reductive elimination reactions. Only from the product mixture of **114b** a few crystals could be obtained showing the same structural motif as observed in **116a-c**. Treatment of **114a-c** with $[\text{Rh}(\text{CO})_2\text{Cl}]_2$ finally led in case of **114a** to the uniform conversion to the unprecedented Si_7 rhodium complex

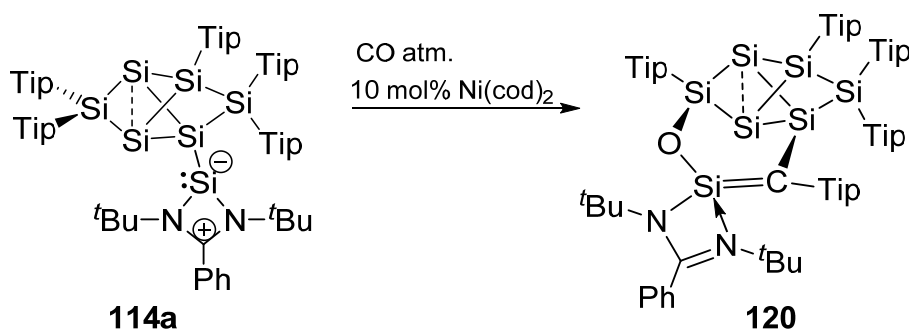
117 and inseparable mixture of products for **114b,c** (Scheme 58). Structure **117** could be analyzed by x-ray crystallography and exhibits an unprecedented pentacoordination of the Rh centre, which is fully incorporated into the cluster core in contrast to the iridium complexes **116a-c**.

Monitoring of the initial product **117** via ^1H NMR spectroscopy shows the rearrangement to a second product **118** with a restored benzpolarene framework. According to an x-ray diffraction study, the structure of **118** exhibits a covalently attached rhodium atom in the *ligato*-position (Scheme 58). Mechanistic considerations for the formation of **116a-c** and **117** through oxidative addition followed by reductive elimination have been proposed based on the structurally characterized products. Notably, while conversion of **117** to **118** was observed in solution, crystalline samples of **117** require the addition of 10 mol% of **114a** and additional 0.4 equivalents of $[\text{Rh}(\text{CO})_2\text{Cl}]_2$ to result in uniform conversion to **118**.



Scheme 58. Synthesis of Si_7 rhodium complexes **117** and **118** from silylene-functionalized Si_6 siliconoid **114a**.

A second central aspect of this project was the investigation to apply siliconoids in a catalytic cycle. With respect to the establishment of N-heterocyclic silylenes in catalysis, we focused on the silylene-functionalized siliconoid **114a** and the thus obtained Group 9 transition metal complexes **116a**, **117** and **118**. The Group 9 metallasiliconoids **116a**, **117** and **118** were thus employed as catalysts in the isomerization of terminal alkenes to 2-alkenes showing especially in case of **116a**



Scheme 60. Synthesis of the *privo-ligato* silanolether-bridged siliconoid **120**.

When the sililyene/siliconoid hybrid **114a** was treated with carbon monoxide in the presence of 10 mol% of Ni(cod)_2 , the full reductive cleavage of the $\text{C}\equiv\text{O}$ triple bond is observed. The structure **120** was confirmed by x-ray diffraction confirming the integrity of the benzpolarene scaffold with a peripheral connection of the *privo*- and *ligato*-positions by a $\text{Si}=\text{C}$ enol ether bridge (Scheme 60). We proposed a reaction mechanism stating that formation of an initial $\text{114a} \rightarrow \text{Ni(CO)}_3$ complex is the starting point based on the experimental observation that the reaction requires 10 mol% of Ni(cod)_2 . The mechanistic considerations have been supported by the optimization of the electronic structures of all proposed intermediates at the BP86-D3(BJ)/def2-SVP level of theory. The persistence of the hexasilabenzpolarene scaffold during the full cleavage of the $\text{C}\equiv\text{O}$ triple bond and the reorganization in the periphery of the cluster scaffold strongly supports the privileged role of the benzpolarene structural motif. This observation may add further support for its use as a functional ligand in homogeneous catalytic processes.

5 References

- [1] W. W. Emmett, Geolocigal Survey (US), Geological Survey Professional Paper **1975**, 870-A, A54.
- [2] J. Berzelius, Kongliga Vetenskaps-Academiens Handlingar [*Proceedings of the Royal Science Academy*] **1824**, 12, 46-98.
- [3] C. B. Carter, M. G. Norton, Ceramic materials: science and engineering, *Springer* **2007**.
- [4] R. G. Blezard, "The History of Calcareous Cements" in Hewlett, C. Peter, ed. Lea's chemistry of cement and concrete. 4. Ed. Amsterdam: *Elsevier Butterworth-Heinemann*, **2004**, 1-24.
- [5] A. Thomson, A System of Chemistry in Four Volumes, 5th ed. **1817**, 1, 252.
- [6] H.-H. Moretto, M. Schulze, G. Wagner „Silicones“ in Ullmann's Encyclopedia of Industrial Chemistry, *Wiley-VCH, Weinheim*, **2000**.
- [7] P. Siffert, E. F. Krimmel, Science & Business Media, Silicon: Evolution and future of a technology, *Springer*, **2004**.
- [8] G. W. Pickard, Patent US836531: Means For Receiving Intelligence Communicated By Electric Waves, **1905**.
- [9] L. Bo, History of Semiconductor Engineering. *Springer Science & Business Media*, **2007**, pp. 120 & 321-323. ISBN: 978-3-540-34258-8.
- [10] G. Feher, *Phys. Rev.* **1959**, 114, 1219-1244.
- [11] A. M. Tyryshkin, S. A. Lyon, A. V. Astashkin, A. M. Raitsimring, *Phys. Rev.* **2003**, B 68, 193207/1-193207/4.
- [12] Example for Arsenic: (a) C. C. Lo, V. Lang, R. E. George, J. J. L. Morton, A. M. Tyryshkin, S. A. Lyon, J. Bokor, T. Schenkel, *Phys. Rev. Lett.* **2011**, 106, 207601/1-207601/4.
Antimony: (b) C. C. Lo, J. Bokor, T. Schenkel, A. m. Tyryshkin, S. A. Lyon, *Appl. Phys. Lett.* **2007**, 91, 242106/1-242106/3;
Bismuth: (c) G. W. Morley, M. Warner, A. M. stoneham, P. T. Greenlang, J. van Tol, C. W. M. Kay, G. Aeppli, *Nature Mater.* **2010**, 9, 725-729.
- [13] For examples see: (a) A. Höfer, T. Feudel, N. Strecker, W. Fichtner, K.-H. Stegemann, H. Syhre, G. Dallmann, *J. Appl. Phys.* **1995**, 78, 3671-3679;
(b) R. Tiwari, S. Chandra, B. R. Chakraborty, *Mat. Sci. Semicon. Proc.*

- 2013**, 16, 2013-2020.
- [14] Example for Aluminium: (a) U. Landman, R. N. Barnett, A. G. Scherbakov, P. Avouris, *Phys. Rev. Lett.* **2000**, 85, 1958-1961.
Gallium: (b) S. W. Glunz, S. Rein, J. Knobloch, W. Wettling, T. Abe, *Prog. Photovolt. Res. Appl.* **1999**, 7, 463-469.
Indium: (c) S. Scalese, M. Italia, A. La Magna, G. Mannino, V. Privitera, M. Bersani, D. Giubertoni, M. Barozzi, S. Solmi, P. Pichler, *J. Appl. Phys.* **2003**, 93, 9773-9782.
- [15] H. Queisser, *Kristalline Krisen*, **1985**, S. 8, München.
- [16] J. Dabrowski, H.-J. Müssig, *Silicon Surfaces and Formation of Interfaces: Basic Science in the Industrial World. World Scientific*, **2000**, pp 3-13. ISBN 978-981-02-3286-3.
- [17] J. S. Hill in: *Multicrystalline Silicon Modules To Dominate Solar PV Industry In 2014*, **2012**, <http://cleantechnica.com>.
- [18] J. A. del Alamo, *Nature* **2011**, 479, 317-323.
- [19] L. C. Feldman, *Fundamental Aspects of Silicon Oxidation. Springer Science & business Media*, **2001**, pp 1-11, ISBN: 978-3-540-41682-1.
- [20] W. Lu, C. M. Lieber, *Nature Mat.* **2007**, 6, 841-850.
- [21] For examples see: (a) N. Cheng, S. Stambula, D. Wang, M. N. Banis, J. Liu, A. Riese, B. Xiao, R. Li, T.-K. Sham, L.-M. Liu, G. A. Botton, X. Sun, *Nat. Commun.* **2016**, 7, 13638; (b) S. Stavric, M. Belic, Z. Sljivancanin, *Carbon*, **2016**, 96, 216-222; (c) M. R. Friedfeld, J. L. Stein, B. M. Croissairt, *Inorg. Chem.*, **2017**, 56, 8689-8697.
- [22] For examples see: a) S. E. Weitzner, L. Dabo, *Phys. Rev. B*, **2017**, 96, 205134; b) T. Eom, W. J. Kim, H.-K. Lim, M. H. Han, K. H. Han, E.-K. Lee, S. Lebègue, Y. J. Hwanh, B. K. Min, H. Kim, *J. Phys. Chem. C*, **2018**, 122, 9245-9254.
- [23] F. S. Kipping, J. E. Sands, *J. Chem. Soc., Trans.* **1921**, 119, 830-847.
- [24] F. S. Kipping, *J. Chem. Soc. Trans.* **1924**, 125, 2291-2297.
- [25] F. S. Kipping, *Proc. R. Soc. A.* **1937**, 159, 139-148.
- [26] J. J. Daly, J. Maier, *Nature*, **1964**, 203, 1167-1168.
- [27] J. J. Daly, *J. Chem. Soc. Suppl.* **1964**, 6147-6166.
- [28] J. J. Daly, *J. Chem. Soc.* **1965**, 4789-4799.
- [29] J. J. Daly, L. Maier, *Nature* **1965**, 208, 383-384.

- [30] S. K. Pitzer, *J. Am. Chem. Soc.* **1975**, *70*, 2140-2145.
- [31] R. S. Mulliken, *J. Am. Chem. Soc.* **1955**, *77*, 884-887.
- [32] R. S. Mulliken, *J. Chem. Phys.* **1950**, *72*, 4493-4503.
- [33] P. Jutzi, *Angew. Chem. Int. Ed.* **1975**, *14*, 232-245.
- [34] A. G. Brook, S. C. Nyburg, F. Abdesaken, B. Gutekunst, G. Gutekunst, R. Krishna, M. R. Kallury, Y. C. Poon, Y. M. Chang, W. N. Winnie, *J. Am. Chem. Soc., Chem. Commun.* **1981**, *104*, 191-192.
- [35] R. West, J. M. Fink, J. Michl, *Science*, **1981**, *214*, 1343-1344.
- [36] M. Yoshifuji, I. Shima, N. Inamoto, K. Hirotsu, T. Higuchi, *J. Am. Chem. Soc.* **1981**, *103*, 4587-4589.
- [37] Review: R. C. Fischer, P. P. Power, *Chem. Rev.* **2010**, *110*, 3877-3923.
- [38] Reviews: (a) M. Weidenbruch in: The Chemistry of Organic Silicon Compounds, Vol. 3 (Eds.: Z. Rappoport, Y. Apeloig), Wiley, Chichester, UK, **2001**, Chapter 5; (b) M. Karni, Y. Apeloig, J. Kapp, von R. Schleyer in: The Chemistry of Organo Silicon Compounds, Vol. 3. (Eds.: Z. Rappoport, Y. Apeloig), John Wiley & Sons, Ltd. Chichester, **2001**, Chapter 1; (c) M. Kira, T. Iwamoto, *Adv. Organomet. Chem.* **2006**, *54*, 73-148; (d) V. Ya. Lee, A. Sekiguchi in: Organometallic Compounds of Low-coordinate Si, Ge, Sn and Pb: From Phantom Species to Stable Compounds, Wiley, Chichester, UK, **2010**, Chapter 5; (e) T. Iwamoto, S. Ishida in: Functional Molecular Silicon Compounds II, D. Scheschkewitz (ed), *Struct. Bonding* **2013**, *156*, 125-202; (f) S. Ishida, T. Iwamoto, *Coord. Chem. Rev.* **2016**, *314*, 34-63.
- [39] N. Wiberg, S. K. Vasisht, G. Fischer, P. Meyer, *Z. Anorg. Allg. Chem.* **2004**, *630*, 1823-1828.
- [40] A. Sekiguchi, R. Kinjo, M. Ichinohe, *Science*, **2004**, *305*, 1755-1757.
- [41] E. Fritz-Langhals, P. Jutzi, R. Weidner, *WACKER Chemie A.G. EP3*, 440, 088A1, **2017**.
- [42] B.-X. Leong, J. Lee, M.-C. Yang, C.-K. Siu, M.-D. Su, C.-W. So, *J. Am. Chem. Soc.* **2019**, *141*, 44, 17629-17636.
- [43] E. Fritz-Langhals, *Org. Process Res. Dev.* **2019**, *23*, 2369.
- [44] Y. Xiong, S. Yao, T. Szilvási, A. Ruzucka, M. Driess, *Chem. Commun.* **2020**, *56*, 747-750.
- [45] M. Majumdar, I. Omlor, C. B. Yildiz, A. Azizoglu, V. Huch, D. Scheschkewitz,

- Angew. Chem. Int. Ed.* **2015**, *54*, 8746-8750; *Angew. Chem.* **2015**, *127*, 8870-8874.
- [46] Y. Wang, A. Kostenko, T. J. Hadlington, M.-P. Luecke, S. Yao, M. Driess, *J. Am. Chem. Soc.* **2019**, *141*, 626-634.
- [47] A. V. Protschenko, P. Vasko, D. C. Huan Do, J. Hicks, M. Ángeles Fuentes, C. Jones, S. Aldridge, *Angew. Chem. Int. Ed.* **2019**, *58*, 1808-1812; *Angew. Chem.* **2019**, *131*, 1822-1826.
- [48] T. M. I Davidson, *J. Organomet. Chem.* **1970**, *24*, 97-100.
- [49] H. Murakami, T. Kanayama, *Appl. Phys. Lett.* **1995**, *67*, 2341-2343.
- [50] W. Watanabe, H. Murakami, T. Miyazaki, T. Kanayama, *Appl. Phys. Lett.* **1997**, *71*, 1207-1209.
- [51] W. M. M. Kessels, M. C. M. Van de Sanden, D. V. Schram, *Appl. Phys. Lett.* **1998**, *72*, 2397-2399.
- [52] G. A. Rechtsteiner, O. Hampe, M. F. Jarrold, *J. Phys. Chem. B.* **2001**, *105*, 4188-4194.
- [53] P. Willmes, K. Leszczyńska, Y. Heider, K. Abersfelder, M. Zimmer, V. Huch, D. Scheschkewitz, *Angew. Chem. Int. Ed.* **2016**, *55*, 2907-2910; *Angew. Chem.* **2016**, *128*, 2959-2963.
- [54] L. Klemmer, V. Huch, A. Jana, D. Scheschkewitz, *Chem. Commun.* **2019**, *55*, 10100-10103.
- [55] Recent reviews: (a) A. Rammo, D. Scheschkewitz, *Chem. Eur. J.* **2018**, *24*, 6866-6885; (b) T. Matsuo, N. Hayakawa, *Sci. Technol. Adv. Mat.* **2018**, *19*, 108-129; (c) C. Präsang, D. Scheschkewitz, *Chem. Soc. Rev.* **2016**, *45*, 900-921.
- [56] Recent reviews: (a) E. Rivard, *Chem. Soc. Rev.* **2016**, *45*, 989-1003; (b) B. Blom, M. Driess in: Functional Molecular Silicon Compounds II, D. Scheschkewitz (ed), *Struct. Bonding* **2013**, *156*, 85-123; (c) S. Mandal, H. W. Roesky, *Acc. Chem. Res.* **2012**, *45*, 298-307; (d) M. Asay, C. Jones, M. Driess, *Chem. Rev.* **2011**, *111*, 354-396; (e) Y. Mizuhata, T. Sasamori, N. Tokito, *Chem. Rev.* **2009**, *109*, 3479-3511.
- [57] P. Jutzi, D. Kanne, C. Krüger, *Angew. Chem. Int. Ed. Engl.* **1986**, *25*, 164-165; *Angew. Chem.* **1986**, *98*, 163-164.
- [58] M. Denk, R. Lennon, R. Hayashi, R. West, A. V. Belyakov, H. P. Verne, A. Haaland, M. Wagner, N. Metzler, *J. Am. Chem. Soc.* **1994**, *116*, 2691.

- [59] M. Kira, S. Ishida, T. Iwamoto, C. Kabuto, *J. Am. Chem. Soc.* **1999**, *121*, 9722-9723.
- [60] C.-W. So, H. W. Roesky, J. Magull, R. B. Oswald, *Angew. Chem. Int. Ed.* **2006**, *45*, 3948-3950; *Angew. Chem.* **2006**, *118*, 4052-4054.
- [61] S. S. Sen, H. W. Roesky, D. Stern, J. Henn, D. Stalke, *J. Am. Chem. Soc.* **2010**, *132*, 1123-1126.
- [62] B. Gehrhus, M. F. Lappert, J. Heinicke, R. Boese, D. Bläser, *J. Chem. Soc., Chem. Commun.* **1995**, 1931-1932.
- [63] M. Driess, S. Yao, M. Brym, C. van Wüllen, D. Lentz, *J. Am. Chem. Soc.* **2006**, *128*, 9628-9629.
- [64] G. Schmid, E. Welz, *Angew. Chem. Int. Ed. Engl.* **1977**, *16*, 785-786; *Angew. Chem.* **1977**, *59*, 823.
- [65] Review: B. Blom, M. Stoelzel, M. Driess, *Chem. Eur. J.* **2013**, *19*, 40-62.
- [66] Selected examples: a) J. A. Baus, F. M. Mück, H. Schneider, R. Tacke, *Chem. Eur. J.* **2016**, *23*, 296-303; b) Y.-P. Zhou, Z. Mo, M.-P. Luecke, M. Driess, *Chem. Eur. J.* **2017**, *24*, 4780-4784; c) S. Takahashi, E. Bellan, A. Baceiredo, N. Saffon-Merceron, S. Massou, N. Nakata, D. Hashizume, V. Branchadell, T. Kato, *Angew. Chem. Int. Ed.* **2019**, *58*, 10310-10314; *Angew. Chem.* **2019**, *131*, 10416-10420.
- [67] S. D. Grumbine, T. D. Tilley, A. L. Rheingold, *J. Am. Chem. Soc.* **1993**, *115*, 358-360.
- [68] S. D. Grumbine, T. D. Tilley, F. P. Arnold, A. L. Rheingold, *J. Am. Chem. Soc.* **1993**, *115*, 7884-7885.
- [69] S. D. Grumbine, T. D. Tilley, F. P. Arnold, A. L. Rheingold, *J. Am. Chem. Soc.* **1994**, *116*, 5495-5496.
- [70] C. Zybille, G. Müller, *Angew. Chem.* 1987, *99*, 683-684.
- [71] R. Azhakar, R. S. Ghadwal, H. W. Roesky, J. Hey, D. Stalke, *J. Chem. Asian*, **2012**, *7*, 528-533.
- [72] G. L. Geoffroy, M. G. Bradley, *Inorg. Chem.* **1978**, *17*, 2410-2414.
- [73] T. A. Schmedake, M. Haaf, B. J. Paradise, A. J. Millevolte, D. R. Powell, R. West, *J. Organomet. Chem.* **2001**, *636*, 17-25.
- [74] A.-K. Jungton, A. Meltzer, C. Präsang, T. Braun, M. Driess, A. Penner, *Dalton Trans.* **2010**, *39*, 5436-5438.
- [75] M. Zhang, X. Liu, C. Shi, C. Ren, Y. Ding, H. W. Roesky, *Z. Anorg. Allg.*

- Chem.* **2008**, *634*, 1755-1758.
- [76] G. Avent, B. Gehrhus, P. B. Hitchcock, M. F. Lappert, H. Maciejewski, *J. Organomet. Chem.* **2003**, *686*, 321-331.
- [77] G. Tan, B. Blom, D. Gallego, M. Driess, *Organometallics*, **2014**, *33*, 1, 363-369.
- [78] A. N. Paesch, A.-K. Kreyenschmidt, R. Herbst-Irmer, D. Stalke, *Inorg. Chem.* **2019**, *58*, 10, 7000-7009.
- [79] B. Blom, S. Inoue, D. Gallego, M. Driess, *Chem. Eur. J.* **2012**, *18*, 13355-13360.
- [80] R. Azhakar, S. P. Sarish, H. W. Roesky, J. Hey, D. Stalke, *Inorg. Chem.* **2011**, *50*, 5039-5043.
- [81] C. Boehme, G. Frenking, *Organometallics*, **1998**, *17*, 5801-5809.
- [82] S. Schäfer, R. Köppe, M. T. Gamer, P. W. Roesky, *Chem. Commun.* **2014**, *50*, 11401-11403.
- [83] D. Sheberla, B. Tumanskii, A. C. Tomasik, A. Mitra, N. J. Hill, R. West, Y. Apeloig, *Chem. Sci.*, **2010**, *1*, 234-241.
- [84] Y. Wang, Y. Xie, P. Wei, R. B. King, H. F. Schaefer III, P. v. R. Schleyer, G. H. Robinson, *Science*, **2008**, *321*, 1069-1071.
- [85] S. S. Sen, A. Jana, H. W. Roesky, C. Schulzke, *Angew. Chem. Int. Ed.* **2009**, *48*, 8536-8538; *Angew. Chem.* **2009**, *121*, 8688-8690.
- [86] D. Gau, R. Rodriguez, T. Kato, N. Saffon-Merceron, A. De Cózar, A. Baceiredo, *Angew. Chem. Int. Ed.* **2011**, *50*, 1092-1096; *Angew. Chem.* **2011**, *123*, 1124-1128.
- [87] C. Jones, S. J. Bonyhady, N. Holzman, G. Frenking, A. Stasch, *Inorg. Chem.* **2011**, *50*, 12315-12325.
- [88] S. S. Sen, S. Khan, S. Nagendran, H. W. Roesky, *Acc. Chem. Res.* **2012**, *45*, 4, 578-587.
- [89] B. Gehrhus, P. B. Hitchcock, M. F. Lappert, *Z. Anorg. Allg. Chem.* **2005**, *631*, 1383-1386.
- [90] W. Wang, S. Inoue, S. Yao, M. Driess, *J. Am. Chem. Soc.* **2010**, *132*, 45, 15890-15892.
- [91] W. Wang, S. Inoue, S. Enthaler, M. Driess, *Angew. Chem. Int. Ed.*, **2012**, *51*, 6167-6171; *Angew. Chem.* **2012**, *124*, 6271-6275.

-
- [92] D. Gallego, S. Inoue, B. Blom, M. Driess, *Organometallics* **2014**, *33*, 23, 6885–6897.
- [93] R. Kinjo, M. Ichinohe, A. Sekiguchi, N. Takagi, M. Sumimoto, S. Nagase, *J. Am. Chem. Soc.* **2007**, *129*, 7766–7767.
- [94] S. S. Sen, H. W. Roesky, K. Meindl, D. Stern, J. Henn, A. C. Stückl, D. Stalke, *Chem. Commun.* **2010**, 46, 5873–5875.
- [95] W. Wang, S. Inoue, E. Irran, M. Driess, *Angew. Chem. Int. Ed.* **2012**, *51*, 3691–3694; *Angew. Chem.* **2012**, *124*, 3751–3754.
- [96] Y.-P. Zhou, S. Raoufmoghaddam, T. Szilvási, M. Driess, *Angew. Chem. Int. Ed.*, **2016**, *55*, 12868–12872, *Angew. Chem.*, **2016**, *128*, 13060–13064.
- [97] H. Ren, Y.-P. Zhou, Y. Bai, C. Cui, M. Driess, *Chem. Eur. J.* **2017**, *23*, 5663–5667.
- [98] M. N. Hopkinson, C. Richter, M. Schedler, F. Glorius, *Nature*, **2014**, *510*, 485–496.
- [99] G. C. Fortman, S. P. Nolan, *Chem. Soc. Rev.* **2011**, *40*, 5151–5169.
- [100] F. E. Hahn, M. C. Jahnke, *Angew. Chem. Int. Ed.* **2008**, *47*, 3122–3172; *Angew. Chem.* **2008**, *120*, 3166–3216.
- [101] D. J. Nelson, S. P. Nolan, *Chem. Soc. Rev.* **2013**, *42*, 6723–6753.
- [102] S. Diez-Gonzalez, N. Marion, S. P. Nolan, *Chem. Rev.* **2009**, *109*, 3612–3676.
- [103] N. Marion, S. P. Nolan, *Chem. Soc. Rev.* **2008**, *37*, 1776–1782.
- [104] C. Valente, S. Calimsiz, K. H. Hoi, D. Mallik, M. Sayah, M. G. Organ, *Angew. Chem. Int. Ed.* **2012**, *51*, 3314–3332; *Angew. Chem.* **2012**, *124*, 3370–3388.
- [105] H. D. Velazquez, F. Verpoort, *Chem. Soc. Rev.* **2012**, *41*, 7032–7060.
- [106] Recent reviews: (a) Y.-P. Zhou, M. Driess, *Angew. Chem. Int. Ed.* **2019**, *58*, 3715–3728; (b) S. Raoufmoghaddam, Y.-P. Zhou, Y. Wang, M. Driess, *J. Organomet. Chem.* **2017**, *829*, 2–10.
- [107] A. Fürstner, H. Krause, C.W. Lehmann, *Chem. Commun.* **2001**, 2372–2373.
- [108] A. Brück, D. Gallego, W. Wang, E. Irran, M. Driess, J. F. Hartwig, *Angew. Chem. Int. Ed.* **2012**, *51*, 11478–11482; *Angew. Chem.* **2012**, *124*, 11645–11649.
- [109] B. Blom, D. Gallego, M. Driess, *Inorg. Chem. Front.* **2014**, *1*, 134–148.
- [110] D. Gallego, A. Brück, E. Irran, F. Meier, M. Kaupp, M. Driess, J. F.
-

- Hartwig, *J. Am. Chem. Soc.* **2013**, *135*, 15617-15626.
- [111] B. Blom, S. Enthaler, S. Inoue, E. Irran, M. Driess, *J. Am. Chem. Soc.* **2013**, *135*, 6703-6713.
- [112] P. B. Glaser, T. D. Tilley, *J. Am. Chem. Soc.* **2003**, *125*, 45, 13640-13641.
- [113] P. G. Hayes, C. Beddie, M. B. Hall, R. Waterman, T. D. Tilley, *J. Am. Chem. Soc.* **2006**, *128*, 2, 428-429.
- [114] E. Calimano, T. D. Tilley, *J. Am. Chem. Soc.* **2009**, *131*, 31, 11161-11173.
- [115] M. Stoelzel, C. Praesang, B. Blom, M. Driess, *Aust. J. Chem.* **2013**, *66*, 1163.
- [116] C. I. Someya, M. Haberberger, W. Wang, S. Enthaler, S. Inoue, *Chem. Lett.* **2013**, *42*, 286.
- [117] Y.-P. Zhou, Z. Mo, M.-P. Luecke, M. Driess, *Chem. Eur. J.* **2018**, *24*, 4780-4784.
- [118] A. Wang, A. Kostenko, S. Yao, M. Driess, *J. Am. Chem. Soc.* **2017**, *139*, 38, 13499-13506.
- [119] J. E. Carey, C. H. Crouch, M. Shen, E. Mazur, *Opt. Lett.* **2005**, *30*, 1773-1775.
- [120] Z. Huang, J. E. Carey, M. Liu, Y. Guo, E. Mazur, J. C. Campbell, *Appl. Phys. Lett.* **2006**, *89*, 033506.
- [121] A. J. Said, D. Recht, J. T. Sullivan, J. M. Warrender, T. Buonassisi, P. D. Persans, M. J. Aziz, *Appl. Phys. Lett.* **2011**, *99*, 073503.
- [122] K. Eom, J. Lee, M. Oschatz, F. Wu, S. Kaskel, G. Yushin, T. F. Fuller, *Nat. Commun.* **2017**, *8*, 1-9.
- [123] Y. Wang, M. Chen, Y. Xie, P. Wie, H. F. Schaefer, P. von R. Schleyer, G. H. Robinson, *Nature Chemistry*, **2015**, *7*, 509-513.
- [124] M. Haaf, A. Schmiedl, T. A. Schmedake, D. R. Powell, A. J. Millevolte, M. Denk, R. West, *J. Am. Chem. Soc.* **1998**, *120*, 12714-12719.
- [125] P. Zark, A. Schöfer, A. Mitra, D. Haase, W. Saak, R. West, T. Müller, *J. Organomet. Chem.* **2010**, *695*, 398-408.
- [126] S. Yao, Y. Xiong, M. Driess, *Chem. Eur. J.* **2010**, *16*, 1281-1288.
- [127] S.-H. Zhang, H.-X. Yeong, C.-W. So, *Chem. Eur. J.* **2011**, *17*, 3490-3499.
- [128] R. Tacke, C. Kobelt, J. A. Baus, R. Bertemann, C. Burschka, *Dalton Trans.* **2015**, *44*, 14959-14974.
- [129] S. Kaufmann, S. Schäfer, M. T. Gamer, P. W. Roesky, *Dalton Trans.* **2017**, *46*, 8861-8867.

- [130] H. Suzuki, N. Tokitoh, S. Nagase, R. Okazaki, *J. Am. Chem. Soc.* **1994**, *116*, 11578-11579.
- [131] C. Filippou, B. Baars, O. Chernov, Y. N. Lebedev, G. Schnakenburg, *Angew. Chem.* **2014**, *126*, 576-581; *Angew. Chem. Int. Ed.* **2014**, *53*, 565-570.
- [132] R. Kobayashi, S. Ishida, T. Iwamoto, *Angew. Chem.* **2019**, *131*, 9525-9528; *Angew. Chem. Int. Ed.* **2019**, *58*, 9425-9428
- [133] T. M. I. Davidson, *J. Organomet. Chem.* **1970**, *24*, 97-100.
- [134] H. Murakami, T. Kanayama, *Appl. Phys. Lett.* **1995**, *67*, 2341-2343.
- [135] M. Watanabe, H. Murakami, T. Miyazaki, T. Kanayama, *Appl. Phys. Lett.* **1997**, *71*, 1207-1209.
- [136] W. M. M. Kessels, M. C. M. Van De Sanden, D. C. Schram, *Appl. Phys. Lett.* **1998**, *72*, 2397-2399.
- [137] G. A. Rechtsteiner, O. Hampe, M. F. Jarrold, *J. Phys. Chem. B* **2001**, *105*, 4188-4194.
- [138] A. A. Adesina, *Appl. Catal. A*, **1996**, *138*, 345–367.
- [139] H. Schulz, *Appl. Catal. A* **1999**, *186*, 3–12.
- [140] P. M. Maitlis, *J. Organomet. Chem.* **2004**, *689*, 4366–4374.
- [141] P. M. Maitlis, V. Zanotti, *Chem. Commun.* **2009**, 1619–1634.
- [142] A. F. Holleman, E. Wiberg, N. Wiberg, *Lehrbuch der Anorganischen Chemie*, 102 ed., de Gruyter, Berlin, **2007**.
- [143] Selected examples: (a) W. J. Evans, J. W. Grate, L. A. Hughes, H. Zhang, J. L. Atwood, *J. Am. Chem. Soc.* **1985**, *107*, 3728– 3730; (b) W. J. Evans, D. S. Lee, J. W. Ziller, N. Kaltsoyannis, *J. Am. Chem. Soc.* **2006**, *128*, 14176– 14184; (c) P. A. Bianconi, R. N. Vrtis, C. P. Rao, I. D. Williams, M. P. Engeler, S. J. Lippard, *Organometallics* **1987**, *6*, 1968– 1977; (d) O. T. Summerscales, F. G. N. Cloke, P. B. Hitchcock, J. C. Green, N. Hazari, *Science* **2006**, *311*, 829– 831; (e) T. Watanabe, Y. Ishida, T. Matsuo, H. Kawaguchi, *J. Am. Chem. Soc.* **2009**, *131*, 3474– 3475; (f) P. L. Arnold, Z. R. Turner, R. M. Bellabarba, R. P. Tooze, *Chem. Sci.* **2011**, *2*, 77– 79.
- [144] R. E. LaPointe, P. T. Wolczanski, J. F. Mitchell, *J. Am. Chem. Soc.* **1986**, *108*, 6382– 6384.
- [145] R. Toreki, R. E. LaPointe, P. T. Wolczanski, *J. Am. Chem. Soc.* **1987**, *109*, 7558– 7560.

- [146] R. L. Miller, P. T. Wolczanski, *J. Am. Chem. Soc.* **1993**, *115*, 10422–10423.
- [147] M. J. Cowley, Y. Ohmori, V. Huch, M. Ichinohe, A. Sekiguchi, D. Scheschkewitz, *Angew. Chem. Int. Ed.* **2013**, *52*, 13247-13250; *Angew. Chem.* **2013**, *50*, 13489-13492.
- [148] X. Wang, Z. Zhu, Y. Peng, H. Lei, J. C. Fettinger, P. P. Power, *J. Am. Chem. Soc.* **2009**, *131*, 6912-6913.
- [149] A. Fukazawa, J. L. Dutton, C. Fan, L. G. Mercier, A. Y. Houghton, Q. Wu, W. E. Piers, M. Parvez, *Chem. Sci.* **2012**, *3*, 1814-1818.
- [150] M. Sajid, L. M. Elmer, C. Rosorius, C. G. Daniliuc, S. Grimme, G. Kehr, G. Erker, *Angew. Chem. Int. Ed.* **2013**, *52*, 2243-2246; *Angew. Chem.* **2013**, *125*, 2299-2302.
- [151] R. Dobrovetsky, D. W. Stephan, *J. Am. Chem. Soc.* **2013**, *135*, 4974-4977.
- [152] J. Böhnke, H. Braunschweig, T. Dellermann, W. C. Ewing, K. Hammond, J. O. C. Jimenez-Halla, T. Kramer, J. Mies, *Angew. Chem. Int. Ed.* **2015**, *54*, 13801-13805; *Angew. Chem.* **2015**, *127*, 14006-14010.
- [153] H. Braunschweig, R. D. Dewhurst, F. Hupp, M. Nutz, K. Radacki, C. W. Tate, A. Vargas, Q. Ye, *Nature*, **2015**, *522*, 237-330.
- [154] M. M. Hansmann, R. Jazzar, G. Bertrand, *J. Am. Chem. Soc.* **2016**, *138*, 8356-8359.
- [155] W. Lu, H. Hu, Y. Li, R. Ganguly, R. Kinjo, *J. Am. Chem. Soc.* **2016**, *138*, 6650-6661.
- [156] M. Arrowsmith, J. Böhnke, M. A. Elik, H. Braunschweig, *Angew. Chem. Int. Ed.* **2017**, *56*, 14287-14292; *Angew. Chem.* **2017**, *129*, 14475-14480.
- [157] M. Devillard, B. de Bruin, M. A. Siegler, I. J. I. van der Vlugt, *Chem. Eur. J.* **2017**, *23*, 13628-13632.
- [158] A. L. Kenward, W. E. Piers, *Angew. Chem. Int. Ed.* **2008**, *47*, 38–41; *Angew. Chem.* **2008**, *120*, 38–42.
- [159] P. P. Power, *Nature* **2010**, *463*, 171–177.
- [160] D. Martin, M. Soleilhavoup, G. Bertrand, *Chem. Sci.* **2011**, *2*, 389–399.
- [161] S. Yao, Y. Xiong, M. Driess, *Organometallics* **2011**, *30*, 1748–1767.
- [162] P. P. Power, *Acc. Chem. Res.* **2011**, *44*, 627–637.

- [163] S. K. Mandal, H. W. Roesky, *Acc. Chem. Res.* **2012**, *45*, 298–307.
- [164] W. F. Sager, A. Fatiadi, P. C. Parks, D. G. White, T. P. Perros, *J. Inorg. Nucl. Chem.* **1963**, *25*, 187–194.
- [165] H. Braunschweig, T. Dellermann, R. D. Dewhurst, W. C. Ewing, K. Hammond, J. O. C. Jimenez-Halla, T. Kramer, I. Krummenacher, J. Mies, A. K. Phukan, A. Vargas, *Nat. Chem.* **2013**, *5*, 1025–1028.
- [166] M. A. Pearsall, R. West, *J. Am. Chem. Soc.* **1988**, *110*, 7228–7229.
- [167] M. Tacke, C. Klein, D. J. Stufkens, A. Oskam, A. Bunte, P. Jutzi, *Z. Anorg. Allg. Chem.* **1993**, *619*, 865–868.
- [168] C. A. Arrington, J. T. Petty, S. E. Payne, W.C.K. Haskins, *J. Am. Chem. Soc.* **1988**, *110*, 6240–6241.
- [169] H. Bornemann, W. Sander, *J. Organomet. Chem.* **2002**, *641*, 156–164.
- [170] C. Ganesamoorthy, J. Schoening, C. Wölper, L. Song, P. R. Schreiner, S. Schulz, *Nat. Chem.* **2020**, *12*, 608–614.
- [171] A. G. Brook, *J. Am. Chem. Soc.* **1958**, *80*, 1886–1889.
- [172] D. K. Yu, R. Q. Zhang, S. T. Lee, *J. Appl. Phys.* **2002**, *92*, 7453–7458.
- [173] A. C. R. Joanis, *Acad. Sci.* **1891**, *113*, 795–798.
- [174] E. Zintl, J. Goubeau, W. Dullenkopf, *Z. Phys. Chem., Abt. A* **1931**, *154*, 1.
- [175] E. Zintl, A. Harder, *Z. Phys. Chem., Abt. A*, **1931**, *154*, 47.
- [176] E. Zintl, W. Dullenkopf, *Z. Phys. Chem., Abt. B*, **1932**, *16*, 183.
- [177] E. Zintl, H. Kaiser, *Z. Anorg. Allg. Chem.*, **1933**, *211*, 113–131.
- [178] E. Zintl, A. Harder, S. Neumayr, *Z. Phys. Chem., Abt. A*, **1931**, *154*, 92.
- [179] J. M. Goicoechea, S. C. Sevov, *J. Am. Chem. Soc.* **2004**, *126*, 6860–6861.
- [180] J. M. Goicoechea, S. C. Sevov, *Inorg. Chem.* **2005**, *44*, 2654–2658.
- [181] S. Scharfe, T. F. Fässler, *Philos. Trans. R. Soc. London Ser. A* **2010**, *328*, 1265–1284.
- [182] S. Scharfe, T. F. Fässler, in *Nanoparticles - From Theory to Application* Vol. 2 (Ed.: G. Schmid), *WILEY-VCH*, Weinheim, **2010**, pp. 49.
- [183] C. Lorenz, F. Hastreiter, K. Hioe, N. Lokesh, S. Gärtner, N. Korber, R. M. Gschwind, *Angew. Chem. Int. Ed.* **2018**, *57*, 12956–12960; *Angew. Chem.* **2018**, *130*, 13138–13142.
- [184] T. Henneberger, W. Klein, T. F. Fässler, *Z. Anorg. Allg. Chem.* **2018**, *644*, 1018–1027.
- [185] F. Hastreiter, C. Lorenz, J. Hioe, S. Gärtner, N. Lokesh, N. Korber, R. M.

- Gschwind, *Angew. Chem. Int. Ed.* **2019**, *58*, 3133-3137; *Angew. Chem.* **2019**, *131*, 3165-3169.
- [186] L. J. Schiegerl, A. J. Karttunen, W. Klein, T. F. Fässler, *Chem. Eur. J.* **2018**, *24*, 19171-19174.
- [187] M. Waibel, G. Raudaschl-Sieber and T. F. Fässler, *Chem. Eur. J.* **2011**, *17*, 13391–13394.
- [188] M. Waibel and T. F. Fässler, *Inorg. Chem.*, **2013**, *52*, 5861–5866.
- [189] M. Waibel, C. B. Benda, B. Wahl, T. F. Fässler, *Chem. Eur. J.* **2011**, *17*, 12928-12931.
- [190] D. Nied, P. Oña-Burgos, W. Kloppe, F. Breher, *Organometallics* **2011**, *30*, 1419-1428.
- [191] S. Nagase, M. Nakano, and T. Kudo, *J. Chem. Soc., Chem. Commun.*, **1987**, 60-62.
- [192] H. Matsumoto, K. Higuchi, Y. Hoshino, H. Koike, Y. Naoi, Y. Nagai, J. Chem. Soc., *Chem. Commun.* **1988**, 1083–1084.
- [193] Selected Reviews: (a) A. Sekiguchi, H. Sakurai, *Adv. Organomet. Chem.* **1995**, *37*, 1–38; (b) N. Wiberg, P. P. Power, in *Molecular Clusters of the Main Group Elements*, (Ed.: M. Dries and H. Nöth), *Wiley-VCH*, New York, **2004**, pp. 188.
- [194] N. Wiberg, C. M. M. Finger, K. Polborn, *Angew. Chem., Int. Ed. Engl.* **1993**, *32*, 1054–1056; *Angew. Chem.* **1993**, *105*, 1140–1142.
- [195] N. Wiberg, W. Hochmuth, H. Nöth, M. Schmidt-Amelunxen, *Angew. Chem. Int. Ed. Engl.* **1996**, *35*, 1333-1334; *Angew. Chem.* **1996**, *108*, 1437–1438.
- [196] M. Ichinohe, M. Toyoshima, R. Kinjo, A. Sekiguchi, *J. Am. Chem. Soc.* **2003**, *125*, 13328–13329.
- [197] Y. Ito, V. Y. Lee, H. Gornitzka, C. Goedecke, G. Frenking, A. Sekiguchi, *J. Am. Chem. Soc.* **2013**, *135*, 6770-6773.
- [198] A. Jana, V. Huch, M. Repisky, R. J. F. Berger, D. Scheschkewitz, *Angew. Chem. Int. Ed.* **2014**, *53*, 3514-3518; *Angew. Chem.* **2014**, *126*, 3583-3588.
- [199] H. Schnöckel, *Dalton Trans.* 2005, 3131–3136.
- [200] Reviews: (a) A. Schnepf, *Chem. Soc. Rev.* **2007**, *36*, 745–758; (b) A. Schnepf, *New J. Chem.* **2010**, *34*, 2079–2092.
- [201] For reviews concerning Zintl Ions, cage compounds, and intermetalloid

- Clusters of Group 14 and Group 15 Elements see: (a) S. Scharfe, F. Kraus, S. Stegmaier, A. Schier, T. F. Fässler, *Angew. Chem. Int. Ed.* **2011**, *50*, 3630–3670; *Angew. Chem.* **2011**, *123*, 3712–3754;; (b) T. F. Fässler, *Struct. Bond.* **2011**, *140*, 91–131.
- [202] K. Abersfelder, A. Russell, H. S. Rzepa, A. J. P. White, P. R. Haycock, D. Scheschkewitz, *J. Am. Chem. Soc.* **2012**, *134*, 16008–16016.
- [203] Y. Heider, D. Scheschkewitz, *Dalton. Trans.* **2018**, *47*, 7104-7112.
- [204] W. Wu, G. J. J. Song, S. S., C. P. Hiberty, *Angew. Chem. Int. Ed.* **2009**, *48*, 1407-1410; *Angew. Chem.* **2009**, *48*, 1435-1438..
- [205] S. Shaik, P. Maitr, G. Sini, C. P. Hiberty, *J. Am. Chem. Soc.* **1992**, *114*, 7861.
- [206] N. Wiberg, H.-W. Lemer, S. Wagner, H. Nöth, T. Seifert, *Z. Naturforsch.* **1999**, *54b*, 877–880.
- [207] B. E. Eichler, Philip P. Power, *Angew. Chem. Int. Ed.* **2001**, *40*, 796–797; *Angew. Chem.* **2001**, *113*, 818–819.
- [208] F. Li, A. Muçoz-Castro, S. C. Sevov, *Angew. Chem. Int. Ed.* **2012**, *51*, 8581–8584; *Angew. Chem.* **2012**, *124*, 8709–8712.
- [209] F. Li, S. C. Sevov, *J. Am. Chem. Soc.* **2014**, *136*, 12056–12063.
- [210] S. C. Sevov, J. M. Goicoechea, *Organometallics* **2006**, *25*, 5678-5692.
- [211] O. Kysliak, C. Schrenk, A. Schnepf, *Inorg. Chem.* **2015**, *54*, 7083-7088.
- [212] O. Kysliak, A. Schnepf, *Dalton Trans.* **2016**, *45*, 2404-2408.
- [213] F. S. Geitner, J. V. Dums, T. F. Fässler, *J. Am. Chem. Soc.* **2017**, *139*, 11933-11940.
- [214] F. S. Geitner, W. Klein, T. F. Fässler, *Angew. Chem. Int. Ed.* **2018**, *57*, 14509-14513; *Angew. Chem.* **2018**, *130*, 14717-14721.
- [215] S. Frischhut, W. Klein, M. Drees, T. F. Fässler, *Chem. Eur. J.* **2018**, *24*, 9009-9014.
- [216] B. W. Eichhorn, R. C. Haushalter, W. T. Pennington, *J. Am. Chem. Soc.* **1988**, *110*, 8704.
- [217] B. Schiemenz, G. Huttner, *Angew. Chem. Int. Ed. Engl.* **1993**, *32*, 297-298; *Angew. Chem.* **1993**, *105*, 295-296.
- [218] G. Renner, P. Kircher, G. Huttner, P. Rutsch, K. Heinze, *Eur. J. Inorg. Chem.* **2001**, 973-980.
- [219] B. Kesanli, J. Fettingner, B. Eichhorn, *Chem. Eur. J.*, **2001**, *7*, 5277-5285.

- [220] Recent review: R. J. Wilson, B. Weinert, S. Dehnen, *Dalton. Trans.* **2018**, 47, 14861-14869.
- [221] S. Joseph, M. Hamberger, F. Mutzbaurer, O. Härtl, M. Meier, N. Korber, *Angew. Chem. Int. Ed.* **2009**, 48, 8770-8772; *Angew. Chem.* **2009**, 121, 8926-8929.
- [222] Recent reviews: (a) S. D. Hoffmann, T. F. Fässler, *Angew. Chem. Int. Ed.* **2004**, 43, 6242-6247; (b) K. Mayer, J. Weßing, T. F. Fässler, R. A. Fischer, *Angew. Chem. Int. Ed.* **2018**, 57, 14372-14393; *Angew. Chem.* **2018**, 130, 14570-14593.
- [223] J. M. Goicoechea, S. C. Sevov, *Angew. Chem. Int. Ed.* **2005**, 44, 4026-4028; *Angew. Chem.* **2005**, 117, 4094-4096.
- [224] J. M. Goicoechea, S. C. Sevov, *J. Am. Chem. Soc.* **2006**, 128, 4155-4161.
- [225] S. Scharfe, T. F. Fässler, S. Stegmaier, S. D. Hoffman, K. Ruhland, *Chem. Eur. J.* **2008**, 14, 4479-4482.
- [226] E. N. Esenturk, J. Fettinger, Y. F. Lam, B. Eichhorn, *Angew. Chem. Int. Ed.* **2004**, 43, 2132-2134; *Angew. Chem.* **2004**, 116, 2184-2186.
- [227] E. N. Esenturk, J. Fettinger, B. Eichhorn, *Chem. Commun.* **2005**, 247-249.
- [228] E. N. Esenturk, J. Fettinger, B. Eichhorn, *J. Am. Chem. Soc.* **2006**, 128, 9178-9186.
- [229] E. N. Esenturk, J. C. Fettinger, B. W. Eichhorn, *J. Am. Chem. Soc.* **2006**, 128, 12-13.
- [230] B. Kesanli, J. E. Halsig, P. Zavalij, J. C. Fettinger, Y.-F. Lam, B. W. Eichhorn, *J. Am. Chem. Soc.* **2007**, 129, 4567-4574.
- [231] Germanium: J. M. Goicoechea, S. C. Sevov, *J. Am. Chem. Soc.* **2005**, 127, 7676-7677.
- [232] Tin: Z. M. Sun, H. Xiao, J. Li, L. S. Wang, *J. Am. Chem. Soc.* **2007**, 129, 9560-9561.
- [233] F. S. Kocak, P. Zavalij, Y.-F. Lam, B. W. Eichhorn, *Inorg. Chem.* **2008**, 47, 3515-3520.
- [234] J.-Q. Wang, S. Stegmaier, B. Wahl, T. F. Fässler, *Chem. Eur. J.* **2010**, 1793-1798.
- [235] H. N. Waltenburg, J. T. Yates, Jr., *Chem. Rev.* **1995**, 95, 1589-1673.
- [236] N. F. Borrelli, D. W. Hall, H. J. Holland, D. W. Smith, *J. Appl. Phys.* **1987**,

- 61, 12, 5399-5409.
- [237] W. L. Wilson, P. F. Szajowski, L. E. Brus, *Science*, **1993**, 262, 1242-1244.
- [238] T. Iwamoto, M. Tamura, C. Kabuto, M. Kira, *Science*, **2000**, 290, 504-506.
- [239] D. Scheschkewitz, *Angew. Chem. Int. Ed.* **2005**, 44, 2954-2956; *Angew. Chem.* **2005**, 117, 3014-3016.
- [240] M. Weidenbruch, S. Willms, W. Saak, G. Henkel, *Angew. Chemie Int. Ed. Engl.*, **1997**, 36, 2503-2504.
- [241] G. Fischer, V. Huch, P. Mayer, S. K. Vasisht, M. Veith, N. Wiberg, *Angew. Chem. Int. Ed.*, **2005**, 44, 7884-7887; *Angew. Chem.* **2005**, 117, 8096-8099.
- [242] D. Nied, R. Koppe, W. Kloppe, H. Schnöckel, F. Breher, *J. Am. Chem. Soc.*, **2010**, 132, 10264-10265.
- [243] K. Wakita, N. Tokitoh, R. Okazaki, S. Nagase, *Angew. Chem. Int. Ed.* **2000**, 39, 634-636.
- [244] K. Abersfelder, A. J. P. White, H. S. Rzepa, D. Scheschkewitz, *Science*, **2010**, 327, 564-566.
- [245] D. Kratzert, D. Leusser, J. J. Holstein, Birger Dittrich, K. Abersfelder, D. Scheschkewitz, D. Stalke, *Angew. Chem. Int. Ed.* **2013**, 52, 4478-4482; *Angew. Chem.* **2013**, 125, 4574-457.
- [246] E. Niecke, P. Becker, M. Nieger, D. Stalke, W. W. Schoeller, *Angew. Chem. Int. Ed.* **1995**, 34, 1849-1852; *Angew. Chem.* **1995**, 107, 2012-2015.
- [247] P. Jutzi, A. Mix, B. Rummel, W. W. Schoeller, B. Neumann, H.-G. Stammler, *Science* **2004**, 305, 849-851.
- [248] K. Leszczyńska, K. Abersfelder, A. Mix, B. Neumann, H.-G. Stammler, M. J. Cowley, P. Jutzi, D. Scheschkewitz, *Angew. Chem. Int. Ed.* **2012**, 51, 6785-6788; *Angew. Chem.* **2012**, 124, 6891-6895.
- [249] K. Leszczyńska, K. Abersfelder, M. Majumdar, B. Neumann, H.-G. Stammler, H. S. Rzepa, P. Jutzi, D. Scheschkewitz, *Chem. Commun.* **2012**, 48, 7820-7822.
- [250] K. Abersfelder, A. J. P. White, R. J. F. Berger, H. S. Rzepa, D. Scheschkewitz, *Angew. Chem. Int. Ed.* **2011**, 50, 7936-7939; *Angew. Chem.* **2011**, 123, 8082-8086.
- [251] T. Iwamoto, N. Akasaka, S. Ishida, *Nat. Commun.* **2014**, 5, 5353.

- [252] A. Tsurusaki, C. Iizuka, K. Otsuka, S. Kyushin, *J. Am. Chem. Soc.* **2013**, *135*, 16340-16343.
- [253] A. Tsurusaki, J. Kamiyama, S. Kysushin, *J. Am. Chem. Soc.* **2014**, *136*, 12896-12898.
- [254] J. Keuter, K. Schwedtmann, A. Hepp, K. Bergander, O. Janka, C. Doerenkamp, H. Eckert, C. Mück-Lichtenfeld, F. Lips, *Angew. Chem. Int. Ed.* **2017**, *56*, 13866-13871; *Angew. Chem.* **2017**, *129*, 14054-14059.
- [255] J. Keuter, C. Schwermann, A. Hepp, K. Bergander, J. Droste, M. R. Hansen, N. L. Doltsinis, C. Mück-Lichtenfeld, F. Lips, *Chem. Sci.* **2020**, *11*, 5895-5901.
- [256] D. Scheschkewitz, *Angew. Chem. Int. Ed.* **2004**, *43*, 2965-2967.
- [257] C. Strohmann, D. Schildbach, D. Auer, *J. Am. Chem. Soc.* **2005**, *127*, 7968-7971.
- [258] C. Strohmann, J. Hörnig, D. Auer, *Chem. Commun.* **2002**, 766-767.
- [259] K. I. Leszczyńska, V. Huch, C. Präsang, J. Schwabedissen, R. J. F. Berger, D. Scheschkewitz, *Angew. Chem. Int. Ed.* **2019**, *58*, 5124-5128; *Angew. Chem.* **2019**, *131*, 5178-5182.
- [260] N. X. Truong, M. Haertelt, B. K. A. Jaeger, S. Gewinner, W. Schöllkopf, A. Fielicke, O. Dopfer, *Int. J. Mass Spectrom.* **2016**, *395*, 1–6.
- [261] S.-J. Lu, X.-L. Xu, G.-J. Cao, H.-G. Xu, W.-J. Zheng, *J. Chem. Phys.* **2018**, *149*, 174314.
- [262] Y. Chang, G. Li, A. Gao, H. Chen, Q. Li, *Theor. Chem. Acc.* **2011**, *130*, 1009–1022.
- [263] S. Nigam, C. Majumder, S. K. Kulshreshtha, *J. Chem. Phys.* **2006**, *125*, 074303.
- [264] Y. Heider, P. Willmes, V. Huch, M. Zimmer, D. Scheschkewitz, *J. Am. Chem. Soc.* **2019**, *141*, 49, 19498-19504.
- [265] M. Weidenbruch, A. Schäfer, R. Rankers, *J. Organomet. Chem.* **1980** *195*, 171-184.
- [266] E. Hengge, H. G. Schuster, *J. Organomet. Chem.* **1982**, *231*, 17-20.
- [267] D. Seyferth, E. W. Goldman, J. Escudie, *J. Organomet. Chem.* **1984**, *271*, 337-352.
- [268] C. W. Carlson, R. West, *Organometallics* **1983**, *2*, 1798-1801.
- [269] B. Wrackmeyer, E. V. Klimkina, W. Milius, *Z. Anorg. Allg. Chem.* **2012**,

- 638, 1080-1092.
- [270] M. Unn, Phosphorus Sulfur and Silicon 2011, 186, 1259-1262.
- [271] H. Yodhida, Y. Takahara, T. Erata, W. Ando, *J. Am. Chem. Soc.* **1992**, *114*, 1098-1100.
- [272] N. Choi, K. Asano, W. Ando, *Organometallics* **1995**, *14*, 3146-3148.
- [273] N. Choi, K. Asano, N. Sato, W. Ando, *J. Organomet. Chem.* **1996**, *516*, 155-165.
- [274] L. C. Siemes, J. Keuter, A. Hepp, F. Lips, *Inorg. Chem.* **2019**, *58*, 13142-13149.
- [275] K. Schwedtmann, A. Hepp, K. Schwedtmann, J. J. Weigand, F. Lips, *Eur. J. Inorg. Chem.* **2019**, 4719-4726.
- [276] W. Wojnowski, B. Dręczewski, A. Herman, K. Peters, E.-M. Peters, H. G. von Schnering, *Angew. Chem. Int. Ed.* **1985**, *24*, 992-993; *Angew. Chem.* **1985**, *97*, 978-979.

6 Supporting Information

6.1 Site-selective functionalization of Si₆R₆ siliconoids

Electronic Supplementary Material (ESI) for Chemical Science.
This journal is © The Royal Society of Chemistry 2019

Supporting Information:

Site-Selective Functionalization of Si₆R₆ Siliconoids

Yannic Heider,[‡] Nadine E. Poitiers,[‡] Philipp Willmes, Kinga Leszczyńska, Volker Huch,
and David Scheschkewitz*

Krupp-Chair of General and Inorganic Chemistry, Saarland University, D-66123 Saarbrücken, Germany

Contents

<u>General Methods</u>	<u>S2</u>
<u>1. Preparation, data and spectra (NMR, UV-vis, IR) of:</u>	<u>S3</u>
<i>ligato</i> -TMS-substituted siliconoid 5a	S3
<i>ligato</i> -Benzoyl-substituted siliconoid 5b	S7
<i>privo</i> -Lithiated Anionic siliconoid 4Li	S11
<i>privo</i> -TMS-substituted siliconoid 6a	S16
<i>privo</i> -Benzoyl-substituted siliconoid 6b	S20
<i>privo</i> -Pivaloyl-substituted siliconoid 6c	S22
<i>privo</i> -Bis(dimethylamino)phosphinyl-substituted siliconoid 6d	S28
<i>privo</i> -Trichlorosilyl-substituted siliconoid 6e	S31
<i>privo</i> -Borate-substituted siliconoid 6f	S34
<u>2. Details on X-ray Diffraction Studies</u>	<u>S40</u>
<u>3. Plots of the Hammett parameter σ_m/σ_p vs ^{29}Si chemical shift of Si2</u>	<u>S46</u>

General

All manipulations were carried out under a protective atmosphere of argon, by using a glovebox or standard Schlenk techniques. Ethereal solvents were dried by heating to reflux over Na/benzophenone and distilled and stored under an atmosphere of argon. Hydrocarbons were dried over sodium or potassium. NMR spectra were recorded on a Bruker Avance III 300 NMR spectrometer (^1H = 300.13 MHz, ^{13}C = 75.46 MHz, ^{29}Si = 59.6 MHz, ^7Li = 116.64 MHz, ^{11}B = 96.3 MHz) and/or a Bruker Avance IV 400 NMR spectrometer (^1H = 400.13 MHz, ^{13}C = 100.6 MHz, ^{29}Si = 59.6 MHz) UV/Vis spectra were recorded on a Perkin-Elmer Lambda 35 spectrometer in quartz cells with a path length of 0.1 cm. Infrared spectra were measured with a Bruker Vertex 79 in a platinum ATR diamond cell. Elemental analyses were performed on an elemental analyzer Leco CHN-900 and/or an elemental vario Micro Cube. They are mostly low in carbon, which is tentatively attributed to incomplete combustion due to the formation of silicon carbide. Compounds **1**, **2** and **3** were prepared according to our published procedures.^{21, 22, 31, 32}

General procedure for the synthesis of *privo* and *ligato* functionalized siliconoids **5a-b** and **6a-f**.

The respective compounds are prepared by treating 1 equivalent of the anionic siliconoid **3Li** or **4Li** with 1 equivalent of Me_3SiCl (**5a**, **6a**), benzoylchloride (**5b**, **6b**), pivaloyl chloride (**6c**), $(\text{Me}_2\text{N})_2\text{PCl}$ (**6d**), SiCl_4 (**6e**), or $\text{H}_3\text{B}\cdot\text{SMe}_2$ (**6f**) in benzene or toluene at room temperature. After stirring for the indicated period of time, all volatiles are removed in vacuo and the crude product is filtered from hexane and crystallized from hexane or pentane.

Preparation of *ligato*-Trimethylsilyl-2,2,5,5,6-pentakis(2',4',6'-triisopropylphenyl)tetracyclo**[2.2.0.0^{1,3}.0^{3,6}]hexasilane (5a)**

Quantities: **3Li**, 325 mg (0.21 mmol); Me₃SiCl 25.24 mg (0.23 mmol); benzene (5 mL); stirring 4 h; crystallization from pentane. Yield: 120 mg (45 %) red crystals. **¹H-NMR** (300.13 MHz, tol-d₈, 223 K): δ = 7.61, 7.28 (C₁₀H₈), 7.21 (m, overlapping with C₁₀H₈, 3 H, Ar-H), 7.09 – 6.81 (m, overlapping with benzene-d₆, 12 H, Tip-CH), 5.32 (sept, ³J_{HH} = 6.44, 1H, Tip-*i*Pr-CHMe₂), 5.07 (sept, ³J_{HH} = 6.44, 1 H, Tip-*i*Pr-CHMe₂), 4.44 (sept, ³J_{HH} = 6.44, 2 H, Tip-*i*Pr-CHMe₂), 3.96 (sept, ³J_{HH} = 6.44, 2 H, Tip-*i*Pr-CH₃), 3.55 (sept, ³J_{HH} = 6.44, 1H, Tip-*i*Pr-CHMe₂), 3.28 (m, overlapping, together 3H, Tip-*i*Pr-CHMe₂), 2.73 (m, overlapping, together 6H, Tip-*i*Pr-CHMe₂), 2.22 (br, 2H, Tip-*i*Pr-CH₃), 1.98 (br, 2H, Tip-*i*Pr-CH₃), 1.76 (br, 3H, Tip-*i*Pr-CH₃), 1.53 - 1.07 (br, together 96H, Tip-*i*Pr-CH₃), 0.22 (s, 9H, Si-CH₃). **¹³C-NMR** (75.46 MHz, tol-d₈, 223 K): δ = 156.47, 155.65, 154.41, 154.15, 153.82, 153.15, 152.95, 151.94, 151.59, 150.59, 150.42, 150.14, 148.99, 148.89, 139.32, 139.07 (Ar-C), 133.88, 128.15, 126.06 (C₁₀H₈), 123.61, 123.45, 123.21, 123.04, 122.47, 122.08, 121.91, 121.24, 121.05 (Ar-CH), 38.37, 36.22, 36.09, 35.90, 35.14, 34.84, 34.46, 34.25, 32.05, 29.31 (Tip-*i*Pr-CH), 29.1884, 28.49, 27.26, 26.23, 25.35, 24.96, 24.58, 24.24, 24.05, 23.85, 23.42, 22.80 (Tip-*i*Pr-CH₃), 22.56 (Tip-*i*Pr-CH₂), 14.12 (Tip-*i*Pr-CH₃), 2.94 (Si-CH₃). **²⁹Si-NMR** (59.62 MHz, tol-d₈, 223 K): δ = 169.9 (s, *privo*-SiTip₂), 25.8 (s, *remoto*-SiTip₂), 11.3 (s, *ligato*-SiTip), -3.7 (s, *ligato*-Si-SiMe₃), -42.5 (s, SiMe₃), -257.8 (s, *nudo*-Si), -266.6 (s, *nudo*-Si). **Elemental analysis** calculated for C₈₁H₁₃₀Si₇: C, 74.81; H, 10.08. Found: C, 74.1; H, 9.95.

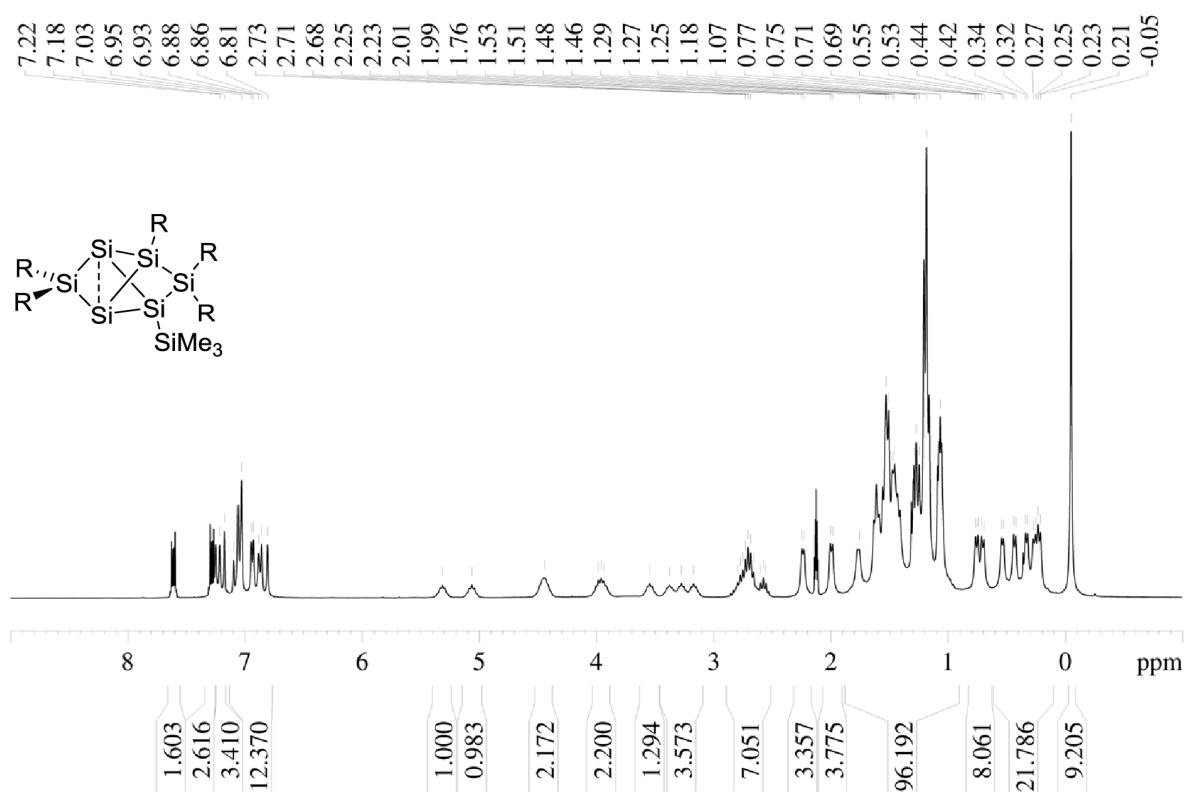


Figure S1: ¹H NMR of **5a** in C₆D₆ (300 MHz).

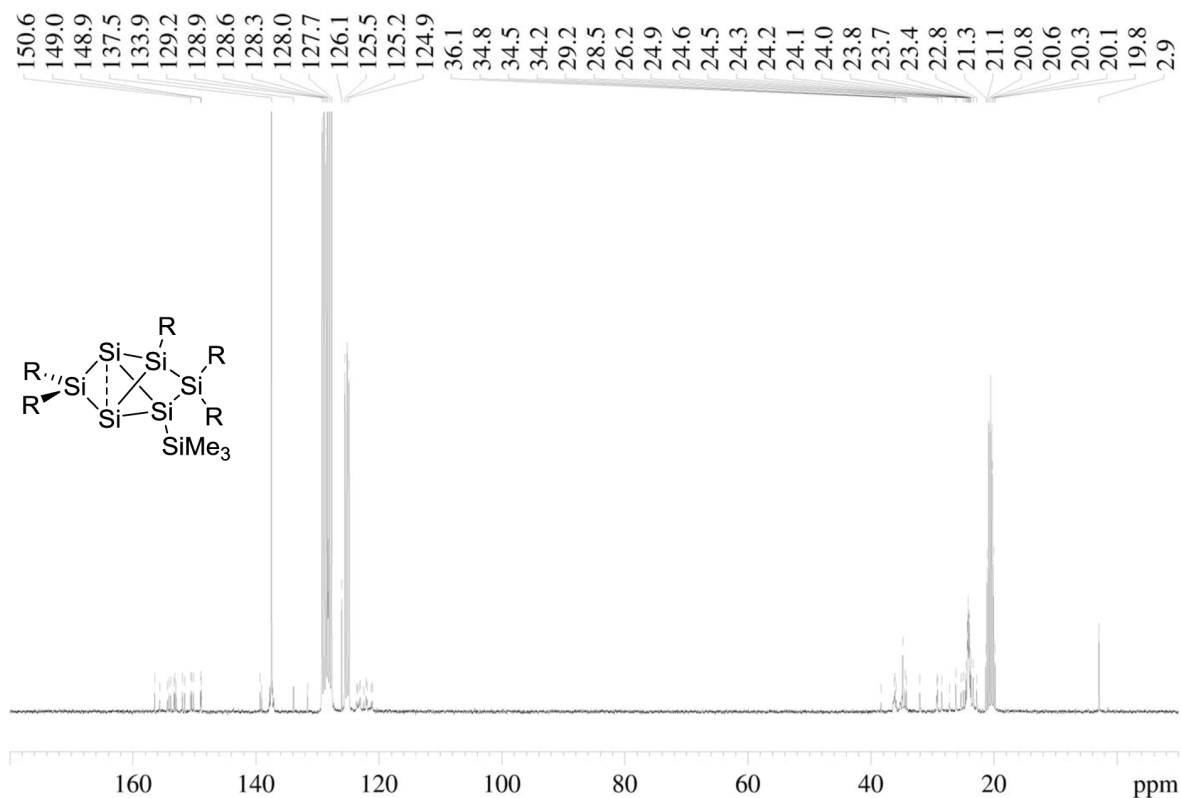


Figure S2: ¹³C NMR of **5a** in C₆D₆ (75.5 MHz).

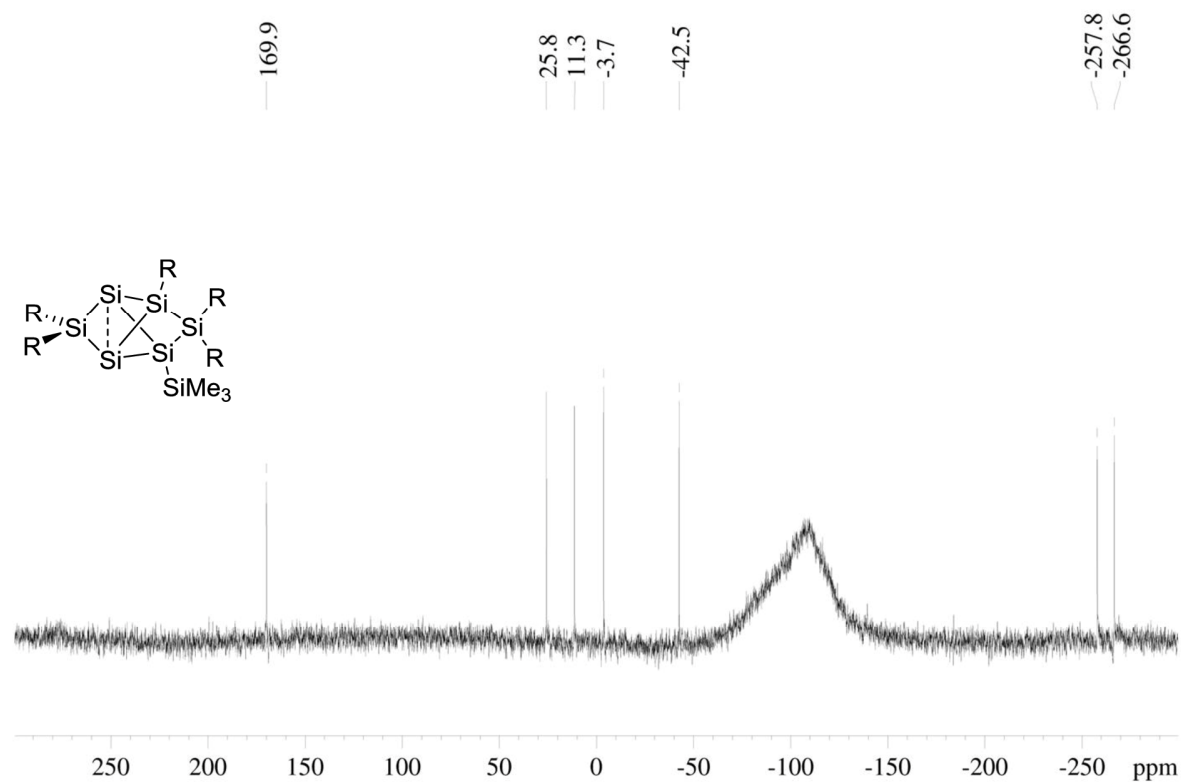


Figure S3: ²⁹Si NMR of **5a** in C₆D₆ (59.6 MHz).

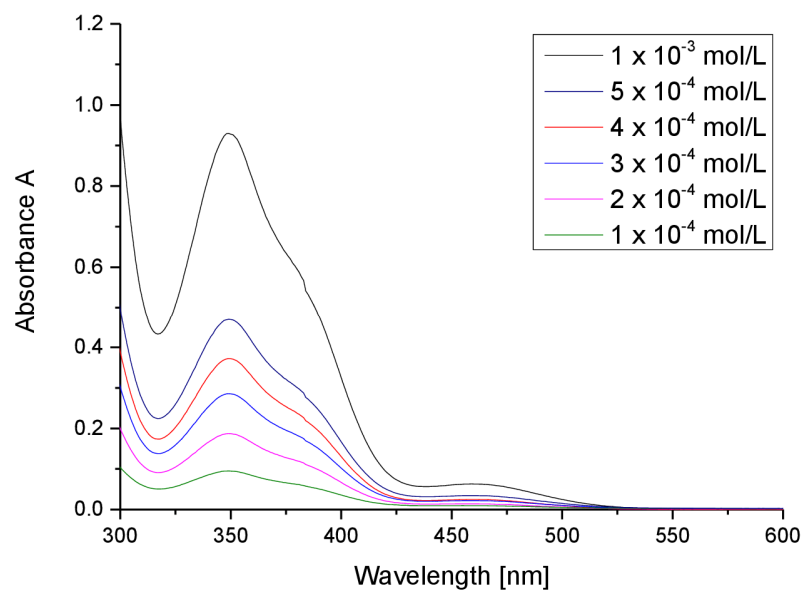


Figure S4: UV-Vis spectrum of **5a** in hexane at different concentrations.

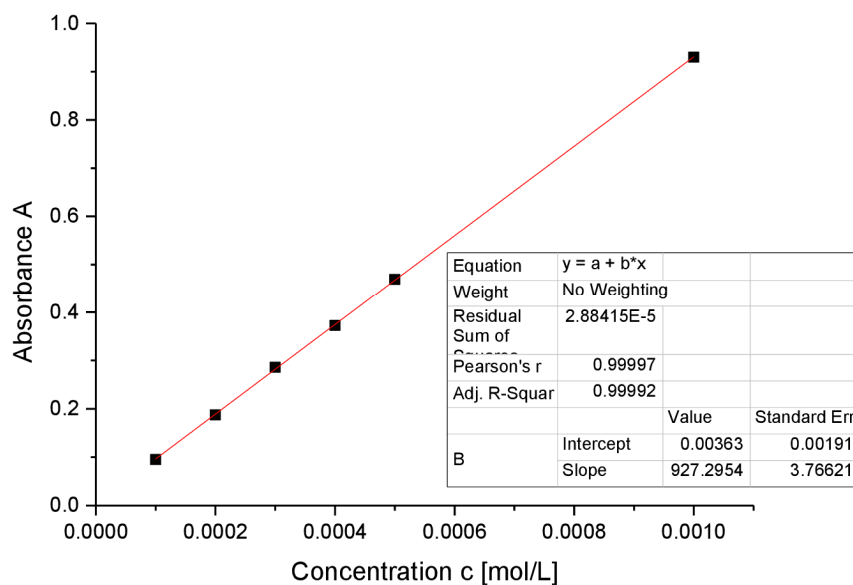


Figure S5: Determination of ε ($9273 \text{ M}^{-1} \text{ cm}^{-1}$) by linear regression of absorptions ($\lambda = 349 \text{ nm}$) of **5a** against concentration.

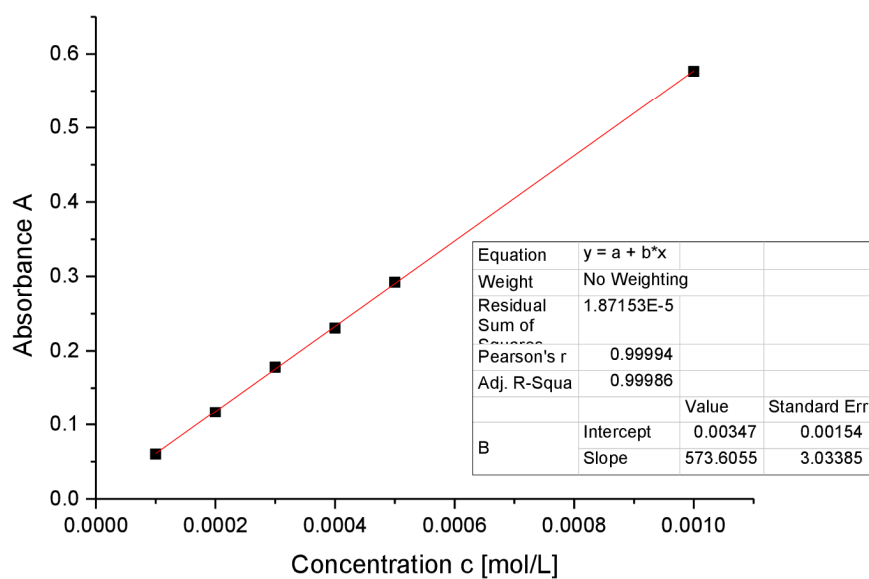


Figure S6: Determination of ε ($5736 \text{ M}^{-1} \text{ cm}^{-1}$) by linear regression of absorptions ($\lambda = 382 \text{ nm}$) of **5a** against concentration.

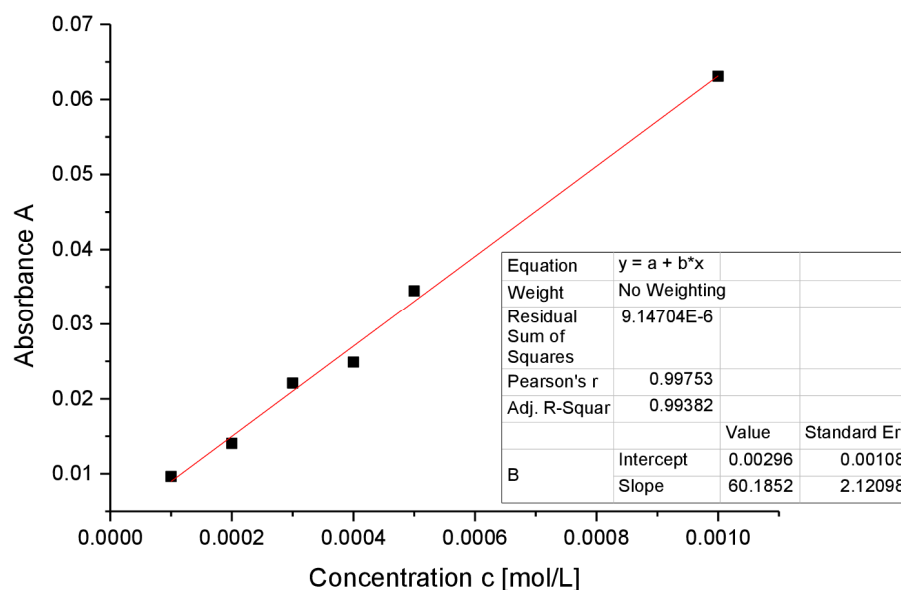


Figure S7: Determination of ϵ ($602 \text{ M}^{-1} \text{ cm}^{-1}$) by linear regression of absorptions ($\lambda = 459 \text{ nm}$) of **5a** against concentration.

Preparation of ligato-Benzoyl-2,2,5,5,6-pentakis(2',4',6'-triisopropyl-phenyl)tetracyclo

[2.2.0.0^{1,3}.0^{3,6}] hexasilane (5b)

Quantities: **3Li**, 500 mg (0.32 mmol); benzoylchloride 49.24 mg (0.35 mmol); benzene; stirring 4 h; crystallization from pentane. Yield: 270 mg (66 %) red crystals.

¹H-NMR (300.13 MHz, benzene-d₆, 300 K): δ = 7.87 (m, 1H, Ar-H) 7.62, 7.24 (C₁₀H₈), 7.07 - 6.79 (br, overlapping with benzene-d₆, 8H Tip-CH), 6.73 (s, 1H, Tip-CH), 5.05 - 4.82 (m, 2H, Tip-ⁱPr-CHMe₂), 4.38 - 4.13 (m, 2H, Tip-ⁱPr-CHMe₂), 4.03 - 3.48 (m, 4H, Tip-ⁱPr-CHMe₂), 3.22 - 2.89 (m, 2H, Tip-ⁱPr-CHMe₂), 2.82 - 2.48 (m, 5H, Tip-ⁱPr-CHMe₂) 2.33 (sept, ³J_{HH} = 6.8 Hz, 1H, Tip-ⁱPr-CHMe₂), 2.1, 2.07 (br, 3H, Tip-ⁱPr-CH₃), 1.87 - 0.12 (m, overlapping with hexane, 112H, Tip-ⁱPr-CH₃). **¹³C-NMR** (75.46 MHz, benzene-d₆, 300 K): δ = 155.99, 154.64, 152.59, 151.01, 150.59, 150.23, 149.53, 143.49, 136.75, 136.38, 136.09 (Ar-C), 133.90 (C₁₀H₈), 132.42, 128.89 (Ar-CH), 128.19 (C₁₀H₈), 127.87, 127.55 (Ar-C), 125.88 (C₁₀H₈), 123.55, 123.09, 122.51, 122.24, 122.04, 121.32, 120.99 (br, Ar-CH), 37.61, 36.79, 36.39, 35.99, 35.52, 34.34, 34.59, 34.49, 34.27, 34.17, 33.86 (Tip-ⁱPr-CH), 28.21, 28.11, 27.34, 27.19, 27.09, 25.54, 24.92, 24.74, 24.28, 24.05, 23.86, 23.76, 23.53, 23.24 (Tip-ⁱPr-CH₃), 22.54 (Tip-ⁱPr-CH₂), 22.43, 14.11 (Tip-ⁱPr-CH₃). **²⁹Si-NMR** (59.62 MHz, benzene-d₆, 300 K): δ = 174.7 (s, *privo*-SiTip₂), 17.1 (s, *ligato*-SiTip), 8.7 (s, *remoto*-SiTip₂), -26.5 (s, *ligato*-Si-C=O), -263.0 (s, *nudo*-Si), -279.0 (s, *nudo*-Si).

Elemental analysis calculated for C₈₂H₁₂₀OSi₆: C, 76.33; H, 8.91. Found: C, 74.96; H, 9.60.

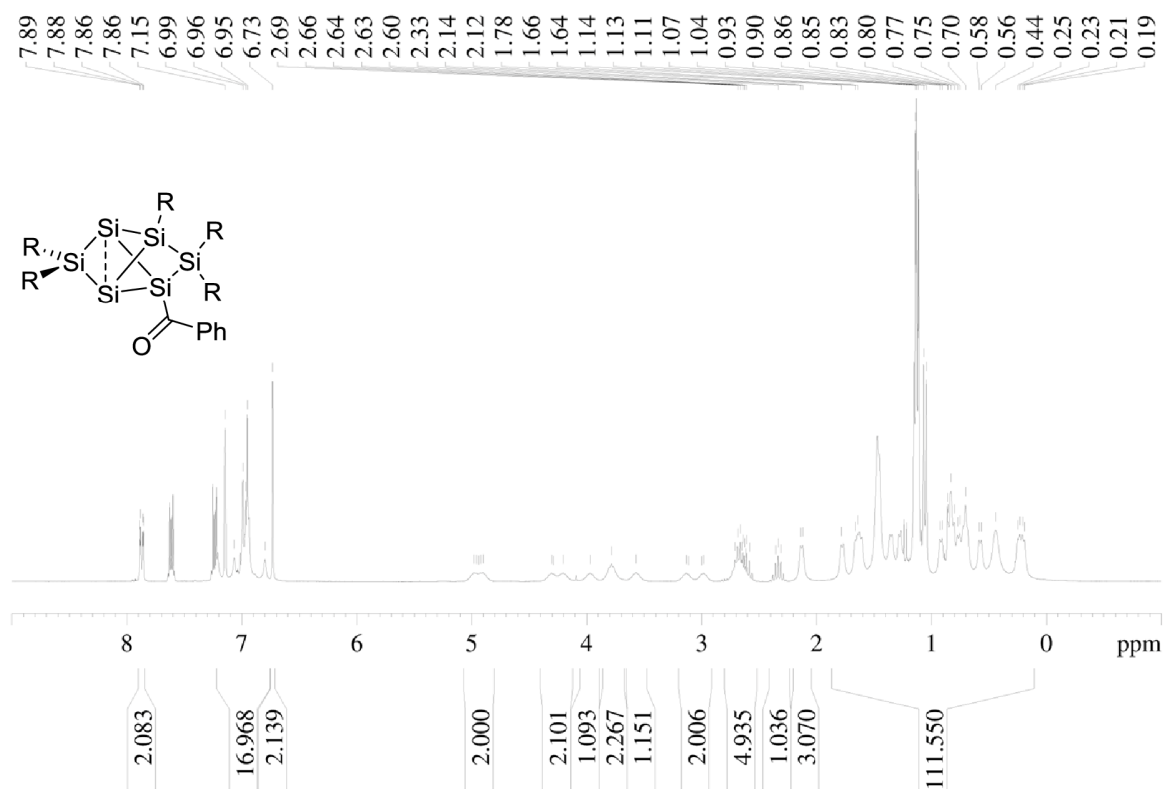


Figure S8: ¹H NMR of **5b** in C₆D₆ (300 MHz).

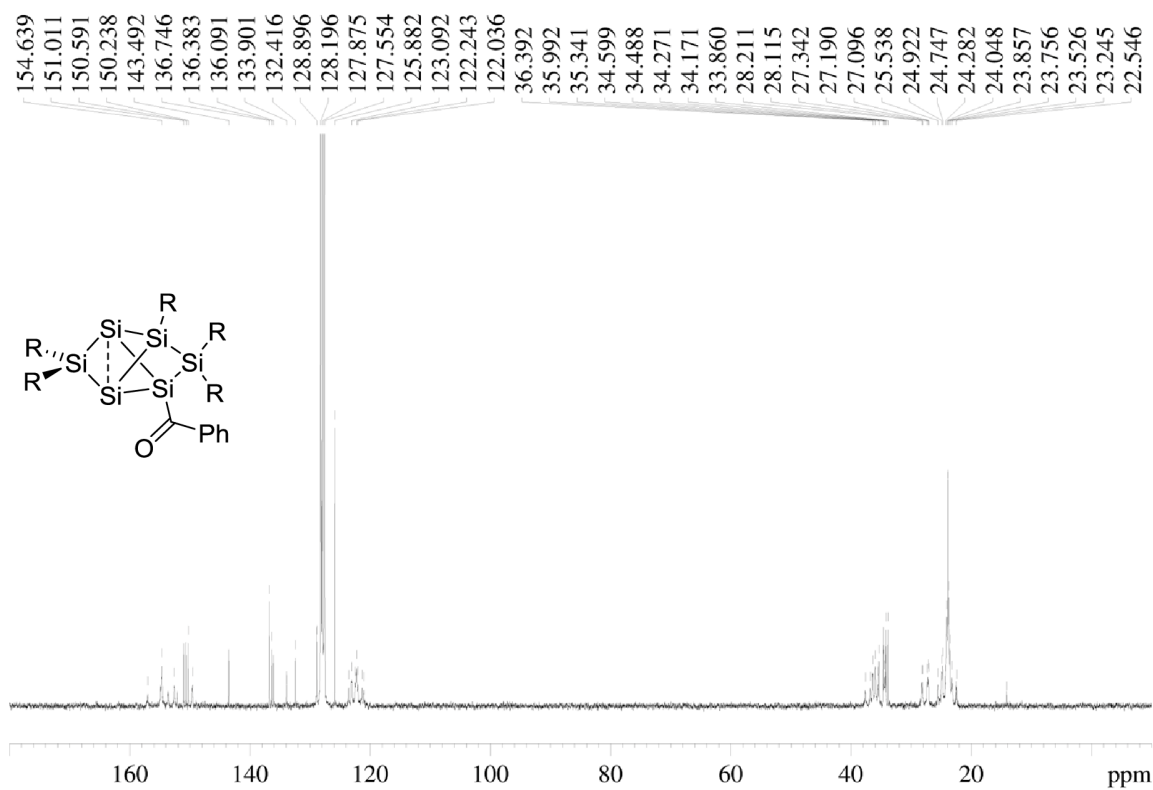


Figure S9: ¹³C NMR of **5b** in C₆D₆ (75.5 MHz).

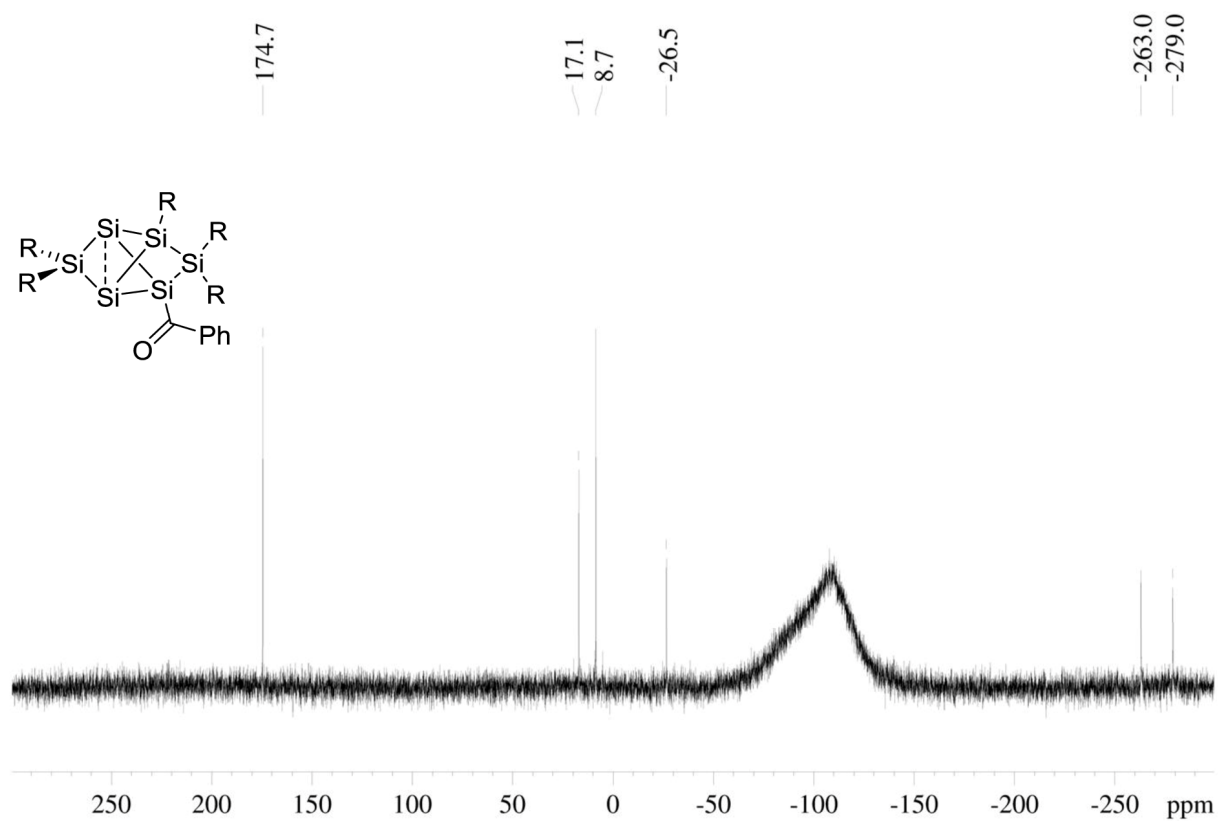


Figure S10: ^{29}Si NMR of **5b** in C_6D_6 (59.6 MHz).

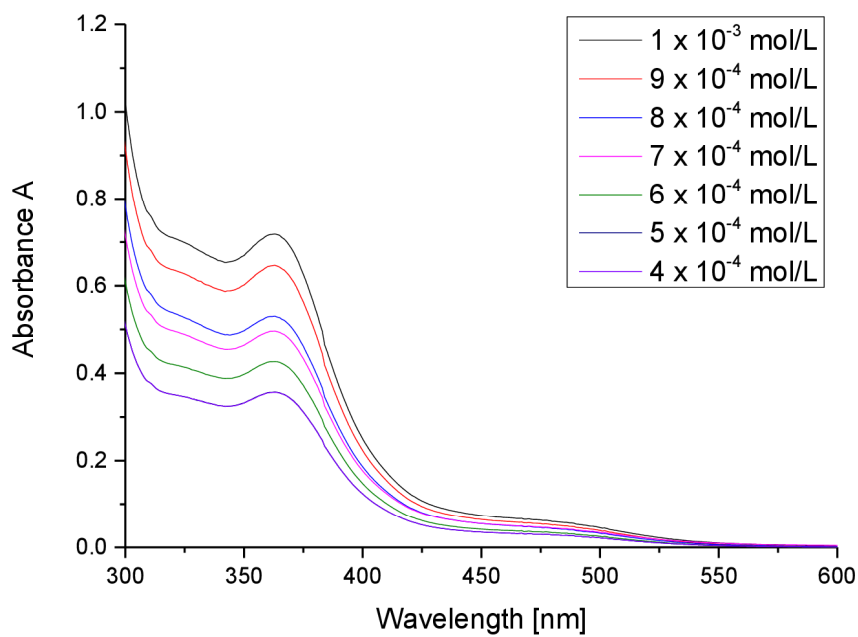


Figure S11: UV-Vis spectrum of **5b** in hexane at different concentrations.

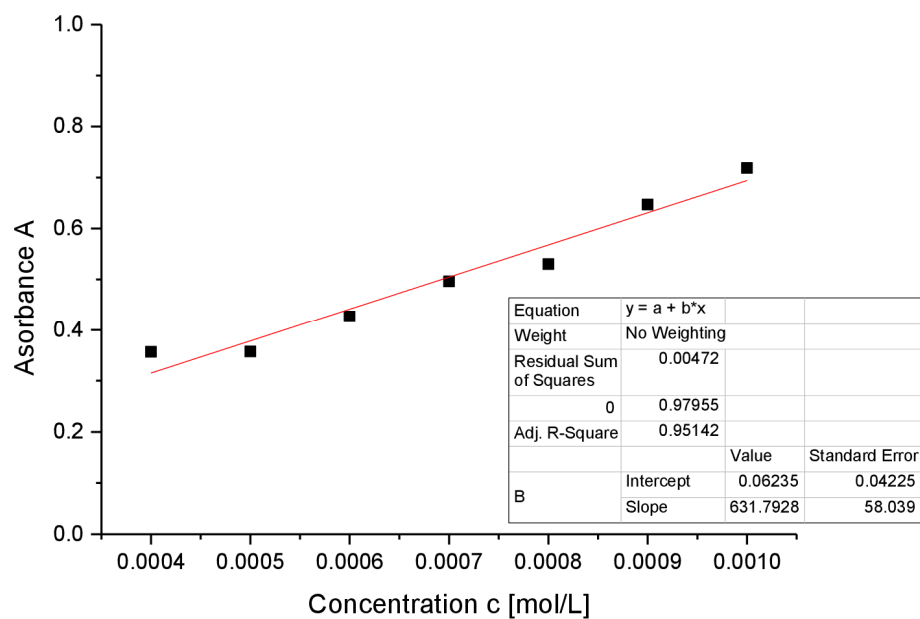


Figure S12: Determination of ϵ ($6318 \text{ M}^{-1} \text{ cm}^{-1}$) by linear regression of absorptions ($\lambda = 363 \text{ nm}$) of **5b** against concentration.

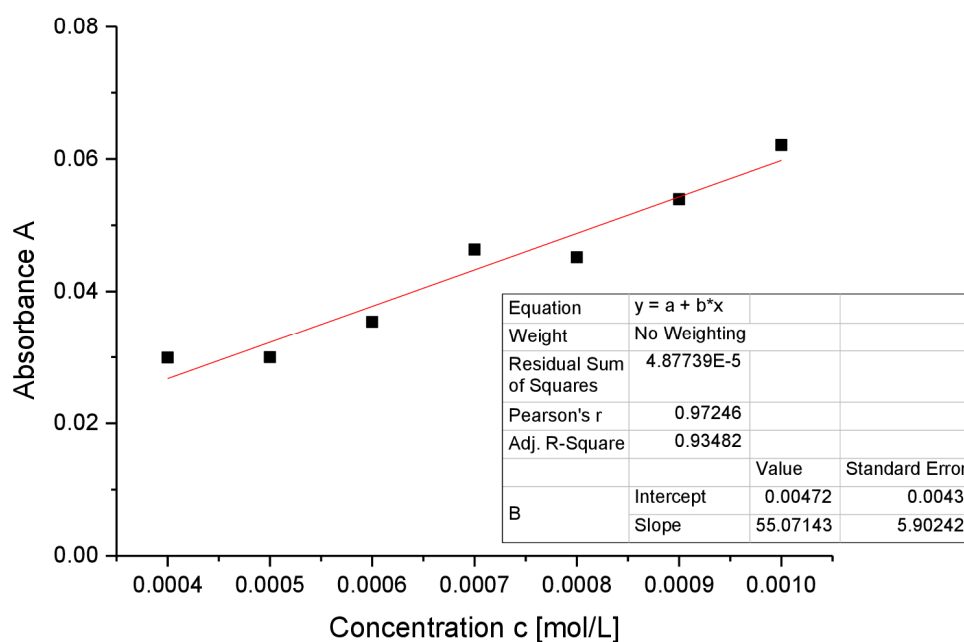


Figure S13: Determination of ϵ ($551 \text{ M}^{-1} \text{ cm}^{-1}$) by linear regression of absorptions ($\lambda = 477 \text{ nm}$) of **5b** against concentration.

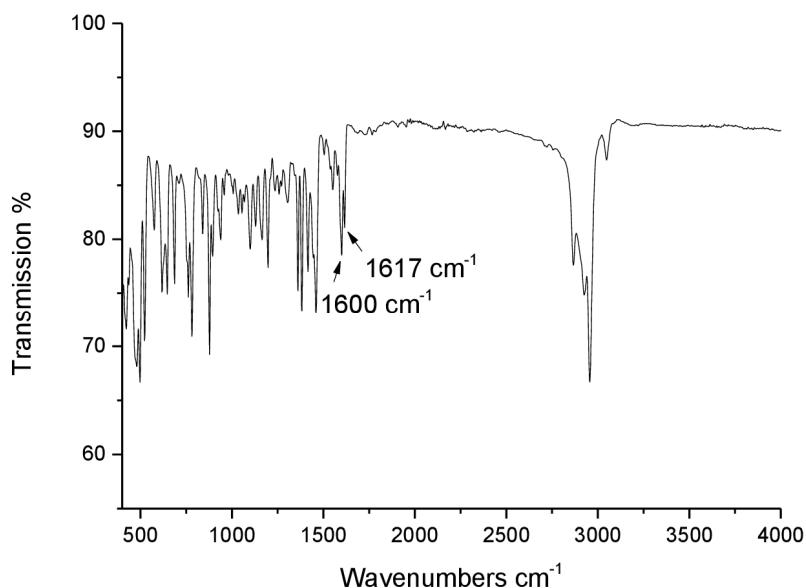


Figure S14: Infrared spectrum of **5b** (powder).

Preparation of *privo*-Lithiated anionic siliconoid **4Li**

***privo*-Lithio-2,4,5,5,6-pentakis(2',4',6'-triisopropylphenyl) tetracyclo [2.2.0.0^{1,3}.0^{3,6}]hexasilane (**4Li**)**

A solution of 2.39 g of siliconoid **3** (1.72 mmol) in 6 mL of Et₂O is cooled to -78°C . Lithium/naphthalene solution in thf (7.6 mL, 0.5 M, 3.78 mmol) is added dropwise and the resulting reaction mixture allowed warming to room temperature overnight with vigorous stirring. All volatiles are removed in vacuum and the resulting residue is washed three times with hexane. The final product **4Li** remains as pale-orange microcrystals. (1.42 g; 60% yield). ¹H NMR (300.13 MHz, benzene-d₆, 300K): δ = 7.28 (d, 1H, Tip-H), 7.27 (d, 1H, Tip-H), 7.05 (d, 1H, Tip-H), 7.00 (s, 2H, Tip-H), 6.94 (d, 1H, Tip-H), 6.93 (s, 1H, Tip-H), 6.84, 6.83 (each d, each 1H, Tip-H), 5.45 (sept, 1H, ⁱPr-CH), 5.15 – 5.00 (m, 2H, ⁱPr-CH), 4.57 (sept, 1H, ⁱPr-CH), 4.45 (sept, 1H, ⁱPr-CH), 4.18 (sept, 2H, ⁱPr-CH), 3.64 (sept, 1H, ⁱPr-CH), 3.44 – 3.30 (m, 2H, ⁱPr-CH), 3.04 (t, 8H, thf), 2.83 – 2.65 (m, 5H, ⁱPr-CH), 2.17, 2.14 (each d, together 6H, ⁱPr-CH₃), 1.74 (t, 6H, ⁱPr-CH₃), 1.67, 1.62, 1.57 (each d, each 3H, ⁱPr-CH₃), 1.50 (d, 9H, ⁱPr-CH₃), 1.45 (d, 3H, ⁱPr-CH₃) 1.25 – 1.11 (m, 38H, ⁱPr-CH₃ and thf), 0.95 (d, 6H, ⁱPr-CH₃), 0.75 (t, 6H, ⁱPr-CH₃), 0.69 – 0.62 (m, 9H, ⁱPr-CH₃) 0.37, 0.34 (each d, together 6H, ⁱPr-CH₃). ⁷Li NMR (116.6 MHz, benzene-d₆, 300K): δ = 0.29 (s). ¹³C NMR (75.5 MHz, benzene-d₆, 300K): δ = 158.3, 156.4, 156.1, 156.0, 153.8, 153.5, 152.5, 152.5, 151.0, 149.3, 148.8, 148.4, 148.3, 147.5, 146.3, 140.9, 139.8, 131.7, 131.5 (Ar-C), 123.0, 122.6, 122.4, 122.2, 121.4, 121.3, 120.9, 120.1, 119.8 (Ar-CH), 68.5 (thf), 36.8, 36.7, 36.5, 36.3, 36.1, 36.0, 35.1, 34.9, 34.8, 34.7, 34.6, 30.2, 28.1, 27.8, 27.5, 27.1, 26.7, 25.6 (Tip-ⁱPr-CH and Tip-ⁱPr-CH₃), 25.2 (thf), 25.2, 24.9, 24.9, 24.8, 24.7, 24.6, 24.5, 24.3, 24.2 23.6, 22.6, 22.0 (Tip-

i Pr-CH and Tip- i Pr-CH₃). **^{29}Si NMR** (59.6 MHz, benzene- d_6 , 300K): δ = 267.9 (br, *privo*-SiTipLi), 100.2 (s, *ligato*-Si), 15.3 (s, *remoto*-Si), -43.8 (s, *ligato*-Si), -222.2 (s, *nudo*-Si), -231.4 (s, *nudo*-Si). **Elemental analysis** calculated for C₈₃H₁₃₁LiO₂Si₆: C, 74.60; H, 9.88. Found: C, 72.68; H, 9.51.

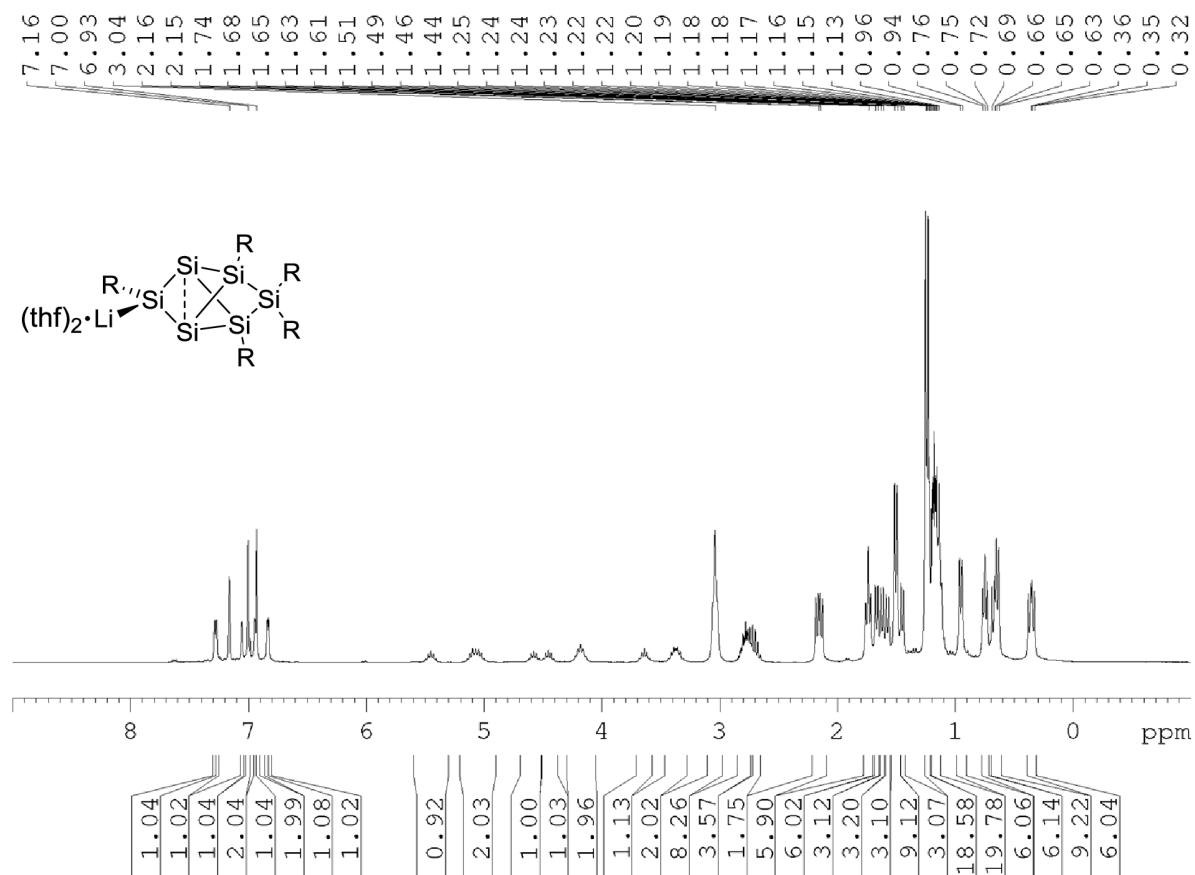


Figure S15: ^1H NMR of **4Li** in C_6D_6 (300 MHz).

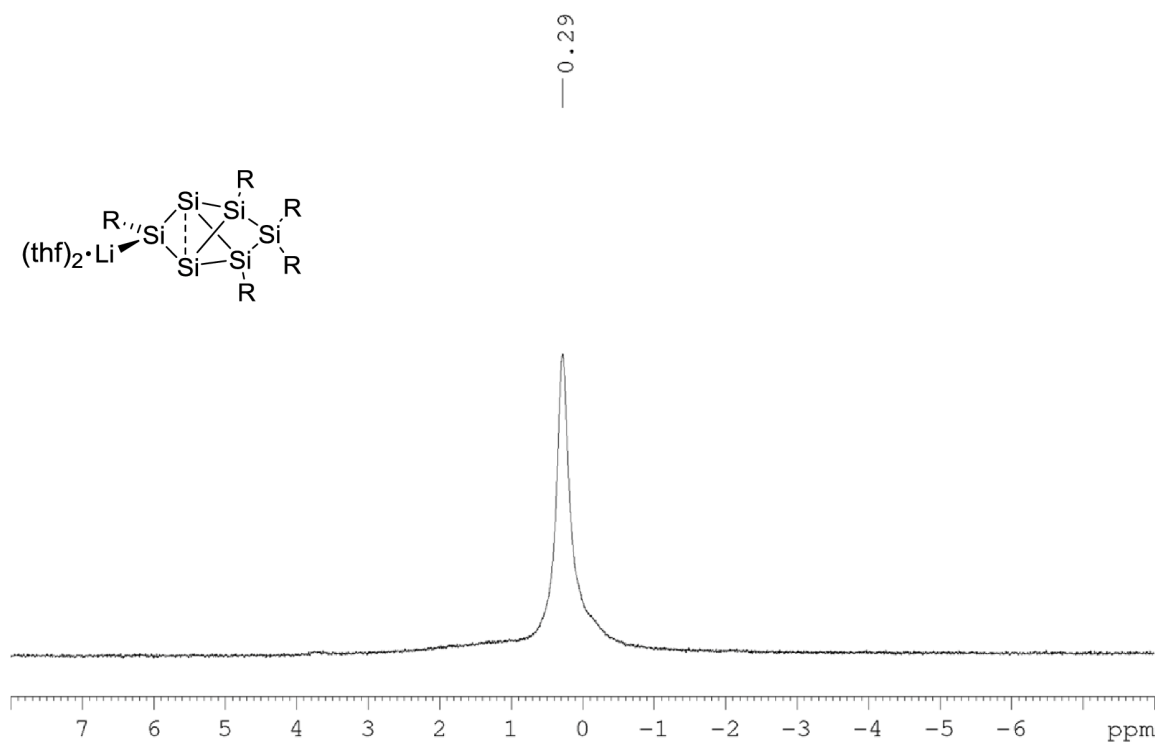


Figure S16: ^7Li NMR of **4Li** in C_6D_6 (116.6 MHz).

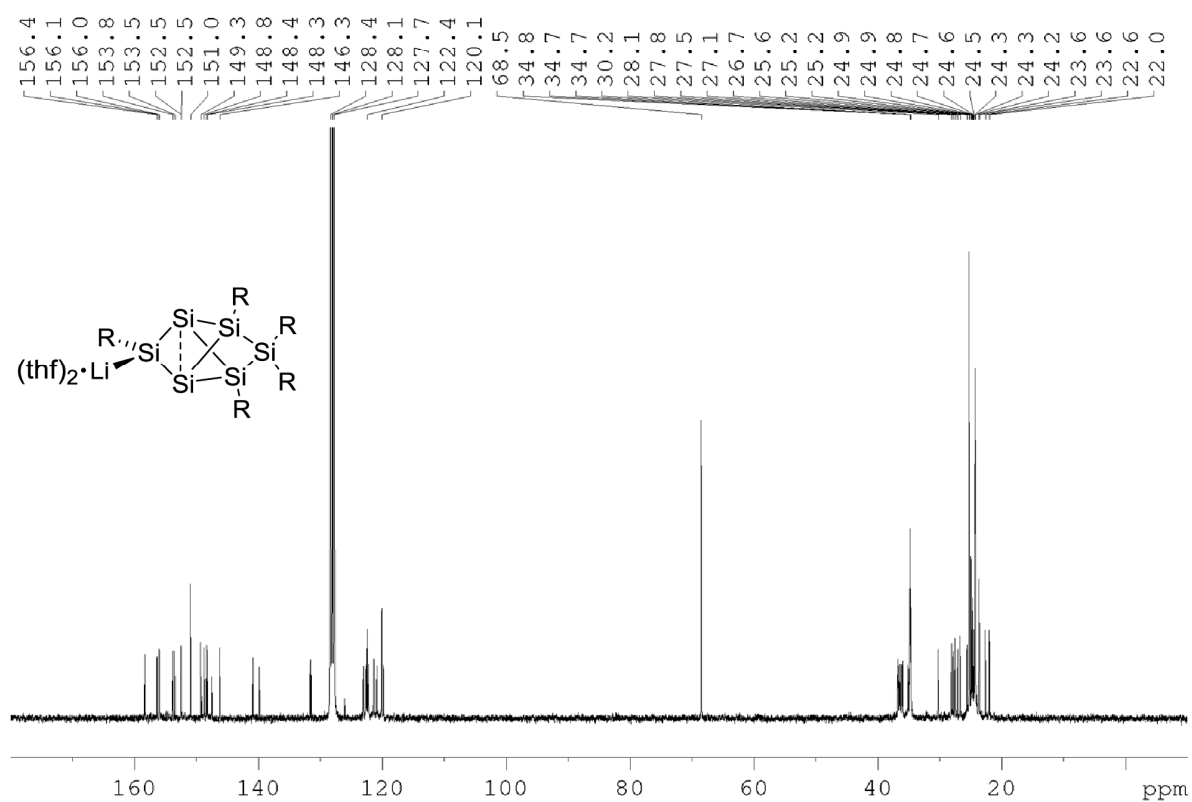


Figure S17: ^{13}C NMR of **4Li** in C_6D_6 (75.5 MHz).

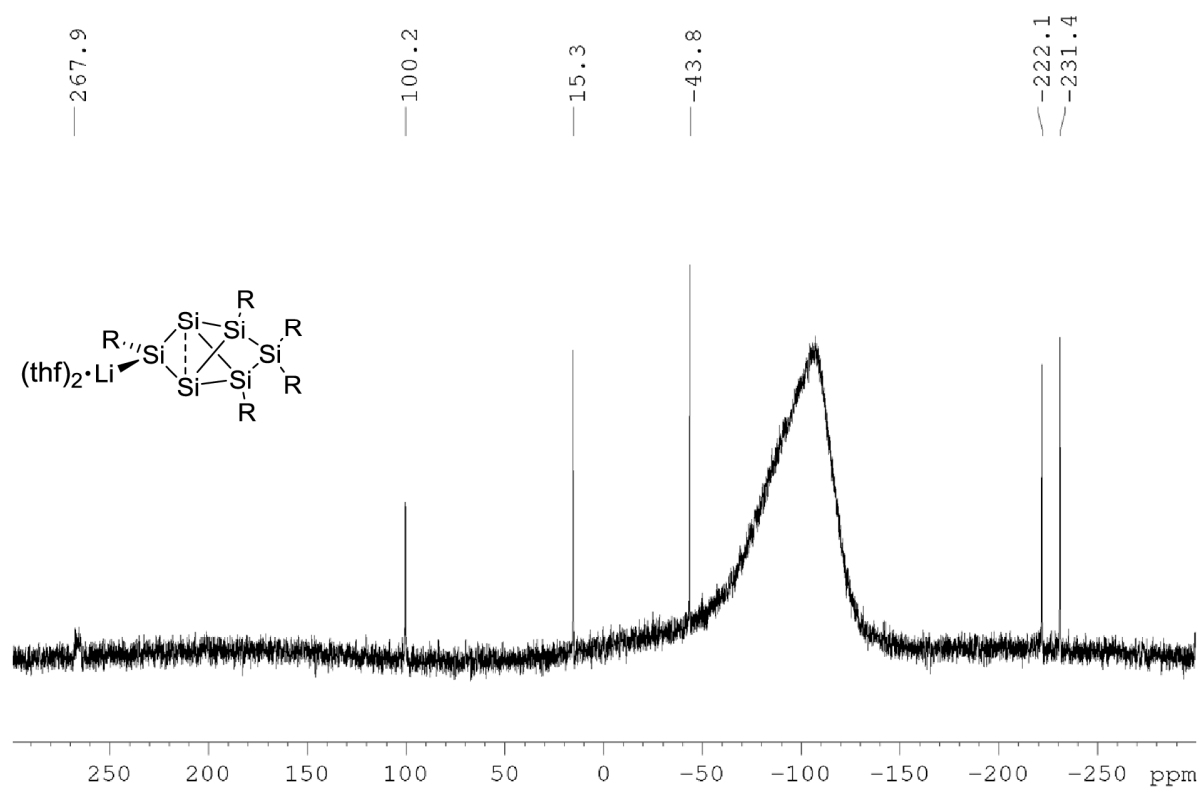


Figure S18: ^{29}Si NMR of **4Li** in C_6D_6 (59.6 MHz).

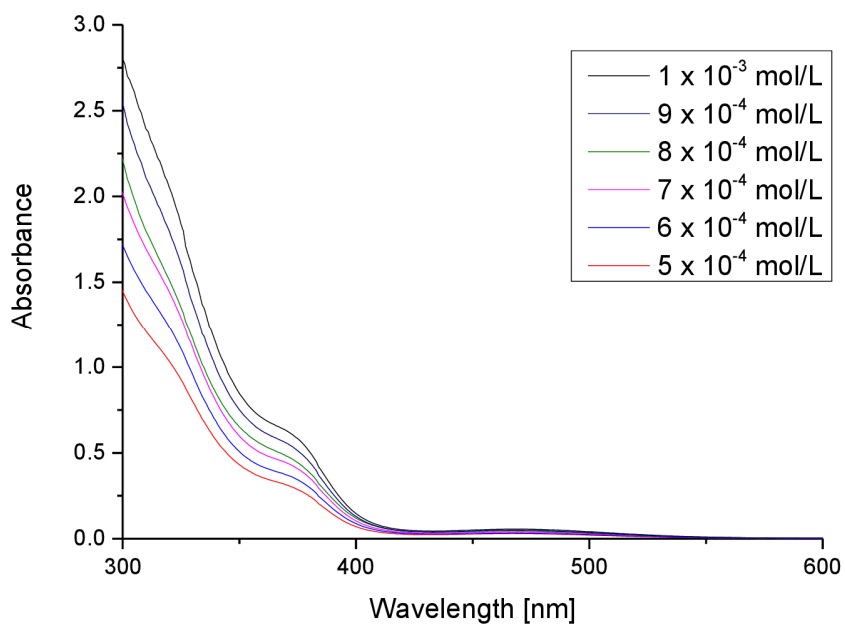


Figure S19: UV-Vis spectrum of **4Li** in hexane at different concentrations.

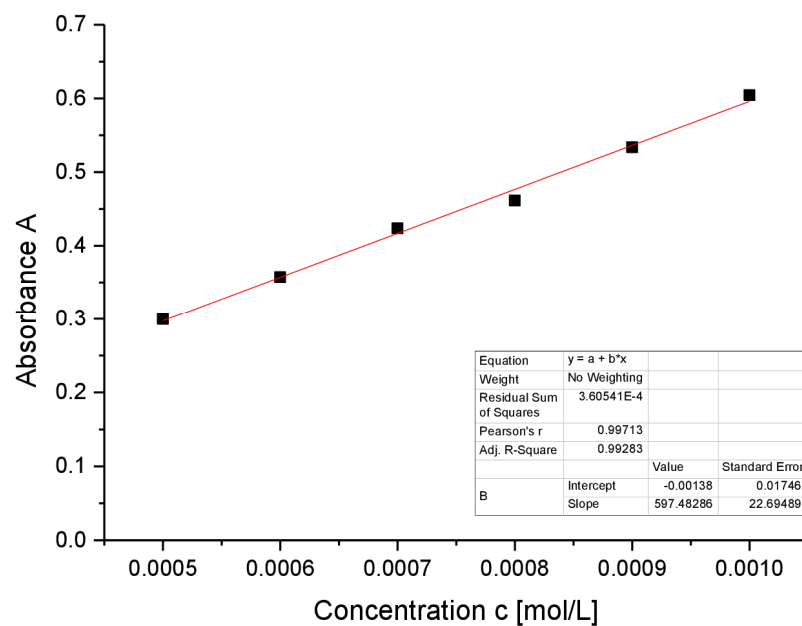


Figure S20: Determination of ε ($5974 \text{ M}^{-1} \text{ cm}^{-1}$) by linear regression of absorptions ($\lambda = 373 \text{ nm}$) of **4Li** against concentration.

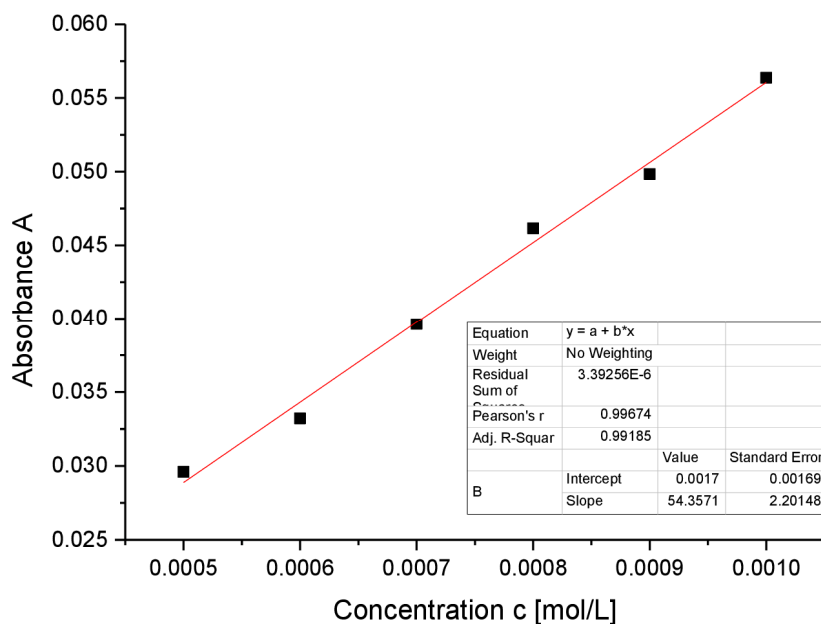


Figure S21: Determination of ε ($543 \text{ M}^{-1} \text{ cm}^{-1}$) by linear regression of absorptions ($\lambda = 468 \text{ nm}$) of **4Li** against concentration.

Preparation of *privo*-Trimethylsilyl-2,4,5,5,6-pentakis(2',4',6'-triisopropylphenyl)tetracyclo**[2.2.0.0^{1,3}.0^{3,6}]hexasilane (6a)**

Quantities: **4Li**, 104 mg (0.078 mmol); Me₃SiCl 11 g (9.39 mg, 0.086 mmol); toluene (2 mL); stirring 2.5 h; crystallization from hexane. Yield: 65 mg (66 %) orange crystals.

¹H NMR (300.13 MHz, benzene-d₆, 300K): δ = 7.27 (d, 2H, Tip-H), 7.07, 7.01, 6.97, 6.91, 6.83 (each d, each 1H, Tip-H), 6.80 (d, 2H, Tip-H), 6.75 (d, 1H, Tip-H), 4.93 (m, 2H, ⁱPr-CH), 4.37 (sept, 1H, ⁱPr-CH), 4.06 (sept, 2H, ⁱPr-CH), 3.74, 3.63 (each m, each 1H, ⁱPr-CH), 3.57 (t, 10H, thf), 3.37 (m, 2H, ⁱPr-CH), 2.71 (m, 6H, ⁱPr-CH), 2.14 (d, 3H, ⁱPr-CH₃), 2.05 (d, 3H, ⁱPr-CH₃), 1.82 (d, 3H, ⁱPr-CH₃), 1.67 (m, 7H, ⁱPr-CH₃), 1.57 (m, 14H, ⁱPr-CH₃), 1.43 (br, 10H, thf), 1.24, 1.21, 1.20, 1.18, 1.17, 1.16, 1.15, 1.13, 1.11, 1.08 (each d, overall 36H, ⁱPr-CH₃), 0.79 (d, 3H, ⁱPr-CH₃), 0.67 (t, 6H, ⁱPr-CH₃), 0.51 (m, 6H, ⁱPr-CH₃), 0.40, 0.38 (each d, overall 6H, ⁱPr-CH₃), 0.29 (d, 3H, ⁱPr-CH₃), -0.15 (s, 9H, Si(CH₃)₃). **¹³C NMR** (75.5 MHz, benzene-d₆, 300K): δ = 157.1, 156.9, 156.6, 156.1, 153.7, 153.2, 152.6, 152.0, 150.7, 150.2, 149.9, 149.4, 149.2, 138.7, 138.3, 134.8, 129.1, 126.9, 123.7 (Ar-C), 123.1, 122.8, 122.6, 122.4, 122.2, 122.1, 121.7, 121.6, 121.3, 121.0 (Ar-CH), 37.7, 37.6, 37.3, 36.9, 36.7, 36.4, 35.1, 35.0, 34.8, 34.7, 34.6, 34.5, 27.8, 27.6, 27.4, 27.1, 27.0, 26.5, 26.4, 26.2, 25.7, 25.4, 25.3, 25.1, 25.0, 24.9, 24.6, 24.4, 24.3, 24.1, 24.0, 23.9, 22.6 (Tip-ⁱPr-CH and Tip-ⁱPr-CH₃), 1.5 (Si(CH₃)₃). **²⁹Si NMR** (59.6 MHz, benzene-d₆, 300K): δ = 193.6 (s, *privo*-Si(Tip)SiMe₃), 29.2 (s, *remoto*-SiTip₂), 22.4 (s, *ligato*-SiTip), -11.2 (s, SiMe₃), -15.9 (s, *ligato*-SiTip), -242.0 (s, *nudo*-Si), -253.3 (s, *nudo*-Si). **Elemental analysis** calculated for C₇₈H₁₂₄Si₇: C, 74.45; H, 9.93. Found: C, 71.65; H, 9.83.

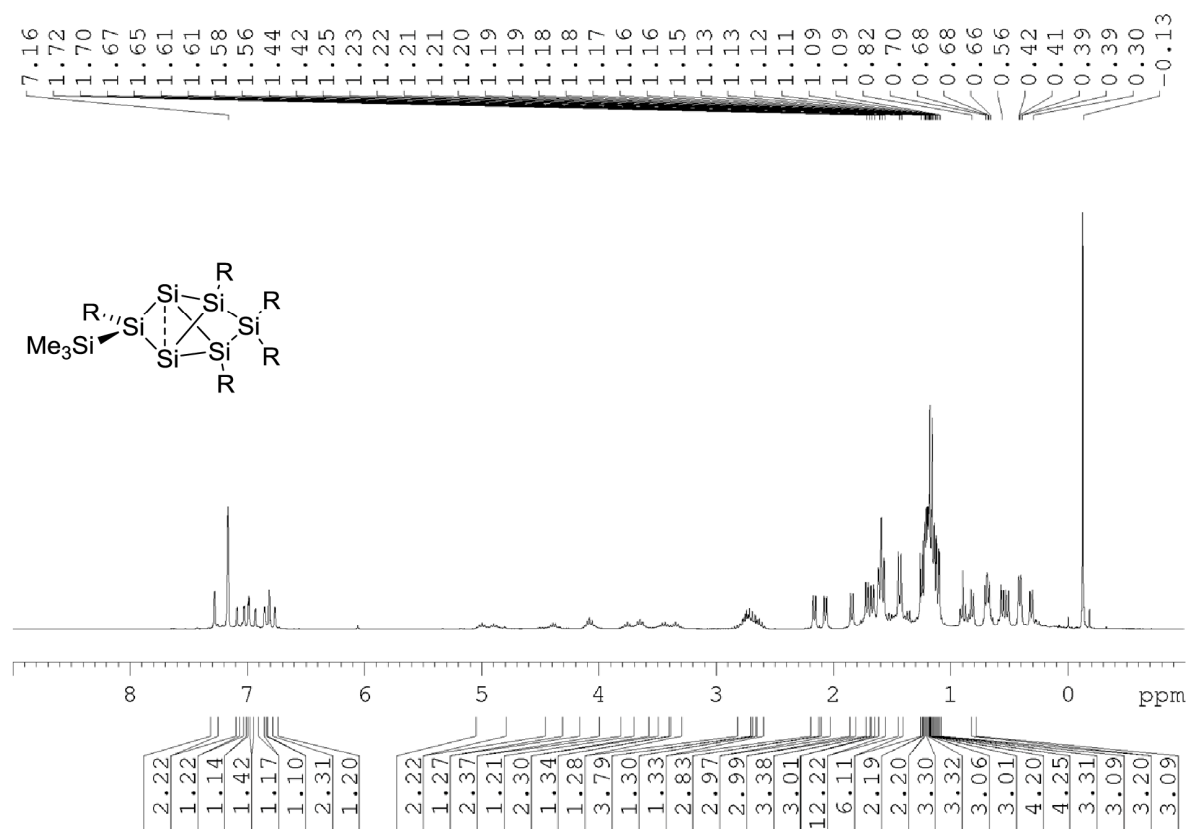


Figure S22: ^1H NMR of **6a** in C_6D_6 (300 MHz).

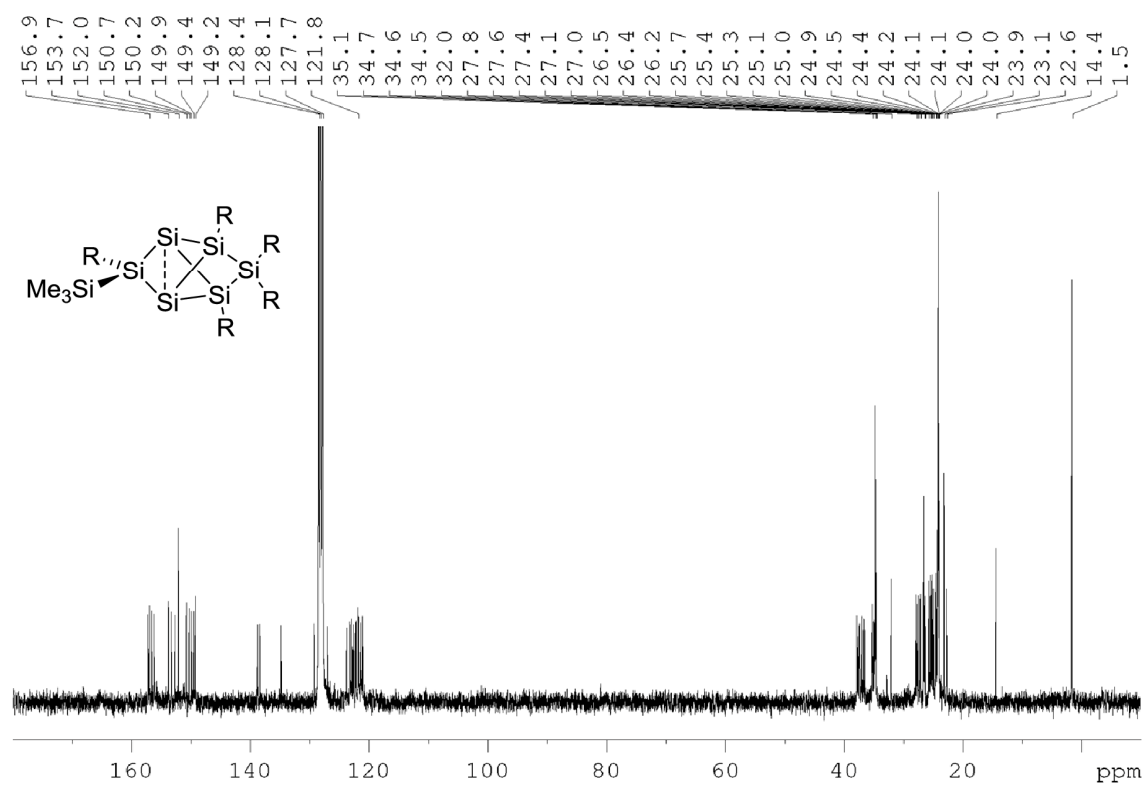


Figure S23: ^{13}C NMR of **6a** in C_6D_6 (75.5 MHz).

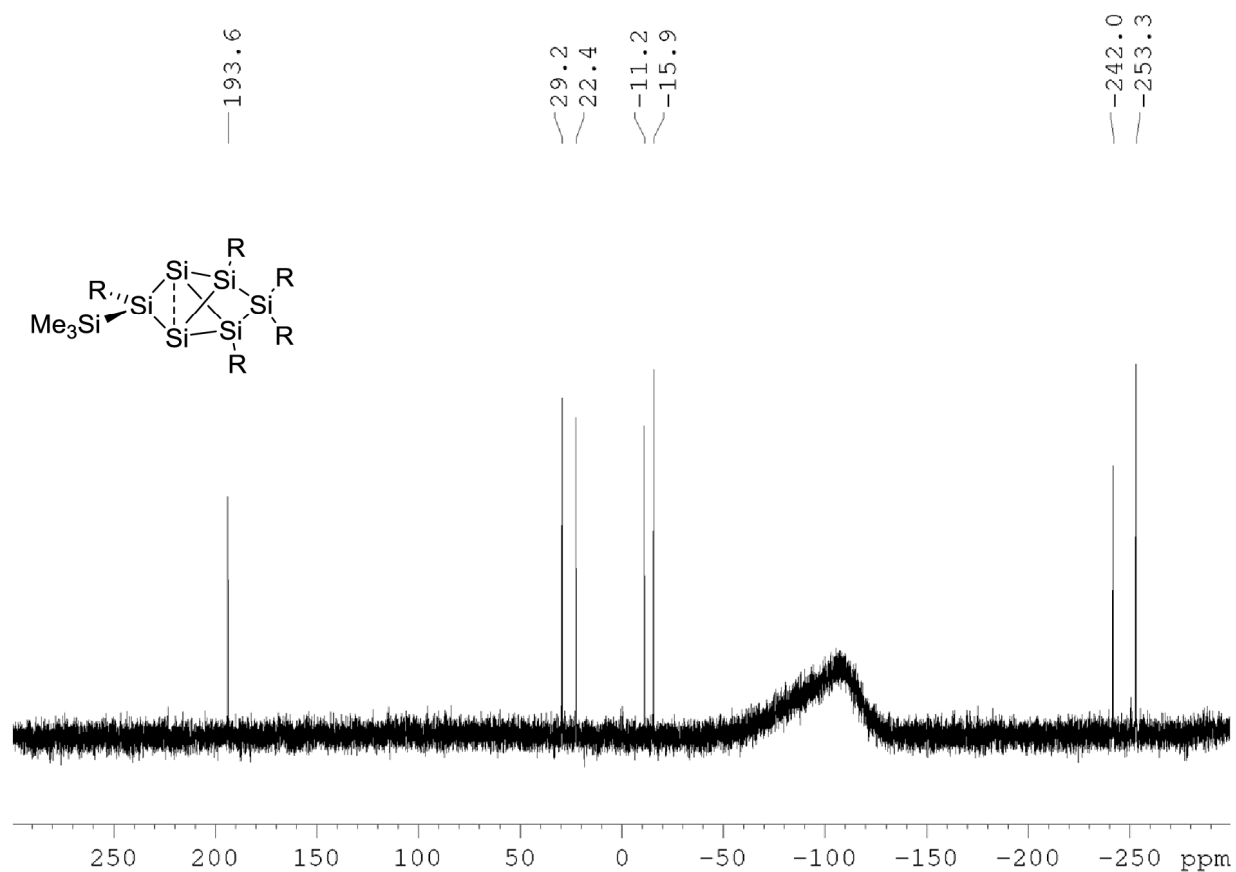


Figure S24: ^{29}Si NMR of **6a** in C_6D_6 (59.6 MHz).

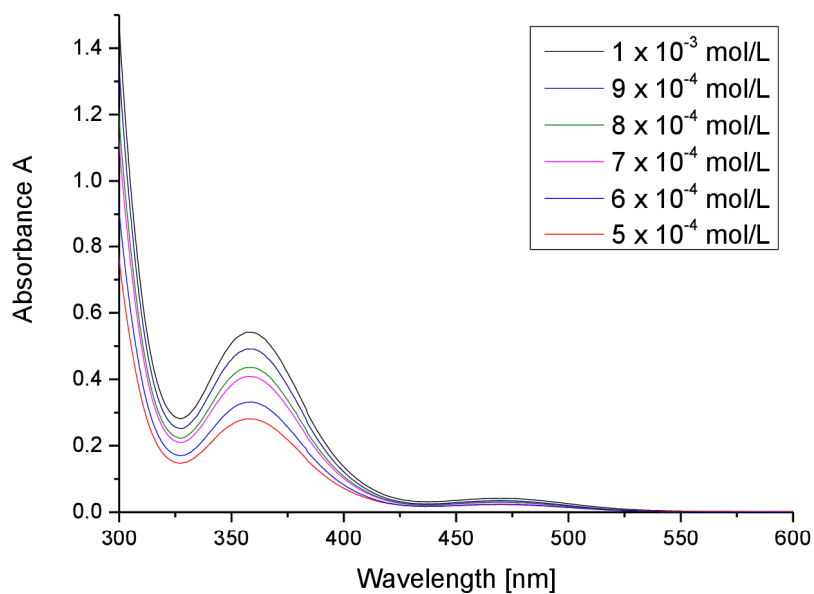


Figure S25: UV-Vis spectrum of **6a** in hexane at different concentrations.

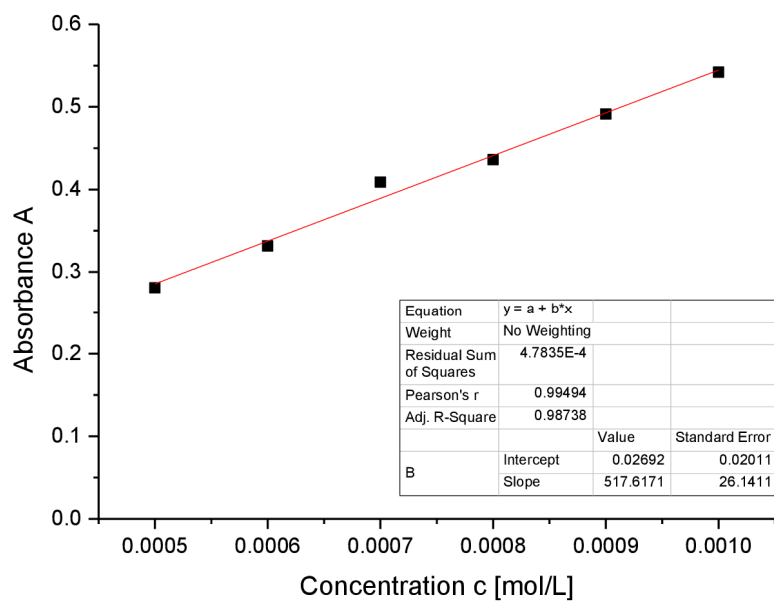


Figure S26: Determination of ε ($5176 \text{ M}^{-1} \text{ cm}^{-1}$) by linear regression of absorptions ($\lambda = 357 \text{ nm}$) of **6a** against concentration.

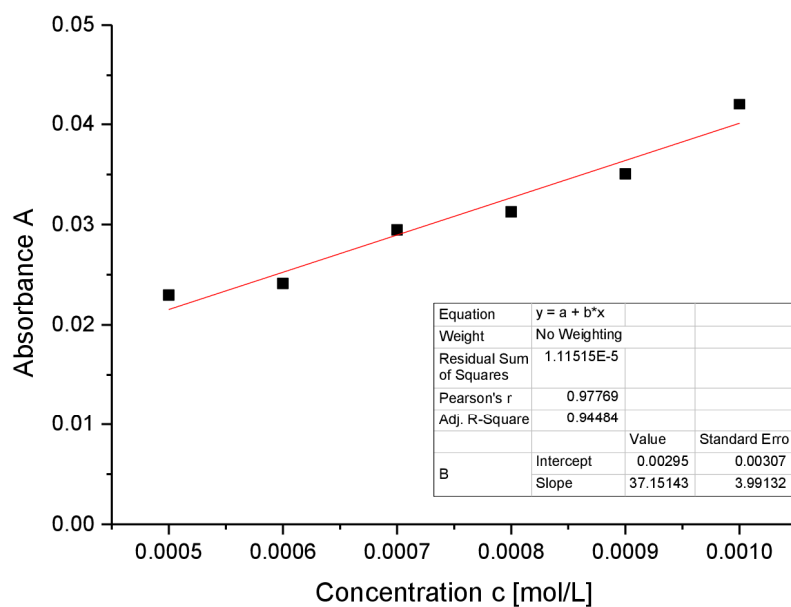


Figure S27: Determination of ε ($371 \text{ M}^{-1} \text{ cm}^{-1}$) by linear regression of absorptions ($\lambda = 469 \text{ nm}$) of **6a** against concentration.

Preparation of *privo*-Benzoyl-2,4,5,5,6-pentakis(2',4',6'-tri-*iso*-propylphenyl)tetracyclo**[2.2.0.0^{1,3}.0^{3,6}] hexasilane (6b)**

Quantities: **4Li**, 89.5 mg (0.06 mmol); benzoyl chloride 7.5 μ L (9.1 mg, 0.065 mmol); toluene; stirring 0.5 h; The crude product was thoroughly dried in vacuo and characterized by multinuclear NMR spectroscopy.

¹H NMR (300.13 MHz, benzene-*d*₆, 300K): δ = 7.72 (s), 7.70 (d), 7.26 (d), 7.24 (br), 7.07 (d), 6.96 (d), 6.89 (d), 6.87 (s), 6.81 (t), 6.77 (m), 6.74 (s), 5.06 – 5.02 (m), 4.90 – 4.85 (m), 4.30 – 4.20 (m), 4.15 – 4.02 (m), 3.70 – 3.63 (m), 3.30 – 3.19 (m), 2.86 – 2.55 (m), 2.14 (d), 2.04 (d), 1.87 (d), 1.63 – 1.33 (m), 1.25 – 1.06 (m), 0.80 (d), 0.74 (d), 0.70 – 0.62 (m), 0.47 (d), 0.39 (d), 0.31 (d). **¹³C NMR** (75.5 MHz, benzene-*d*₆, 300 K): δ = 226.9 (CO), 156.8, 156.5, 156.1, 156.1, 154.3, 153.7, 153.4, 153.3, 152.2, 152.0, 151.4, 150.8, 150.6, 149.6, 149.5, 149.1, 140.5, 138.5, 138.4, 133.5, 132.4, 128.9, 126.5, 126.1, 123.5, 123.2, 122.9, 122.4, 122.2, 121.9, 121.5, 121.3, 121.2 (Ar-C and Ar-CH), 37.4, 37.1, 36.6, 35.2, 34.8, 34.6, 34.5 (Tip-*i*Pr-CH and Tip-*i*Pr-CH₃), 32.0 (hexane), 27.6, 27.4, 27.1, 26.7, 26.5, 26.1, 25.9, 25.7, 25.6, 25.4, 25.3, 24.9, 24.7, 24.5, 24.1, 24.1, 24.0, 23.9, 23.5, 23.1, 22.9, 22.7, 22.6 (Tip-*i*Pr-CH and Tip-*i*Pr-CH₃), 14.4 (hexane). **²⁹Si NMR** (59.6 MHz, benzene-*d*₆, 300 K): δ = 166.2 (s, *privo*-Si(Tip)COPh), 30.9 (s, *remoto*-SiTip₂), -3.6 (s, *ligato*-SiTip), -16.2 (s, *ligato*-SiTip) -269.5 (s, *nudo*-Si) -271.1 (s, *nudo*-Si).

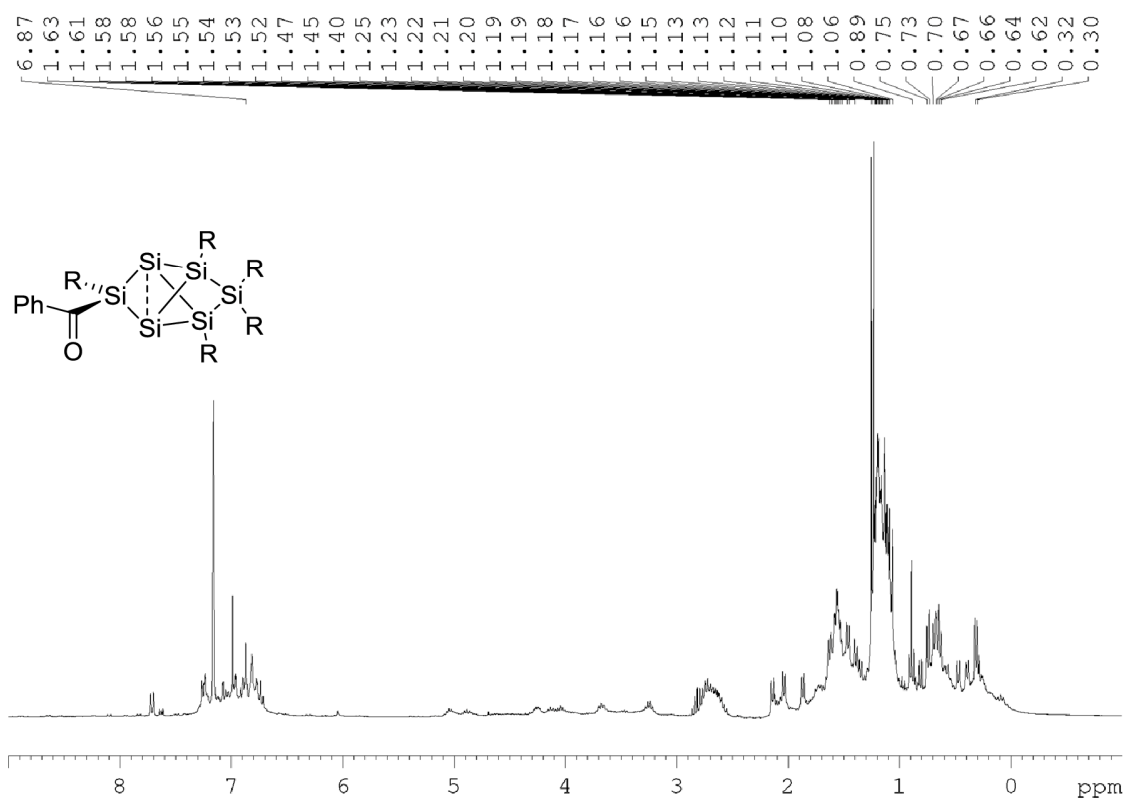
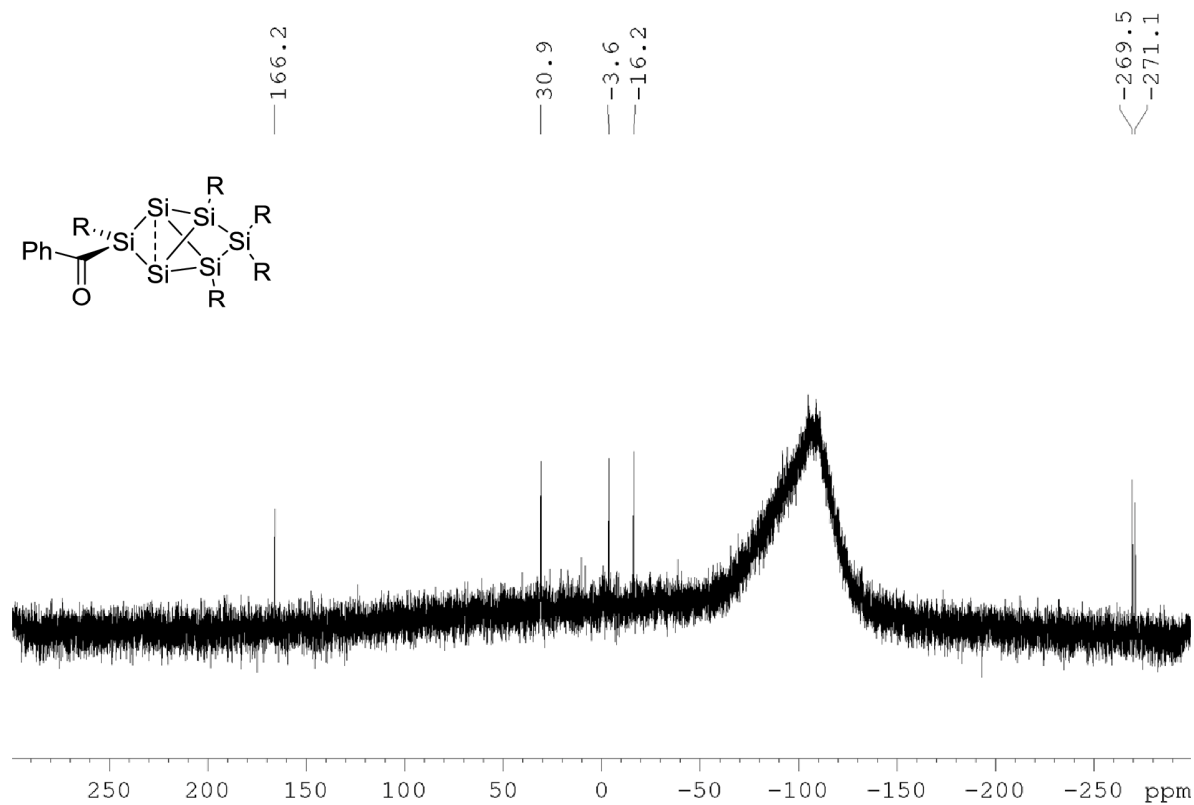
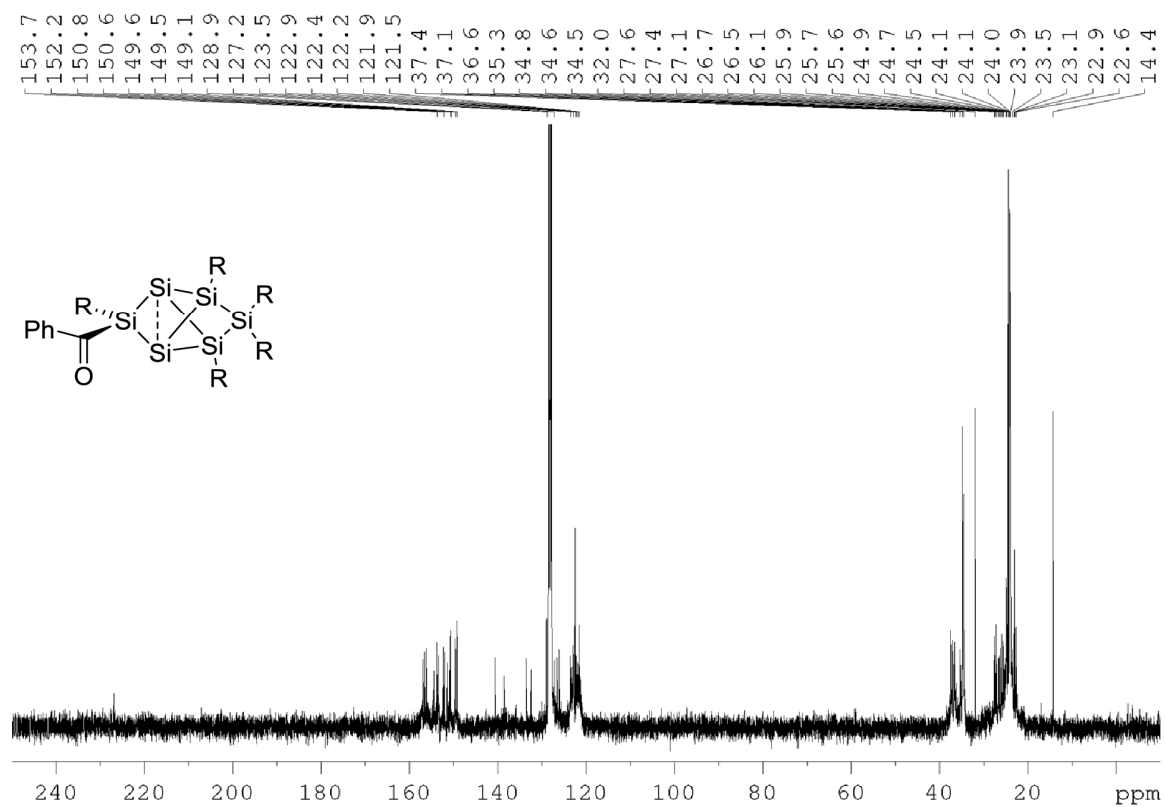


Figure S28: ¹H NMR of **6b** in C₆D₆ (300 MHz).



Preparation of privo-Pivaloyl-2,4,5,5,6-pentakis(2',4',6'-triisopropylphenyl)tetracyclo[2.2.0.0^{1,3}.0^{3,6}]hexasilane (6c)

Quantities: **4Li**, 150.7 mg (0.11 mmol); pivaloyl chloride 13.9 μ L (13.6 mg, 0.11 mmol); toluene (2.5 mL); stirring 0.5 h; crystallization from hexane. Yield: 39 mg (27 %) orange crystals.

¹H NMR (400.13 MHz, benzene-d₆, 300K): δ = 7.27, 7.25, 7.12, 7.07, 7.01, 6.92, 6.86, 6.85 (each d, each 1H, Tip-H), 6.80 (t, 2H, Tip-H), 5.07, 4.86, 4.35 (each sept, each 1H, ⁱPr-CH), 4.18 – 4.06 (m, 2H, ⁱPr-CH), 3.96 – 3.87 (m, 2H, ⁱPr-CH), 3.65 (s, 1H, ⁱPr CH), 3.32 – 3.23 (m, 2H, ⁱPr-CH), 2.78 – 2.70 (m, 3H, ⁱPr-CH), 2.65 – 2.58 (m, 2H, ⁱPr-CH), 2.17, 2.05, 1.81, 1.78 (each d, each 3H, ⁱPr-CH₃), 1.64 – 1.56 (m, 12H, ⁱPr-CH₃), 1.44, 1.41, 1.32 (each d, each 3H, ⁱPr-CH₃), 1.25 – 1.17 (m, 21H, ⁱPr-CH₃), 1.11 – 1.08 (m, 12H, ⁱPr-CH₃), 0.89 (s, 9H, ^tBu-CH₃), 0.75, 0.69, 0.67, 0.58 (each d, each 3H, ⁱPr-CH₃), 0.36 – 0.28 (m, 12H, ⁱPr-CH₃). **¹³C NMR** (100.6 MHz, benzene-d₆, 300K): δ = 238.7 (CO), 157.1, 156.9, 155.9, 155.4, 154.2, 153.8, 153.5, 153.2, 152.1 151.8, 151.6, 150.6, 150.5, 149.5, 149.3, 138.5, 138.4, 133.6, 128.2, 127.9 (Ar-C), 126.6, 123.6, 123.0, 122.9, 122.7, 122.4, 122.2, 122.0, 121.5, 120.6 (Ar-CH), 49.4 (CMe₃), 37.7, 37.5, 37.3, 37.2, 37.0, 36.7, 36.5, 35.3, 35.0, 35.0, 34.7, 34.6, 34.6, 32.0, 29.0, 27.4, 26.8 (Tip-ⁱPr-CH and Tip-ⁱPr-CH₃), 26.8 (^tBu-CH₃), 26.2, 26.1, 25.7, 25.7, 25.5, 25.4, 25.2, 25.1, 25.0, 24.9, 24.8, 24.5, 24.1, 24.1, 24.1, 24.0, 23.9, 23.6, 23.1, 22.4, 14.4 (Tip-ⁱPr-CH and Tip-ⁱPr-CH₃). **²⁹Si NMR** (59.6 MHz, benzene-d₆, 300 K): δ = 173.1 (s, *privo*-Si(Tip)CO^tBu) 30.9 (s, *remoto*-SiTip₂), –1.7 (s, *ligato*-SiTip), –14.5 (s, *ligato*-SiTip) –263.1 (s, *nudo*-Si) –265.8 (s, *nudo*-Si). Elemental analysis calculated for C₈₀H₁₂₄OSi₆: C, 75.64, H; 9.84. Found: C, 74.29; H, 10.05.

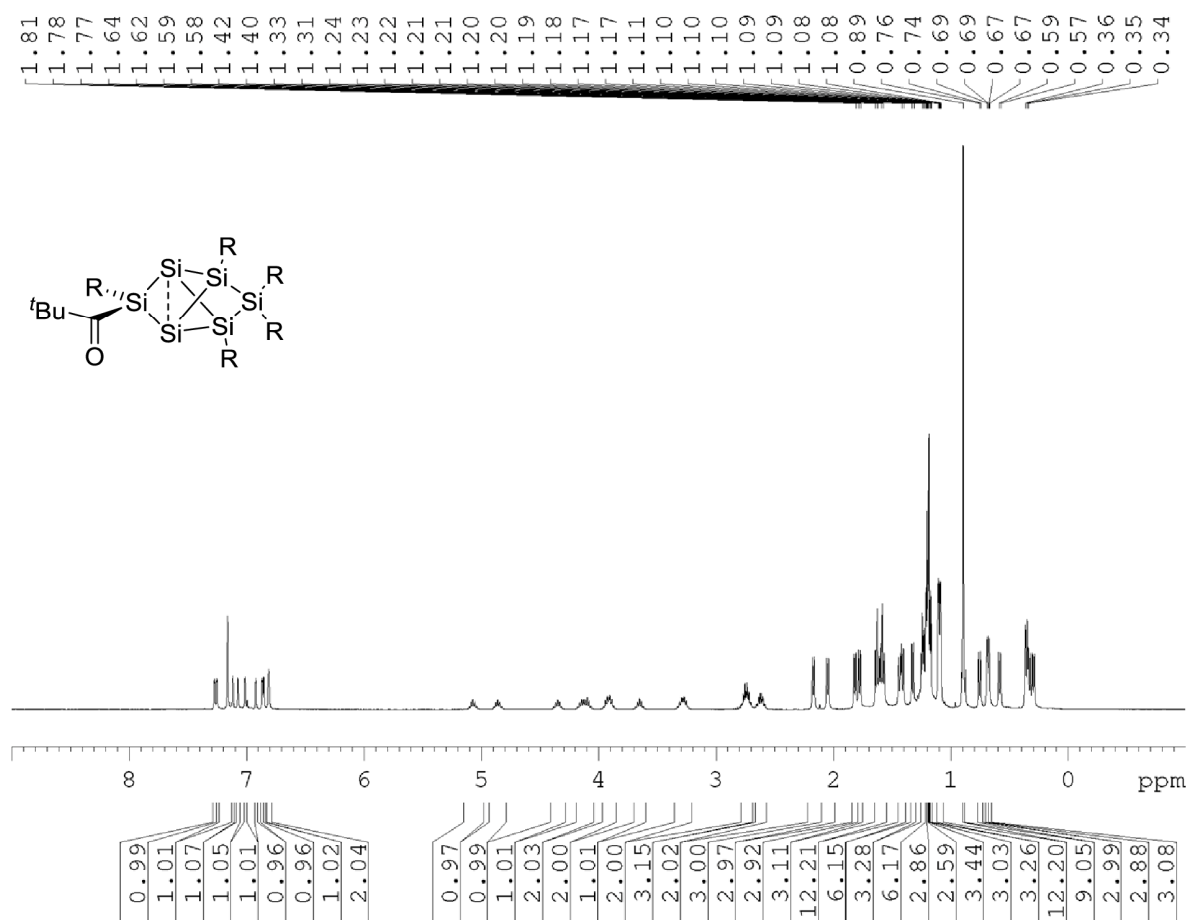


Figure S31: ^1H NMR of **6c** in C_6D_6 (400 MHz).

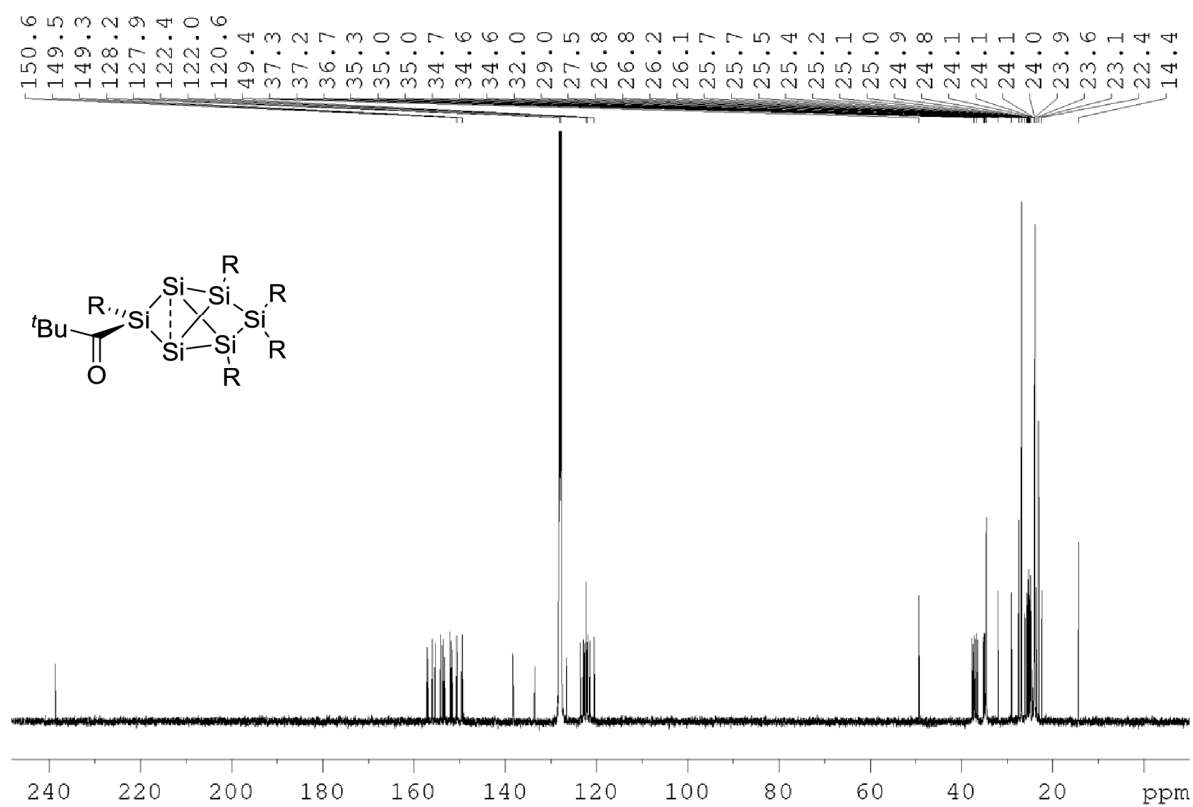


Figure S32: ¹³C NMR of **6c** in C₆D₆ (100.6 MHz).

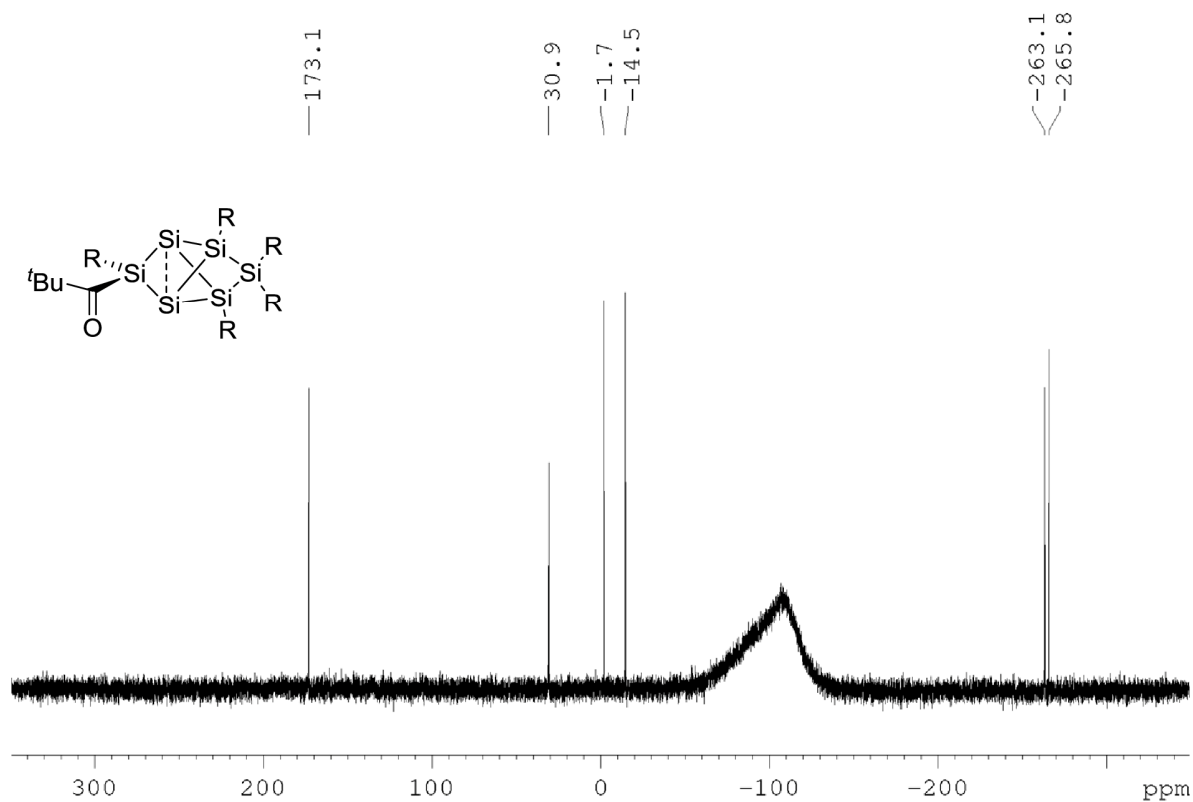


Figure S33: ²⁹Si NMR of **6c** in C₆D₆ (59.6 MHz).

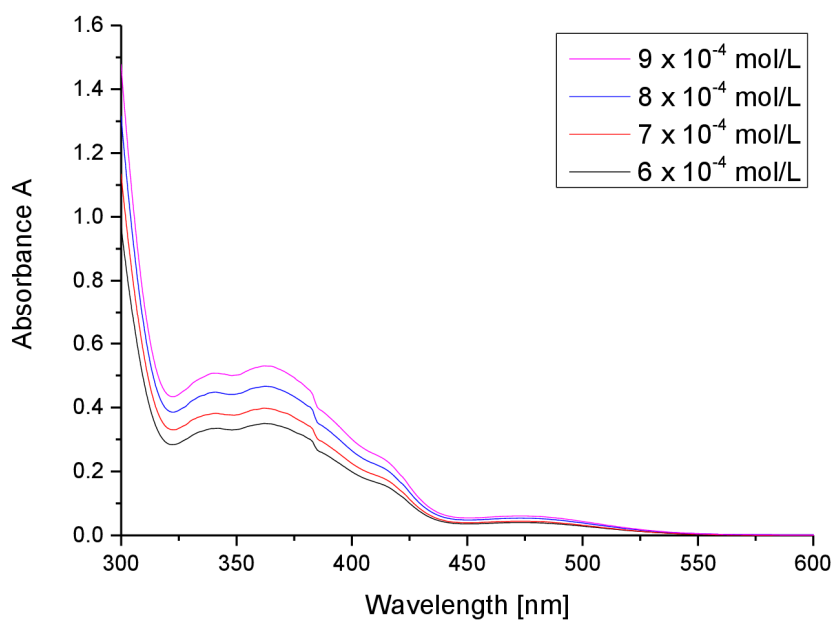


Figure S34: UV-Vis spectrum of **6c** in hexane at different concentrations.

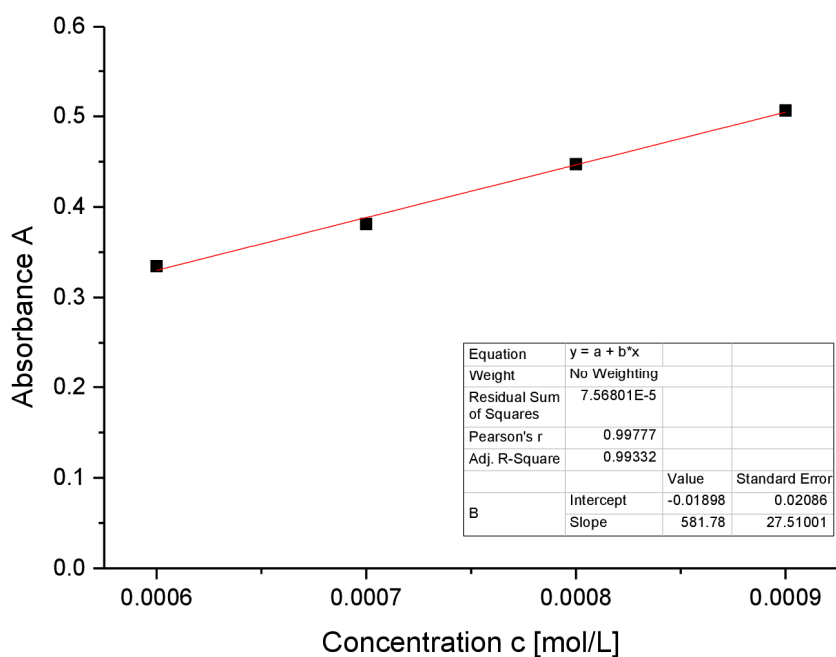


Figure S35: Determination of ϵ ($5817 \text{ M}^{-1} \text{ cm}^{-1}$) by linear regression of absorptions ($\lambda = 342 \text{ nm}$) of **6c** against concentration.

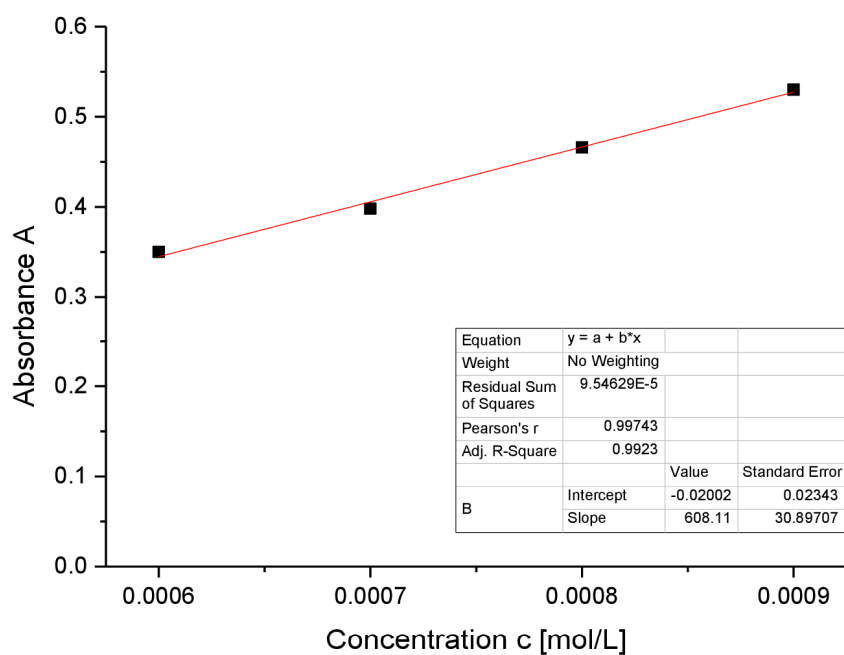


Figure S36: Determination of ε ($6081 \text{ M}^{-1} \text{ cm}^{-1}$) by linear regression of absorptions ($\lambda = 362 \text{ nm}$) of **6c** against concentration.

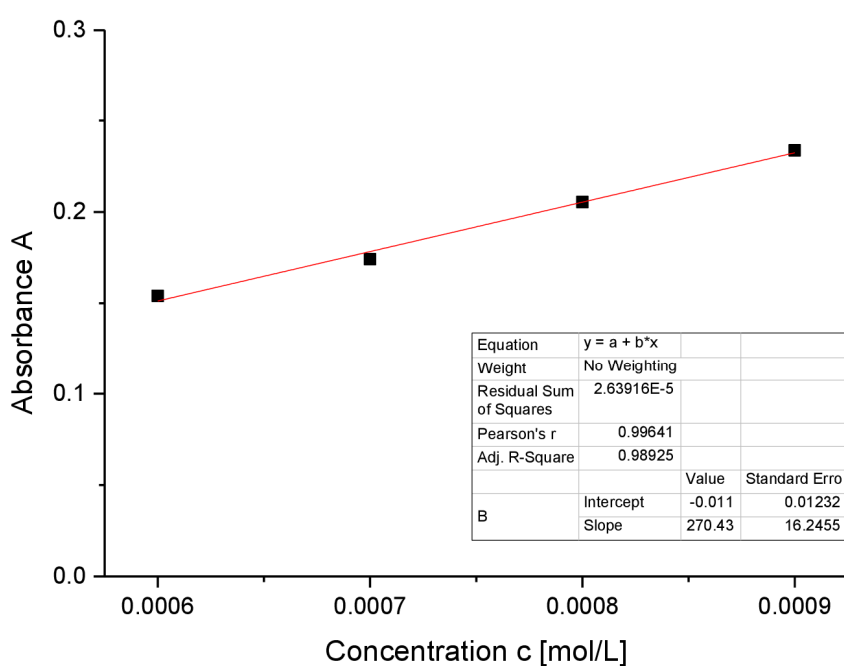


Figure S37: Determination of ε ($2704 \text{ M}^{-1} \text{ cm}^{-1}$) by linear regression of absorptions ($\lambda = 415 \text{ nm}$) of **6c** against concentration.

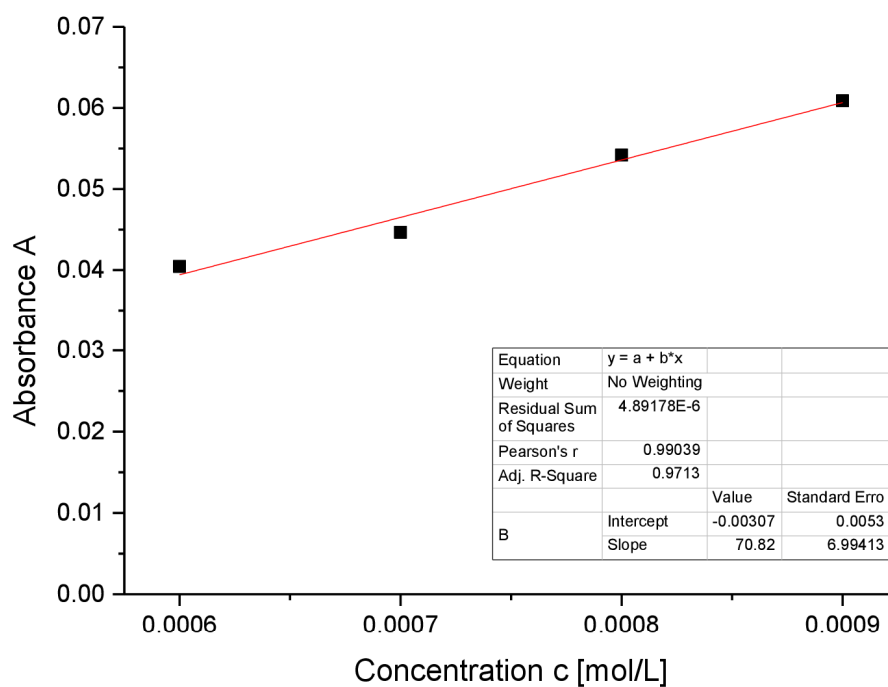


Figure S38: Determination of ϵ ($708 \text{ M}^{-1} \text{ cm}^{-1}$) by linear regression of absorptions ($\lambda = 473 \text{ nm}$) of **6c** against concentrations.

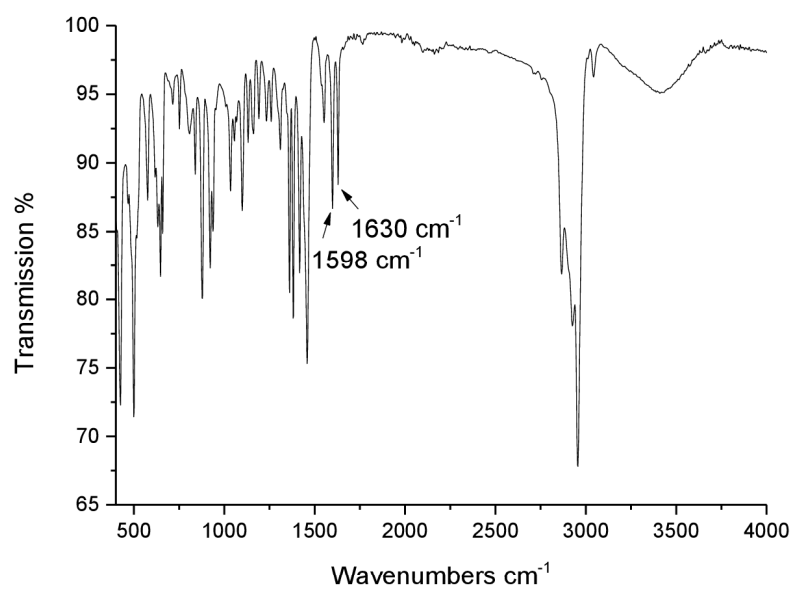


Figure S39: Infrared spectrum of **6c** (powder).

Preparation of *privo*-Bis(dimethylamino)phosphanyl-2,4,5,5,6-pentakis(2',4',6'-tri-*iso*-propyl-phenyl)-tetracyclo[2.2.0.0^{1,3}.0^{3,6}] hexasilane (6d)

Quantities: **4Li**, 102.8 mg (0.077 mmol); (Me₂N)₂PCl 11.2 μ L (11.9 mg, 0.077 mmol); benzene-d₆ (0.6 mL); NMR scale. The crude product was thoroughly dried in vacuum and characterized by multinuclear NMR spectroscopy.

¹H NMR (300.13 MHz, benzene-d₆, 300K): δ = 7.28 (d, 2H, Tip-H), 7.09 (s, 1H, Tip-H), 6.99 (s, 1H, Tip-H), 6.91 (s, 1H, Tip-H), 6.87 (s, 1H, Tip-H), 6.81 (s, 2H, Tip-H), 6.79 (s, 1H, Tip-H), 5.06 (sept, 1H, ⁱPr-CH), 4.88 (sept, 1H, ⁱPr-CH), 4.41 (sept, 1H, ⁱPr-CH), 4.19 – 4.08 (m, 2H, ⁱPr-CH), 4.01 – 3.95 (m, 2H, ⁱPr-CH), 3.65 (sept, 1H, ⁱPr-CH), 3.47 (sept, 1H, ⁱPr-CH), 3.35 (sept, 1H, ⁱPr-CH), 2.78 – 2.65 (m, 5H, ⁱPr-CH), 2.58 (d, ³J_{PH} = 9.89 Hz, 6H, N(CH₃)₂), 2.30 (d, ³J_{PH} = 9.19 Hz, 6H, N(CH₃)₂), 2.19 (d, 3H, ⁱPr-CH₃), 2.06 (d, 3H, ⁱPr-CH₃), 1.86 (d, 3H, ⁱPr-CH₃), 1.79 (d, 3H, ⁱPr-CH₃), 1.70 (d, 3H, ⁱPr-CH₃), 1.65 – 1.57 (m, 12H, ⁱPr-CH₃), 1.44 (t, 6H, ⁱPr-CH₃), 1.22 – 1.14 (m, 27H, ⁱPr-CH₃), 1.11 – 1.07 (m, 6H, ⁱPr-CH₃), 0.84 (d, 3H, ⁱPr-CH₃), 0.72 (d, 3H, ⁱPr-CH₃), 0.68 (d, 3H, ⁱPr-CH₃), 0.55 (d, 3H, ⁱPr-CH₃), 0.45 – 0.39 (m, 9H, ⁱPr-CH₃), 0.31 (d, 3H, ⁱPr-CH₃). **¹³C NMR** (75.5 MHz, benzene-d₆, 300 K): δ = 157.4, 157.1, 156.9, 156.5, 156.3, 156.0, 155.9, 154.5, 153.7, 153.6, 153.3, 152.0, 151.8, 151.2, 151.0, 150.7, 150.3, 149.9, 149.3, 149.1 (Ar-C), 123.7, 123.1, 122.8, 122.5, 122.2, 122.1, 121.9, 121.7, 121.6, 121.4 (Ar-CH), 47.2 (d, ²J_{CP} = 9.54 Hz, N(CH₃)₂), 46.0 (d, ²J_{C-P} = 14.79 Hz, N(CH₃)₂), 40.7, 39.5, 38.4, 37.6, 37.4, 37.2, 37.1, 36.9, 36.4, 35.2, 34.8, 34.7, 34.6, 34.5, 28.4, 27.8, 27.4, 26.9, 26.6, 26.4, 26.3, 25.6, 25.4, 25.3, 25.2, 25.1, 25.0, 24.9, 24.8, 24.5, 24.5, 24.1, 24.1, 24.0, 24.0, 22.4 (Tip-ⁱPr-CH and Tip-ⁱPr-CH₃). **²⁹Si NMR** (59.6 MHz, benzene-d₆, 300 K): δ = 186.5 (d, ¹J_{SIP} = 97.44 Hz, *privo*-Si(Tip)P(NMe₂)₂), 28.0 (d, ¹J_{SIP} = 7.52 Hz, *remoto*-SiTip₂), 13.7 (d, ¹J_{SIP} = 20.87 Hz, *ligato*-SiTip), –16.9 (s, *ligato*-SiTip), –246.0 (d, ¹J_{SIP} = 33.40 Hz, *nudo*-Si), –256.1 (d, ¹J_{SIP} = 8.28 Hz, *nudo*-Si). **³¹P NMR** (121.5 MHz, benzene-d₆, 300 K): δ = 121.3 (s, ¹J_{SIP} = 97.44 Hz).

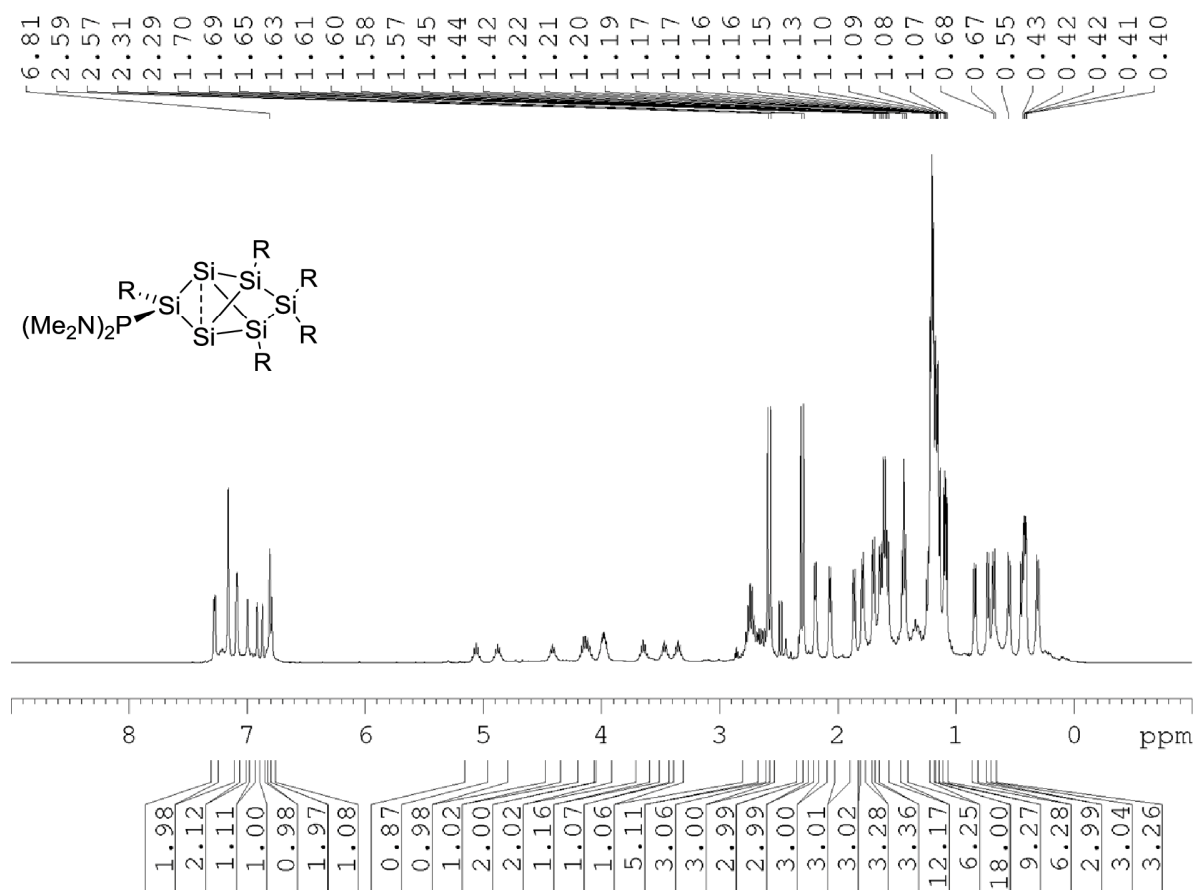


Figure S40: ^1H NMR of **6d** in C_6D_6 (400 MHz).

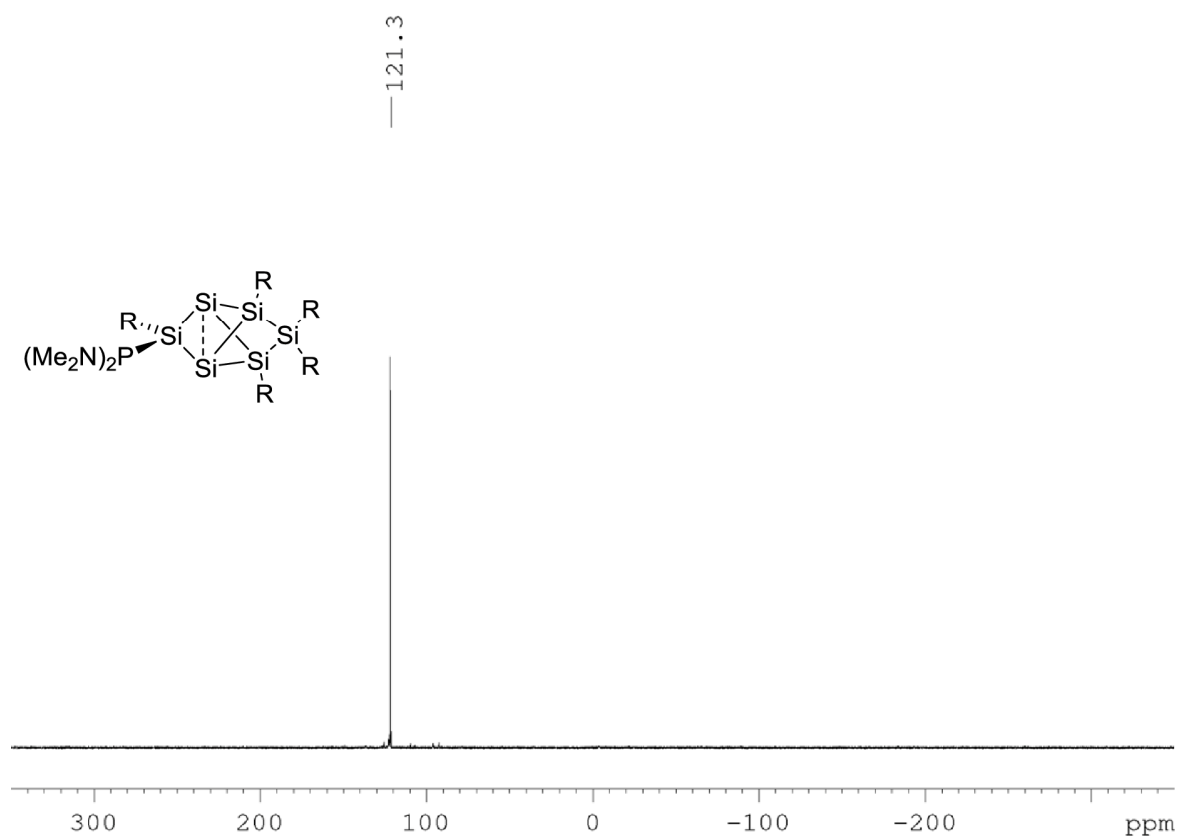


Figure S41: ^{31}P NMR of **6d** in C_6D_6 (121.5 MHz).

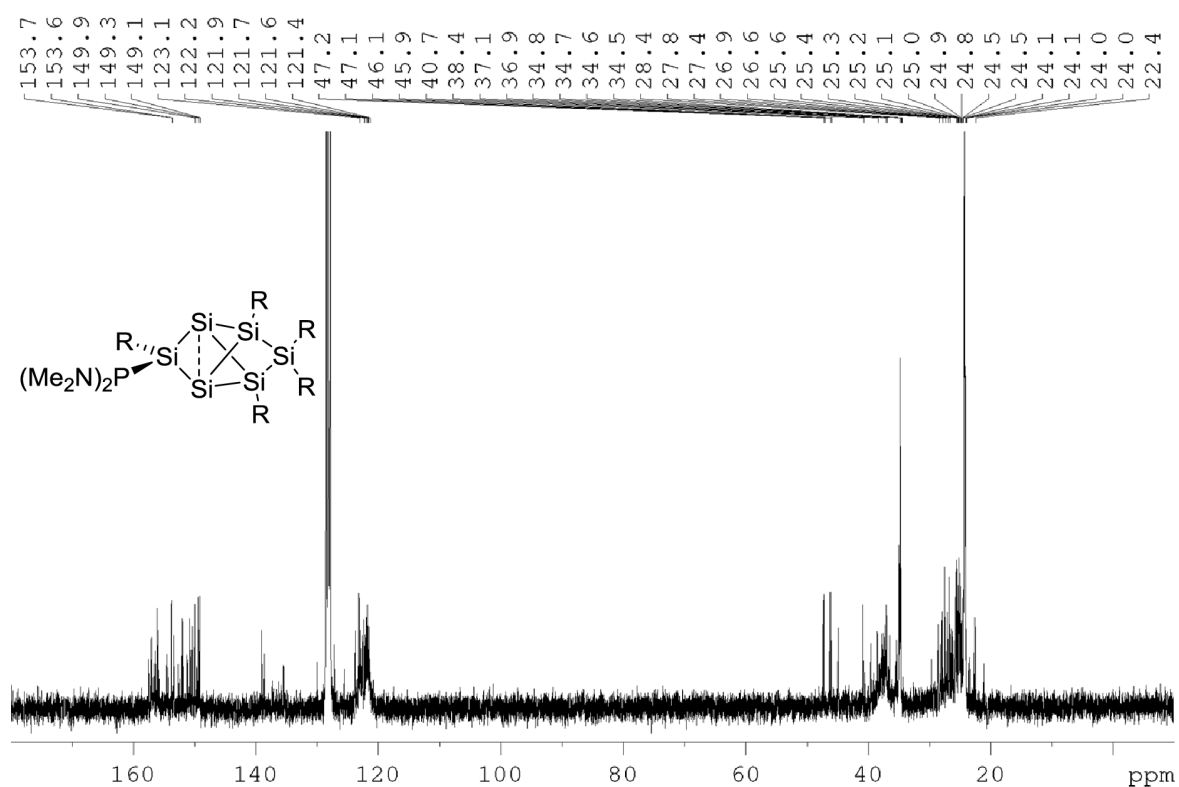


Figure S42: ^{13}C NMR of **6d** in C_6D_6 (75.5 MHz).

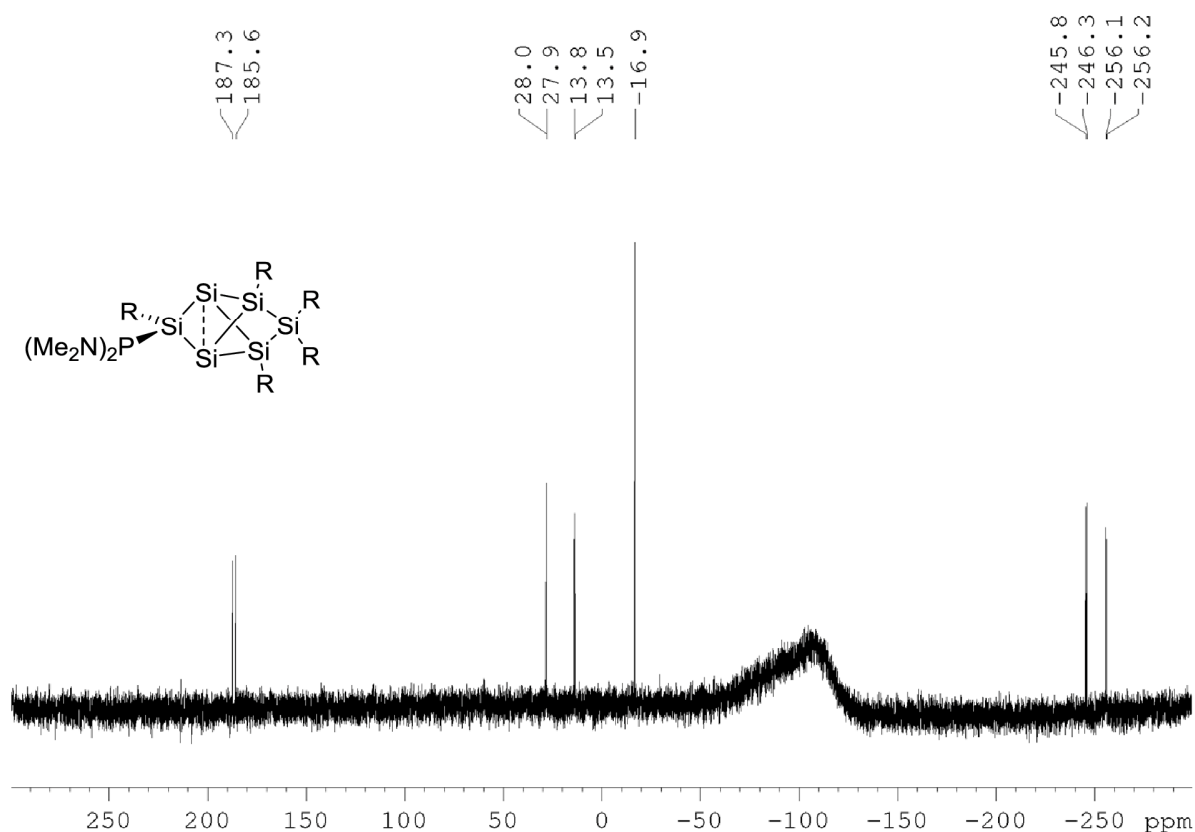


Figure S43: ^{29}Si NMR of **6d** in C_6D_6 (59.6 MHz).

***privo*-Trichlorosilyl-2,4,5,5,6-pentakis(2',4',6'-tri-*iso*-propyl-phenyl)tetracyclo[2.2.0.0^{1,3}.0^{3,6}]hexasilane (**6e**)**

Quantities: **4Li**, 81.8 mg (0.061 mmol); SiCl_4 7.7 μL (11.4 mg, 0.067 mmol); benzene- d_6 (0.6 mL); NMR scale. The crude product was thoroughly dried in vacuo and characterized by multinuclear NMR spectroscopy.

^1H NMR (300.13 MHz, benzene- d_6 , 300K): δ = 7.25 (s, 2H, Tip-H), 7.10 (d, 1H, Tip-H), 7.04 (d, 1H, Tip-H), 6.97 (d, 1H, Tip-H), 6.90 (d, 1H, Tip-H), 6.82 (d, 1H, Tip-H), 6.78 (s, 2H, Tip-H), 6.74 (d, 1H, Tip-H), 4.89 (sept, 1H, ^iPr -CH), 4.74 (sept, 1H, ^iPr -CH), 4.28 (sept, 1H, ^iPr -CH), 4.01 – 3.79 (m, 3H, ^iPr -CH), 3.72 – 3.52 (m, 2H, ^iPr -CH), 3.39 – 3.20 (m, 2H, ^iPr -CH), 2.78 – 2.52 (m, 5H, ^iPr -CH), 2.13 (d, 3H, ^iPr -CH₃), 2.03 (d, 3H, ^iPr -CH₃), 1.81 (d, 6H, ^iPr -CH₃), 1.62 (d, 3H, ^iPr -CH₃), 1.60 – 1.50 (m, 15H, ^iPr -CH₃), 1.39 (d, 3H, ^iPr -CH₃), 1.24 (d, 3H, ^iPr -CH₃), 1.21 – 1.05 (m, 30H, ^iPr -CH₃), 0.77 (d, 3H, ^iPr -CH₃), 0.65 (d, 6H, ^iPr -CH₃), 0.53 (d, 3H, ^iPr -CH₃), 0.46 (d, 3H, ^iPr -CH₃), 0.38 – 0.35 (m, 6H, ^iPr -CH₃), 0.28 (d, 3H, ^iPr -CH₃). **^{13}C NMR** (75.5 MHz, benzene- d_6 , 300 K): δ = 157.0, 156.7, 156.6, 156.2, 154.4, 154.1, 153.8, 153.6, 152.0, 151.8, 151.3, 150.8, 149.9, 149.7, 137.8, 137.5, 130.1, 127.6, 125.3(Ar-C), 123.9, 123.3, 122.9, 122.8, 122.4, 122.3, 122.2, 122.1, 121.5 (Ar-CH), 38.3, 37.8, 37.6, 37.5, 37.1, 36.5, 36.5, 35.4, 35.1, 34.7, 34.7, 34.6, 34.6, 34.5, 27.8, 27.4, 27.3, 27.1, 27.0, 26.7, 26.5, 26.1, 25.6, 25.2, 25.1, 25.0, 24.6, 24.1,

24.0, 23.9, 23.8, 23.7, 22.9, 22.5 (Tip-ⁱPr-CH and Tip-ⁱPr-CH₃). ²⁹Si NMR (59.6 MHz, benzene-d₆, 300 K):
δ = 161.7 (privo-Si(Tip)SiCl₃), 35.2 (s, *remoto*-SiTip₂), 12.0 (s, *ligato*-SiTip), 7.4 (SiCl₃), -6.4 (s, *ligato*-
SiTip), -251.6 (s, *nudo*-Si), -258.9 (s, *nudo*-Si).

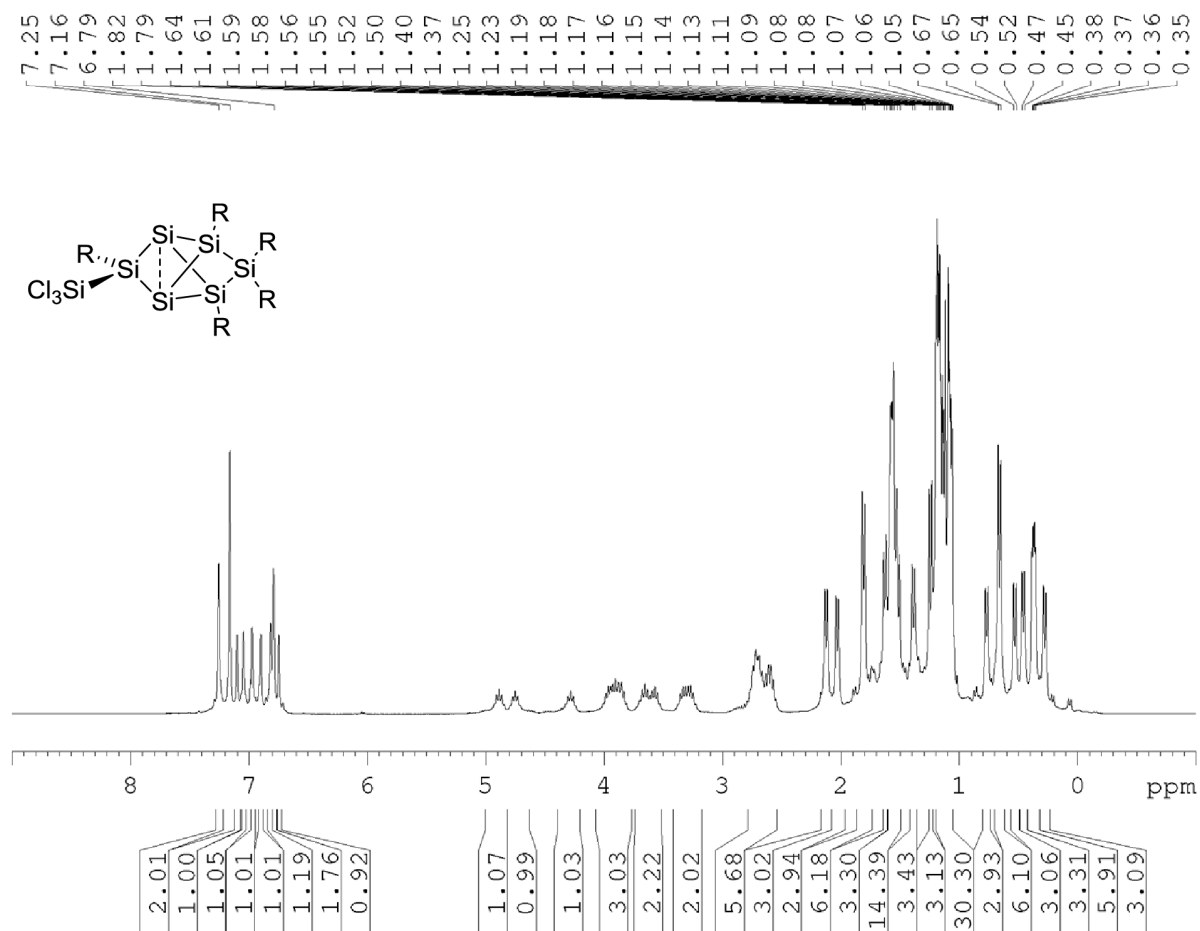


Figure S44: ¹H NMR of **6e** in C₆D₆ (300 MHz).

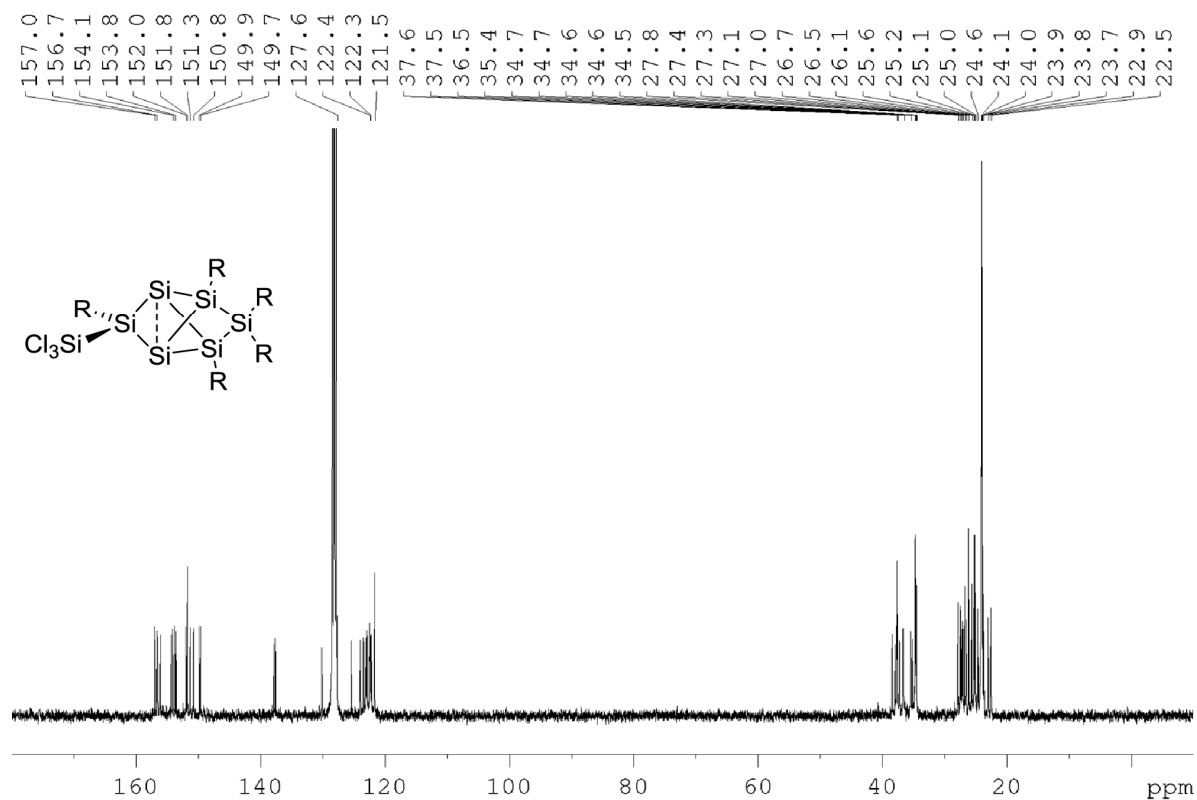


Figure S45: ¹³C NMR of **6e** in C₆D₆ (75.5 MHz).

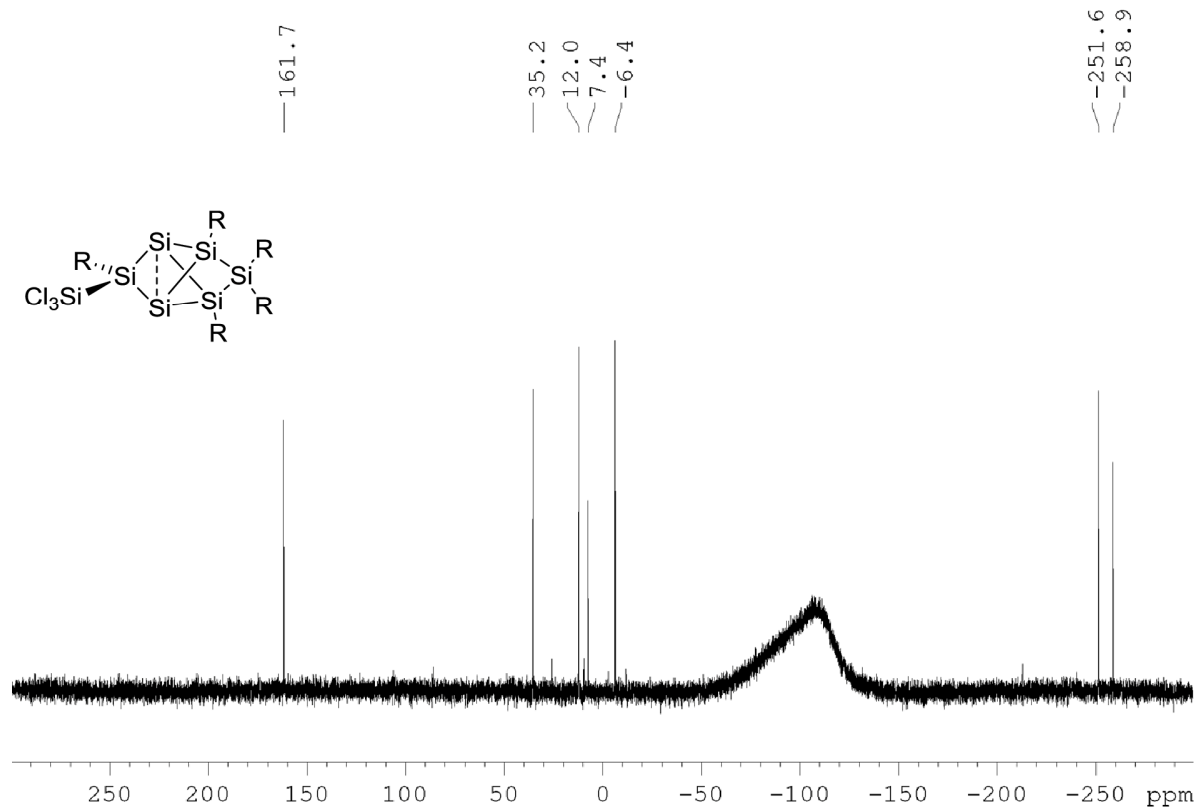


Figure S46: ²⁹Si NMR of **6e** in C₆D₆ (59.6 MHz).

Preparation of *privo*-Lithium-2,4,5,5,6-pentakis(2',4',6'-triisopropylphenyl)tetracyclo[2.2.0.0^{1,3}.0^{3,6}]hexasilan-2-ylborate (6f)

Quantities: **4Li**, 53.4 mg (0.04 mmol); H₃B·SMe₂ 4.2 μL (3.4 mg, 0.04 mmol); toluene (1 mL); stirring 1 h; crystallization from hexane. Yield: 40 mg (78 %) yellow crystals.

¹H NMR (300.13 MHz, benzene-d₆, 300K): δ = 7.27, 7.24, 7.09, 6.97, 6.94 (each d, each 1H, Tip-H), 6.89 (s, 2H, Tip-H), 6.81, 6.80, 6.68 (each d, each 1 H, Tip-H), 5.16, 5.05, 4.77 (each sept, each 1H, ⁱPr-CH), 4.30 (m, 3H, ⁱPr-CH), 3.79, 3.69 (each sept, each 1H, ⁱPr-CH), 3.33 (m, 2H, ⁱPr-CH), 3.07 (br, 7H, thf), 2.72 (m, 5H, ⁱPr-CH), 2.14, 2.10, 1.78, 1.71 (each d, each 3H, ⁱPr-CH₃), 1.61 (m, 12H, ⁱPr-CH₃), 1.47, 1.42, 1.37 (each d, each 3H, ⁱPr-CH₃), 1.20 (m, 30H, ⁱPr-CH₃), 1.19 (m, thf), 0.63 (m, 18H, ⁱPr-CH₃), 0.35 (m, 9H, ⁱPr-CH₃). **⁷Li NMR** (116.6 MHz, benzene-d₆, 300K): δ = -0.58 (s). **¹¹B NMR** (96.3 MHz, benzene-d₆, 300K): δ = -36.4 (q, ¹J_{BH} = 82.3 Hz, BH₃). **¹³C NMR** (75.5 MHz, benzene-d₆, 300K): δ = 156.8, 156.5, 156.4, 155.9, 153.5, 153.3, 152.0, 151.9, 149.3, 149.0, 148.8, 148.6, 148.4, 148.1, 142.7, 139.9, 139.4, 130.6, 128.8 (Ar-C), 123.1, 122.7, 122.4, 122.2, 121.6, 121.0, 120.8, 120.3, 119.6 (Ar-CH), 36.9, 36.7, 36.6, 36.1, 35.9, 35.2, 34.7, 34.6, 34.5, 34.4, 33.8, 28.5, 27.5, 27.5, 27.3, 27.0, 26.4, 26.3, 25.7, 25.5, 25.2, 25.1, 25.0, 24.9, 24.8, 24.7, 24.6, 24.4, 24.3, 24.1, 24.0, 24.0, 23.9, 23.9, 23.8, 23.6, 22.5, 22.0 (Tip-ⁱPr-CH and Tip-ⁱPr-CH₃). **²⁹Si NMR** (59.6 MHz, benzene-d₆, 300K): δ = 237.3 (br, *privo*-Si(Tip)BH₃), 21.7 (s, *ligato*-SiTip), 21.1 (s, *remoto*-SiTip₂), -28.8 (s, *ligato*-SiTip), -243.3 (s, *nudo*-Si), -255.6 (s, *nudo*-Si). **Elemental analysis** calculated for C₇₉H₁₂₆BLiOSi₆: C, 74.24; H, 9.94. Found: C, 70.10; H, 9.50.

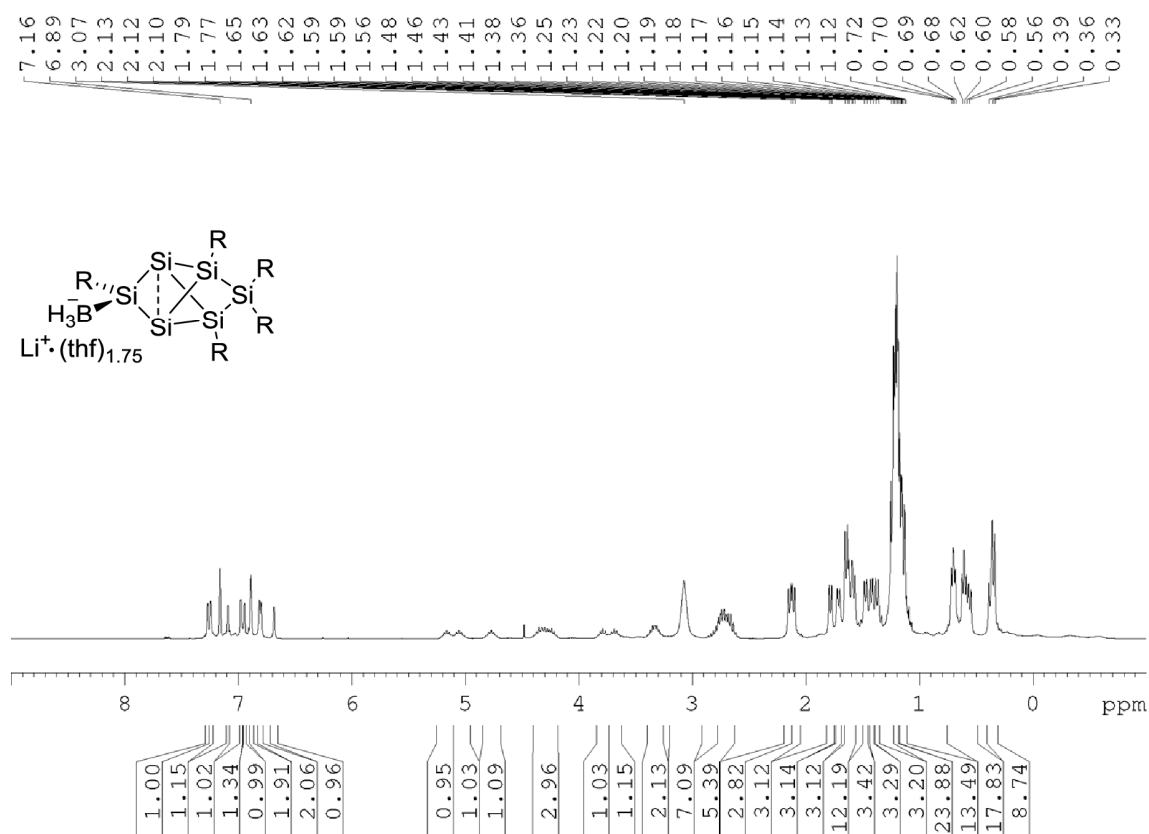


Figure S47: ¹H NMR of **6f** in C₆D₆ (300 MHz).

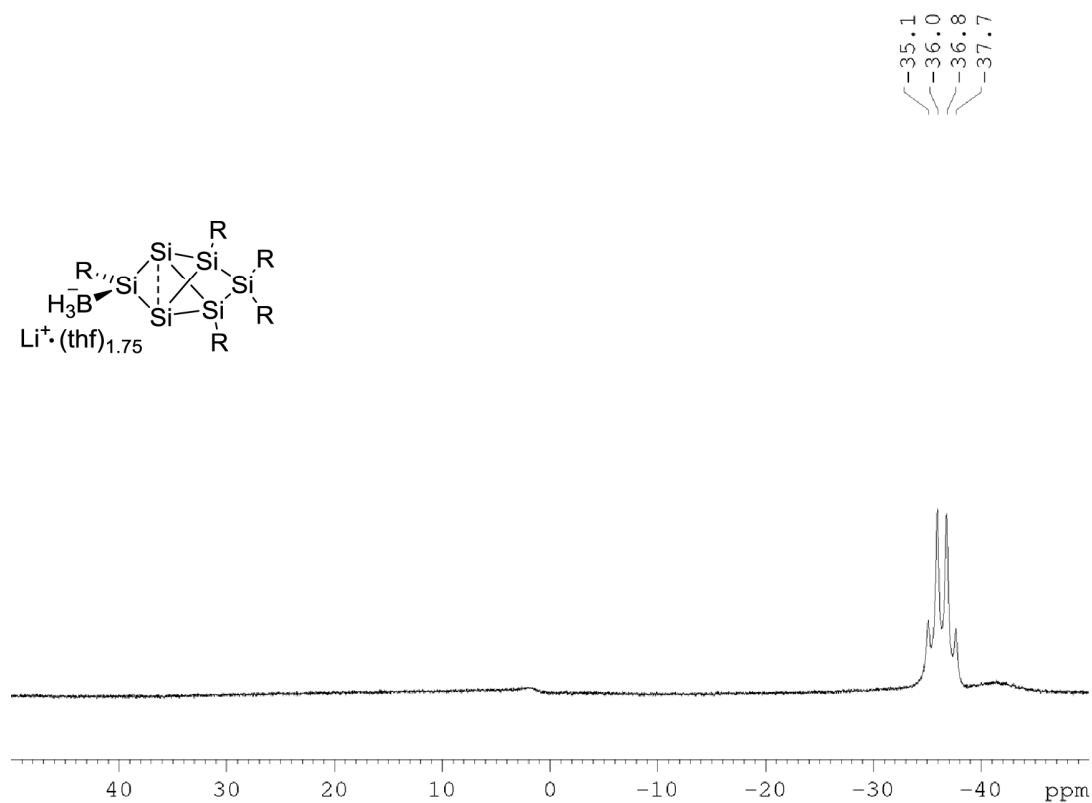


Figure S48: ¹¹B NMR of **6f** in C₆D₆ (96.3 MHz).

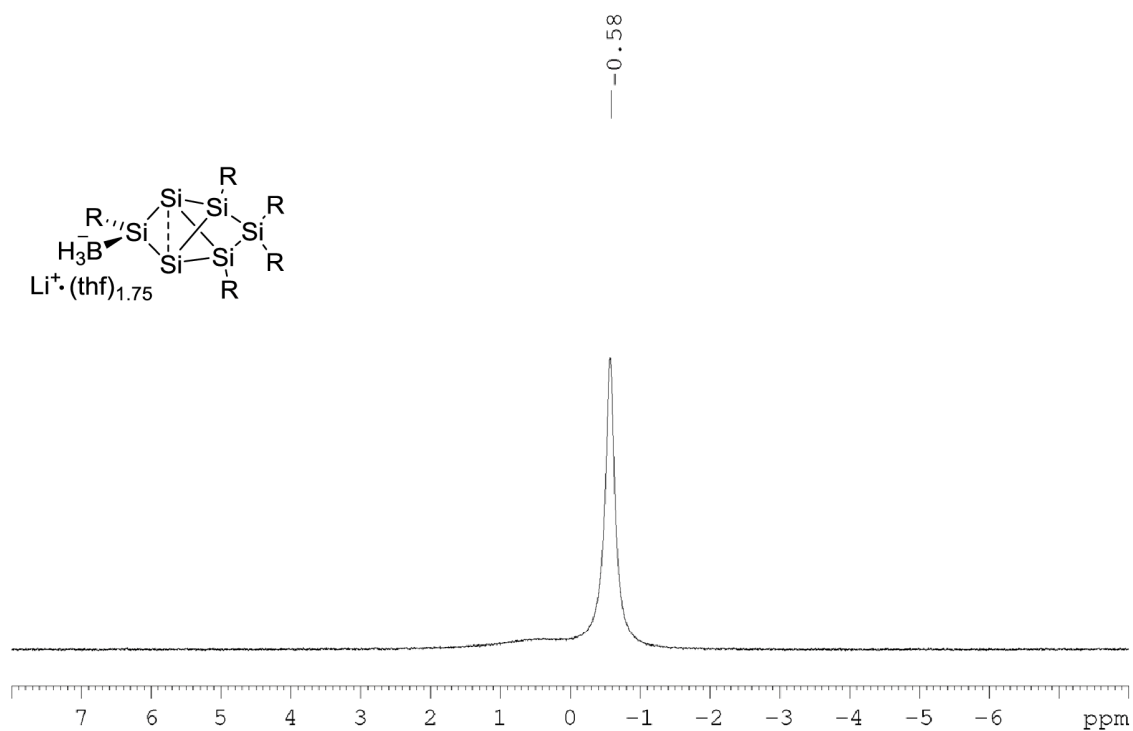


Figure S49: ⁷Li NMR of **6f** in C₆D₆ (116.6 MHz).

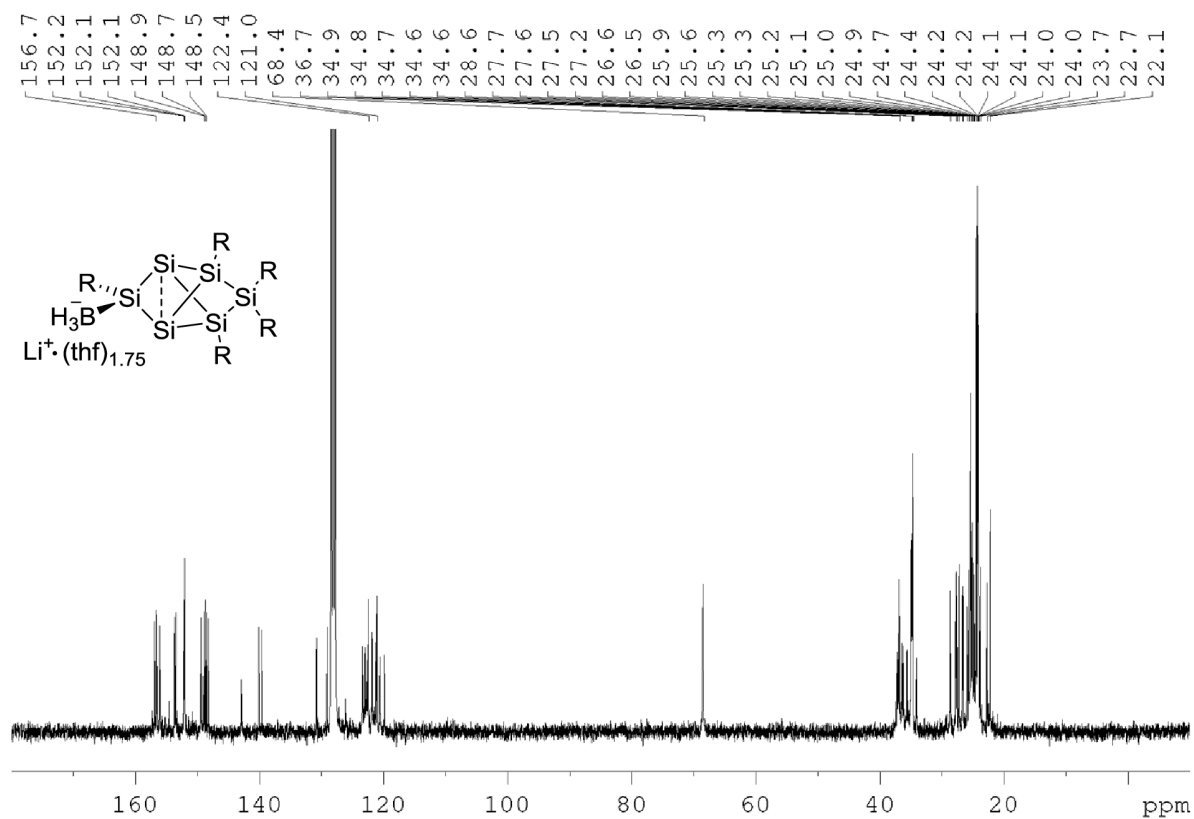


Figure S50: ¹³C NMR of **6f** in C₆D₆ (75.5 MHz).

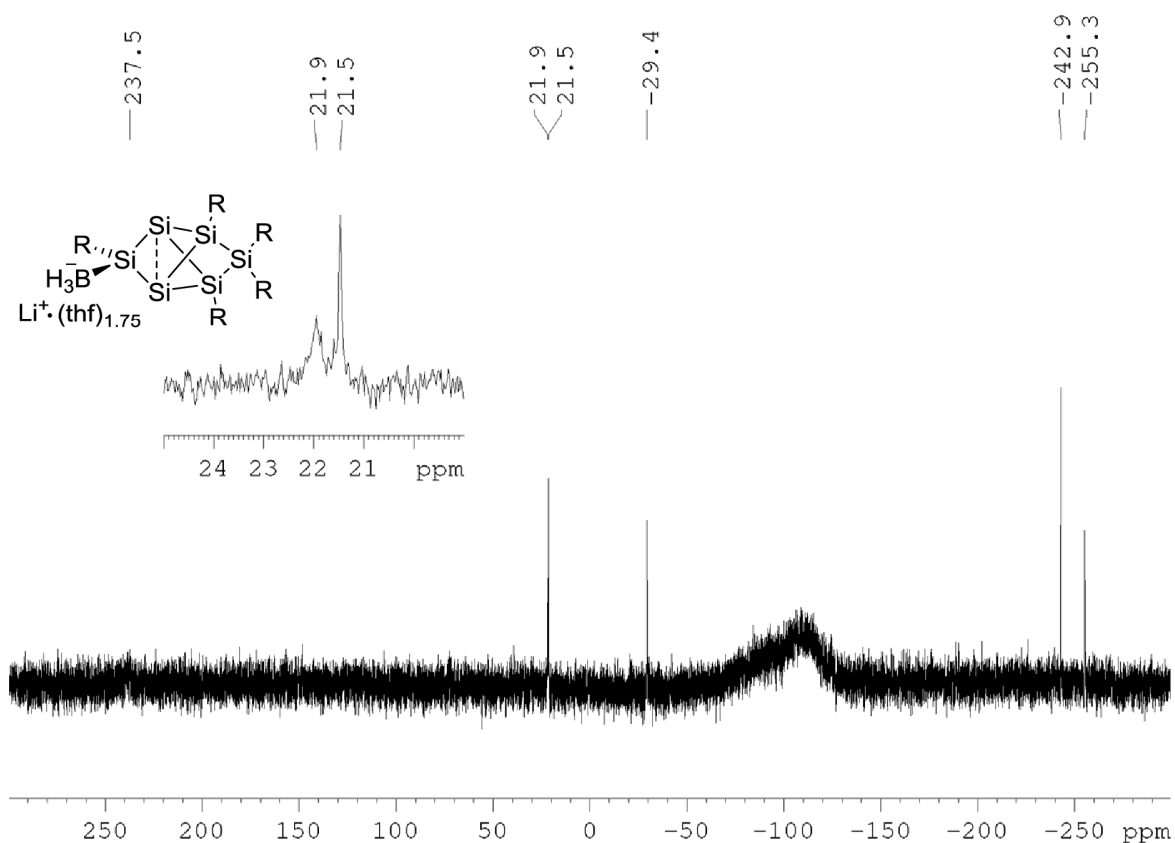


Figure S51: ^{29}Si NMR of **6f** in C_6D_6 (59.6 MHz; $I_b = 1$)

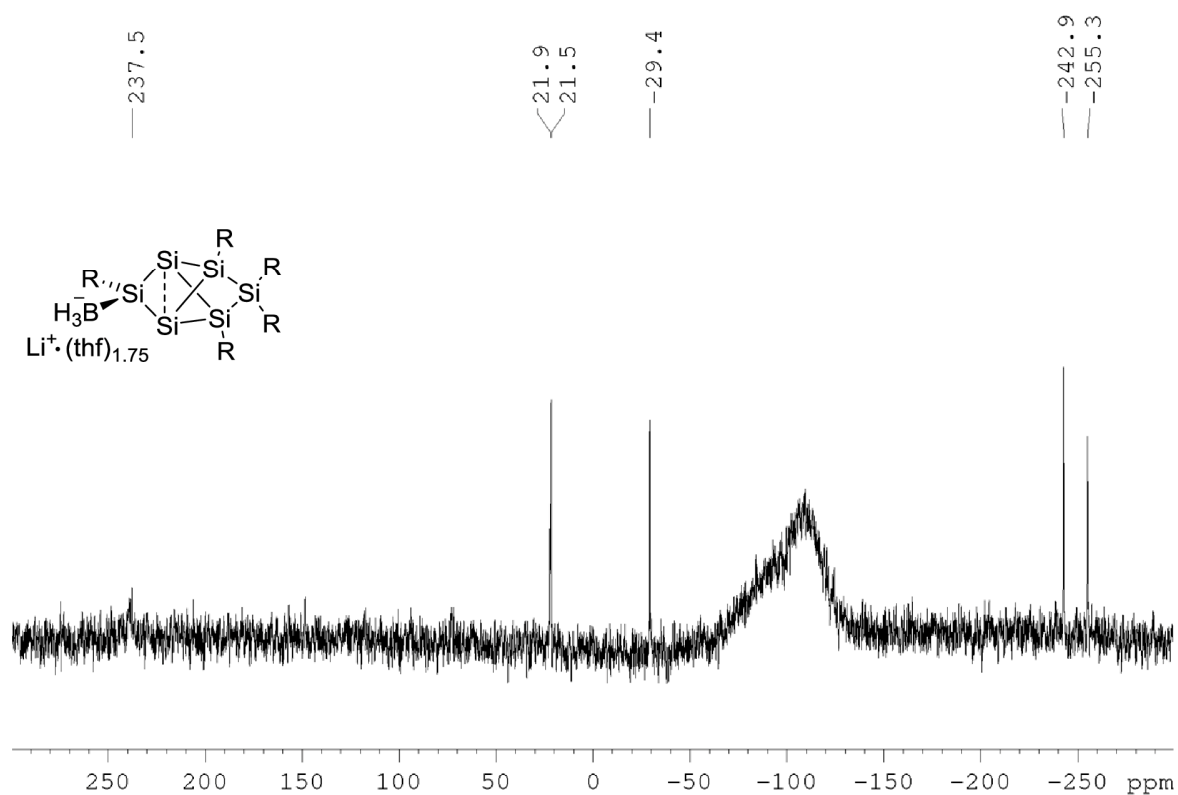


Figure S52: ^{29}Si NMR of **6f** in C_6D_6 (59.6 MHz; $I_b = 6$)

S37

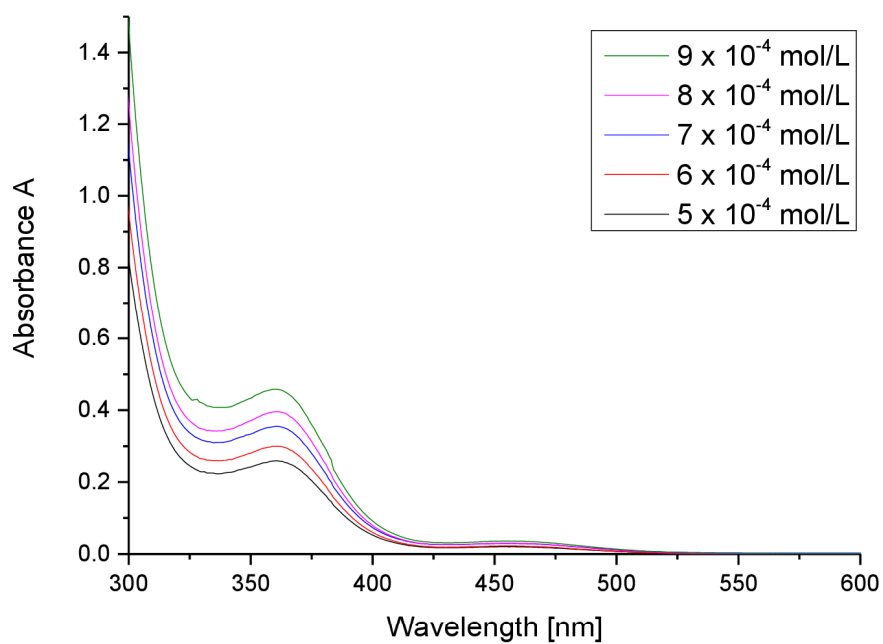


Figure S53: UV-Vis spectrum of **6f** in hexane at different concentrations.

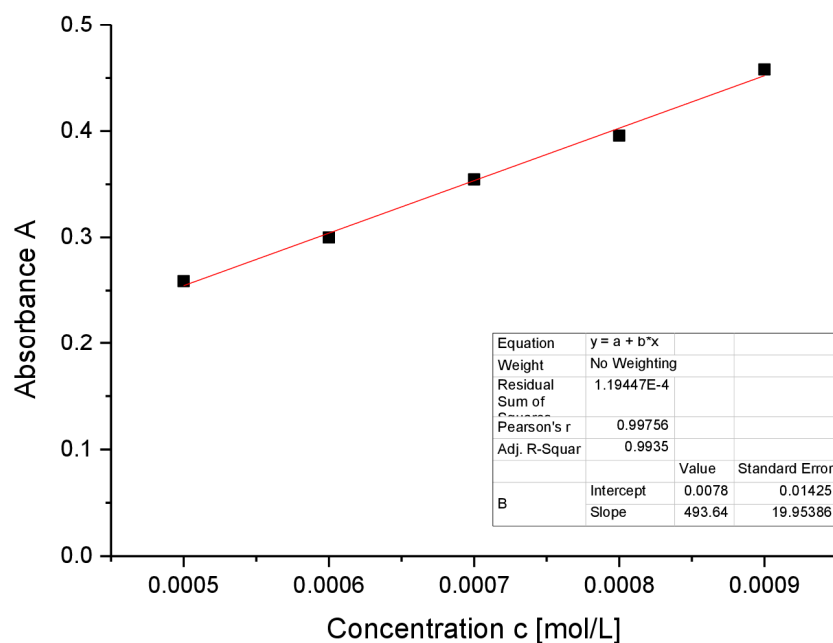


Figure S54: Determination of ϵ ($4936 \text{ M}^{-1} \text{cm}^{-1}$) by linear regression of absorptions ($\lambda = 361 \text{ nm}$) of **6f** against concentration.

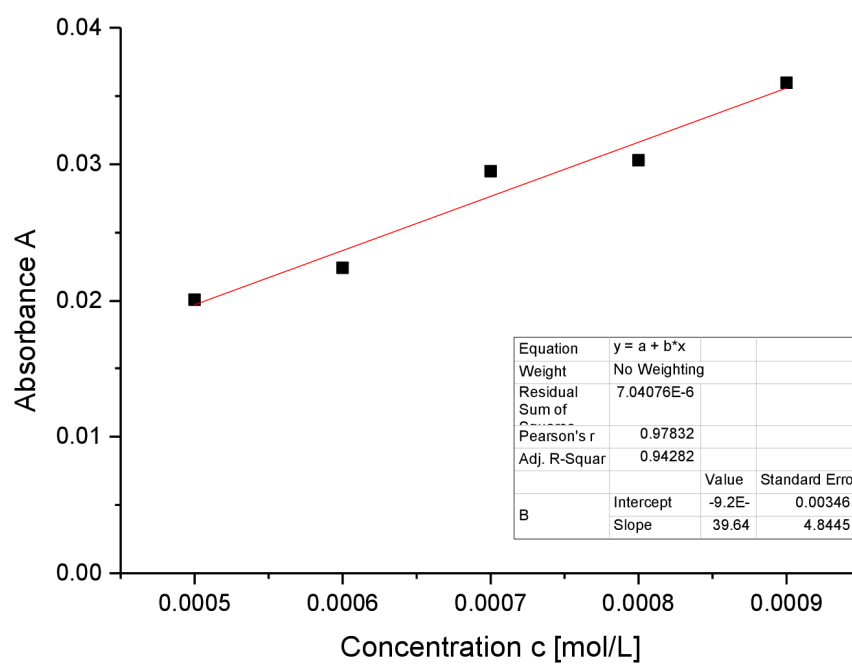


Figure S55: Determination of $\varepsilon(396 \text{ M}^{-1} \text{ cm}^{-1})$ by linear regression of absorptions ($\lambda = 454 \text{ nm}$) of **6f** against concentration.

Details on X-ray Diffraction Studies**Table S1.** Crystal data and structure refinement for *ligato*-TMS-substituted siliconoid **5a** (CCDC-1877380).

Identification code	sh3711	
Empirical formula	C ₇₈ H ₁₂₄ Si ₇ , 0.5(C ₅ H ₁₂)	
Formula weight	1294.47	
Temperature	132(2) K	
Wavelength	0.71073 Å	
Crystal system	Monoclinic	
Space group	C2/c	
Unit cell dimensions	a = 38.1514(15) Å	$\alpha = 90^\circ$.
	b = 12.7134(5) Å	$\beta = 94.456(3)^\circ$.
	c = 33.8416(11) Å	$\gamma = 90^\circ$.
Volume	16364.7(11) Å ³	
Z	8	
Density (calculated)	1.051 Mg/m ³	
Absorption coefficient	0.155 mm ⁻¹	
F(000)	5688	
Crystal size	0.546 x 0.393 x 0.223 mm ³	
Theta range for data collection	1.071 to 29.218°.	
Index ranges	-52 ≤ h ≤ 52, -17 ≤ k ≤ 17, -46 ≤ l ≤ 46	
Reflections collected	160059	
Independent reflections	22155 [R(int) = 0.0358]	
Completeness to theta = 25.242°	100.0 %	
Absorption correction	Semi-empirical from equivalents	
Max. and min. transmission	0.7458 and 0.7025	
Refinement method	Full-matrix least-squares on F ²	
Data / restraints / parameters	22155 / 83 / 836	
Goodness-of-fit on F ²	1.031	
Final R indices [I > 2σ(I)]	R1 = 0.0431, wR2 = 0.1036	
R indices (all data)	R1 = 0.0584, wR2 = 0.1118	
Extinction coefficient	n/a	
Largest diff. peak and hole	0.779 and -0.649 e.Å ⁻³	

Table S2. Crystal data and structure refinement for *ligato*-benzoyl-substituted siliconoid **5b** (CCDC-1877381).

Identification code	sh3716	
Empirical formula	C ₈₂ H ₁₂₀ O Si ₆	
Formula weight	1290.31	
Temperature	132(2) K	
Wavelength	0.71073 Å	
Crystal system	Monoclinic	
Space group	P2 ₁ /c	
Unit cell dimensions	a = 18.8229(6) Å	α = 90°.
	b = 28.6659(10) Å	β = 107.786(2)°.
	c = 30.7990(12) Å	γ = 90°.
Volume	15824.1(10) Å ³	
Z	8	
Density (calculated)	1.083 Mg/m ³	
Absorption coefficient	0.147 mm ⁻¹	
F(000)	5632	
Crystal size	0.672 x 0.453 x 0.385 mm ³	
Theta range for data collection	0.993 to 27.929°.	
Index ranges	-22 ≤ h ≤ 24, -37 ≤ k ≤ 35, -40 ≤ l ≤ 40	
Reflections collected	152878	
Independent reflections	37861 [R(int) = 0.0485]	
Completeness to theta = 25.242°	99.9 %	
Absorption correction	Semi-empirical from equivalents	
Max. and min. transmission	0.7456 and 0.6696	
Refinement method	Full-matrix least-squares on F ²	
Data / restraints / parameters	37861 / 192 / 1743	
Goodness-of-fit on F ²	1.081	
Final R indices [I > 2σ(I)]	R1 = 0.0648, wR2 = 0.1395	
R indices (all data)	R1 = 0.1038, wR2 = 0.1598	
Extinction coefficient	n/a	
Largest diff. peak and hole	0.801 and -0.476 e.Å ⁻³	

Table S3. Crystal data and structure refinement for *privo*-lithiated anionic siliconoid **4Li** (CCDC-1877378).

Identification code	sh3618	
Empirical formula	C ₈₇ H ₁₃₉ Li O ₃ Si ₆	
Formula weight	1408.45	
Temperature	175(2) K	
Wavelength	0.71073 Å	
Crystal system	Triclinic	
Space group	P-1	
Unit cell dimensions	a = 14.2918(16) Å	α = 109.652(5)°.
	b = 16.4145(18) Å	β = 104.243(4)°.
	c = 21.516(3) Å	γ = 99.970(4)°.
Volume	4422.6(9) Å ³	
Z	2	
Density (calculated)	1.058 Mg/m ³	
Absorption coefficient	0.138 mm ⁻¹	
F(000)	1544	
Crystal size	0.696 x 0.647 x 0.466 mm ³	
Theta range for data collection	1.362 to 27.284°.	
Index ranges	-18 ≤ h ≤ 18, -21 ≤ k ≤ 20, -27 ≤ l ≤ 27	
Reflections collected	69055	
Independent reflections	19545 [R(int) = 0.0443]	
Completeness to theta = 25.242°	100.0 %	
Absorption correction	Semi-empirical from equivalents	
Max. and min. transmission	0.7455 and 0.6196	
Refinement method	Full-matrix least-squares on F ²	
Data / restraints / parameters	19545 / 411 / 1006	
Goodness-of-fit on F ²	1.064	
Final R indices [I > 2σ(I)]	R1 = 0.0628, wR2 = 0.1581	
R indices (all data)	R1 = 0.0952, wR2 = 0.1885	
Extinction coefficient	n/a	
Largest diff. peak and hole	0.975 and -0.428 e.Å ⁻³	

Table S4. Crystal data and structure refinement for *privo*-TMS-substituted siliconoid **6a** (CCDC-1877379).

Identification code	sh3668	
Empirical formula	C ₇₈ H ₁₂₄ Si ₇ , C ₆ H ₁₄	
Formula weight	1344.57	
Temperature	152(2) K	
Wavelength	0.71073 Å	
Crystal system	Monoclinic	
Space group	P2 ₁ /c	
Unit cell dimensions	a = 21.0070(7) Å	α = 90°.
	b = 20.4182(7) Å	β = 95.4324(13)°.
	c = 19.9183(7) Å	γ = 90°.
Volume	8505.1(5) Å ³	
Z	4	
Density (calculated)	1.050 Mg/m ³	
Absorption coefficient	0.152 mm ⁻¹	
F(000)	2960	
Crystal size	0.480 x 0.380 x 0.166 mm ³	
Theta range for data collection	0.974 to 28.755°.	
Index ranges	-27 ≤ h ≤ 28, -27 ≤ k ≤ 25, -24 ≤ l ≤ 26	
Reflections collected	68739	
Independent reflections	22100 [R(int) = 0.0376]	
Completeness to theta = 25.242°	100.0 %	
Absorption correction	Semi-empirical from equivalents	
Max. and min. transmission	0.7458 and 0.6844	
Refinement method	Full-matrix least-squares on F ²	
Data / restraints / parameters	22100 / 26 / 1278	
Goodness-of-fit on F ²	1.032	
Final R indices [I > 2σ(I)]	R1 = 0.0473, wR2 = 0.1158	
R indices (all data)	R1 = 0.0737, wR2 = 0.1319	
Extinction coefficient	n/a	
Largest diff. peak and hole	0.783 and -0.504 e.Å ⁻³	

Table S5. Crystal data and structure refinement for *privo*-pivaloyl-substituted siliconoid **6c** (CCDC-1877382).

Identification code	sh3824	
Empirical formula	C ₈₀ H ₁₂₄ O Si ₆ , 0.5(C ₆ H ₁₄)	
Formula weight	1313.41	
Temperature	152(2) K	
Wavelength	0.71073 Å	
Crystal system	Triclinic	
Space group	P-1	
Unit cell dimensions	a = 13.3961(3) Å	α = 67.9010(10)°.
	b = 18.2592(5) Å	β = 70.1540(10)°.
	c = 19.4141(4) Å	γ = 76.3090(10)°.
Volume	4106.08(17) Å ³	
Z	2	
Density (calculated)	1.062 Mg/m ³	
Absorption coefficient	0.143 mm ⁻¹	
F(000)	1442	
Crystal size	0.374 x 0.306 x 0.220 mm ³	
Theta range for data collection	1.179 to 33.864°.	
Index ranges	-20 ≤ h ≤ 20, -28 ≤ k ≤ 28, -30 ≤ l ≤ 30	
Reflections collected	127205	
Independent reflections	33036 [R(int) = 0.0356]	
Completeness to theta = 25.242°	100.0 %	
Absorption correction	Semi-empirical from equivalents	
Max. and min. transmission	0.7467 and 0.7205	
Refinement method	Full-matrix least-squares on F ²	
Data / restraints / parameters	33036 / 77 / 872	
Goodness-of-fit on F ²	1.032	
Final R indices [I > 2σ(I)]	R1 = 0.0544, wR2 = 0.1381	
R indices (all data)	R1 = 0.0908, wR2 = 0.1578	
Extinction coefficient	n/a	
Largest diff. peak and hole	1.580 and -0.722 e.Å ⁻³	

Table S6. Crystal data and structure refinement for *privo*-borate-substituted siliconoid **6f** (CCDC-1877383).

Identification code	sh3732	
Empirical formula	C ₁₅₈ H ₂₅₂ B ₂ Li ₂ O ₂ Si ₁₂ , 2(C ₆ H ₆)	
Formula weight	2712.38	
Temperature	192(2) K	
Wavelength	0.71073 Å	
Crystal system	Monoclinic	
Space group	P2 ₁ /c	
Unit cell dimensions	a = 17.8496(8) Å	α = 90°.
	b = 24.9370(10) Å	β = 99.856(2)°.
	c = 20.3519(9) Å	γ = 90°.
Volume	8925.2(7) Å ³	
Z	2	
Density (calculated)	1.009 Mg/m ³	
Absorption coefficient	0.133 mm ⁻¹	
F(000)	2968	
Crystal size	0.778 x 0.754 x 0.306 mm ³	
Theta range for data collection	1.158 to 29.617°.	
Index ranges	-24 ≤ h ≤ 24, -34 ≤ k ≤ 22, -28 ≤ l ≤ 28	
Reflections collected	96855	
Independent reflections	25096 [R(int) = 0.0341]	
Completeness to theta = 25.242°	100.0 %	
Absorption correction	Semi-empirical from equivalents	
Max. and min. transmission	0.7459 and 0.6970	
Refinement method	Full-matrix least-squares on F ²	
Data / restraints / parameters	25096 / 192 / 950	
Goodness-of-fit on F ²	1.403	
Final R indices [I > 2σ(I)]	R1 = 0.0643, wR2 = 0.1752	
R indices (all data)	R1 = 0.0991, wR2 = 0.1926	
Extinction coefficient	n/a	
Largest diff. peak and hole	1.192 and -0.383 e.Å ⁻³	

Plot of the Hammett parameter σ_m/σ_p vs ^{29}Si chemical shift of Si2

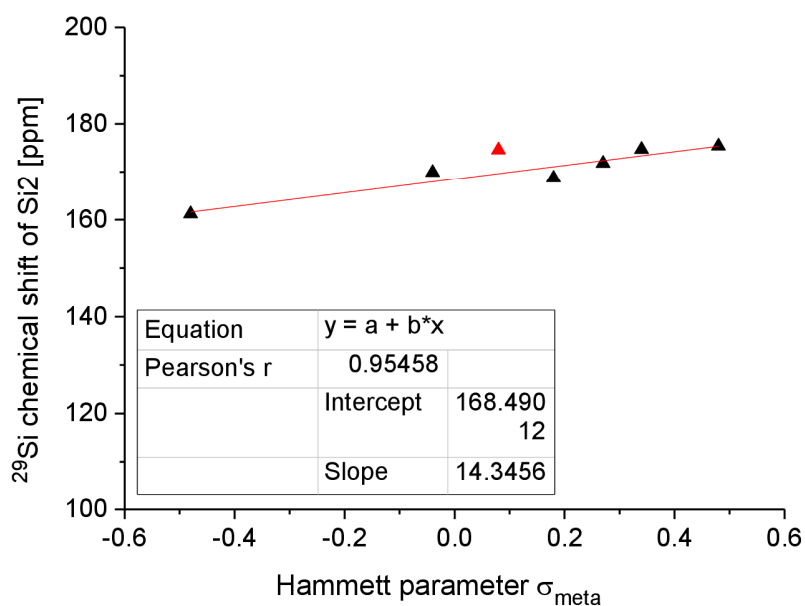


Figure S56: Plot of the Hammett parameter σ_m vs ^{29}Si chemical shift of Si2 for substituents in *ligato* position of **5a-f** and **2**.

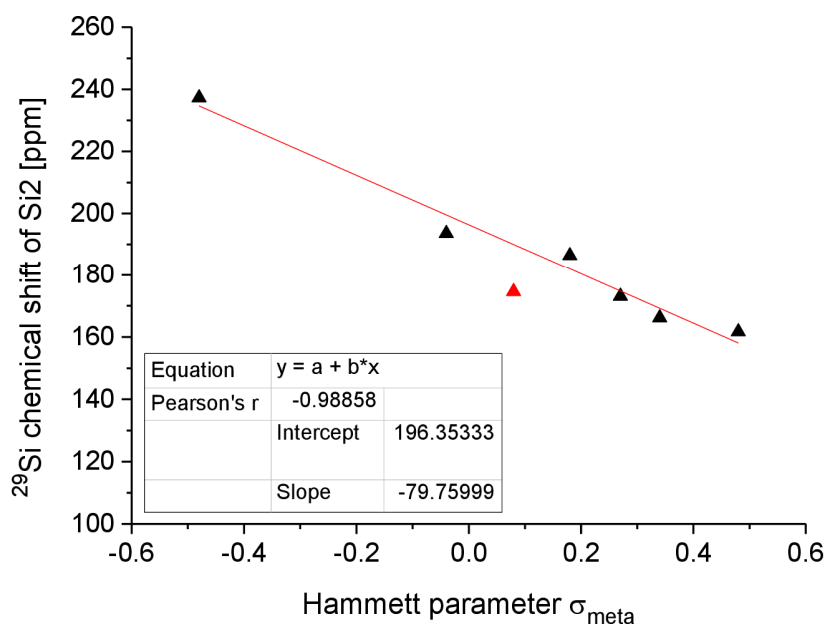


Figure S57: Plot of the Hammett parameter σ_m vs ^{29}Si chemical shift of Si2 for substituents in *privo* position of **6a-f** and **2**.

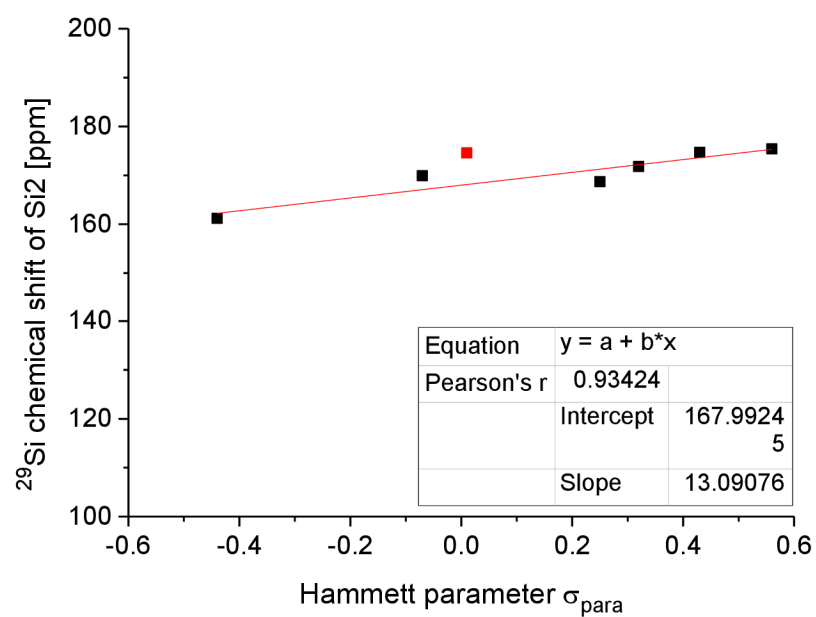


Figure S58: Plot of the Hammett parameter σ_p vs ^{29}Si chemical shift of Si2 for substituents in *ligato* position of **5a-f** and **2**.

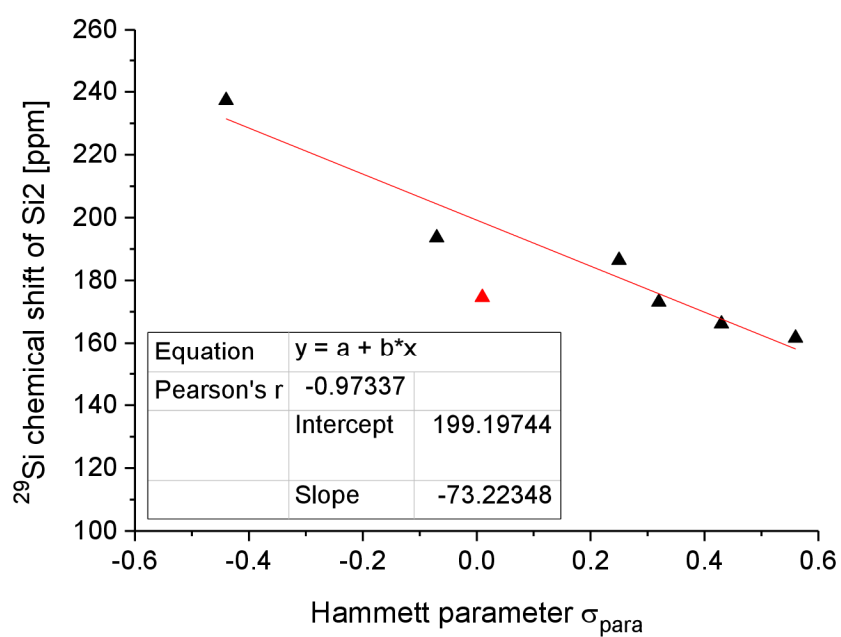


Figure S59: Plot of the Hammett parameter σ_p vs ^{29}Si chemical shift of Si2 for substituents in *privo* position of **6a-f** and **2**.

6.2 Indirect and Direct Grafting of Transition Metals to Siliconoids



Supporting Information

Indirect and Direct Grafting of Transition Metals to Siliconoids

*Nadine E. Poitiers, Luisa Giarrana, Kinga I. Leszczyńska, Volker Huch, Michael Zimmer, and David Scheschkewitz**

anie_202001178_sm_miscellaneous_information.pdf

Table of Contents

<u>1. Experimental Procedures</u>	S3
<u>2. Preparation, data and spectra (NMR, UV-vis, IR) of:</u>	
• <i>ligato</i> -Zirconocene-substituted siliconoid (2a)	S3
• <i>ligato</i> -Hafnocene-substituted siliconoid (2b)	S8
• General procedure for tetrylene-substituted siliconoids	S13
• <i>ligato</i> -Silylene-substituted siliconoid (3a)	S13
• <i>ligato</i> -Germylene-substituted siliconoid (3b)	S18
• <i>ligato</i> -Stannylene-substituted siliconoid (3c)	S23
• <i>ligato</i> -Silylene-substituted siliconoid Fe(CO) ₄ complex (4a)	S29
• <i>ligato</i> -Germylene-substituted siliconoid Fe(CO) ₄ complex (4b)	S34
• <i>ligato</i> -Stannylene-substituted siliconoid Fe(CO) ₄ complex (4c)	S39
<u>3. Details on Structure optimization at BP86+D3(BJ)/def2-SVP level of theory</u>	S48
• <i>ligato</i> -Zirconocene-substituted siliconoid (2a)	S48
• <i>ligato</i> -Hafnocene-substituted siliconoid (2b)	S52
<u>4. Details on X-Ray Diffraction Studies</u>	S56
• <i>ligato</i> -Zirconocene-substituted siliconoid (2a)	S56
• <i>ligato</i> -Hafnocene-substituted siliconoid (2b)	S58
• <i>ligato</i> -Silylene-substituted siliconoid (3a)	S60
• <i>ligato</i> -Germylene-substituted siliconoid (3b)	S62
• <i>ligato</i> -Stannylene-substituted siliconoid (3c)	S64
• <i>ligato</i> -Silylene-substituted siliconoid Fe(CO) ₄ complex (4a)	S66
• <i>ligato</i> -Germylene-substituted siliconoid Fe(CO) ₄ complex (4b)	S68
• <i>ligato</i> -Stannylene-substituted siliconoid Fe(CO) ₄ complex (4c)	S70
<u>5. References</u>	S71
<u>6. Author Contributions</u>	S71

1. Experimental Procedures

All manipulations were carried out under a protective atmosphere of argon, by using a glovebox or standard Schlenk techniques. Ethereal solvents were dried by heating to reflux over Na/benzophenone and distilled and stored under an atmosphere of argon. Hydrocarbons were dried over sodium or potassium. NMR spectra were recorded on a Bruker Avance IV 400 NMR spectrometer (^1H = 400.13 MHz, ^{13}C = 100.6 MHz, ^{29}Si = 59.6 MHz, ^{119}Sn = 149.21 MHz) and a Bruker Avance III 400 WB spectrometer (^{29}Si = 79.53 MHz, ^{119}Sn = 149.27 MHz). UV/Vis spectra were recorded on a Shimadzu UV-2600 spectrometer in quartz cells with a path length of 0.1 cm. Infrared spectra were measured with a Shimadzu IRAffinity-1S in a platinum ATR diamond cell. Elemental analyses were performed on an elemental analyzer Leco CHN-900 and/or an elemental vario Micro Cube. The anionic siliconoid **1Li**^[1] and NH_4SiCl (**a**), NH_4GeCl (**b**), NH_4SnCl (**c**)^[2] were prepared following the literature protocols.

2. Preparation, data and spectra (NMR, UV-vis, IR)

Preparation of *ligato*-zirconocene-substituted siliconoid (**2a**)

The anionic siliconoid **1Li** (300 mg; 0.203 mmol) and 1 eq (59.39 mg; 0.203 mmol) of bis(cyclopentadienyl)zirconium(IV) dichloride were dissolved in 5 mL benzene under stirring. The solution turned instantly dark red and was stirred overnight at room temperature. The solvent was removed in vacuo and the dark red residue was filtered from 3 mL hexane. The solution was concentrated to 1 mL and stored at -26°C for one day to obtain dark red crystals of **2a** (185 mg; 0.128 mmol) in 63 % yield (mp. 115°C , dec.).

^1H -NMR (400.13 MHz, C_6D_6 , 300 K) δ = 7.625 (q, 5H, C_{10}H_8), 7.326 – 7.322 (m, 1H, Ar-H), 7.251 (q, 5H, C_{10}H_8), 7.203 – 7.200 (m, 1H, Ar-H), 7.057 (m, 1H, Ar-H), 6.989 – 6.973 (m, 3H, Ar-H), 6.894 (bs, 1H, Ar-H), 6.862 – 6.859 (m, 1H, Ar-H), 6.806 – 6.803 (m, 1H, Ar-H), 6.772 – 6.769 (m, 1H, Ar-H), 6.038 (sept, 1H, $^3J_{\text{HH}} = 6.70$ Hz, Tip-*i*Pr-CH₂), 5.915 (s, 5H, Cp), 5.478 (s, 5H, Cp), 5.027 (sept, 1H, $^3J_{\text{HH}} = 6.65$ Hz, Tip-*i*Pr-CH₂), 4.648 (sept, 1H, $^3J_{\text{HH}} = 6.61$ Hz, Tip-*i*Pr-CH₂), 4.143 (sept, 1H, $^3J_{\text{HH}} = 6.61$ Hz, Tip-*i*Pr-CH₂), 4.103 (s, 0.2H, Si-H), 3.934 (sept, 1H, $J = 6.45$ Hz, Tip-*i*Pr-CH₂), 3.744 (sept, 1H, $^3J_{\text{HH}} = 6.45$ Hz, Tip-*i*Pr-CH₂), 3.453 (sept, 1H, $^3J_{\text{HH}} = 6.45$ Hz, Tip-*i*Pr-CH₂), 3.391 – 3.289 (m, 2H, Tip-*i*Pr-CH₂), 2.937 (sept, 1H, $^3J_{\text{HH}} = 6.43$ Hz, Tip-*i*Pr-CH₂), 2.846 – 2.540 (m, 7 H, Tip-*i*Pr-CH₂), 2.284 (d, 3H, $^3J_{\text{HH}} = 6.60$ Hz, Tip-*i*Pr-CH₃), 2.029 (d, 3H, $^3J_{\text{HH}} = 6.60$ Hz, Tip-*i*Pr-CH₃), 1.732 (d, 3H, $^3J_{\text{HH}} = 6.37$ Hz, Tip-*i*Pr-CH₃), 1.690 – 1.465 (m, 30H, Tip-*i*Pr-CH₃ overlapping with hexane), 1.282 – 1.016 (m, 62 H, Tip-*i*Pr-CH₃), 0.891 (t, 4H, hexane), 0.678 (d, 3H, $^3J_{\text{HH}} = 6.31$ Hz, Tip-*i*Pr-CH₃), 0.602 (d, 3H, $^3J_{\text{HH}} = 6.31$ Hz, Tip-*i*Pr-CH₃), 0.495 (d, 3H, $^3J_{\text{HH}} = 6.31$ Hz, Tip-*i*Pr-CH₃), 0.394 (d, 3H, $^3J_{\text{HH}} = 6.66$ Hz, Tip-*i*Pr-CH₃), 0.337 (d, 3H, $^3J_{\text{HH}} = 6.31$ Hz, Tip-*i*Pr-CH₃), 0.233 (d, 3H, $^3J_{\text{HH}} = 6.31$ Hz, Tip-*i*Pr-CH₃), 0.154 (d, 3H, $^3J_{\text{HH}} = 6.31$ Hz, Tip-*i*Pr-CH₃) ppm.

^{13}C -NMR (100.61 MHz, C_6D_6 , 300 K) δ = 156.20, 155.96, 154.57, 154.38, 154.16, 153.97, 153.52, 153.32, 152.87, 152.05, 151.12, 150.54 (s, each 1C, Ar-C), 150.36, 150.32 (s, each 1C, Ar-C), 150.01, 149.76, 149.35, 149.05, 148.83 (s, each 1C, Ar-C), 143.09, 141.06, 139.37, 138.63, 136.89, 136.48, 134.21, 133.99 (s, each 1C, Ar-C), 129.07, 128.17, 128.09, 127.86 (s, each 1C, Ar-CH, overlapping with C_6D_6), 125.99 (s, 1C, Ar-CH), 123.81, 123.36, 123.28, 123.20, 122.77, 122.61, 122.34, 122.28, 122.21, 121.12 (bs, each 1C, Ar-CH), 115.64 (s, 1C, Ar-CH), 114.08 (s, 2C, Ar-CH), 112.49 (s, 1C, Ar-C-Zr), 111.80 (s, 1C, Ar-C-Zr), 37.86, 37.36, 36.37, 36.13, 35.99, 35.66, 35.54, 35.33 (s, each 1C, Tip-*i*Pr-CH) 34.71, 34.64, 34.60, 34.49, 34.38, 34.34, 34.31, 34.05, 33.12 (s, each 1C, Tip-*i*Pr-CH), 31.90 (s, 1C, Tip-*i*Pr-CH), 29.32, 28.87, 28.84 (s, each 1C, Tip-*i*Pr-CH₃), 27.14, 27.11 (bs, each 1C, Tip-*i*Pr-CH₃), 26.51, 26.09, 25.67 (s, each 1C, Tip-*i*Pr-CH₃), 25.21, 25.13, 25.09 (bs, each 1C, Tip-*i*Pr-CH₃), 24.61 (s, 1C, Tip-*i*Pr-CH₃), 24.39, 24.22, 24.18, 24.13, 24.07, 24.01, 23.97, 23.91, 23.89, 23.84, 23.69, 23.68, 23.49 (s, each 1C, overlapping, Tip-*i*Pr-CH₃), 22.99 (s, 1C, Tip-*i*Pr-CH₃), 14.30 (s, 1C, Tip-*i*Pr-CH₃) ppm.

^{29}Si -NMR (79.49 MHz, C_6D_6 , 300 K) δ = 162.6 (s, *privo*-Si(Tip)₂), 29.5 (s, *ligato*-SiTip), 23.7 (s, *remoto*-Si(Tip)₂), 21.4 (s, *ligato*-Si-Zr(Cp₂Cl), -233.5 (s, *nudo*-Si), -240.6 (s, *nudo*-Si) ppm.

CP-MAS ^{29}Si -NMR (79.53 MHz, 300K) δ = 161.7 (s, *privo*-Si(Tip)₂), 30.2 (s, *ligato*-SiTip), 22.1 (s, *remoto*-Si(Tip)₂), 18.8 (s, *ligato*-Si-Zr(Cp₂Cl), -234.6 (s, *nudo*-Si), -243.7 (s, *nudo*-Si) ppm.

Elemental analysis: calculated for $\text{C}_{85}\text{H}_{125}\text{ClZrSi}_6$ (additional 0.4 eq C_{10}H_8): C: 71.59 % ; H: 8.64 %. Found: C: 72.70 % ; H: 9.01 %.

UV/VIS (hexane): λ_{max} (ϵ) = 521 nm ($1700 \text{ M}^{-1} \text{ cm}^{-1}$).

SUPPORTING INFORMATION

WILEY-VCH

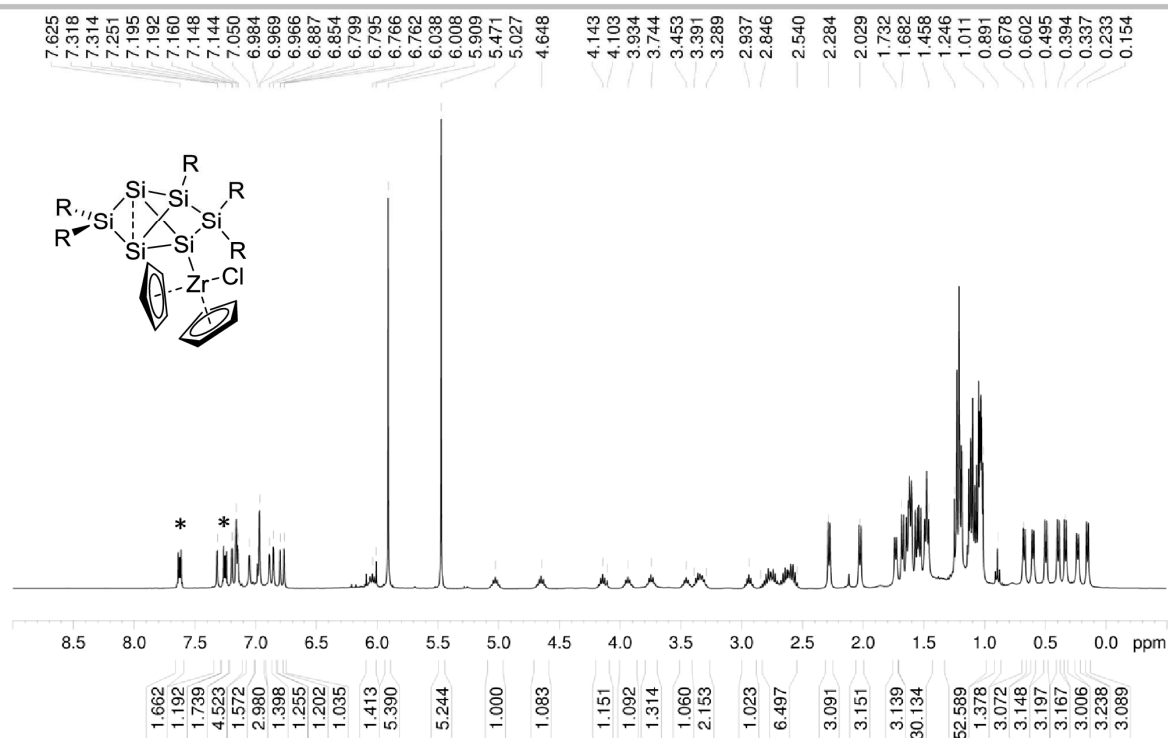


Figure S1. ¹H NMR of **2a** in C₆D₆ (400.13 MHz, 300 K). Residual naphthalene (C₁₀H₈) marked with asterisk (*).

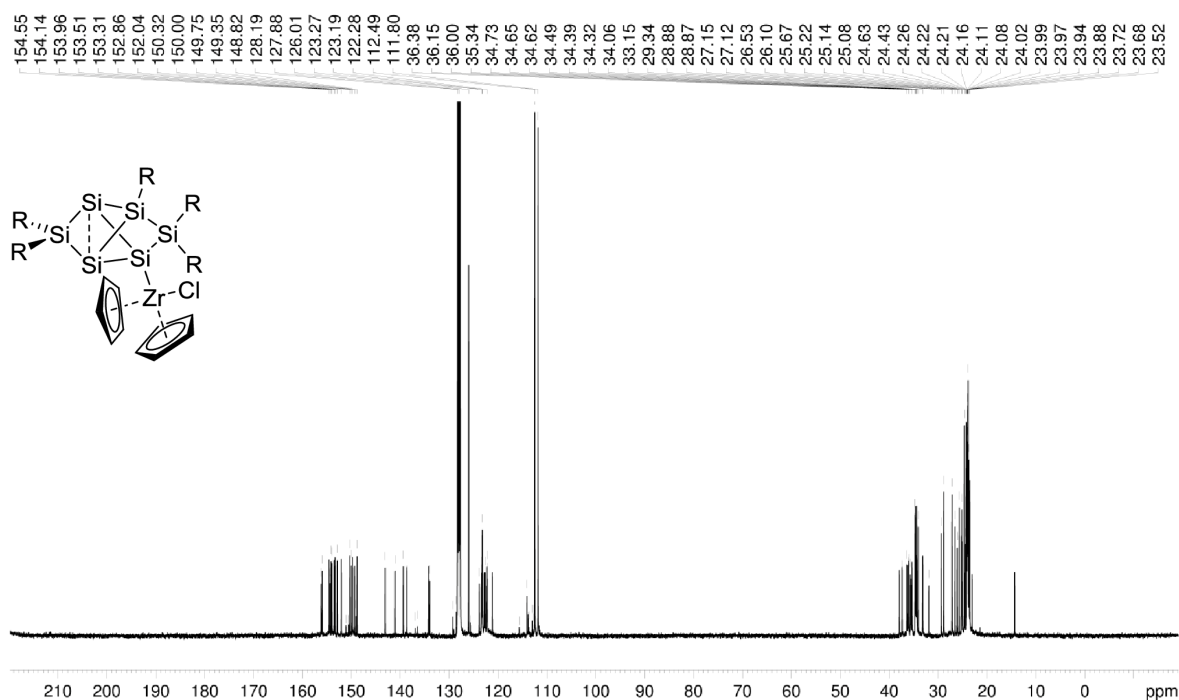


Figure S2. ¹³C NMR of **2a** in C₆D₆ (100.61 MHz, 300 K).

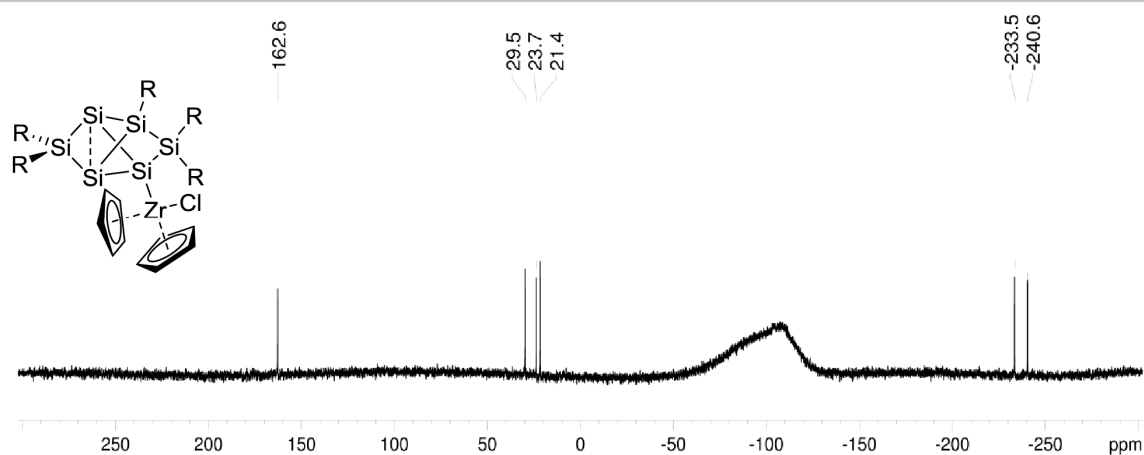


Figure S3. ^{29}Si NMR of **2a** in C_6D_6 (79.49 MHz, 300 K).

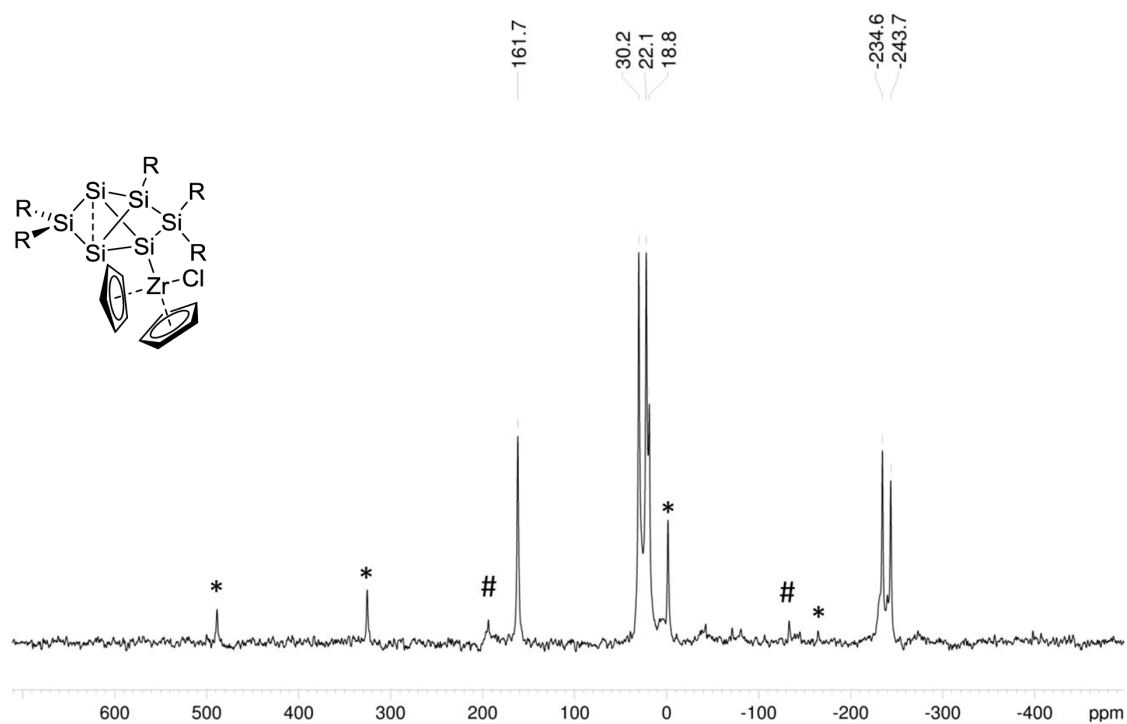


Figure S4. CP-MAS ^{29}Si NMR of **2a** in C_6D_6 (79.53 MHz, 14 KHz, 300 K), side spinning bands of: * *privo*-SiTip₂ (161.7 ppm), # *ligato*-SiTip (30.2 ppm).

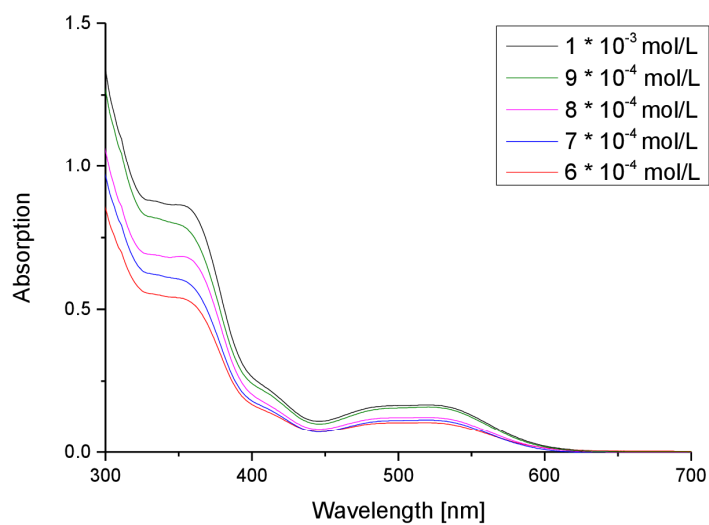


Figure S5. UV-Vis spectrum of **2a** in hexane at different concentrations.

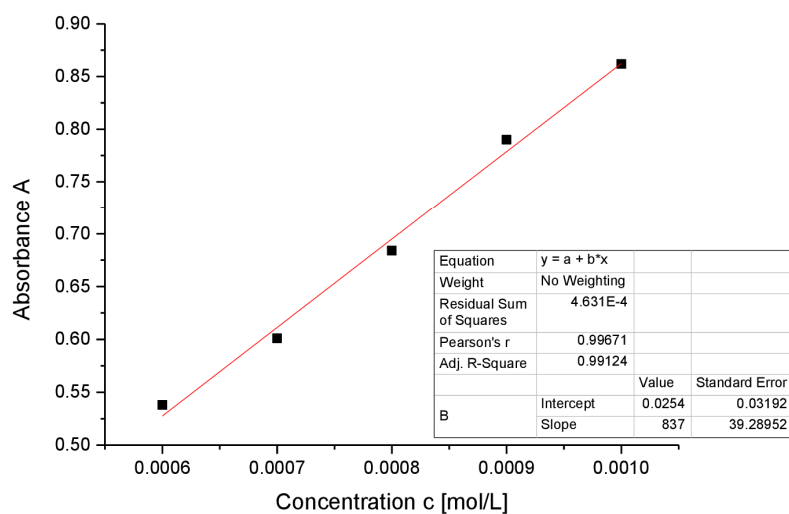


Figure S6. Determination of ε ($8370 \text{ M}^{-1} \text{ cm}^{-1}$) by linear regression of absorptions ($\lambda = 353 \text{ nm}$) of **2a** against concentration.

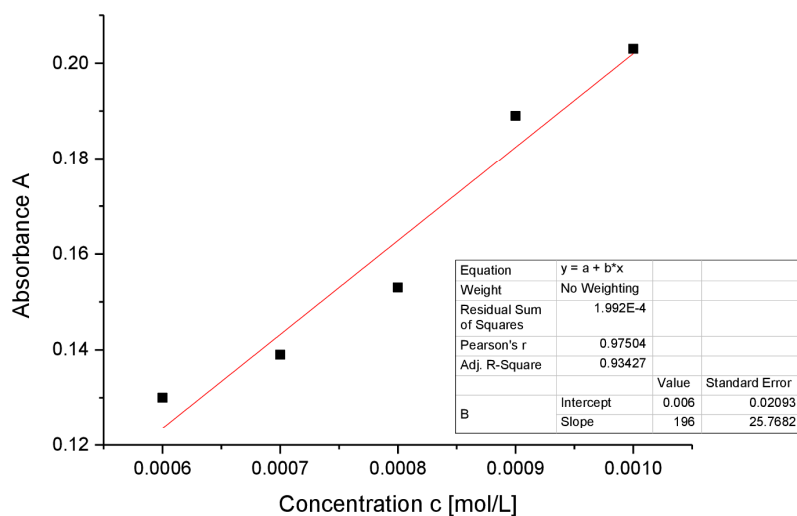


Figure S7. Determination of ϵ ($1960 \text{ M}^{-1} \text{ cm}^{-1}$) by linear regression of absorptions ($\lambda = 416 \text{ nm}$) of **2a** against concentration.

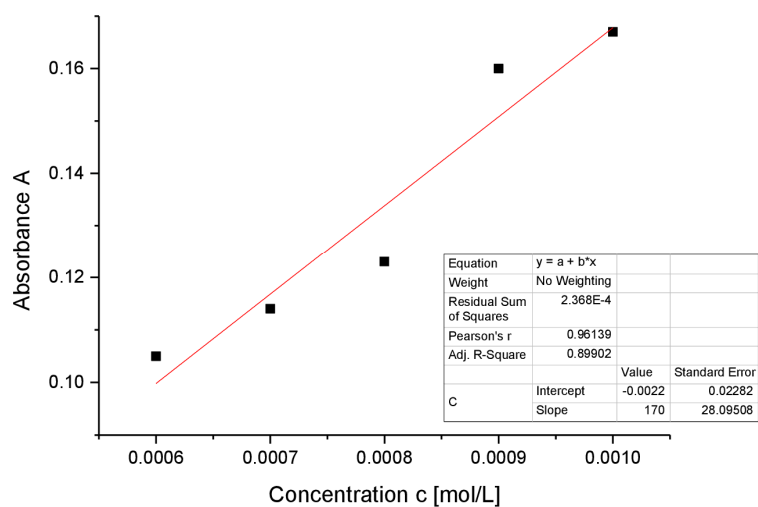


Figure S8. Determination of ϵ ($1700 \text{ M}^{-1} \text{ cm}^{-1}$) by linear regression of absorptions ($\lambda = 521 \text{ nm}$) of **2a** against concentration.

SUPPORTING INFORMATION

WILEY-VCH

Preparation of *ligato*-Hafnocence-substituted siliconoid (2b)

The anionic siliconoid **1Li** (365 mg; 0.237 mmol) and 1 eq (90.15 mg; 0.237 mmol) of bis(cyclopentadienyl)hafnium(IV)dichloride were dissolved in 4 mL benzene under stirring at room temperature. The solution turned instantly dark purple and was stirred 2h. The solvent was removed in vacuo and the dark red residue was filtered from 6 mL hexane. The solution was concentrated to 1 mL and stored at -26°C for one day to yield bright red crystals of the hafnium-functionalized siliconoid **2b** (225 mg; 0.147 mmol). A second batch of crystals was isolated by reducing the mother liquor (15 mg, 0.01 mmol) giving a total amount of 66 % (240 mg; 0.157 mmol) of compound **2b** (mp. $> 270^{\circ}\text{C}$, dec.).

$^1\text{H-NMR}$ (400.13 MHz, C_6D_6 , 300 K) δ = 7.628 (q, 1H, C_{10}H_8), 7.316 – 7.312 (m, 1H, Ar-H), 7.251 (q, 1H C_{10}H_8), 7.203 – 7.199 (m, 1H, Ar-H), 7.160 – 7.131 (m, 1H, Ar-H), 7.049 (bs, 1H, Ar-H), 6.986 – 6.970 (m, 2H, Ar-H), 6.891 (bs, 1H, Ar-H), 6.861 – 6.857 (m, 1H, Ar-H), 6.807 – 6.803 (m, 1H, Ar-H), 6.757 – 6.753 (m, 1H, Ar-H), 6.039 (sept, 1H, $^3J_{\text{HH}} = 6.45$ Hz, Tip-*i*Pr- CH_2), 5.949 (s, 0.5 H, Cp), 5.829 (s, 5H, Cp), 5.382 (s, 5H, Cp), 5.041 (sept, 1H, $^3J_{\text{HH}} = 6.69$ Hz, Tip-*i*Pr- CH_2), 4.645 (sept, 1H, $^3J_{\text{HH}} = 6.67$ Hz, Tip-*i*Pr- CH_2), 4.137 (sept, 1H, $^3J_{\text{HH}} = 6.67$ Hz, Tip-*i*Pr- CH_2), 4.092 (s, 0.1H, Si-H), 3.939 (sept, 1H, $^3J_{\text{HH}} = 6.05$ Hz, Tip-*i*Pr- CH_2), 3.782 (sept, 1H, $^3J_{\text{HH}} = 6.36$ Hz, Tip-*i*Pr- CH_2), 3.472 (sept, 1H, $^3J_{\text{HH}} = 6.36$ Hz, Tip-*i*Pr- CH_2), 3.354 (sept, 1H, $^3J_{\text{HH}} = 6.36$ Hz, Tip-*i*Pr- CH_2), 2.939 (sept, 1H, $^3J_{\text{HH}} = 6.49$ Hz, Tip-*i*Pr- CH_2), 2.830 – 2.529 (m, 5 H, Tip-*i*Pr- CH_2), 2.279 (d, 3H, $^3J_{\text{HH}} = 6.50$ Hz, Tip-*i*Pr- CH_3), 2.028 (d, 3H, $^3J_{\text{HH}} = 6.50$ Hz, Tip-*i*Pr- CH_3), 1.738 (d, 3H, $^3J_{\text{HH}} = 6.44$ Hz, Tip-*i*Pr- CH_3), 1.653 – 1.565 (m, 16H, Tip-*i*Pr- CH_3), 1.527 – 1.463 (m, 10 H, Tip-*i*Pr- CH_3), 1.280 – 1.180 (m, 27 H, Tip-*i*Pr- CH_3), 1.129 – 1.102 (m, 27 H, Tip-*i*Pr- CH_3), 0.889 (t, 10H, hexane), 0.676 (d, 3H, $^3J_{\text{HH}} = 6.48$ Hz, Tip-*i*Pr- CH_3), 0.602 (d, 3H, $^3J_{\text{HH}} = 6.05$ Hz, Tip-*i*Pr- CH_3), 0.504 (d, 3H, $^3J_{\text{HH}} = 6.65$ Hz, Tip-*i*Pr- CH_3), 0.391 (d, 3H, $^3J_{\text{HH}} = 6.35$ Hz, Tip-*i*Pr- CH_3), 0.337 (d, 3H, $^3J_{\text{HH}} = 6.35$ Hz, Tip-*i*Pr- CH_3), 0.241 (d, 3H, $^3J_{\text{HH}} = 6.35$ Hz, Tip-*i*Pr- CH_3), 0.151 (d, 3H, $^3J_{\text{HH}} = 6.05$ Hz, Tip-*i*Pr- CH_3) ppm.

$^{13}\text{C-NMR}$ (100.61 MHz, C_6D_6 , 300 K) δ = 156.22, 155.99, 154.55, 154.42, 154.16, 154.06, 153.55, 153.35, 153.00, 152.07 (s, each 1C, Ar-C), 150.30, 149.98, 149.74, 149.30, 148.80 (s, each 1C, Ar-C), 143.19, 141.17, 139.49, 138.80, 135.27, 134.00 (s, each 1C, Ar-C), 128.51, 128.09, 127.86 (s, each 1C, Ar-CH, overlapping with C_6D_6), 125.99 (s, 1C, Ar-CH), 123.82, 123.41, 123.26, 123.20, 122.79, 122.62 (s, each 1C, Ar-CH), 122.28 (bs, 2C, Ar-CH), 121.14 (s, 1C, Ar-CH), 114.30 (s, 1C, Ar-CH), 112.84 (s, 1C, Ar-CH), 111.42 (s, 1C, Ar-C-Hf), 110.84 (s, 1C, Ar-C-Hf), 37.84, 37.23, 36.42, 36.09, 35.97 (s, each 1C, Tip-*i*Pr-CH), 35.65, 35.57 (bs, each 1C, Tip-*i*Pr-CH), 35.35 (s, 1C, Tip-*i*Pr-CH), 34.71, 34.64, 34.59, 34.50, 34.37, 34.30, 34.05 (s, each 1C, Tip-*i*Pr-CH), 33.17 (s, 1C, Tip-*i*Pr-CH), 31.90 (s, 2C, Tip-*i*Pr-CH), 29.31, 28.84, 27.15, 26.51, 26.09, 25.68, 25.26, 25.12 (s, each 1C, Tip-*i*Pr- CH_3), 24.63, 24.59 (bs, each 1C, Tip-*i*Pr- CH_3), 24.38 (bs, 1C, Tip-*i*Pr- CH_3), 24.21, 24.19, 24.17, 24.12, 24.07, 24.03, 23.99, 23.95, 23.84 (s, each 1C, overlapping, Tip-*i*Pr- CH_3), 23.70, 23.49 (s, each 1C, Tip-*i*Pr- CH_3), 22.99 (s, 2C, Tip-*i*Pr- CH_3) ppm.

$^{29}\text{Si-NMR}$ (79.49 MHz, C_6D_6 , 300 K) δ = 162.8 (s, *privo*-Si(Tip) $_2$), 35.9 (s, *ligato*-SiTip), 31.0 (s, *remoto*-Si(Tip) $_2$), 28.4 (s, *ligato*-Si-Zr(Cp_2Cl), -232.1 (s, *nudo*-Si), -240.3 (s, *nudo*-Si) ppm.

CP-MAS $^{29}\text{Si-NMR}$ (79.53 MHz, 300K) δ = 162.0 (s, *privo*-Si(Tip) $_2$), 36.3 (s, *ligato*-SiTip), 30.5 (s, *remoto*-Si(Tip) $_2$), 27.6 (s, *ligato*-Si-Zr(Cp_2Cl), -229.4 (s, *nudo*-Si), -239.9 (s, *nudo*-Si) ppm.

Elemental analysis: calculated for $\text{C}_{85}\text{H}_{125}\text{ClHfSi}_6$: C: 66.75 % ; H: 8.24 % . Found: C:65.54 % ; H: 7.85 % .

UV/VIS (hexane): λ_{max} (ε) = 497 nm ($2710 \text{ M}^{-1} \text{ cm}^{-1}$).

SUPPORTING INFORMATION

WILEY-VCH

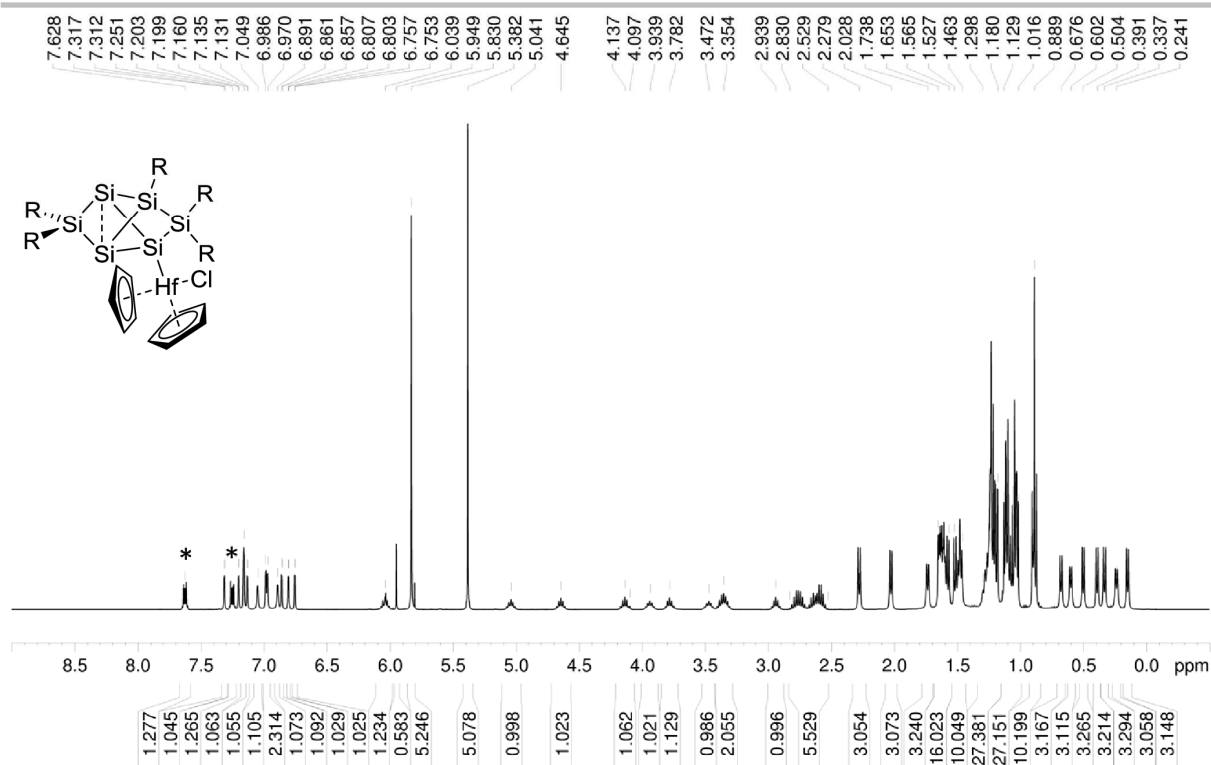


Figure S9. ¹H NMR of **2b** in C₆D₆ (400.13 MHz, 300 K). Residual naphthalene (C₁₀H₈) marked with asterisk (*).

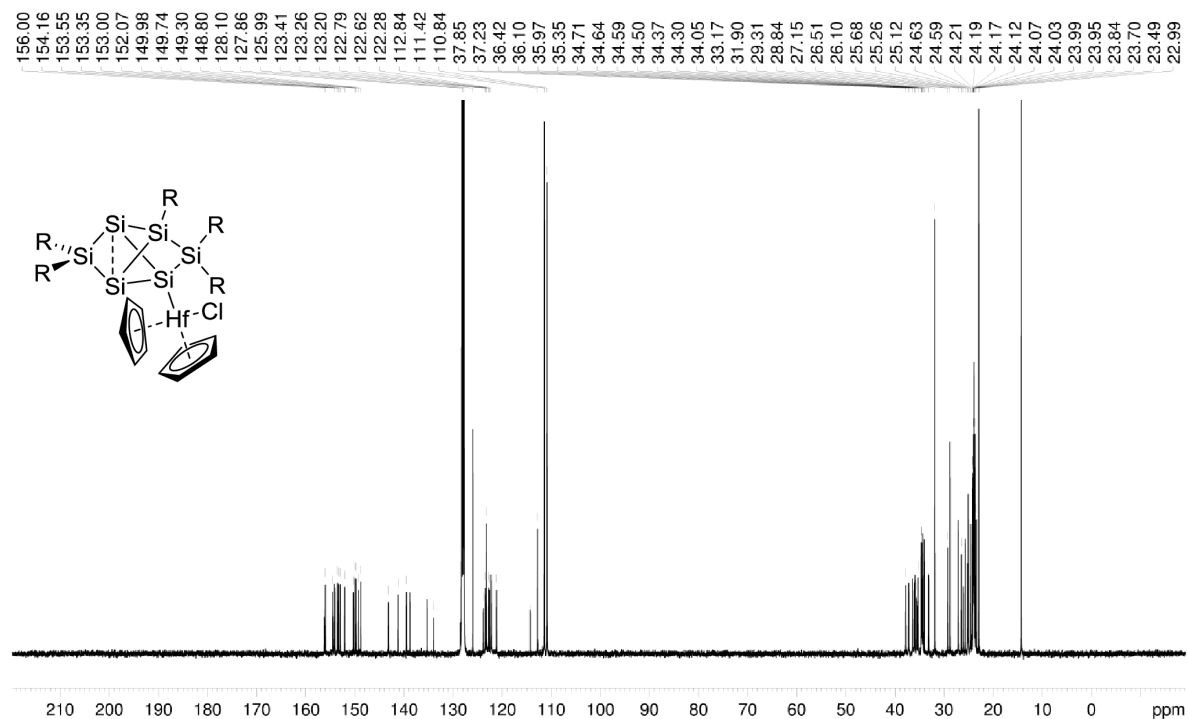


Figure S10. ¹³C NMR of **2b** in C₆D₆ (100.61 MHz, 300 K).

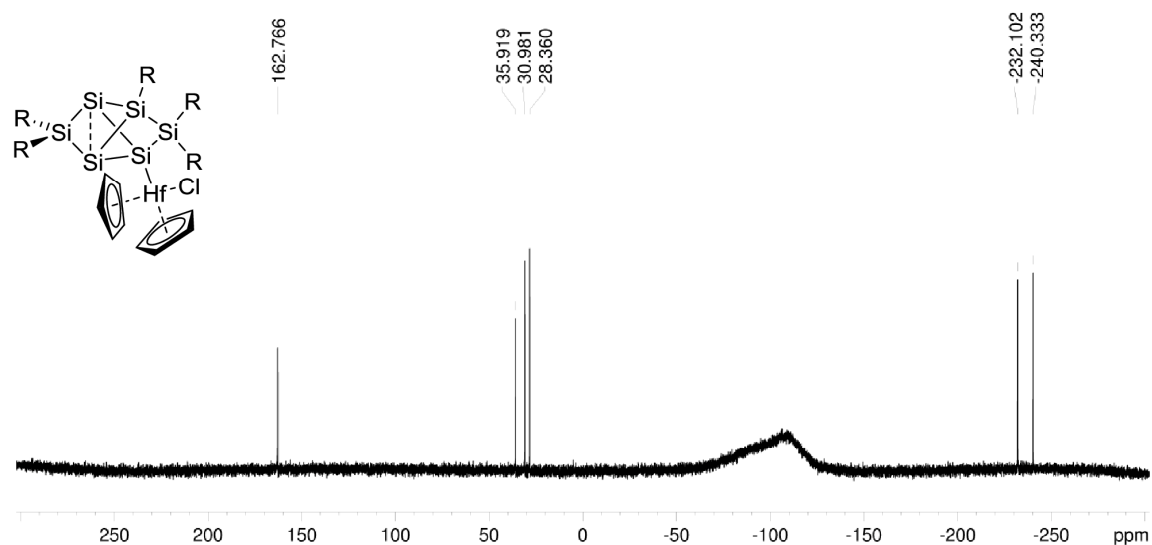


Figure S11. ^{29}Si NMR of **2b** in C_6D_6 (79.49 MHz, 300 K).

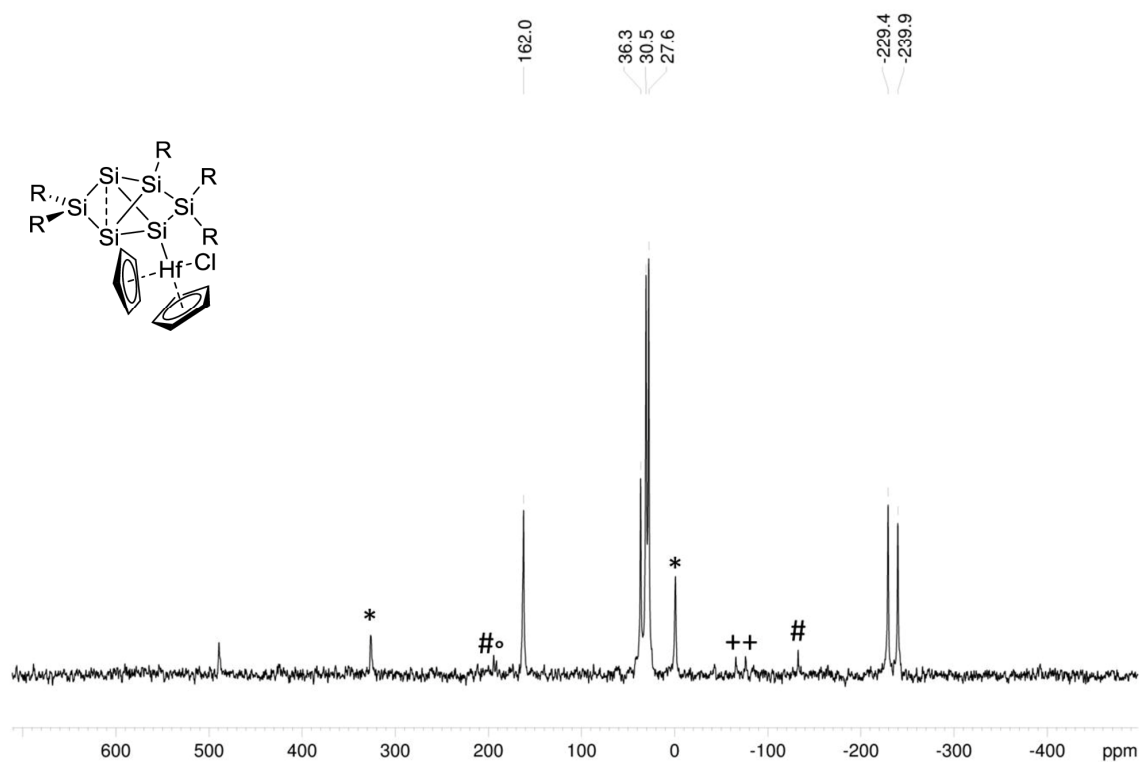


Figure S12. CP-MAS ^{29}Si NMR of **2b** in C_6D_6 (79.53 MHz, 13 KHz, 300 K), side spinning bands of: * *privo*- SiTip_2 (162.0 ppm), # *remoto*- $\text{Si}(\text{Tip})_2$ (30.5 ppm), ° *ligato*- $\text{Si-Zr}(\text{Cp}_2\text{Cl})$ (27.6 ppm), + *nudo*-Si (229.4 ppm, 239.9 ppm).

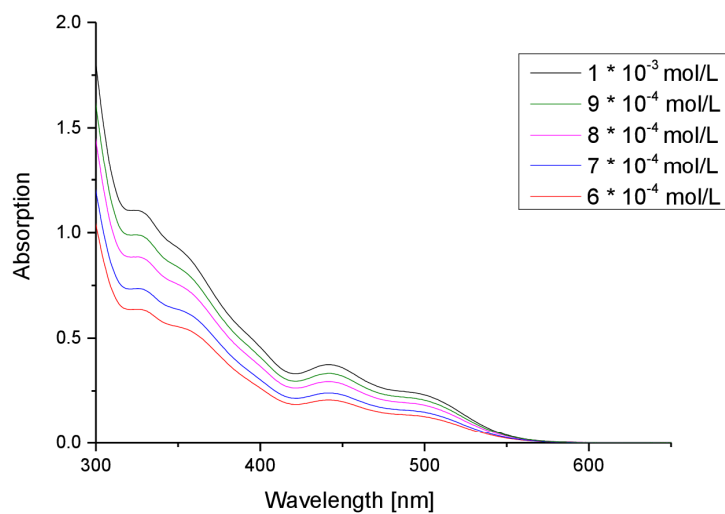


Figure S13. UV-Vis spectrum of **2a** in hexane at different concentrations.

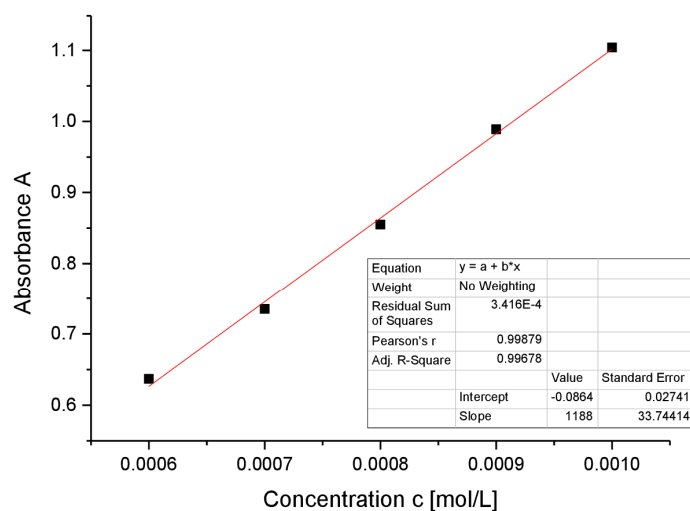


Figure S14. Determination of ϵ ($11880 \text{ M}^{-1} \text{ cm}^{-1}$) by linear regression of absorptions ($\lambda = 325 \text{ nm}$) of **2b** against concentration.

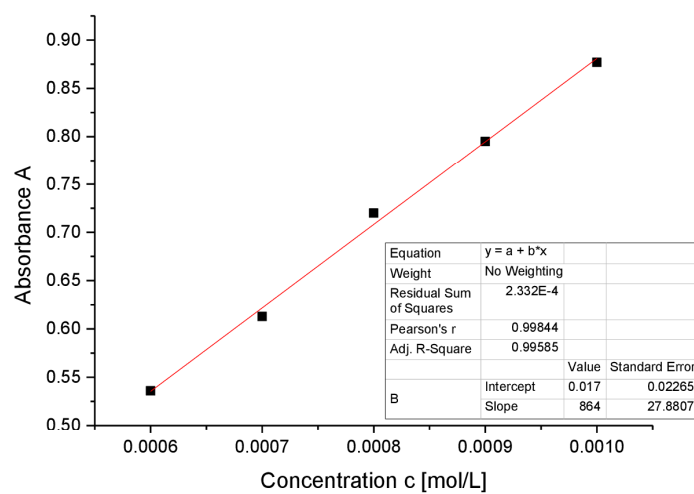


Figure S15. Determination of ϵ ($8640 \text{ M}^{-1} \text{ cm}^{-1}$) by linear regression of absorptions ($\lambda = 357 \text{ nm}$) of **2b** against concentration.

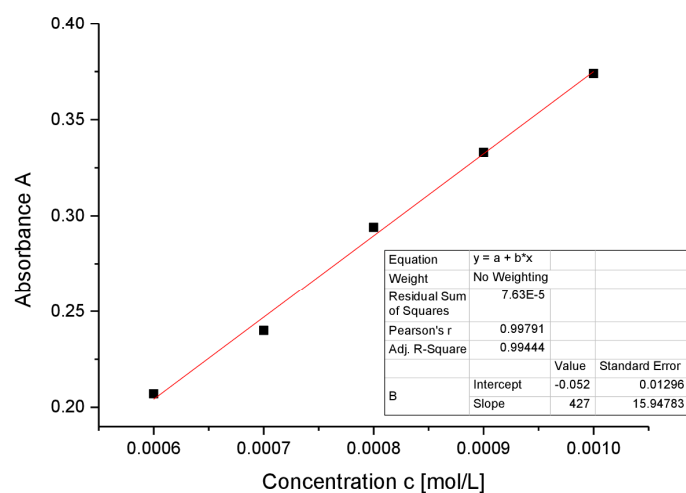


Figure S16. Determination of ϵ ($4270 \text{ M}^{-1} \text{ cm}^{-1}$) by linear regression of absorptions ($\lambda = 443 \text{ nm}$) of **2b** against concentration.

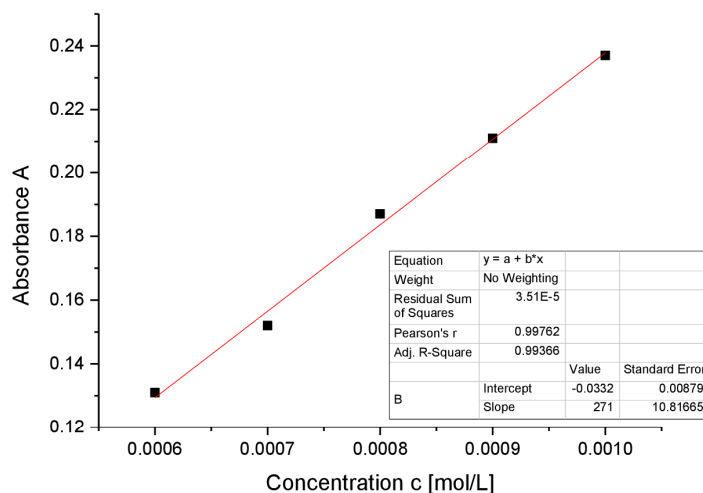


Figure S17. Determination of ε ($2710 \text{ M}^{-1} \text{ cm}^{-1}$) by linear regression of absorptions ($\lambda = 497 \text{ nm}$) of **2b** against concentration.

Procedure for the synthesis of *ligato*-tetrylene-substituted Si_6 siliconoids **3a-b**

Compounds **3a-c** are prepared by treating 1 equivalent of the anionic siliconoid **1Li** with 1.1 equivalent of chlorosilylene (**a**) or chlorogermylene (**b**) in benzene. The solution of the appropriate tetrylene in benzene was added slowly with a syringe to the solution of **1Li** in benzene at room temperature such that the tetrylene forms a layer below the **1Li** solution. Keeping the mixture under argon atmosphere over night without stirring afforded the respective products **3a-b** as crystals. After removing the mother liquor by cannula, the crystals were washed twice using the indicated amount of benzene each to remove the precipitated lithium salt. A second fraction was obtained by hot filtration of the mother liquor from benzene followed by concentration of the filtrate.

Procedure for the synthesis of *ligato*-tetrylene-substituted Si_6 siliconoid **3c**

The solution of chlorostannylene (**c**) was added to the solution of **1Li** in benzene and stirred overnight while the color changed from brown to orange-brown. Benzene was removed in vacuo and the orange residue was filtered from the indicated amount of hexane. The solution was concentrated and stored at -26°C overnight to yield orange crystals of the *ligato*-stannylene-substituted siliconoid **3c**. Concentration of the mother liquor affords a second batch of orange crystals at -26°C .

Preparation of *ligato*-NHSilylene-substituted siliconoid (**3a**)

Quantities: **1Li**, 3 g (1.9 mmol), chlorosilylene 0.62 g (2.1 mmol), benzene 6 mL + 6 mL, direct crystallization from the reaction mixture, washed twice with 4 mL benzene each. Yield: 1.97 g (1.33 mmol ; 72 %) bright red crystals (mp. $> 220^\circ\text{C}$, dec.).

$^1\text{H-NMR}$ (400.13 MHz, C_6D_6 , 300 K) δ = 7.265 (q, 0.2H, C_{10}H_8), 7.366 – 7.336 (m, 2H, Ar-H), 7.286 – 7.233 (m, 1 H, Ar-H overlapping with C_{10}H_8), 7.188 – 7.185 (m, 1H, Ar-H), 7.110 – 7.072 (t, 1 H, $J = 7.58 \text{ Hz}$, Ar-H), 7.036 – 6.995 (m, 4H, Ar-H), 6.965 – 6.928 (t, 1H, $J = 7.42 \text{ Hz}$, Ar-H), 6.903 – 6.881 (m, 4H, Ar-H), 6.828 – 6.790 (m, 1 H, Ar-H), 6.759 – 6.756 (m, 1H, Ar-H), 5.538 – 5.375 (m, 3H, Tip-*i*Pr- CH_2), 4.521 (sept, 1H, $^3J_{\text{HH}} = 6.78 \text{ Hz}$, Tip-*i*Pr- CH_2), 3.8802 (sept, 1H, $^3J_{\text{HH}} = 6.62 \text{ Hz}$, Tip-*i*Pr- CH_2), 3.819 (sept, 1H, $^3J_{\text{HH}} = 6.62 \text{ Hz}$, Tip-*i*Pr- CH_2), 3.734 (sept, 1H, $^3J_{\text{HH}} = 6.66 \text{ Hz}$, Tip-*i*Pr- CH_2), 3.650 (sept, 1H, $^3J_{\text{HH}} = 6.66 \text{ Hz}$, Tip-*i*Pr- CH_2), 3.492 (sept, 1H, $^3J_{\text{HH}} = 6.64 \text{ Hz}$, Tip-*i*Pr- CH_2), 3.411 (sept, 1H, $^3J_{\text{HH}} = 6.54 \text{ Hz}$, Tip-*i*Pr- CH_2), 2.857 – 2.553 (m, 6H, Tip-*i*Pr- CH_3), 2.167 – 2.117 (dd, 6H, $^3J_{\text{HH}} = 13.32 \text{ Hz}$, $^3J_{\text{HH}} = 6.52 \text{ Hz}$, Tip-*i*Pr- CH_3), 1.896 – 1.879 (d, 3H, $^3J_{\text{HH}} = 6.02 \text{ Hz}$, Tip-*i*Pr- CH_3), 1.784 – 1.768 (m, 6H, Tip-*i*Pr- CH_3), 1.624 – 1.608 (d, 3H, $^3J_{\text{HH}} = 6.27 \text{ Hz}$ Tip-*i*Pr- CH_3), 1.555 – 1.459 (m, 19H, Tip-*i*Pr- CH_3), 1.396 – 1.360 (m, 6H, Tip-*i*Pr- CH_3), 1.301 – 1.246 (m, 16H, Tip-*i*Pr- CH_3), 1.201 – 1.034 (m, 30H, Tip-*i*Pr- CH_3), 0.958 (s, 12 H, $\text{C}(\text{CH}_3)_3$ overlapping with Tip-*i*Pr- CH_3), 0.857 (s, 9H, $\text{C}(\text{CH}_3)_3$), 0.787 – 0.771 (d, 3 H, $^3J_{\text{HH}} = 6.44 \text{ Hz}$, Tip-*i*Pr- CH_3), 0.661 – 0.645 (d, 3 H, $^3J_{\text{HH}} = 6.60 \text{ Hz}$, Tip-*i*Pr- CH_3), 0.555 – 0.539 (d, 3

SUPPORTING INFORMATION

WILEY-VCH

H, $^3J_{\text{HH}} = 6.28$ Hz, Tip-*i*Pr-CH₃), 0.428 – 0.412 (d, 3 H, $^3J_{\text{HH}} = 6.40$ Hz, Tip-*i*Pr-CH₃), 0.366 – 0.349 (d, 3 H, $^3J_{\text{HH}} = 6.48$ Hz, Tip-*i*Pr-CH₃), 0.313 – 0.297 (d, 3 H, $^3J_{\text{HH}} = 6.32$ Hz, Tip-*i*Pr-CH₃), 0.201 – 0.185 (d, 3 H, $^3J_{\text{HH}} = 6.48$ Hz, Tip-*i*Pr-CH₃) ppm.

^{13}C -NMR (100.61 MHz, C₆D₆, 300 K) δ = 156.07, 155.12, 154.36, 153.73, 153.71, 153.62, 253.48, 153.48, 153.35, 153.03, 152.66, 152.25 (s, each 1C, Ar-C), 149.99, 149.39, 148.96, 148.53, 148.03 (s, each 1C, Ar-C), 141.65 (s, 1C, Ar-C), 140.75 (bs, 1C, Ar-C), 140.45, 140.17 (bs, each 1C, Ar-C), 138.60, 138.06 (s, each 1C, Ar-C), 136.89 (bs, 1C, Ar-C), 134.12 (s, 1C, Ar-C), 133.05 (bs, 1C, Ar-C), 129.37, 129.24, 128.72 (s, each 1C, Ar-CH), 128.22, 127.81, 127.57, 127.02 (s, each 1C overlapping with C₆D₆, Ar-CH), 123.16, 122.97, 122.73, 122.29, 122.17, 122.09, 121.74, 121.43, 121.35, 120.64 (bs, each 1C, Ar-CH), 53.97 (s, 1C, C(CH₃)₃), 53.51 (s, 1C, C(CH₃)₃), 37.33 (s, 1C Tip-*i*Pr-CH), 36.57 36.17, 35.96, 35.73, 35.64, 35.40 (bs, each 1C Tip-*i*Pr-CH), 34.86, 34.75, 34.55, 34.42, 34.26, 34.19, 33.85 (bs, each 1C Tip-*i*Pr-CH), 32.47 (s, 1C Tip-*i*Pr-CH), 31.47, 30.79 (s, each 3C, Tip-*i*Pr-CH), 28.23, 28.11, 27.90, 27.64, 26.97 (s, each 1C, Tip-*i*Pr-CH₃), 25.25, 25.19 (bs, each 1C, Tip-*i*Pr-CH₃), 24.81 (s, 1C, Tip-*i*Pr-CH₃), 24.49, 24.35, 24.14, 24.07, 24.03, 23.97, 23.87, 23.80, 23.73, 23.69, 23.65, 23.59, 23.55, 23.22, 23.17 (bs, each 1C, Tip-*i*Pr-CH₃), 22.92 (s, 1C, Tip-*i*Pr-CH₃) ppm.

^{29}Si -NMR (79.49 MHz, C₆D₆, 300 K) δ = 166.7 (s, *privo*-Si(Tip)₂), 48.0 (s, NHSi), 23.6 (s, *ligato*-SiTip), 13.9 (s, *remoto*-Si(Tip)₂), -36.9 (s, *ligato*-Si-NHSi), -244.6 (s, *nudo*-Si), -260.7 (s, *nudo*-Si) ppm.

CP-MAS ^{29}Si -NMR (79.53 MHz, 14KHz, 300K) δ = 160.0 (s, *privo*-Si), 47.2 (s, NHSi), 25.2 (s, *ligato*-SiTip), 10.8 (*remoto*-Si(Tip)₂), -44.7 (s, *ligato*-Si-NHSi), -250.5 (s, *nudo*-Si), -262.6 (s, *nudo*-Si) ppm.

Elemental analysis: calculated for C₉₀H₁₃₈N₂Si₇: C, 74.77 %; H, 9.69 %; N, 1.94 %. Found: C, 73.91 %; H, 9.40 %; N, 1.63 %.

UV/VIS (toluene): λ_{max} (ϵ) = 472 nm (2420 M⁻¹ cm⁻¹).

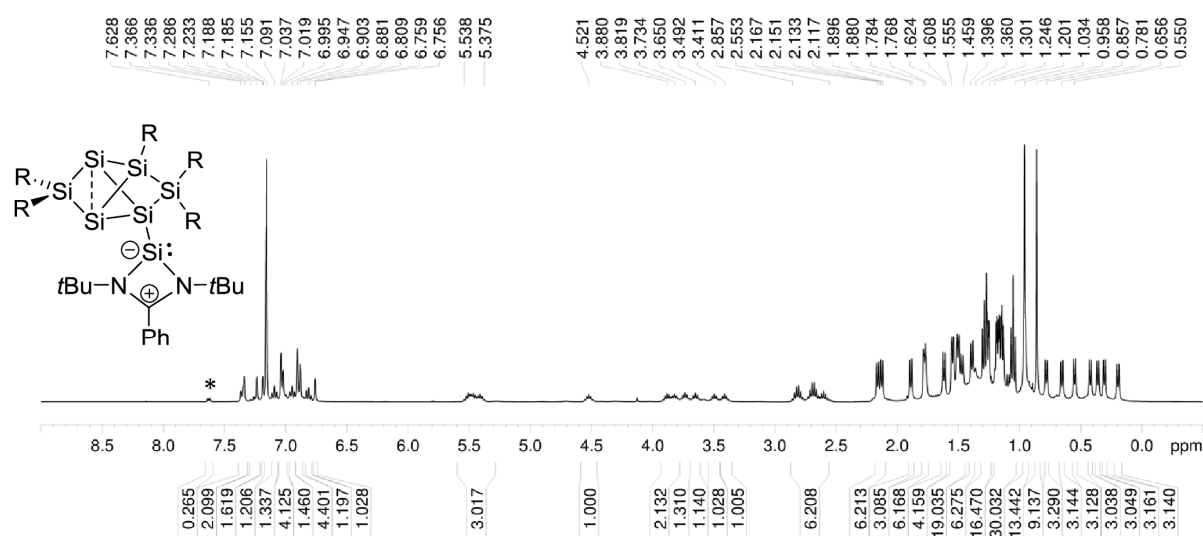
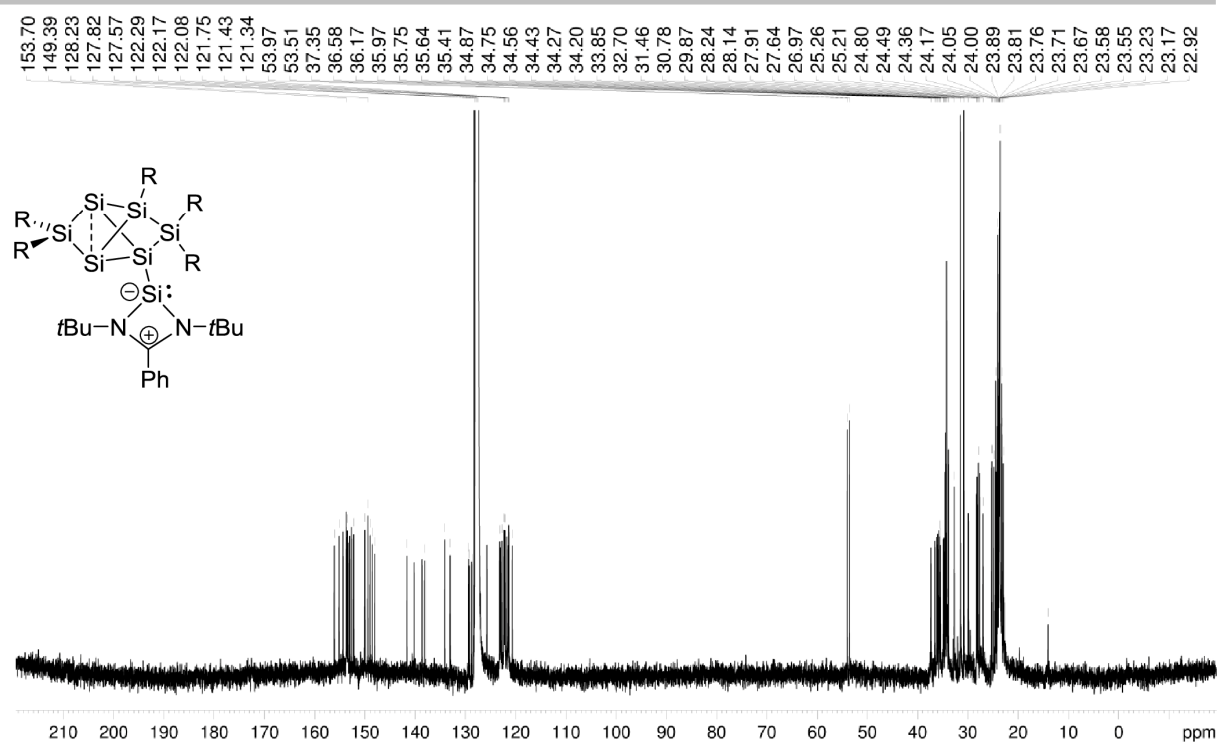
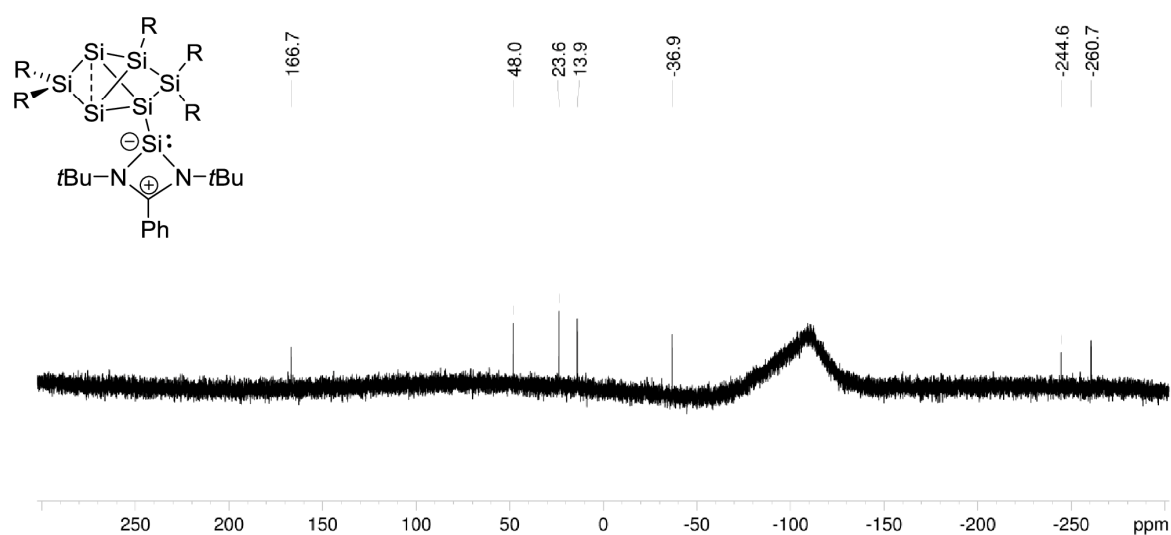


Figure S18. ^1H NMR of **3a** in C₆D₆ (400.13 MHz, 300 K). Residual naphthalene (C₁₀H₈) marked with asterisk (*).

SUPPORTING INFORMATION

WILEY-VCH

Figure S19. ^{13}C NMR of **3a** in C_6D_6 (100.61 MHz, 300 K).Figure S20. ^{29}Si NMR of **3a** in C_6D_6 (79.49 MHz, 300 K).

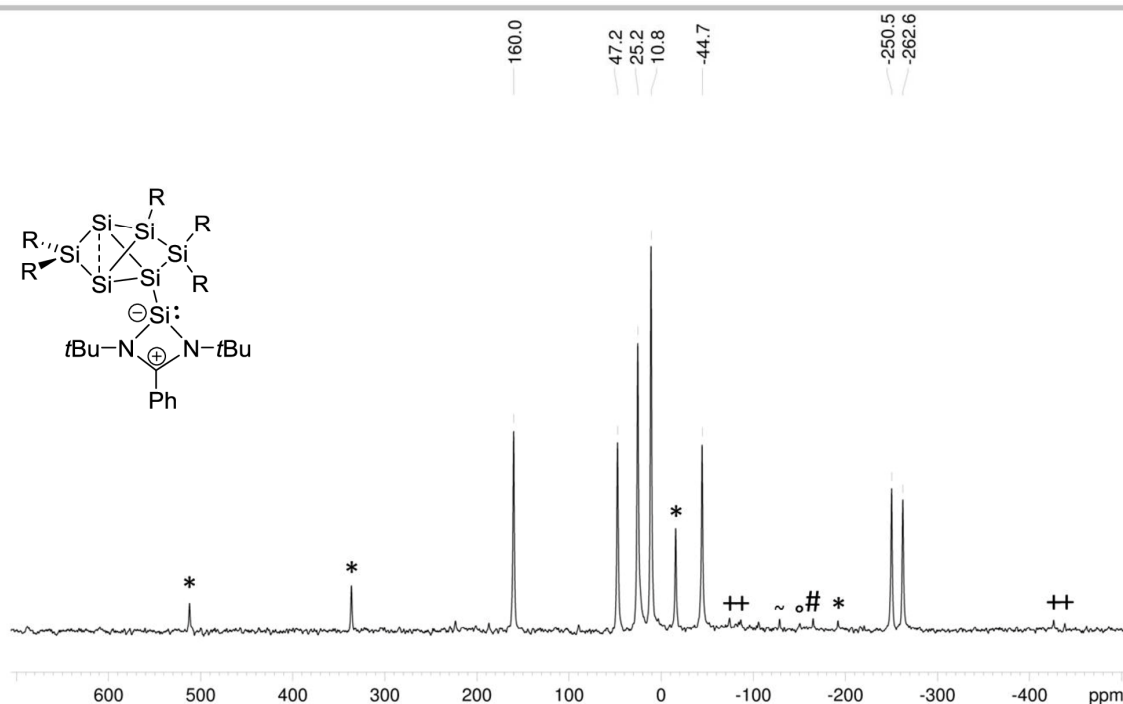


Figure S21. CP-MAS ^{29}Si NMR of **3a** in C_6D_6 (79.53 MHz, 14 KHz, 300 K), *side spinning bands of: * *privo*-SiTip₂ (160.0 ppm), # *remoto*-SiTip (10.8 ppm), ° *ligato*-SiTip (25.2 ppm), ~ NHSi (47.2 ppm), + *nudo*-Si (250.5 ppm, 262.6 ppm).

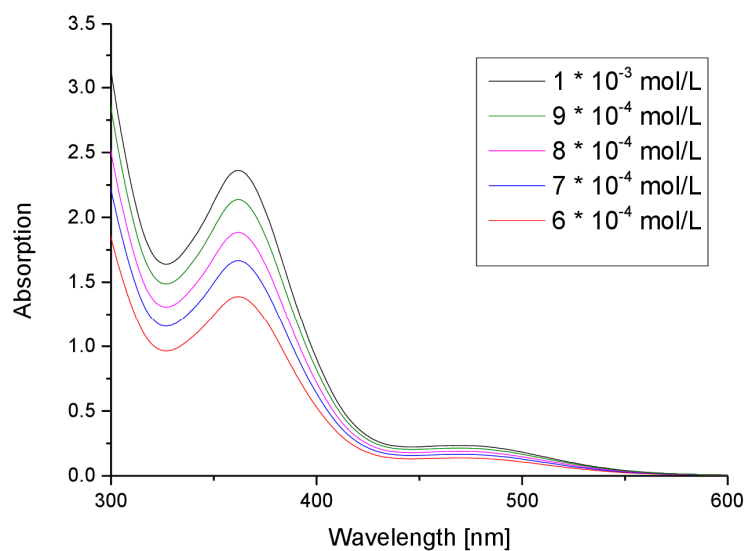


Figure S22. UV-Vis spectrum of **3a** in toluene at different concentrations.

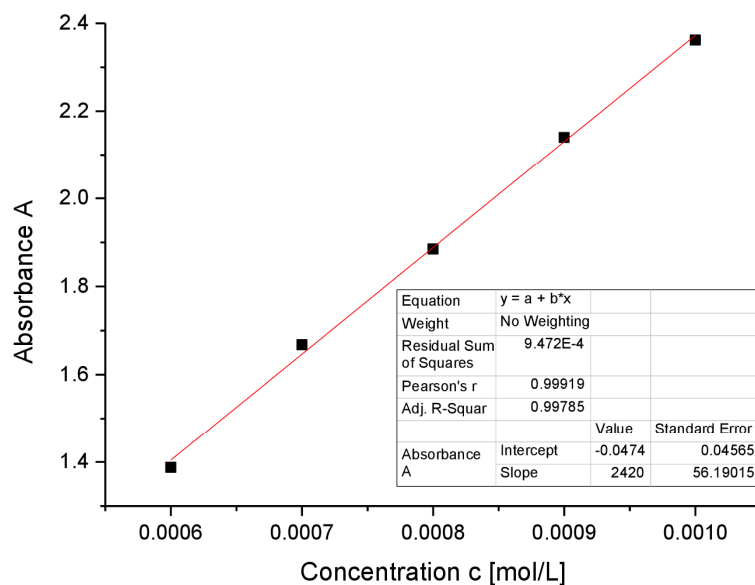


Figure S23. Determination of ε ($24200 \text{ M}^{-1} \text{ cm}^{-1}$) by linear regression of absorptions ($\lambda = 362 \text{ nm}$) of **3a** against concentration.

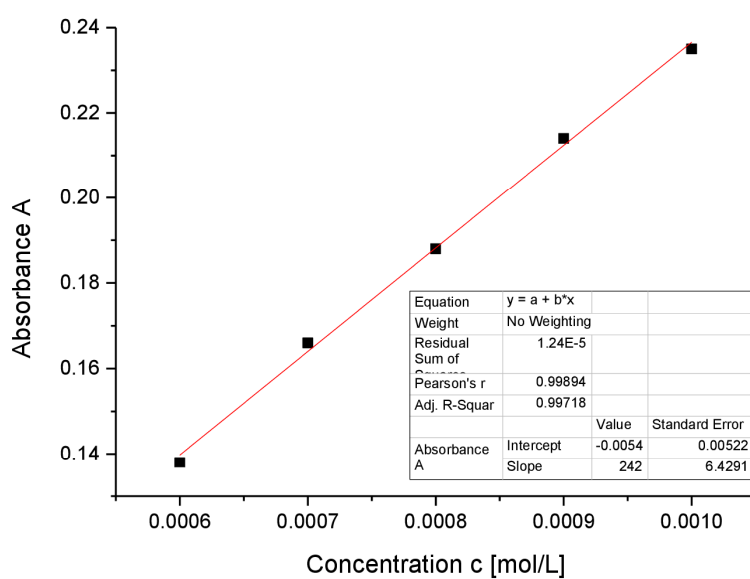


Figure S24. Determination of ε ($2420 \text{ M}^{-1} \text{ cm}^{-1}$) by linear regression of absorptions ($\lambda = 472 \text{ nm}$) of **3a** against concentration.

SUPPORTING INFORMATION

WILEY-VCH

Preparation of *ligato*-NHGermylene-substituted siliconoid (3b)

Quantities: 1Li, 2 g (1.244 mmol), chlorogermylene 0.47 g (1.368 mmol), benzene 5 mL + 5 mL, direct crystallization from the reaction mixture, washed with 4 mL benzene each. Yield: 1.45 g (0.974 mmol ; 78 %) bright orange crystals (mp. > 220°C, dec.).

¹H-NMR (400.13 MHz, C₆D₆, 300 K) δ = 7.631 (q, 0.6H, C₁₀H₈), 7.348–7.242 (m, 5 H, Ar-H), 7.197–7.194 (m, 1H, Ar-H), 7.137–7.097 (m, 1H, Ar-H), 7.057–6.962 (m, 7H, Ar-H), 6.936–6.855 (m, 6H, Ar-H), 6.764–6.761 (bs, 1H, Ar-H), 5.471–5.371 (m, 3H, Tip-*i*Pr-CHMe₂), 5.264 (sept, 0.4H, ³J_{HH} = 6.27 Hz, Tip-*i*Pr-CHMe₂), 4.902 (sept, 0.4H, ³J_{HH} = 6.27 Hz, Tip-*i*Pr-CHMe₂), 4.769 (sept, 0.8H, ³J_{HH} = 6.27 Hz, Tip-*i*Pr-CHMe₂), 4.522 (sept, 1H, ³J_{HH} = 6.17 Hz, Tip-*i*Pr-CHMe₂), 4.228 (sept, 0.4H, ³J_{HH} = 6.17 Hz, Tip-*i*Pr-CHMe₂), 4.086–4.055 (m, 0.8H, Tip-*i*Pr-CHMe₂), 3.899–3.744 (m, 3H, Tip-*i*Pr-CHMe₂), 3.654–3.475 (m, 3H, Tip-*i*Pr-CHMe₂), 3.435–3.475 (m, 3H, Tip-*i*Pr-CHMe₂), 3.435–3.346 (m, 1H, Tip-*i*Pr-CHMe₂), 2.873–2.559 (m, 7H, Tip-*i*Pr-CHMe₂), 2.06–2.170 (m, 5H, Tip-*i*Pr-CH₃), 2.102–2.057 (m, 4H Tip-*i*Pr-CH₃), 1.859–1.842 (d, 3H, ³J_{HH} = 6.60, Tip-*i*Pr-CH₃), 1.771–1.683 (m, 8H, Tip-*i*Pr-CH₃), 1.635–1.603 (m, 7 H, Tip-*i*Pr-CH₃), 1.554–1.496 (m, 18H, Tip-*i*Pr-CH₃), 1.393–1.377 (d, 1H, ³J_{HH} = 6.56, Tip-*i*Pr-CH₃), 1.297–1.042 (m, 50H, Tip-*i*Pr-CH₃), 0.950–0.934 (d, 1H, ³J_{HH} = 6.60, Tip-*i*Pr-CH₃), 0.907 (s, 9H, C(CH₃)₃), 0.824–0.638 (m, 24H, Tip-*i*Pr-CH₃ overlapping with C(CH₃)₃), 0.550–0.534 (d, 3H, ³J_{HH} = 6.23, Tip-*i*Pr-CH₃), 0.425–0.367 (each d, 8H, ³J_{HH} = 6.50, Tip-*i*Pr-CH₃), 0.307–0.292 (d, 1H, ³J_{HH} = 6.04, Tip-*i*Pr-CH₃), 0.207–0.190 (d, 1H, ³J_{HH} = 6.48, Tip-*i*Pr-CH₃).

¹³C-NMR (100.61 MHz, C₆D₆, 300 K) δ = 160.23 (s, 1C, Ar-C), 156.01, 155.84, 155.44, 155.08, 154.30, 153.65, 153.35, 153.28, 153.17, 153.14, 152.85, 152.53, 152.39, 152.29 (s, each Ar-C), 151.75, 151.68 (s, each 1C, Ar-C), 150.02, 149.83, 149.69, 149.43, 148.96, 148.59, 148.42, 148.19, 148.04 (s, each 1C, Ar-C), 141.30, 141.26 (bs, each 1C, Ar-C), 140.41 (bs, 1C, Ar-C), 140.23 (bs, 1C, Ar-C), 138.39, 138.31, 138.00, 137.15, 136.78, 135.83 (s, each 1C, Ar-C), 133.70, 133.30, 132.68 (s, each 1C, Ar-C), 129.35, 129.03, 128.93, 128.83, 128.69 (bs, each 1C, Ar-CH), 128.44 (s, 1C, Ar-CH), 127.81, 127.57 (s, each 1C, overlapping with C₆D₆, Ar-CH), 125.71 (s, 1C, Ar-CH), 124.42 (bs, 1C, Ar-CH), 123.11 (s, 1C, Ar-CH), 122.83–122.74 (d, 1C, J = 8.64 Hz, Ar-CH), 122.70 (bs, 1C, Ar-CH), 122.52, 122.40, 122.29 (bs, each 1C, Ar-CH), 122.11, 122.07, 121.79, 121.68 (s, each 1C, Ar-CH), 121.50–121.41 (d, 1C, J = 9.79 Hz, Ar-CH), 120.86, 120.68, 120.64 (bs, each 1C, Ar-CH), 54.21, 53.87, 53.83, 53.40 (s, each 1C, C(CH₃)₃), 37.56 (bs, 1C, Tip-*i*Pr-CH), 37.39 (s, 1C, Tip-*i*Pr-CH), 36.61 (s, 1C, Tip-*i*Pr-CH), 36.13, 36.01, 35.88, 35.76, 35.61, 35.49 (s, each 1C, Tip-*i*Pr-CH), 34.82, 34.62, 34.54, 34.43, 34.36 (s, each 1C, Tip-*i*Pr-CH), 34.24, 34.19 (bs, each 1C, Tip-*i*Pr-CH), 33.93, 33.87, 33.77 (s, each 1C, Tip-*i*Pr-CH), 32.61 (s, 1C, Tip-*i*Pr-CH), 32.04, 31.98 (bs, each 1C, Tip-*i*Pr-CH), 31.77 (bs, 1C, Tip-*i*Pr-CH), 31.67, 31.09 (s, each 1C, Tip-*i*Pr-CH), 29.87, 28.28, 28.14 (s, each 2C, Tip-*i*Pr-CH₃), 27.94 (bs, 1C, Tip-*i*Pr-CH₃), 27.82 (s, 2C, Tip-*i*Pr-CH₃), 27.68, 27.59 (bs, each 1C, Tip-*i*Pr-CH₃), 27.28, 26.93 (bs, each 1C, Tip-*i*Pr-CH₃), 25.55 (s, 1C, Tip-*i*Pr-CH₃), 25.45–25.37 (bs, 3C, Tip-*i*Pr-CH₃), 25.22, 25.09 (s, each 1C, Tip-*i*Pr-CH₃), 24.89, 24.83, 24.72, 24.66, 24.54, 24.49, 24.41, 24.34 (bs, each 1C, Tip-*i*Pr-CH₃), 24.15, 24.10, 24.04, 24.03, 23.99, 12.96, 23.88, 23.82, 23.78, 23.72, 23.67, 23.59, 23.44, 23.39, 23.34 (bs, each 1C, Tip-*i*Pr-CH₃), 23.24, 23.20 (s, each 1C, Tip-*i*Pr-CH₃), 22.80 (s, 1C, Tip-*i*Pr-CH₃), 14.04 (s, 1C, Tip-*i*Pr-CH₃).

²⁹Si-NMR (79.49 MHz, C₆D₆, 300 K) δ = 167.3 (s, *privo*-Si), 24.2 (s, *ligato*-SiTip), 13.3 (s, *remoto*-Si(Tip)₂), –23.0 (s, *ligato*-Si-NHGe), –245.4 (s, *nudo*-Si), –261.1 (s, *nudo*-Si) ppm.

²⁹Si-NMR (79.49 MHz, toluene-d₈, 300 K) δ = 167.3 (s, major, *privo*-Si), 165.6 (s, minor, *privo*-Si), 26.7 (s, minor, *ligato*-SiTip), 24.5 (s, major, *ligato*-SiTip), 16.2 (s, minor, *remoto*-Si(Tip)₂), 13.2 (s, major, *remoto*-Si(Tip)₂), –23.4 (s, major, *ligato*-Si-NHGe), –35.0 (s, minor, *ligato*-Si-NHGe), –233.9 (s, minor, *nudo*-Si), –238.1 (s, minor, *nudo*-Si), –245.9 (s, major, *nudo*-Si), –261.1 (s, major, *nudo*-Si) ppm.

CP-MAS ²⁹Si-NMR (79.53 MHz, 300K) δ = 163.4 (s, *privo*-Si), 29.7 (s, *ligato*-SiTip), 12.8 (*remoto*-Si(Tip)₂), –29.5 (s, *ligato*-Si-NHSi), –248.9 (s, *nudo*-Si), –261.2 (s, *nudo*-Si) ppm.

Elemental analysis: calculated for C₉₀H₁₃₈GeN₂Si₆: C: 72.59 % ; H: 9.34 % ; N: 1.88 %. Found: C: 71.59 % ; H: 8.82 % ; N: 1.88 %.

UV/VIS (toluene): λ_{max} (ϵ) = 436 nm (2240 M^{–1} cm^{–1}).

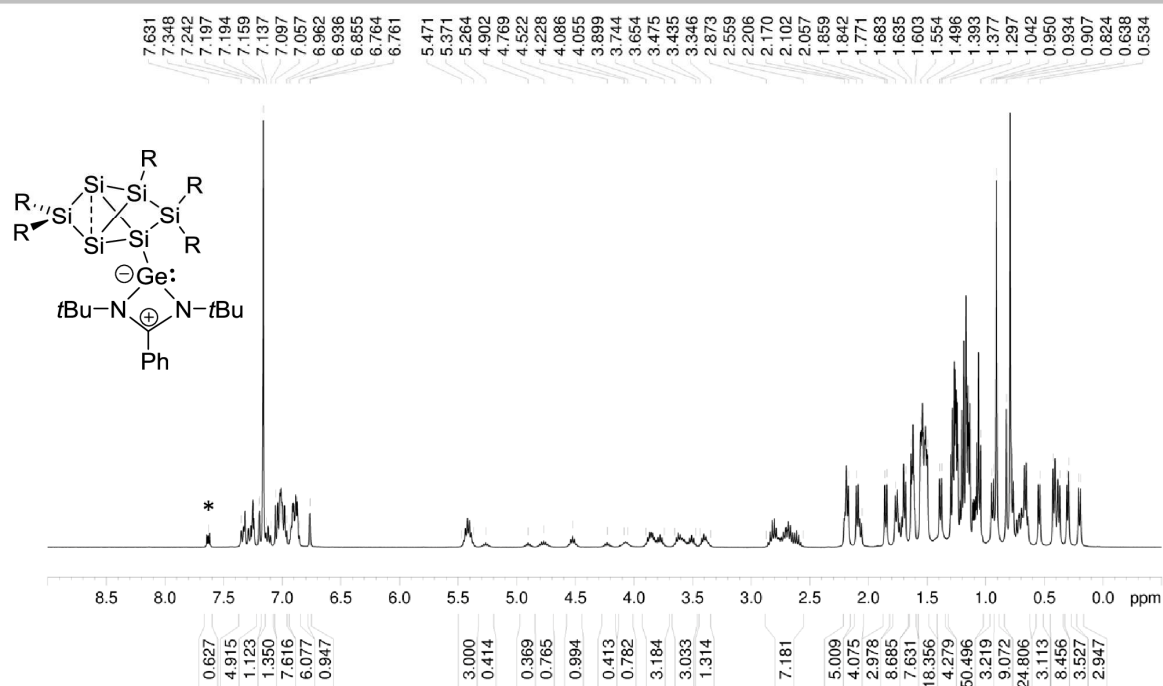


Figure S25. ^1H NMR of **3b** in C_6D_6 (400.13 MHz, 300 K). Residual naphthalene (C_{10}H_8) marked with asterisk (*).

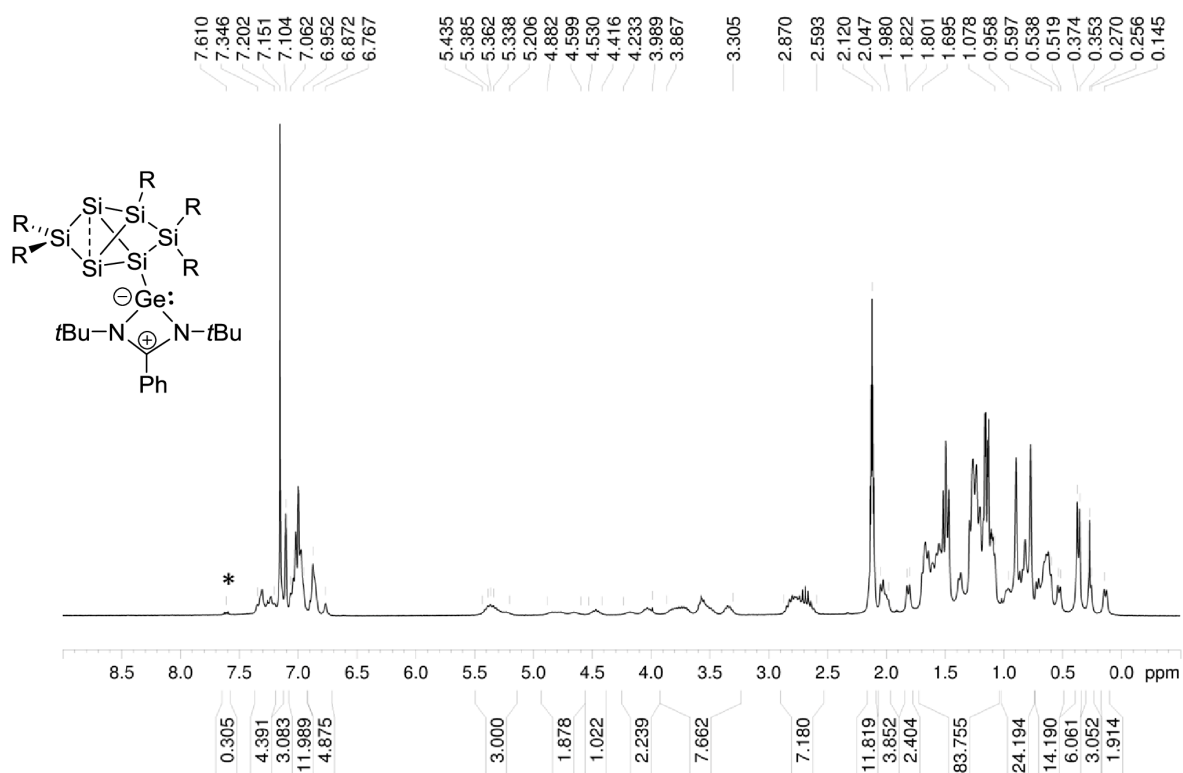
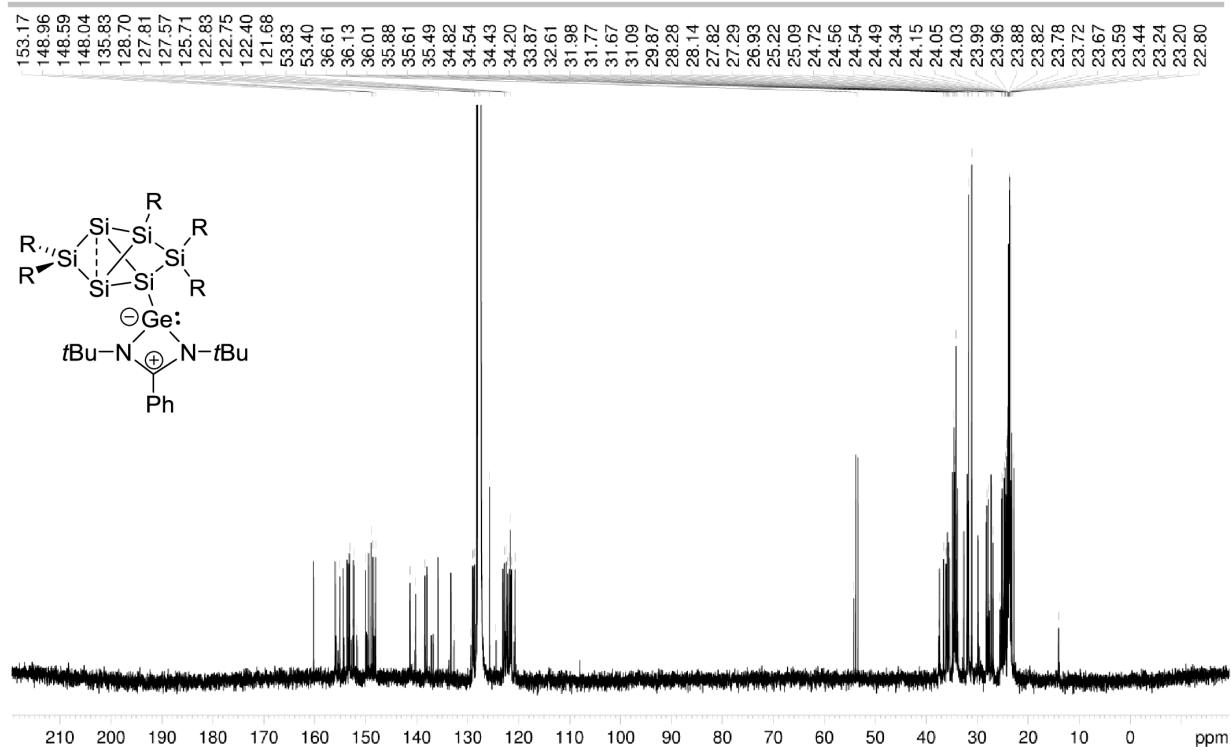
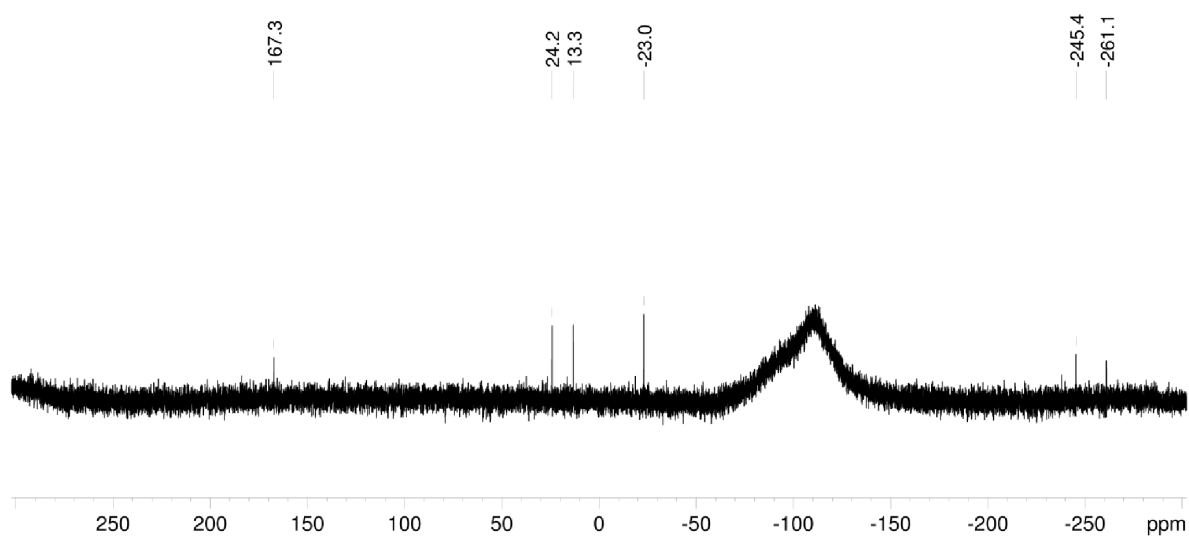


Figure S26. ^1H NMR of **3b** in toluene- d_8 (300.13 MHz, 343 K). Residual naphthalene (C_{10}H_8) marked with asterisk (*).

SUPPORTING INFORMATION

WILEY-VCH

Figure S27. ¹³C NMR of **3b** in C₆D₆ (100.61 MHz, 300 K).Figure S28. ²⁹Si NMR of **3b** in C₆D₆ (79.49 MHz, 300 K).

SUPPORTING INFORMATION

WILEY-VCH

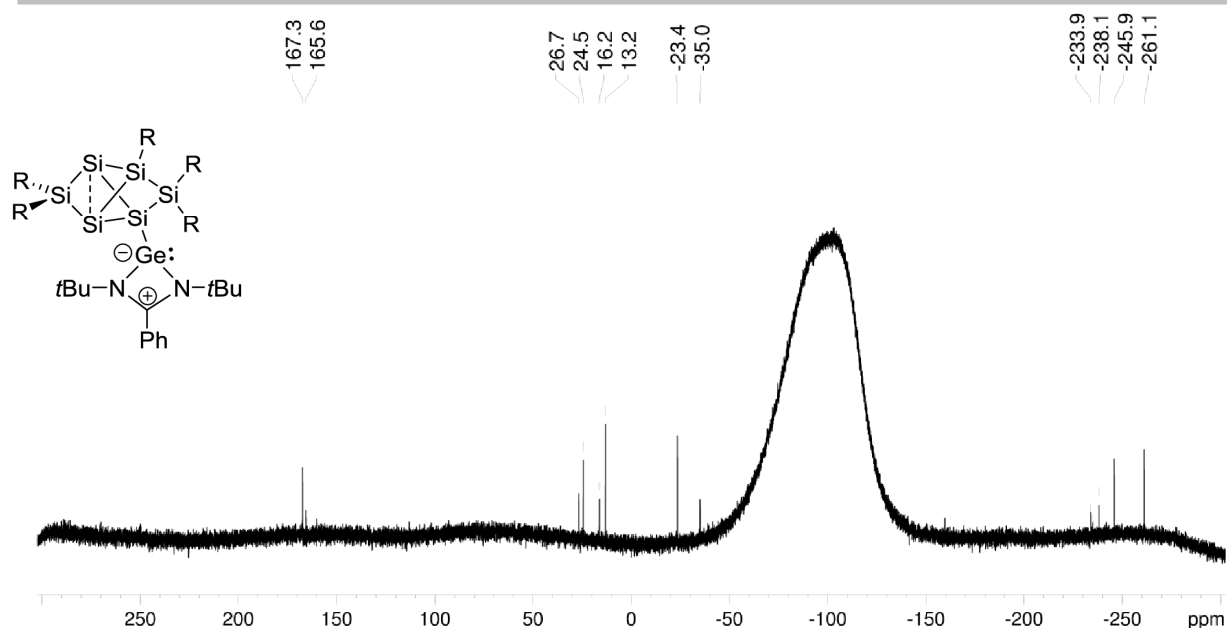


Figure S29. ^{26}Si NMR of **3b** in toluene- d_8 (79.49 MHz, 300 K).

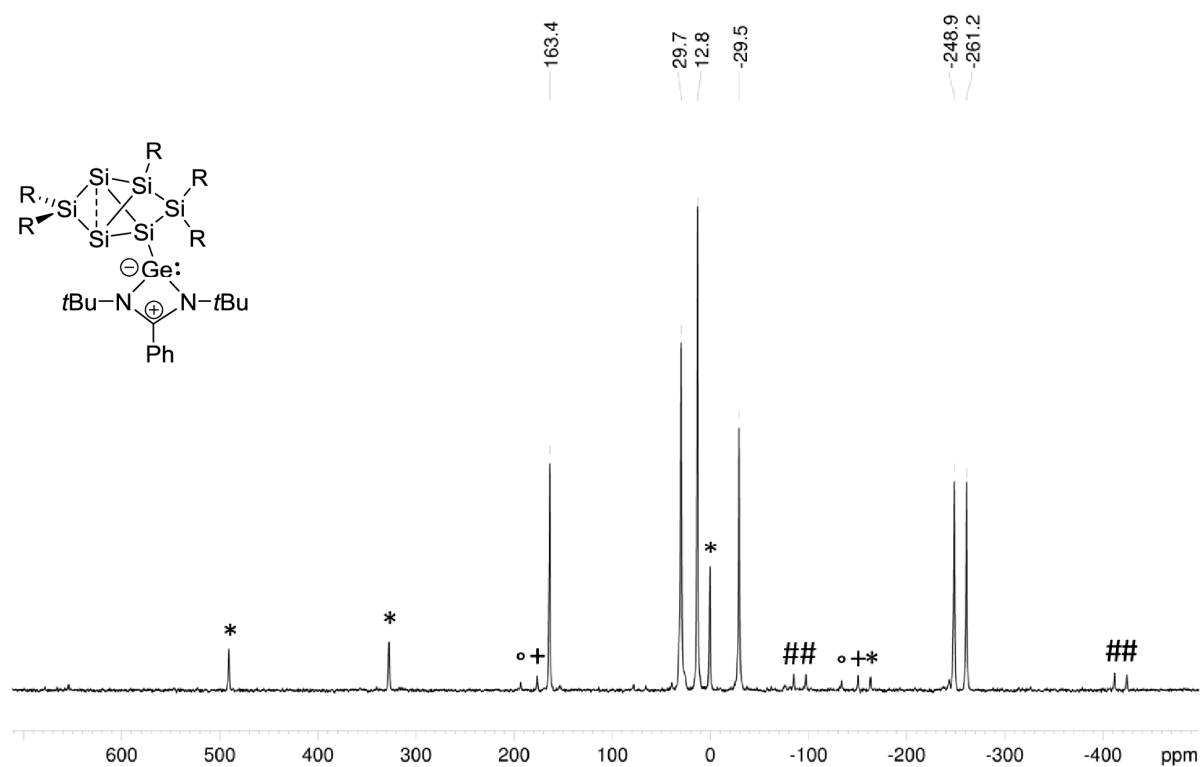


Figure S30. CP-MAS ^{26}Si NMR of **3b** in C_6D_6 (79.53 MHz, 300 K), side spinning bands of: * *privo*-Si(Tip)₂ (163.4 ppm), # *nudo*-Si (-248.6 ppm ; -261.2 ppm), + *remoto*-Si(Tip)₂ (12.8 ppm), ° *ligato*-SiTip (29.7 ppm).

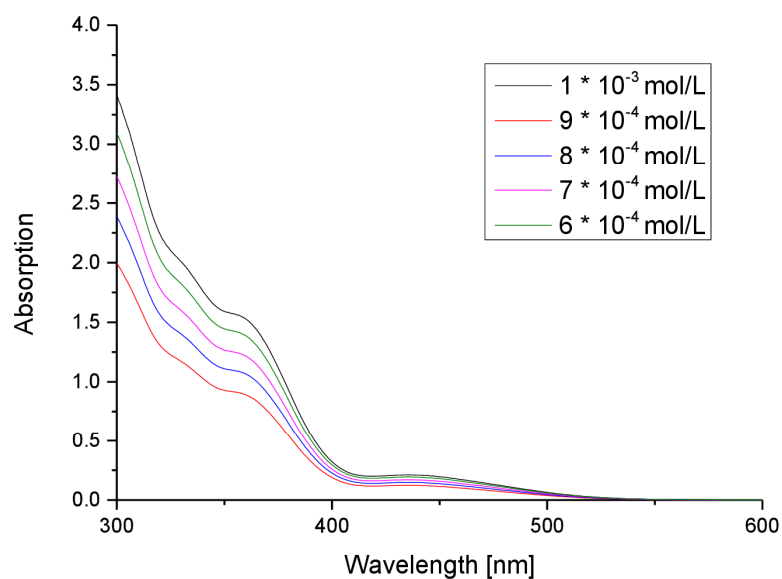


Figure S31. UV-Vis spectrum of **3b** in toluene at different concentrations.

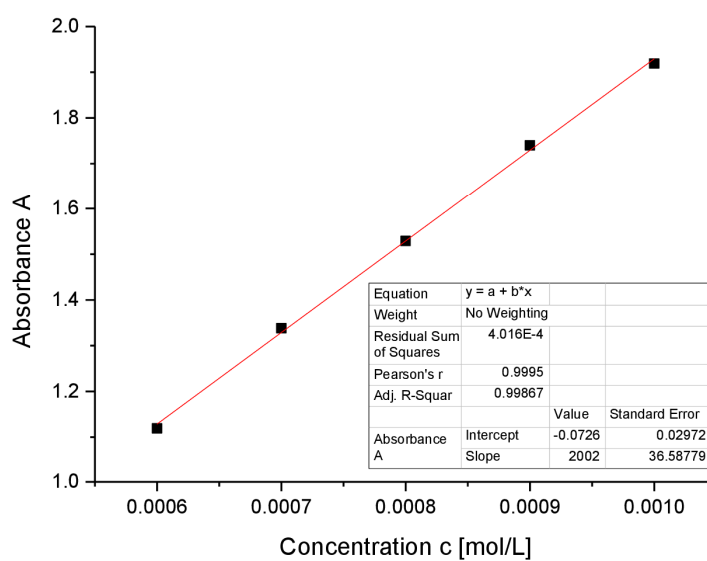


Figure S32. Determination of ϵ ($20020 \text{ M}^{-1} \text{ cm}^{-1}$) by linear regression of absorptions ($\lambda = 334 \text{ nm}$) of **3b** against concentration.

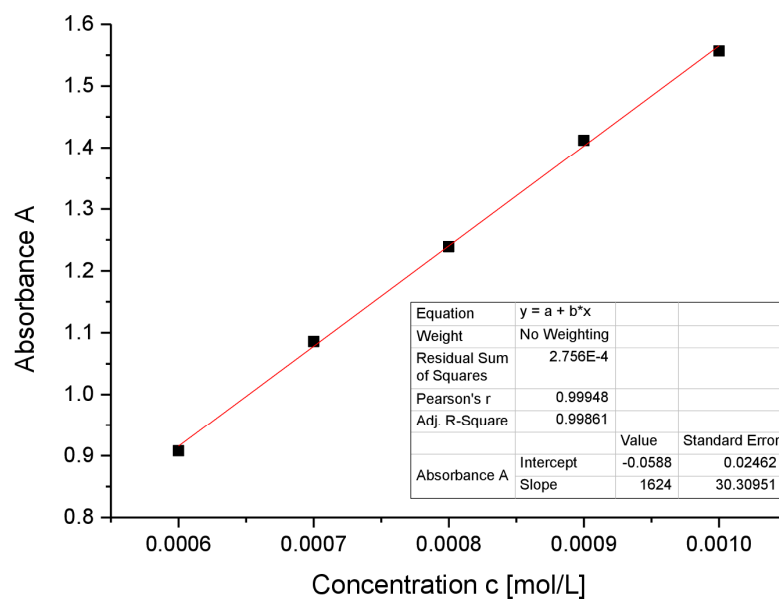


Figure S33. Determination of ϵ ($16240 \text{ M}^{-1} \text{ cm}^{-1}$) by linear regression of absorptions ($\lambda = 357 \text{ nm}$) of **3b** against concentration.

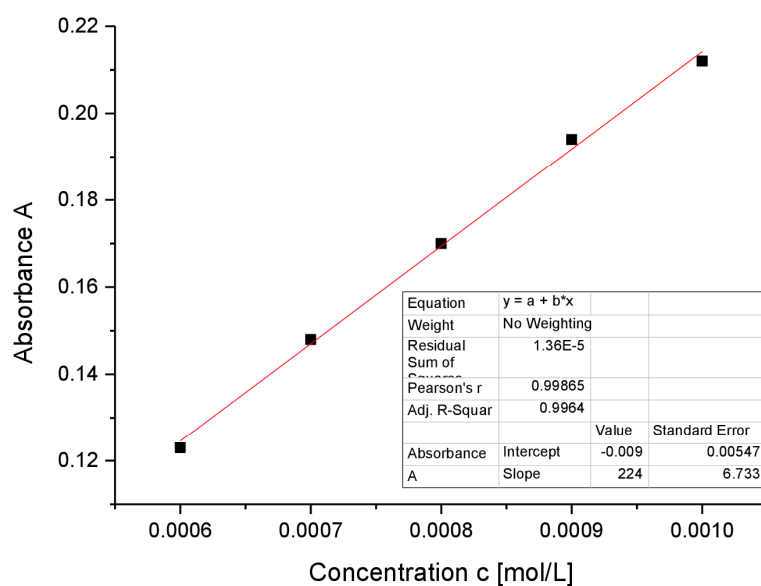


Figure S34. Determination of ϵ ($2240 \text{ M}^{-1} \text{ cm}^{-1}$) by linear regression of absorptions ($\lambda = 436 \text{ nm}$) of **3b** against concentration.

Preparation of *ligato*-NHStannylene-substituted siliconoid (**3c**)

Quantities: **1Li**, 750 mg (0.51 mmol), chlorostannylene 0.215 g (0.559 mmol), benzene 4 mL + 4 mL, stirred overnight, filtered from 15 mL hexane, crystallization from hexane. Yield: 0.59 g (0.373 mmol ; 74 %) orange-brown crystals (mp. > 300 °C).

SUPPORTING INFORMATION

WILEY-VCH

$^1\text{H-NMR}$ (400.13 MHz, C_6D_6 , 300 K) δ = 7.625 (C_{10}H_8), 7.297 – 7.158 (m, 7H, Ar-H overlapping with C_{10}H_8), 7.036 – 6.868 (m, 17H, Ar-H), 5.464 – 5.175 (bs, 1H, Tip-*i*Pr-CHMe₂), 4.883 (bs, 2H, Tip-*i*Pr-CHMe₂), 4.695 (bs, 1H, Tip-*i*Pr-CHMe₂), 4.317 (bs, 1H, Tip-*i*Pr-CHMe₂), 4.114 (bs, 2H, Tip-*i*Pr-CHMe₂), 3.709 – 3.611 (m, 3H, Tip-*i*Pr-CHMe₂), 3.330 (sept, 1H, $^3J_{\text{HH}}$ = 6.13 Hz, Tip-*i*Pr-CHMe₂), 2.844 – 2.598 (m, 7H, Tip-*i*Pr-CHMe₂), 2.229 – 2.15 (d, 4H, $^3J_{\text{HH}}$ = 5.68, Tip-*i*Pr-CH₃), 2.107 – 2.042 (m, 7H, Tip-*i*Pr-CH₃), 1.745 – 0.385 (m, 164 H, Tip-*i*Pr-CH₃ overlapping with $\text{C}(\text{CH}_3)_3$).

$^{13}\text{C-NMR}$ (100.61 MHz, C_6D_6 , 300 K) δ = 165.02 (s, 1C, Ar-C), 155.83, 155.41, 153.94, 153.67, 152.76, 152.46, 152.10, 151.51, 149.89, 149.76, 148.76, 148.50, 148.17 (broad, each 1C, Ar-C), 140.56 (s, 1C, Ar-C), 139.45, 138.50, 136.75, 134.11 (broad, each 1C, Ar-C), 133.68 (s, 1C, Ar-C), 129.60 (bs, 1C, Ar-CH), 128.74, 128.45, 128.09, 127.98, 127.87, 127.68, 127.64, 127.17, 127.07 (s, each 1C, Ar-CH), 125.70 (s, 1C, Ar-CH), 124.80 (bs, 1C, Ar-CH), 122.64, 122.48, 122.31, 122.06, 121.49, 121.29, 120.7 (bs, 7C, Ar-CH), 53.38 (s, 1C, $\text{C}(\text{CH}_3)_3$), 52.88 (s, 1C, $\text{C}(\text{CH}_3)_3$), 37.48 (s, 1C, Tip-*i*Pr-CH), 35.86 bs, 3C, Tip-*i*Pr-CH), 35.17 (bs, 1C, Tip-*i*Pr-CH), 34.71, 34.45, 34.38, 34.21, 33.95 (broad, each 1C, Tip-*i*Pr-CH), 33.48, 32.23, 32.04 (broad, each 1C, Tip-*i*Pr-CH), 31.61 (s, each 1C, Tip-*i*Pr-CH), 28.05, 27.77, 27.51, 27.26 (broad, each 1C, Tip-*i*Pr-CH₃), 25.39, 25.09, 24.87, 24.51 (broad, each 1C, Tip-*i*Pr-CH₃), 24.11 (s, 3C, CH₃), 24.04, 23.89 (broad, each 1C, Tip-*i*Pr-CH₃), 23.83 (s, 3C, CH₃), 23.79, 23.63, 23.38 (broad, each 1C, Tip-*i*Pr-CH₃), 22.57 (s, 1C, Tip-*i*Pr-CH₃).

$^{29}\text{Si-NMR}$ (79.49 MHz, C_6D_6 , 300 K) δ = 162.3 (s, *privo*-Si), 35.8 (s, *ligato*-SiTip), 20.6 (*remoto*-Si(Tip)₂), -19.77 (s, *ligato*-Si-NHSi), -232.8 (s, *nudo*-Si), -237.01 (s, *nudo*-Si) ppm.

$^{119}\text{Sn-NMR}$ (149.21 MHz, C_6D_6 , 300 K) δ = 336.51 (bs), 267.84 (s).

CP-MAS $^{29}\text{Si-NMR}$ (79.53 MHz, 13KHz, 300K) δ = 162.9 (s, *privo*-Si), 40.1 (s, *ligato*-SiTip), 14.3 (*remoto*-Si(Tip)₂), -12.0 (s, *ligato*-Si-NHSi), -244.3 (s, *nudo*-Si), -259.9 (s, *nudo*-Si) ppm.

CP-MAS $^{119}\text{Sn-NMR}$ (149.27 MHz, 13KHz, 300K) δ = 332.1 (s).

CP-MAS $^{119}\text{Sn-NMR}$ (149.27 MHz, 11KHz, 300K) δ = 332.0 (s).

Elemental analysis: calculated for $\text{C}_{90}\text{H}_{138}\text{N}_2\text{Si}_6\text{Sn}$: C, 70.41 % ; H, 9.06 % ; N, 1.82 %. Found: C, 70.80 % ; H, 8.57 % ; N, 1.80 %.

UV/VIS (hexane): λ_{max} (ϵ) = 436 nm ($2160 \text{ M}^{-1} \text{ cm}^{-1}$).

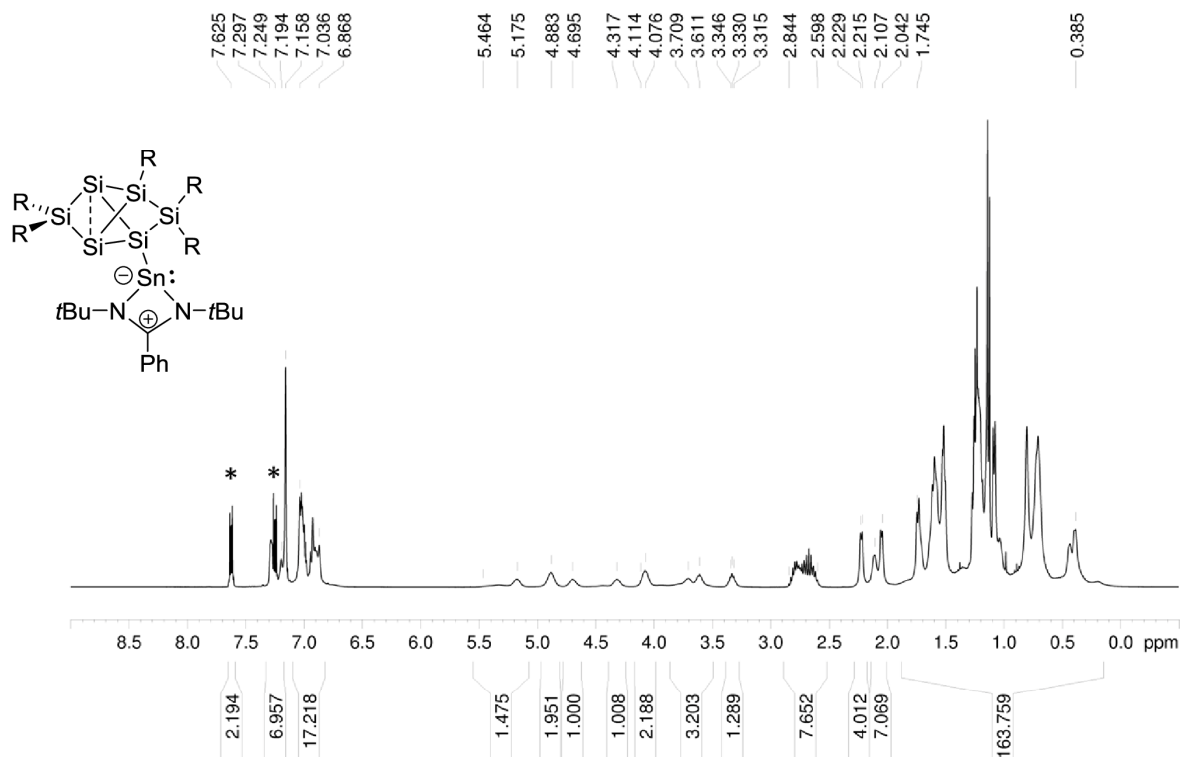
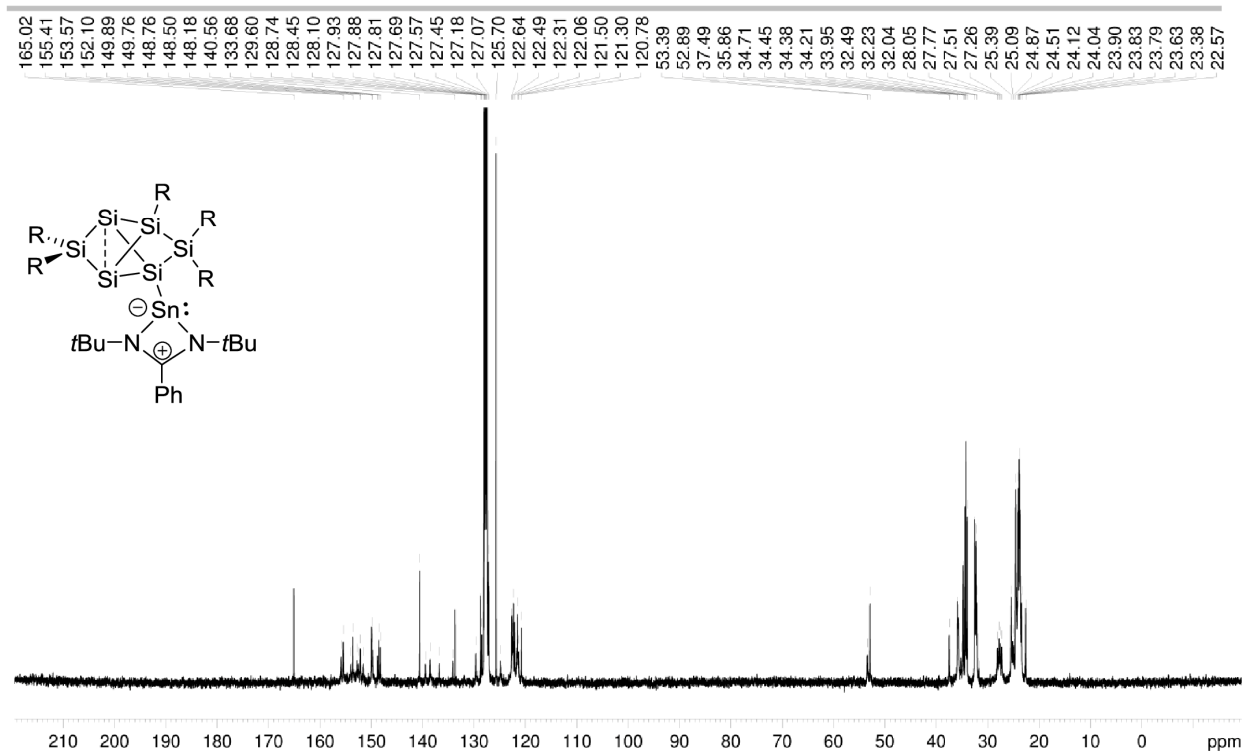
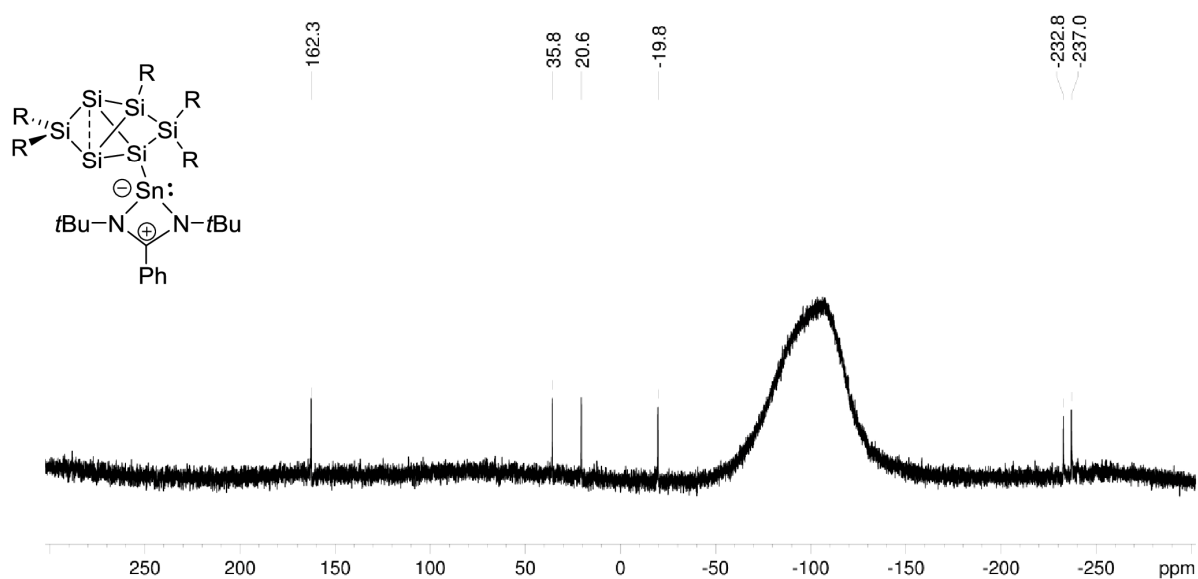


Figure S35. ^1H NMR of **3c** in C_6D_6 (400.13 MHz, 300 K). Residual naphthalene (C_{10}H_8) marked with asterisk (*).

SUPPORTING INFORMATION

WILEY-VCH

Figure S36. ¹³C NMR of **3c** in C₆D₆ (100.61 MHz, 300 K).Figure S37. ²⁹Si NMR of **3c** in C₆D₆ (79.49 MHz, 300 K).

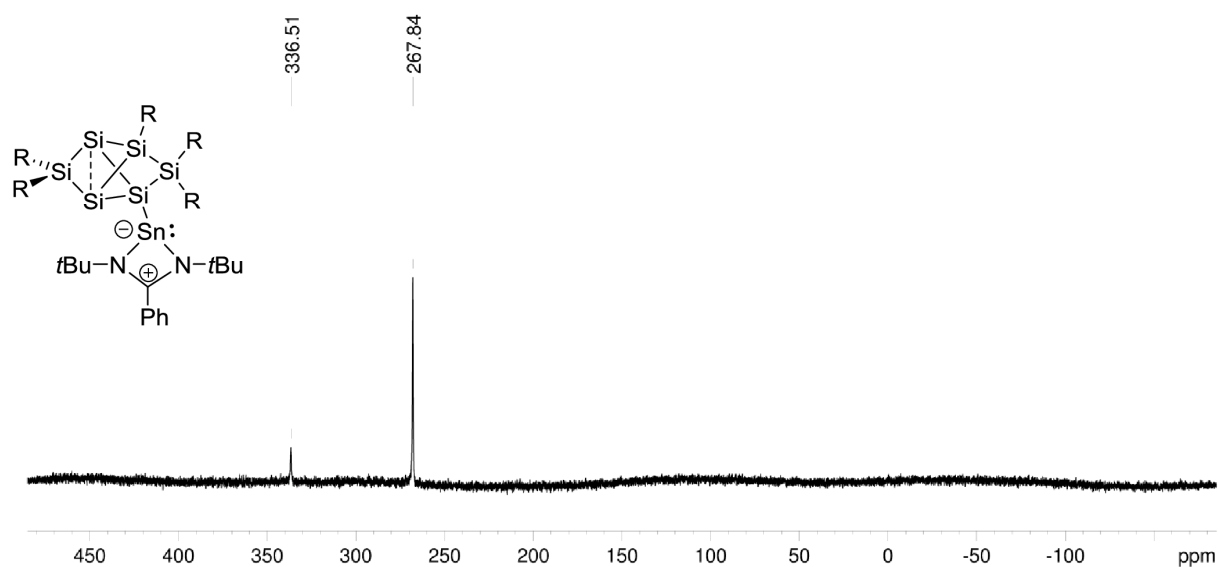


Figure S38 ^{119}Sn NMR of **3c** in C_6D_6 (79.49 MHz, 300 K).

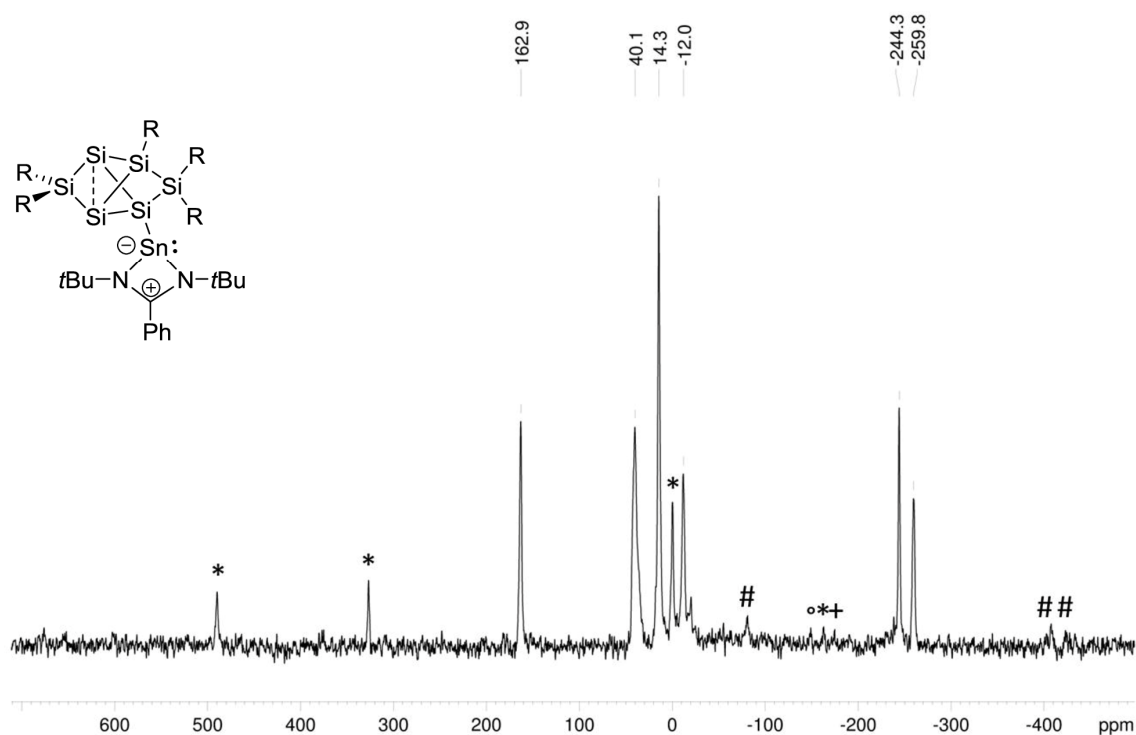
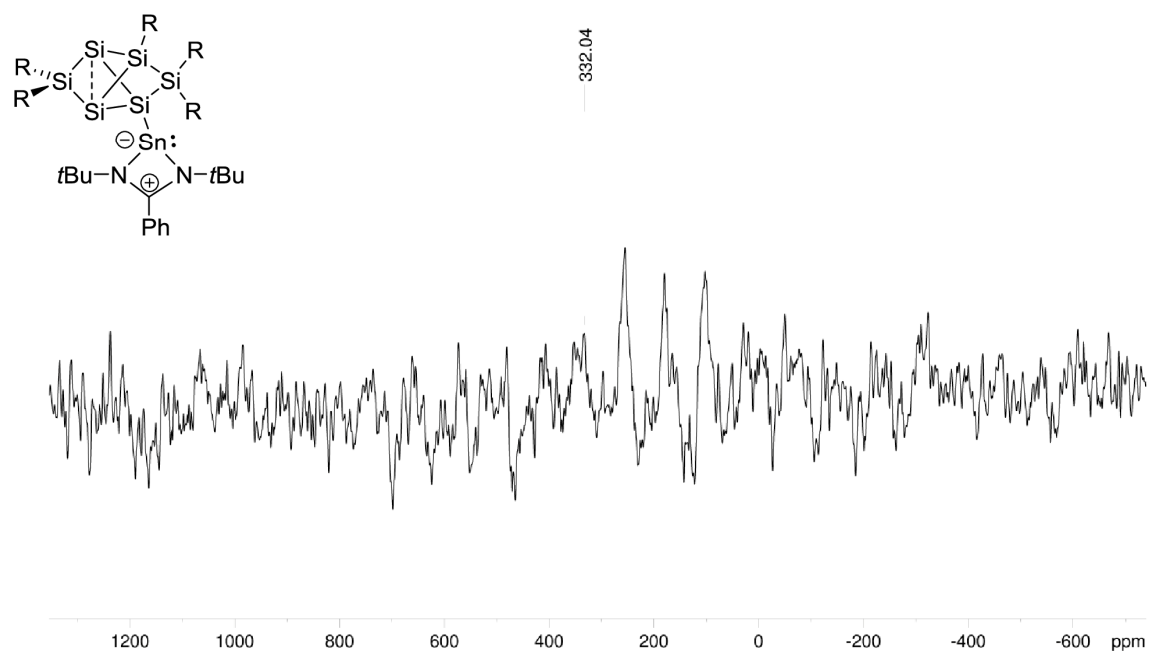
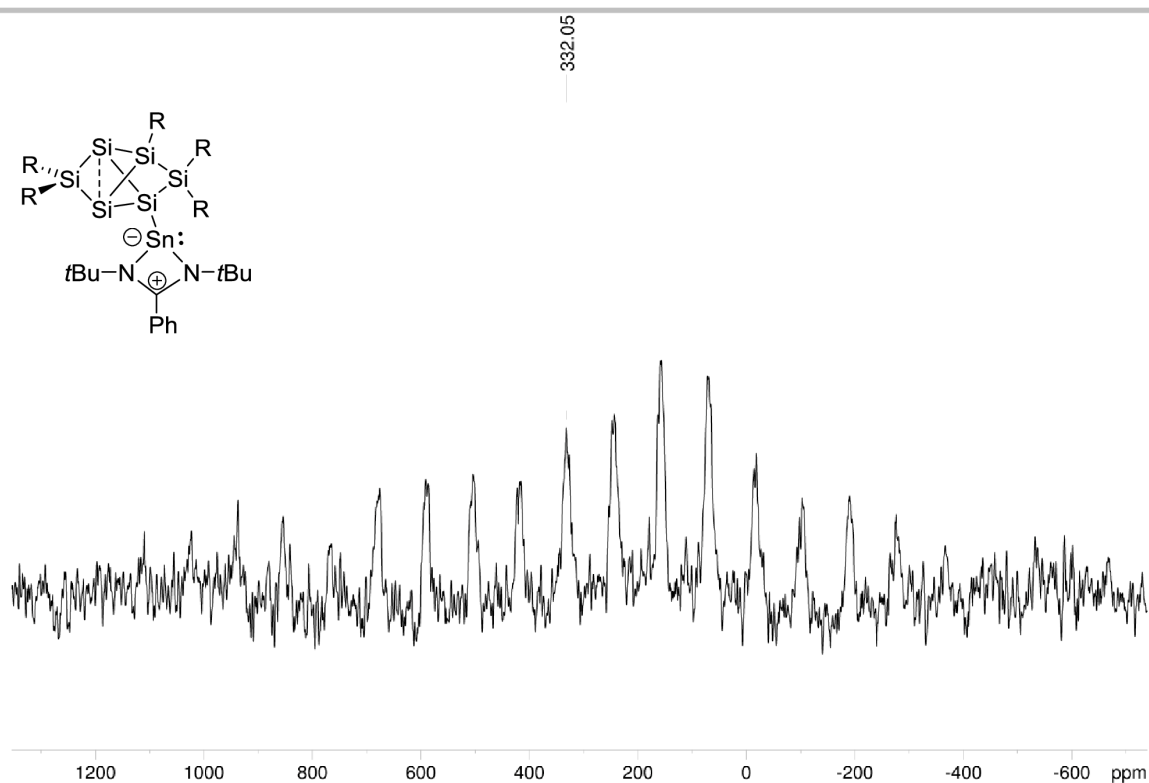


Figure S39. CP-MAS ^{29}Si NMR of **3c** in C_6D_6 (79.53 MHz, 13 KHz, 300 K), side spinning bands: * *privo*-Si(Tip)₂ (162.9 ppm), # *nudo*-Si (-244.3 ppm ; -259.9 ppm), ° *remoto*-Si(Tip)₂ (12.8 ppm), + *ligato*-SiTip (-12.0 ppm).



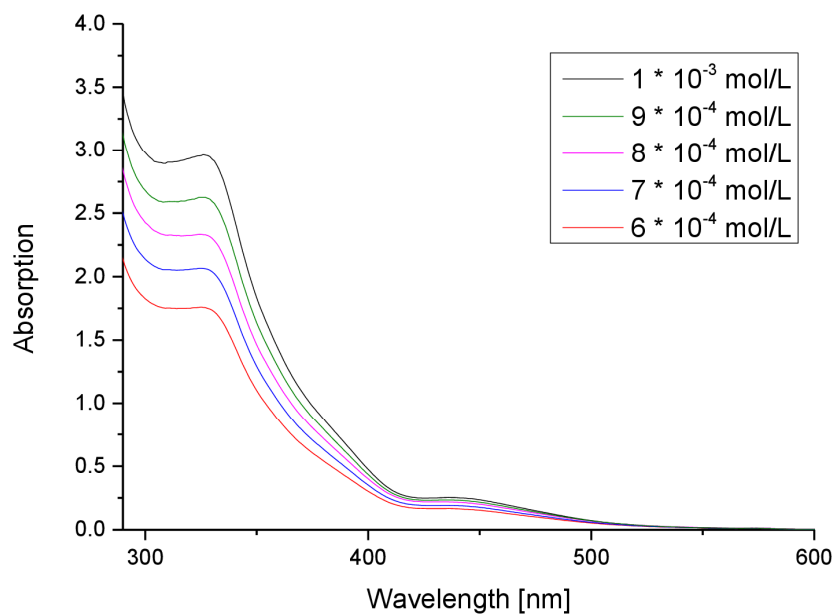


Figure S42. UV-Vis spectrum of **3c** in hexane at different concentrations.

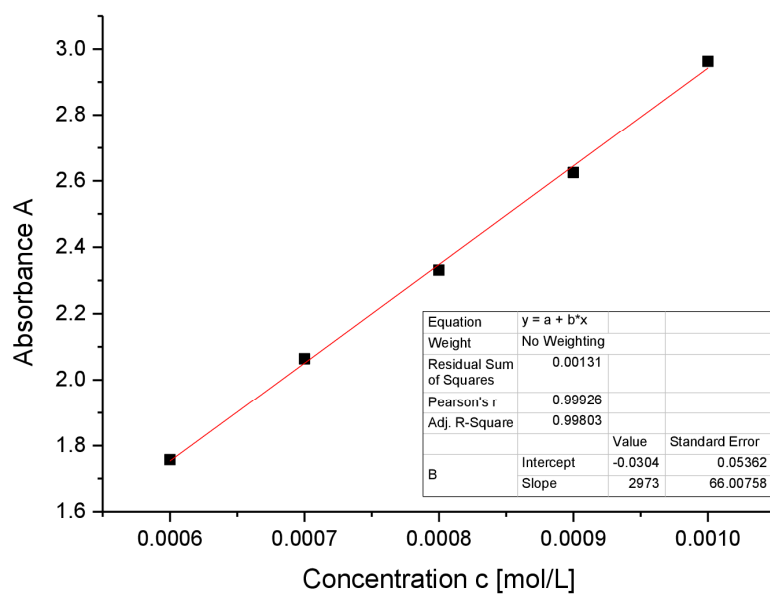


Figure S43. Determination of ε ($29730 \text{ M}^{-1} \text{ cm}^{-1}$) by linear regression of absorptions ($\lambda = 326 \text{ nm}$) of **3c** against concentration.

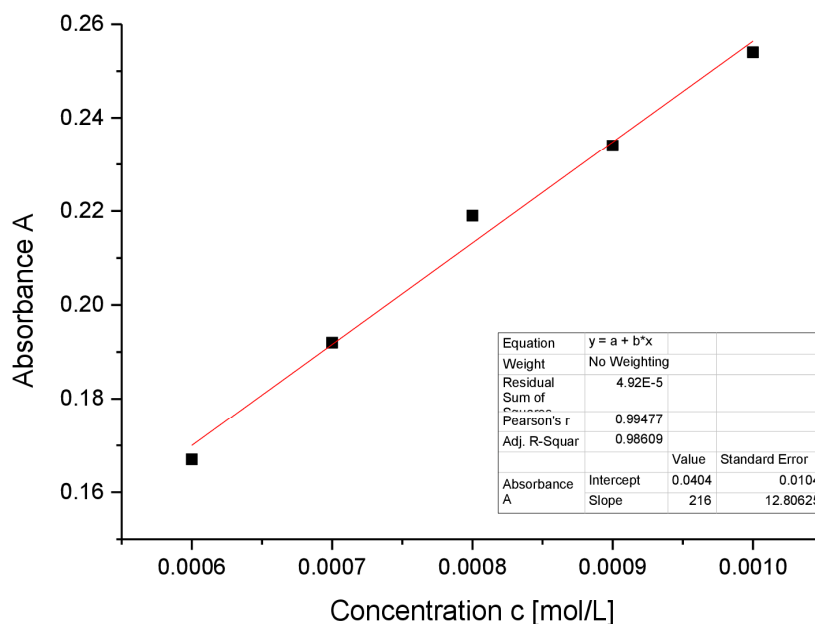


Figure S44. Determination of ε ($2160 \text{ M}^{-1} \text{ cm}^{-1}$) by linear regression of absorptions ($\lambda = 436 \text{ nm}$) of **3c** against concentration.

General procedure for the synthesis of *ligato*-Tetrylene-substituted siliconoid $\text{Fe}(\text{CO})_4$ complexes

The respective compounds **4a-c** are prepared by treating 1 equivalent of **3a**, **3b** or **3c** with the respective amount of diironnonacarbonyl ($\text{Fe}_2(\text{CO})_9$) in benzene at 40°C overnight. A color change was observed from red/orange to a dark brown-greenish solution. Benzene was removed under reduced pressure and the brown residue was filtered from the indicated amount of hexane. Hexane was removed under vacuum and the crude product was crystallized from the indicated amount of benzene at room temperature or hexane at -26°C .

Preparation of *ligato*-NHSilylene-substituted siliconoid $\text{Fe}(\text{CO})_4$ complex (**4a**)

Quantities: **3a**, 250 mg (0.173 mmol) ; $\text{Fe}_2(\text{CO})_9$ 251.84 mg (0.692 mmol) ; benzene 6 mL, filtered from 20 mL hexane, Crystallization from 1 mL hexane at -26°C overnight . Yield: 210 mg (0.130 mmol ; 75 %) orange crystals (mp. $> 220^\circ\text{C}$, dec.).

$^1\text{H-NMR}$ (400.13 MHz, C_6D_6 , 300 K) δ = 7.956 – 7.993 (d, 2H, $^3J_{\text{HH}}$ = 7.88 Hz, 1H, Ar-H), 7.487 – 7.445 (m, 2H, Ar-H), 7.355 – 7.333 (m, 1H, Ar-H), 7.280 (bs, 1H, Ar-H), 7.218 – 7.214 (m, 1H, Ar-H), 6.928 – 6.886 (m, 3H, Ar-H), 6.855 – 6.796 (m, 2H, Ar-H), 6.770 – 6.750 (m, 2H, Ar-H), 6.578 – 6.575 (m, 1H, Ar-H), 6.299 (sept, 1H, $^3J_{\text{HH}}$ = 6.89 Hz, Tip-*i*Pr-CHMe₂), 6.060 (sept, 1H, $^3J_{\text{HH}}$ = 6.59 Hz, Tip-*i*Pr-CHMe₂), 5.356 (sept, 1H, $^3J_{\text{HH}}$ = 6.35 Hz, Tip-*i*Pr-CHMe₂), 4.850 (sept, 1H, $^3J_{\text{HH}}$ = 6.35 Hz, Tip-*i*Pr-CHMe₂), 4.172 (sept, 1H, $^3J_{\text{HH}}$ = 6.39 Hz, Tip-*i*Pr-CHMe₂), 3.777 (sept, 1H, $^3J_{\text{HH}}$ = 6.39 Hz, Tip-*i*Pr-CHMe₂), 3.583 (sept, 1H, $^3J_{\text{HH}}$ = 6.88 Hz, Tip-*i*Pr-CHMe₂), 3.497-3.435 (m, 2H, Tip-*i*Pr-CHMe₂), 3.217 (sept, 1H, $^3J_{\text{HH}}$ = 6.61 Hz, Tip-*i*Pr-CHMe₂), 2.885 (sept, 1H, $^3J_{\text{HH}}$ = 6.61 Hz, Tip-*i*Pr-CHMe₂), 2.737 (sept, 1H, $^3J_{\text{HH}}$ = 6.90 Hz, Tip-*i*Pr-CHMe₂), 2.677 – 2.544 (m, 3H, Tip-*i*Pr-CHMe₂), 2.235 – 2.219 (d, 3H, $^3J_{\text{HH}}$ = 6.25 Hz, Tip-*i*Pr-CHMe₃), 2.176 – 2.144 (t, 6H, $^3J_{\text{HH}}$ = 6.77 Hz, Tip-*i*Pr-CHMe₃), 2.115 – 2.099 (d, 3H, $^3J_{\text{HH}}$ = 6.77 Hz, Tip-*i*Pr-CHMe₃), 1.919 – 1.904 (d, 3H, $^3J_{\text{HH}}$ = 6.69 Hz, Tip-*i*Pr-CHMe₃), 1.758 – 1.742 (d, 3H, $^3J_{\text{HH}}$ = 6.63 Hz, Tip-*i*Pr-CHMe₃), 1.719 – 1.703 (d, 3H, $^3J_{\text{HH}}$ = 6.48 Hz, Tip-*i*Pr-CHMe₃), 1.664 – 1.5986 (m, 9H, Tip-*i*Pr-CHMe₃), 1.559 – 1.542 (d, 3H, $^3J_{\text{HH}}$ = 6.78 Hz, Tip-*i*Pr-CHMe₃), 1.398 – 1.382 (d, 3H, $^3J_{\text{HH}}$ = 6.41 Hz, Tip-*i*Pr-CHMe₃), 1.352 – 1.060 (m, 52H, Tip-*i*Pr-CHMe₃ and $\text{C}(\text{CH}_3)_3$), 0.999 (s, 9H, $\text{C}(\text{CH}_3)_3$), 0.907 –

SUPPORTING INFORMATION

WILEY-VCH

0.857 (m, 10H, Tip-*i*Pr-CHMe₃), 0.529-0.515 (d, 9H, ³J_{HH} = 6.10 Hz, Tip-*i*Pr-CHMe₃), 0.453 – 0.408 (m, 6H, Tip-*i*Pr-CHMe₃), 0.321 – 0.299 (m, 6H, Tip-*i*Pr-CHMe₃).

¹³C-NMR (100.61 MHz, C₆D₆, 300 K) δ = 210.11 (C-O), 166.59 (s, 1C, Ar-C), 156.58, 156.34, 155.90, 154.96, 154.77, 153.38, 152.99, 152.64, 151.21, 149.78, 149.54, 149.42, 149.19, 148.72 (s, each 1C, Ar-C), 140.51 (s, 1C, Ar-C), 138.35 (s, 1C, Ar-C), 137.79 (s, 1C, Ar-C), 135.82 (C₁₀H₈), 131.37 (s, 1C, Ar-CH), 130.22, 130.12 (bs, each 1C, Ar-CH), 128.21, (s, each 1C, Ar-CH), 128.45 (C₁₀H₈), 128.21, 127.97, 127.89, 127.05 (s, each 1C, Ar-CH overlapping with C₆D₆), 125.45, 125.69, 125.26, 123.77, 123.35, 122.79, 122.44, 122.04, 120.91, 120.83, 120.47 (s, each 1C, Ar-CH), 55.74, 55.52 (s, each 1C, C(CH₃)₃), 38.83, 37.58, 36.65, 36.16 (s, each 1C, Tip-*i*Pr-CH), 34.95, 34.79, 34.75, 24.50, 24.47, 34.32, 34.25, 34.03, 33.98 (bs, each 1C, Tip-*i*Pr-CH), 31.59 (s, 3C, Tip-*i*Pr-CH), 31.53, 31.21, 30.91 (s, each 1C, Tip-*i*Pr-CH), 29.90, 29.03, 28.47, 28.05, 27.96 (s, each 1C, Tip-*i*Pr-CH₃), 26.95, 26.88, 26.82 (s, each 1C, Tip-*i*Pr-CH₃), 25.93, 25.27, 25.03, 24.69, 24.66, 24.49 (s, each 1C, Tip-*i*Pr-CH₃), 23.82, 23.74, 23.72, 23.62, 23.57, 23.43, 23.87 (bs, each 1C, Tip-*i*Pr-CH₃), 22.87 (s, 1C, Tip-*i*Pr-CH₃), 22.69 (s, 3C, CH₃), 22.63, 22.09 (s, each 1C, Tip-*i*Pr-CH₃), 13.98 (s, 3C, CH₃).

²⁹Si-NMR (79.49 MHz, C₆D₆, 300 K) δ = 165.1 (s, *privo*-Si(Tip)₂), 110.0 (s, NHSi), 28.1 (s, *ligato*-SiTip), -22.0 (s, *remoto*-Si(Tip)₂), -26.1 (s, *ligato*-Si-NHSi), -198.2 (s, *nudo*-Si), -230.4 (s, *nudo*-Si) ppm.

CP-MAS ²⁹Si-NMR (79.53 MHz, 300K) δ = 158.2 (s, *privo*-Si), 109.5 (s, NHSi), 27.1 (s, *ligato*-SiTip), -23.4 (bs, 2Si, *remoto*-Si(Tip)₂ + *ligato*-Si-NHSi), -195.9 (s, *nudo*-Si), -231.2 (s, *nudo*-Si) ppm.

Elemental analysis: calculated for C₉₄H₁₃₈FeN₂O₄Si₇: C: 70.01 % ; H: 8.63 % ; N: 1.74 %. Found: C: 71.12 % ; H: 8.71 % ; N: 1.54 %.

UV/VIS (hexane): λ_{max} (ε) = 591 nm (680 M⁻¹ cm⁻¹).

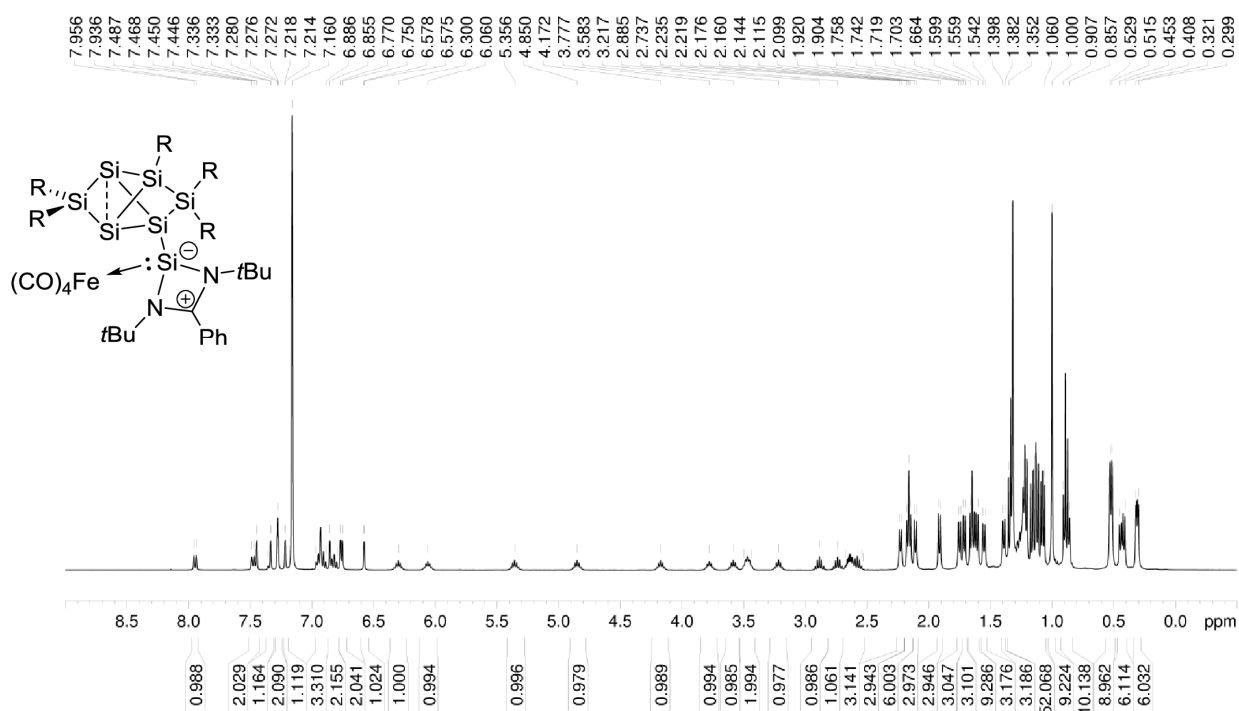
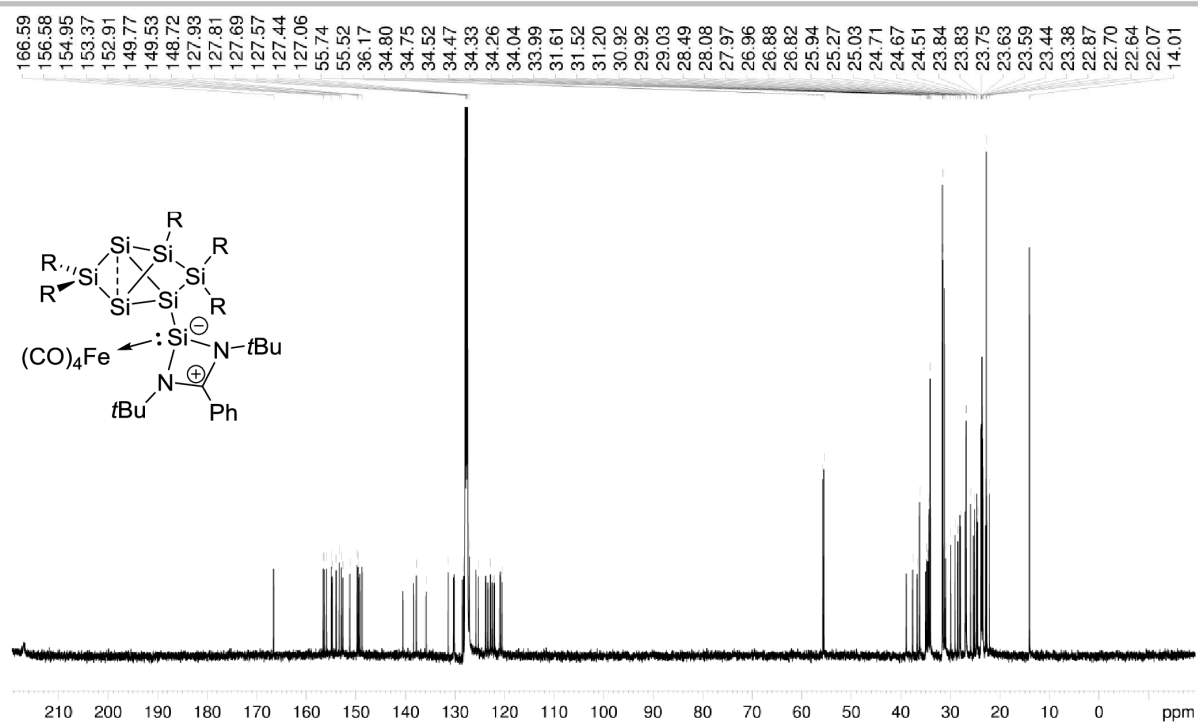
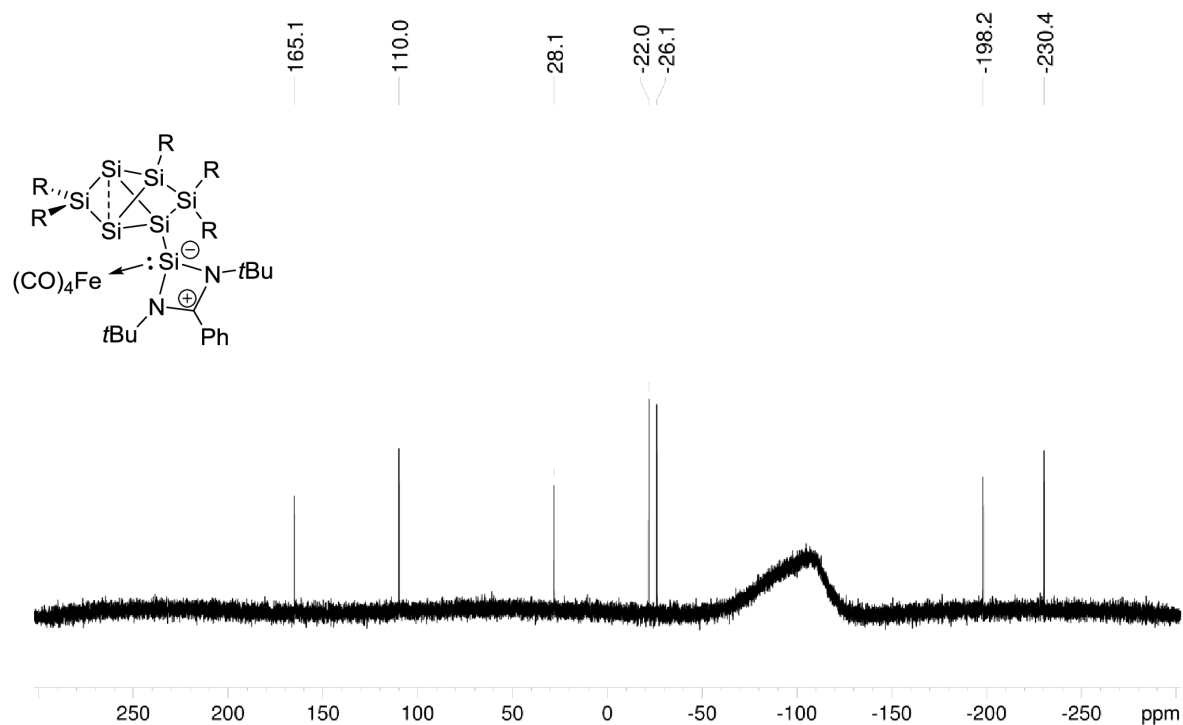


Figure S45. ¹H NMR of 4a in C₆D₆ (400.13 MHz, 300 K).

SUPPORTING INFORMATION

WILEY-VCH

Figure S46. ^{13}C NMR of **4a** in C_6D_6 (100.61 MHz, 300 K).Figure S47. ^{29}Si NMR of **4a** in C_6D_6 (79.49 MHz, 300 K).

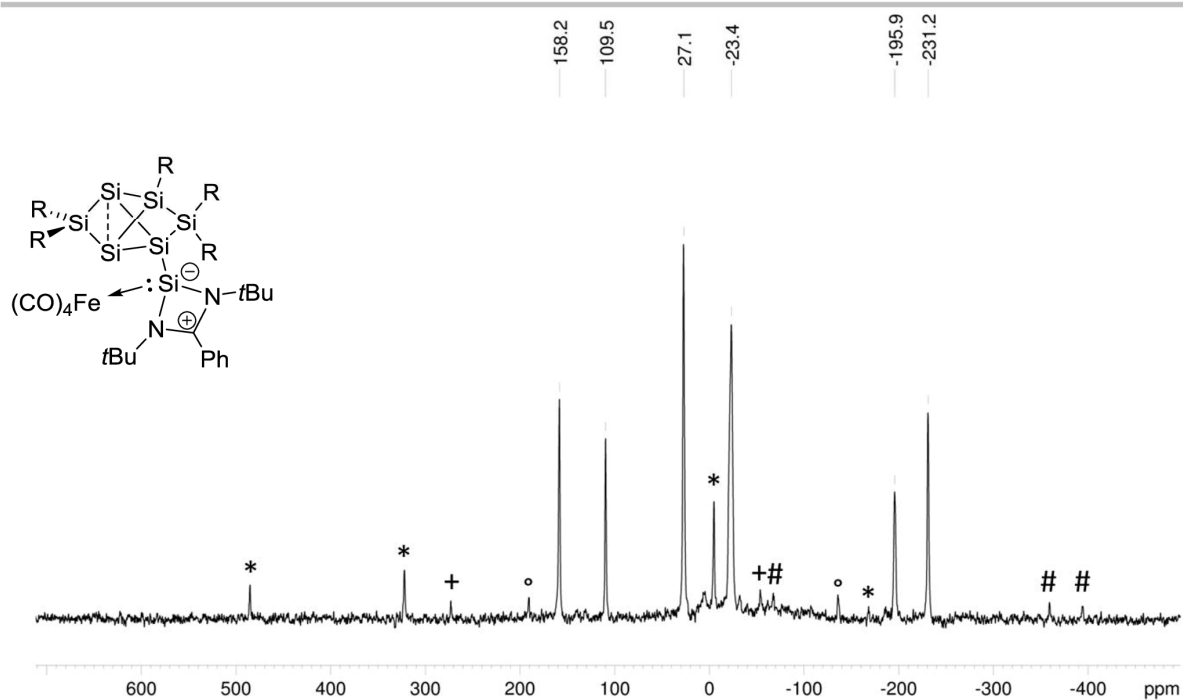


Figure S48. CP-MAS ^{29}Si NMR of **4a** (79.53 MHz, 300 K), side spinning bands: * *privo*-Si(Tip) $_2$ (158.2 ppm), # *nudo*-Si (-195.9 ppm ; -231.2 ppm), + NHSi (109.5 ppm), ° *ligato*-SiTip (27.1 ppm).

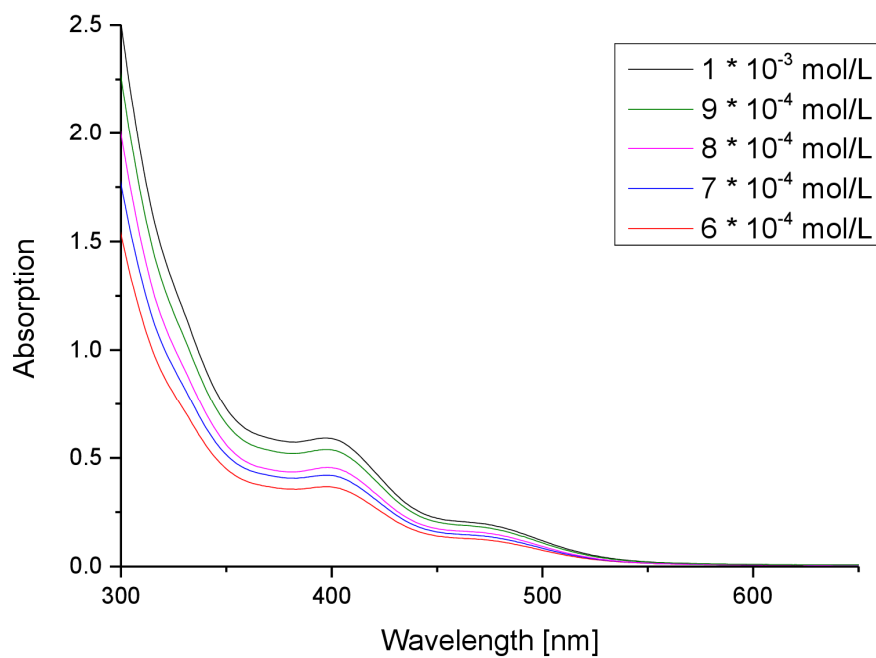


Figure S49. UV-Vis spectrum of **4a** in hexane at different concentrations.

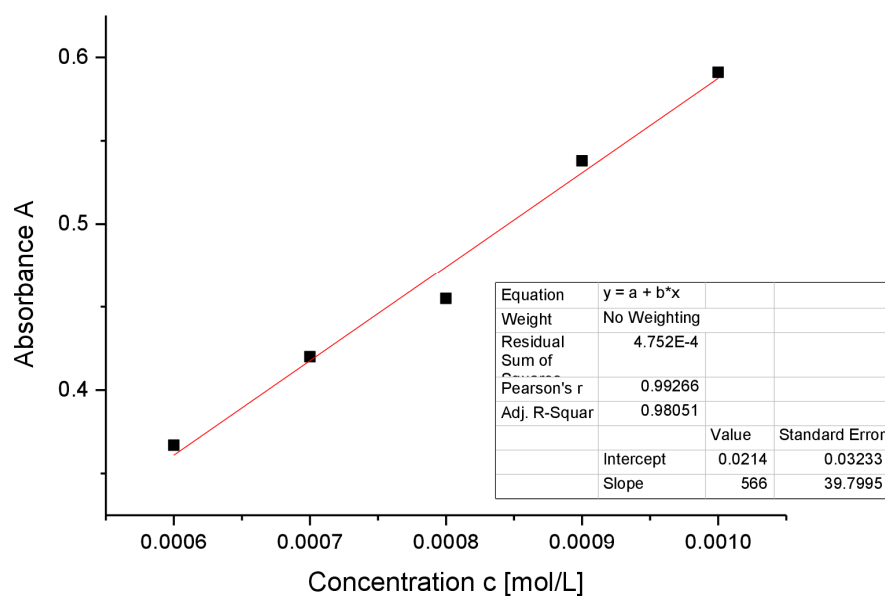


Figure S50. Determination of ϵ ($5660 \text{ M}^{-1} \text{ cm}^{-1}$) by linear regression of absorptions ($\lambda = 397 \text{ nm}$) of **4a** against concentration.

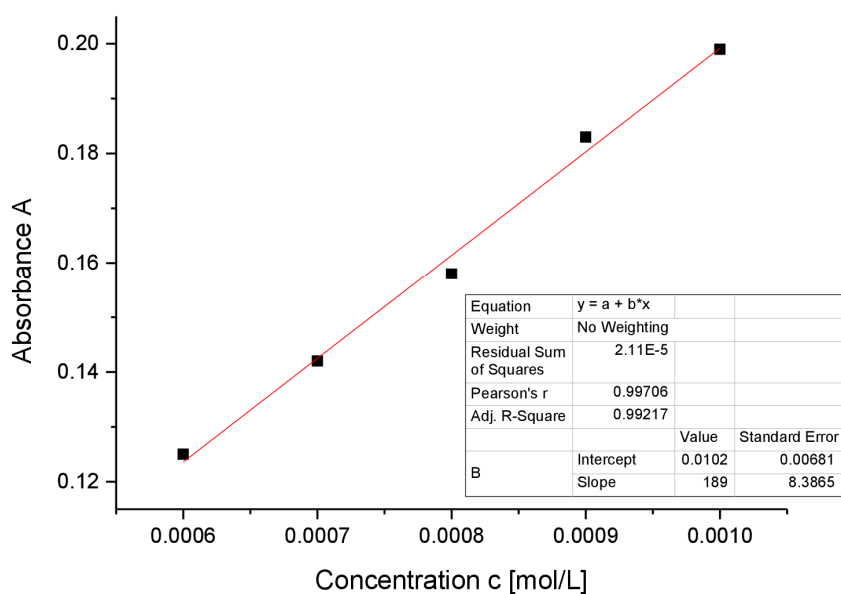
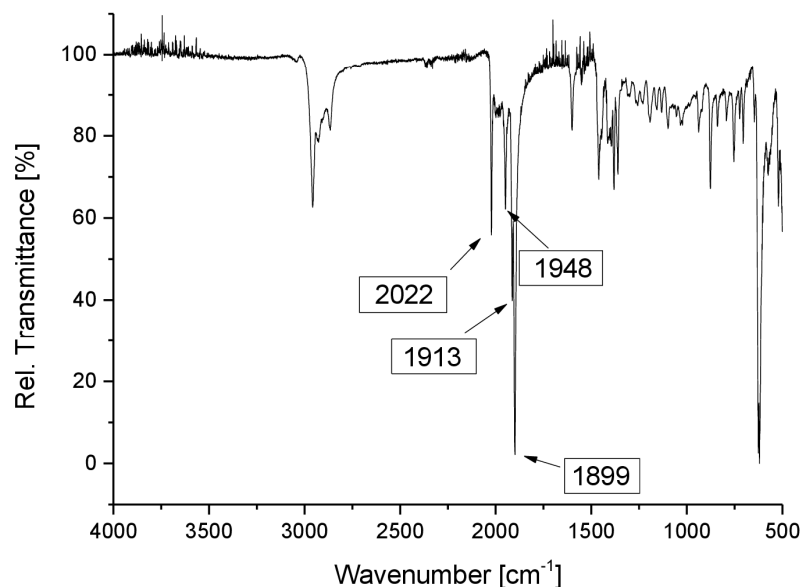


Figure S51. Determination of ϵ ($1890 \text{ M}^{-1} \text{ cm}^{-1}$) by linear regression of absorptions ($\lambda = 470 \text{ nm}$) of **4a** against concentration.

Figure S52. Ir spectrum of **4a****Preparation of *ligato*-NHGermylene-substituted siliconoid Fe(CO)₄ complex (**4b**)**

Quantities: **3b**, 250 mg (0.164 mmol) ; Fe₂(CO)₉ 297.68 mg (0.818 mmol) ; benzene 5 mL, filtered from 10 mL hexane, crystallization from 1 mL hexane at -26°C. Yield: 166 mg (0.098 mmol ; 60 %) orange-brown crystals (mp. > 210 °C, dec.).

¹H-NMR (400.13 MHz, C₆D₆, 300 K) δ = 7.942-7.922 (d, 1H, J = 7.73, Ar-H), 7.465 - 7.440 (m, 2 H, Ar-H), 7.342 - 7.338 (m, 1H, Ar-H), 7.264-7.251 (m, 2H, Ar-H), 7.009 – 6.924 (m, 3H, Ar-H), 6.889 – 6.858 (m, 2H, Ar-H), 6.767 – 6.740 (m, 2H, Ar-H), 6.557 – 6.553 (m, 1H, Ar-H), 6.387 (sept, ³J_{HH} = 6.42 Hz, 1H, Tip-*i*Pr-CHMe₂), 5.977 (sept, ³J_{HH} = 6.21 Hz, 1H, Tip-*i*Pr-CHMe₂), 5.318 (sept, ³J_{HH} = 6.67 Hz, 1H, Tip-*i*Pr-CHMe₂), 4.951 (sept, ³J_{HH} = 6.67 Hz, 1H, Tip-*i*Pr-CHMe₂), 4.135 (sept, ³J_{HH} = 6.49 Hz, 1H, Tip-*i*Pr-CHMe₂), 3.746 (sept, ³J_{HH} = 6.39 Hz, 1H, Tip-*i*Pr-CHMe₂), 3.597 – 3.454 (m, 3H, Tip-*i*Pr-CHMe₂), 3.191 (sept, ³J_{HH} = 6.83 Hz, 1H, Tip-*i*Pr-CHMe₂), 2.873 (sept, ³J_{HH} = 6.69 Hz, 1H, Tip-*i*Pr-CHMe₂), 2.738 (sept, ³J_{HH} = 6.91 Hz, 1H, Tip-*i*Pr-CHMe₂), 2.663 – 2.539 (m, 3H, Tip-*i*Pr-CHMe₂), 2.218 – 2.202 (d, 3H, ³J_{HH} = 6.51 Hz, Tip-*i*Pr-CH₃), 2.125 – 2.081 (m, 9H, Tip-*i*Pr-CH₃), 1.903 – 1.887 (d, 3H, ³J_{HH} = 6.63 Hz, Tip-*i*Pr-CH₃), 1.772 – 1.756 (d, 3H, ³J_{HH} = 6.63 Hz, Tip-*i*Pr-CH₃), 1.707 – 1.662 (m, 9H, Tip-*i*Pr-CH₃), 1.606 (t, 6 H, ³J_{HH} = 7.04 Hz, Tip-*i*Pr-CH₃), 1.383 – 1.367 (d, 3H, ³J_{HH} = 6.13 Hz, Tip-*i*Pr-CH₃), 1.325 (t, 6 H, ³J_{HH} = 6.96 Hz, Tip-*i*Pr-CH₃), 1.271 (s, 9H, C(CH₃)₃), 1.219 – 1.201 (d, 6H, ³J_{HH} = 6.96 Hz, Tip-*i*Pr-CH₃), 1.167 – 1.055 (m, 20H, Tip-*i*Pr-CH₃), 0.935 (s, 9H, C(CH₃)₃), 0.821 – 0.805 (d, 3H, ³J_{HH} = 6.11 Hz, Tip-*i*Pr-CH₃), 0.573 – 0.481 (m, 13H, Tip-*i*Pr-CH₃), 0.410 – 0.395 (d, 3H, ³J_{HH} = 6.58 Hz, Tip-*i*Pr-CH₃), 0.336 – 0.295 (dd, 6H, ³J_{HH} = 6.58 Hz, ³J_{HH} = 6.34 Hz, Tip-*i*Pr-CH₃) ppm.

¹³C-NMR (100.61 MHz, C₆D₆, 300 K) δ = 216.63 (C-O) 211.85 (Fe(CO)₅) 165.38 (s, 1C, Ar-C), 156.42, 156.20, 155.86, 155.26, 154.56, 153.76, 153.38, 152.92, 152.84, 151.51, 149.98, 149.63, 149.53, 149.41, 149.01 (s, each 1C, Ar-C), 139.77, 138.05, 137.06, 135.42, 133.24, (s, each 1C, Ar-C), 130.30, 129.65 (s, each 1C, Ar-CH), 128.07, 128.01, 127.96 (bs, each 1C, Ar-CH), 126.94, 125.72 125.68, 125.22, 123.80, 123.26, 122.84, 122.35, 122.21, 121.24, 120.82, 120.39 (s, each 1C, Ar-CH), 55.68, 55.22 (s, each 1C, C(CH₃)₃), 38.87, 37.69, 36.70, 36.34, 36.03 (s, each 1C, Tip-*i*Pr-CH), 35.18, 35.07, 34.80, 34.69, 34.65, 34.33, 34.22, 34.05, 34.01, 33.97 (bs, each 1C, Tip-*i*Pr-CH), 31.69, 31.58, 31.41 (s, each 1C, Tip-*i*Pr-CH), 30.80 (s, 1C, Tip-*i*Pr-CH), 29.87 (s, 1C, Tip-*i*Pr-CH₃), 28.53 – 28.47 (d, 1C, J = 5.49 Hz, Tip-*i*Pr-CH₃), 28.03, 27.85 (s, each 1C, Tip-*i*Pr-CH₃), 26.99, 26.89, 26.79, 26.74, 26.47 (s,

SUPPORTING INFORMATION

WILEY-VCH

each 1C, Tip-*i*Pr-CH₃), 25.56, 25.22, 24.96, 24.69 (s, each 1C, Tip-*i*Pr-CH₃), 24.63 (d, 1C, J = 6.14 Hz, Tip-*i*Pr-CH₃), 24.38 (s, 1C, Tip-*i*Pr-CH₃), 23.74, 23.68, 23.58, 23.49, 23.41 (bs, each 1C, Tip-*i*Pr-CH₃), 22.89, 22.71 (s, each 1C, Tip-*i*Pr-CH₃), 22.67 (s, 3C, CH₃), 22.34, 13.96 (s, 3C, CH₃) ppm.

²⁹Si-NMR (79.49 MHz, C₆D₆, 300 K) δ = 163.7 (s, *privo*-Si), 31.7 (s, *ligato*-SiTip), -13.6 (*remoto*-Si(Tip)₂), -24.1 (s, *ligato*-Si-NHSi), -203.2 (s, *nudo*-Si), -231.6 (s, *nudo*-Si) ppm.

CP-MAS ²⁹Si-NMR (79.53 MHz, 300K) δ = 156.7 (s, *privo*-Si), 29.9 (s, *ligato*-SiTip), -9.4 (*remoto*-Si(Tip)₂), -25.6 (s, *ligato*-Si-NHSi), -202.2 (s, *nudo*-Si), -232.8 (s, *nudo*-Si) ppm.

Elemental analysis: calculated for C₉₄H₁₃₈FeGeN₂O₄Si₆: C: 68.13 % ; H: 8.39 % ; N: 1.69 %. Found: C, 69.28 % ; H, 8.76 % ; N, 1.79 %.

UV/VIS (hexane): λ_{max} (ε) = 469nm (2090 M⁻¹ cm⁻¹).

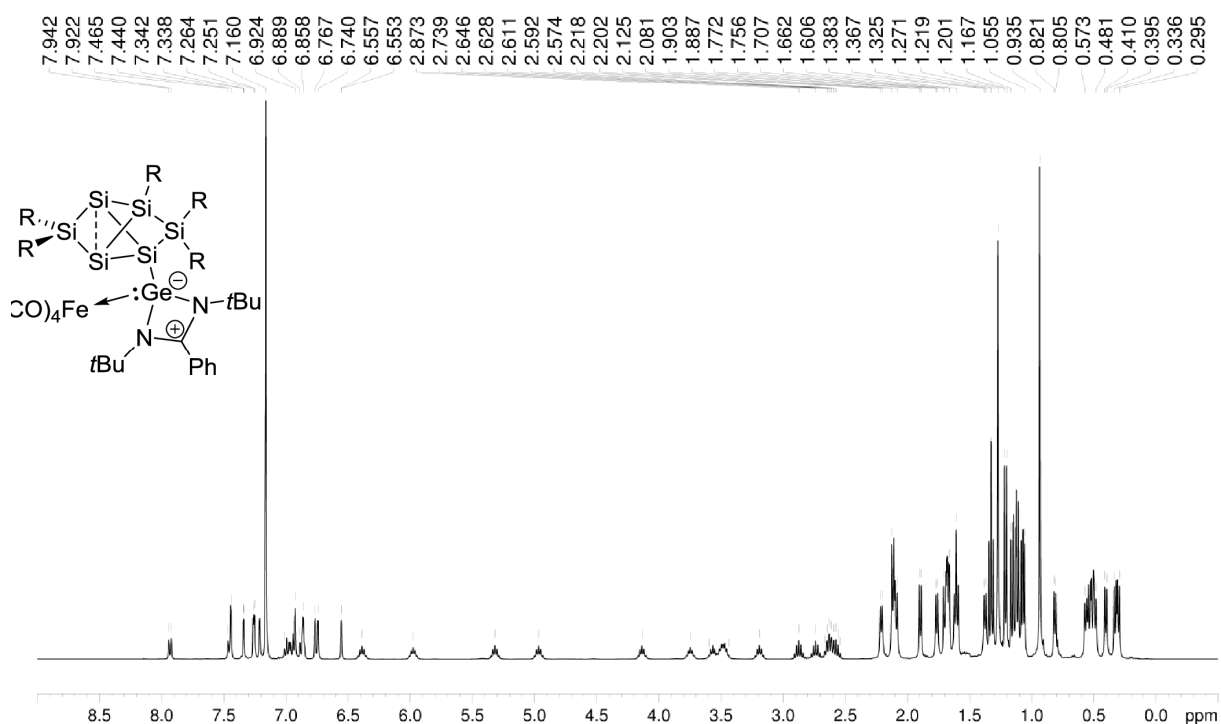
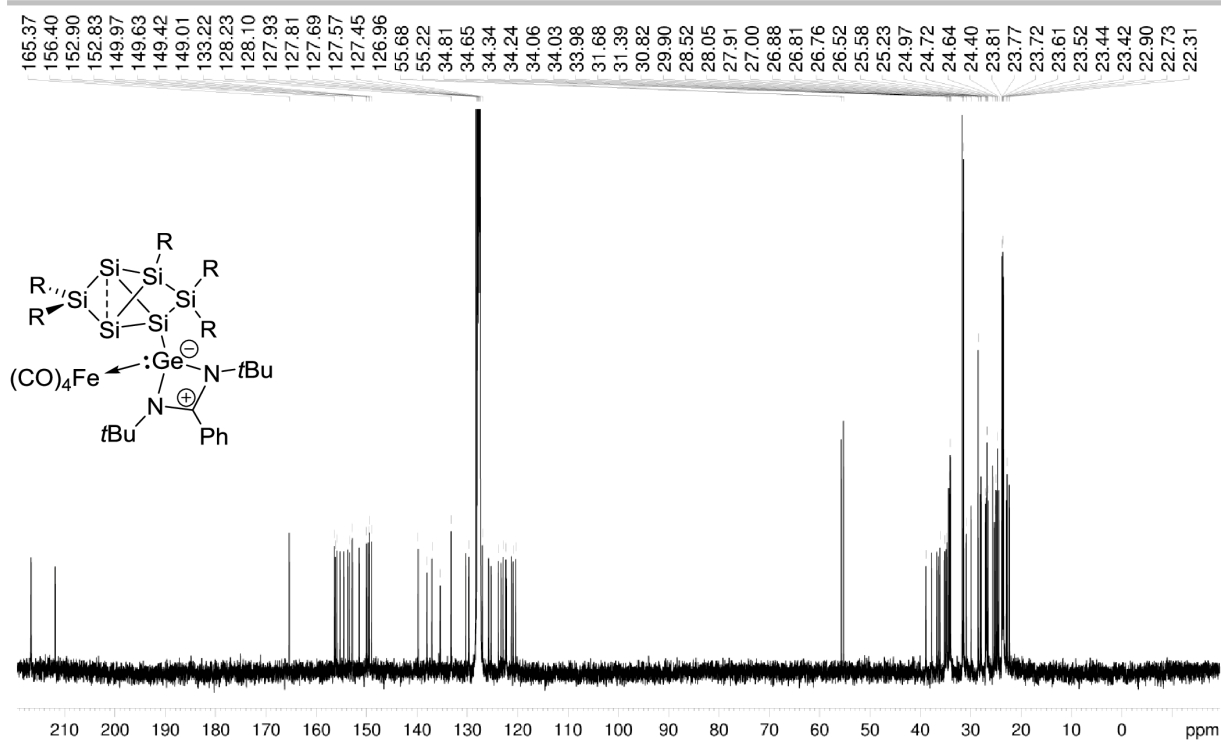
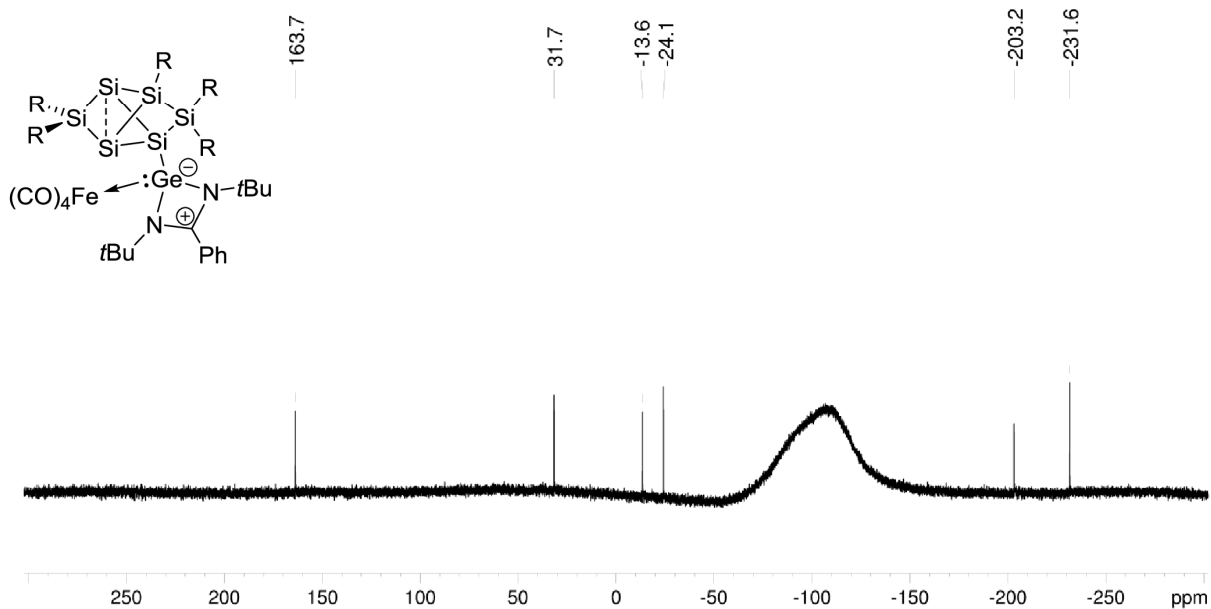


Figure S53. ¹H NMR of **4b** in C₆D₆ (400.13 MHz, 300 K).

SUPPORTING INFORMATION

WILEY-VCH

Figure S54. ^{13}C NMR of **4b** in C_6D_6 (100.61 MHz, 300 K).Figure S55. ^{29}Si NMR of **4b** in C_6D_6 (79.49 MHz, 300 K).

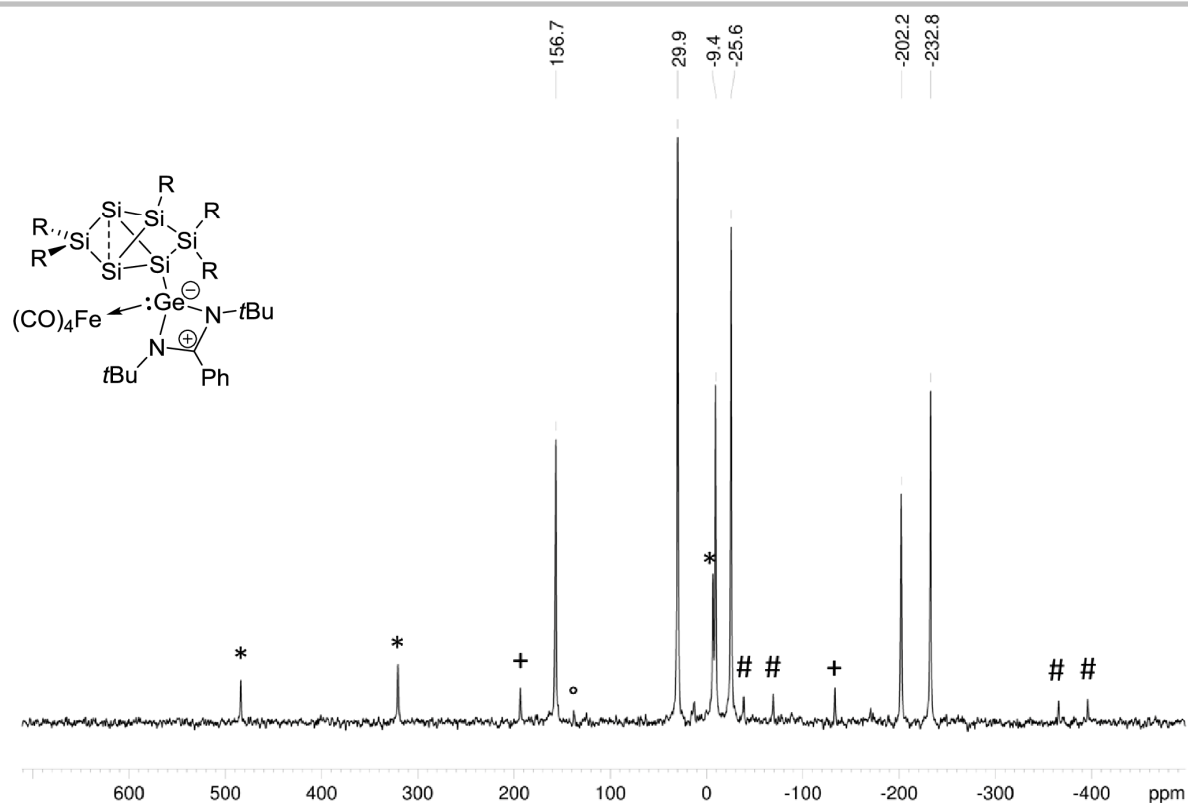


Figure S56. CP-MAS ^{29}Si NMR of **4b** in C_6D_6 (79.53 MHz, 300 K), side spinning bands: * *privo*-Si(Tip) $_2$ (156.7 ppm), # *nudo*-Si (-202.2 ppm ; -232.8 ppm), + *ligato*-SiTip, (29.9 ppm), ° *ligato*-Si-NHGe (-25.6 ppm).

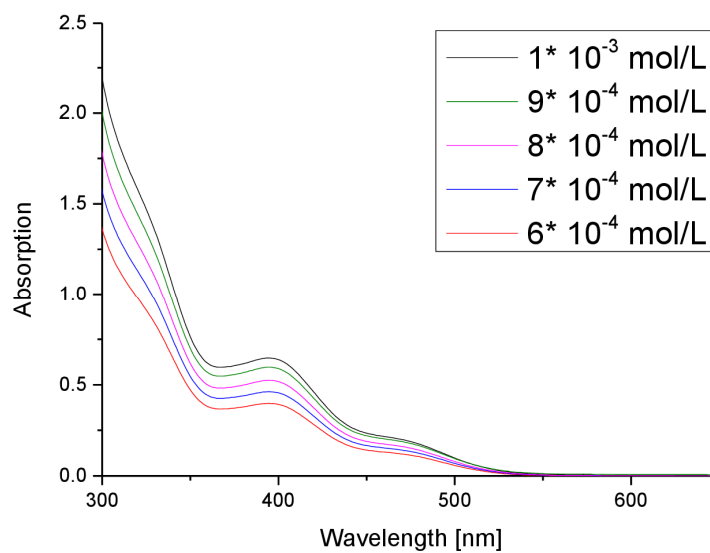


Figure S57. UV-Vis spectrum of **4b** in hexane at different concentrations.

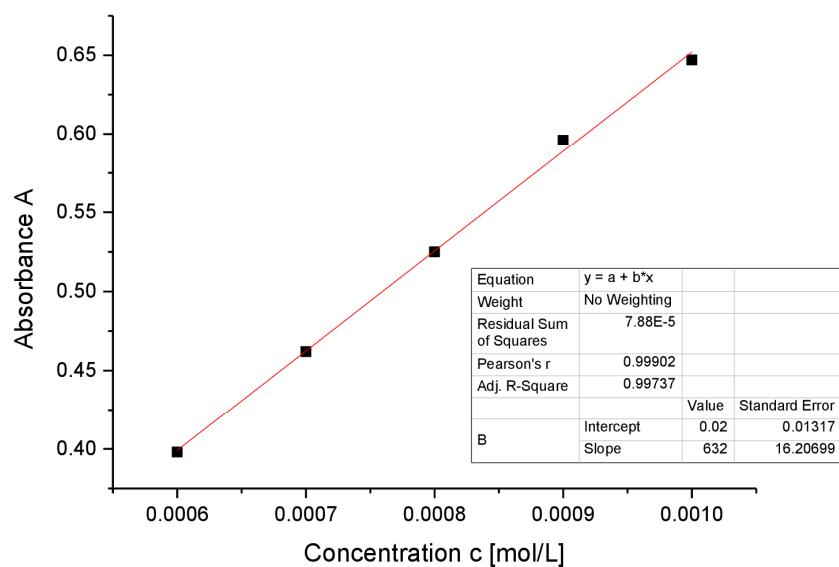


Figure S58. Determination of ϵ ($6320 \text{ M}^{-1} \text{ cm}^{-1}$) by linear regression of absorptions ($\lambda = 394 \text{ nm}$) of **4b** against concentration.

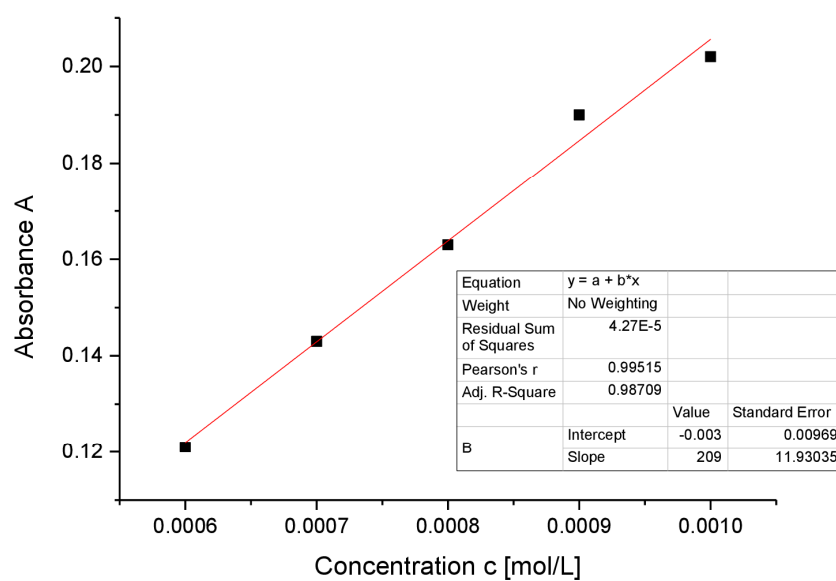
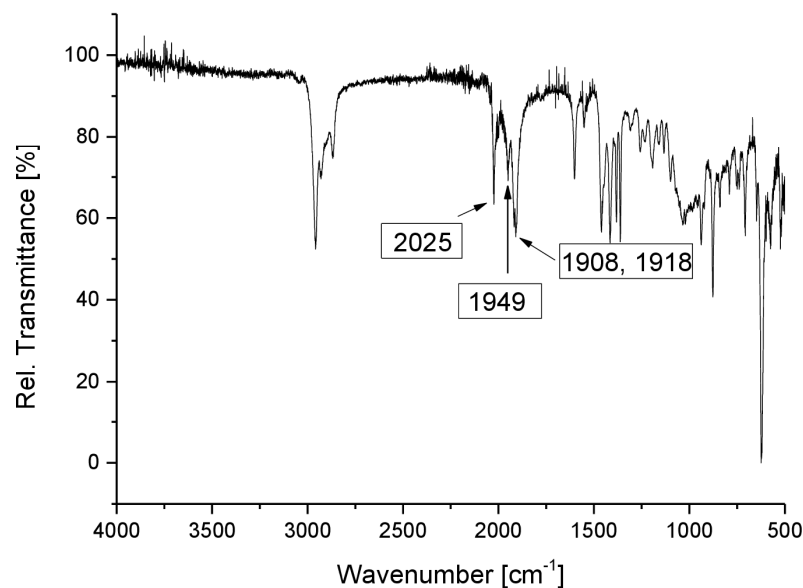


Figure S59. Determination of ϵ ($2090 \text{ M}^{-1} \text{ cm}^{-1}$) by linear regression of absorptions ($\lambda = 469 \text{ nm}$) of **4b** against concentration.

Figure S60. IR spectrum of **4b****Preparation of *ligato*-NHStannylene-substituted siliconoid Fe(CO)₄ complex (**4c**)**

Quantities: **3c**, 250 mg (0.15 mmol) ; Fe₂(CO)₉ 82.02 mg (0.225 mmol) ; benzene 10 mL, filtered from 10 mL hexane, crystallization from 0.8 mL benzene. Yield: 181 mg (0.106 mmol ; 70 %) orange crystals (mp. > 230 °C, dec.).

¹H-NMR (400.13 MHz, C₆D₆, 300 K) δ = 7.829 – 7.809 (d, ⁴J_{HH} = 7.56 Hz, 1H, Ar-H), 7.389 – 7.330 (m, 3 H, Ar-H), 7.194 – 7.173 (m, 3H, Ar-H), 7.042 – 6.944 (m, 2H, Ar-H), 6.905 – 6.868 (m, 2H, Ar-H), 6.835 – 6.832 (m, 1H, Ar-H), 6.762 – 6.678 (m, 1H, Ar-H), 6.521 (bs, 1H, Ar-H), 6.336 (sept, 1H, ³J_{HH} = 6.40 Hz, Tip-*i*Pr-CHMe₂), 5.716 – 5.685 (m, 1H, Tip-*i*Pr-CHMe₂), 5.329 (sept, 1H, ³J_{HH} = 6.69 Hz, Tip-*i*Pr-CHMe₂), 5.191 (sept, 1H, ³J_{HH} = 6.69 Hz, Tip-*i*Pr-CHMe₂), 4.137 (sept, 1H, ³J_{HH} = 6.38 Hz, Tip-*i*Pr-CHMe₂), 3.761 (sept, 1H, ³J_{HH} = 6.38 Hz, Tip-*i*Pr-CHMe₂), 3.581 (sept, 1H, ³J_{HH} = 6.28 Hz, Tip-*i*Pr-CHMe₂), 3.512 – 3.421 (m, 2 H, Tip-*i*Pr-CHMe₂), 3.117 (sept, 1H, ³J_{HH} = 6.40 Hz, Tip-*i*Pr-CHMe₂), 2.818, 2.738 (each sept, together 2H, ³J_{HH} = 6.67 Hz, ³J_{HH} = 6.78 Hz, Tip-*i*Pr-CHMe₂), 2.640 – 2.523 (m, 3H, Tip-*i*Pr-CHMe₂), 2.141 – 2.125 (d, 6H, ³J_{HH} = 6.34 Hz, Tip-*i*Pr-CHMe₃), 2.059 – 2.044 (d, 3H, ³J_{HH} = 6.74 Hz, Tip-*i*Pr-CHMe₃), 1.849 (t, 6H, ³J_{HH} = 6.95 Hz, Tip-*i*Pr-CHMe₃), 1.776 – 1.635 (m, 17 H, Tip-*i*Pr-CHMe₃), 1.585 – 1.568 (d, 3H, ³J_{HH} = 6.96 Hz, Tip-*i*Pr-CHMe₃), 1.383 – 1.367 (d, 3H, ³J_{HH} = 6.54 Hz, Tip-*i*Pr-CHMe₃), 1.289 – 1.199 (m, 17H, Tip-*i*Pr-CHMe₃), 1.156 – 1.033 (m, 30H, Tip-*i*Pr-CHMe₃ and C(CH₃)₃), 0.907 – 0.872 (t, hexane), 0.822 (s, 9H, C(CH₃)₃), 0.688 – 0.673 (d, 3H, ³J_{HH} = Hz, Tip-*i*Pr-CHMe₃), 0.626 (t, 6H, ³J_{HH} = 6.64 Hz, Tip-*i*Pr-CHMe₃), 0.570 – 0.554 (d, 3H, ³J_{HH} = 6.54 Hz, Tip-*i*Pr-CHMe₃), 0.514 – 0.498 (d, 3H, ³J_{HH} = 6.30 Hz, Tip-*i*Pr-CHMe₃), 0.388 – 0.373 (d, 3H, ³J_{HH} = 6.13 Hz, Tip-*i*Pr-CHMe₃), 0.333 – 0.317 (d, 3H, ³J_{HH} = 6.24 Hz, Tip-*i*Pr-CHMe₃), 0.273 – 0.257 (d, 3H, ³J_{HH} = 6.36 Hz, Tip-*i*Pr-CHMe₃) ppm.

¹³C-NMR (100.61 MHz, C₆D₆, 300 K) δ = 215.96 (C=O), 167.46 (s, 1C, Ar-C), 156.18, 155.83, 155.32, 154.25 (s, each 1C, Ar-C), 153.25 - 153.2 (d, 1C, J = 6.15 Hz, Ar-C), 152.93 - 152.89 (d, 1C, J = 4.72 Hz, Ar-C), 151.96, 150.33, 149.79, 149.63, 149.48, 149.35 (s, each 1C, Ar-C), 139.02, 137.72, 136.73, 135.53, 135.24 (s, each 1C, Ar-C), 130.17, 129.30, (s, each 1C, Ar-C), 129.21 (s, 1C, Ar-C), 128.10, 127.99, 127.94, 127.81, 127.57 (bs, each 1C, overlapping with C₆D₆, Ar-CH), 126.8, 124.99, 123.75, 123.09, 122.70, 122.41, 122.24, 120.61, 120.32 (s, each 1C, Ar-CH), 54.55, 54.01 (s, each 1C, C(CH₃)₃), 38.60, 37.60, 36.95, 36.31, 35.70, 35.65, 35.58, 35.36 (s, each 1C, Tip-*i*Pr-CH), 35.06 - 35.96 (d, 1C, J = 10.19 Hz, Tip-*i*Pr-CH), 34.36, 34.14 (s, each 1C, Tip-*i*Pr-CH), 33.99, 33.96 (s, 1C, Tip-*i*Pr-CH), 32.14 – 31.04 (d, 1C, J = 9.53 Hz, Tip-*i*Pr-CH), 30.33 (s, 1C, Tip-*i*Pr-CH), 28.66 (s, 1C, Tip-*i*Pr-CH₃), 28.24-

SUPPORTING INFORMATION

WILEY-VCH

28.19 (d, 1C, $J = 5.70$ Hz, Tip-*i*Pr-CH₃), 27.69 (s, 1C, Tip-*i*Pr-CH₃), 27.19, 27.19 (s, each 1C, Tip-*i*Pr-CH₃), 26.90, 26.72, 26.17 (s, each 1C, Tip-*i*Pr-CH₃), 25.36 – 25.09 (t, 1C, $J = 13.13$ Hz, Tip-*i*Pr-CH₃), 24.68–24.60 (d, 1C, $J = 8.35$ Hz, Tip-*i*Pr-CH₃), 24.45, 24.17 (s, each 1C, Tip-*i*Pr-CH₃), 23.80, 23.76, 23.67, 23.63, 23.55, 23.49, 23.47, 23.41 (bs, each 1C, Tip-*i*Pr-CH₃ and C(CH₃)₃), 22.93 – 22.86 (d, 1C, $J = 7.25$ Hz, Tip-*i*Pr-CH₃) ppm.

²⁹Si-NMR (79.49 MHz, C₆D₆, 300 K) $\delta = 160.2$ (s, *privo*-Si), 37.9 (s, *ligato*-SiTip), -4.2 (*remoto*-Si(Tip)₂), -34.8 (s, *ligato*-Si-NHSi), -201.7 (s, *nudo*-Si), -230.7 (s, *nudo*-Si) ppm.

¹¹⁹Sn-NMR (149.21 MHz, C₆D₆, 300 K) $\delta = 456.3$ (s) ppm.

¹H-NMR (400.13 MHz, thf-d₈, 300 K) $\delta = 7.626 - 7.606$ (d, $^4J_{\text{HH}} = 6.71$ Hz, 1H, Ar-H), 7.423 – 7.7335 (m, 4 H, Ar-H, overlapping with C₆D₆ residue), 7.1251 (s, 1H, Ar-H), 7.114 – 7.099 (m, 3H, Ar-H), 6.947 (s, 1H, Ar-H), 6.876 (s, 1H, Ar-H), 6.747 (s, 1H, Ar-H), 6.695 (s, 1H, Ar-H), 6.622 (s, 1H, Ar-H), 6.464 (s, 1H, Ar-H), 6.046 – 5.983 (sept, 1H, $^3J_{\text{HH}} = 6.97$ Hz, Tip-*i*Pr-CHMe₂), 5.378 (bs, 1H, Tip-*i*Pr-CHMe₂), 5.157 – 5.104 (sept, 1H, $^3J_{\text{HH}} = 6.68$ Hz, Tip-*i*Pr-CHMe₂), 4.967 – 4.918 (sept, 1H, $^3J_{\text{HH}} = 6.45$ Hz, Tip-*i*Pr-CHMe₂), 3.902 – 3.837 (sept, 1H, $^3J_{\text{HH}} = 6.63$ Hz, Tip-*i*Pr-CHMe₂), 3.579 – 3.523 (m, 5H, Tip-*i*Pr-CHMe₂ overlapping with thf-d₈), 3.307 – 3.243 (m, 2H, Tip-*i*Pr-CHMe₂), 3.192 – 3.133 (sept, 1H, $^3J_{\text{HH}} = 6.60$ Hz, Tip-*i*Pr-CHMe₂), 2.929 – 2.869 (sept, 1H, $^3J_{\text{HH}} = 6.60$ Hz, Tip-*i*Pr-CHMe₂), 2.806 – 2.588 (m, 6H, Tip-*i*Pr-CHMe₂), 1.919 – 1.1883 (m, 6H, Tip-*i*Pr-CHMe₃), 1.779 – 1.763 (d, 3H, $^3J_{\text{HH}} = 6.80$ Hz, Tip-*i*Pr-CHMe₃), 1.724 (bs, 4H, Tip-*i*Pr-CHMe₃), 1.584 – 1.567 (d, 6H, $^3J_{\text{HH}} = 6.96$ Hz, Tip-*i*Pr-CHMe₃), 1.508 – 1.456 (m, 16H, Tip-*i*Pr-CHMe₃), 1.402 – 1.385 (d, 3H, $^3J_{\text{HH}} = 6.30$ Hz, Tip-*i*Pr-CHMe₃), 1.188 – 1.031 (m, 48H, Tip-*i*Pr-CHMe₃ and C(CH₃)₃), 0.662 (s, 9H, C(CH₃)₃), 0.508 – 0.492 (d, 3H, $^3J_{\text{HH}} = 6.03$ Hz, Tip-*i*Pr-CHMe₃), 0.461 – 0.445 (d, 3H, $^3J_{\text{HH}} = 6.03$ Hz, Tip-*i*Pr-CHMe₃), 0.369 – 0.340 (t, 6H, $^3J_{\text{HH}} = 5.69$ Hz, Tip-*i*Pr-CHMe₃), 0.224 – 0.208 (d, 3H, $^3J_{\text{HH}} = 6.37$ Hz, Tip-*i*Pr-CHMe₃), 0.135 – 0.45 (d, together 9H, $^3J_{\text{HH}} = 6.36$ Hz, $^3J_{\text{HH}} = 6.10$ Hz, $^3J_{\text{HH}} = 6.23$ Hz, Tip-*i*Pr-CHMe₃) ppm.

¹³C-NMR (100.61 MHz, thf-d₈, 300 K) $\delta = 216.57$ (C=O), 211.52 (Fe-(CO)₅), 168.51 (s, 1C, Ar-C), 156.90, 156.34, 156.07, 154.89 (s, each 1C, Ar-C), 153.95 – 153.90 (d, 1C, $J = 4.80$ Hz, Ar-C), 153.81, 153.59, 152.76, 150.80, 150.61 (s, each 1C, Ar-C), 150.51 – 150.43 (d, 1C, $J = 7.57$ Hz, Ar-C), 150.23 (s, 1C, Ar-C), 139.72, 138.52, 137.39, 136.25, 130.80, 130.45 (s, each 1C, Ar-C), 129.89, 129.85, 129.39 (bs, each 1C, Ar-CH), 129.02 (C₆D₆ residue), 128.78, 128.10, 127.97, 127.92, 125.81, 125.58, 124.72, 124.01, 123.45, 123.08, 122.78, 121.42, 121.14 (s, each 1C, Ar-CH), 55.34, 55.89 (s, each 1C, C(CH₃)₃), 39.29, 38.34, 37.54, 37.03 (s, each 1C, Tip-*i*Pr-CH), 36.43 (bs, 2C, Tip-*i*Pr-CH), 36.29, 36.14 (s, each 1C, Tip-*i*Pr-CH), 35.84 – 35.77 (d, 1C, $J = 7.36$ Hz, Tip-*i*Pr-CH), 35.27, 35.09 (s, each 1C, Tip-*i*Pr-CH), 34.97, 34.95, 34.92 (bs, each 1C, Tip-*i*Pr-CH), 32.75 – 32.64 (d, 2C, $J = 10.4$ Hz, Tip-*i*Pr-CH), 30.87 (s, 1C, Tip-*i*Pr-CH), 28.93, 28.74, 28.59, 28.34 (s, each 1C, Tip-*i*Pr-CH₃), 27.75, 27.71 (bs, each 1C, Tip-*i*Pr-CH₃), 27.51, 26.92, 26.49 (s, each 1C, Tip-*i*Pr-CH₃), 25.60, 25.04, 24.81, 24.64 (s, each 1C, overlapping with thf-d₈), 24.33, 24.78, 24.13, 24.11, 24.07, 23.92 (bs, each 1C, Tip-*i*Pr-CH₃ and C(CH₃)₃), 23.31 – 23.27 (d, 1C, $J = 4.71$ Hz, Tip-*i*Pr-CH₃) ppm.

²⁹Si-NMR (79.49 MHz, thf-d₈, 300 K) $\delta = 159.2$ (s, *privo*-Si), 38.4 (s, *ligato*-SiTip), -4.0 (*remoto*-Si(Tip)₂), -35.1 (s, *ligato*-Si-NHSi), -202.1 (s, *nudo*-Si), -230.5 (s, *nudo*-Si) ppm.

¹¹⁹Sn-NMR (149.21 MHz, thf-d₈, 300 K) $\delta = 453.4$ (s) ppm.

CP-MAS ²⁹Si-NMR (79.53 MHz, 300K) $\delta = 154.1$ (s, *privo*-Si), 36.4 (s, *ligato*-SiTip), -3.7 (*remoto*-Si(Tip)₂), -31.6 (s, *ligato*-Si-NHSi), -200.3 (s, *nudo*-Si), -232.8 (s, *nudo*-Si) ppm.

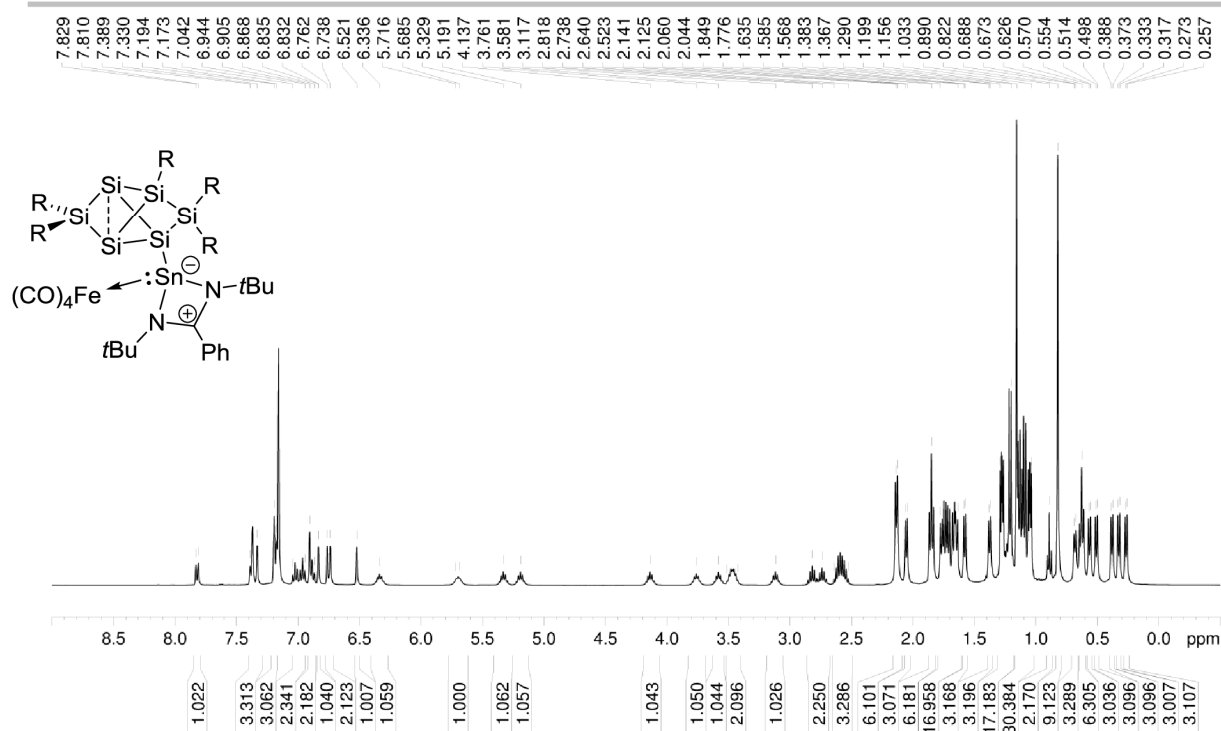
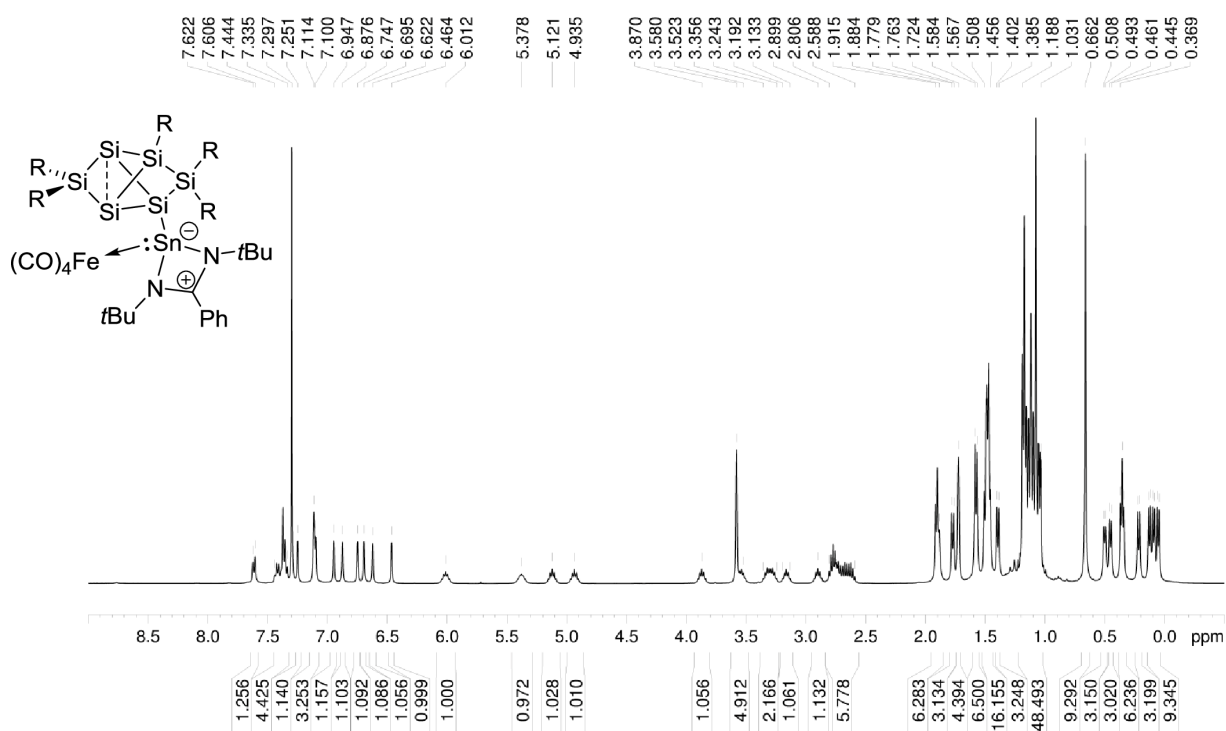
CP-MAS ¹¹⁹Sn-NMR (149.27 MHz, 300K) $\delta = 469.2$ (s) ppm.

Elemental analysis: calculated for C₉₄H₁₃₈FeN₂O₄Si₆Sn: C, 66.29 % ; H, 8.17 % ; N, 1.64 %. Found: C, 66.31 % ; H, 7.84 % ; N, 1.89 %.

UV/VIS (hexane): λ_{max} (ϵ) = 466 nm (3010 M⁻¹ cm⁻¹).

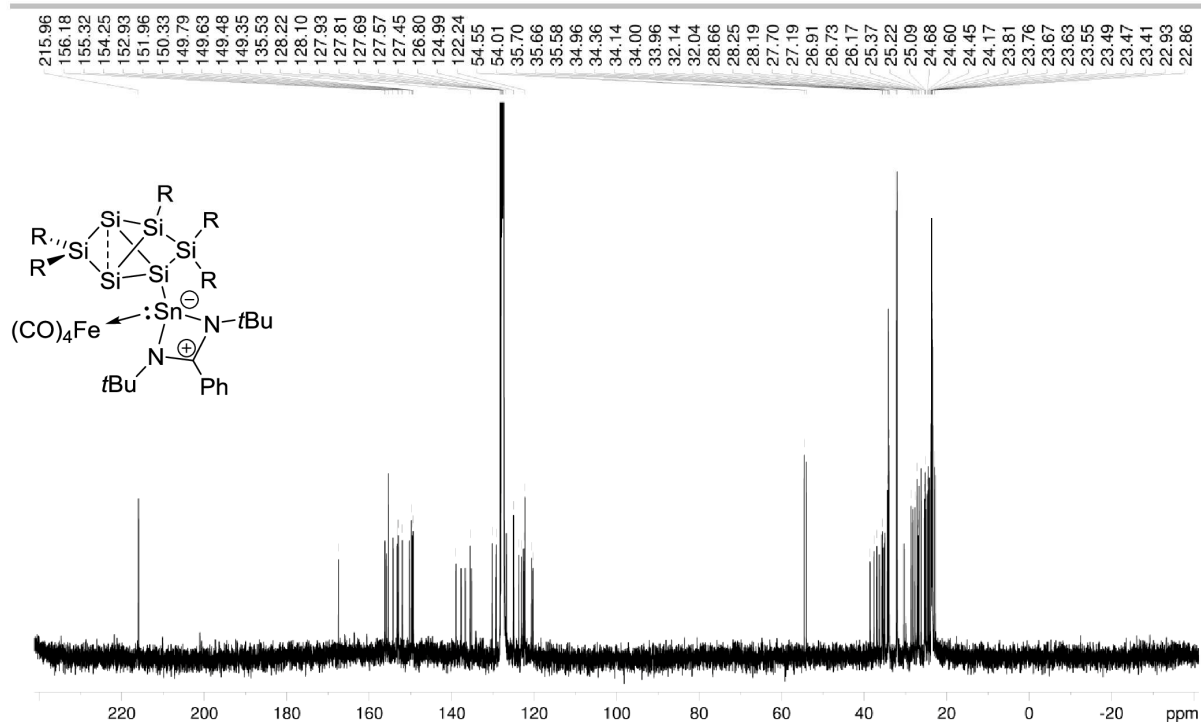
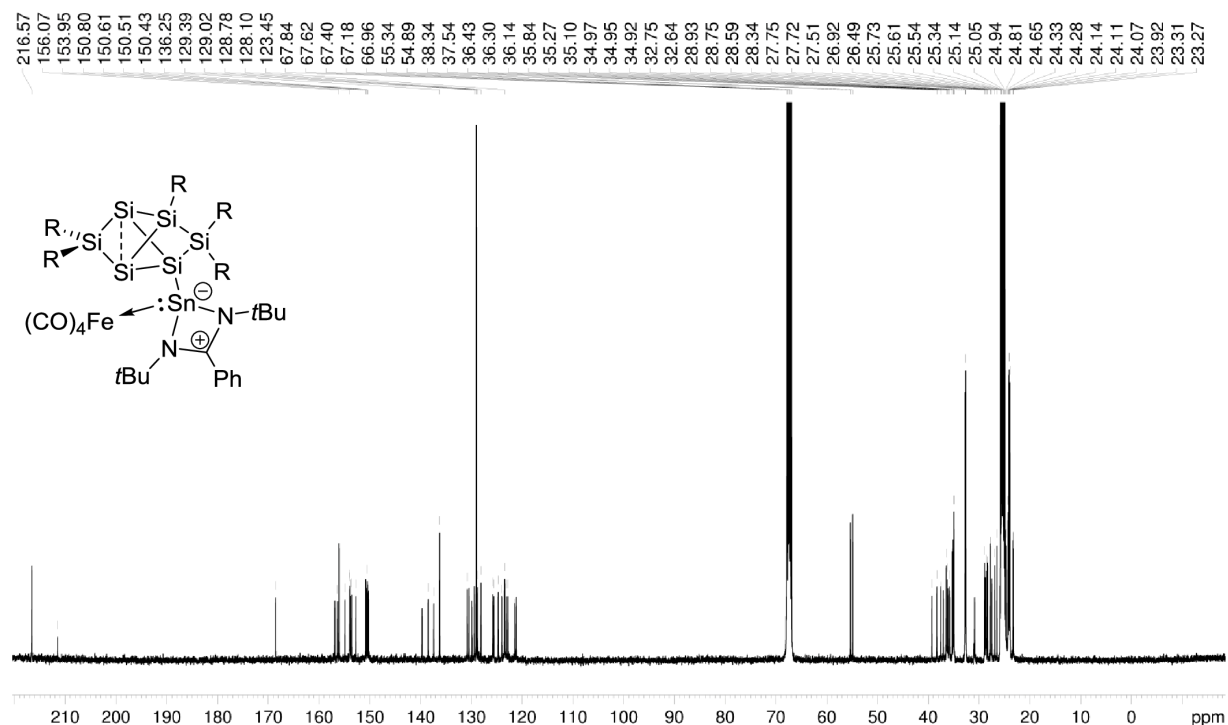
SUPPORTING INFORMATION

WILEY-VCH

Figure S61. ¹H NMR of **4c** in C₆D₆ (400.13 MHz, 300 K).Figure S62. ¹H NMR of **4c** in thf-d₈ (400.13 MHz, 300 K).

SUPPORTING INFORMATION

WILEY-VCH

Figure S63. ¹³C NMR of 4c in C₆D₆ (100.61 MHz, 300 K).Figure S64. ¹³C NMR of 4c in thf-d₈ (100.61 MHz, 300 K).

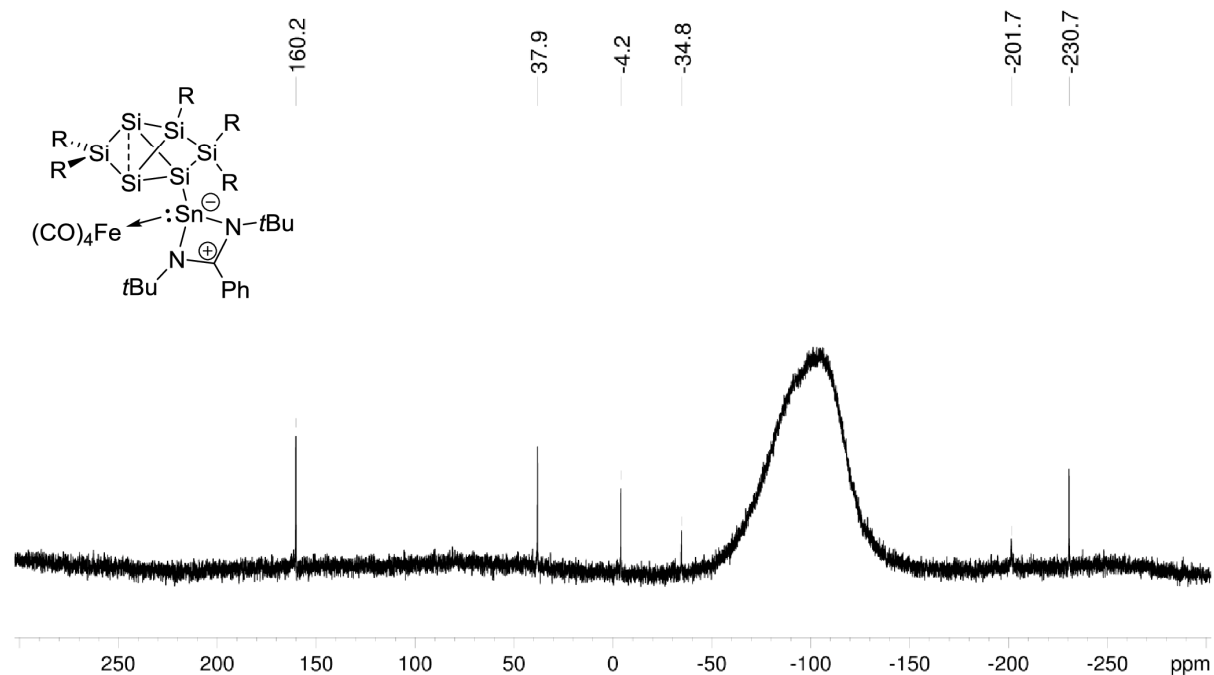


Figure S65. ²⁹Si NMR of **4c** in C₆D₆ (79.49 MHz, 300 K).

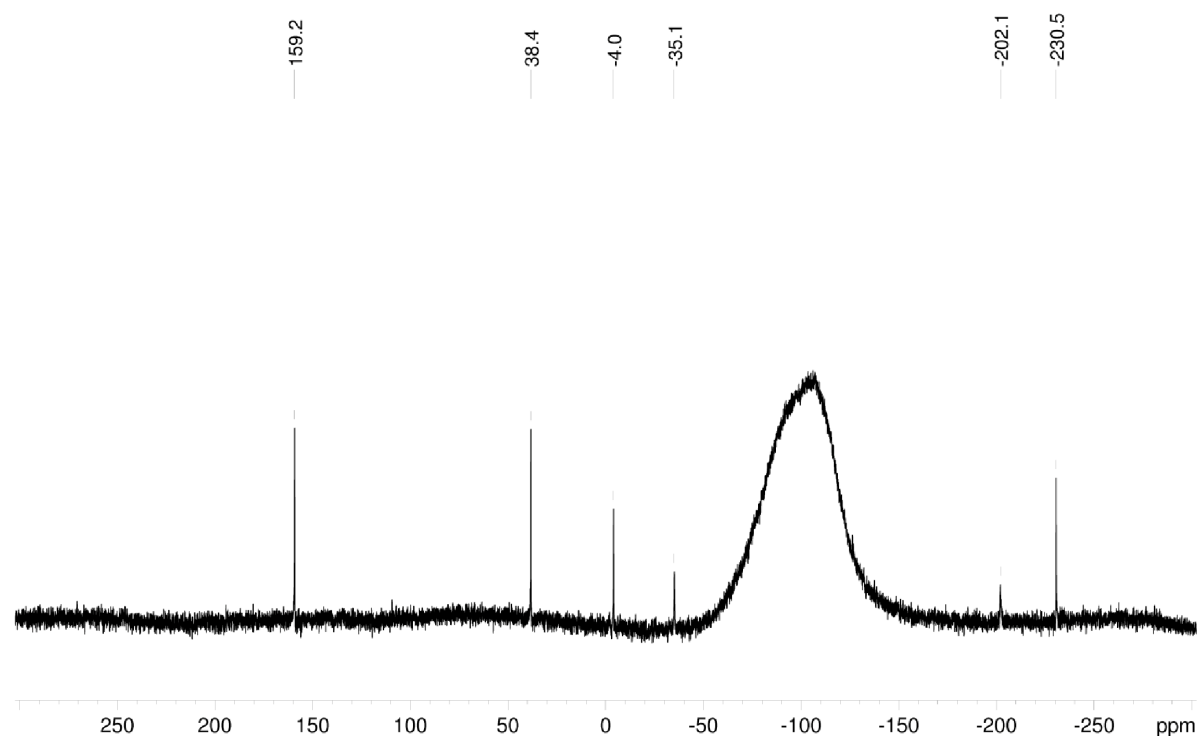


Figure S66. ²⁹Si NMR of **4c** in thf-d₈ (79.49 MHz, 300 K).

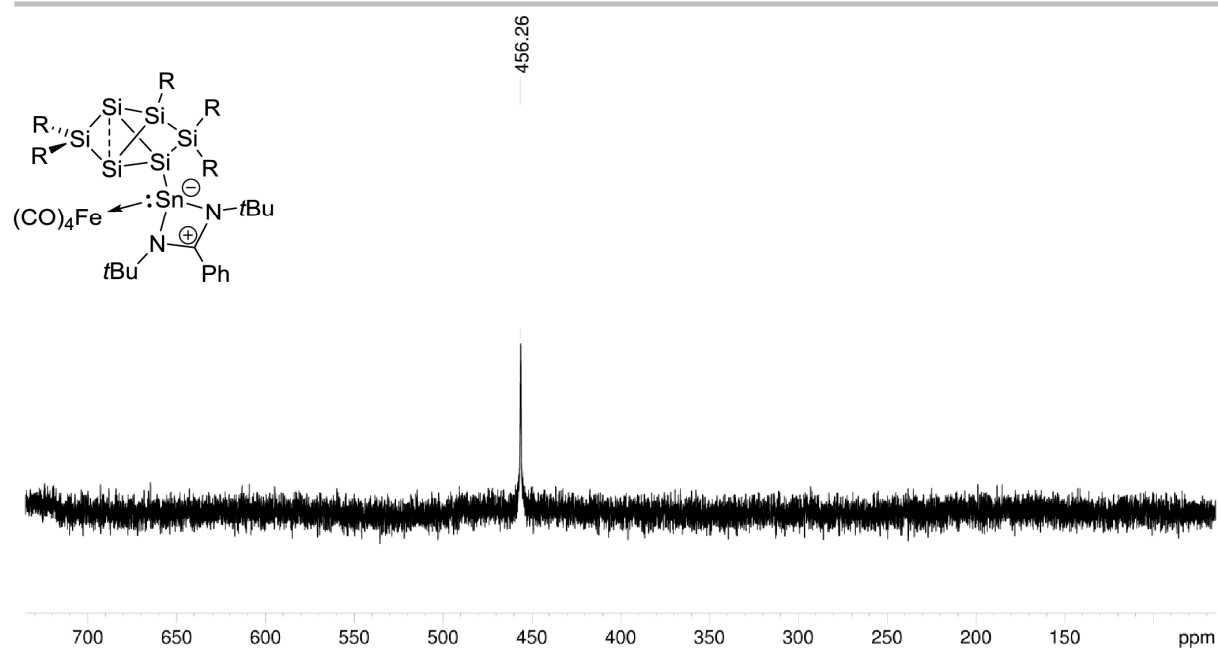


Figure S67. ^{119}Sn NMR of **4c** in C_6D_6 (79.49 MHz, 300 K).

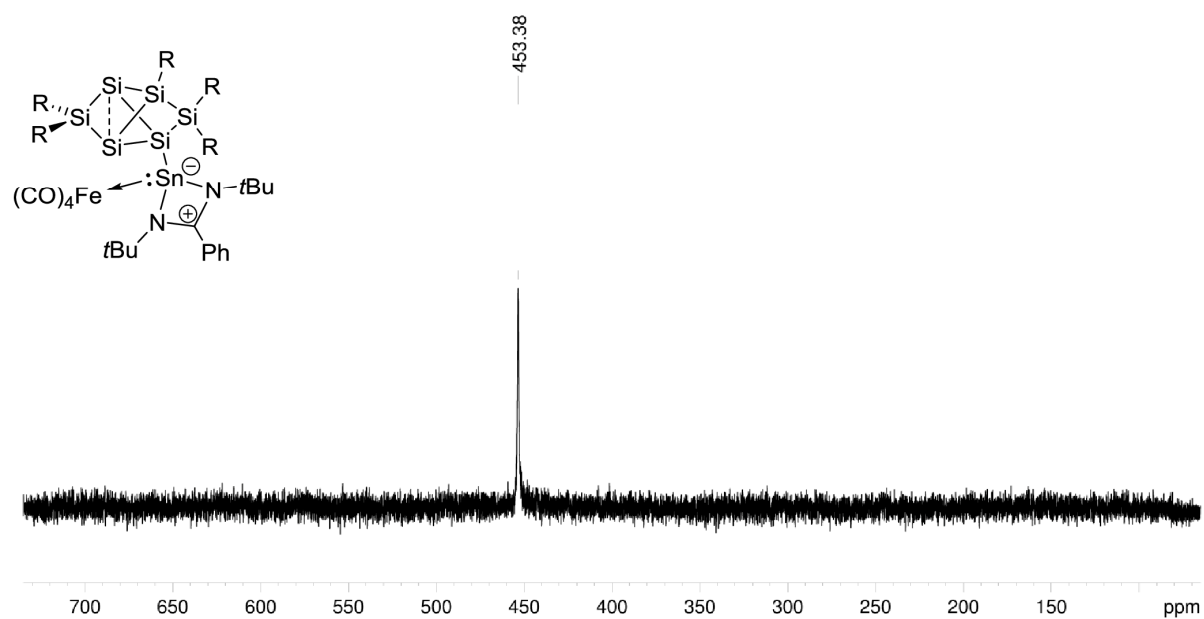


Figure S68. ^{119}Sn NMR of **4c** in thf-d_8 (79.49 MHz, 300 K).

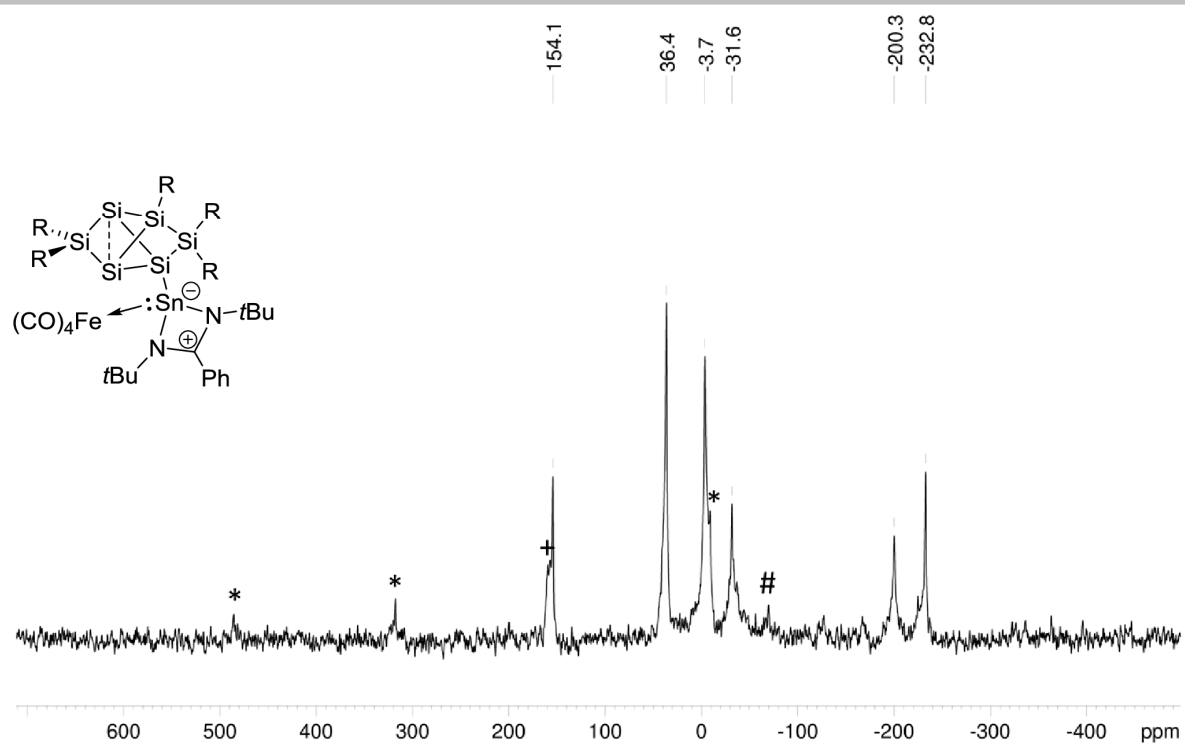


Figure S69. CP-MAS ^{29}Si NMR of **4c** (79.53 MHz, 13 KHz, 300 K), side spinning bands: * *privo*-SiTip₂ (154.1 ppm), + *remoto*-Si(Tip)₂ (-3.7 ppm), # *nudo*-Si (-200.3 ppm; -232.8 ppm).

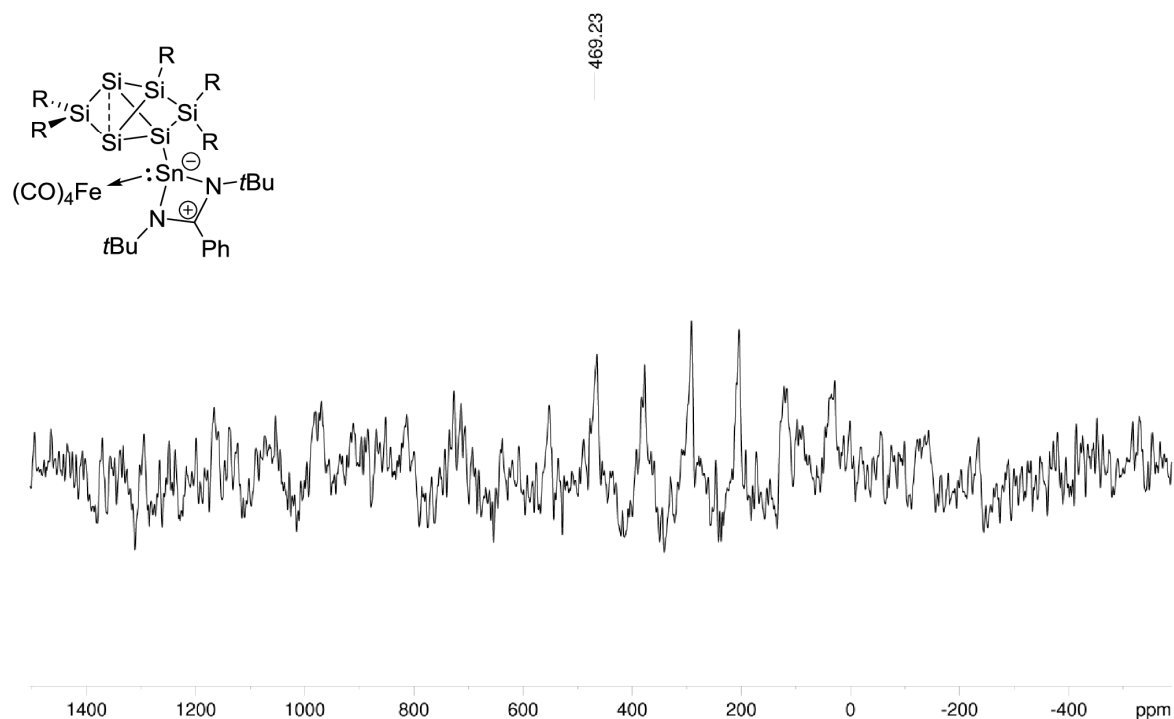


Figure S70. CP-MAS ^{119}Sn NMR of **4c** (149.27 MHz, 13 KHz, 300 K).

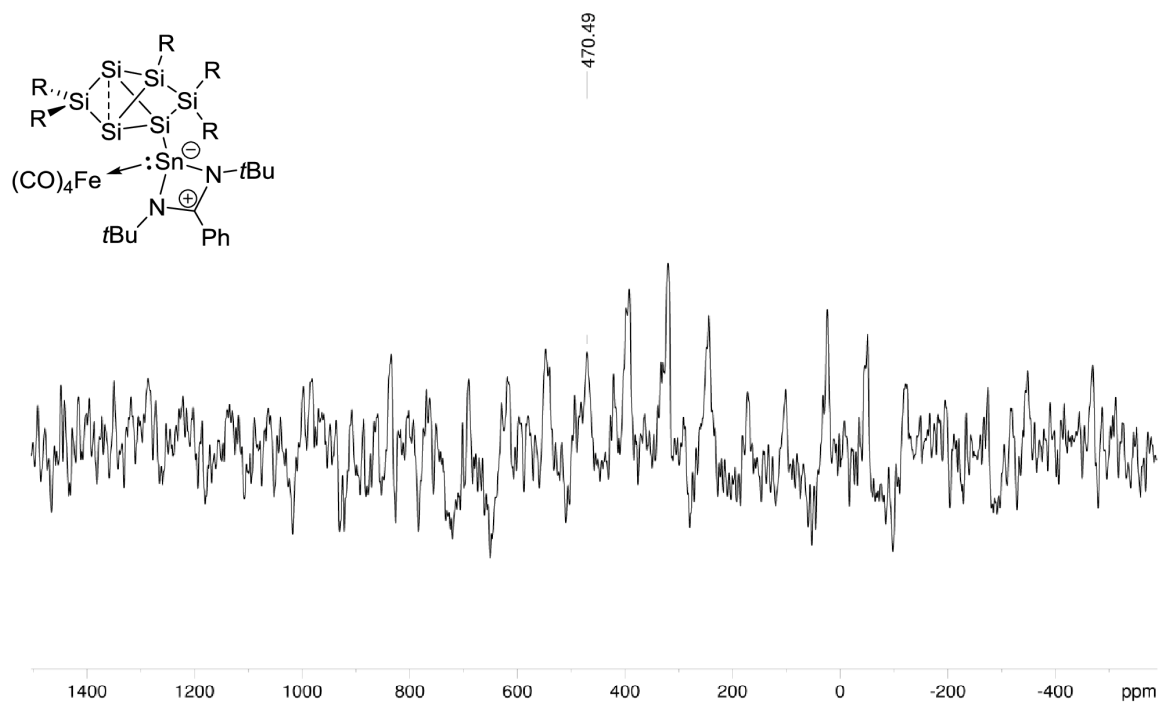


Figure S71. CP-MAS ^{119}Sn NMR of **4c** (149.27 MHz, 11 KHz, 300 K).

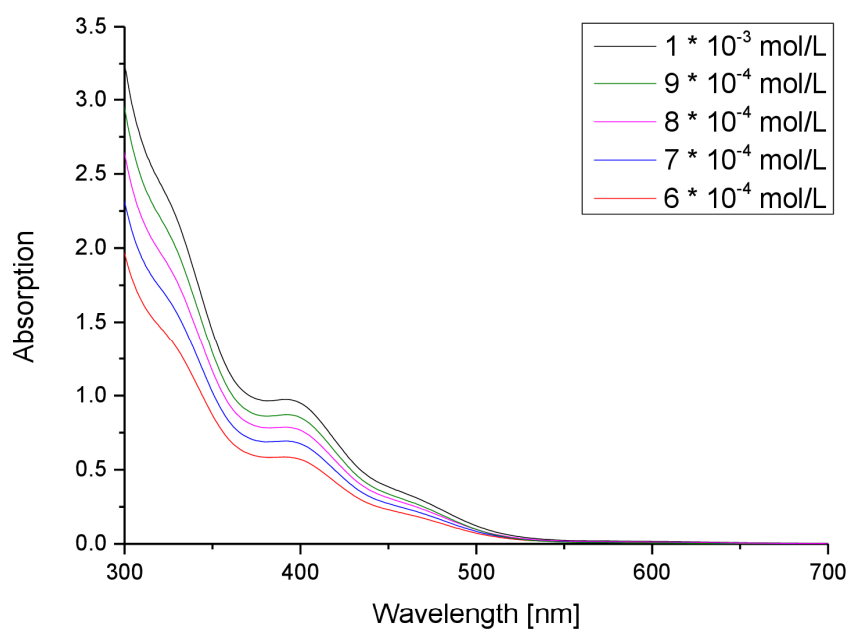


Figure S72. UV-Vis spectrum of **4c** in hexane at different concentrations.

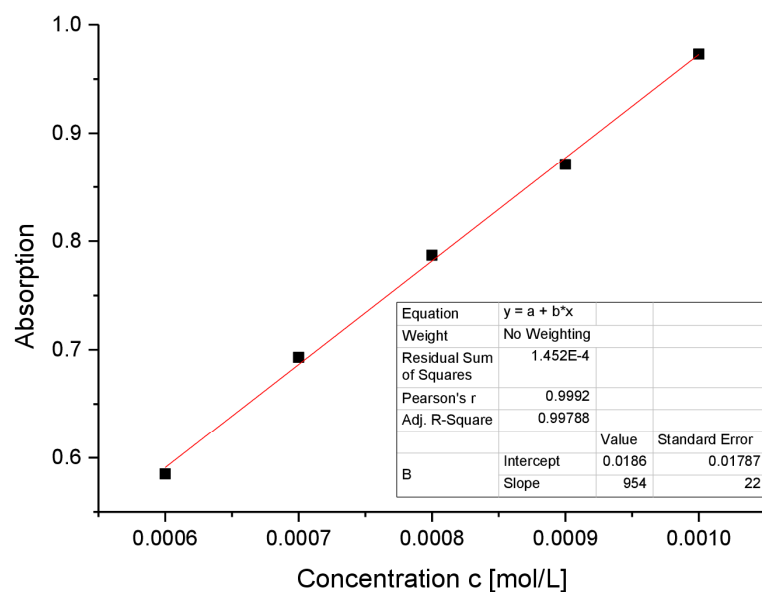


Figure S73. Determination of ϵ ($9540 \text{ M}^{-1} \text{ cm}^{-1}$) by linear regression of absorptions ($\lambda = 392 \text{ nm}$) of **4c** against concentration.

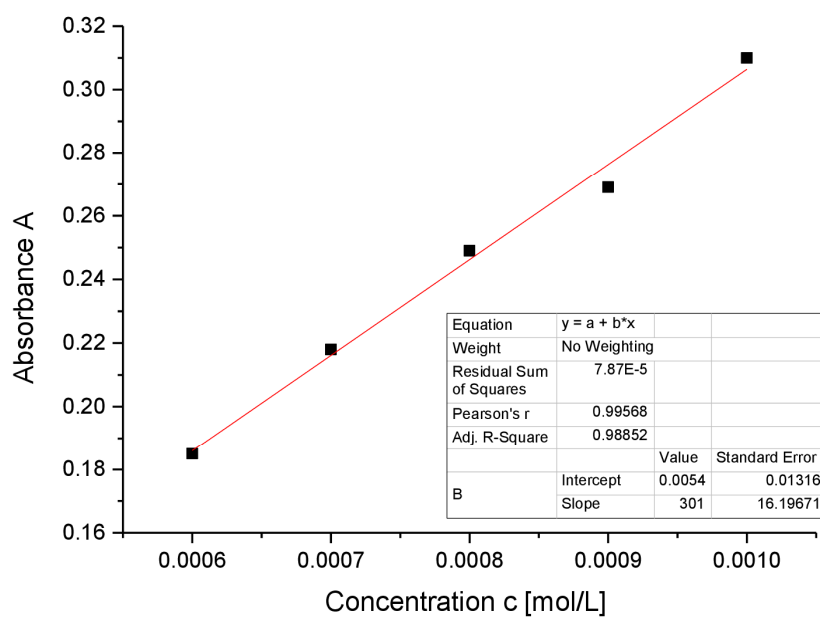


Figure S74. Determination of ϵ ($3010 \text{ M}^{-1} \text{ cm}^{-1}$) by linear regression of absorptions ($\lambda = 466 \text{ nm}$) of **4c** against concentration.

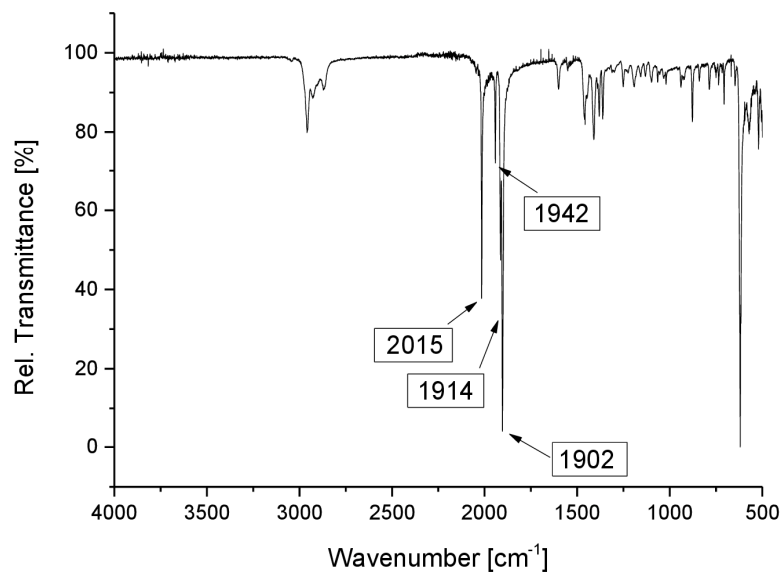


Figure S75. Ir spectrum of **4c**.

3. Computational Details

Geometry optimizations were performed using the Gaussian 09 optimizer^[3] together with TurboMole V7.0.^[4] energies and gradients. All geometry optimizations were computed using the functional BP86^[5,6] functional with Grimme dispersion corrections D3^[7] and the Becke-Jonson damping function^[8] in combination with the def2-SVP basis set.^[9] The stationary points were located with the Berny algorithm^[10] using redundant internal coordinates. Analytical Hessians were computed to determine the nature of stationary points (one and zero imaginary frequencies for transition states and minima, respectively)^[11] and to calculate unscaled zero-point energies (ZPEs) as well as thermal corrections and entropy effects using the standard statistical-mechanics relationships for an ideal gas.

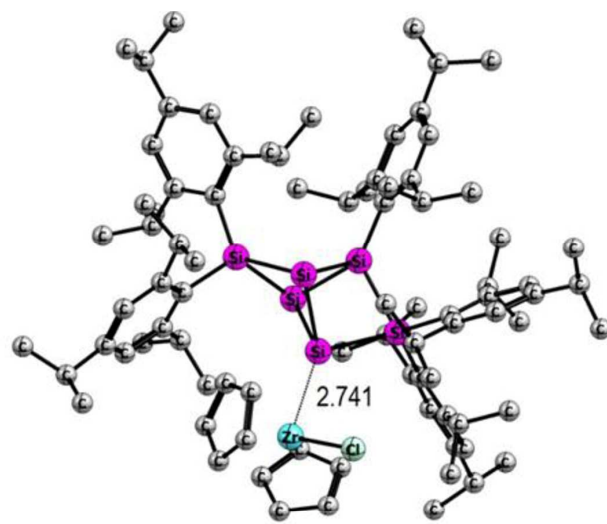


Figure S76. Optimized structures at the BP86+D3(BJ)/def2-SVP level of theory for **2a**. Bond distances are in [Å]. Hydrogen atoms were omitted for clarity.

SUPPORTING INFORMATION

WILEY-VCH

Table S1. Coordinates of *ligato*-Zirconocene-substituted siliconoid (2a) Si₆-ZrClCp₂

E (BP86+D3(BJ)/def2-SVP) = -5556.8010875510

C	6.615806	-3.645905	-2.623523
C	0.237089	2.725865	-2.647041
C	4.658251	-2.030846	-2.359199
C	2.702938	-0.485735	-2.353045
C	0.820990	5.151431	-2.264417
C	1.259166	7.649635	-2.046128
C	5.787123	-2.659253	-1.815220
C	0.826732	3.830793	-1.777215
C	3.875555	-1.124979	-1.621221
C	1.317180	6.226514	-1.512255
C	-4.709322	0.320304	-0.645437
C	5.035157	2.268439	-0.855681
C	-5.523778	2.626984	-0.211949
C	6.110541	-2.357526	-0.485589
C	1.341885	3.568366	-0.474253
C	-4.466170	1.709126	-0.074362
C	-6.607823	4.907048	0.138971
C	1.855845	5.948421	-0.245676
C	-2.690990	-2.419672	-0.044308
C	4.202007	-0.826707	-0.265155
C	-5.436515	3.944039	0.252783
C	5.348224	-1.475594	0.306089
C	1.884726	4.648145	0.286631
C	5.232288	2.347514	0.659481
C	-3.242432	2.101394	0.551665
C	6.265485	3.178743	1.133327
C	-4.216868	4.338323	0.817997
C	-3.118819	3.468430	0.950973
C	-3.218648	-1.978933	1.322413
C	1.739884	-3.944762	0.739214
C	4.463300	1.584498	1.590153
C	3.071092	-3.873090	1.248881
C	-3.921566	-2.934919	2.079222
C	2.502752	4.450660	1.669100
C	5.842805	-1.264134	1.741696
C	-3.017134	-0.673797	1.867294
C	-1.856832	4.095235	1.530996
C	1.048689	-4.962090	1.458915
C	6.555783	3.306457	2.498013
C	7.705994	4.178949	2.978649
C	3.207329	-4.851754	2.270420
C	-4.448819	-2.656487	3.349671
C	1.953455	-5.514300	2.421925
C	4.729330	1.728532	2.980199
C	-3.599800	-0.365899	3.131317
C	5.758787	2.587301	3.404819
C	-5.136517	-3.738850	4.167273
C	-4.297241	-1.352517	3.847755
C	-3.483374	1.025845	3.739282
C	-0.870457	-3.702211	3.642517
C	-0.761879	-2.289085	3.769004
C	3.930471	0.967578	4.032261
C	-0.086521	-4.304105	4.680116
C	0.086379	-2.014151	4.886084
C	0.480976	-3.253030	5.460725
Cl	3.420021	-2.532148	4.488914
Si	-0.074023	-0.057905	-0.183447
Si	1.333393	1.811048	0.261723
Si	3.169191	0.392488	0.824413
Si	-1.982571	0.721635	1.056465
Si	1.278355	-0.804663	1.785302
Si	0.112283	1.248288	2.281423
Zr	1.513405	-3.173033	3.145867
H	3.837601	-3.173250	0.898859
H	1.347047	-3.333319	-0.078217
H	0.018991	-5.288665	1.288920
H	1.736592	-6.334300	3.116539
H	4.104265	-5.034125	2.872675
H	1.154967	-3.378442	6.315513

SUPPORTING INFORMATION

WILEY-VCH

H	0.018455	-5.378237	4.872661
H	-1.476629	-4.224170	2.896924
H	0.400715	-1.017224	5.216163
H	-1.274945	-1.548998	3.148900
H	-2.341778	-1.511663	-0.579007
H	-4.065027	-3.946700	1.666337
H	-5.158536	-4.655024	3.536540
H	-4.721460	-1.096622	4.831370
H	-2.817118	1.617217	3.076288
H	-3.802594	-0.280103	-0.451786
H	-6.457691	2.299410	-0.696125
H	-7.434108	4.353777	-0.359389
H	-4.104926	5.376161	1.166297
H	-1.028122	3.362359	1.429255
H	0.716786	1.776189	-2.325440
H	2.809673	3.386003	1.741681
H	2.269583	6.773916	0.352227
H	0.413865	5.356862	-3.266319
H	0.856314	7.590533	-3.081133
H	8.156081	4.645069	2.074675
H	6.875779	3.742564	0.409457
H	4.114232	1.677197	-1.043693
H	3.458653	0.096948	3.523634
H	5.961453	2.679725	4.482332
H	5.024922	-0.787342	2.316321
H	6.994186	-2.841676	-0.041805
H	7.475889	-3.944092	-1.984286
H	4.375576	-2.243645	-3.402387
H	2.213569	0.211767	-1.642156
C	3.760358	5.303844	1.895640
H	4.277630	4.964838	2.813236
H	4.474943	5.219394	1.056734
H	3.507320	6.376020	2.031925
C	1.493786	4.717870	2.794699
H	0.652475	4.001359	2.754964
H	1.979727	4.613886	3.784997
H	1.083861	5.746747	2.724144
C	0.517483	2.900941	-4.146813
H	1.593480	3.076918	-4.344344
H	0.206519	1.992861	-4.702562
H	-0.050176	3.750472	-4.579542
C	-1.270895	2.581730	-2.381336
H	-1.695947	1.725402	-2.945386
H	-1.481575	2.410734	-1.309038
H	-1.816678	3.500662	-2.680321
C	2.655257	8.293102	-2.122463
H	3.105329	8.399223	-1.113683
H	3.346705	7.679848	-2.734246
H	2.600855	9.306427	-2.571134
C	0.285773	8.506077	-1.213658
H	-0.723600	8.049333	-1.183789
H	0.638739	8.603124	-0.165875
H	0.193204	9.528647	-1.634638
C	7.182919	-3.004305	-3.902608
H	7.778449	-2.099586	-3.667539
H	7.835081	-3.716835	-4.448611
H	6.370105	-2.699980	-4.594373
C	5.805658	-4.917481	-2.940043
H	6.426952	-5.663385	-3.477791
H	5.421779	-5.388280	-2.012956
H	4.931046	-4.682204	-3.581774
C	6.194088	-2.572782	2.471932
H	5.360220	-3.293931	2.466747
H	7.085181	-3.063903	2.030509
H	6.429100	-2.356055	3.532546
C	7.074702	-0.339076	1.775742
H	7.377184	-0.134496	2.822448
H	7.930128	-0.824804	1.261095
H	6.886360	0.630134	1.284594
C	1.648311	-1.528033	-2.759881
H	2.042045	-2.231352	-3.523197
H	1.319933	-2.123802	-1.884779

SUPPORTING INFORMATION

WILEY-VCH

H	0.749521	-1.033716	-3.183957
C	3.156168	0.344119	-3.565597
H	3.843942	1.157138	-3.263491
H	3.683525	-0.280960	-4.315313
H	2.284949	0.805869	-4.069183
C	4.804801	3.644933	-1.503218
H	5.699694	4.294868	-1.413618
H	4.591260	3.526692	-2.585470
H	3.945851	4.172533	-1.050120
C	6.207405	1.534557	-1.533827
H	7.154351	2.095963	-1.393229
H	6.346821	0.517468	-1.123454
H	6.031273	1.438467	-2.624653
C	2.788181	1.832236	4.587469
H	2.123215	2.187784	3.776214
H	2.166375	1.253331	5.301151
H	3.185331	2.724026	5.116479
C	4.800698	0.422202	5.174294
H	4.196752	-0.225263	5.838441
H	5.644305	-0.183522	4.788304
H	5.222045	1.238564	5.796706
C	8.796218	3.328697	3.657792
H	8.407303	2.840848	4.575717
H	9.156491	2.527547	2.981937
H	9.665196	3.953496	3.951228
C	7.223407	5.315356	3.898039
H	6.471145	5.951429	3.390712
H	6.756059	4.913795	4.821168
H	8.070122	5.962437	4.207184
C	-1.468759	-3.325944	0.120401
H	-1.761009	-4.286514	0.593169
H	-1.006744	-3.557793	-0.861122
H	-0.704262	-2.838568	0.752341
C	-3.738208	-3.113661	-0.930777
H	-3.304846	-3.329920	-1.928380
H	-4.064488	-4.082511	-0.499942
H	-4.640362	-2.493299	-1.077840
C	-4.323363	-4.062030	5.435896
H	-4.779227	-4.903350	5.997716
H	-3.278187	-4.332456	5.185102
H	-4.282841	-3.185548	6.115257
C	-6.591566	-3.368316	4.505423
H	-7.175827	-3.155972	3.587798
H	-7.093266	-4.192488	5.053044
H	-6.637161	-2.465202	5.148824
C	-4.838535	1.751308	3.752621
H	-5.257476	1.815292	2.728704
H	-5.574272	1.224809	4.395901
H	-4.724827	2.785069	4.137737
C	-2.796211	1.005905	5.112441
H	-3.379397	0.430475	5.860438
H	-1.789975	0.545678	5.039312
H	-2.673416	2.036525	5.504163
C	-7.106005	5.340712	1.530350
H	-7.996902	5.996952	1.447493
H	-7.377700	4.463108	2.150319
H	-6.322238	5.905993	2.076229
C	-6.260285	6.122606	-0.740132
H	-5.445432	6.725085	-0.287621
H	-5.922246	5.806241	-1.747138
H	-7.139746	6.787873	-0.862546
C	-5.896416	-0.364856	0.054177
H	-6.066305	-1.386501	-0.339504
H	-5.719335	-0.447207	1.144229
H	-6.834104	0.206966	-0.099513
C	-4.877199	0.366818	-2.175152
H	-4.001260	0.849092	-2.653224
H	-4.977219	-0.656934	-2.590821
H	-5.779926	0.939630	-2.471270
C	-1.447630	5.346755	0.736585
H	-0.487511	5.745324	1.109035
H	-1.313671	5.113863	-0.337206

SUPPORTING INFORMATION

WILEY-VCH

H	-2.200488	6.156575	0.823068
C	-2.037761	4.410605	3.027578
H	-2.937841	5.037262	3.193441
H	-2.155700	3.485576	3.624335
H	-1.165984	4.960349	3.430436

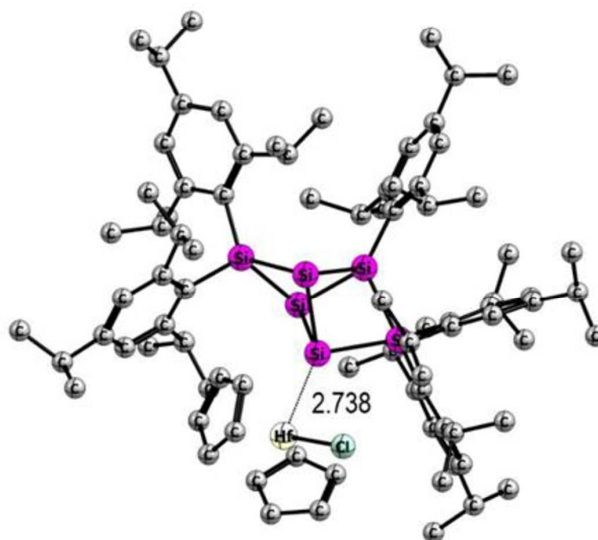


Figure S77. Optimized structures at the BP86+D3(BJ)/def2-SVP level of theory for **2b**. Bond distances are in [Å]. Hydrogen atoms were omitted for clarity.

Table S2. *ligato*-Zirconocene-substituted siliconoid (**2b**) Si₆-HfClCp₂

E (BP86+D3(BJ)/def2-SVP) = -5557.7688670110

C	6.615439	-3.649632	-2.614586
C	0.233564	2.722996	-2.649845
C	4.660899	-2.030203	-2.354583
C	2.708123	-0.481696	-2.352198
C	0.813850	5.150080	-2.272562
C	1.248393	7.649420	-2.060019
C	5.787830	-2.660250	-1.808505
C	0.823094	3.830315	-1.782990
C	3.878685	-1.122460	-1.618365
C	1.310655	6.227317	-1.523894
C	-4.708410	0.324412	-0.642459
C	5.041246	2.267830	-0.853727
C	-5.522802	2.629923	-0.203113
C	6.109934	-2.358026	-0.478656
C	1.342035	3.570986	-0.480885
C	-4.464551	1.712245	-0.069276
C	-6.607217	4.908809	0.154309
C	1.853835	5.952307	-0.258542
C	-2.688632	-2.415268	-0.047691
C	4.203417	-0.824023	-0.261939
C	-5.435052	3.946296	0.263468
C	5.347858	-1.474246	0.311231
C	1.885898	4.653121	0.276148
C	5.235697	2.349323	0.661697
C	-3.239526	2.104000	0.554632
C	6.268233	3.180965	1.136156
C	-4.214156	4.340302	0.826125
C	-3.115449	3.470627	0.955136
C	-3.216397	-1.975958	1.319524
C	1.742563	-3.960699	0.728819
C	4.464602	1.588151	1.592215
C	3.071764	-3.884417	1.243391
C	-3.920899	-2.932092	2.074606

SUPPORTING INFORMATION

WILEY-VCH

C	2.508439	4.458921	1.657141
C	5.840428	-1.262677	1.747496
C	-3.013801	-0.671722	1.866336
C	-1.852087	4.097229	1.532323
C	1.049873	-4.978188	1.447005
C	6.555888	3.311097	2.501239
C	7.705719	4.183825	2.982429
C	3.204575	-4.858754	2.269820
C	-4.448811	-2.654709	3.345052
C	1.950824	-5.523697	2.417479
C	4.728031	1.734625	2.982438
C	-3.597197	-0.364789	3.130242
C	5.756843	2.593880	3.407744
C	-5.137210	-3.737696	4.161244
C	-4.296395	-1.351529	3.844846
C	-3.478777	1.025692	3.740700
C	-0.882333	-3.726421	3.637077
C	-0.782438	-2.313576	3.776271
C	3.926949	0.975428	4.033977
C	-0.090968	-4.331724	4.667122
C	0.063928	-2.041844	4.895194
C	0.470444	-3.283305	5.456541
Cl	3.398766	-2.521052	4.473407
Si	-0.069882	-0.054379	-0.182135
Si	1.336803	1.816146	0.260509
Si	3.170080	0.396301	0.826434
Si	-1.978597	0.724269	1.057645
Si	1.281276	-0.800871	1.786992
Si	0.116738	1.252370	2.281795
Hf	1.501925	-3.174348	3.134478
H	3.838410	-3.184469	0.893666
H	1.351242	-3.349884	-0.089927
H	0.021730	-5.307483	1.272452
H	1.733683	-6.343237	3.112473
H	4.099251	-5.038676	2.876243
H	1.145072	-3.412273	6.310361
H	0.020660	-5.406530	4.851560
H	-1.486340	-4.246015	2.888063
H	0.370656	-1.045522	5.234051
H	-1.295987	-1.571112	3.159226
H	-2.339711	-1.506617	-0.581505
H	-4.065110	-3.943238	1.660437
H	-5.162751	-4.652109	3.528089
H	-4.720900	-1.096510	4.828563
H	-2.813916	1.618190	3.077361
H	-3.801368	-0.276203	-0.451144
H	-6.457682	2.302749	-0.685686
H	-7.434249	4.356085	-0.343426
H	-4.101731	5.377721	1.175518
H	-1.023363	3.364786	1.427603
H	0.713826	1.774319	-2.326250
H	2.816619	3.394710	1.730981
H	2.268496	6.779460	0.336426
H	0.403386	5.353036	-3.273623
H	0.843349	7.587741	-3.094023
H	8.156500	4.649573	2.078611
H	6.880099	3.743412	0.412533
H	4.121193	1.675624	-1.042462
H	3.450756	0.108497	3.523356
H	5.957284	2.688197	4.485556
H	5.021862	-0.784993	2.320488
H	6.992146	-2.843355	-0.033313
H	7.474557	-3.948233	-1.974230
H	4.379321	-2.243327	-3.398009
H	2.219439	0.217658	-1.642636
C	3.765812	5.313827	1.878397
H	4.285608	4.977400	2.795504
H	4.478392	5.228093	1.037909
H	3.512149	6.386103	2.012749
C	1.502637	4.727114	2.785349
H	0.661694	4.010040	2.749029
H	1.991616	4.624797	3.774323

SUPPORTING INFORMATION

WILEY-VCH

H	1.091892	5.755655	2.714656
C	0.513419	2.894714	-4.150161
H	1.589171	3.071514	-4.348312
H	0.203449	1.984875	-4.703596
H	-0.055254	3.742546	-4.584903
C	-1.274212	2.578711	-2.383222
H	-1.698983	1.720765	-2.945025
H	-1.484360	2.410232	-1.310421
H	-1.820627	3.496612	-2.684224
C	2.642845	8.295923	-2.140517
H	3.094896	8.404829	-1.132914
H	3.334359	7.683217	-2.752778
H	2.585139	9.308360	-2.590779
C	0.274940	8.505045	-1.226767
H	-0.733385	8.046193	-1.194085
H	0.629911	8.604372	-0.179877
H	0.179296	9.526791	-1.649069
C	7.184533	-3.011374	-3.894448
H	7.781596	-2.107338	-3.660630
H	7.835703	-3.726075	-4.438802
H	6.372709	-2.706768	-4.587246
C	5.803206	-4.920339	-2.929296
H	6.423582	-5.668516	-3.464952
H	5.417469	-5.388442	-2.001627
H	4.929650	-4.684675	-3.572334
C	6.189778	-2.571746	2.478105
H	5.358288	-3.295693	2.464758
H	7.085154	-3.059714	2.041958
H	6.416986	-2.356651	3.540792
C	7.072927	-0.338493	1.783854
H	7.374534	-0.135052	2.831058
H	7.928536	-0.824308	1.269605
H	6.885725	0.631320	1.293491
C	1.651863	-1.522512	-2.758581
H	2.045214	-2.228026	-3.520074
H	1.321115	-2.115910	-1.882722
H	0.754625	-1.027145	-3.184750
C	3.164131	0.345655	-3.565416
H	3.854397	1.156783	-3.263879
H	3.689669	-0.281689	-4.314528
H	2.294409	0.809702	-4.069499
C	4.810811	3.643043	-1.503904
H	5.704114	4.294843	-1.412008
H	4.601347	3.522943	-2.586762
H	3.949148	4.169563	-1.054700
C	6.215106	1.533560	-1.528613
H	7.161511	2.095799	-1.387672
H	6.354436	0.517336	-1.116031
H	6.040712	1.435137	-2.619514
C	2.788766	1.843748	4.591884
H	2.125122	2.203708	3.781533
H	2.164656	1.265956	5.304423
H	3.189910	2.732789	5.122534
C	4.796479	0.423758	5.173554
H	4.190540	-0.220402	5.839196
H	5.635773	-0.186392	4.785084
H	5.224220	1.237076	5.795557
C	8.795385	3.333656	3.662601
H	8.405674	2.846081	4.580340
H	9.156074	2.532289	2.987223
H	9.664217	3.958432	3.956537
C	7.222744	5.320606	3.901122
H	6.470774	5.956535	3.393175
H	6.754965	4.919512	4.824235
H	8.069340	5.967780	4.210391
C	-1.466182	-3.321583	0.115249
H	-1.757005	-4.281583	0.589861
H	-1.006248	-3.554347	-0.867043
H	-0.699944	-2.832954	0.744352
C	-3.735949	-3.108453	-0.934731
H	-3.302981	-3.322919	-1.932892
H	-4.061633	-4.078120	-0.505298

SUPPORTING INFORMATION

WILEY-VCH

H	-4.638417	-2.488212	-1.080380
C	-4.321476	-4.065987	5.426950
H	-4.778272	-4.907168	5.988228
H	-3.277801	-4.338820	5.172700
H	-4.276550	-3.190975	6.107932
C	-6.590589	-3.365018	4.504047
H	-7.176628	-3.148428	3.588545
H	-7.092734	-4.189875	5.050213
H	-6.632740	-2.463967	5.150571
C	-4.833442	1.751906	3.758953
H	-5.254915	1.818108	2.736209
H	-5.567946	1.224777	4.403121
H	-4.718036	2.784866	4.145710
C	-2.787931	1.002255	5.111947
H	-3.368375	0.423828	5.859764
H	-1.781436	0.543291	5.034424
H	-2.664915	2.031788	5.506444
C	-7.102560	5.339019	1.547788
H	-7.994077	5.994857	1.468438
H	-7.372265	4.459835	2.166389
H	-6.317915	5.903561	2.093170
C	-6.262476	6.126565	-0.722842
H	-5.447121	6.728664	-0.270732
H	-5.926341	5.812675	-1.731257
H	-7.142693	6.791441	-0.841905
C	-5.894602	-0.362189	0.057274
H	-6.064283	-1.383448	-0.337528
H	-5.716727	-0.445822	1.147090
H	-6.832714	0.209311	-0.095038
C	-4.878398	0.373798	-2.171874
H	-4.003143	0.856981	-2.650254
H	-4.979015	-0.649176	-2.589328
H	-5.781538	0.947175	-2.465625
C	-1.445432	5.349441	0.737684
H	-0.484670	5.748354	1.108055
H	-1.313846	5.117027	-0.336518
H	-2.198542	6.158784	0.826233
C	-2.029081	4.410889	3.029710
H	-2.928457	5.037738	3.198668
H	-2.146008	3.485079	3.625490
H	-1.156046	4.959644	3.431196

4. Details on X-Ray Diffraction Studies

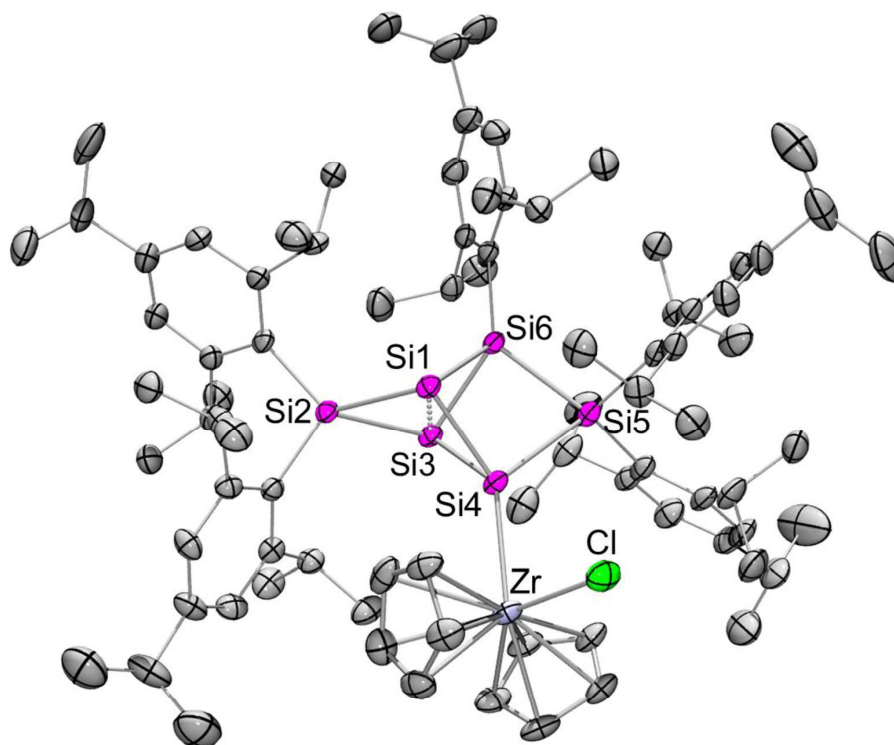


Figure S78. Molecular structure of siliconoid **2a** in the solid state. Hydrogen atoms omitted for clarity. Thermal ellipsoids represent 50% probability.

Table S3. Crystal data and structure refinement for **2a** (CCDC: 1978002).

Identification code	sh3962	
Empirical formula	C ₉₅ H _{144.50} Cl Si ₆ Zr	
Formula weight	1581.81	
Temperature	142(2) K	
Wavelength	0.71073 Å	
Crystal system	Monoclinic	
Space group	P2 ₁ /n	
Unit cell dimensions	a = 22.3173(9) Å	$\alpha = 90^\circ$.
	b = 19.6898(10) Å	$\beta = 111.7090(10)^\circ$.
	c = 26.1198(13) Å	$\gamma = 90^\circ$.
Volume	10663.6(9) Å ³	
Z	4	
Density (calculated)	0.985 Mg/m ³	
Absorption coefficient	0.232 mm ⁻¹	
F(000)	3422	
Crystal size	0.240 x 0.200 x 0.084 mm ³	
Theta range for data collection	1.332 to 26.416°.	

SUPPORTING INFORMATION

WILEY-VCH

Index ranges	-22<=h<=27, -24<=k<=24, -32<=l<=32
Reflections collected	89012
Independent reflections	21834 [R(int) = 0.0701]
Completeness to theta = 25.242°	100.0 %
Absorption correction	Semi-empirical from equivalents
Max. and min. transmission	0.7454 and 0.6852
Refinement method	Full-matrix least-squares on F ²
Data / restraints / parameters	21834 / 477 / 1027
Goodness-of-fit on F ²	1.085
Final R indices [I>2sigma(I)]	R1 = 0.0676, wR2 = 0.1985
R indices (all data)	R1 = 0.1161, wR2 = 0.2279
Extinction coefficient	n/a
Largest diff. peak and hole	0.896 and -0.486 e.Å ⁻³

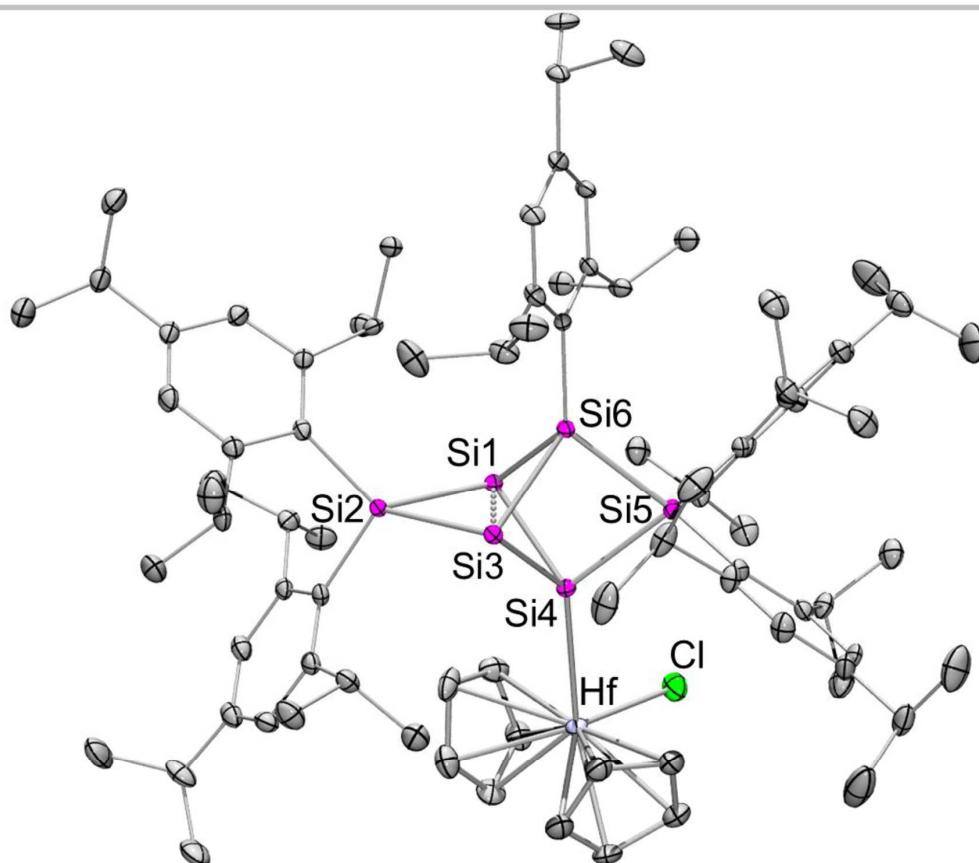


Figure S79. Molecular structure of siliconoid **2b** in the solid state. Hydrogen atoms omitted for clarity. Thermal ellipsoids represent 50% probability.

Table S4. Crystal data and structure refinement for **2b** (CCDC: 1978003).

Identification code	sh3983	
Empirical formula	C ₈₅ H ₁₂₅ Cl Hf Si ₆ , 0.75(C ₆ H ₁₄), 0.25(C ₇ H ₈)	
Formula weight	1616.98	
Temperature	133(2) K	
Wavelength	0.71073 Å	
Crystal system	Monoclinic	
Space group	P2 ₁ /c	
Unit cell dimensions	a = 21.8827(15) Å	α = 90°.
	b = 15.7650(11) Å	β = 101.965(2)°.
	c = 26.6938(16) Å	γ = 90°.
Volume	9008.8(10) Å ³	
Z	4	
Density (calculated)	1.192 Mg/m ³	
Absorption coefficient	1.309 mm ⁻¹	
F(000)	3432	

SUPPORTING INFORMATION

WILEY-VCH

Crystal size	0.224 x 0.193 x 0.058 mm ³
Theta range for data collection	0.951 to 28.310°.
Index ranges	-29<=h<=29, -21<=k<=18, -27<=l<=35
Reflections collected	90445
Independent reflections	22373 [R(int) = 0.0586]
Completeness to theta = 25.242°	100.0 %
Absorption correction	Semi-empirical from equivalents
Max. and min. transmission	0.7457 and 0.6882
Refinement method	Full-matrix least-squares on F ²
Data / restraints / parameters	22373 / 74 / 918
Goodness-of-fit on F ²	1.037
Final R indices [I>2sigma(I)]	R1 = 0.0405, wR2 = 0.1001
R indices (all data)	R1 = 0.0704, wR2 = 0.1128
Extinction coefficient	n/a
Largest diff. peak and hole	1.132 and -0.838 e.Å ⁻³

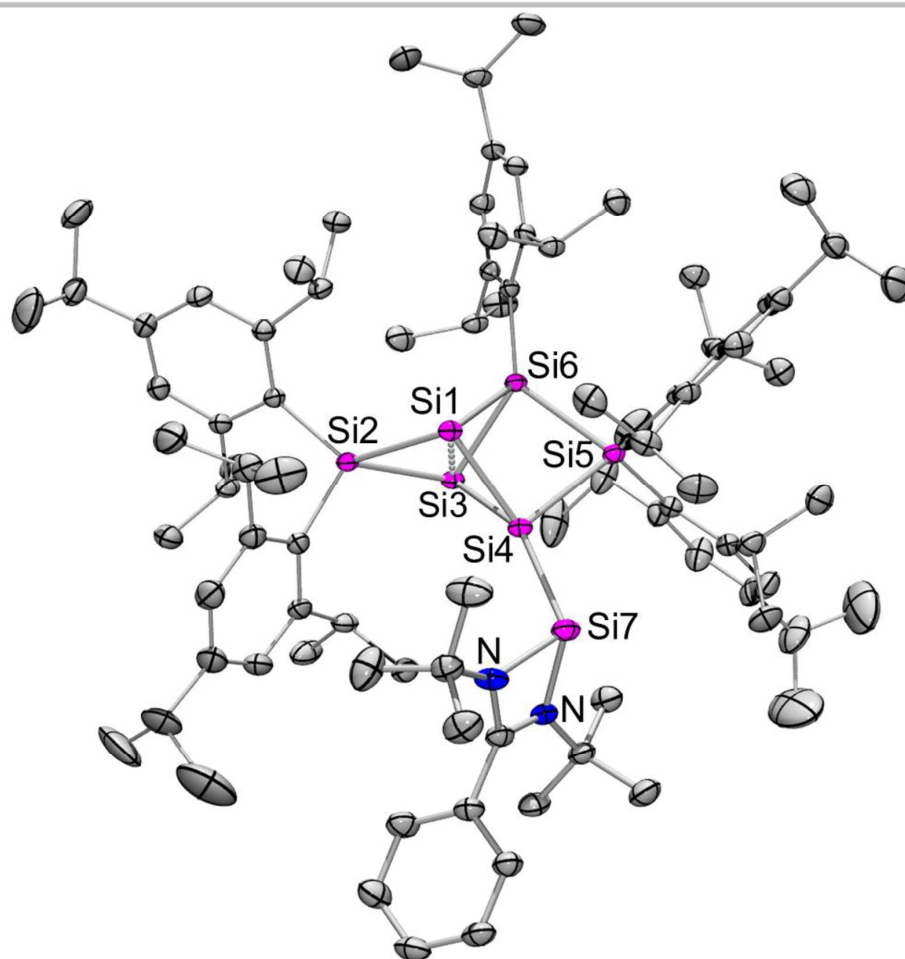


Figure S80. Molecular structure of siliconoid **3a** in the solid state. Hydrogen atoms omitted for clarity. Thermal ellipsoids represent 50% probability.

Table S5. Crystal data and structure refinement for $\text{Si}_6\text{NHSi } \mathbf{3a}$ (CCDC: 1978004).

Identification code	sh3825	
Empirical formula	$\text{C}_{90} \text{H}_{138} \text{N}_2 \text{Si}_7, \text{C}_6 \text{H}_6$	
Formula weight	1522.75	
Temperature	153(2) K	
Wavelength	0.71073 Å	
Crystal system	Triclinic	
Space group	P-1	
Unit cell dimensions	$a = 15.2632(6) \text{ Å}$	$\alpha = 75.024(2)^\circ$
	$b = 17.4776(7) \text{ Å}$	$\beta = 76.782(2)^\circ$
	$c = 18.7820(8) \text{ Å}$	$\gamma = 78.320(2)^\circ$
Volume	$4656.9(3) \text{ Å}^3$	
Z	2	
Density (calculated)	1.086 Mg/m^3	

SUPPORTING INFORMATION

WILEY-VCH

Absorption coefficient	0.146 mm ⁻¹
F(000)	1664
Crystal size	0.499 x 0.120 x 0.094 mm ³
Theta range for data collection	1.142 to 27.197°.
Index ranges	-19<=h<=19, -22<=k<=22, -24<=l<=24
Reflections collected	79046
Independent reflections	20558 [R(int) = 0.0562]
Completeness to theta = 25.242°	99.9 %
Absorption correction	Semi-empirical from equivalents
Max. and min. transmission	0.7455 and 0.7133
Refinement method	Full-matrix least-squares on F ²
Data / restraints / parameters	20558 / 43 / 973
Goodness-of-fit on F ²	1.029
Final R indices [I>2sigma(I)]	R1 = 0.0541, wR2 = 0.1288
R indices (all data)	R1 = 0.0950, wR2 = 0.1481
Extinction coefficient	n/a
Largest diff. peak and hole	0.703 and -0.605 e.Å ⁻³

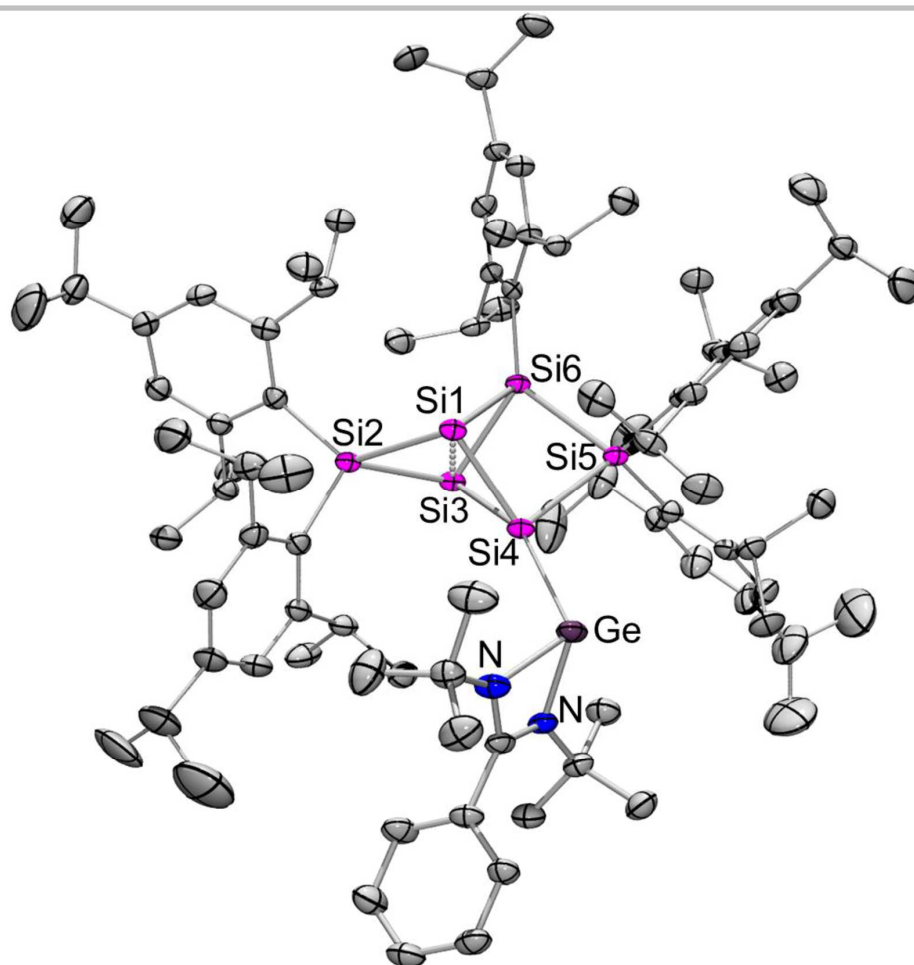


Figure S81. Molecular structure of siliconoid **3b** in the solid state. Hydrogen atoms omitted for clarity. Thermal ellipsoids represent 50% probability.

Table S6. Crystal data and structure refinement for $\text{Si}_6\text{NHGe } \mathbf{3b}$ (CCDC: 1978005).

Identification code	sh3963a	
Empirical formula	$\text{C}_{90}\text{H}_{138}\text{GeN}_2\text{Si}_6$, C_6H_6	
Formula weight	1567.25	
Temperature	172(2) K	
Wavelength	0.71073 Å	
Crystal system	Triclinic	
Space group	P-1	
Unit cell dimensions	$a = 15.309(7)$ Å	$\alpha = 75.056(13)^\circ$
	$b = 17.430(8)$ Å	$\beta = 76.627(14)^\circ$
	$c = 18.845(9)$ Å	$\gamma = 78.843(13)^\circ$
Volume	$4678(4)$ Å ³	
Z	2	
Density (calculated)	1.113 Mg/m ³	

SUPPORTING INFORMATION

WILEY-VCH

Absorption coefficient	0.448 mm ⁻¹
F(000)	1700
Crystal size	0.233 x 0.083 x 0.047 mm ³
Theta range for data collection	1.139 to 26.789°.
Index ranges	-19<=h<=19, -21<=k<=22, -23<=l<=23
Reflections collected	92059
Independent reflections	18674 [R(int) = 0.0852]
Completeness to theta = 25.242°	96.8 %
Absorption correction	Semi-empirical from equivalents
Max. and min. transmission	0.8620 and 0.7809
Refinement method	Full-matrix least-squares on F ²
Data / restraints / parameters	18674 / 78 / 990
Goodness-of-fit on F ²	1.018
Final R indices [I>2sigma(I)]	R1 = 0.0588, wR2 = 0.1459
R indices (all data)	R1 = 0.1170, wR2 = 0.1746
Extinction coefficient	n/a
Largest diff. peak and hole	0.633 and -0.630 e.Å ⁻³

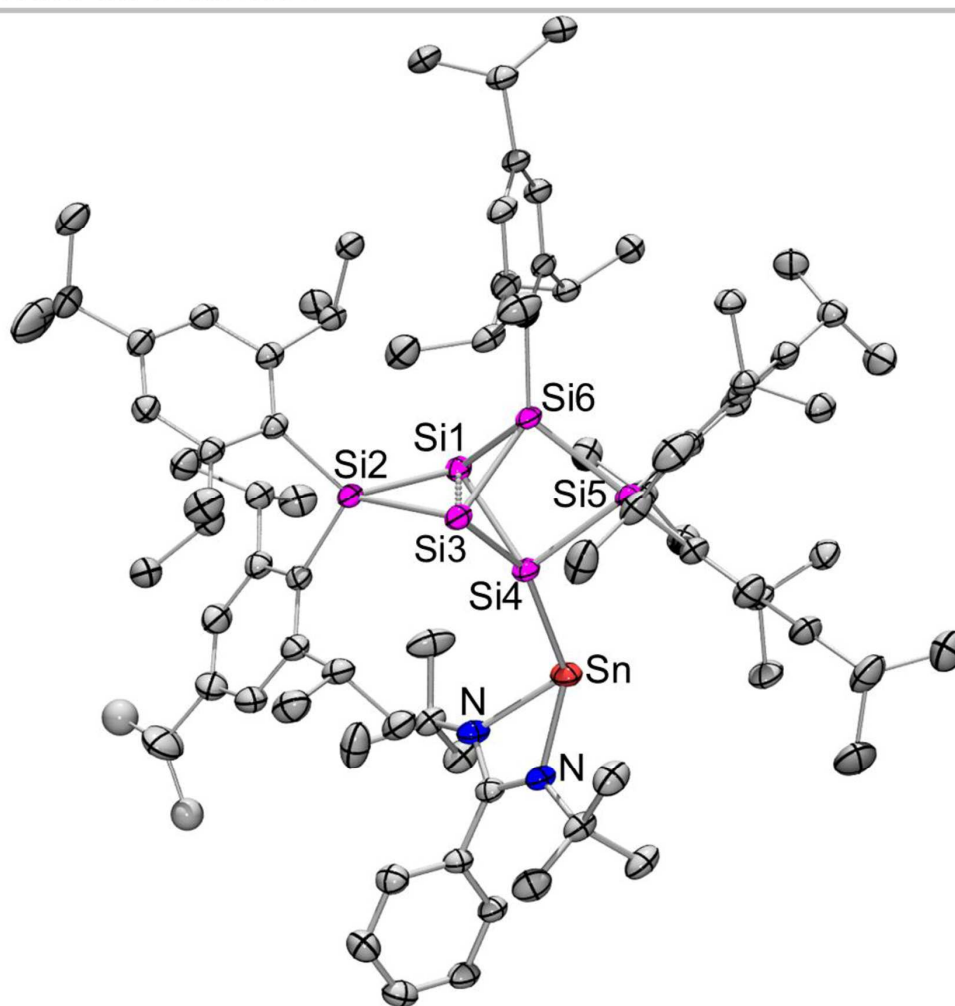


Figure S82. Molecular structure of siliconoid **3c** in the solid state. Hydrogen atoms omitted for clarity. Thermal ellipsoids represent 50% probability.

Table S7. Crystal data and structure refinement for $\text{Si}_6\text{NHSn } \mathbf{3c}$ (CCDC: 1978006).

Identification code	sh4153cu	
Empirical formula	$\text{C}_{93} \text{H}_{141} \text{N}_2 \text{Si}_6 \text{Sn}$	
Formula weight	1574.30	
Temperature	133(2) K	
Wavelength	1.54178 Å	
Crystal system	Triclinic	
Space group	P-1	
Unit cell dimensions	$a = 15.6171(7) \text{ Å}$	$\alpha = 63.047(2)^\circ$
	$b = 17.9450(9) \text{ Å}$	$\beta = 86.806(4)^\circ$
	$c = 18.8679(14) \text{ Å}$	$\gamma = 76.562(2)^\circ$
Volume	$4576.8(5) \text{ Å}^3$	
Z	2	

SUPPORTING INFORMATION

WILEY-VCH

Density (calculated)	1.142 Mg/m ³
Absorption coefficient	3.287 mm ⁻¹
F(000)	1694
Crystal size	0.216 x 0.053 x 0.025 mm ³
Theta range for data collection	2.631 to 81.246°.
Index ranges	-19<=h<=19, -22<=k<=22, -23<=l<=24
Reflections collected	89251
Independent reflections	19644 [R(int) = 0.0615]
Completeness to theta = 67.679°	99.3 %
Absorption correction	Semi-empirical from equivalents
Max. and min. transmission	0.7543 and 0.6543
Refinement method	Full-matrix least-squares on F ²
Data / restraints / parameters	19644 / 22 / 968
Goodness-of-fit on F ²	1.047
Final R indices [I>2sigma(I)]	R1 = 0.0420, wR2 = 0.1072
R indices (all data)	R1 = 0.0493, wR2 = 0.1133
Extinction coefficient	n/a
Largest diff. peak and hole	1.314 and -0.629 e.Å ⁻³

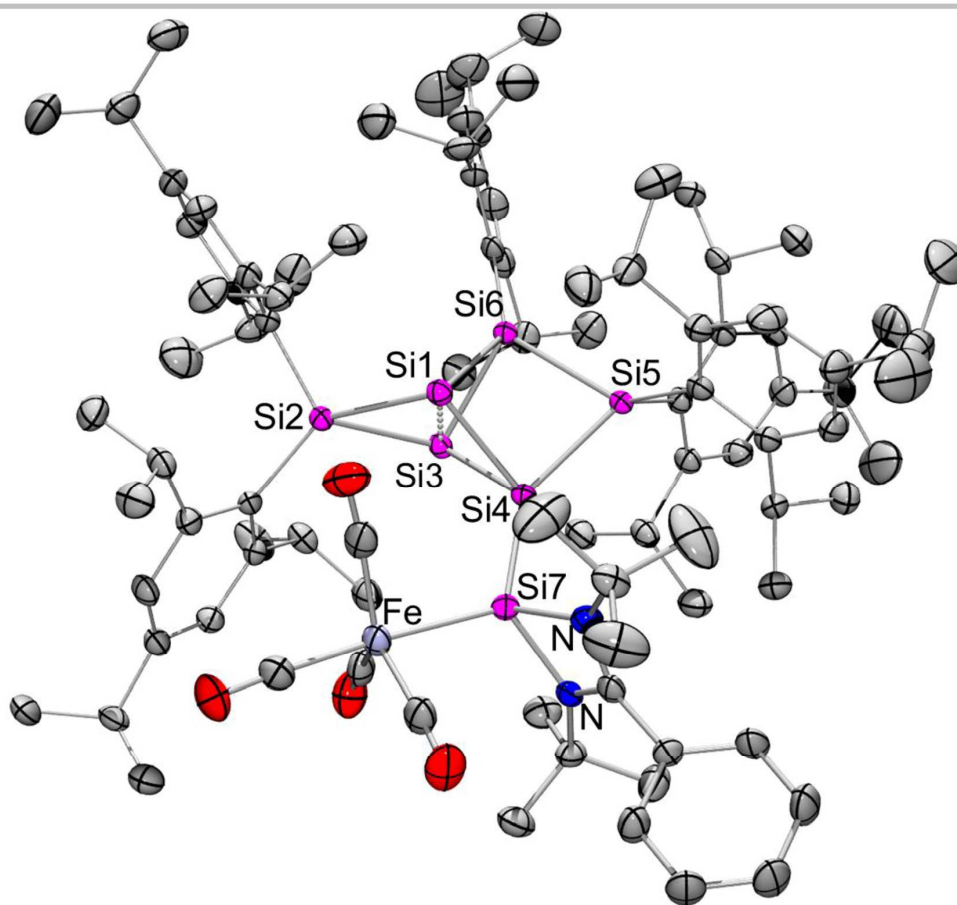


Figure S83. Molecular structure of siliconoid **4a** in the solid state. Hydrogen atoms omitted for clarity. Thermal ellipsoids represent 50% probability.

Table S8. Crystal data and structure refinement for $\text{Si}_6\text{NHSi-Fe(CO)}_4$ **4a** (CCDC: 1978007).

Identification code	sh3964	
Empirical formula	$\text{C}_{94} \text{H}_{138} \text{Fe} \text{N}_2 \text{O}_4 \text{Si}_7$, $\text{C}_6 \text{H}_{14}$	
Formula weight	1698.71	
Temperature	162(2) K	
Wavelength	0.71073 Å	
Crystal system	Triclinic	
Space group	P-1	
Unit cell dimensions	$a = 16.0595(7)$ Å	$\angle = 76.092(3)^\circ$
	$b = 17.5648(8)$ Å	$\angle = 78.970(3)^\circ$
	$c = 19.8297(9)$ Å	$\angle = 88.051(2)^\circ$
Volume	$5328.9(4)$ Å ³	
Z	2	
Density (calculated)	1.059 Mg/m^3	
Absorption coefficient	0.265 mm^{-1}	

SUPPORTING INFORMATION

WILEY-VCH

F(000)	1844
Crystal size	0.177 x 0.166 x 0.090 mm ³
Theta range for data collection	1.077 to 27.205°.
Index ranges	-15<=h<=20, -22<=k<=22, -25<=l<=25
Reflections collected	86873
Independent reflections	23475 [R(int) = 0.0751]
Completeness to theta = 25.242°	99.5 %
Absorption correction	Semi-empirical from equivalents
Max. and min. transmission	0.8620 and 0.8226
Refinement method	Full-matrix least-squares on F ²
Data / restraints / parameters	23475 / 54 / 1117
Goodness-of-fit on F ²	1.056
Final R indices [I>2sigma(I)]	R1 = 0.0706, wR2 = 0.1897
R indices (all data)	R1 = 0.1354, wR2 = 0.2254
Extinction coefficient	n/a
Largest diff. peak and hole	0.839 and -0.527 e.Å ⁻³

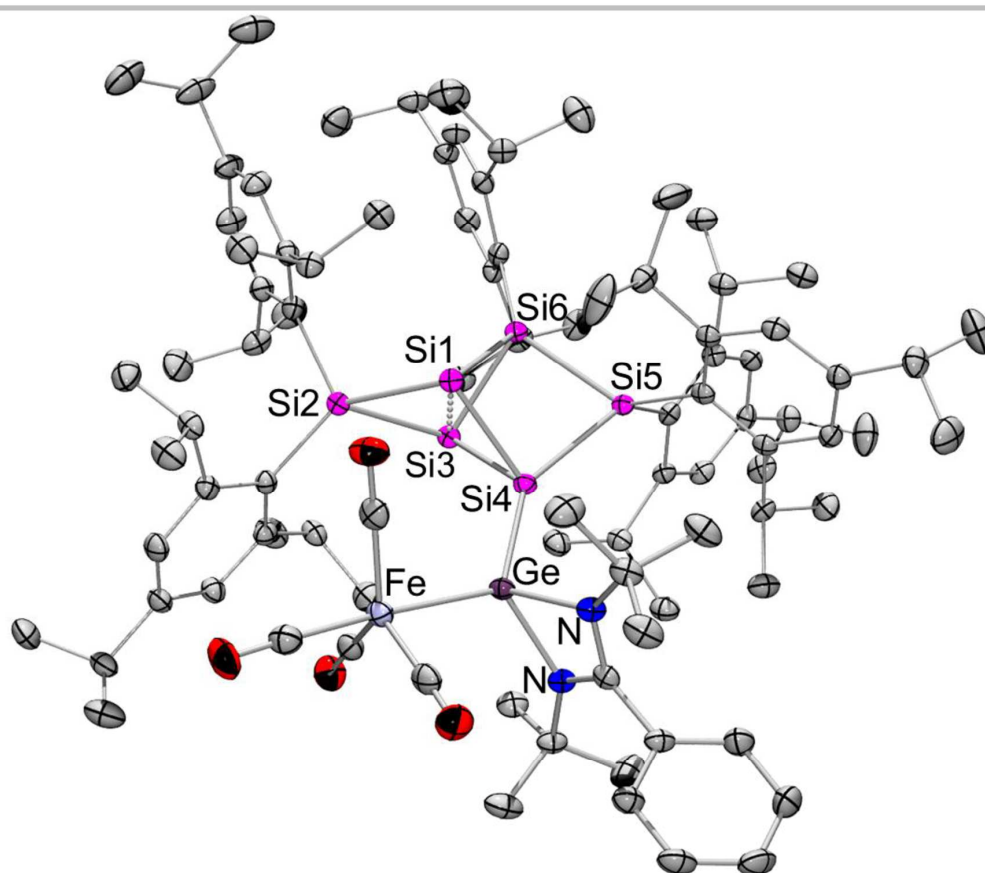


Figure S84. Molecular structure of siliconoid **4b** in the solid state. Hydrogen atoms omitted for clarity. Thermal ellipsoids represent 50% probability.

Table S9. Crystal data and structure refinement for $\text{Si}_6\text{NHGe-Fe(CO)}_4$ **4b** (CCDC: 1978008).

Identification code	sh3980	
Empirical formula	$\text{C}_{94}\text{H}_{138}\text{FeGeN}_2\text{O}_4\text{Si}_6$	
Formula weight	1743.21	
Temperature	142(2) K	
Wavelength	0.71073 Å	
Crystal system	Monoclinic	
Space group	$P2_1/n$	
Unit cell dimensions	$a = 15.0527(18)$ Å	$\alpha = 90^\circ$.
	$b = 32.231(4)$ Å	$\beta = 90.764(7)^\circ$.
	$c = 20.333(3)$ Å	$\gamma = 90^\circ$.
Volume	$9864(2)$ Å ³	
Z	4	
Density (calculated)	1.174 Mg/m ³	
Absorption coefficient	0.574 mm ⁻¹	
F(000)	3760	

SUPPORTING INFORMATION

WILEY-VCH

Crystal size	0.280 x 0.225 x 0.048 mm ³
Theta range for data collection	1.184 to 27.264°.
Index ranges	-19<= <i>h</i> <=19, -40<= <i>k</i> <=41, -24<= <i>l</i> <=25
Reflections collected	150931
Independent reflections	21746 [R(int) = 0.0959]
Completeness to theta = 25.242°	99.8 %
Absorption correction	Semi-empirical from equivalents
Max. and min. transmission	0.8620 and 0.7749
Refinement method	Full-matrix least-squares on F ²
Data / restraints / parameters	21746 / 21 / 1060
Goodness-of-fit on F ²	1.015
Final R indices [I>2sigma(I)]	R1 = 0.0493, wR2 = 0.0983
R indices (all data)	R1 = 0.1017, wR2 = 0.1162
Extinction coefficient	n/a
Largest diff. peak and hole	0.612 and -0.604 e.Å ⁻³

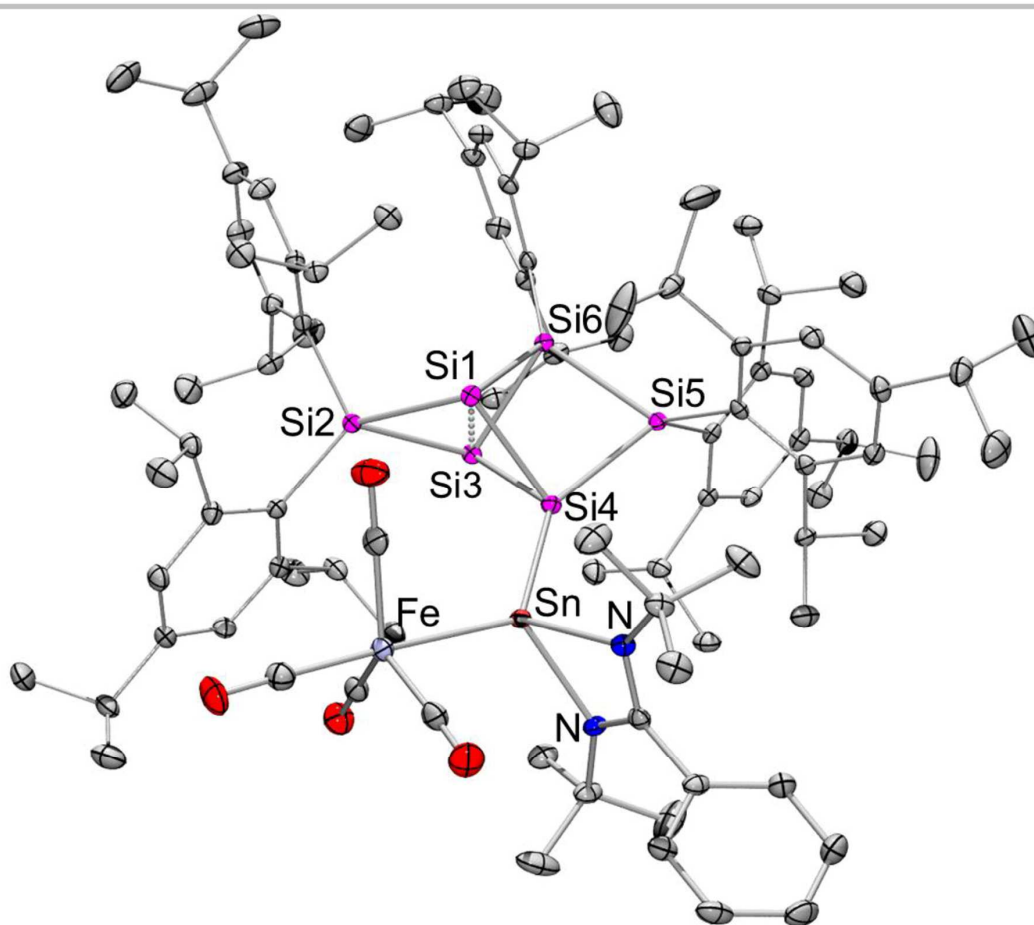


Figure S85. Molecular structure of siliconoid **4c** in the solid state. Hydrogen atoms omitted for clarity. Thermal ellipsoids represent 50% probability.

Table S10. Crystal data and structure refinement for $\text{Si}_6\text{NHSn-Fe(CO)}_4$ **4c** (CCDC: 1978009).

Identification code	sh4100	
Empirical formula	$\text{C}_{94}\text{H}_{138}\text{FeN}_2\text{O}_4\text{Si}_6\text{Sn}$, C_6H_{14}	
Formula weight	1789.31	
Temperature	122(2) K	
Wavelength	0.71073 Å	
Crystal system	Monoclinic	
Space group	$P2_1/n$	
Unit cell dimensions	$a = 15.2343(5)$ Å	$\alpha = 90^\circ$.
	$b = 32.1747(10)$ Å	$\beta = 90.9122(10)^\circ$.
	$c = 20.3411(5)$ Å	$\gamma = 90^\circ$.
Volume	$9969.1(5)$ Å ³	
Z	4	
Density (calculated)	1.192 Mg/m^3	
Absorption coefficient	0.517 mm^{-1}	

SUPPORTING INFORMATION

WILEY-VCH

F(000)	3832
Crystal size	0.307 x 0.200 x 0.184 mm ³
Theta range for data collection	1.184 to 27.883°
Index ranges	-19<=h<=20, -39<=k<=42, -16<=l<=26
Reflections collected	97578
Independent reflections	23765 [R(int) = 0.0385]
Completeness to theta = 25.242°	100.0 %
Absorption correction	Semi-empirical from equivalents
Max. and min. transmission	0.7456 and 0.7002
Refinement method	Full-matrix least-squares on F ²
Data / restraints / parameters	23765 / 21 / 1060
Goodness-of-fit on F ²	1.028
Final R indices [I>2sigma(I)]	R1 = 0.0334, wR2 = 0.0727
R indices (all data)	R1 = 0.0494, wR2 = 0.0791
Extinction coefficient	n/a
Largest diff. peak and hole	0.913 and -0.460 e.Å ⁻³

5. References

- [1] P. Willmes, K. Leszczyńska, Y. Heider, K. Abersfelder, M. Zimmer, V. Huch, D. Scheschke, *Angew. Chem. Int. Ed.* **2016**, *55*, 2907-2910.
- [2] C.-W. So, H. W. Roesky, J. Magull, R. B. Oswald, *Angew. Chem. Int. Ed.* **2006**, *45*, 3948-3950; b) S. S. Sen, H. W. Roesky, D. Stern, J. Henn, D. Stalke, *J. Am. Chem. Soc.* **2010**, *132*, 1123-1126; c) S. Nagendran, S. S. Sen, H. W. Roesky, D. Koley, H. Grubenmüller, A. Pal, R. Herbst-Irmer, *Organometallics* **2008**, *27*, 5459-5463; d) S. S. Sen, M. P. Kritzler-Kosch, S. Nagendran, H. W. Roesky, T. Beck, A. Pal, R. Herbst-Irmer, *Eur. J. Inorg. Chem.* **2010**, 5304-5311.
- [3] M. J. Frisch, G. W. Trucks, H. B. Schlegel, G. E. Scuseria, M. A. Robb, J. R. Cheeseman, G. Scalmani, V. Barone, B. Mennucci, G. A. Petersson, H. P. Hratchian, A. F. Izmaylov, J. Bloino, G. Zheng, J. L. Sonnenberg, M. Hada, M. Ehara, K. Toyota, R. Fukuda, J. Hasegawa, M. Ishida, T. Najajima, Y. Honda, O. Kitao, H. Nakai, T. Vreven, J. A. Montgomery, J. E. Peralta, F. Ogliaro, M. Bearpark, J. J. Heyd, E. Brothers, K. N. Kudin, V. N. Staroverov, R. Kobayashi, J. Normand, K. Raghavachari, A. Rendell, J. C. Burant, S. S. Iyengar, J. Tomasi, M. Cossi, N. Rega, J. M. Millam, M. Klene, J. E. Knox, J. B. Cross, V. Bakken, C. Adamo, J. Jaramillo, R. Gomperts, R. E. Stratman, O. Yazyev, A. J. Austin, R. Cammi, C. Pomelli, J. W. Ochterski, R. L. Martin, K. Morokuma, V. G. Zakrzewski, G. A. Voth, P. Salvador, J. J. Dannenberg, S. Dapprich, A. D. Daniels, O. Farkas, J. B. Foresman, J. V. Ortiz, J. Cioslowski, D. J. Fox, *Gaussian09, Revision C.01. Gaussian, Inc.: Wallingford CT*, **2009**.
- [4] TURBOMOLE V7.0 2015 a development of University of Karlsruhe and Forschungszentrum Karlsruhe GmbH, 1989-2007; TURBOMOLE GmbH, since **2007**, available from <http://www.turbomole.com>; Karlsruhe.
- [5] A. D. Becke, *Phys. Rev. A* **1988**, *38* (6), 3098-3100.
- [6] J. P. Perdew, *Phys. Rev. B* **1986**, *33* (12), 8822-8824.
- [7] S. Grimme, J. Antony, S. Ehrlich, H. Krieg, *J. Chem. Phys.* **2010**, *132* (15), 154104.
- [8] S. Grimme, S. Ehrlich, L. Goerigk, *J. Comp. Chem.* **2011**, *32* (7), 1456-1465.
- [9] F. Weigend, R. Ahlrichs, *Phys. Chem. Chem. Phys.* **2005**, *7* (18), 3297-3305.
- [10] C. Y. Peng, P. Y. Ayala, H. B. Schlegel, M. J. Frisch, *J. Comp. Chem.* **1996**, *17* (1), 49-56.
- [11] J. W. McIver, A. Komornic, *J. Am. Chem. Soc.* **1972**, *94* (8), 2625-2633.

6. Author Contributions

N. P. Conceptualization: Equal, Data curation: Lead; Formal analysis: Lead; Investigation: Lead; Methodology: Lead; Validation: Lead; Visualization: Lead; Writing original draft: Lead; Writing review & editing: Lead. L.G. Investigation: Supporting; Data curation: Supporting; Formal analysis: Supporting. K. I. Methodology: Supporting. V.H. Data curation: Lead; Formal analysis: Lead, X-ray structures: Lead. M. Z. VT NMR studies: Lead. D. S. Conceptualization: Lead, Funding acquisition: Lead; Methodology: Supporting; Project administration: Lead; Resources: Lead; Supervision: Lead; Writing original draft: Supporting; Writing review & edition: Supporting.

6.3 Exohedral functionalization vs. core expansion of siliconoids with Group 9 metals: catalytic activity in alkene isomerization

Electronic Supplementary Material (ESI) for Chemical Science.
This journal is © The Royal Society of Chemistry 2020

**Exohedral functionalization vs. core expansion of siliconoids
with Group 9 metals: catalytic activity in alkene isomerization**

Nadine Poitiers, Luisa Giarrana, Volker Huch, Michael Zimmer and David Scheschkewitz*

Krupp-Chair of General and Inorganic Chemistry, Saarland University, 66123 Saarbrücken, Germany

Supporting Information

Table of Contents

1. General	S3
2. Preparation, data and spectra (NMR, UV-vis, IR):	S3
<ul style="list-style-type: none"> (5-(Chlorobis(2,4,6-triisopropylphenyl)silyl)-2-(1,3-di-<i>tert</i>-butyl-4-phenyl-1,3,2λ^3-diazasilet-1-ium-2(3<i>H</i>)-yl)-3,3,4-tris(2,4,6-triisopropylphenyl)tricyclo[2.1.0.0^{2,5}]pentasilane-1-yl-iridium (2a) 	S3
<ul style="list-style-type: none"> (5-(Chlorobis(2,4,6-triisopropylphenyl)silyl)-2-(1,3-di-<i>tert</i>-butyl-4-phenyl-1,3,2λ^3-diazagermet-1-ium-2(3<i>H</i>)-yl)-3,3,4-tris(2,4,6-triisopropylphenyl)tricyclo[2.1.0.0^{2,5}]pentasilane-1-yl-iridium (2b) 	S8
<ul style="list-style-type: none"> (5-(Chlorobis(2,4,6-triisopropylphenyl)silyl)-2-(1,3-di-<i>tert</i>-butyl-4-phenyl-1,3,2λ^3-diazastannet-1-ium-2(3<i>H</i>)-yl)-3,3,4-tris(2,4,6-triisopropylphenyl)tricyclo[2.1.0.0^{2,5}]pentasilane-1-yl-iridium (2c) 	S14
<ul style="list-style-type: none"> η^5-((2-(Chloro-λ^2-silyl)-4-(1,3-di-<i>tert</i>-butyl-4-phenyl-1,3,2-diazasilet-1-ium-2-id-2(3<i>H</i>)-yl)-1,1,2-tris(2,4,6-triisopropylphenyl)-1,2-dihydro tetrasilet-3-yl)bis(2,4,6-triisopropylphenyl)silyl)rhodium (3) 	S21
<ul style="list-style-type: none"> 1.2 <i>trans</i>-Dicarbonyl-(1,3-di-<i>tert</i>-butyl-2-chloro-4-phenyl-2,3-dihydro-1,3,2-diazasilet-1-ium-2-ide)-<i>ligato</i>-(2,2,5,5,6-pentakis(2,4,6-triisopropylphenyl)tetracyclo[2.2.0.0^{1,3}.0^{3,6}]hexasilan -4-yl)rhodium (4) 	S26
<ul style="list-style-type: none"> (5-(Chlorobis(2,4,6-triisopropylphenyl)silyl)-2-(1,3-di-<i>tert</i>-butyl-4-phenyl-1,3,2λ^3-diazagermet-1-ium-2(3<i>H</i>)-yl)-3,3,4-tris(2,4,6-triisopropylphenyl)tricyclo[2.1.0.0^{2,5}]pentasilane-1-yl-rhodium 	S31
3. Data and Plots of spectroscopic conversion in alkene isomerization	S32
4. Details on X-ray Diffraction Studies	S43
<ul style="list-style-type: none"> (5-(Chlorobis(2,4,6-triisopropylphenyl)silyl)-2-(1,3-di-<i>tert</i>-butyl-4-phenyl-1,3,2λ^3-diazasilet-1-ium-2(3<i>H</i>)-yl)-3,3,4-tris(2,4,6-triisopropylphenyl)tricyclo[2.1.0.0^{2,5}]pentasilane-1-yl-iridium (2a) 	S43
<ul style="list-style-type: none"> (5-(Chlorobis(2,4,6-triisopropylphenyl)silyl)-2-(1,3-di-<i>tert</i>-butyl-4-phenyl-1,3,2λ^3-diazagermet-1-ium-2(3<i>H</i>)-yl)-3,3,4-tris(2,4,6-triisopropylphenyl)tricyclo[2.1.0.0^{2,5}]pentasilane-1-yl-iridium (2b) 	S45
<ul style="list-style-type: none"> (5-(Chlorobis(2,4,6-triisopropylphenyl)silyl)-2-(1,3-di-<i>tert</i>-butyl-4-phenyl-1,3,2λ^3-diazastannet-1-ium-2(3<i>H</i>)-yl)-3,3,4-tris(2,4,6-triisopropylphenyl)tricyclo[2.1.0.0^{2,5}]pentasilane-1-yl-iridium (2c) 	S46
<ul style="list-style-type: none"> η^5-((2-(Chloro-λ^2-silyl)-4-(1,3-di-<i>tert</i>-butyl-4-phenyl-1,3,2-diazasilet-1-ium-2-id-2(3<i>H</i>)-yl)-1,1,2-tris(2,4,6-triisopropylphenyl)-1,2-dihydro tetrasilet-3-yl)bis(2,4,6-triisopropylphenyl)silyl)rhodium (3) 	S48
<ul style="list-style-type: none"> <i>trans</i>-Dicarbonyl-(1,3-di-<i>tert</i>-butyl-2-chloro-4-phenyl-2,3-dihydro-1,3,2-diazasilet-1-ium-2-ide)-<i>ligato</i>-(2,2,5,5,6-pentakis(2,4,6-triisopropylphenyl)tetracyclo[2.2.0.0^{1,3}.0^{3,6}]hexasilan -4-yl)rhodium (4) 	S50
<ul style="list-style-type: none"> (5-(Chlorobis(2,4,6-triisopropylphenyl)silyl)-2-(1,3-di-<i>tert</i>-butyl-4-phenyl-1,3,2λ^3-diazagermet-1-ium-2(3<i>H</i>)-yl)-3,3,4-tris(2,4,6-triisopropylphenyl)tricyclo[2.1.0.0^{2,5}]pentasilane-1-yl-rhodium 	S51
5. References	S53

1. General

All manipulations were carried out under a protective atmosphere of argon, by using a glovebox or standard Schlenk techniques. Ethereal solvents were dried by heating to reflux over Na/benzophenone and distilled and stored under an atmosphere of argon. Hydrocarbons were dried over sodium or potassium. Solution NMR spectra were recorded on a Bruker Avance IV 400 NMR spectrometer (^1H = 400.13 MHz, ^{13}C = 100.6 MHz, ^{29}Si = 79.49 MHz, ^{119}Sn = 149.21 MHz) and solid state NMR spectra on a Bruker Avance III 400 WB spectrometer (^{29}Si = 79.53 MHz, ^{119}Sn = 149.27 MHz). UV/Vis spectra were recorded on a Shimadzu UV-2600 spectrometer in quartz cells with a path length of 0.1 cm. Infrared spectra were measured with a Shimadzu IR Affinity-1S in a platinum ATR diamond cell. Elemental analyses were performed on an elemental analyzer Leco CHN-900 and/or an elemental vario Micro Cube. Compounds **1a-c** were prepared according to our published procedures.¹

2. Preparation, data and spectra (NMR, UV-vis, IR)

Procedure for the synthesis of tetrylene-functionalized iridium siliconoid complexes **2a-c**

The respective compounds **2a-c** are prepared by treating 1 equivalent of the *ligato*-tetrylene-functionalized siliconoids **1a-c** with the corresponding amount of chloro(1,5-cyclooctadiene)iridium(I) dimer [(cod)IrCl]₂ in benzene. The suspension is heated to 40°C for 5 minutes and then stirred at room temperature overnight. After removing all volatiles in vacuum, the crude product is filtered from the indicated amount of hexane and crystallized from hexane at -26°C overnight. Concentration of the mother liquor typically affords a second batch of crystalline **2a-c**.

(5-(Chlorobis(2,4,6-triisopropylphenyl)silyl)-2-(1,3-di-*tert*-butyl-4-phenyl-1,3,2λ³-diazasilet-1-ium-2(3*H*)-yl)-3,3,4-tris(2,4,6-triisopropylphenyl)tricyclo[2.1.0.0^{2,5}] pentasilane-1-yl-iridium (**2a**)

Quantities: Si₆NHSi **1a**, 700 mg (0.485 mmol), [(cod)IrCl]₂ 162.76 mg (0.243 mmol), benzene 10 mL, filtration four times from hexane 15 mL each, crystallization from hexane. Yield: 568 mg (0.328 mmol ; 68 %) violet crystals (mp. > 147 °C, dec.).

¹H-NMR (400.13 MHz, C₆D₆, 300 K) δ = 7.391 (bs, 1H, Ar-H), 7.193 – 7.189 (m, 2H, Ar-H), 7.142 – 7.138 (m, 1H, Ar-H), 7.052 – 7.047 (m, 1H, Ar-H), 7.002 – 6.917 (m, 6H, Ar-H), 6.838 – 6.802 (m, 3H, Ar-H), 6.773 (bs, 1H, Ar-H), 5.831 (sept, 1H, $^3J_{\text{HH}}$ = 6.16 Hz, Tip-*i*Pr-CH₂), 5.185 (sept, 1H, $^3J_{\text{HH}}$ = 6.80 Hz, Tip-*i*Pr-CH₂), 4.913 (sept, 1H, $^3J_{\text{HH}}$ = 6.44 Hz, Tip-*i*Pr-CH₂), 4.583 – 4.433 (m, 4H, Tip-*i*Pr-CH₂), 3.819 (sept, 1H, $^3J_{\text{HH}}$ = 6.98 Hz, Tip-*i*Pr-CH₂), 3.668 (sept, 1H, $^3J_{\text{HH}}$ = 6.39 Hz, Tip-*i*Pr-CH₂), 3.161 (sept, 1H, $^3J_{\text{HH}}$ = 6.07 Hz, Tip-*i*Pr-CH₂), 2.854 – 2.569 (m, 7H, Tip-*i*Pr-CH₂), 2.363 (bs, 2H, Tip-*i*Pr-CH₂), 2.101 – 2.021 (m, 14H, Tip-*i*Pr-CH₃), 1.929 (d, 3H, $^3J_{\text{HH}}$ = 6.47 Hz, Tip-*i*Pr-CH₃), 1.836 (d, 3H, $^3J_{\text{HH}}$ = 6.56 Hz, Tip-*i*Pr-CH₃), 1.804 – 1.775 (m, 6H, Tip-*i*Pr-CH₃), 1.578 (d, 3H, $^3J_{\text{HH}}$ = 6.35 Hz, Tip-*i*Pr-CH₃), 1.513 (d, 6H, $^3J_{\text{HH}}$ = 6.35 Hz, Tip-*i*Pr-CH₃), 1.465 (d, 3H, $^3J_{\text{HH}}$ = 6.70 Hz, Tip-*i*Pr-CH₃), 1.384 – 1.360 (m, 6H, Tip-*i*Pr-CH₃), 1.278 – 1.134 (m, 36H, Tip-*i*Pr-CH₃), 1.077 – 1.058 (m, 7H, Tip-*i*Pr-CH₃), 0.890 (t, 6H, $^3J_{\text{HH}}$ = 7.18 Hz, Tip-*i*Pr-CH₃), 0.830 (s, 9H, C(CH₃)₃), 0.723 (d, together 6H, Tip-*i*Pr-CH₃), 0.683 (m, 12 H, Tip-*i*Pr-CH₃ overlapping with C(CH₃)₃), 0.460 – 0.438 (m, 6H, Tip-*i*Pr-CH₃), 0.281 (d, 3H, $^3J_{\text{HH}}$ = 6.49 Hz, Tip-*i*Pr-CH₃), 0.167 (d, 3H, $^3J_{\text{HH}}$ = 6.49 Hz, Tip-*i*Pr-CH₃) ppm.

¹³C-NMR (100.61 MHz, C₆D₆, 300 K) δ = 169.70 (s, 1C, C-Ph), 156.15, 155.41 (s, each 1C, Ar-C), 154.42, 154.37 (s, each 1C, Ar-C), 154.14, 153.76, 153.22, 153.14, 152.90 (s, each 1C, Ar-C), 150.20, 149.91, 148.77, 147.98 (s, each 1C, Ar-C), 143.56 (s, 1C, Ar-C), 141.46 (s, 1C, Ar-C), 137.92, 137.13, 135.43, 132.13, 131.19 (s, each 1C, Ar-C), 130.03, 129.69 (s, each 1C, Ar-CH), 128.12, 127.88 (s, each 1C, Ar-CH overlapping with C₆D₆), 127.43, 127.40 (s, each 1C, Ar-CH), 123.62, 123.54, 123.51, 123.08, 122.88, 122.74, 122.57, 122.49, 122.08, 120.62 (s,

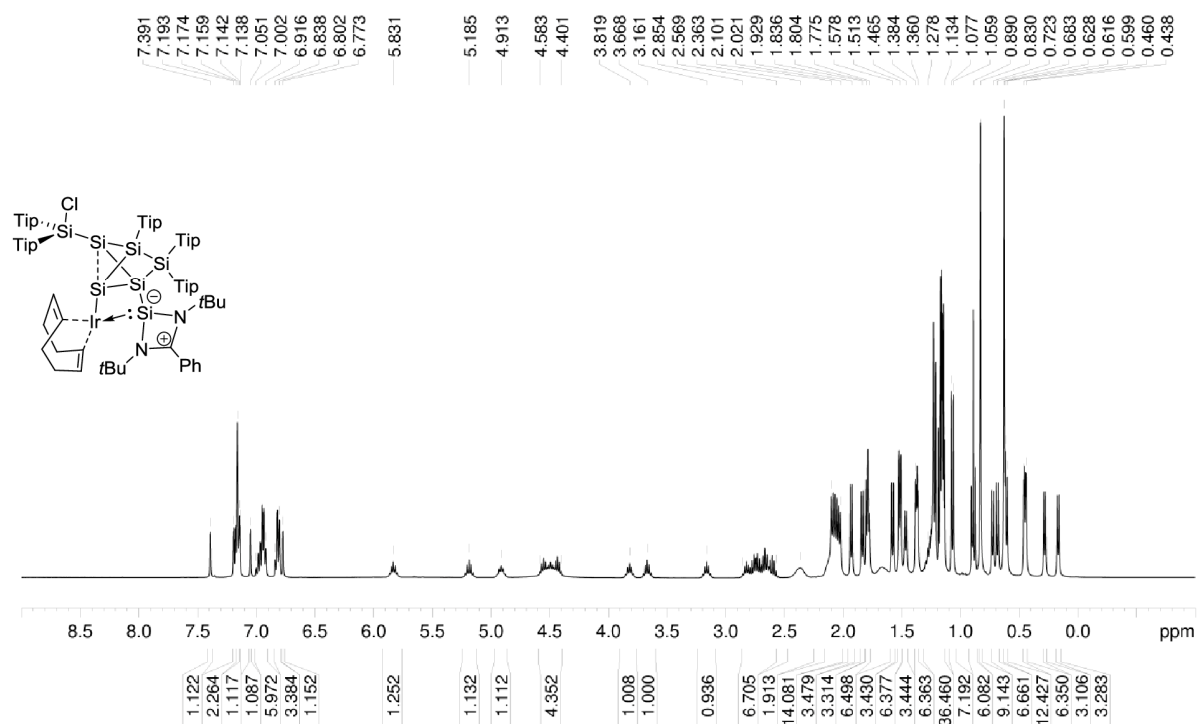
each 1C, Ar-CH), 53.81 (s, 1C, C(CH₃)₃), 53.67 (s, 1C, C(CH₃)₃), 38.12 (s, 1C, Tip-*i*Pr-CH), 35.72, 35.69 (s, each 1C, (s, 1C, Tip-*i*Pr-CH), 35.33, 34.79, 34.70, 34.59, 34.44, 34.31, 33.85, 33.57 (s, each 1C, (s, 1C, Tip-*i*Pr-CH), 32.98 (s, 1C, (s, 1C, Tip-*i*Pr-CH), 32.17 (s, 1C, (s, 1C, Tip-*i*Pr-CH), 31.92 (s, 1C, Tip-*i*Pr-CH), 31.79 (s, 1C, Tip-*i*Pr-CH), 31.18 (s, 1C, (s, 1C, Tip-*i*Pr-CH), 30.6 (s, 1C, Tip-*i*Pr-CH), 30.04, 29.09, 29.02 (s, each 1C, Tip-*i*Pr-CH₃), 28.41 (s, 1C, Tip-*i*Pr-CH₃), 27.28 (s, 1C, Tip-*i*Pr-CH₃), 26.15, 25.91, 25.69, 25.15 (s, each 1C, Tip-*i*Pr-CH₃), 24.76, 24.68, 24.61, 24.49, 24.46, 24.37, 24.26, 24.21, 24.18, 24.15, 24.13, 24.03, 23.96, 23.84, 23.74 (s, each 1C, Tip-*i*Pr-CH₃), 23.11, 23.01, 22.73, 22.40, (s, each 1C, Tip-*i*Pr-CH₃), 14.32 (s, 1C, Tip-*i*Pr-CH₃) ppm.

²⁹Si-NMR (79.49 MHz, C₆D₆, 300 K) δ = 56.7 (s, SiTip₂), 33.4 (s, NHSi), 13.3 (s, SiTip₂Cl), -38.4 (s, SiTip), -88.9 (s, Si-NHSi), -125.4 (s, unsubstituted Si), -128.7 (s, Si-Ir) ppm.

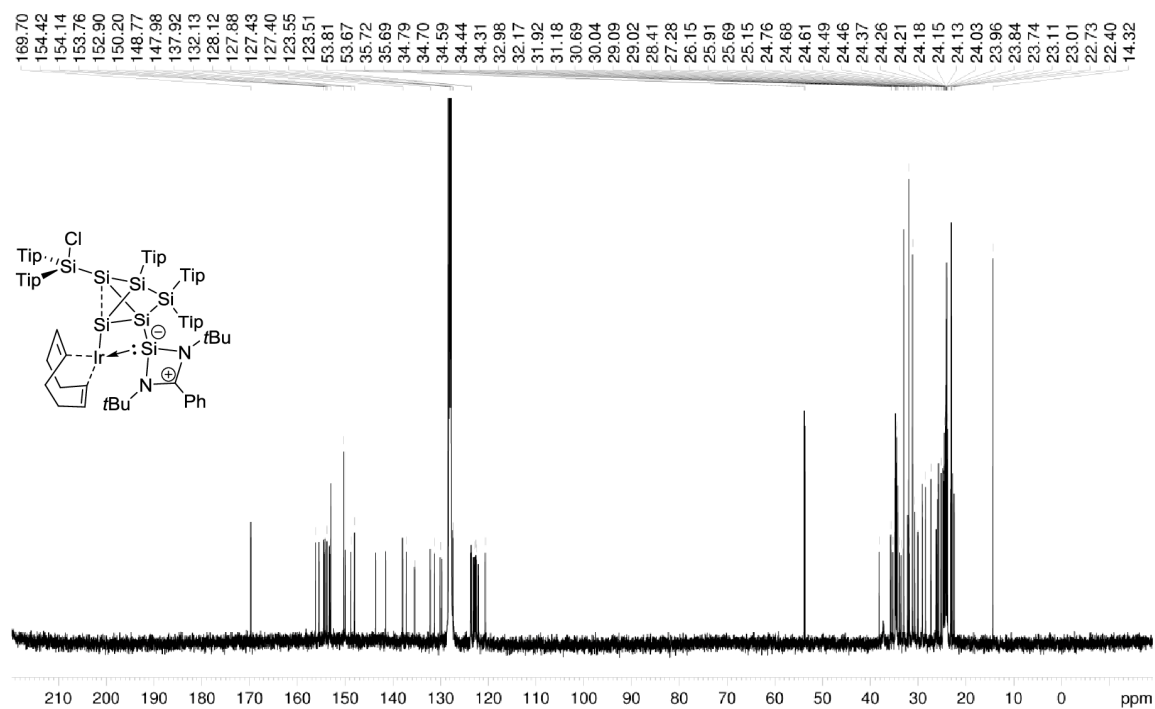
CP-MAS ²⁹Si-NMR (79.53 MHz, 13KHz, 300K) δ = 55.3 (s, SiTip₂), 32.9 (s, NHSi), 11.5 (s, SiTip₂Cl), -41.6 (s, SiTip), -88.6 (s, Si-NHSi), -126.8 (s, unsubstituted Si), -128.2 (s, unsubstituted Si) ppm.

Elemental analysis: calculated for C₉₇H₁₄₆ClIrN₂Si₇: C, 66.03 % ; H, 8.34 % ; N, 1.59 %. Found: C, 65.55, % ; H, 8.03 % ; N: 1.73 %.

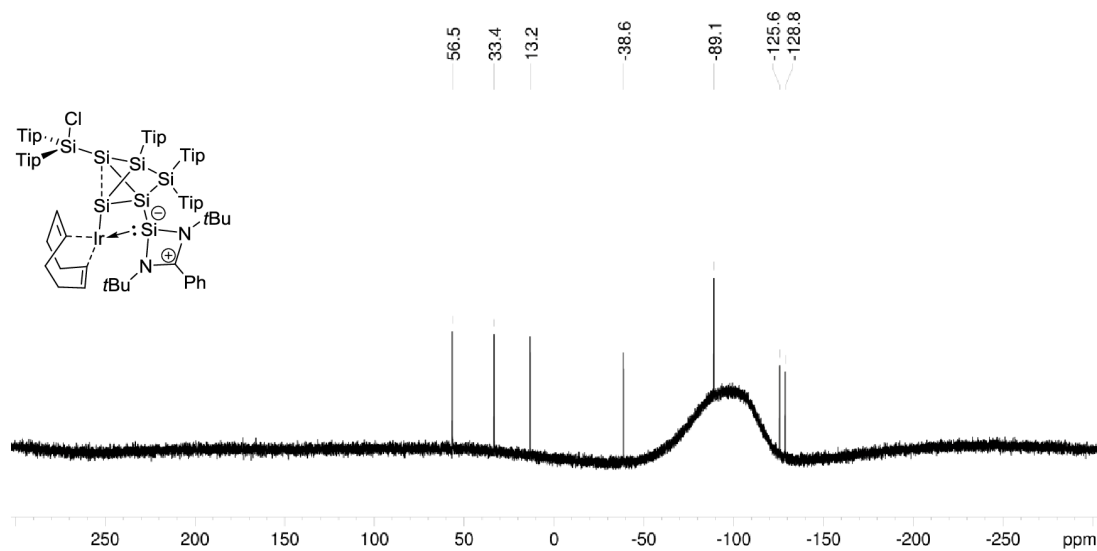
UV/VIS (hexane): $\lambda_{\max}(\epsilon)$ = 576 nm (1200 M⁻¹ cm⁻¹).



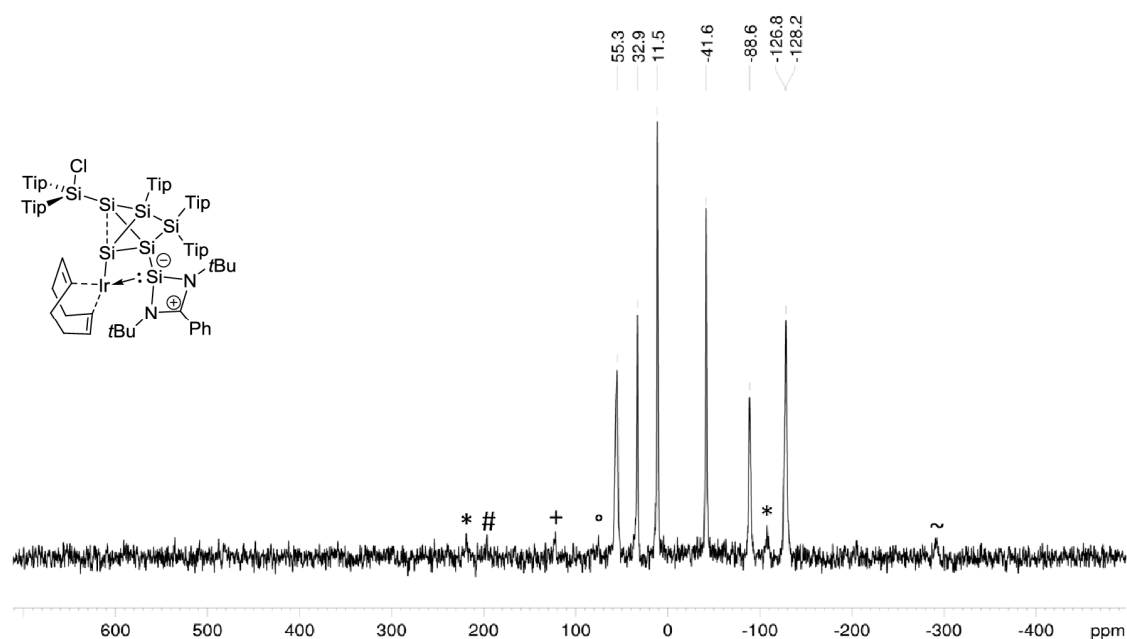
Supplementary Figure 1: ¹H NMR spectrum of **2a** in C₆D₆ (400.13 MHz, 300 K).



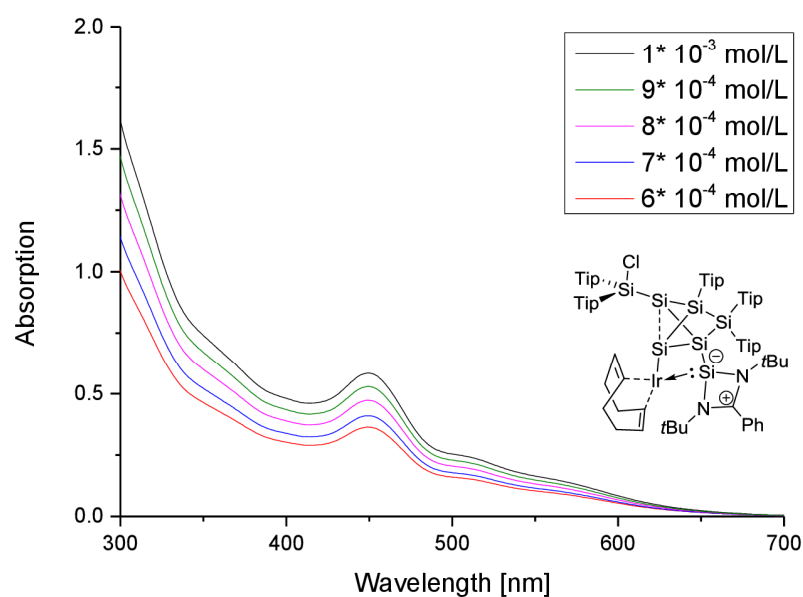
Supplementary Figure 2: ¹³C NMR spectrum of **2a** in C₆D₆ (100.61 MHz, 300 K).



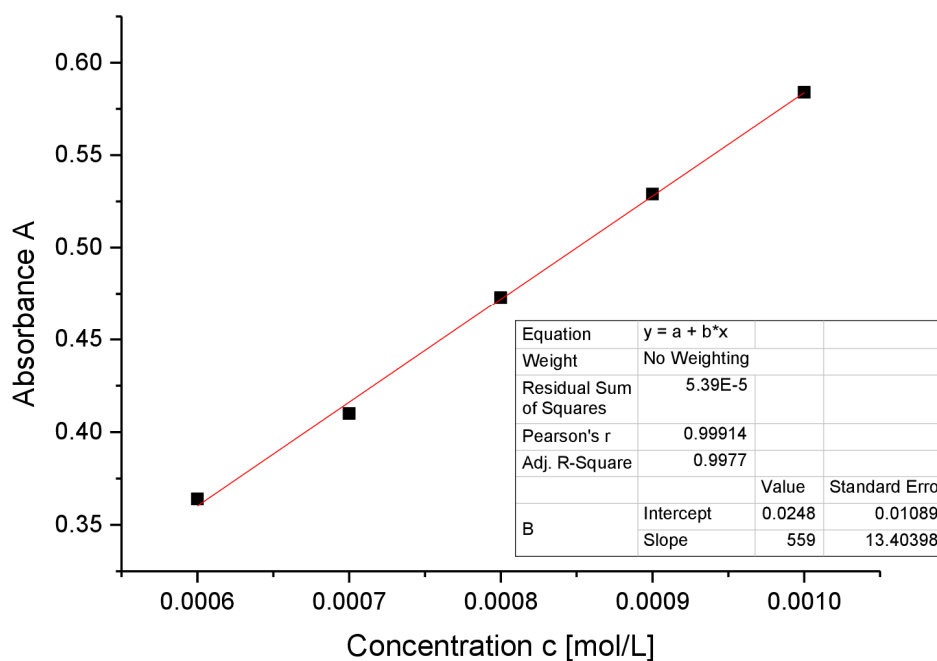
Supplementary Figure 3: ²⁹Si NMR spectrum of **2a** in C₆D₆ (79.49 MHz, 300 K).



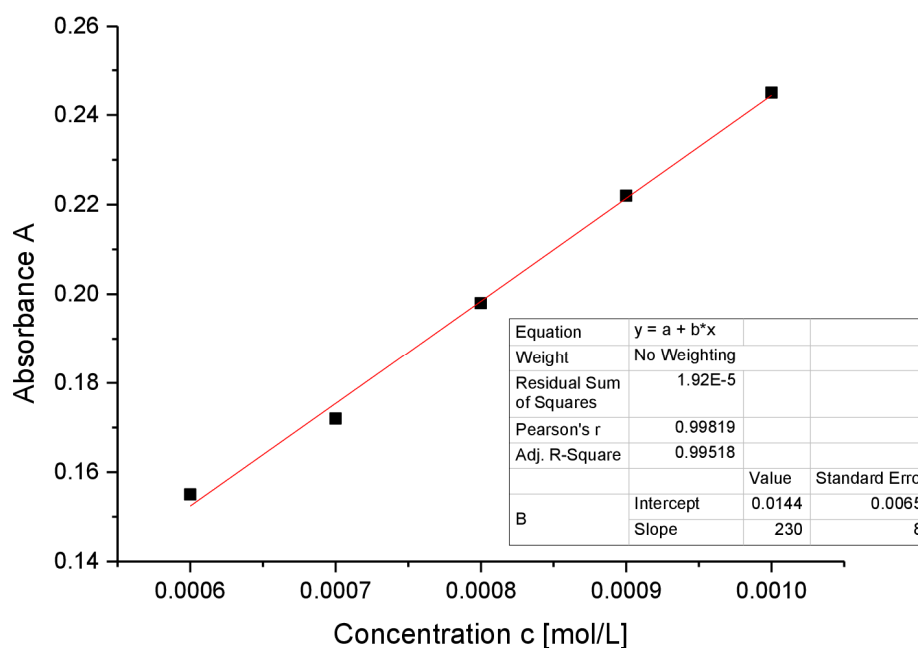
Supplementary Figure 4: CP MAS ^{29}Si NMR spectrum of **2a** (79.53 MHz, 13 KHz, 300 K), side spinning bands of: * SiTip_2 (55.3 ppm), # NHSi (32.9 ppm), + SiTip (-41.6 ppm), ° unsubstituted Si (-88.6 ppm), ~ unsubstituted Si (-126.8 ppm, -128.2 ppm).



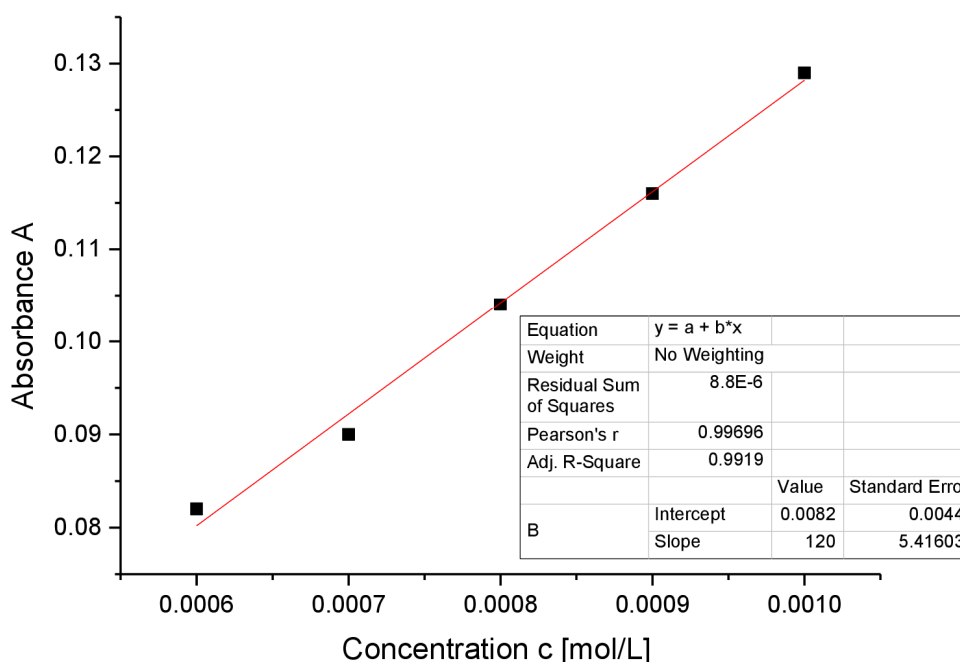
Supplementary Figure 5: UV-Vis spectrum of **2a** in hexane at different concentrations.



Supplementary Figure 6: Determination of ϵ ($5590 \text{ M}^{-1} \text{ cm}^{-1}$) by linear regression of absorptions ($\lambda = 449 \text{ nm}$) of **2a** against concentration.



Supplementary Figure 7: Determination of ϵ ($2300 \text{ M}^{-1} \text{ cm}^{-1}$) by linear regression of absorptions ($\lambda = 508 \text{ nm}$) of **2a** against concentration.



Supplementary Figure 8: Determination of ε ($1200 \text{ M}^{-1} \text{ cm}^{-1}$) by linear regression of absorptions ($\lambda = 576 \text{ nm}$) of **2a** against concentration.

(5-(Chlorobis(2,4,6-triisopropylphenyl)silyl)-2-(1,3-di-*tert*-butyl-4-phenyl-1,3,2 λ^3 -diazagermet-1-ium-2(3*H*)-yl)-3,3,4-tris(2,4,6-triisopropylphenyl)tricyclo [2.1.0.0^{2,5}]pentasilane-1-yl-iridium (2b**)**

Quantities: Si₆NHGe **1b**, 500 mg (0.327 mmol), [(cod)IrCl]₂ 140.92 mg (0.21 mmol), benzene 10 mL, filtration two times from hexane 8 mL each, crystallization from hexane at -26 °C. Yield: 362 mg (0.198 mmol; 61 %) violet-brown crystals (mp. 154 °C, dec.).

¹H-NMR (400.13 MHz, C₆D₆, 300 K) δ = 7.375 (bs, 1H, Ar-H), 7.164 – 7.141 (m, 7H, Ar-H overlapping with C₆D₆), 7.047 – 6.907 (m, 7H, Ar-H), 6.871 – 6.814 (m, 3H, Ar-H), 6.753 (bs, 1H, Ar-H), 5.829 (sept, 1H, ³J_{HH} = 6.36 Hz, Tip-*i*Pr-CH₂), 5.156 (sept, 1H, ³J_{HH} = 6.89 Hz, Tip-*i*Pr-CH₂), 4.918 (sept, 1H, ³J_{HH} = 6.97 Hz, Tip-*i*Pr-CH₂), 4.641 (bs, 1H, Tip-*i*Pr-CH₂), 4.468 (m, 3H, Tip-*i*Pr-CH₂), 3.867 (sept, 1H, ³J_{HH} = 6.42 Hz, Tip-*i*Pr-CH₂), 3.575 (sept, 1H, ³J_{HH} = 6.42 Hz, Tip-*i*Pr-CH₂), 3.192 (sept, 1H, ³J_{HH} = 6.42 Hz, Tip-*i*Pr-CH₂), 2.849 – 2.576 (m, 7H, Tip-*i*Pr-CH₂), 2.329 (bs, 2H, Tip-*i*Pr-CH₂), 2.103, 2.051, 2.001 (each d, together 12H, each ³J_{HH} = 6.34 Hz, Tip-*i*Pr-CH₃), 1.927 (d, 4H, ³J_{HH} = 6.67 Hz, Tip-*i*Pr-CH₃), 1.840 (d, ³J_{HH} = 6.67 Hz, Tip-*i*Pr-CH₃), 1.793, 1.755 (each d, together 6H, each ³J_{HH} = 6.67 Hz, Tip-*i*Pr-CH₃), 1.605 – 1.506 (m, 16H, Tip-*i*Pr-CH₃), 1.390 (d, 3H, ³J_{HH} = 6.61 Hz, Tip-*i*Pr-CH₃), 1.352 (d, 3H, ³J_{HH} = 6.61 Hz, Tip-*i*Pr-CH₃), 1.299 – 1.136 (m, 37H, Tip-*i*Pr-CH₃), 1.087 – 1.066 (m, 6H, Tip-*i*Pr-CH₃), 0.889 (dd, 6H, ³J_{HH} = 6.55 Hz, Tip-*i*Pr-CH₃), 0.783 (s, 9H, C(CH₃)₃), 0.710 (d, 3H, ³J_{HH} = 6.59 Hz, Tip-*i*Pr-CH₃), 0.674 (d, 3H, ³J_{HH} = 6.59 Hz, Tip-*i*Pr-CH₃), 0.581 – 0.567 (m, 12H, Tip-*i*Pr-CH₃ overlapping with C(CH₃)₃), 0.484 (d, 3H, ³J_{HH} = 6.59 Hz, Tip-*i*Pr-CH₃), 0.441 (d, 3H, ³J_{HH} = 6.59 Hz, Tip-*i*Pr-CH₃), 0.301 (d, 3H, ³J_{HH} = 6.27 Hz, Tip-*i*Pr-CH₃), 0.176 (d, 3H, ³J_{HH} = 6.27 Hz, Tip-*i*Pr-CH₃) ppm.

¹³C-NMR (100.61 MHz, C₆D₆, 300 K) δ = 169.08 (s, 1C, C-Ph), 156.22, 155.45, 154.58, 154.41, 154.13, 153.71, 153.60, 153.29, 152.83 (s, each 1C, Ar-C), 150.35, 150.22, 150.02, 148.94, 148.04 (s, each 1C, Ar-C), 142.89 (s, 1C, Ar-C), 140.71 (s, 1C, Ar-C), 137.58, 135.81, 134.98, 134.06 (s, each 1C, Ar-C), 130.99 (s, 1C, Ar-C), 129.79,

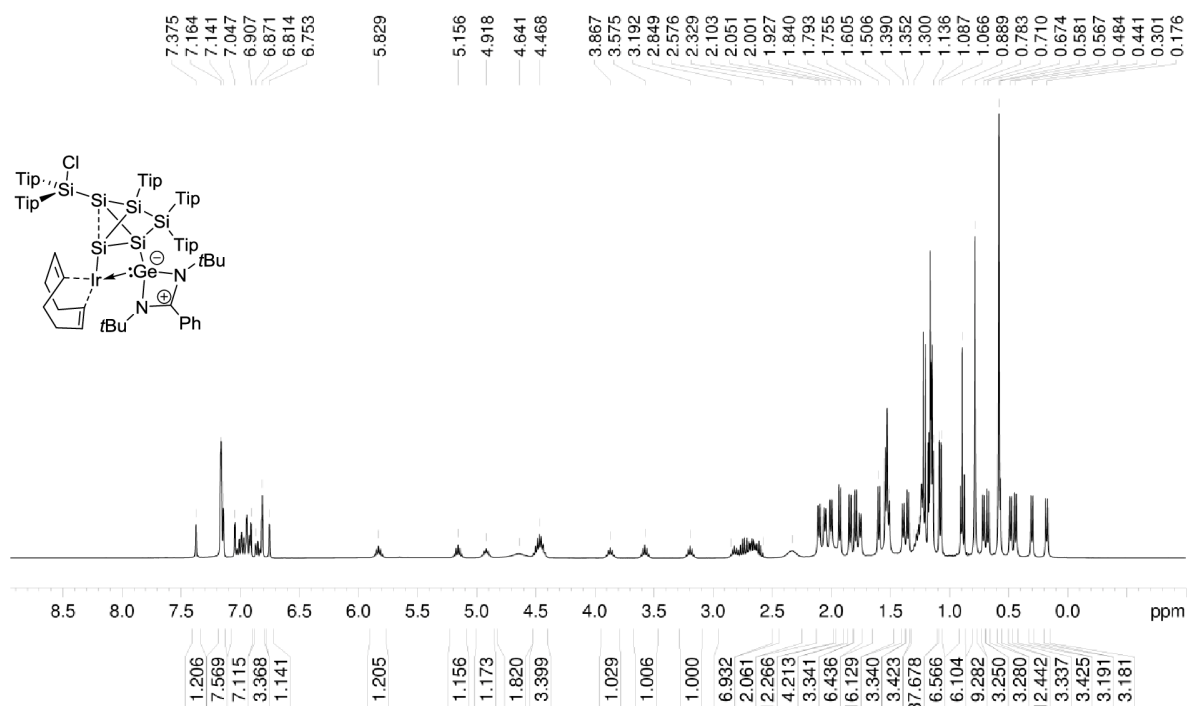
129.5 (s, each 1C, Ar-CH), 128.14, 127.89 (s, each 1C, Ar-CH overlapping with C₆D₆), 127.34, 127.24 (s, each 1C, Ar-CH), 123.66, 123.53, 123.43, 123.16, 122.94, 122.70, 122.40, 121.94 (s, each 1C, Ar-CH), 120.67 (s, 1C, Ar-CH), 54.06 (s, 1C, C(CH₃)₃), 53.63 (s, 1C, C(CH₃)₃), 38.47 (s, 1C, Tip-*i*Pr-CH), 36.38 (bs, 1C, Tip-*i*Pr-CH), 35.93, 35.75, 35.65 (s, each 1C, Tip-*i*Pr-CH), 34.79, 34.75, 34.71 (bs, each 1C, Tip-*i*Pr-CH), 34.60, 34.39, 34.34 (s, each 1C, Tip-*i*Pr-CH), 33.94, 33.76 (s, each 1C, Tip-*i*Pr-CH), 32.57 (s, 1C, Tip-*i*Pr-CH), 31.97 (s, 1C, Tip-*i*Pr-CH), 31.92 (s, 1C, Tip-*i*Pr-CH), 31.75 (s, 1C, Tip-*i*Pr-CH), 31.21 (s, 1C, Tip-*i*Pr-CH), 30.37, 29.89 (s, each 1C, Tip-*i*Pr-CH₃), 29.68 (bs, 1C, Tip-*i*Pr-CH₃), 29.25, 28.51, 27.43 (s, each 1C, Tip-*i*Pr-CH₃), 26.00, 25.89, 25.65 (s, each 1C, Tip-*i*Pr-CH₃), 25.11, 24.83 (s, each 1C, Tip-*i*Pr-CH₃), 24.72, 24.55, 24.48, 24.43, 24.36, 24.30 (s, each 1C, Tip-*i*Pr-CH₃), 24.19, 24.17 (bs, each 1C, Tip-*i*Pr-CH₃), 24.07, 24.03, 23.97, 23.92 (bs, each 1C, Tip-*i*Pr-CH₃), 23.77, 23.74 (s, each 1C, Tip-*i*Pr-CH₃), 23.20, (s, 1C, Tip-*i*Pr-CH₃), 23.01 (s, 1C, Tip-*i*Pr-CH₃), 22.51, 22.48 (bs, each 1C, Tip-*i*Pr-CH₃), 14.32 (s, 1C, Tip-*i*Pr-CH₃) ppm.

²⁹Si-NMR (79.49 MHz, C₆D₆, 300 K) δ = 54.6 (s, SiTip₂), 12.8 (s, SiTip₂Cl), -41.6 (s, SiTip), -90.5 (s, Si1), -91.3 (s, Si-NHGe), -121.6 (s, Si-Ir) ppm.

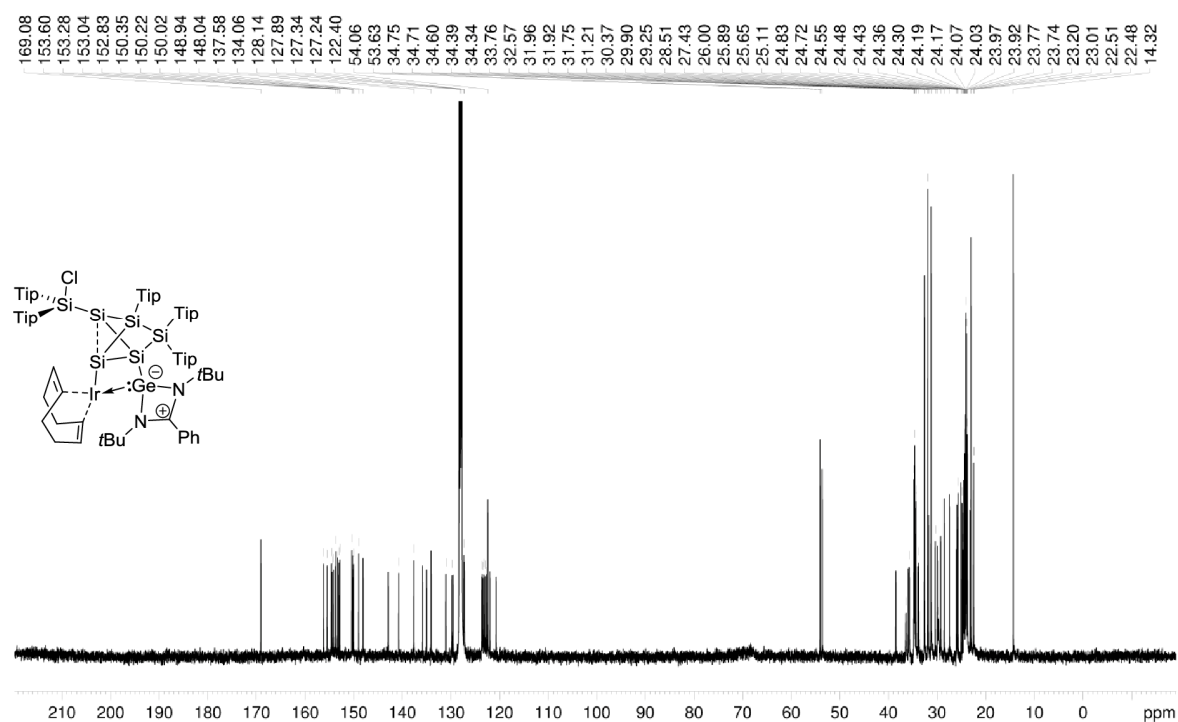
CP-MAS ²⁹Si-NMR (79.53 MHz, 14KHz, 300K) δ = 52.6 (s, SiTip₂), 12.3 (s, SiTip₂Cl), -41.5 (d, SiTip), -90.0 (s, Si-NHGe), -90.8 (s, unsubstituted Si), -121.7 (s, unsubstituted Si) ppm.

Elemental analysis: calculated for C₉₇H₁₄₆ClGeIrN₂Si₆: C: 64.40 % ; H: 8.14 % ; N: 1.55 %. Found: C: 64.68 % ; H: 8.18 % ; N: 1.35 %.

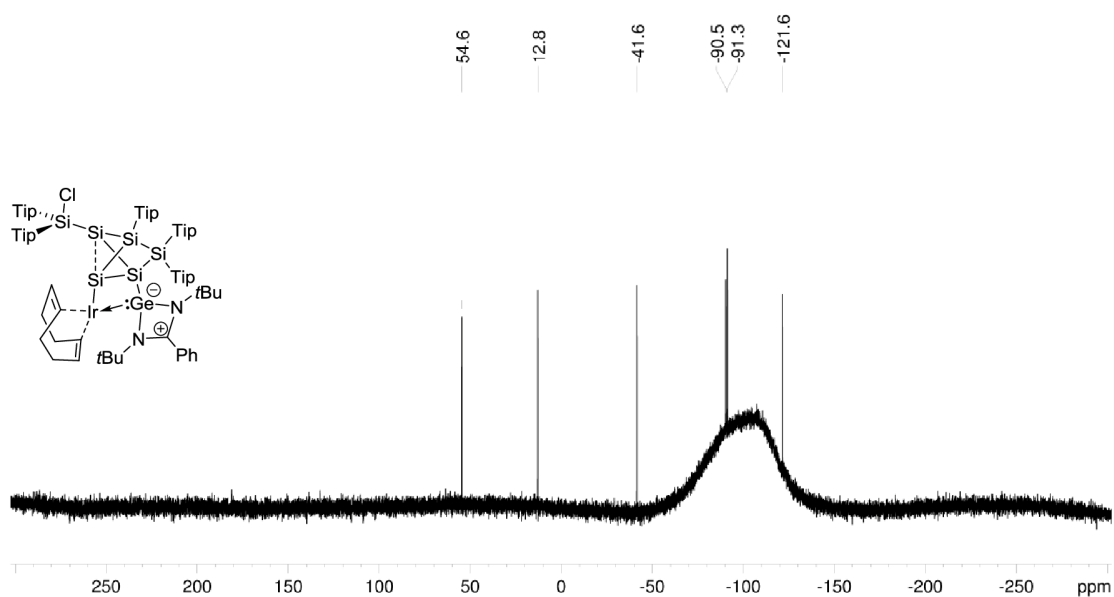
UV/VIS (hexane): λ_{\max} (ϵ) = 580 nm (2500 M⁻¹ cm⁻¹).



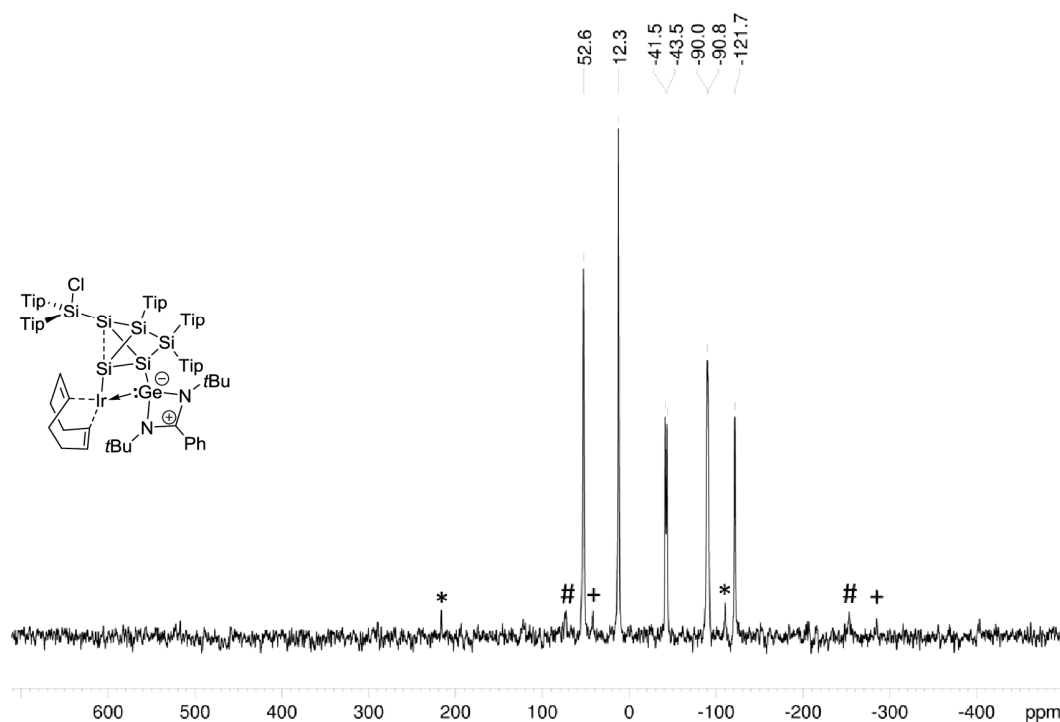
Supplementary Figure 9: ¹H NMR spectrum of **2b** in C₆D₆ (400.13 MHz, 300 K).



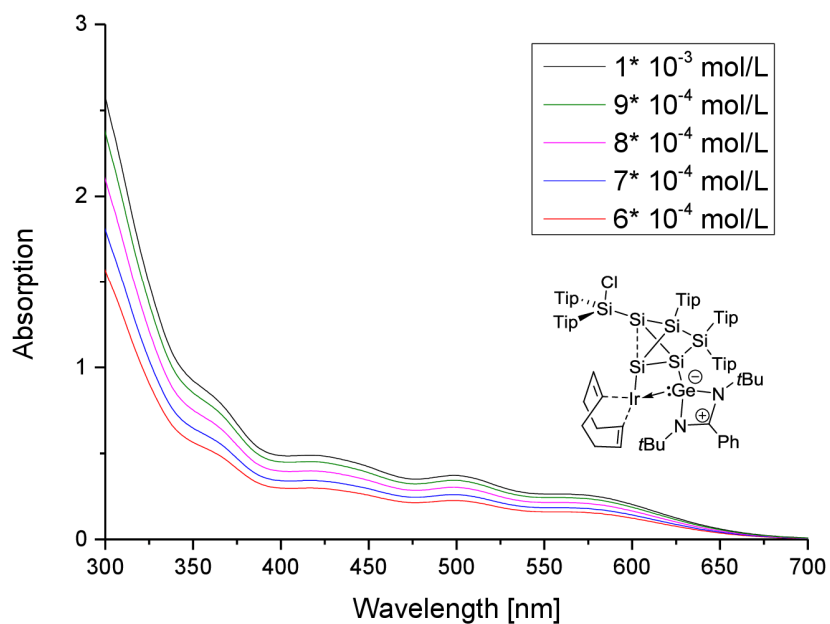
Supplementary Figure 10: ¹³C NMR spectrum of **2b** in C₆D₆ at (100.61 MHz, 300 K).



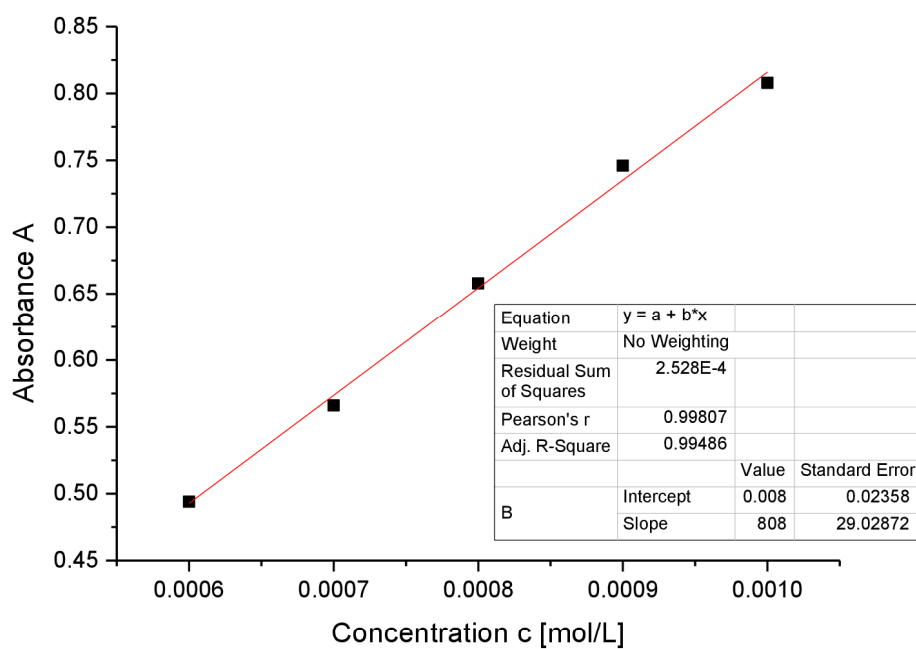
Supplementary Figure 11: ²⁹Si NMR spectrum of **2b** in C₆D₆ (79.49 MHz, 300 K).



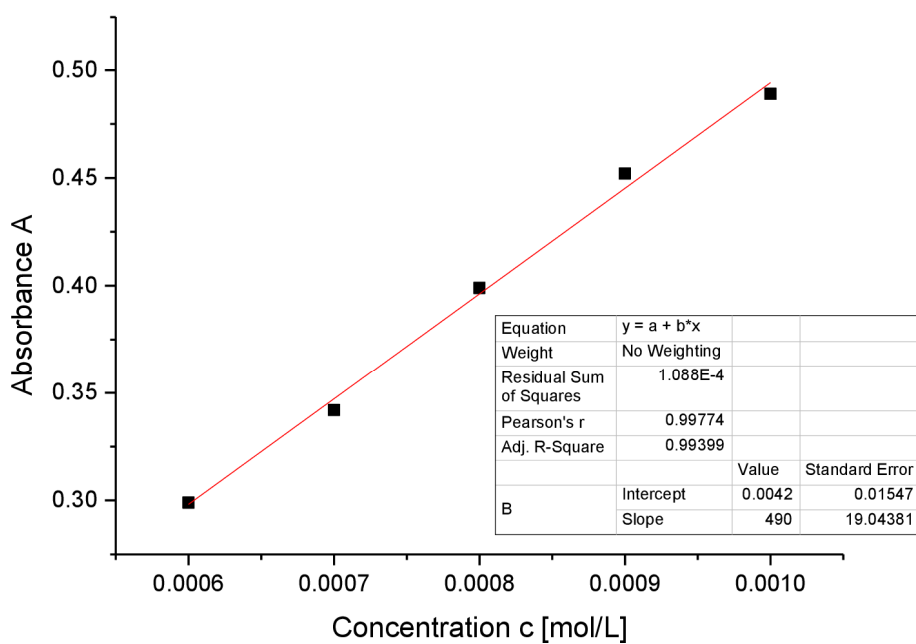
Supplementary Figure 12: CP MAS ^{29}Si NMR spectrum of **2b** (79.53 MHz, 13 KHz, 300 K), side spinning bands of: * SiTip₂ (52.6 ppm), # unsubstituted Si, Si-NHGe (-90.0 ppm, -90.8 ppm), + unsubstituted Si (-121.7 ppm).



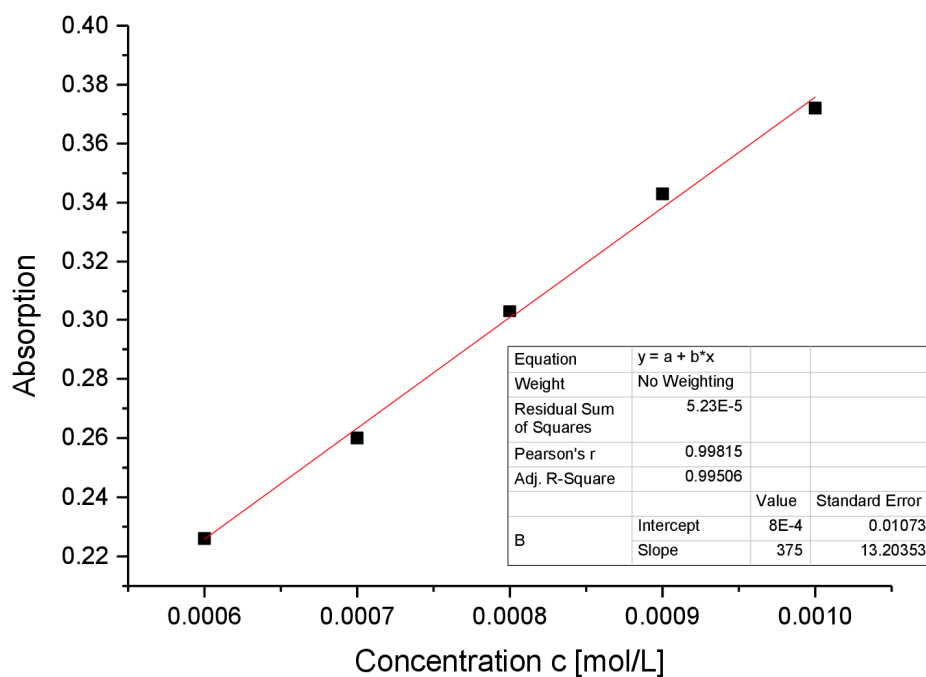
Supplementary Figure 13: UV-Vis spectrum of **2b** in hexane at different concentrations.



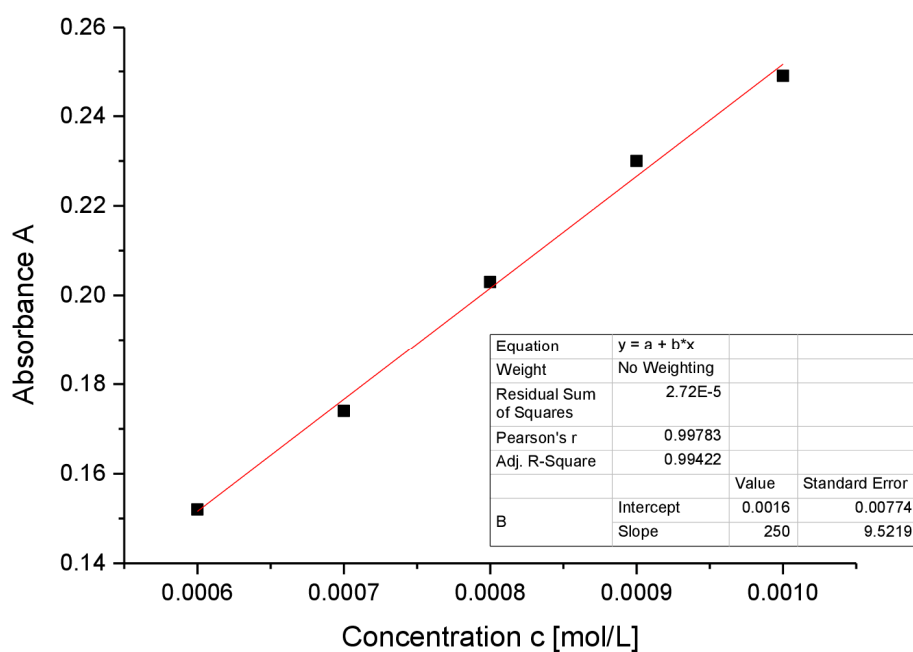
Supplementary Figure 14: Determination of ε ($8080 \text{ M}^{-1} \text{ cm}^{-1}$) by linear regression of absorptions ($\lambda = 364 \text{ nm}$) of **2b** against concentration.



Supplementary Figure 15: Determination of ε ($4900 \text{ M}^{-1} \text{ cm}^{-1}$) by linear regression of absorptions ($\lambda = 417 \text{ nm}$) of **2b** against concentration.



Supplementary Figure 16: Determination of ε ($3750 \text{ M}^{-1} \text{ cm}^{-1}$) by linear regression of absorptions ($\lambda = 499 \text{ nm}$) of **2b** against concentration.



Supplementary Figure 17: Determination of ε ($2500 \text{ M}^{-1} \text{ cm}^{-1}$) by linear regression of absorptions ($\lambda = 580 \text{ nm}$) of **2b** against concentration.

(5-(Chlorobis(2,4,6-triisopropylphenyl)silyl)-2-(1,3-di-*tert*-butyl-4-phenyl-1,3,2λ³-diazastannet-1-ium-2(3*H*)-yl)-3,3,4-tris(2,4,6-triisopropylphenyl)tricyclo [2.1.0.0^{2,5}]pentasilane-1-yl)iridium (2c)

Quantities: Si₆NHSn **1c**, 400 mg (0.24 mmol), [(cod)IrCl]₂ 113.07 mg (0.168 mmol), benzene 10 mL, filtration from hexane 10 mL, crystallization from hexane. Yield: 284 mg (0.152 mmol ; 63 %) violet crystals (mp. 182 °C, dec.).

¹H-NMR (400.13 MHz, C₆D₆, 300 K) δ = 7.637 – 7.613 (C₁₀H₈), 7.364 – 7.237 (m, 1H, Ar-H), 7.261 – 7.237 (C₁₀H₈), 7.157 – 7.7126 (m, 8H, Ar-H overlapping with C₆D₆), 7.050 – 7.863 (m, 9H, Ar-H), 6.809 (bs, 2H, Ar-H), 6.709 – 6.705 (m, 1H, Ar-H), 5.841 (sept, 1H, ³J_{HH} = 6.41 Hz, Tip-*i*Pr-CH₂), 5.122 (sept, 1H, ³J_{HH} = 6.52 Hz, Tip-*i*Pr-CH₂), 4.947 – 4.862 (m, 3H, Tip-*i*Pr-CH₂), 4.681 (sept, 1H, ³J_{HH} = 6.41 Hz, Tip-*i*Pr-CH₂), 4.467 – 4.359 (m, 2H, Tip-*i*Pr-CH₂), 3.908 (sept, 1H, ³J_{HH} = 6.74 Hz, Tip-*i*Pr-CH₂), 3.449 (sept, 1H, ³J_{HH} = 6.81 Hz, Tip-*i*Pr-CH₂), 3.148 (sept, 1H, ³J_{HH} = 6.43 Hz, Tip-*i*Pr-CH₂), 2.826 – 2.592 (m, 7H, Tip-*i*Pr-CH₂), 2.133 (d, 3H, ³J_{HH} = 6.58 Hz, Tip-*i*Pr-CH₃), 2.070 (d, 3H, ³J_{HH} = 6.32 Hz, Tip-*i*Pr-CH₃), 1.931 (t, 7 H, ³J_{HH} = 6.58 Hz, Tip-*i*Pr-CH₃), 1.856 (d, 3H, ³J_{HH} = 6.58 Hz, Tip-*i*Pr-CH₃), 1.814 (d, 3H, ³J_{HH} = 6.58 Hz, Tip-*i*Pr-CH₃), 1.728 (d, 3H, ³J_{HH} = 6.58 Hz, Tip-*i*Pr-CH₃), 1.609 (d, 4H, ³J_{HH} = 6.54 Hz, Tip-*i*Pr-CH₃), 1.550 – 1.526 (m, 7H, Tip-*i*Pr-CH₃), 1.475 (d, 4H, ³J_{HH} = 6.54 Hz, Tip-*i*Pr-CH₃), 1.376 (d, 4H, ³J_{HH} = 6.54 Hz, Tip-*i*Pr-CH₃), 1.332 (d, 4H, ³J_{HH} = 6.54 Hz, Tip-*i*Pr-CH₃), 1.277 – 1.083 (m, 44 H, Tip-*i*Pr-CH₃), 0.888 (t, hexane), 0.735 – 0.688 (m, 16H, Tip-*i*Pr-CH₃) overlapping with C(CH₃)₃), 0.580 – 0.567 (m, 12H, Tip-*i*Pr-CH₃) overlapping with C(CH₃)₃), 0.524 (d, 3H, ³J_{HH} = 6.51 Hz, Tip-*i*Pr-CH₃), 0.456 (d, 3H, ³J_{HH} = 6.51 Hz, Tip-*i*Pr-CH₃), 0.310 (d, 3H, ³J_{HH} = 6.51 Hz, Tip-*i*Pr-CH₃), 0.179 (d, 3H, ³J_{HH} = 6.51 Hz, Tip-*i*Pr-CH₃) ppm.

¹³C-NMR (100.61 MHz, C₆D₆, 300 K) δ = 170.51 (s, 1C, C-Ph), 156.34, 155.42, 154.84, 154.60, 154.25, 154.06, 153.66, 153.42, 152.67 (s, each 1C, Ar-C), 150.47, 150.14, 150.06, 149.04, 148.01 (s, each 1C, Ar-C), 141.45, 139.90, 136.96, 136.21, 135.42, 134.38 (s, each 1C, Ar-C), 130.41, 129.87, 129.10 (s, each 1C, Ar-CH), 128.11, 127.87 (s, each 1C, overlapping with C₆D₆, Ar-CH), 127.29, 127.13 (bs, each 1C, Ar-CH), 126.00 (s, 1C, Ar-CH), 123.76, 123.49, 123.14, 122.98, 122.38, 122.29, 122.18, 121.81, 120.42 (s, each 1C, Ar-CH), 53.35 (s, 1C, C(CH₃)₃), 52.82 (s, 1C, C(CH₃)₃), 38.54 (s, 1C, Tip-*i*Pr-CH), 36.11, 35.95 (s, each 1C, Tip-*i*Pr-CH), 35.17 (s, 1C, Tip-*i*Pr-CH), 34.80, 34.71, 34.62, 34.58, 34.38, 34.29, 34.15, 34.07 (bs, each 1C, Tip-*i*Pr-CH), 32.34 (s, 1C, Tip-*i*Pr-CH), 31.91, 31.89 (bs, overlapping, together 2C, Tip-*i*Pr-CH), 31.16 (s, 1C, Tip-*i*Pr-CH), 29.97, 29.77 (s, each 1C, Tip-*i*Pr-CH₃), 28.16, 27.76 (s, each 1C, Tip-*i*Pr-CH₃), 26.21, 25.89, 25.73, 25.60, 25.24, 25.06, 24.87 (s, each 1C, Tip-*i*Pr-CH₃), 24.52, 254.40, 24.30, 24.15, 23.99, 23.88, 23.80, 23.77 (bs, each 1C, Tip-*i*Pr-CH₃), 23.50 (s, 1C, Tip-*i*Pr-CH₃), 23.19 (s, 1C, Tip-*i*Pr-CH₃), 23.00 (s, 1C, Tip-*i*Pr-CH₃), 22.71, 22.21 (s, 1C, Tip-*i*Pr-CH₃), 14.3 (s, 1C, Tip-*i*Pr-CH₃) ppm.

²⁹Si-NMR (79.49 MHz, C₆D₆, 300 K) δ = 50.2 (s, SiTip₂), 12.2 (s, SiTip₂Cl), -42.1 (s, SiTip), -80.4 (s, Si1), -95.6 (s, Si-NHSn), -116.0 (s, Si-Ir) ppm.

¹¹⁹Sn-NMR (149.21 MHz, C₆D₆, 300 K) δ = 180.3 (s) ppm.

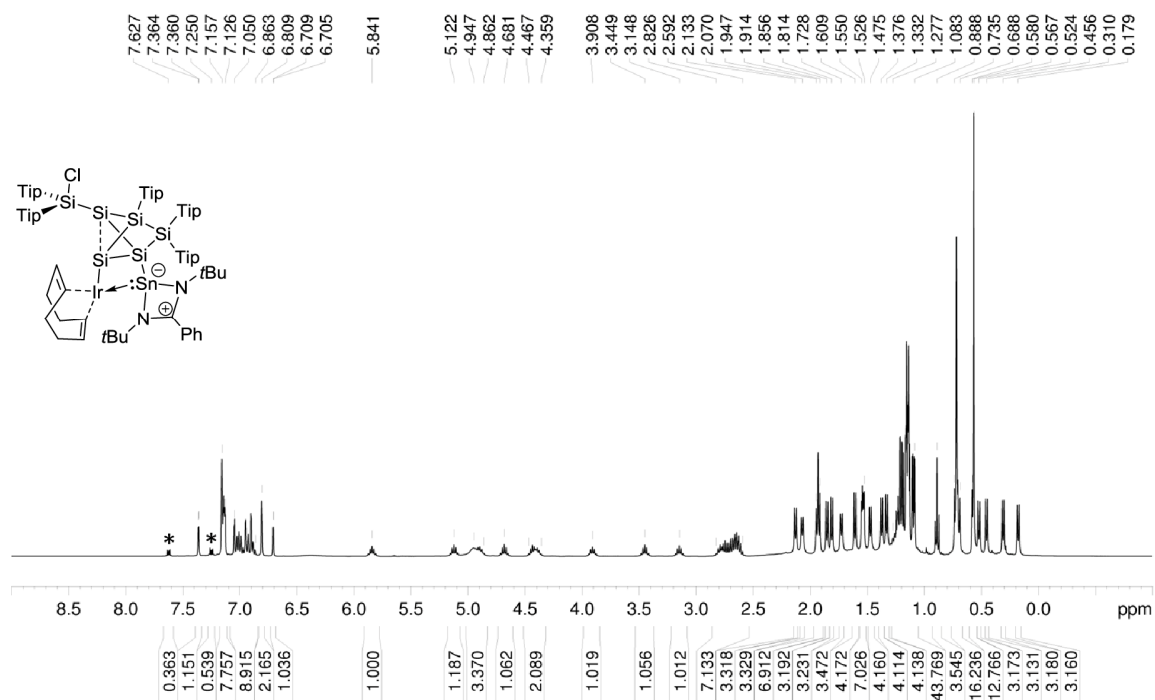
CP-MAS ²⁹Si-NMR (79.53 MHz, 14KHz, 300K) δ = 50.6 (s, SiTip₂), 42.4 (s, SiTip₂), 10.3 (s, SiTip), -42.2 (s, SiTip₂), -43.5 (s, SiTip₂), -68.1 (bs, Si-NHSn), -77.0 (bs, Si-NHSn), -94.6 (bs, unsubstituted-Si), -103.8 (s, unsubstituted-Si), -120.2 (s, unsubstituted-Si) ppm.

CP-MAS ¹¹⁹Sn-NMR (149.27 MHz, 13KHz, 300K) δ = 204.2 (s), 181.7 (s) ppm.

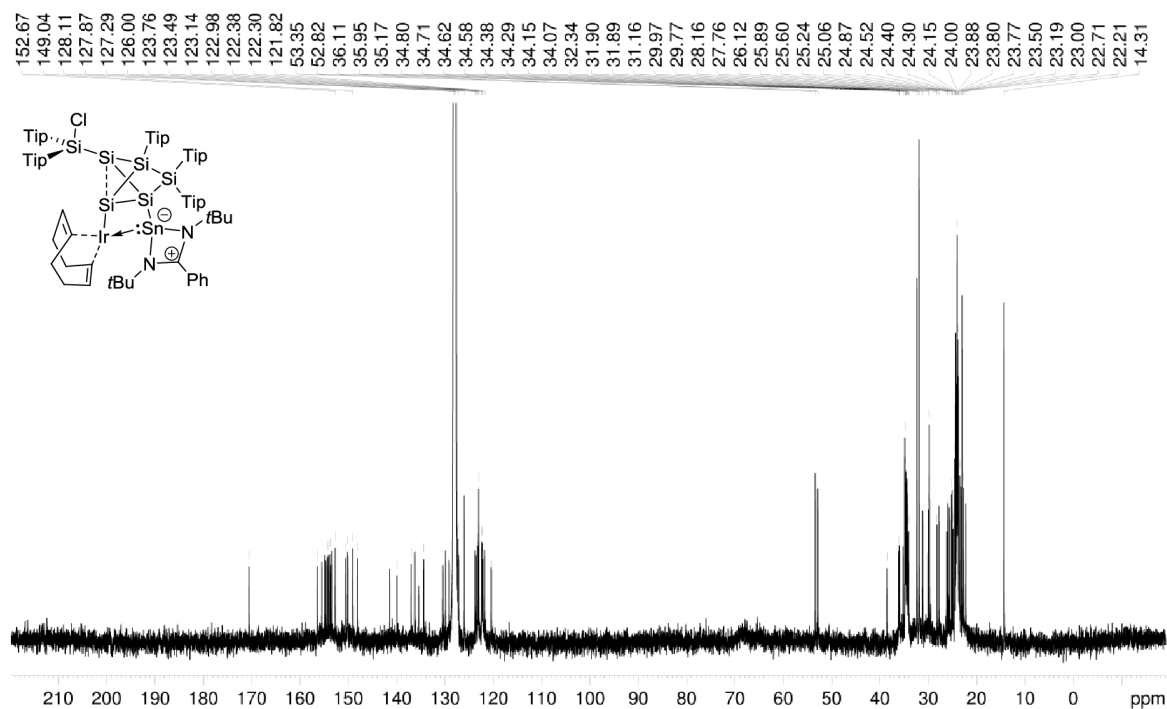
CP-MAS ¹¹⁹Sn-NMR (149.27 MHz, 11KHz, 300K) δ = 204.9 (s), 182.6 (s) ppm.

Elemental analysis: calculated for C₉₇H₁₄₆ClIrN₂Si₆Sn: C: 62.80 % ; H: 7.93 % ; N: 1.51 %. Found: C: 62.59 % ; H: 8.02 % ; N: 1.42 %.

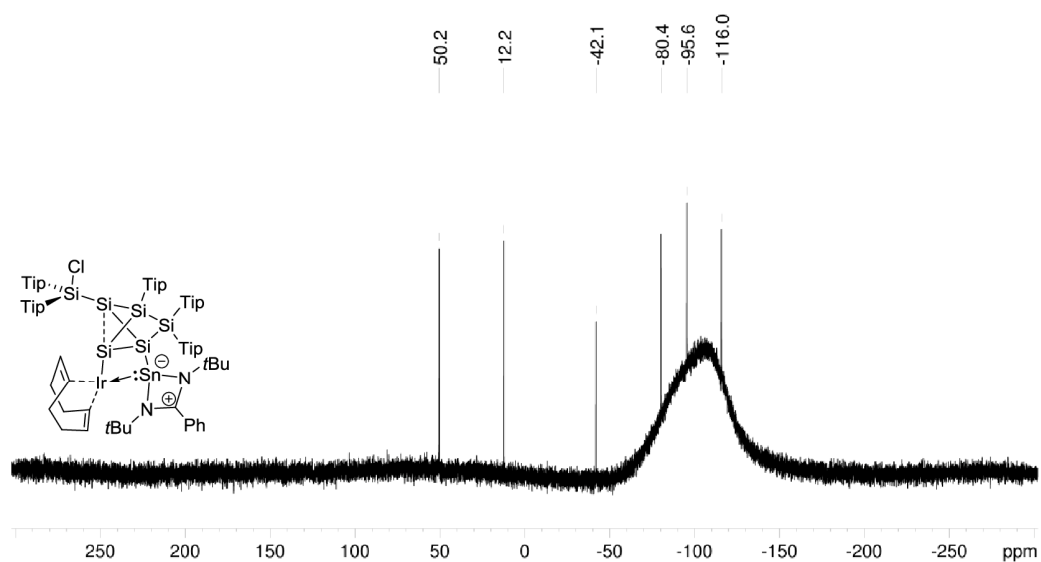
UV/VIS (hexane): λ_{\max} (ϵ) = 592 nm (2660 M⁻¹ cm⁻¹).



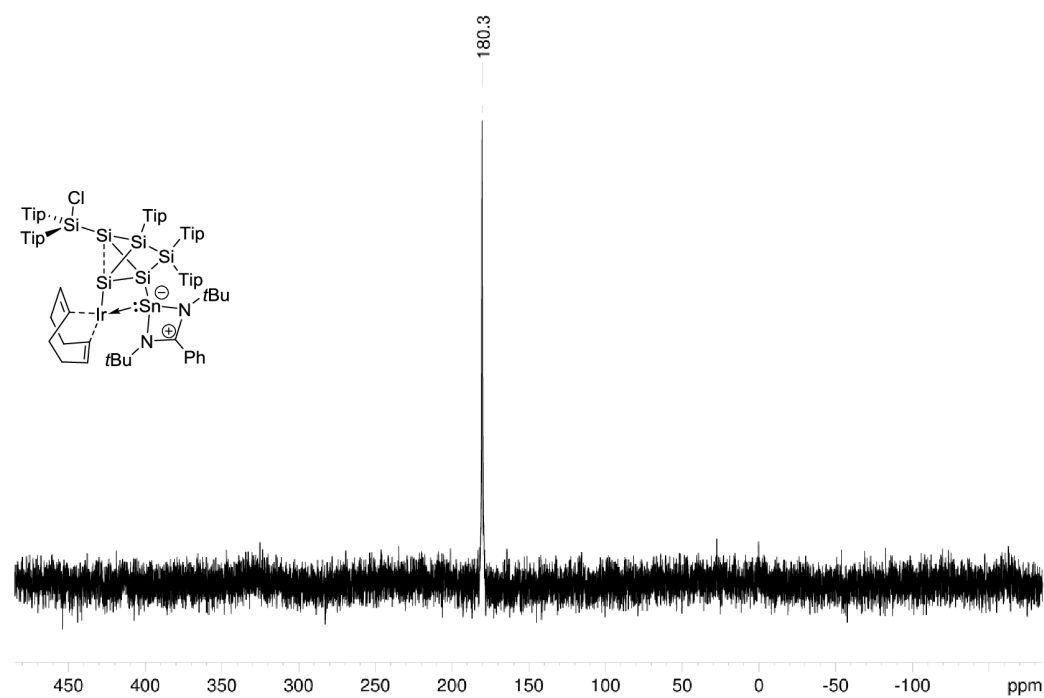
Supplementary Figure 18: ¹H NMR spectrum of **2c** in C₆D₆ (400.13 MHz, 300 K). Residual naphthalene (C₁₀H₈) marked with asterisk (*).



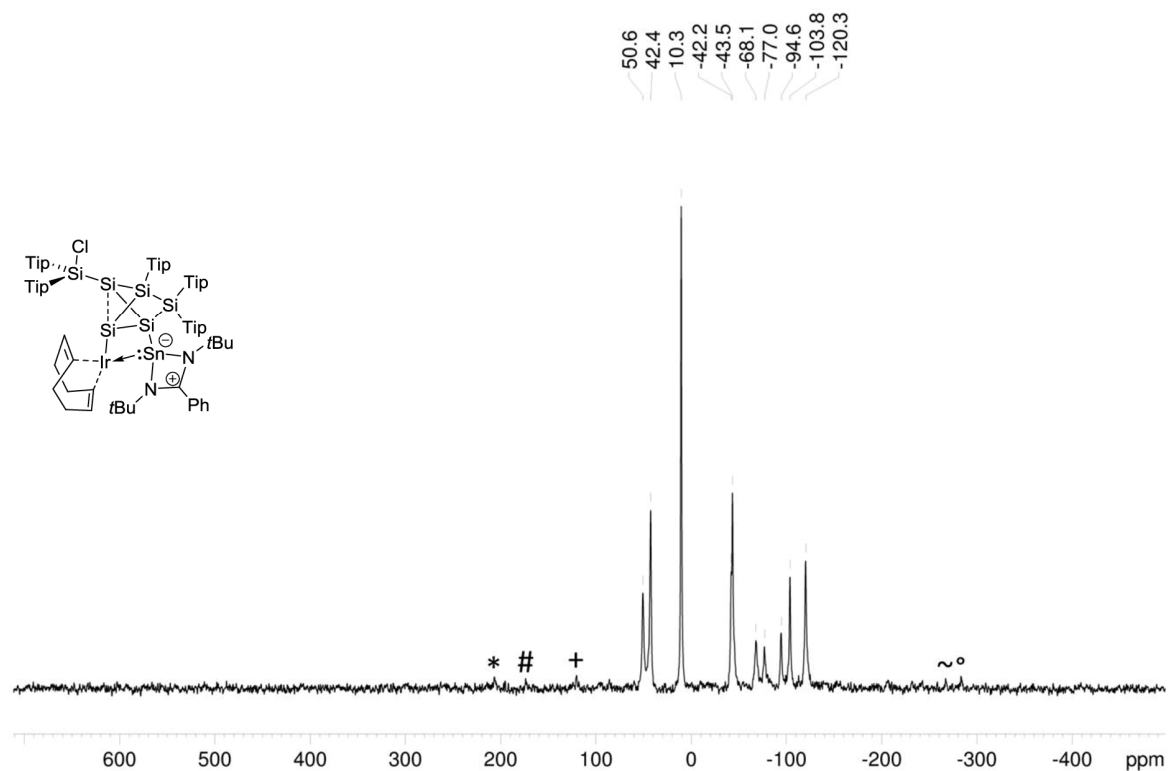
Supplementary Figure 19: ¹³C NMR spectrum of **2c** in C₆D₆ (100.61 MHz, 300 K).



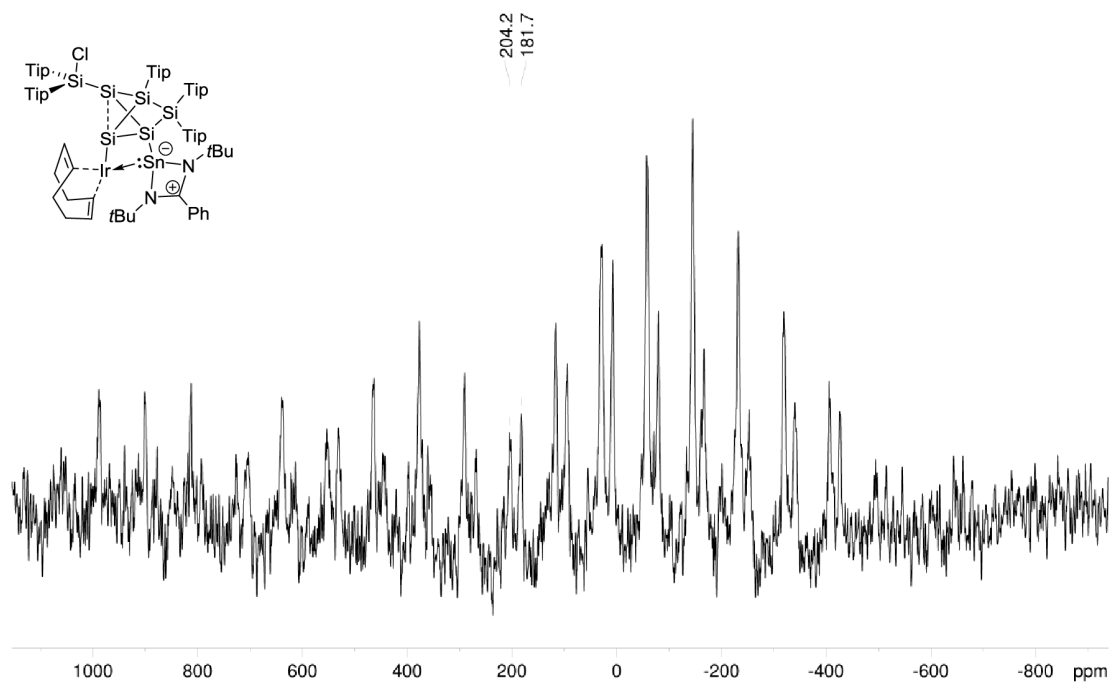
Supplementary Figure 20: ^{29}Si NMR spectrum of **2c** in C_6D_6 (79.49 MHz, 300 K).



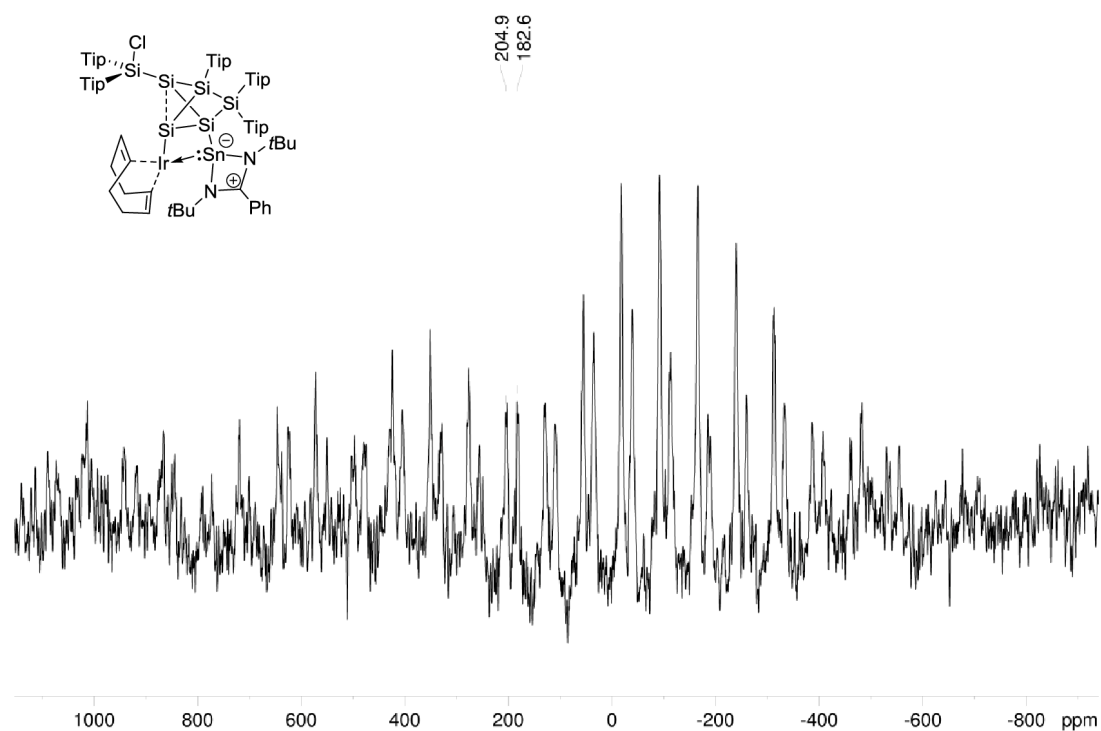
Supplementary Figure 21: ^{119}Sn NMR spectrum of **2c** in C_6D_6 (79.49 MHz, 300 K).



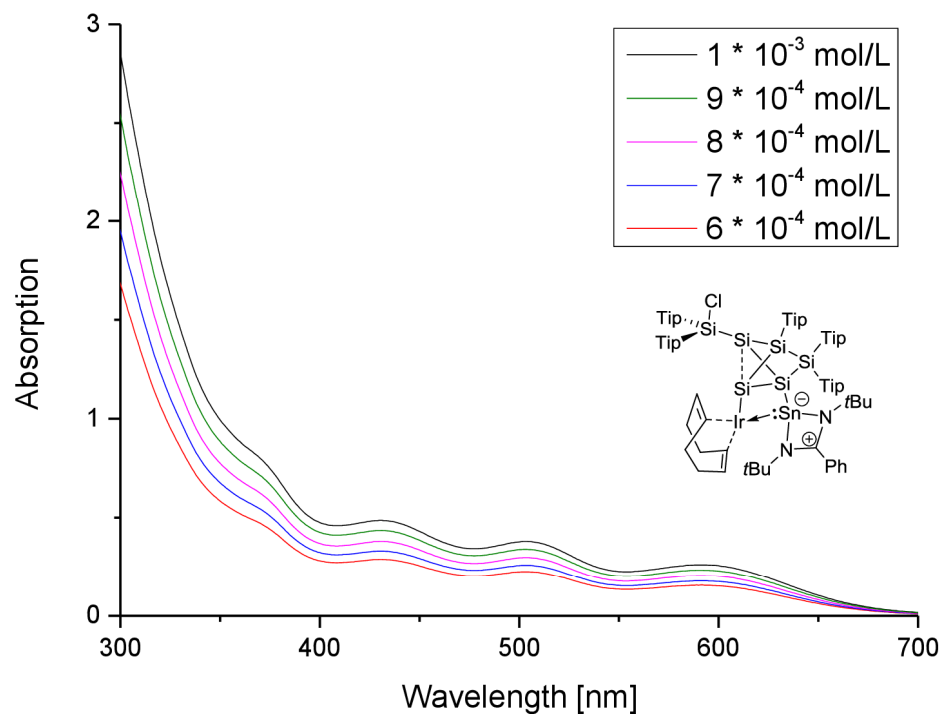
Supplementary Figure 22: CP MAS ^{29}Si NMR spectrum of **2c** (79.53 MHz, 13 KHz, 300 K), side spinning bands of: * SiTip₂ (42.4 ppm), # SiTip (10.3 ppm), + Si-NHSn (-68.1 ppm), ° unsubstituted Si (-120.3 ppm), ~ unsubstituted Si (-103.8 ppm).



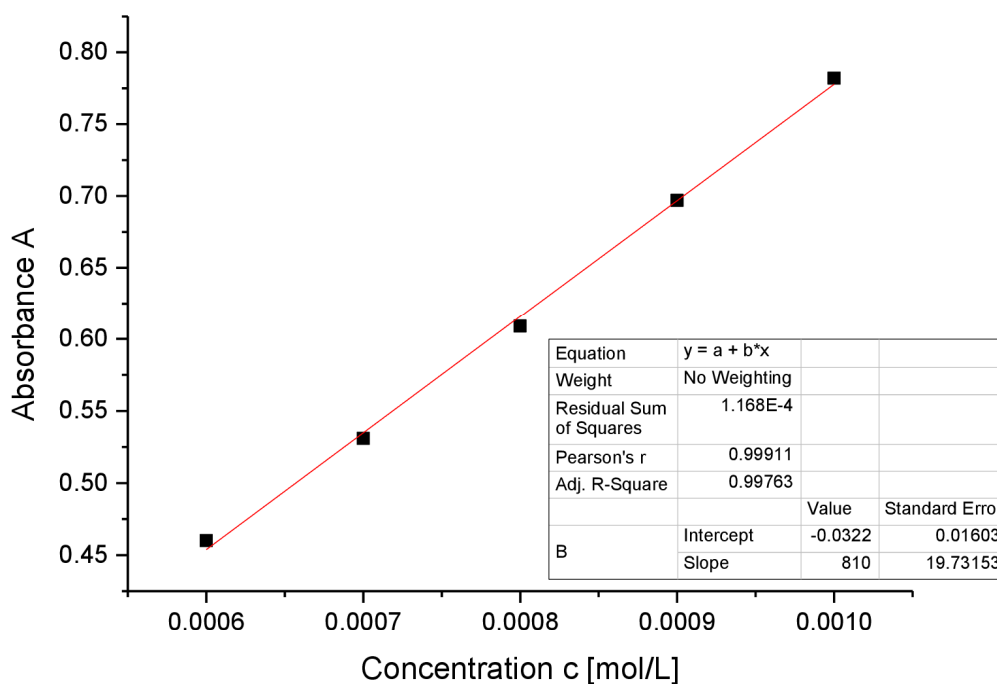
Supplementary Figure 23: CP MAS ^{119}Sn NMR spectrum of **2c** (149.27 MHz, 13 KHz, 300 K).



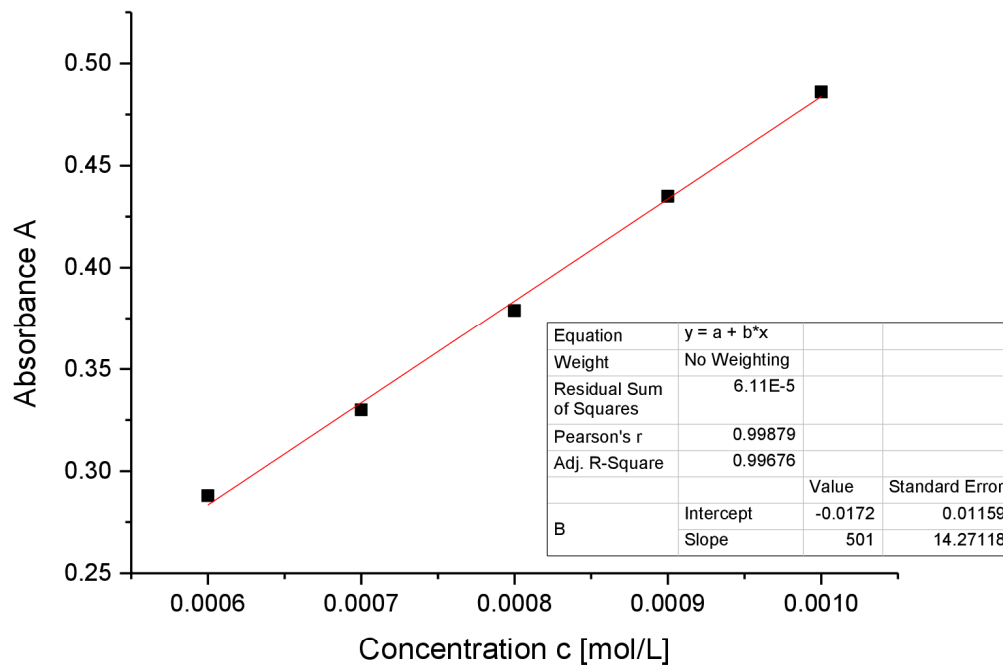
Supplementary Figure 24: CP MAS ^{119}Sn NMR spectrum of **2c** (149.27 MHz, 11 KHz, 300 K).



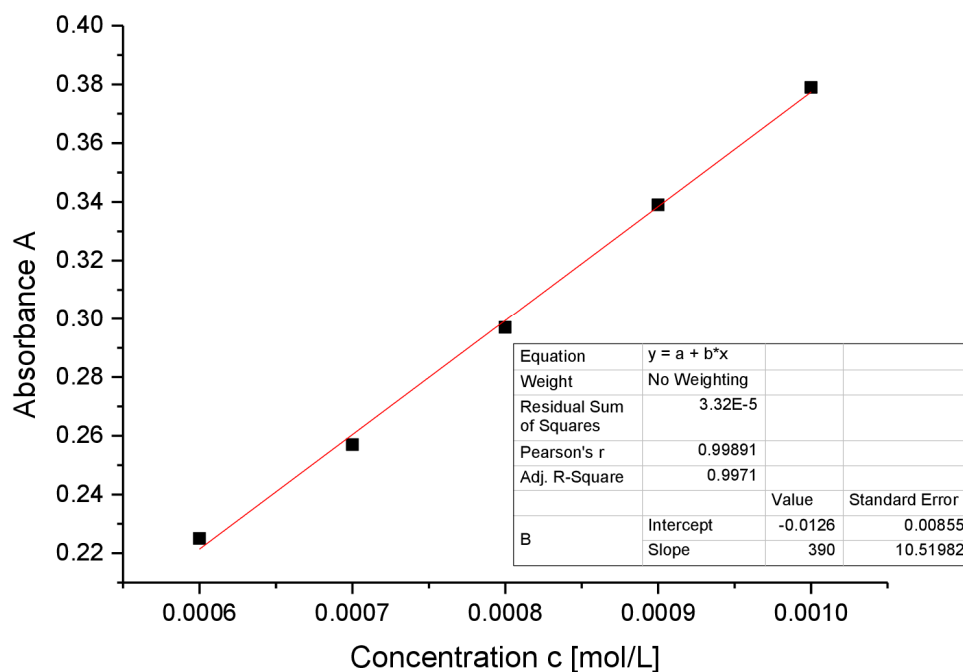
Supplementary Figure 25: UV-Vis spectrum of **2c** in hexane at different concentrations.



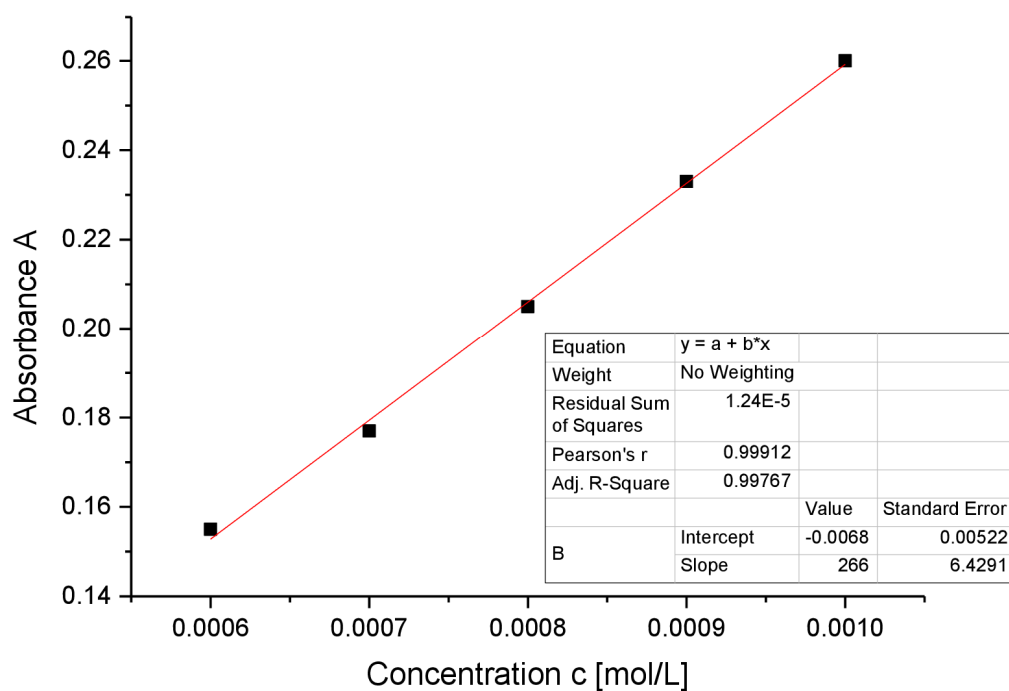
Supplementary Figure 26: Determination of ε ($8100 \text{ M}^{-1} \text{ cm}^{-1}$) by linear regression of absorptions ($\lambda = 372 \text{ nm}$) of **2c** against concentration.



Supplementary Figure 27: Determination of ε ($5010 \text{ M}^{-1} \text{ cm}^{-1}$) by linear regression of absorptions ($\lambda = 431 \text{ nm}$) of **2c** against concentration.



Supplementary Figure 28: Determination of ε ($3390 \text{ M}^{-1} \text{ cm}^{-1}$) by linear regression of absorptions ($\lambda = 504 \text{ nm}$) of **2c** against concentration.



Supplementary Figure 29: Determination of ε ($2660 \text{ M}^{-1} \text{ cm}^{-1}$) by linear regression of absorptions ($\lambda = 592 \text{ nm}$) of **2c** against concentration.

η^5 -((2-(Chloro- λ^2 -silyl)-4-(1,3-di-tert-butyl-4-phenyl-1,3,2-diazasilet-1-ium-2-id-2(3H)-yl)-1,1,2-tris(2,4,6-triisopropylphenyl)-1,2-dihydrotetrasilet-3-yl)bis(2,4,6-triisopropylphenyl)silyl) rhodium (3)

The silylene-substituted siliconoid **1a** (250 mg; 0.346 mmol) and 1 eq (67.29 mg; 0.346 mmol) of $[(\text{CO})_2\text{RhCl}]_2$ were dissolved in 2 mL toluene and stirred for three minutes. The red-brown solution was directly stored at -26°C for crystallization overnight. The mother liquor was removed by cannula and the crystals washed twice with 3 mL toluene each to yield red crystals of **3** (155 mg; 0.09621 mmol) in 56 % yield (mp. 178°C , dec.).

$^1\text{H-NMR}$ (400.13 MHz, C_6D_6 , 300 K) δ = 7.379 (bs, 1H, Ar-H), 7.176 – 7.152 (m, 6H, Ar-H overlapping with C_6D_6), 7.125 – 7.100 (m, 3H, Ar-H), 7.062 (bs, 1H, Ar-H), 7.039 – 6.967 (m, 5H, Ar-H), 6.586 (sept, 1H, $^3J_{\text{HH}} = 6.30$ Hz, Tip-*i*Pr-CH₂), 4.852, 4.685 (each sept, together 4H, $^3J_{\text{HH}} = 5.86$ Hz Tip-*i*Pr-CH₂), 4.227 (sept, 1H, $^3J_{\text{HH}} = 6.55$ Hz, Tip-*i*Pr-CH₂), 3.992 (sept, 1H, $^3J_{\text{HH}} = 6.55$ Hz, Tip-*i*Pr-CH₂), 3.799 – 3.724 (m, 2H, Tip-*i*Pr-CH₂), 3.368 (sept, 1H, $^3J_{\text{HH}} = 6.40$ Hz, Tip-*i*Pr-CH₂), 2.840 – 2.585 (m, 5H, Tip-*i*Pr-CH₂), 2.107 – 1.988 (m, 12H, Tip-*i*Pr-CH₃ overlapping with toluene), 1.707 – 1.643 (m, 11H, Tip-*i*Pr-CH₃), 1.540 – 1.524 (m, 7H, Tip-*i*Pr-CH₃), 1.483 – 1.444 (m, 11H, Tip-*i*Pr-CH₃), 1.241 – 1.116 (m, 35H, Tip-*i*Pr-CH₃), 1.023 (d, 3H, $^3J_{\text{HH}} = 6.37$ Hz, Tip-*i*Pr-CH₃), 0.942 (s, 9H, $\text{C}(\text{CH}_3)_3$), 0.652 – 0.614 (m, 12H, Tip-*i*Pr-CH₃ overlapping with $\text{C}(\text{CH}_3)_3$), 0.527 (d, 3H, $^3J_{\text{HH}} = 6.32$ Hz, Tip-*i*Pr-CH₃), 0.471 (dd, 6H, $^3J_{\text{HH}} = 5.89$ Hz, Tip-*i*Pr-CH₃) ppm.

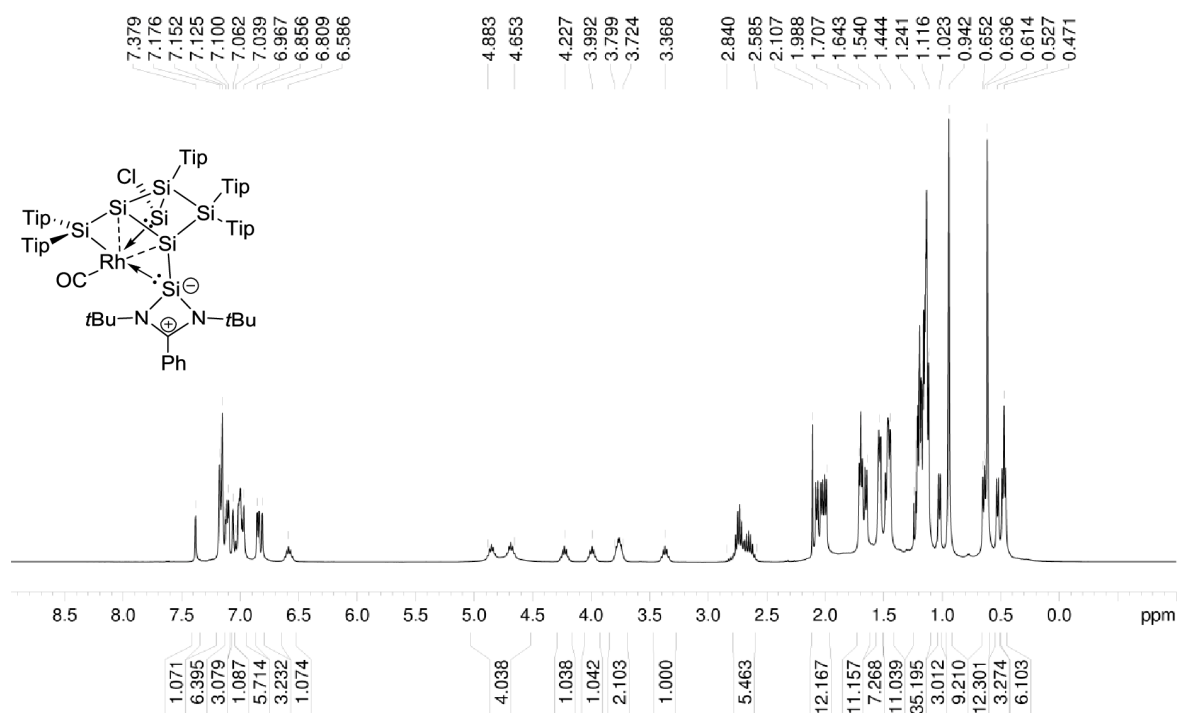
$^{13}\text{C-NMR}$ (100.61 MHz, C_6D_6 , 300 K) δ = 206.72 (s, 1C, CO), 206.03 (s, 1C, CO), 166.97 (s, 1C, Ar-C), 157.40 (s, 1C, Ar-C), 155.42 (s, 1C, Ar-C), 154.08, 153.79, 153.66, 153.44, 152.89 (s, each 1C, Ar-C), 150.95 (s, 1C, Ar-C), 149.33, 148.79, 148.52, 148.27 (s, each 1C, Ar-C), 144.48 (s, 1C, Ar-C), 141.15 – 141.13 (m, 2C, Ar-C), 137.81 (s, 1C, Ar-C), 136.32 – 136.29 (m, 2C, Ar-C), 135.58 (s, 1C, Ar-C), 132.10 – 132.03 (d, 1C, $J = 6.06$ Hz, Ar-C), 130.61 (s, 1C, Ar-C), 129.26 (s, 1C, Ar-CH), 129.22 (s, 1C, Ar-CH), 128.87 (bs, 1C, Ar-CH), 128.49 (s, 1C, Ar-CH), 128.11, 127.87 (s, each 1C, Ar-CH overlapping with C_6D_6), 125.63 (s, 1C, Ar-CH), 124.47, 123.95, 123.54 (s, each 1C, Ar-CH), 122.61 (s, 1C, Ar-CH), 122.35 (s, 1C, Ar-CH), 122.23, 122.15, 122.10 (bs, together 3C, Ar-CH), 121.50 (s, 1C, Ar-CH), 56.21 (s, 1C, $\text{C}(\text{CH}_3)_3$), 55.36 (s, 1C, $\text{C}(\text{CH}_3)_3$), 37.02 – 36.93 (d, 2C, $J = 9.58$ Hz, Tip-*i*Pr-CH), 36.43, 36.32, 36.28 (ns, together 3C, Tip-*i*Pr-CH), 35.90 (s, 1C, Tip-*i*Pr-CH), 34.75 (s, 1C, Tip-*i*Pr-CH), 34.56 – 34.49 (d, 2C, $J = 6.70$ Hz, Tip-*i*Pr-CH), 34.30 – 34.27 (m, 2C, Tip-*i*Pr-CH), 34.18 (s, 1C, Tip-*i*Pr-CH), 33.95 (s, 1C, Tip-*i*Pr-CH), 33.53 (s, 1C, Tip-*i*Pr-CH), 31.05 (s, 1C, Tip-*i*Pr-CH), 29.64, 29.60 (bs, together 2C, Tip-*i*Pr-CH₃), 29.25, 28.68 (s, each 1C, Tip-*i*Pr-CH₃), 28.04 (s, 1C, Tip-*i*Pr-CH₃), 27.49, 27.37 (s, each 1C, Tip-*i*Pr-CH₃), 26.52, 26.48 (s, together 2C, Tip-*i*Pr-CH₃), 26.18, 26.03, 25.95 (s, each 1C, Tip-*i*Pr-CH₃), 25.30 (s, 1C, Tip-*i*Pr-CH₃), 24.87, 24.81, 24.71 (s, each 1C, Tip-*i*Pr-CH₃), 24.41 (s, 1C, Tip-*i*Pr-CH₃), 24.28, 24.26, 24.17, 24.11, 24.03, 23.83, 23.75 (m, together 7C, Tip-*i*Pr-CH₃), 22.99 (s, 1C, Tip-*i*Pr-CH₃), 21.39 (s, 1C, Tip-*i*Pr-CH₃) ppm.

$^{29}\text{Si-NMR}$ (79.49 MHz, C_6D_6 , 300 K) δ = 164.5 (d, 1Si, $^2J_{\text{Si-Rh}} = 53.4$ Hz, Si-Cl), 158.8 (d, 1Si, $^2J_{\text{Si-Rh}} = 41.0$ Hz, SiTip₂), 108.7 (d, 1Si, $^2J_{\text{Si-Rh}} = 59.6$ Hz, NHSi), 58.3 (d, 1Si, $^2J_{\text{Si-Rh}} = 14.3$ Hz, SiTip), -58.3 (s, SiTip₂), -122.1 (s, unsubstituted Si), -140.2 (s, unsubstituted Si) ppm.

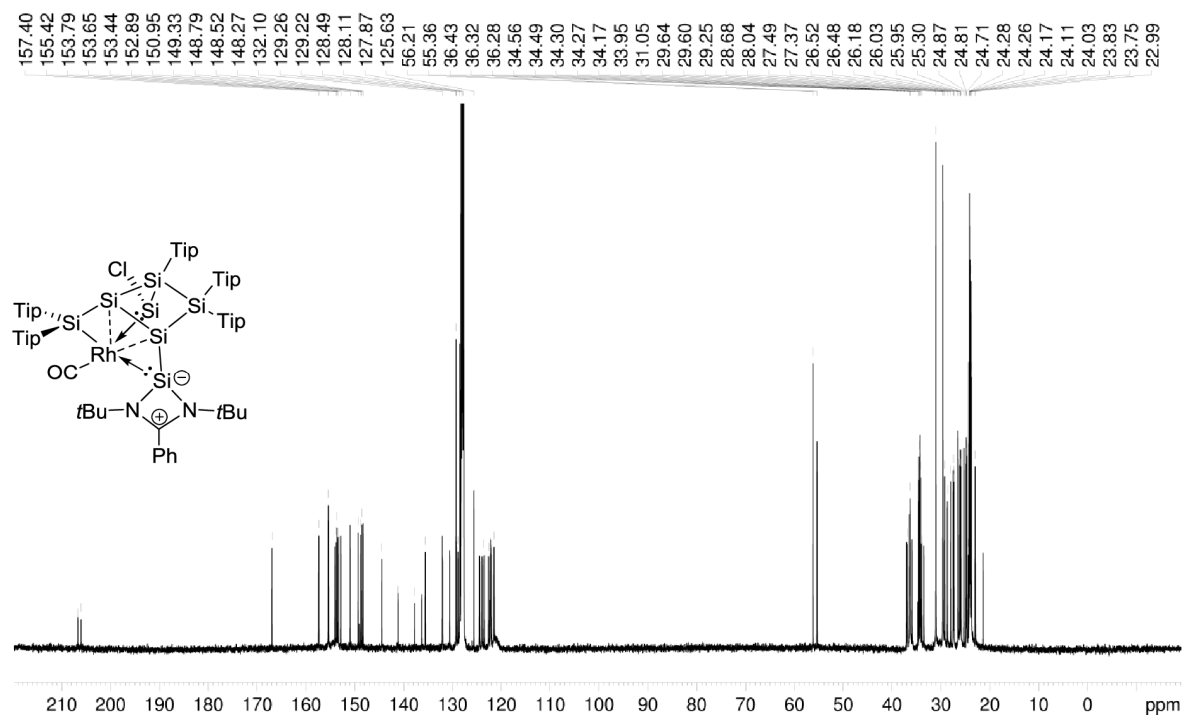
CP-MAS $^{29}\text{Si-NMR}$ (79.53 MHz, 13 KHz, 300K) δ = 165.7 (bs, Si-Cl), 157.3 (bs, SiTip₂), 107.7 (d, 1Si, $^2J_{\text{Si-Rh}} = 62.6$ Hz, NHSi), 54.1 (bs, SiTip), -62.3 (s, SiTip₂), -120.3 (s, unsubstituted Si), -142.1 (s, unsubstituted Si) ppm.

Elemental analysis: calculated for $\text{C}_{91}\text{H}_{138}\text{ClN}_2\text{ORhSi}_7$: C: 67.84 % ; H: 8.63 % ; N: 1.74 %. Found: C: 66.73 % ; H: 7.78 % ; N: 1.63 %.

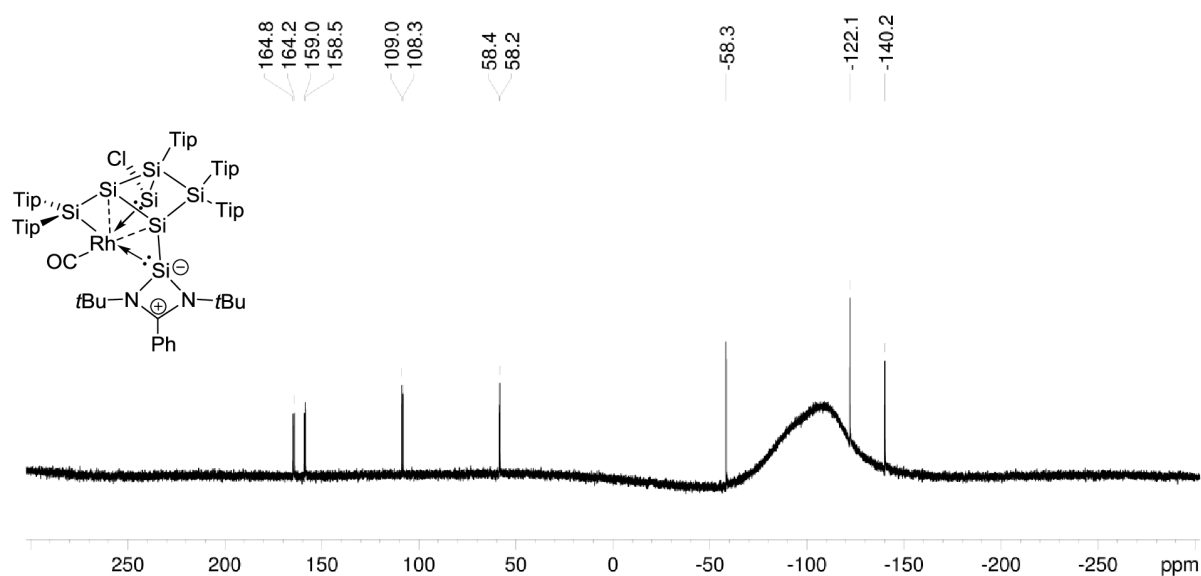
UV/VIS (hexane): $\lambda_{\text{max}} (\epsilon) = 461 \text{ nm } (11630 \text{ M}^{-1} \text{ cm}^{-1})$.



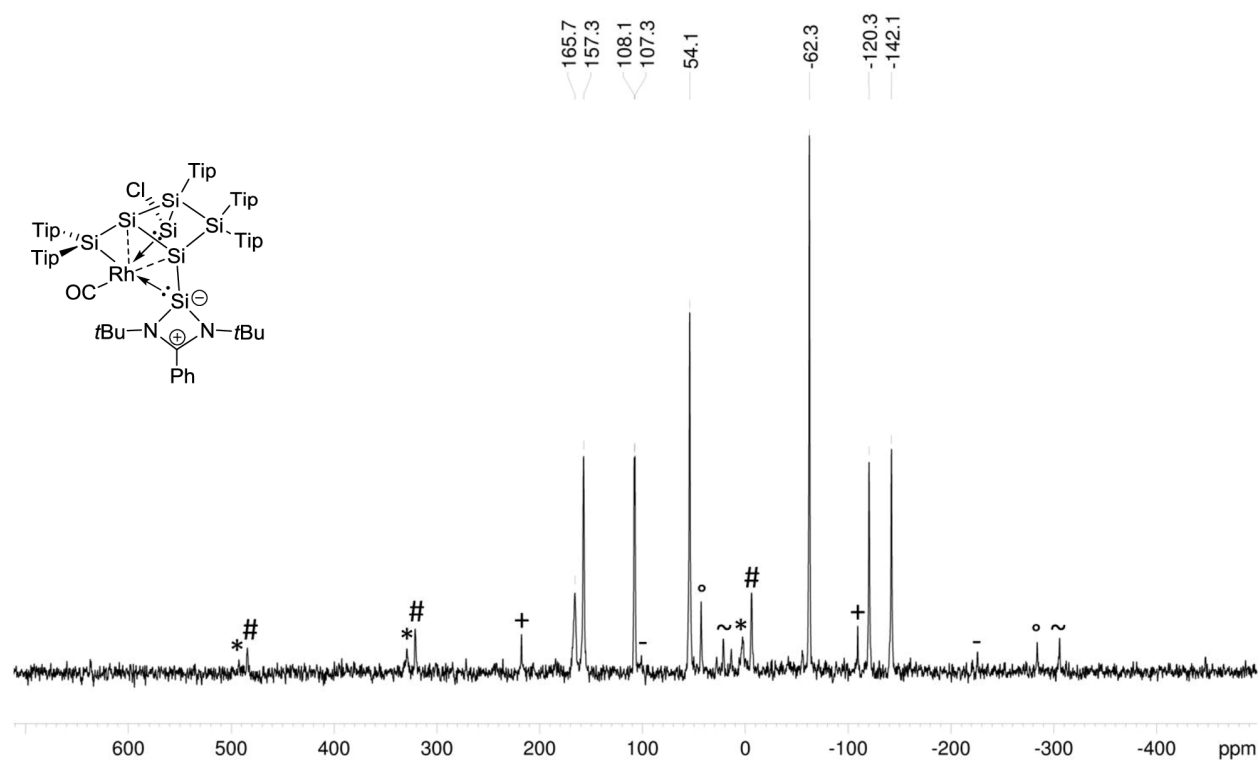
Supplementary Figure 30: ¹H NMR spectrum of **3** in C₆D₆ (400.13 MHz, 300 K).



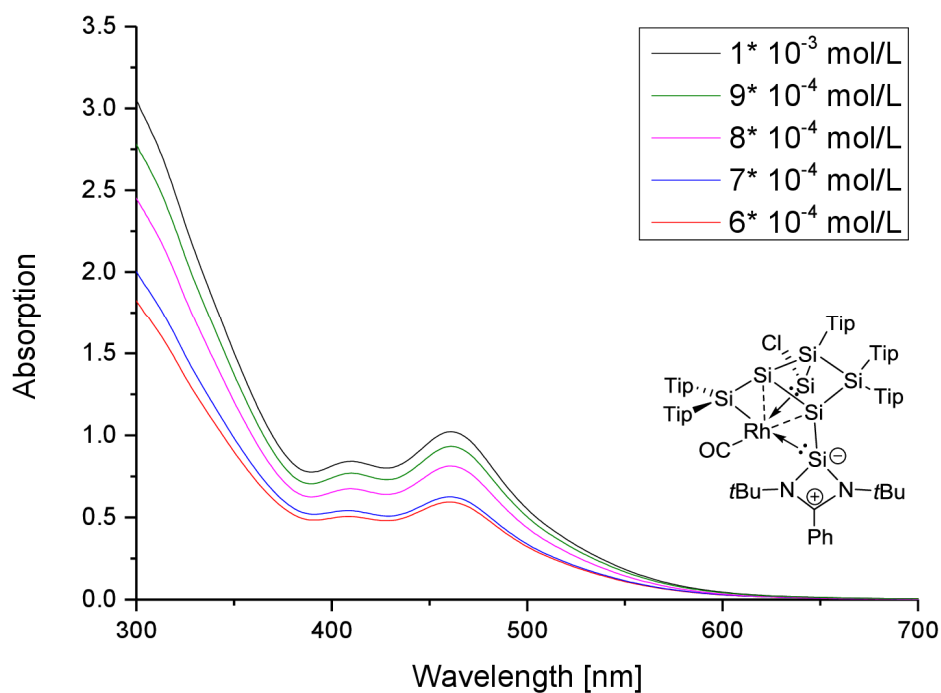
Supplementary Figure 31: ¹³C NMR spectrum of **3** in C₆D₆ (100.61 MHz, 300 K).



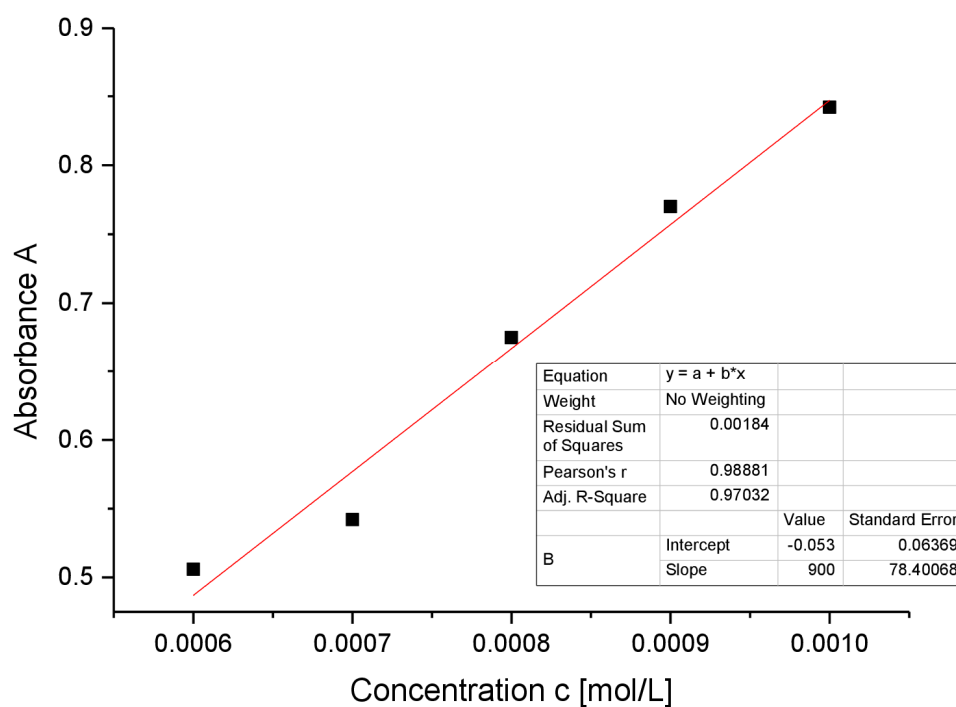
Supplementary Figure 32: ^{29}Si NMR spectrum of **3** in C_6D_6 (79.49 MHz, 300 K).



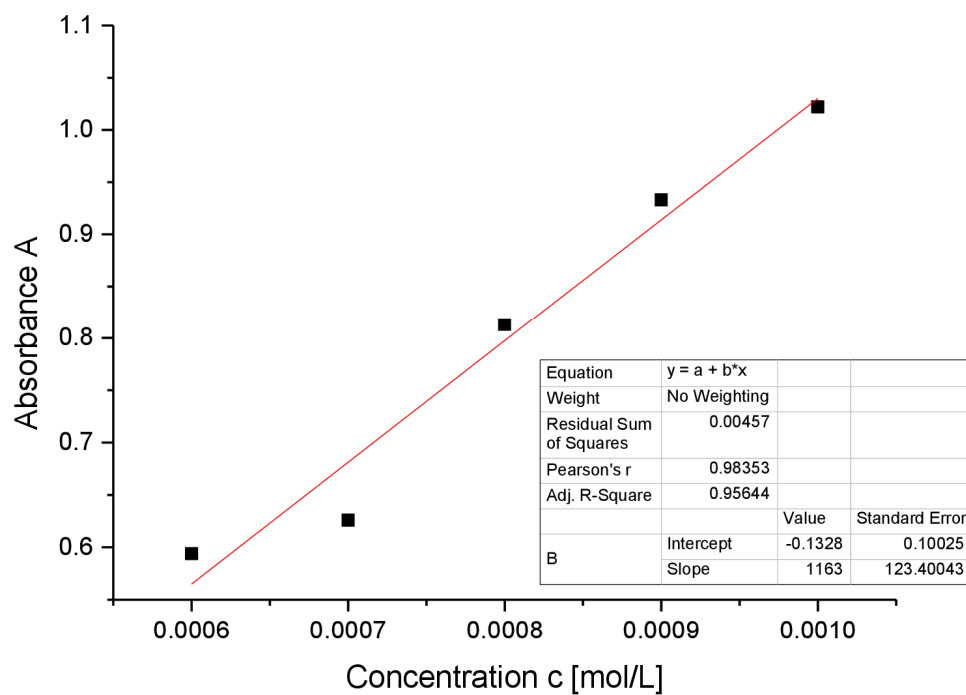
Supplementary Figure 33: CP MAS ^{29}Si NMR spectrum of **3** (79.53 MHz, 13 KHz, 300 K), side spinning bands of: * Si-Cl (165.7 ppm), # SiTip_2 (157.3 ppm), + SiTip (54.1 ppm), - SiTip_2 (-62.3 ppm), ° unsubstituted Si (-120.3 ppm), ~ unsubstituted Si (-124.1 ppm).



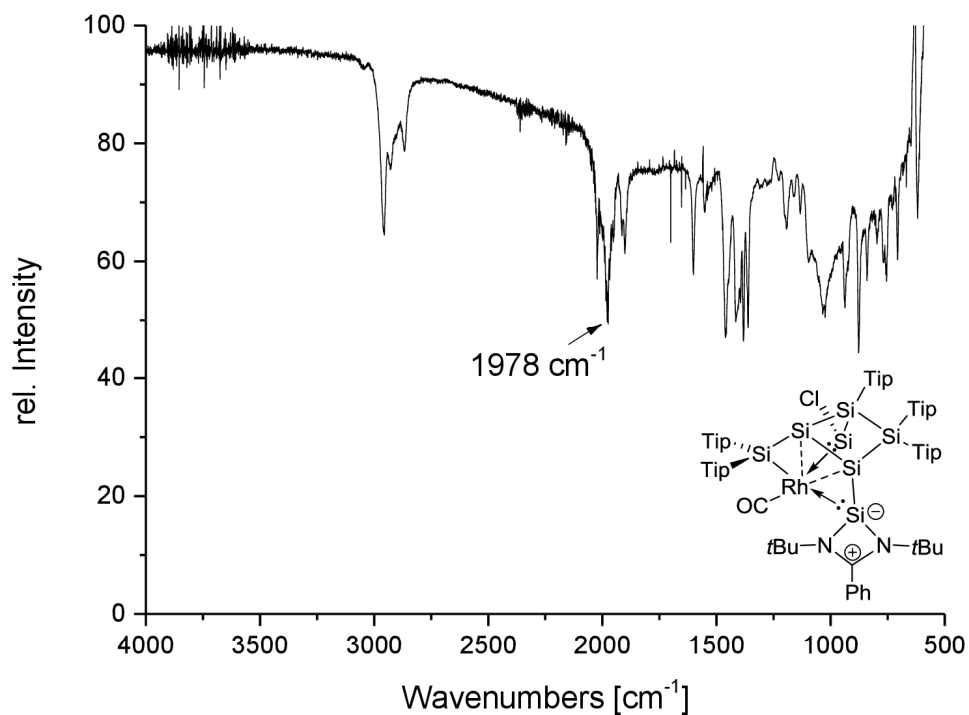
Supplementary Figure 34: UV-Vis spectrum of **3** in hexane at different concentrations.



Supplementary Figure 35: Determination of ε ($9000 \text{ M}^{-1} \text{ cm}^{-1}$) by linear regression of absorptions ($\lambda = 410 \text{ nm}$) of **3** against concentration.



Supplementary Figure 36: Determination of ε ($11630 \text{ M}^{-1} \text{ cm}^{-1}$) by linear regression of absorptions ($\lambda = 461 \text{ nm}$) of **3** against concentration.



Supplementary Figure 37: Infrared spectrum of **3**.

***trans*-Dicarbonyl-(1,3-di-tert-butyl-2-chloro-4-phenyl-2,3-dihydro-1,3,2-diazasilet-1-ium-2-ide)-ligato-(2,2,5,5,6-pentakis(2,4,6-triisopropylphenyl)tetra cyclo[2.2.0.0.1,3.0.3,6]hexasilan-4-yl)rhodium (4)**

The silylene-substituted siliconoid **1a** (500 mg; 0.346 mmol) and 1 eq (134.6 mg; 0.346 mmol) of $[(\text{CO})_2\text{RhCl}]_2$ were dissolved in benzene 10 mL and stirred overnight at room temperature. The solvent was removed in vacuo and the dark red-brownish residue was filtered twice from each 7 mL hexane. The solution was concentrated to 1 mL and stored at $-26\text{ }^\circ\text{C}$ for one day to yield red-brownish crystals of **4** (280 mg; 0.217 mmol) in 63 % yield (mp. $> 192\text{ }^\circ\text{C}$, dec.).

$^1\text{H-NMR}$ (400.13 MHz, C_6D_6 , 300 K) δ = 7.270 (s, 2H, Ar-H), 7.092 – 7.038 (m, 5H, Ar-H), 6.959 (bs, 1H, Ar-H), 6.883 – 6.842 (m, 4H, Ar-H), 6.809 – 6.752 (m, 3H, Ar-H), 5.415 (sept, 1H, $^3J_{\text{HH}} = 6.80\text{ Hz}$, Tip-*i*Pr-CH₂), 5.286 (sept, 1H, $^3J_{\text{HH}} = 6.46\text{ Hz}$, Tip-*i*Pr-CH₂), 5.088 (sept, 1H, $^3J_{\text{HH}} = 6.46\text{ Hz}$, Tip-*i*Pr-CH₂), 4.729 (sept, 1H, $^3J_{\text{HH}} = 6.78\text{ Hz}$, Tip-*i*Pr-CH₂), 4.206 (sept, 1H, $^3J_{\text{HH}} = 6.42\text{ Hz}$, Tip-*i*Pr-CH₂), 4.099 (sept, 1H, $^3J_{\text{HH}} = 6.76\text{ Hz}$, Tip-*i*Pr-CH₂), 3.879 (sept, 1H, $^3J_{\text{HH}} = 6.42\text{ Hz}$, Tip-*i*Pr-CH₂), 3.556 (sept, 1H, $^3J_{\text{HH}} = 6.48\text{ Hz}$, Tip-*i*Pr-CH₂), 3.424 (sept, 2H, $^3J_{\text{HH}} = 6.79\text{ Hz}$, Tip-*i*Pr-CH₂), 2.860 – 2.760 (m, 2H, Tip-*i*Pr-CH₂), 2.738 – 2.562 (m, 3H, Tip-*i*Pr-CH₂), 2.335 (d, 3H, $^3J_{\text{HH}} = 5.69\text{ Hz}$, Tip-*i*Pr-CH₃), 2.153 (d, 3H, $^3J_{\text{HH}} = 6.64\text{ Hz}$, Tip-*i*Pr-CH₃), 1.811 (d, 3H, $^3J_{\text{HH}} = 6.23\text{ Hz}$, Tip-*i*Pr-CH₃), 1.655 – 1.486 (m, 28 H, Tip-*i*Pr-CH₃), 1.276 – 1.228 (m, 16 H, Tip-*i*Pr-CH₃), 1.178 – 1.139 (m, 13H, Tip-*i*Pr-CH₃), 1.076 – 1.042 (m, 19H, Tip-*i*Pr-CH₃ overlapping with $\text{C}(\text{CH}_3)_3$), 0.939 (s, 9H, $\text{C}(\text{CH}_3)_3$), 0.889 (t, hexane), 0.786 – 0.757 (m 6H, Tip-*i*Pr-CH₃), 0.554 – 0.516 (m, 6H, Tip-*i*Pr-CH₃), 0.433 (d, 3H, $^3J_{\text{HH}} = 6.45\text{ Hz}$, Tip-*i*Pr-CH₃), 0.355 (d, 3H, $^3J_{\text{HH}} = 6.45\text{ Hz}$, Tip-*i*Pr-CH₃), 0.280 (d, 3H, $^3J_{\text{HH}} = 6.45\text{ Hz}$, Tip-*i*Pr-CH₃) ppm.

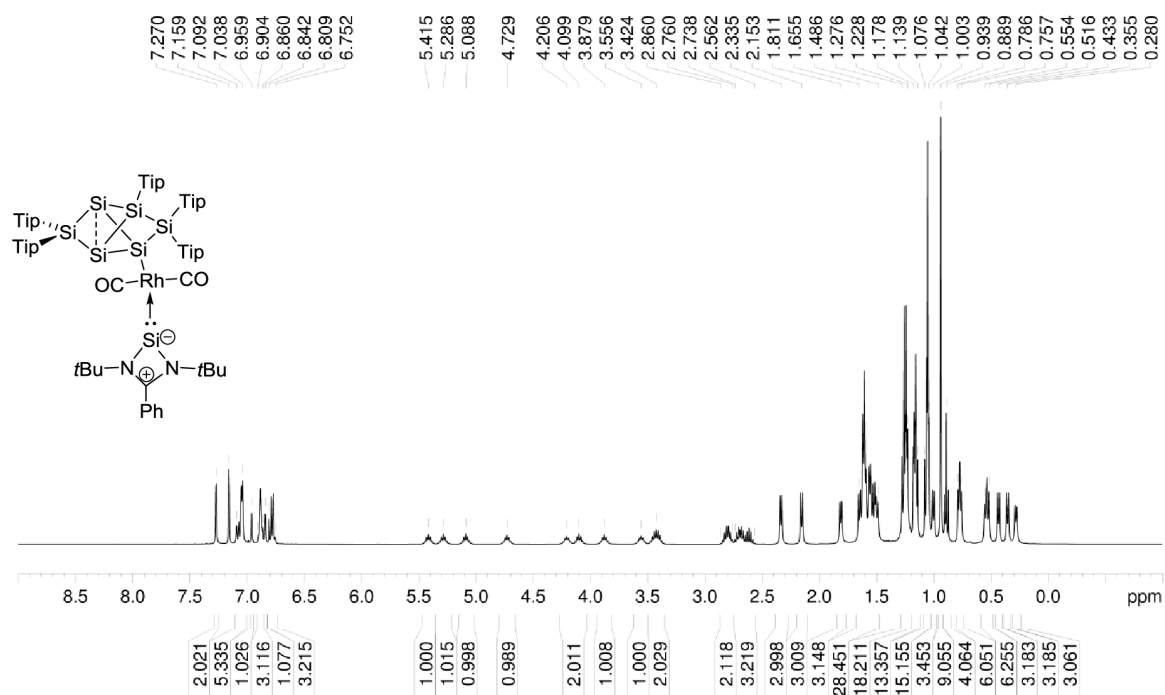
$^{13}\text{C-NMR}$ (100.61 MHz, C_6D_6 , 300 K) δ = 172.72 (s, 1C, Ar-C), 156.04, 155.40, 154.11, 153.86, 153.61, 153.37, 153.06, 152.52, 152.37, 152.24 (s, each 1C, Ar-C), 149.76, 149.18, 148.43, 148.39, 148.23 (s, each 1C, Ar-C), 140.73, 139.98, 138.28, 138.16 (s, each 1C, Ar-C), 133.11, 133.09 (bs, each 1C, Ar-C), 130.46 (s, 1C, Ar-CH), 129.99 (s, 1C, Ar-CH), 128.17 (s, 1C, Ar-CH), 127.82, 127.67 (s, each 1C, overlapping with C_6D_6 , Ar-CH), 122.89, 122.84, 122.63, 122.56, 122.36, 121.69, 121.51, 121.03, 120.75, 120.33 (s, each 1C, Ar-CH), 54.59 (s, 1C, $\text{C}(\text{CH}_3)_3$), 54.54 (s, 1C, $\text{C}(\text{CH}_3)_3$), 37.16 (s, 1C, Tip-*i*Pr-CH), 36.03, 35.94, 35.81, 35.65, 35.20, 34.91, 34.46, 34.41, 34.24, 34.05, 34.02, 33.90, 33.80 (s, each 1C, Tip-*i*Pr-CH), 31.61, 30.88, 30.74 (s, each 1C, Tip-*i*Pr-CH), 28.20, 28.10, 27.48, 27.11, 26.43, 25.61 (s, each 1C, Tip-*i*Pr-CH₃), 24.68, 24.57, 24.51, 24.39, 24.33, 24.15, 23.96, 23.86, 23.74, 23.70 (bs, each 1C, Tip-*i*Pr-CH₃), 23.37, 23.30, 23.01, 22.98 (bs, each 1C, Tip-*i*Pr-CH₃), 22.70, 22.55 (s, each 1C, Tip-*i*Pr-CH₃), 14.02 (s, 1C, Tip-*i*Pr-CH₃) ppm.

$^{29}\text{Si-NMR}$ (79.49 MHz, C_6D_6 , 300 K) δ = 162.6 (s, *privo*-SiTip₂), 48.2 (d, $^2J_{\text{Si-Rh}} = 84.5\text{ Hz}$, NHSi), 21.8 (d, $^2J_{\text{Si-Rh}} = 8.5\text{ Hz}$, *ligato*-SiTip), 17.6 (s, *remoto*-SiTip₂), -9.0 (d, $^2J_{\text{Si-Rh}} = 31.5\text{ Hz}$, *ligato*-Si-NHSi), -256.1 (s, *nudo*-Si1), -258.3 (s, *nudo*-Si3) ppm.

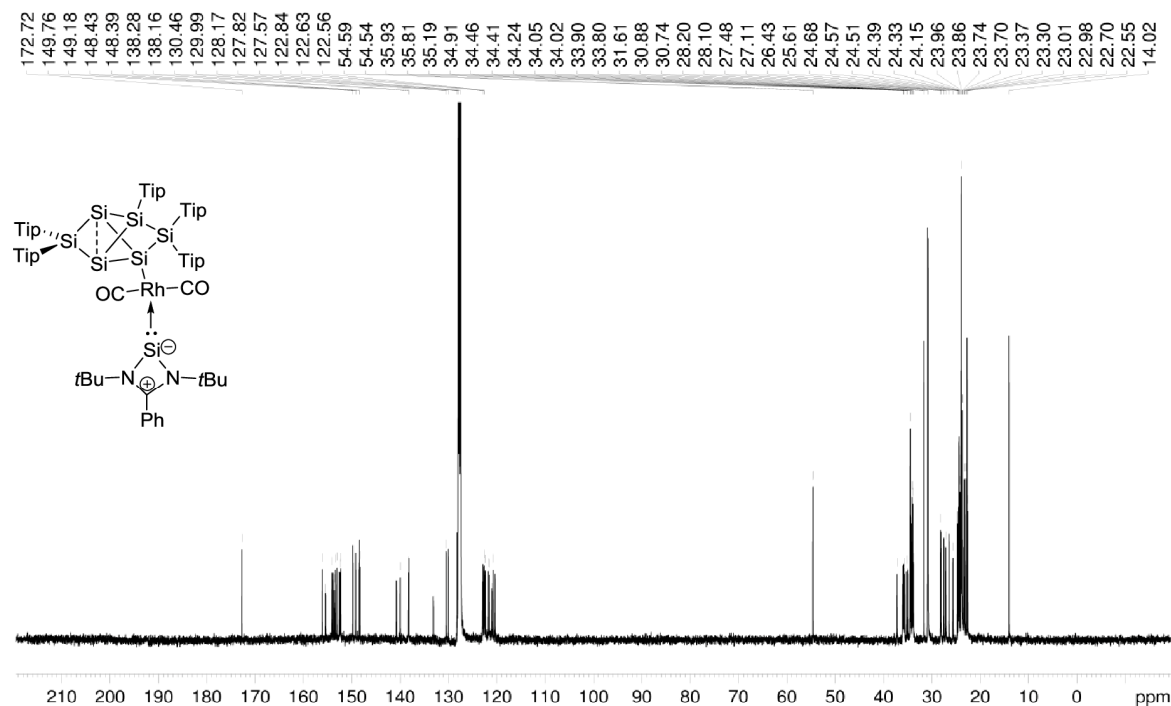
CP-MAS $^{29}\text{Si-NMR}$ (79.53 MHz, 13KHz, 300K) δ = 161.8 (s, *privo*-SiTip₂), 42.7 (d, $^2J_{\text{Si-Rh}} = 69.7\text{ Hz}$, NHSi), 14.5 (s, *ligato*-SiTip), -5.8 (*remoto*-SiTip₂), -23.4 (s, *ligato*-Si-NHSi), -263.8 (s, *nudo*-Si), -266.0 (s, *nudo*-Si) ppm.

Elemental analysis: calculated for $\text{C}_{92}\text{H}_{138}\text{N}_2\text{O}_2\text{RhSi}_7\text{Cl}$: C: 67.42 % ; H: 8.49 % ; N: 1.71 %. Found: C: 67.09 % ; H: 8.38 % ; N: 1.62 %.

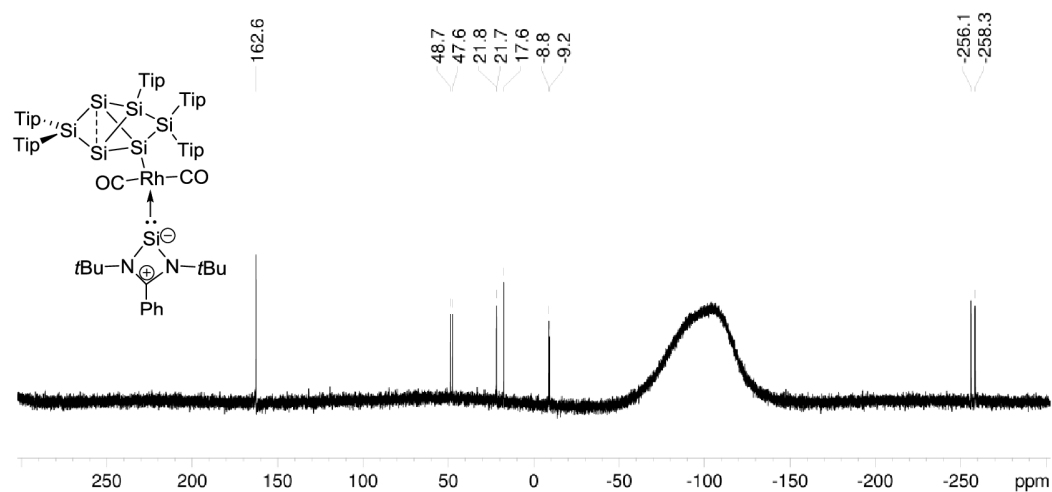
UV/VIS (hexane): $\lambda_{\text{max}}(\epsilon) = 466\text{ nm}$ ($4090\text{ M}^{-1}\text{ cm}^{-1}$).



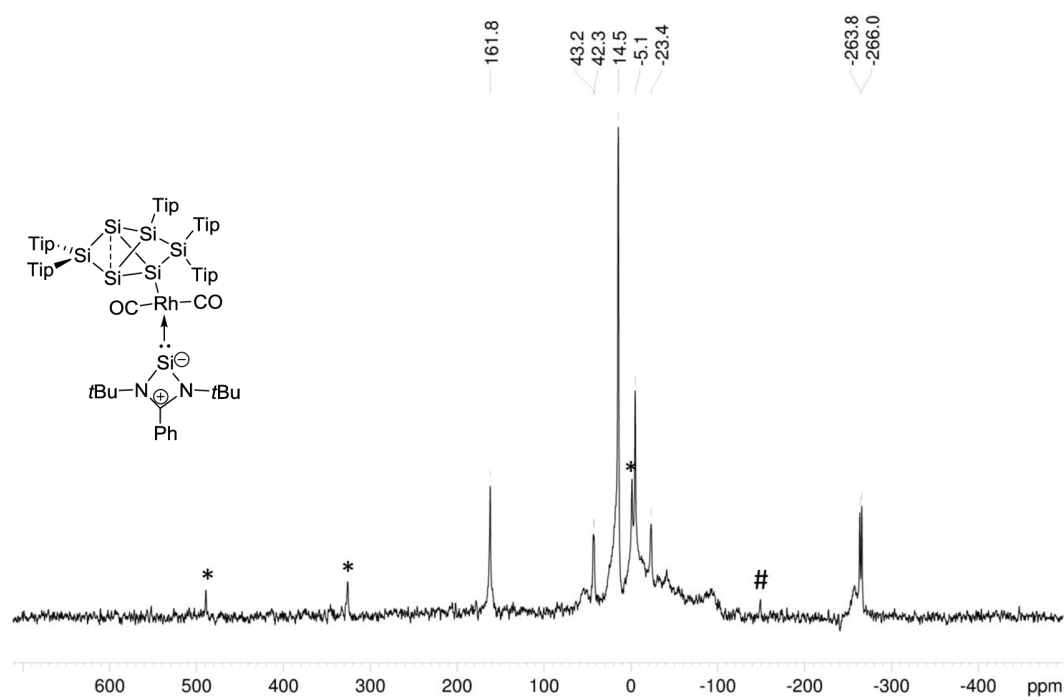
Supplementary Figure 38: ¹H NMR spectrum of **4** in C₆D₆ (400.13 MHz, 300 K).



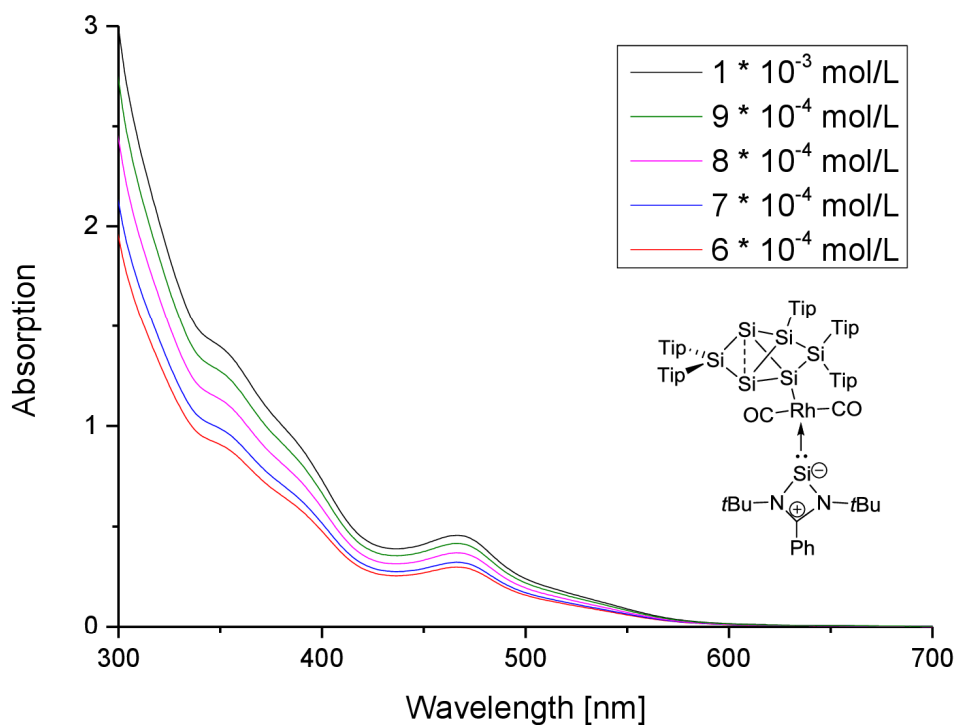
Supplementary Figure 39: ¹³C NMR spectrum of **4** in C₆D₆ (100.61 MHz, 300 K).



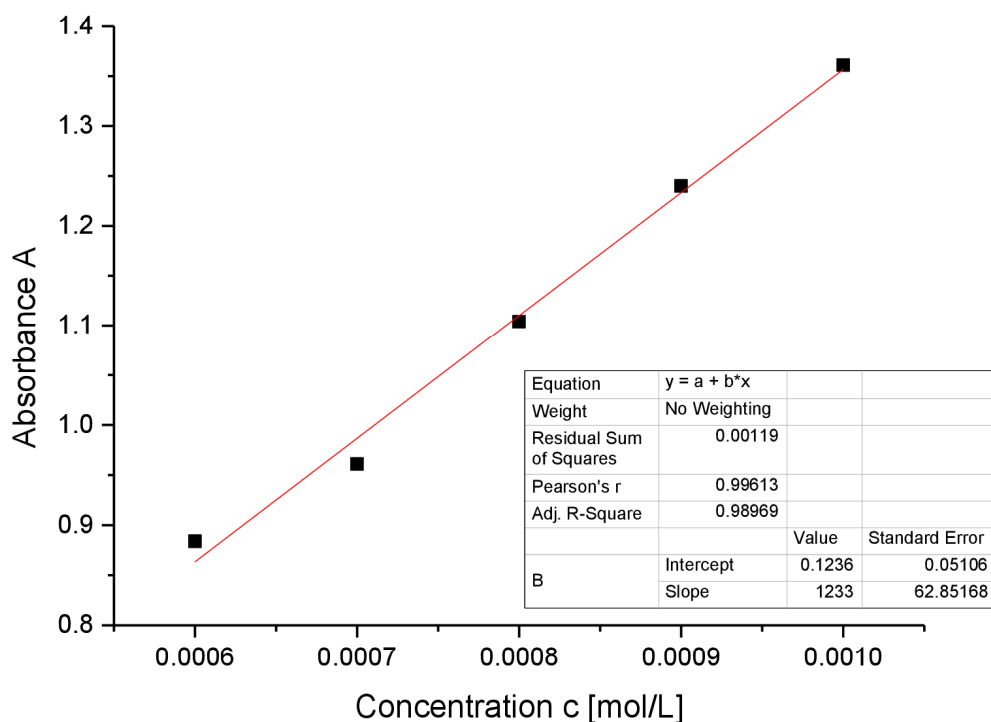
Supplementary Figure 40: ^{29}Si NMR spectrum of **4** in C_6D_6 (79.49 MHz, 300 K).



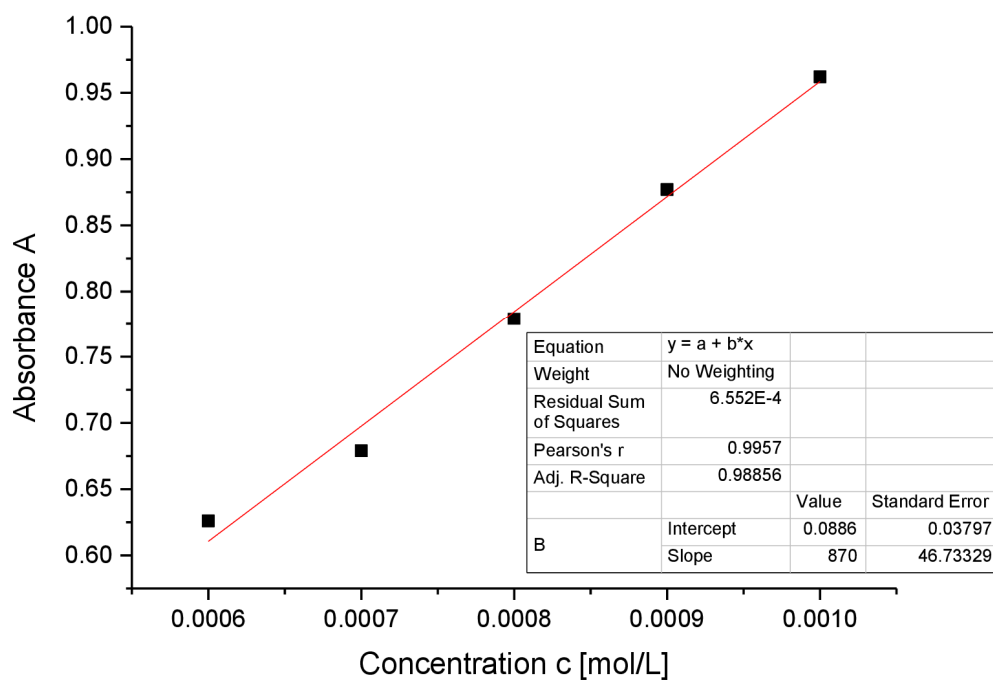
Supplementary Figure 41: CP MAS ^{29}Si NMR spectrum of **4** (79.53 MHz, 13 KHz, 300 K), side spinning bands of: * *privo*-SiTip₂ (161.8 ppm), # *ligato*-SiTip (14.5 ppm).



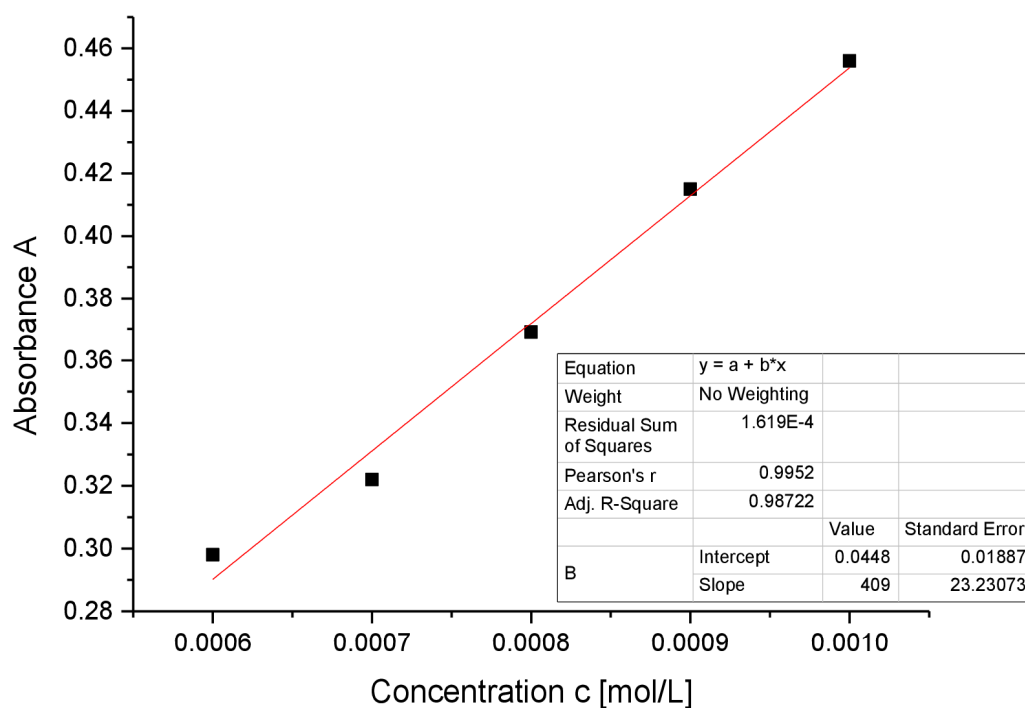
Supplementary Figure 42: UV-Vis spectrum of **4** in hexane at different concentrations.



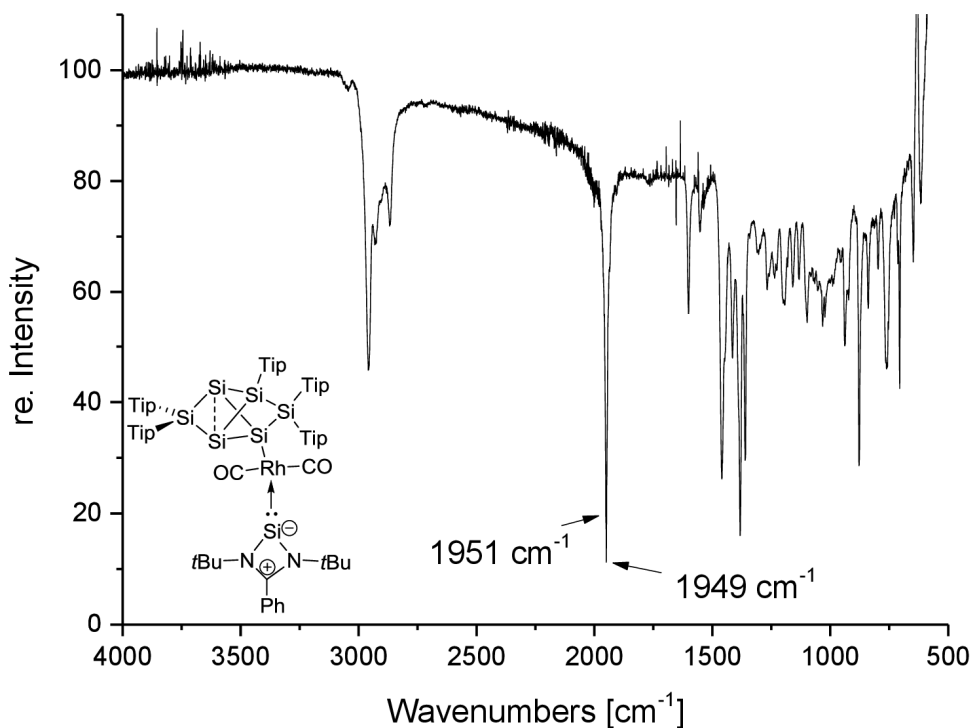
Supplementary Figure 43: Determination of ε ($12330 \text{ M}^{-1} \text{ cm}^{-1}$) by linear regression of absorptions ($\lambda = 354 \text{ nm}$) of **4** against concentration.



Supplementary Figure 44: Determination of ϵ ($8700 \text{ M}^{-1} \text{ cm}^{-1}$) by linear regression of absorptions ($\lambda = 384 \text{ nm}$) of **4** against concentration.



Supplementary Figure 45: Determination of ϵ ($4090 \text{ M}^{-1} \text{ cm}^{-1}$) by linear regression of absorptions ($\lambda = 466 \text{ nm}$) of **4** against concentration.



Supplementary Figure 46: Infrared spectrum of **4**.

(5-(Chlorobis(2,4,6-triisopropylphenyl)silyl)-2-(1,3-di-*tert*-butyl-4-phenyl-1,3,2λ³-diazagermet-1-ium-2(3H)-yl)-3,3,4-tris(2,4,6-triisopropylphenyl)tricyclo [2.1.0.0^{2.5}]pentasilane-1-yl-rhodium

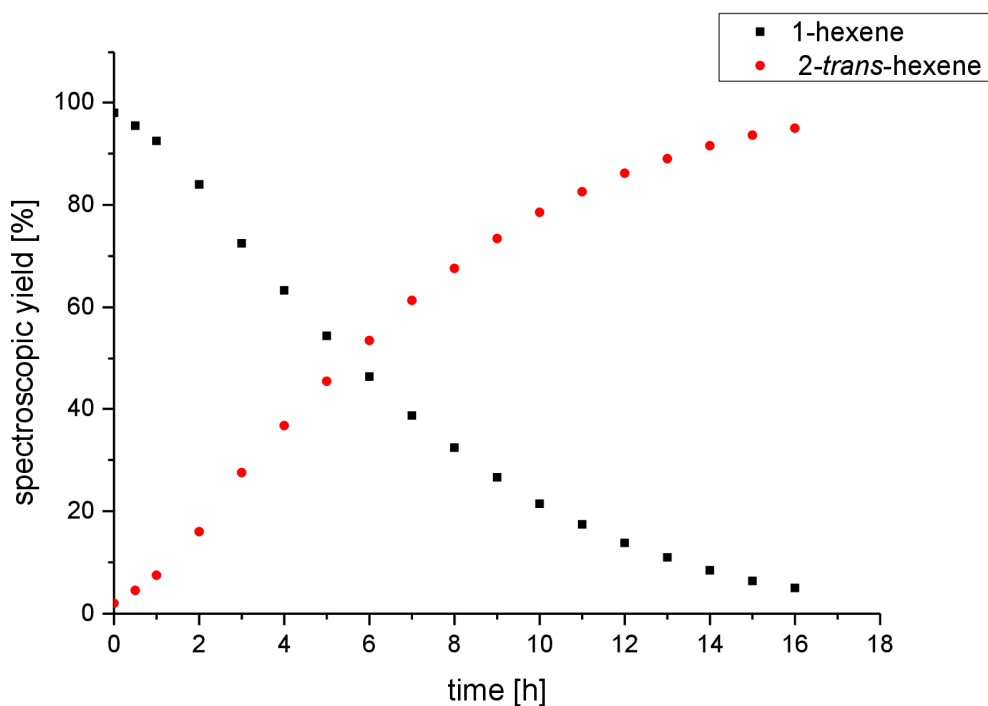
The reaction was prepared in NMR scale. The germylene-substituted siliconoid **1b** (70 mg; 0.046 mmol) and 1 eq (22.59 mg; 0.046 mmol) of [(cod)RhCl]₂ were dissolved in deuterated benzene 0.5 mL and a color change of bright orange to dark red-brown was observed. The solvent was removed in vacuo and the dark red-brownish residue was filtered from 2 mL hexane. The solution was concentrated to 1 mL and stored at -26 °C for eight weeks to yield a few red-brownish crystals of **Si₆Ge-Rh(cod)Cl** which were investigated to X-ray analysis.

3. Data and Plots of spectroscopic conversion in alkene isomerization

Allyltrimethylsilane and 1-hexene were used as neat substrates on an NMR scale using a C₆D₆ capillary as locking signal and the respective amount of the catalysts **2a-c**, **3** and **4**. The yields, turn-over-numbers and turn-over-frequencies were calculated from the ¹H NMR integrations and given in the supplementary tables 2-9.

Supplementary Table 1: Reaction conditions.

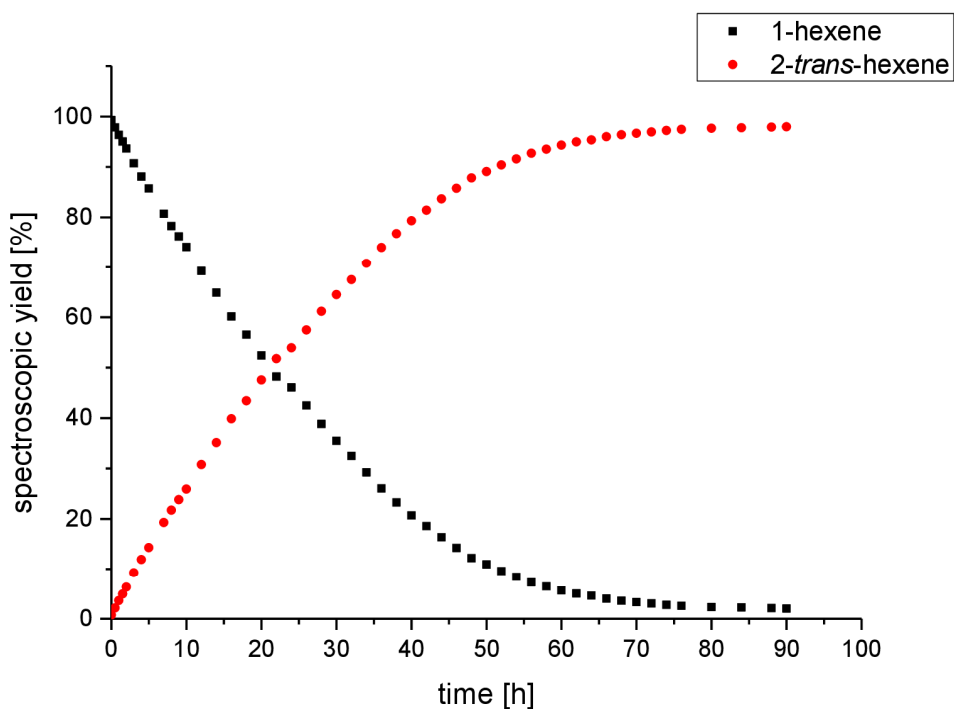
Catalyst	Substrate	Temperature [°C]	n (substrate) [mmol]	n (catalyst) [mmol]	m (substrate) [mg]	m (catalyst) [mg]
2a	1-hexene	25	3.967	0.002	333.87	3.5
2b	1-hexene	25	3.868	0.004	325.53	7
2c	1-hexene	25	3.77	0.004	317.56	7
3	1-hexene	25	2.483	0.006	208.95	10
4	1-hexene	25	2.441	0.006	205.38	10
2a	Allyl-SiMe ₃	60	2.125	0.017	242.81	30
2b	Allyl-SiMe ₃	60	2.073	0.017	236.85	30
2c	Allyl-SiMe ₃	60	2.021	0.016	230.97	30



Supplementary Figure 47: Plot of the spectroscopically determined conversion to 2-*trans*-hexene with 0.05 mol% Si-Ir **2a**.

Supplementary Table 2: Catalytic activity of **2a** with 1-hexene: determined conversion by ^1H NMR spectroscopy, calculated TON and TOF

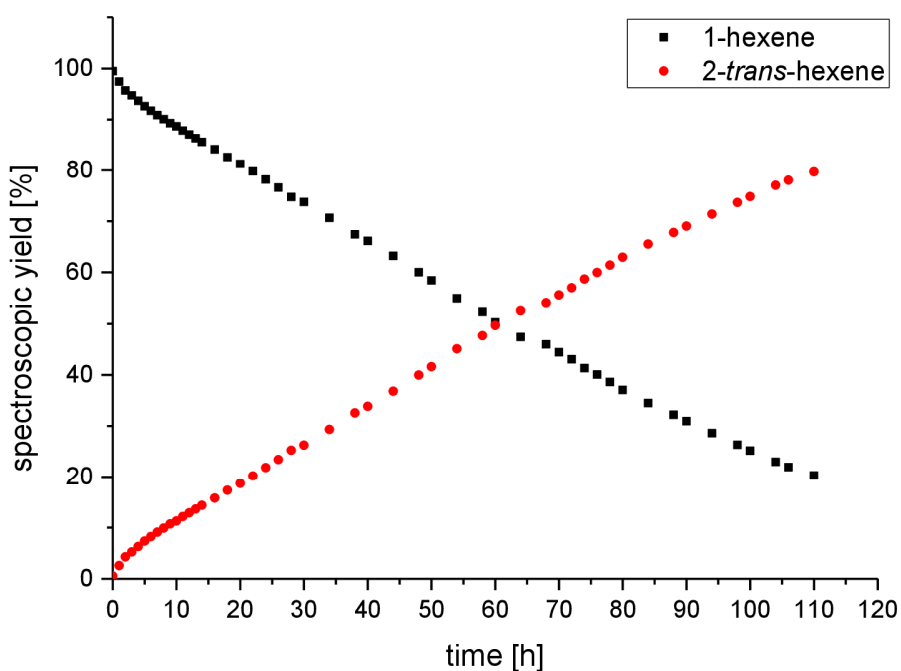
Time [h]	n (1-hexene) [mmol]	n (2-hexene) [mmol]	1-hexene [%]	2-hexene [%]	TON	TOF [h ⁻¹]
0	3.887	0.081	98.00	2.03	40.7	-
0.5	3.786	0.181	95.44	4.55	91.2	182.5
1	3.669	0.298	92.50	7.50	15.3	150.3
2	3.332	0.635	83.99	16.01	320.8	160.4
3	2.875	1.092	72.47	27.53	551.5	183.8
4	2.511	1.456	63.30	36.70	735.2	183.8
5	2.159	1.808	54.43	45.60	912.9	182.6
6	1.844	2.123	46.48	53.50	1072.4	178.7
7	1.534	2.433	38.67	61.33	1228.8	175.5
8	1.285	2.682	32.40	67.60	1354.4	169.3
9	1.055	2.912	26.59	73.41	1470.8	163.4
10	0.851	3.116	21.45	78.55	1573.8	157.4
11	0.691	3.276	17.42	82.58	1654.5	150.4
12	0.548	3.419	13.83	86.18	1726.6	143.9
13	0.436	3.531	10.99	89.02	1783.4	137.2
14	0.336	3.631	8.46	91.54	1834.0	131.0
15	0.253	3.714	6.38	93.62	1875.7	125.1
16	0.200	3.767	5.03	94.97	1902.7	118.9

**Supplementary Figure 48:** Plot of the spectroscopically determined conversion to 2-*trans*-hexene with 0.1 mol% Ge-Ir **2b**.

Supplementary Table 3: Catalytic activity of **2b** with 1-hexene: determined conversion by ^1H NMR spectroscopy, calculated TON and TOF

Time [h]	n (1-hexene) [mmol]	n (2-hexene) [mmol]	1-hexene [%]	2-hexene [%]	TON	TOF [h ⁻¹]
0	3.840	0.028	99.27	0.73	7.3	-
0.5	3.784	0.084	97.84	2.16	21.6	43.2
1	3.727	0.141	96.35	3.65	36.5	36.5
1,5	3.676	0.192	95.03	4.97	49.7	33.1
2	3.622	0.246	93.65	6.35	63.4	31.7
3	3.509	0.359	90.71	9.29	92.8	30.9
4	3.407	0.461	88.08	11.92	119.1	29.8
5	3.315	0.553	85.71	14.29	142.8	28.6
7	3.122	0.746	80.71	19.29	192.8	27.5
8	3.027	0.841	78.25	21.75	217.4	27.2
9	2.947	0.921	76.18	23.82	238.1	26.5
10	2.865	1.003	74.07	25.93	259.2	25.9
12	2.678	1.190	69.23	30.77	307.6	25.6
14	2.509	1.359	64.87	35.13	351.1	25.1
16	2.326	1.542	60.14	39.86	398.4	24.9
18	2.187	1.681	56.55	43.45	434.3	24.1
20	2.028	1.840	52.43	47.57	475.4	23.8
22	1.865	2.003	48.22	51.78	517.5	23.5
24	1.782	2.086	46.07	53.93	539.0	22.5
26	1.644	2.224	42.51	57.49	574.6	22.1
28	1.502	2.366	38.83	61.17	611.4	21.8
30	1.373	2.495	35.49	64.51	644.7	21.5
32	1.257	2.611	32.49	67.51	674.7	21.1
34	1.131	2.737	29.23	70.77	707.3	20.8
36	1.008	2.860	26.05	73.95	739.1	20.5
38	0.900	2.968	23.28	76.72	766.8	20.2
40	0.801	3.067	20.70	79.30	792.6	19.8
42	0.719	3.149	18.59	81.41	813.6	19.4
44	0.633	3.235	16.36	83.64	836.0	19.0
46	0.551	3.317	14.24	85.76	857.1	18.6
48	0.472	3.396	12.19	87.81	877.6	18.3
50	0.423	3.445	10.94	89.06	890.2	17.8
52	0.371	3.497	9.60	90.40	903.5	17.4
54	0.326	3.542	8.43	91.57	915.3	16.9
56	0.282	3.586	7.30	92.70	926.5	16.5
58	0.251	3.617	6.48	93.52	934.8	16.1
60	0.220	3.648	5.68	94.32	942.7	15.7
62	0.195	3.673	5.04	94.96	949.1	15.3
64	0.179	3.689	4.64	95.36	953.1	14.9
66	0.155	3.713	4.01	95.99	959.4	14.5
68	0.140	3.728	3.61	96.39	963.4	14.2

70	0.128	3.740	3.32	96.68	966.3	13.8
72	0.119	3.749	3.07	96.93	968.7	13.5
74	0.107	3.761	2.78	97.22	971.7	13.1
76	0.099	3.769	2.57	97.43	973.8	12.8
80	0.090	3.778	2.32	97.68	976.3	12.2
84	0.087	3.781	2.24	97.76	977.1	11.6
88	0.082	3.786	2.12	97.88	978.3	11.1
90	0.078	3.790	2.03	97.97	979.2	10.9



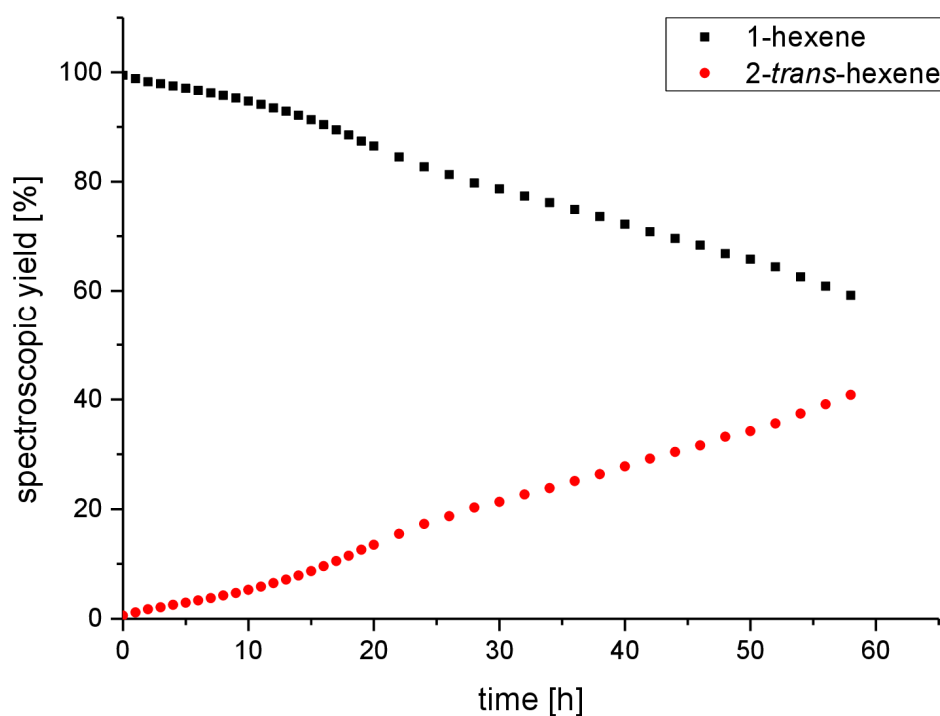
Supplementary Figure 49: Plot of the spectroscopically determined conversion to 2-*trans*-hexene with 0.1 mol% Sn-Ir **2c**.

Supplementary Table 4: Catalytic activity of **2c** with 1-hexene: determined conversion by ^1H NMR spectroscopy, calculated TON and TOF

Time [h]	n (1-hexene) [mmol]	n (2-hexene) [mmol]	1-hexene [%]	2-hexene [%]	TON	TOF [h^{-1}]
0	3.750	0.020	99.46	0.54	5.4	-
1	3.673	0.097	97.43	2.57	25.7	25.7
2	3.609	0.162	95.72	4.28	42.8	21.4
3	3.572	0.198	94.74	5.26	52.6	17.5
4	3.532	0.239	93.67	6.33	63.3	15.8
5	3.492	0.278	92.62	7.38	73.8	14.8
6	3.459	0.311	91.75	8.25	82.5	13.7

6 Supporting Information

7	3.426	0.344	90.87	9.13	91.3	13.0
8	3.397	0.373	90.10	9.90	99.0	12.4
9	3.366	0.404	89.29	10.71	107.1	11.9
10	3.343	0.427	88.68	11.32	113.2	11.3
11	3.311	0.459	87.83	12.17	121.7	11.1
12	3.283	0.487	87.08	12.92	129.2	10.8
13	3.255	0.515	86.34	13.66	136.6	10.5
14	3.227	0.543	85.61	14.39	143.9	10.3
16	3.174	0.596	84.18	15.82	158.2	9.9
18	3.115	0.655	82.63	17.37	173.7	9.6
20	3.065	0.706	81.29	18.71	187.2	9.4
22	3.009	0.761	79.81	20.19	201.9	9.2
24	2.948	0.822	78.18	21.82	218.2	9.1
26	2.888	0.882	76.60	23.40	234.0	9.0
28	2.818	0.952	74.75	25.25	252.5	9.0
30	2.781	0.990	73.77	26.23	262.3	8.7
34	2.664	1.106	70.65	29.35	293.5	8.6
38	2.542	1.228	67.43	32.57	325.7	8.6
40	2.494	1.276	66.15	33.86	338.6	8.5
44	2.383	1.387	63.20	36.80	368.0	8.4
48	2.263	1.507	60.04	39.96	399.6	8.3
50	2.202	1.568	58.41	41.59	415.9	8.3
54	2.069	1.701	54.89	45.11	451.2	8.4
58	1.973	1.797	52.32	47.68	476.8	8.2
60	1.896	1.874	50.30	49.70	497.2	8.3
64	1.789	1.981	47.44	52.56	525.6	8.2
68	1.734	2.036	45.98	54.02	540.2	7.9
70	1.676	2.094	44.45	55.55	555.5	7.9
72	1.623	2.147	43.05	56.95	569.5	7.9
74	1.558	2.212	41.31	58.69	586.9	7.9
76	1.510	2.260	40.05	59.95	599.5	7.9
78	1.455	2.315	38.60	61.40	614.1	7.9
80	1.397	2.373	37.06	62.94	629.4	7.9
84	1.300	2.470	34.50	65.52	655.2	7.8
88	1.214	2.556	32.21	67.79	677.9	7.7
90	1.167	2.603	30.95	69.05	690.5	7.7
94	1.078	2.692	28.60	71.40	714.0	7.6
98	0.992	2.778	26.31	73.69	736.9	7.5
100	0.949	2.821	25.16	74.84	748.4	7.5
104	0.865	2.905	22.95	77.05	770.5	7.4
106	0.827	2.943	21.94	78.06	780.6	7.4
110	0.765	3.005	20.29	79.71	797.1	7.2

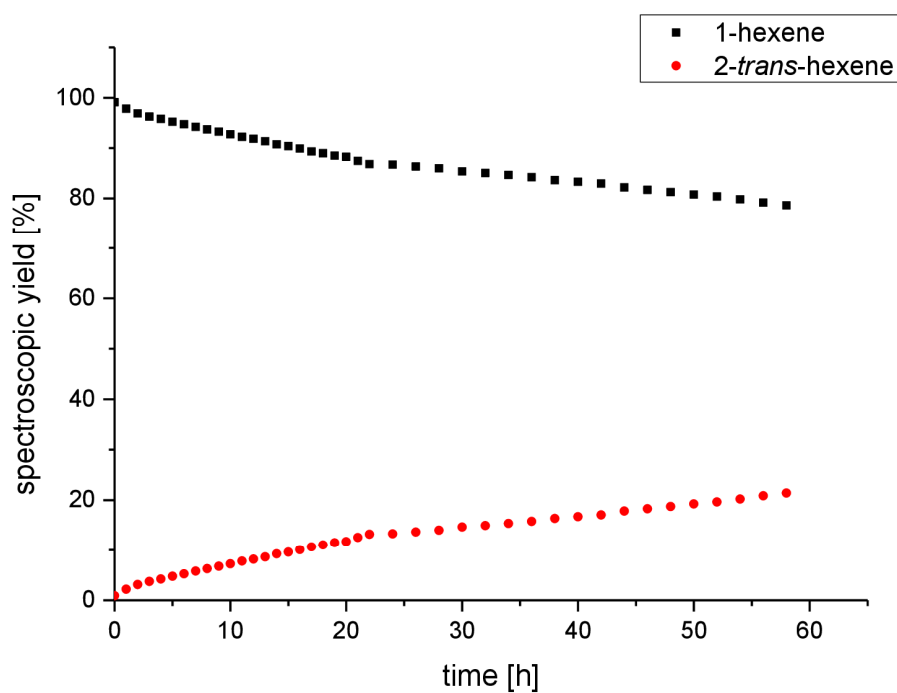


Supplementary Figure 50: Plot of the spectroscopically determined conversion to 2-*trans*-hexene with 0.25 mol% Rh **3**.

Supplementary Table 5: Catalytic activity of Rh-**3** with 1-hexene: determined conversion by ^1H NMR spectroscopy, calculated TON and TOF

Time [h]	n (1-hexene) [mmol]	n (2-hexene) [mmol]	1-hexene [%]	2-hexene [%]	TON	TOF [h ⁻¹]
0	2.469	0.014	99.42	0.58	2.3	-
1	2.454	0.029	98.84	1.16	4.6	4.6
2	2.439	0.043	98.25	1.75	7.0	3.5
3	2.430	0.052	97.89	2.11	8.4	2.8
4	2.420	0.063	97.46	2.54	10.1	2.5
5	2.410	0.073	97.06	2.94	11.7	2.3
6	2.400	0.083	96.66	3.34	13.3	2.2
7	2.389	0.094	96.22	3.78	15.1	2.2
8	2.378	0.105	95.76	4.24	16.9	2.1
9	2.366	0.117	95.29	4.71	18.8	2.1
10	2.352	0.131	94.73	5.27	21.1	2.1
11	2.337	0.146	94.14	5.86	23.4	2.1
12	2.321	0.162	93.49	6.51	26.0	2.2
13	2.305	0.177	92.86	7.14	28.6	2.2
14	2.287	0.196	92.13	7.87	31.5	2.2
15	2.267	0.216	91.32	8.68	34.7	2.3

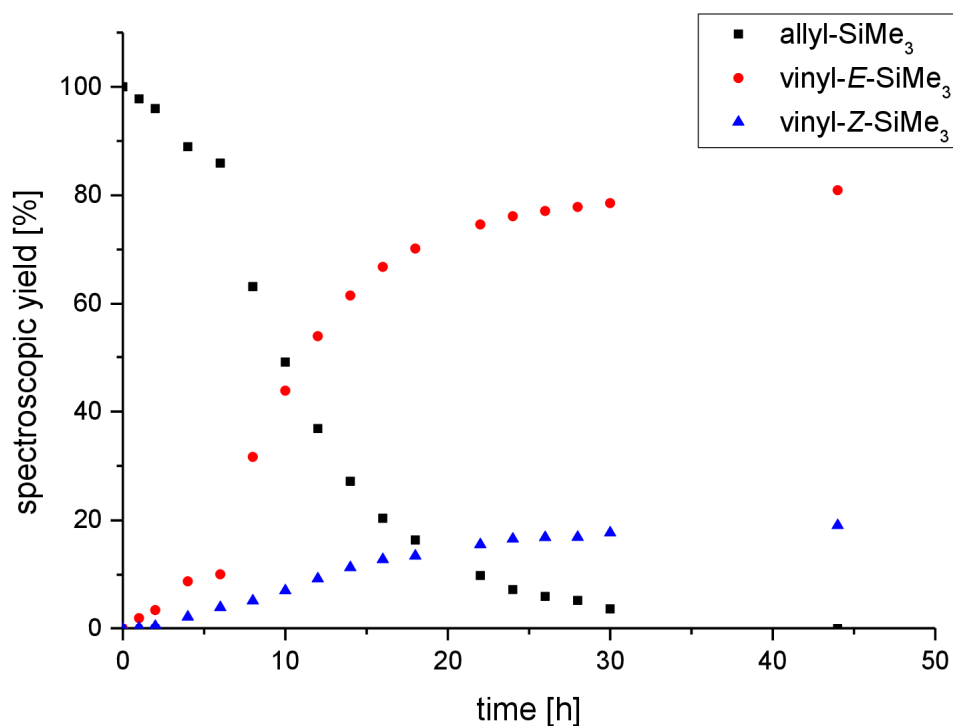
16	2.245	0.238	90.41	9.59	38.3	2.4
17	2.221	0.262	89.46	10.54	42.2	2.5
18	2.197	0.285	88.51	11.49	46.0	2.6
19	2.170	0.313	87.41	12.59	50.3	2.6
20	2.147	0.335	86.49	13.51	54.0	2.7
22	2.098	0.385	84.51	15.49	61.9	2.8
24	2.053	0.430	82.70	17.30	69.2	2.9
26	2.018	0.465	81.28	18.72	74.8	2.9
28	1.979	0.503	79.73	20.27	81.1	2.9
30	1.953	0.530	78.67	21.33	85.3	2.8
32	1.920	0.563	77.34	22.66	90.6	2.8
34	1.891	0.592	76.16	23.84	95.3	2.8
36	1.859	0.623	74.89	25.11	100.4	2.8
38	1.828	0.655	73.62	26.38	105.5	2.8
40	1.793	0.690	72.21	27.79	111.1	2.8
42	1.758	0.725	70.80	29.20	116.7	2.8
44	1.727	0.755	69.58	30.42	121.6	2.8
46	1.698	0.785	68.37	31.63	126.4	2.7
48	1.659	0.824	66.80	33.20	132.7	2.8
50	1.633	0.850	65.77	34.23	136.8	2.7
52	1.599	0.884	64.39	35.61	142.4	2.7
54	1.553	0.929	62.57	37.43	149.7	2.8
56	1.511	0.972	60.87	39.13	156.4	2.8
58	1.469	1.013	59.18	40.82	163.2	2.8



Supplementary Figure 51: Plot of the spectroscopically determined conversion to 2-*trans*-hexene with 0.25 mol% Rh 4.

Supplementary Table 6: Catalytic activity of Rh-4 with 1-hexene: determined conversion by ^1H NMR spectroscopy, calculated TON and TOF.

Time [h]	n (1-hexene) [mmol]	n (2-hexene) [mmol]	1-hexene [%]	2-hexene [%]	TON	TOF [h ⁻¹]
0	2.419	0.022	99.10	0.90	3.6	-
1	2.387	0.053	97.82	2.18	8.7	8.7
2	2.364	0.076	96.88	3.12	12.5	6.2
3	2.349	0.091	96.25	3.75	15.0	5.0
4	2.338	0.103	95.79	4.21	16.9	4.2
5	2.324	0.116	95.23	4.77	19.1	3.8
6	2.312	0.128	94.74	5.26	21.0	3.5
7	2.299	0.141	94.21	5.79	23.2	3.3
8	2.287	0.153	93.72	6.28	25.1	3.1
9	2.276	0.165	93.25	6.75	27.0	3.0
10	2.263	0.177	92.74	7.26	29.0	2.9
11	2.250	0.190	92.21	7.79	31.2	2.8
12	2.241	0.199	91.84	8.16	32.7	2.7
13	2.230	0.211	91.36	8.64	34.6	2.7
14	2.215	0.226	90.75	9.25	37.0	2.6
15	2.206	0.234	90.40	9.60	38.4	2.6
16	2.194	0.246	89.91	10.09	40.4	2.5
17	2.180	0.260	89.34	10.66	42.7	2.5
18	2.171	0.269	88.97	11.03	44.1	2.5
19	2.160	0.281	88.50	11.50	46.0	2.4
20	2.154	0.286	88.27	11.73	46.9	2.3
21	2.134	0.306	87.45	12.55	50.2	2.4
22	2.119	0.322	86.81	13.19	52.8	2.4
24	2.116	0.324	86.71	13.29	53.2	2.2
26	2.107	0.333	86.34	13.66	54.7	2.1
28	2.099	0.342	85.99	14.01	56.0	2.0
30	2.083	0.357	85.36	14.64	58.6	2.0
32	2.076	0.365	85.05	14.95	59.8	1.9
34	2.066	0.375	84.64	15.36	61.4	1.8
36	2.055	0.385	84.22	15.78	63.1	1.8
38	2.041	0.399	83.64	16.36	65.5	1.7
40	2.033	0.408	83.29	16.71	66.9	1.7
42	2.024	0.416	82.94	17.06	68.3	1.6
44	2.005	0.435	82.17	17.83	71.3	1.6
46	1.994	0.446	81.70	18.30	73.2	1.6
48	1.983	0.457	81.26	18.74	75.0	1.6
50	1.971	0.470	80.75	19.25	77.0	1.5
52	1.961	0.479	80.37	19.63	78.5	1.5
54	1.947	0.493	79.78	20.22	80.9	1.5
56	1.931	0.509	79.14	20.86	83.4	1.5
58	1.918	0.522	78.60	21.40	85.6	1.5

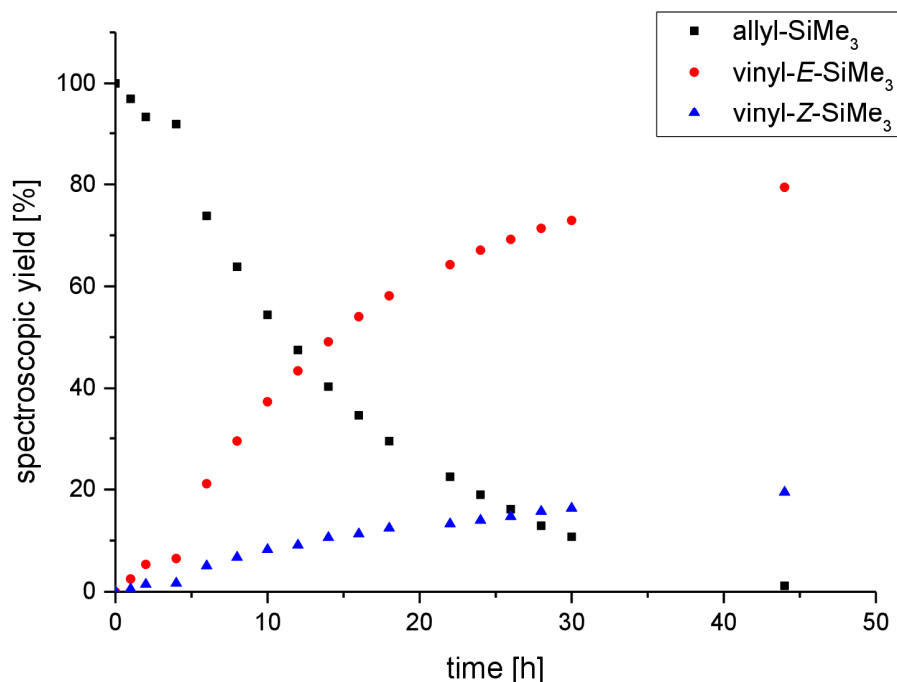


Supplementary Figure 52: Plot of the spectroscopically determined conversion to *E/Z*-vinyltrimethylsilane with 0.8 mol% Si-Ir **2a** at 60 °C. black = allyltrimethylsilane, red = *E*-vinyltrimethylsilane, blue = *Z*-vinyltrimethylsilane.

Supplementary Table 7: Catalytic activity of **2a** with allyltrimethylsilane: determined conversion by ¹H NMR spectroscopy, calculated TON and TOF

Time [h]	n (allyl-SiMe ₃) [mmol]	n (<i>E</i> -vinyl) [mmol]	n (<i>Z</i> -vinyl) [mmol]	allyl-SiMe ₃ [%]	<i>E</i> -vinyl [%]	<i>Z</i> -vinyl [%]	TON	TOF [h ⁻¹]
0	2.125	0.00	0.000	100.00	0.00	0.00	0.0	-
1	2.078	0.04	0.004	97.77	2.02	0.21	2.8	2.8
2	2.039	0.07	0.012	95.95	3.50	0.55	5.1	2.5
4	1.890	0.19	0.048	88.94	8.79	2.27	13.8	3.5
6	1.826	0.21	0.085	85.91	10.09	4.00	17.6	2.9
8	1.342	0.67	0.111	63.13	31.66	5.20	46.1	5.8
10	1.043	0.93	0.151	49.09	43.82	7.10	63.6	6.4
12	0.784	1.14	0.197	36.88	53.84	9.28	78.9	6.6
14	0.577	1.31	0.241	27.17	61.49	11.34	91.0	6.5
16	0.433	1.42	0.273	20.39	66.79	12.82	99.5	6.2
18	0.348	1.49	0.286	16.40	70.15	13.45	104.5	5.8
22	0.209	1.59	0.330	9.85	74.60	15.55	112.7	5.1
24	0.155	1.62	0.353	7.29	76.12	16.60	115.9	4.8
26	0.128	1.64	0.359	6.03	77.09	16.88	117.5	4.5
28	0.112	1.65	0.359	5.27	77.83	16.90	118.4	4.2

30	0.080	1.67	0.377	3.75	78.53	17.72	120.3	4.0
44	0.000	1.72	0.405	0.01	80.93	19.05	125.0	2.8

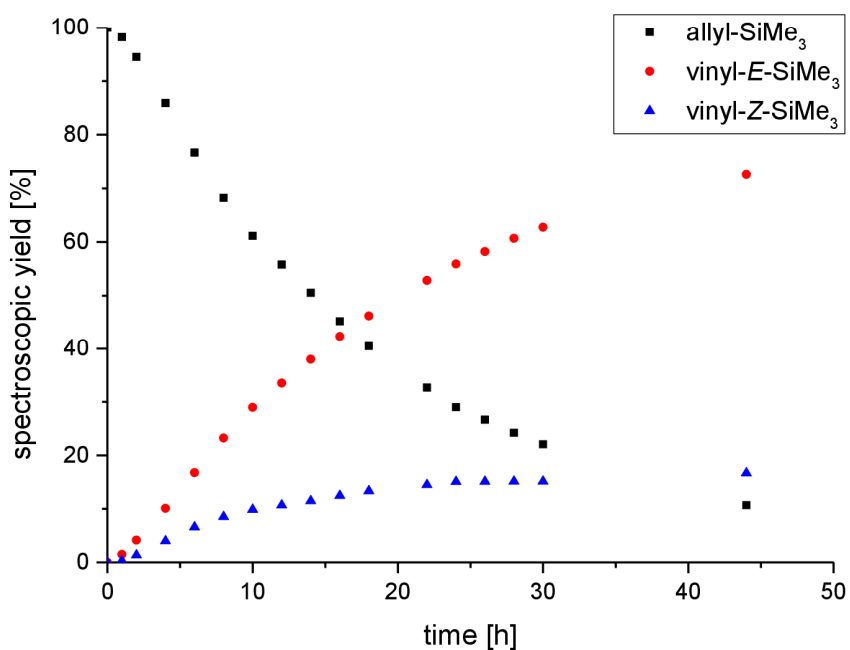


Supplementary Figure 53: Plot of the spectroscopically determined conversion to *E/Z*-vinyltrimethylsilane with 0.8 mol% Ge-Ir **2b** at 60 °C. black = allyltrimethylsilane, red = *E*-vinyltrimethylsilane, blue = *Z*-vinyltrimethylsilane.

Supplementary Table 8: Catalytic activity of **2b** with allyltrimethylsilane: determined conversion by ¹H NMR spectroscopy, calculated TON and TOF

Time [h]	n (allyl-SiMe ₃) [mmol]	n (<i>E</i> -vinyl) [mmol]	n (<i>Z</i> -vinyl) [mmol]	allyl-SiMe ₃ [%]	<i>E</i> -vinyl [%]	<i>Z</i> -vinyl [%]	TON	TOF [h ⁻¹]
0	2.073	0.000	0.000	100.00	0.00	0.00	0.0	-
1	2.010	0.052	0.011	96.96	2.50	0.55	3.8	3.8
2	1.932	0.111	0.030	93.20	5.36	1.44	8.5	4.2
4	1.903	0.135	0.035	91.82	6.50	1.68	10.2	2.6
6	1.530	0.438	0.105	73.82	21.11	5.07	32.7	5.5
8	1.323	0.611	0.139	63.82	29.47	6.72	45.2	5.7
10	1.128	0.774	0.171	54.39	37.35	8.26	57.0	5.7
12	0.984	0.900	0.189	47.48	43.41	9.11	65.7	5.5
14	0.836	1.018	0.219	40.31	49.10	10.59	74.6	5.3
16	0.719	1.120	0.234	34.68	54.02	11.29	81.7	5.1
18	0.610	1.205	0.258	29.44	58.12	12.43	88.2	4.9
22	0.466	1.332	0.275	22.49	64.24	13.27	96.9	4.4
24	0.393	1.390	0.290	18.96	67.07	13.97	101.3	4.2

26	0.334	1.434	0.305	16.12	69.19	14.69	104.9	4.0
28	0.268	1.480	0.326	12.92	71.37	15.70	108.9	3.9
30	0.223	1.511	0.338	10.77	72.91	16.32	111.6	3.7
44	0.024	1.646	0.403	1.16	79.40	19.44	123.6	2.8



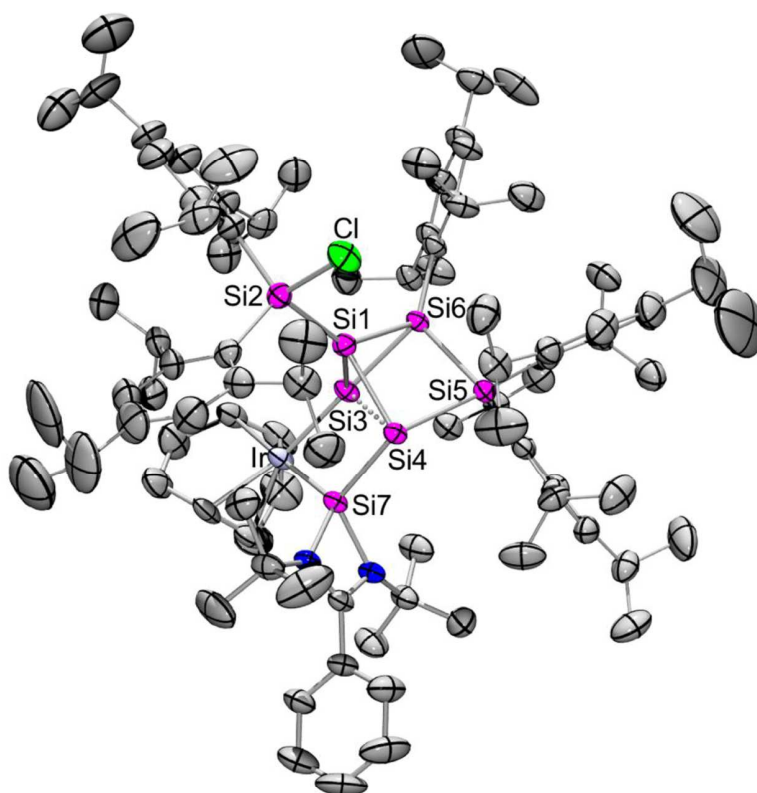
Supplementary Figure 54: Plot of the spectroscopically determined conversion to *E/Z*-vinyltrimethylsilane with 0.8 mol% Sn-Ir **2c** at 60 °C. black = allyltrimethylsilane, red = *E*-vinyltrimethylsilane, blue = *Z*-vinyltrimethylsilane.

Supplementary Table 9: Catalytic activity of **2c** with allyltrimethylsilane: determined conversion by ¹H NMR spectroscopy, calculated TON and TOF

Time [h]	n (allyl-SiMe ₃) [mmol]	n (<i>E</i> -vinyl) [mmol]	n (<i>Z</i> -vinyl) [mmol]	allyl-SiMe ₃ [%]	<i>E</i> -vinyl [%]	<i>Z</i> -vinyl [%]	TON	TOF [h ⁻¹]
0	2.021	0.000	0.000	100.00	0.00	0.00	0.0	-
1	1.985	0.030	0.006	98.21	1.51	0.28	2.2	2.2
2	1.910	0.084	0.027	94.49	4.16	1.35	6.9	3.4
4	1.736	0.204	0.081	85.89	10.11	3.99	17.6	4.4
6	1.549	0.339	0.133	76.66	16.76	6.58	29.2	4.9
8	1.379	0.470	0.172	68.23	23.25	8.53	39.7	5.0
10	1.236	0.586	0.199	61.15	28.98	9.87	48.6	4.9
12	1.128	0.677	0.216	55.79	33.52	10.69	55.2	4.6
14	1.021	0.768	0.232	50.53	37.99	11.47	61.8	4.4
16	0.913	0.856	0.252	45.19	42.35	12.46	68.5	4.3
18	0.818	0.933	0.270	40.47	46.18	13.34	74.4	4.1
22	0.660	1.068	0.293	32.67	52.85	14.48	84.2	3.8

24	0.586	1.130	0.305	29.00	55.92	15.08	88.7	3.7
26	0.539	1.177	0.306	26.66	58.22	15.12	91.7	3.5
28	0.489	1.226	0.306	24.20	60.67	15.12	94.7	3.4
30	0.446	1.269	0.306	22.09	62.77	15.15	97.4	3.2
44	0.216	1.468	0.337	10.70	72.61	16.69	111.6	2.5

4. Details on X-ray Diffraction Studies



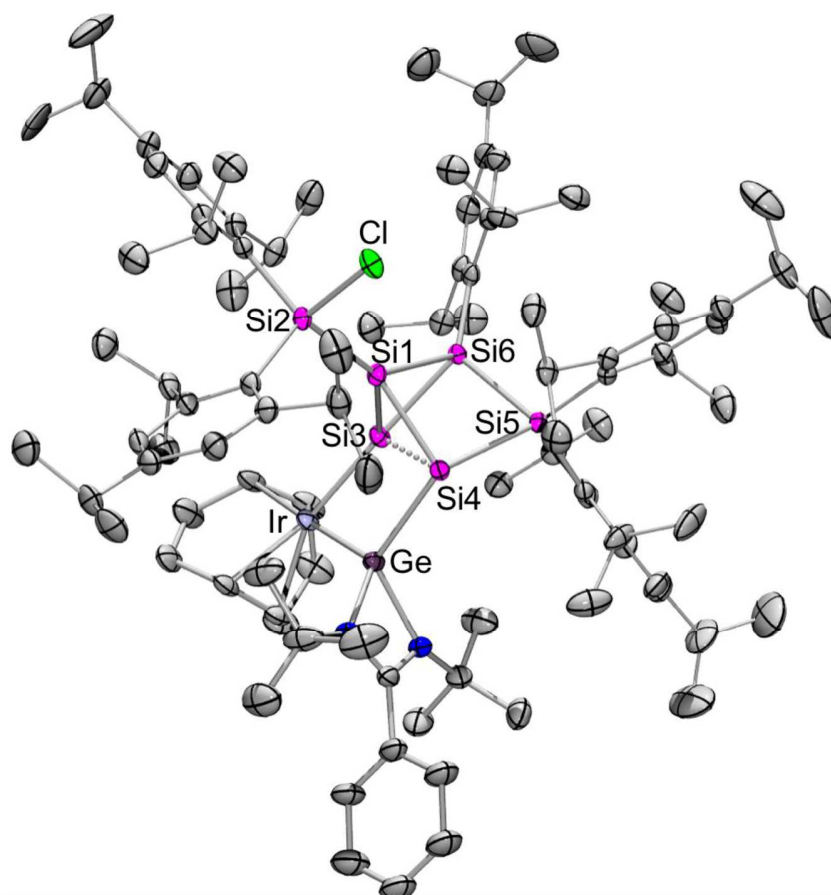
Supplementary Figure 55: Molecular structure of siliconoid **2a** in the solid state. Hydrogen atoms omitted for clarity. Thermal ellipsoids represent 50% probability.

Supplementary Table 10: Crystal data and structure refinement for **2a** (CCDC: 2000911).

Identification code	sh3975
Empirical formula	C ₉₈ H ₁₅₀ Cl Ir N ₂ Si ₇ , 0.5(C ₇ H ₁₄)
Formula weight	1823.56
Temperature	232(2) K
Wavelength	0.71073 Å
Crystal system	Triclinic
Space group	P-1
	S43

6 Supporting Information

Unit cell dimensions	a = 16.5707(18) Å	$\alpha = 105.174(4)^\circ$.
	b = 16.9084(19) Å	$\beta = 96.576(4)^\circ$.
	c = 21.231(2) Å	$\gamma = 109.461(4)^\circ$.
Volume	5278.5(10) Å ³	
Z	2	
Density (calculated)	1.147 Mg/m ³	
Absorption coefficient	1.411 mm ⁻¹	
F(000)	1938	
Crystal size	0.225 x 0.223 x 0.203 mm ³	
Theta range for data collection	1.337 to 27.228°.	
Index ranges	-21 ≤ h ≤ 21, -21 ≤ k ≤ 21, -27 ≤ l ≤ 25	
Reflections collected	86047	
Independent reflections	23228 [R(int) = 0.0613]	
Completeness to theta = 25.242°	99.8 %	
Absorption correction	Semi-empirical from equivalents	
Max. and min. transmission	0.7455 and 0.6468	
Refinement method	Full-matrix least-squares on F ²	
Data / restraints / parameters	23228 / 118 / 1081	
Goodness-of-fit on F ²	1.009	
Final R indices [I > 2σ(I)]	R1 = 0.0491, wR2 = 0.1193	
R indices (all data)	R1 = 0.0797, wR2 = 0.1340	
Extinction coefficient	n/a	
Largest diff. peak and hole	2.194 and -0.953 e.Å ⁻³	

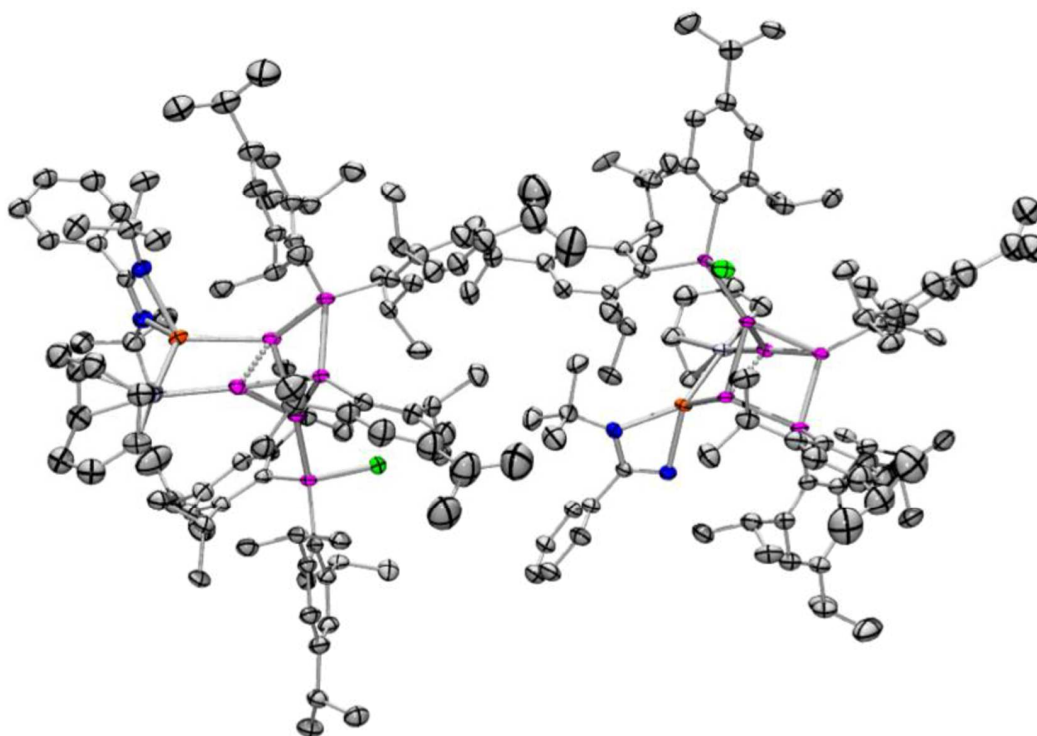


Supplementary Figure 56: Molecular structure of siliconoid **2b** in the solid state. Hydrogen atoms omitted for clarity. Thermal ellipsoids represent 50% probability.

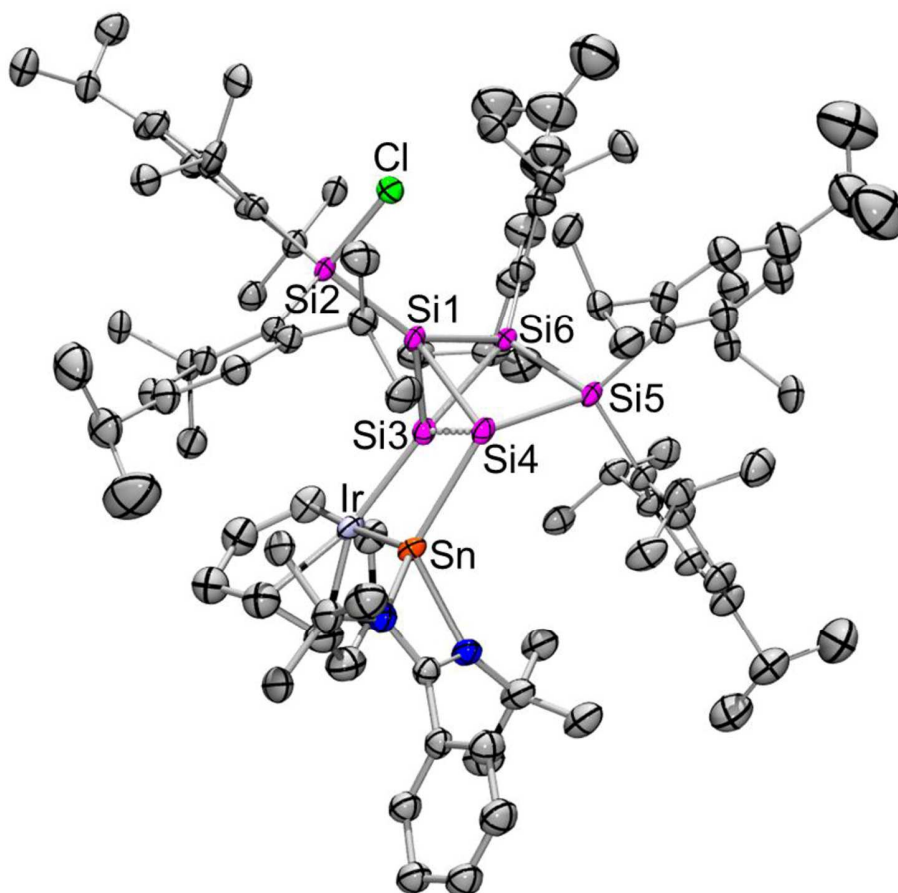
Supplementary Table 11: Crystal data and structure refinement for **2b** (CCDC: 2000912).

Identification code	sh3966	
Empirical formula	C ₉₈ H ₁₅₀ Cl Ge Ir N ₂ Si ₆ , 0.5(C ₆ H ₁₄)	
Formula weight	1868.06	
Temperature	152(2) K	
Wavelength	0.71073 Å	
Crystal system	Monoclinic	
Space group	P2 ₁ /n	
Unit cell dimensions	a = 15.7711(4) Å	$\alpha = 90^\circ$.
	b = 31.3736(8) Å	$\beta = 106.081(2)^\circ$.
	c = 21.3327(6) Å	$\gamma = 90^\circ$.
Volume	10142.3(5) Å ³	
Z	4	
Density (calculated)	1.223 Mg/m ³	
Absorption coefficient	1.748 mm ⁻¹	
F(000)	3948	
	S45	

Crystal size	0.501 x 0.302 x 0.284 mm ³
Theta range for data collection	1.187 to 26.801°
Index ranges	-19<=h<=19, -39<=k<=39, -27<=l<=27
Reflections collected	237683
Independent reflections	21643 [R(int) = 0.0473]
Completeness to theta = 25.242°	100.0 %
Absorption correction	Semi-empirical from equivalents
Max. and min. transmission	0.7454 and 0.6349
Refinement method	Full-matrix least-squares on F ²
Data / restraints / parameters	21643 / 267 / 1147
Goodness-of-fit on F ²	1.144
Final R indices [I>2sigma(I)]	R1 = 0.0332, wR2 = 0.0676
R indices (all data)	R1 = 0.0437, wR2 = 0.0710
Extinction coefficient	n/a
Largest diff. peak and hole	1.172 and -0.942 e.Å ⁻³



Supplementary Figure 57: Molecular structure of siliconoid **2c** in the solid state with two molecules in the asymmetric unit. Hydrogen atoms omitted for clarity. Thermal ellipsoids represent 50% probability.

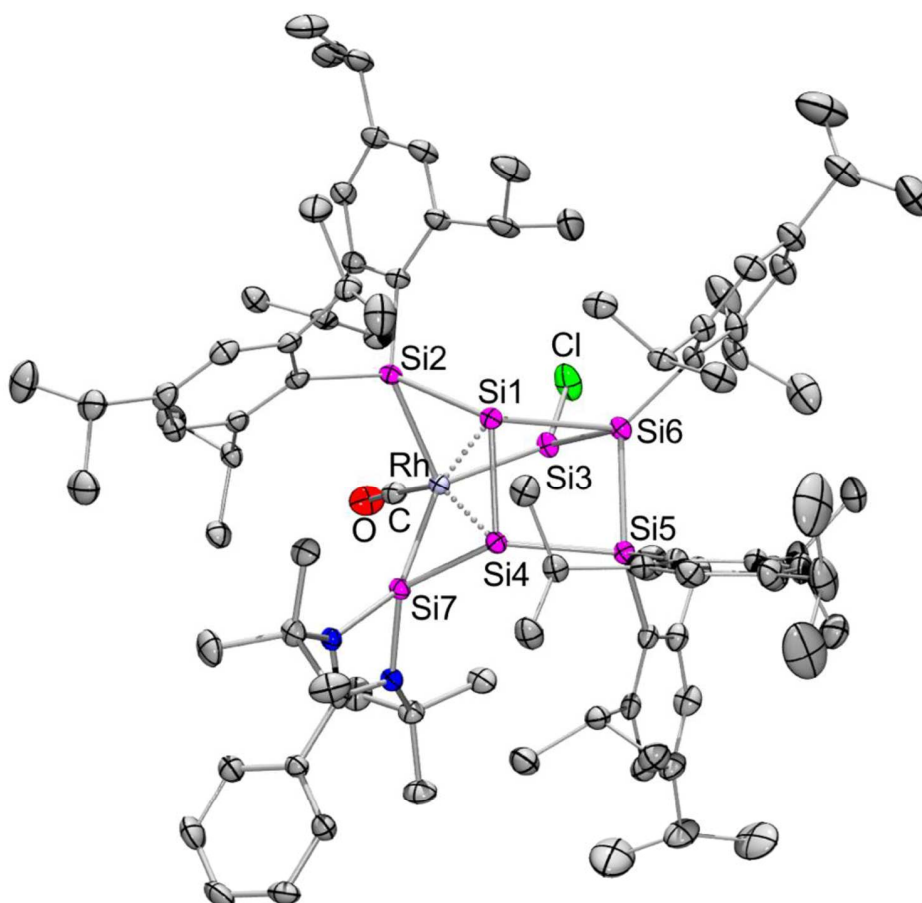


Supplementary Figure 58: Molecular structure of siliconoid **2c** in the solid state. Hydrogen atoms and second molecule omitted for clarity. Thermal ellipsoids represent 50% probability.

Supplementary Table 12: Crystal data and structure refinement for **2c** (CCDC: 2000913).

Identification code	sh4029	
Empirical formula	C ₉₈ H ₁₅₀ Cl Ir N ₂ Si ₆ Sn, 0.5(C ₆ H ₁₄)	
Formula weight	1914.16	
Temperature	100(2) K	
Wavelength	0.71073 Å	
Crystal system	Triclinic	
Space group	P-1	
Unit cell dimensions	a = 15.7798(19) Å	α = 104.327(6)°.
	b = 26.095(3) Å	β = 106.150(6)°.
	c = 27.363(4) Å	γ = 90.156(6)°.
Volume	10455(2) Å ³	
Z	4	
Density (calculated)	1.216 Mg/m ³	
Absorption coefficient	1.647 mm ⁻¹	
F(000)	4020	
	S47	

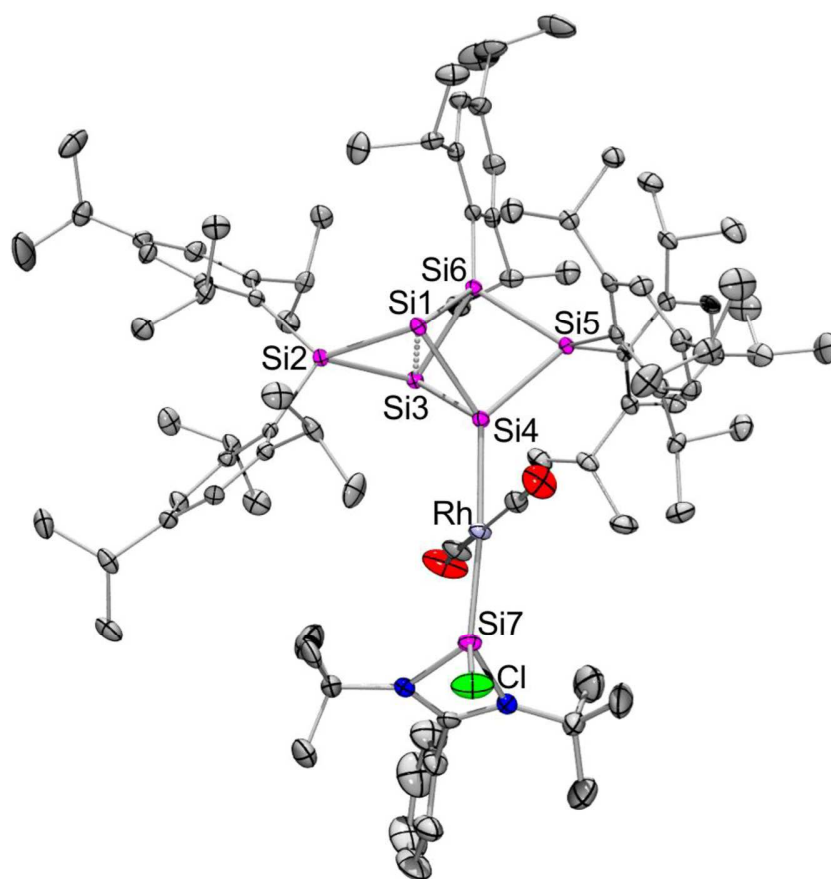
Crystal size	0.432 x 0.317 x 0.197 mm ³
Theta range for data collection	1.277 to 27.832°
Index ranges	-20 ≤ h ≤ 20, -33 ≤ k ≤ 33, -35 ≤ l ≤ 35
Reflections collected	151379
Independent reflections	47657 [R(int) = 0.0833]
Completeness to theta = 25.242°	98.9 %
Absorption correction	Semi-empirical from equivalents
Max. and min. transmission	0.7455 and 0.5496
Refinement method	Full-matrix least-squares on F ²
Data / restraints / parameters	47657 / 4639 / 2128
Goodness-of-fit on F ²	2.470
Final R indices [I > 2σ(I)]	R1 = 0.1685, wR2 = 0.3641
R indices (all data)	R1 = 0.1945, wR2 = 0.3704
Extinction coefficient	n/a
Largest diff. peak and hole	5.451 and -5.133 e.Å ⁻³



Supplementary Figure 59: Molecular structure of siliconoid **3** in the solid state. Hydrogen atoms omitted for clarity. Thermal ellipsoids represent 50% probability.

Supplementary Table 13: Crystal data and structure refinement for **3** (CCDC: 2000914).

Identification code	sh3984	
Empirical formula	C ₉₁ H ₁₃₈ Cl N ₂ O Rh Si ₇ , 2(C ₇ H ₈)	
Formula weight	1795.28	
Temperature	142(2) K	
Wavelength	0.71073 Å	
Crystal system	Triclinic	
Space group	P-1	
Unit cell dimensions	a = 14.9387(8) Å	α = 102.165(3)°.
	b = 17.6518(9) Å	β = 92.721(3)°.
	c = 21.0713(11) Å	γ = 108.260(3)°.
Volume	5119.4(5) Å ³	
Z	2	
Density (calculated)	1.165 Mg/m ³	
Absorption coefficient	0.321 mm ⁻¹	
F(000)	1932	
Crystal size	0.244 x 0.193 x 0.058 mm ³	
Theta range for data collection	1.251 to 27.694°.	
Index ranges	-19 ≤ h ≤ 19, -23 ≤ k ≤ 22, -27 ≤ l ≤ 21	
Reflections collected	86147	
Independent reflections	23261 [R(int) = 0.0620]	
Completeness to theta = 25.242°	98.4 %	
Absorption correction	Semi-empirical from equivalents	
Max. and min. transmission	0.7456 and 0.6703	
Refinement method	Full-matrix least-squares on F ²	
Data / restraints / parameters	23261 / 134 / 1120	
Goodness-of-fit on F ²	1.018	
Final R indices [I > 2σ(I)]	R1 = 0.0487, wR2 = 0.1050	
R indices (all data)	R1 = 0.0847, wR2 = 0.1200	
Extinction coefficient	n/a	
Largest diff. peak and hole	0.786 and -0.692 e.Å ⁻³	

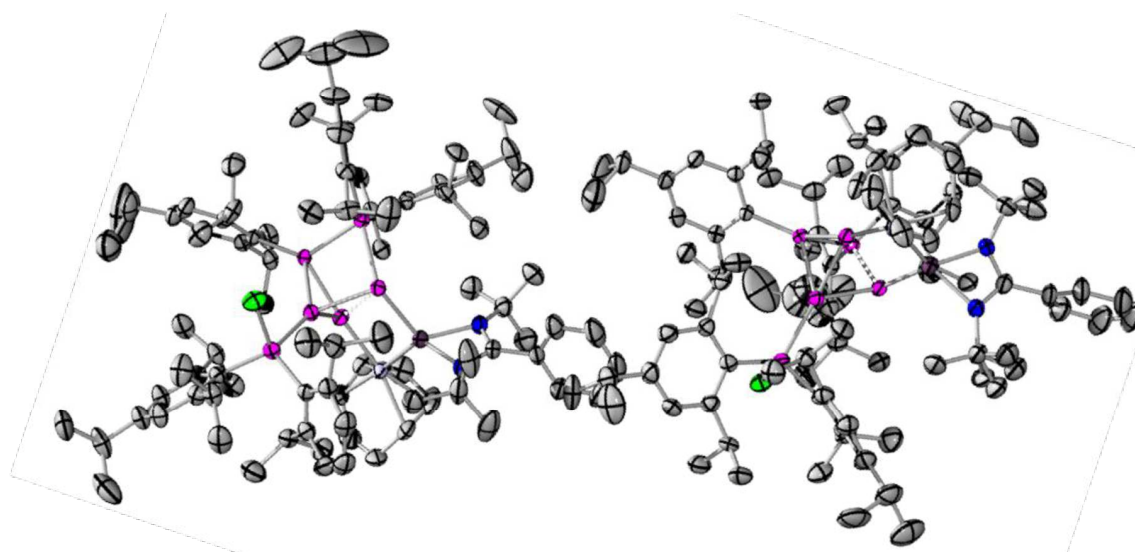


Supplementary Figure 60: Molecular structure of siliconoid **4** in the solid state. Hydrogen atoms omitted for clarity. Thermal ellipsoids represent 50% probability.

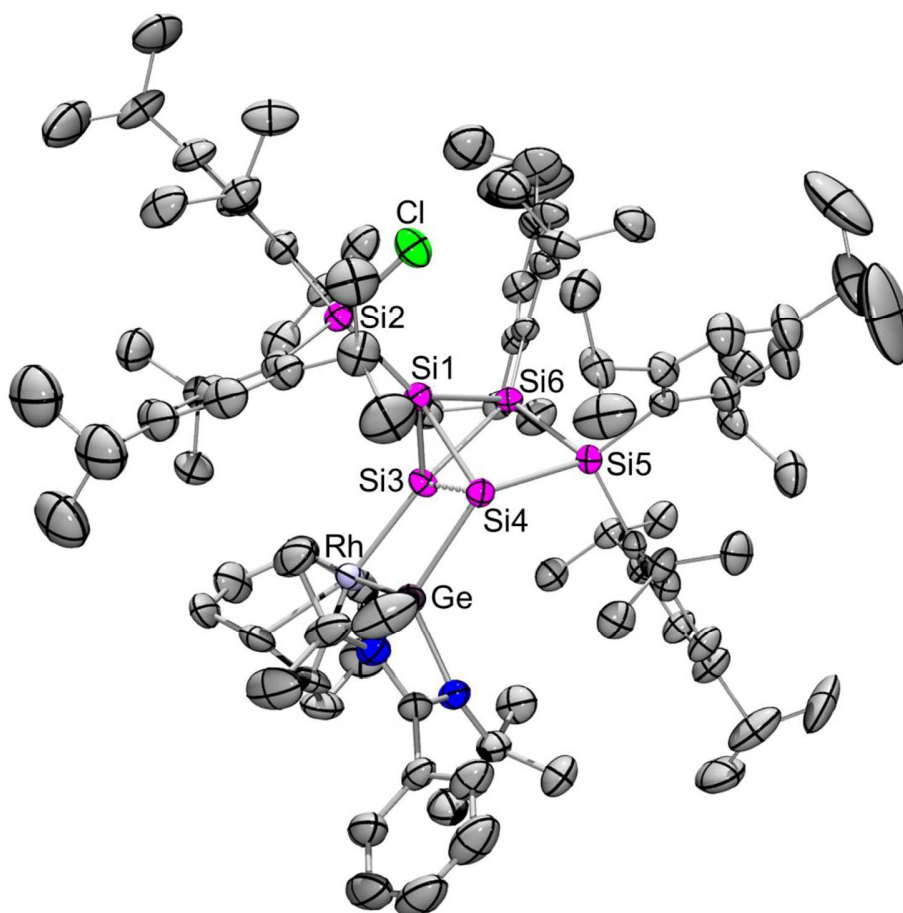
Supplementary Table 14: Crystal data and structure refinement for **4** (CCDC: 2000915).

Identification code	sh3959	
Empirical formula	C ₉₂ H ₁₃₈ Cl N ₂ O ₂ Rh Si ₇	
Formula weight	1639.03	
Temperature	142(2) K	
Wavelength	0.71073 Å	
Crystal system	Orthorhombic	
Space group	Pna2 ₁	
Unit cell dimensions	a = 37.608(4) Å	α = 90°.
	b = 13.6961(14) Å	β = 90°.
	c = 18.1426(19) Å	γ = 90°.
Volume	9345.0(17) Å ³	
Z	4	
Density (calculated)	1.165 Mg/m ³	
Absorption coefficient	0.346 mm ⁻¹	
F(000)	3520	
	S50	

Crystal size	0.375 x 0.222 x 0.054 mm ³
Theta range for data collection	1.560 to 27.934°.
Index ranges	-49<= <i>h</i> <=49, -18<= <i>k</i> <=10, -23<= <i>l</i> <=23
Reflections collected	85115
Independent reflections	22265 [R(int) = 0.0551]
Completeness to theta = 25.242°	100.0 %
Absorption correction	Semi-empirical from equivalents
Max. and min. transmission	0.7456 and 0.6838
Refinement method	Full-matrix least-squares on F ²
Data / restraints / parameters	22265 / 70 / 1034
Goodness-of-fit on F ²	1.008
Final R indices [<i>I</i> >2sigma(<i>I</i>)]	R1 = 0.0408, wR2 = 0.0760
R indices (all data)	R1 = 0.0566, wR2 = 0.0807
Absolute structure parameter	-0.014(8)
Extinction coefficient	n/a
Largest diff. peak and hole	0.645 and -0.493 e.Å ⁻³



Supplementary Figure 61: Molecular structure of siliconoid **4** in the solid state with two molecules in the asymmetric unit. Hydrogen atoms omitted for clarity. Thermal ellipsoids represent 50% probability.



Supplementary Figure 62: Molecular structure of siliconoid **4** in the solid state. Hydrogen atoms and second molecule omitted for clarity. Thermal ellipsoids represent 50% probability.

Supplementary Table 15: Crystal data and structure refinement for **Si₆Ge-[Rh(cod)Cl]** (CCDC: 2000916).

Identification code	sh3988
Empirical formula	C ₉₈ H ₁₅₀ Cl Ge N ₂ Rh Si ₆ , C ₆ H ₁₄
Formula weight	1821.85
Temperature	202(2) K
Wavelength	0.71073 Å
Crystal system	Monoclinic
Space group	P2 ₁ /n
Unit cell dimensions	$a = 29.9006(13) \text{ Å}$ $b = 22.5250(8) \text{ Å}$ $c = 32.5302(12) \text{ Å}$
	$\alpha = 90^\circ$ $\beta = 103.500(2)^\circ$ $\gamma = 90^\circ$
Volume	21304.1(14) Å ³
Z	8
Density (calculated)	1.136 Mg/m ³
Absorption coefficient	0.572 mm ⁻¹

S52

F(000)	7840
Crystal size	0.363 x 0.222 x 0.200 mm ³
Theta range for data collection	1.144 to 27.160°.
Index ranges	-38<=h<=38, -28<=k<=20, -41<=l<=41
Reflections collected	189652
Independent reflections	47061 [R(int) = 0.0881]
Completeness to theta = 25.242°	100.0 %
Absorption correction	Semi-empirical from equivalents
Max. and min. transmission	0.7455 and 0.6530
Refinement method	Full-matrix least-squares on F ²
Data / restraints / parameters	47061 / 457 / 2245
Goodness-of-fit on F ²	1.024
Final R indices [I>2sigma(I)]	R1 = 0.0639, wR2 = 0.1421
R indices (all data)	R1 = 0.1527, wR2 = 0.1768
Extinction coefficient	n/a
Largest diff. peak and hole	1.273 and -0.624 e.Å ⁻³

5. References

- [1] N. E. Poitiers, L. Giarrana, K. I. Leszczyńska, V. Huch, M. Zimmer, D. Scheschkewitz, *Angew. Chem. Int. Ed.* 2020, **59**, 8532-8536.

6.4 Chalcogen-expanded unsaturated silicon clusters: thia-, seleno- and tellurasiliconoids

Chemistry–A European Journal

Supporting Information

Chalcogen-Expanded Unsaturated Silicon Clusters: Thia-, Seleno-, and Tellurasiliconoids

Nadine E. Poitiers, Volker Huch, Michael Zimmer, and David Scheschkewitz^{*[a]}

Author Contributions

N.P. Conceptualization: Equal; Data curation: Lead; Formal analysis: Lead; Investigation: Lead; Methodology: Lead; Validation: Lead; Visualization: Lead; Writing - Original Draft: Lead; Writing - Review & Editing: Lead

V.H. X-ray structures determinations: Lead

M.Z. Solid State NMR acquisition and analysis: Lead.

Table of Contents

1. Experimental Procedures	S2
2. Preparation, data and spectra (NMR, UV-vis, IR) of:	S2
• Thiasiliconoid Si ₇ S (2a)	S2
• Selenasiliconoid Si ₇ Se (2b)	S6
• Tellurasiliconoid Si ₇ Te (2c)	S14
• Comparison of the UV-vis spectra of 1 , 2a , 2b , 2c	S24
3. Computational Details	S25
4. Details on X-Ray Diffraction Studies	S41
• Thiasiliconoid Si ₇ S (2a)	S41
• Selenasiliconoid Si ₇ Se (2b)	S43
• Tellurasiliconoid Si ₇ Te (2c)	S45
4. References	S46
Author Contributions	S46

1. Experimental Procedures

All manipulations were carried out under a protective atmosphere of argon in a glovebox or with standard Schlenk techniques. Ethereal solvents were dried by heating to reflux over Na/benzophenone and distilled and stored under an atmosphere of argon. Hydrocarbons were dried over sodium or potassium. NMR spectra were recorded on a Bruker Avance III 300 NMR spectrometer (^1H = 300.13 MHz, ^{13}C = 75.46 MHz, ^{29}Si = 59.6 MHz) and/or a Bruker Avance IV 400 NMR spectrometer (^1H = 400.13 MHz, ^{13}C = 100.6 MHz, ^{29}Si = 59.6 MHz, ^{77}Se = 76.31 MHz, ^{125}Te = 126.24 MHz). Solid state NMR spectra were recorded on a Bruker Avance III 400 WB spectrometer (^{29}Si = 79.53 MHz, ^{77}Se = 76.34 MHz, ^{125}Te = 126.29 MHz). UV/Vis spectra were recorded on a Shimadzu UV-2600 spectrometer in quartz cells with a path length of 0.1 cm. Elemental analyses were performed on an elemental analyzer Leco CHN-900 and/or an elemental vario Micro Cube. The silylene-substituted Si_6 siliconoid **1** was prepared following the literature protocol.^[1]

2. Preparation, data and spectra (NMR, UV-vis, IR)

General procedure for the synthesis of chalcogen-functionalized Si_7 siliconoids (**2a-c**)

Compounds **2a-c** are prepared by treating 1 equivalent of the *ligato*-silylene-functionalized siliconoid **1** with the indicated amount of sulfur (**2a**), selenium (**2b**), tellurium (**2c**) in benzene. The suspension was stirred at room temperature for the indicated time until the color changed to yellow. All volatiles were removed in vacuo and the crude product is filtered from the indicated amount of hexane and crystallized from hexane at room temperature. Concentration of the mother liquor affords a second batch of yellow crystals of **2a-c**.

Preparation of thiasiliconoid Si_7S (**2a**)

Quantities: Si_6NHSi **1**, 400 mg (0.277 mmol), sulfur 22.2 mg (0.692 mmol), benzene 6 mL, stirred for 4 hours at room temperature, filtered from hexane 6 mL, crystallization from hexane. Yield: 190 mg (0.129 mmol; 74 %) bright yellow crystals (mp. 370°C, no dec.).

^1H -NMR (400.13 MHz, C_6D_6 , 300 K) δ = 7.432 – 7.428 (m, 1H, Ar-H), 7.381– 7.377 (m, 1H, Ar-H), 7.089 (s, 3H, Ar-H), 7.066 – 7.062 (m, 1H, Ar-H), 7.029 – 6.968 (m, 3H, Ar-H), 6.848 – 6.757 (m, 3 H, Ar-H), 6.655 – 6.614 (m, 1H, Ar-H), 6.331 – 6.311 (m, 1 H, Ar-H), 5.858 (sept, 1H, $^3J_{\text{HH}} = 6.24$ Hz, Tip-*i*Pr-CH₂), 5.449(sept, 1H, $^3J_{\text{HH}} = 6.24$ Hz, Tip-*i*Pr-CH₂), 5.169 (sept, 1H, $^3J_{\text{HH}} = 6.24$ Hz, Tip-*i*Pr-CH₂), 4.940 (sept, 1H, $^3J_{\text{HH}} = 6.24$ Hz, Tip-*i*Pr-CH₂), 4.390 (sept, 1H, $^3J_{\text{HH}} = 6.24$ Hz, Tip-*i*Pr-CH₂), 4.041 (sept, 1H, $^3J_{\text{HH}} = 6.24$ Hz, Tip-*i*Pr-CH₂), 3.527 (sept, 1H, $^3J_{\text{HH}} = 6.24$ Hz, Tip-*i*Pr-CH₂), 3.3625 (sept, 2H $^3J_{\text{HH}} = 6.24$ Hz, Tip-*i*Pr-CH₂), 3.204 (sept, 1H, $^3J_{\text{HH}} = 6.24$ Hz, Tip-*i*Pr-CH₂), 2.912 – 2.823 (m, 2 H, Tip-*i*Pr-CH₂), 2.751 – 2.662 (m, 3H, Tip-*i*Pr-CH₂), 2.342 (d, 3H, $^3J_{\text{HH}} = 6.24$ Hz, Tip-*i*Pr-CH₃), 2.021 (d, 3H, $^3J_{\text{HH}} = 6.87$ Hz, Tip-*i*Pr-CH₃), 1.826 (d, 3H, $^3J_{\text{HH}} = 6.87$ Hz, Tip-*i*Pr-CH₃), 1.735 – 1.649 (m, 10 H, Tip-*i*Pr-CH₃), 1.561 – 1.425 (m, 20H, Tip-*i*Pr-CH₃), 1.361 – 1.114 (m, 64 H, Tip-*i*Pr-CH₃ overlapping with $\text{C}(\text{CH}_3)_3$), 0.889 (t, 2H, hexane), 0.768 (d, 3H, $^3J_{\text{HH}} = 6.40$ Hz, Tip-*i*Pr-CH₃), 0.714 (d, 3H, $^3J_{\text{HH}} = 6.86$ Hz, Tip-*i*Pr-CH₃), 0.607 (d, 3H, $^3J_{\text{HH}} = 6.40$ Hz, Tip-*i*Pr-CH₃), 0.474 – 0.442 (m, 6H, Tip-*i*Pr-CH₃), 0.359 (d, 3H, $^3J_{\text{HH}} = 5.95$ Hz, Tip-*i*Pr-CH₃) ppm.

^{13}C -NMR (100.61 MHz, C_6D_6 , 300 K) δ = 172.03 (s, 1C, C-Ph), 157.27, 155.94, 154.70, 154.60, 153.70, 153.46, 152.94, 152.89, 152.45, 152.32, 150.07, 149.54, 149.26, 149.08, 148.96 (s, each 1C, Ar-C), 140.58, 139.54, 139.13, 135.52, 133.32, 132.57 (s, each 1C, Ar-C), 129.52, 129.39 (s, each 1C, Ar-CH), 128.11, 127.87, 127.65 (s, each 1C, overlapping with C_6D_6 , Ar-CH), 127.01 (s, 1C, Ar-CH), 123.70, 122.92, 122.39, 122.32, 122.19, 122.01, 121.83, 121.51, 120.07 (s, each 1C, Ar-CH), 56.63, 56.27 (s, each 1C, $\text{C}(\text{CH}_3)_3$), 36.59, 35.74, 35.69, 35.22, 34.96, 34.84, 34.69, 34.64, 34.60, 34.52, 34.38, 34.31 (s, each 1C, Tip-*i*Pr-CH), 32.72 (s, 2C, Tip-*i*Pr-CH), 31.91, 31.52 (s, each 1C, Tip-*i*Pr-CH), 31.37 (s, 2C, Tip-*i*Pr-CH), 29.64, 29.58, 28.20, 28.83, 27.83, 27.53, 27.06, 26.90, 26.46 (s, each 1C, Tip-*i*Pr-CH₃), 25.63, 25.34, 24.81, 24.73, 24.28, 24.19, 24.15, 24.03, 24.01, 23.99, 23.95, 23.73, 23.49, 23.37, 22.99, 22.28 (s, each 1C, Tip-*i*Pr-CH₃), 14.31 (s, 1C, Tip-*i*Pr-CH₃) ppm.

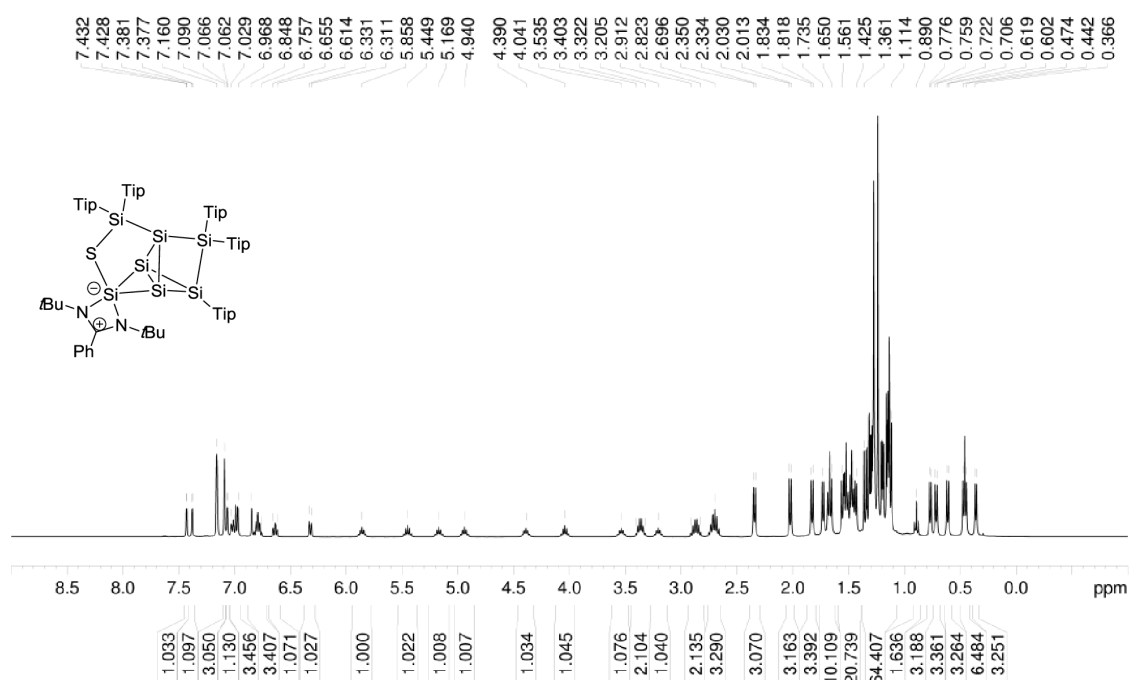
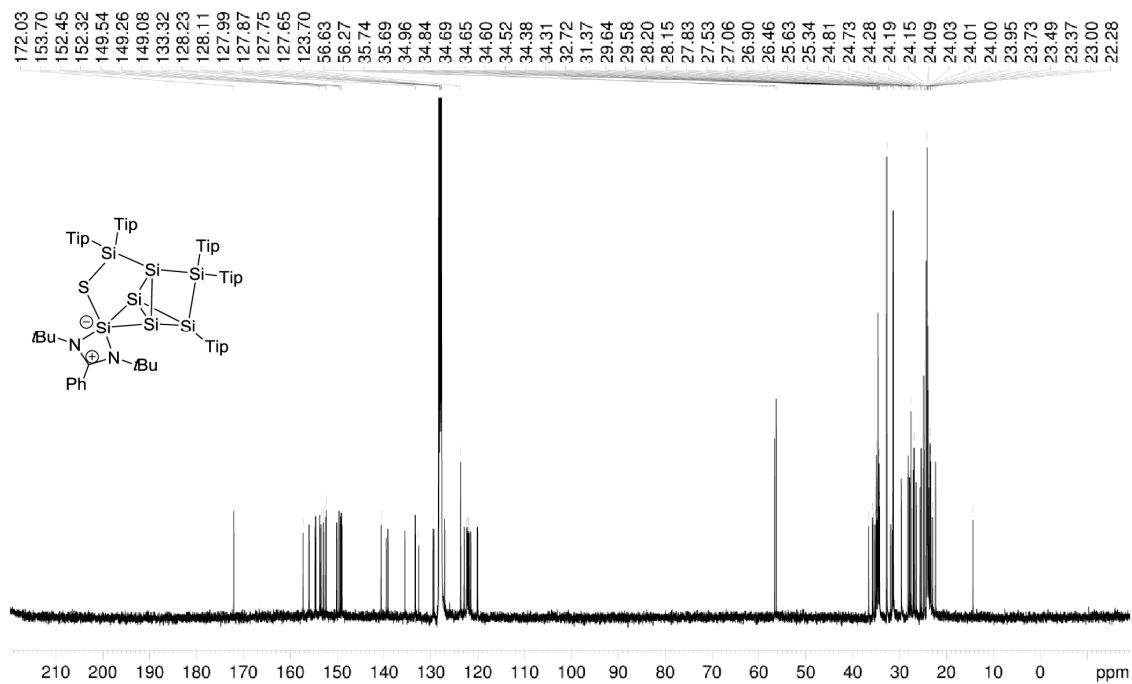
^{29}Si -NMR (79.49 MHz, C_6D_6 , 300 K) δ = 33.5 (s, NHSi), -7.0 (s, SiTip), -11.2 (s, SiTip₂), -13.0 (s, SiTip₂), -109.7 (s, Si), -251.1 (s, Si), -314.9 (s, Si) ppm.

CP-MAS ^{29}Si -NMR (79.53 MHz, 13KHz, 300K) δ = 31.3 (s, NHSi), -7.7 (s, SiTip), -11.1 (s, SiTip₂), -17.3 (SiTip₂), -115.1 (s, Si), -248.4 (s, Si), -316.4 (s, Si) ppm.

Elemental analysis: calculated for $\text{C}_{90}\text{H}_{138}\text{N}_2\text{SSi}_7$: C: 73.20 % ; H: 9.42 % ; N: 1.90 %. Found: C: 72.29 % ; H: 9.63 % ; N: 1.65 %.

SUPPORTING INFORMATION

WILEY-VCH

UV/VIS (hexane): λ_{max} (ϵ) = 394 nm (2870 M⁻¹ cm⁻¹).Figure S1. ¹H NMR of **2a** in C₆D₆ (400.13 MHz, 300 K).Figure S2. ¹³C NMR of **2a** in C₆D₆ (100.61 MHz, 300 K).

SUPPORTING INFORMATION

WILEY-VCH

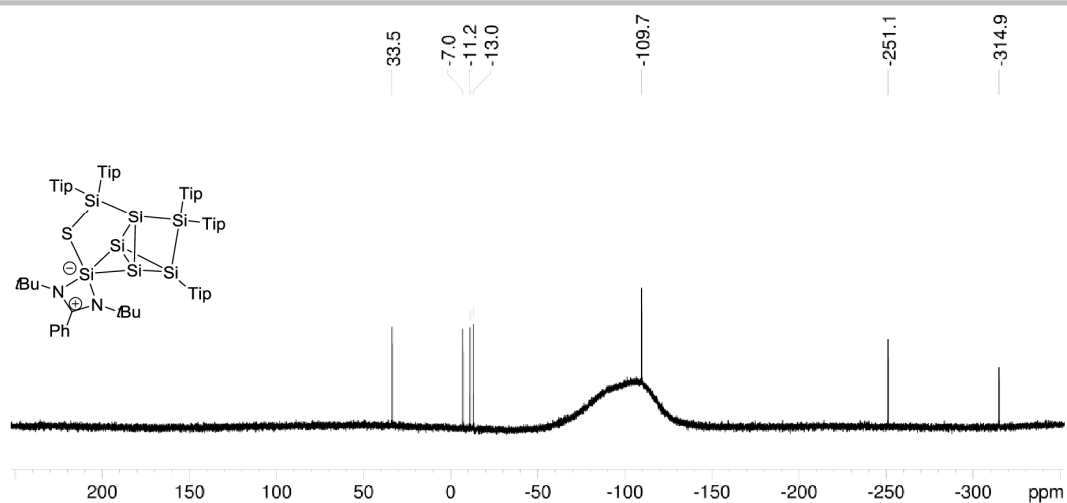


Figure S3. ^{29}Si NMR of **2a** in C_6D_6 (79.49 MHz, 300 K).

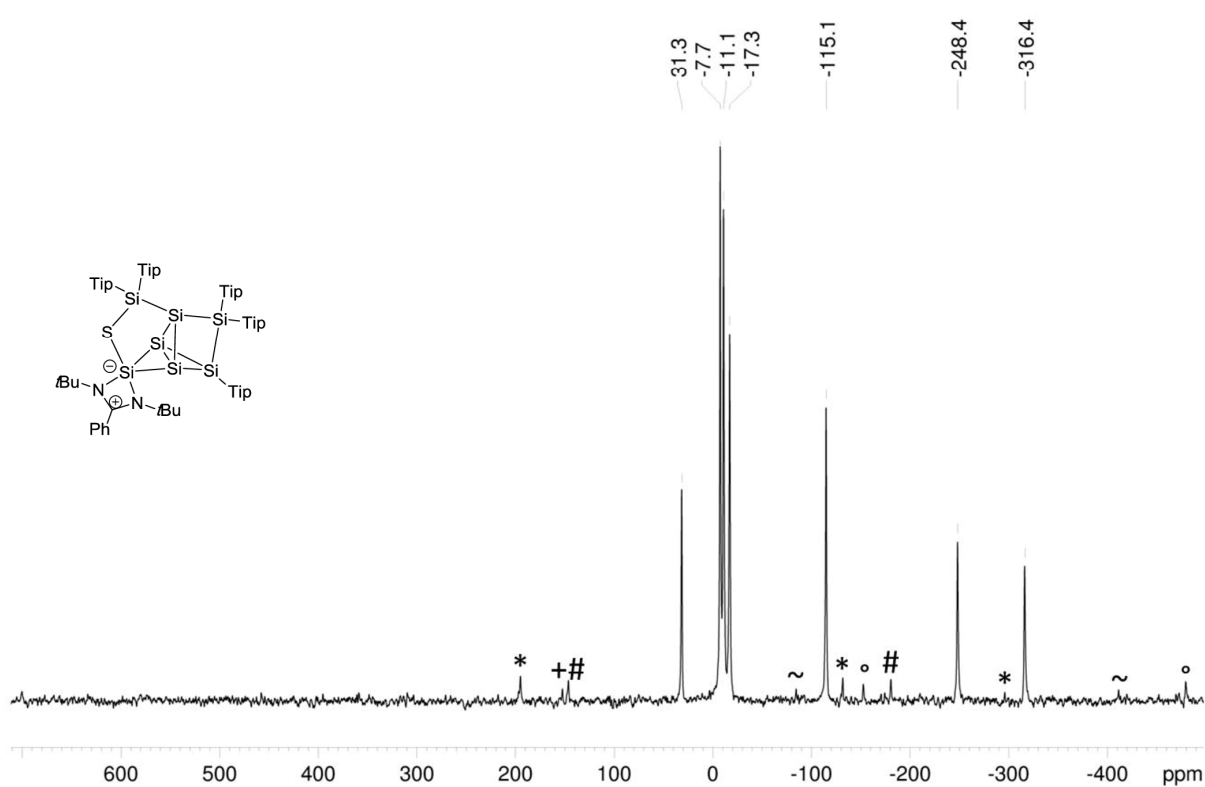


Figure S4. CP-MAS ^{29}Si NMR of **2a** (79.53 MHz, 13 KHz, 300 K), side spinning bands of: * NHSi (31.3 ppm), + SiTip_2 (-11.1 ppm), # SiTip (-17.3 ppm), ° unsubstituted Si (-316.4 ppm), ~ unsubstituted Si (-248.8 ppm).

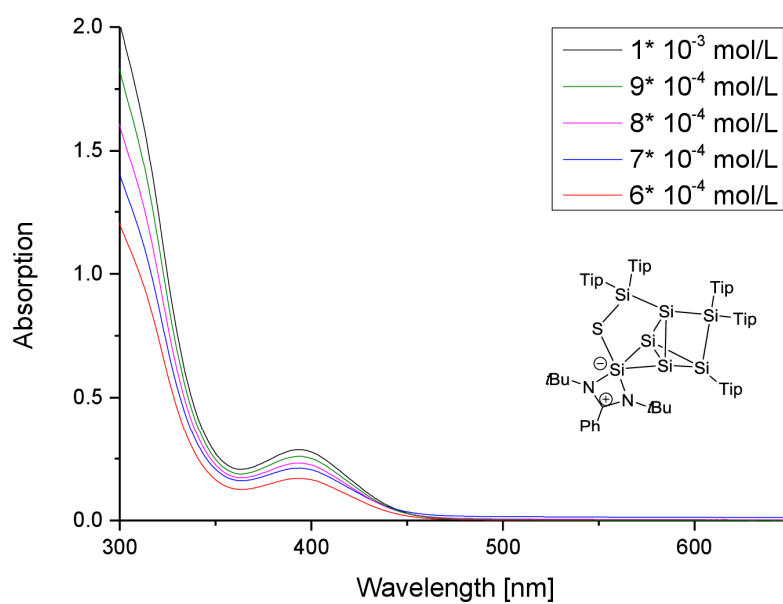


Figure S5. UV-Vis spectrum of **2a** in toluene at different concentrations.

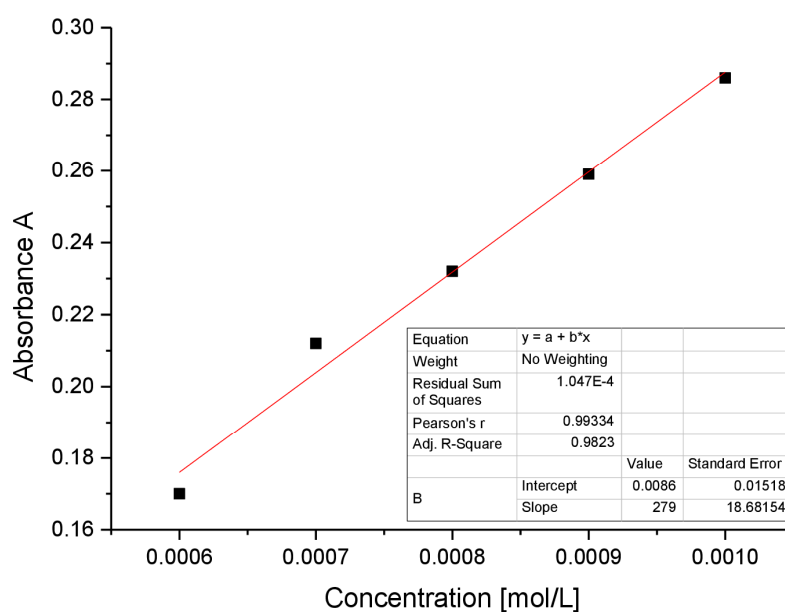


Figure S6. Determination of ϵ (2790 l cm^{-1}) by linear regression of absorptions ($\lambda = 394 \text{ nm}$) of **2a** against concentration.

SUPPORTING INFORMATION

WILEY-VCH

Preparation of selenasiliconoid Si₇Se (2b)

Quantities: Si₆NHSi 1, 400 mg (0.277 mmol), selenium 54.66 mg (0.692 mmol), benzene 6 mL, stirred overnight at room temperature, filtered from hexane 6 mL, crystallization from hexane. Yield: 295 mg (0.194 mmol; 70 %) bright yellow crystals (mp. 380°C, no dec.).

¹H-NMR (400.13 MHz, C₆D₆, 300 K) δ = 7.448 – 7.444 (m, 1H, Ar-H), 7.397 – 7.393 (m, 1H, Ar-H), 7.104 – 7.088 (m, 3H, Ar-H), 7.070 – 7.066 (m, 1H, Ar-H), 7.021 – 6.986 (m, 2 H, Ar-H), 6.955 – 6.951 (m, 1H, Ar-H), 6.841 – 6.838 (m, 1 H, Ar-H), 6.822 – 6.738 (m, 2H, Ar-H), 6.662 – 6.621 (m, 1H, Ar-H), 6.304 – 6.285 (m, 1H, Ar-H), 6.049 (sept, 1H, ³J_{HH} = 6.75 Hz, Tip-*i*Pr-CH₂), 5.565 (sept, 1H, ³J_{HH} = 6.13 Hz, Tip-*i*Pr-CH₂), 5.064 (sept, 1H, ³J_{HH} = 6.31 Hz, Tip-*i*Pr-CH₂), 4.881 (sept, 1H, ³J_{HH} = 6.31 Hz, Tip-*i*Pr-CH₂), 4.350 (sept, 1H, ³J_{HH} = 6.31 Hz, Tip-*i*Pr-CH₂), 3.967 (sept, 1H, ³J_{HH} = 6.31 Hz, Tip-*i*Pr-CH₂), 3.481 – 3.405 (m, 2H, Tip-*i*Pr-CH₂), 3.351 (sept, 1H ³J_{HH} = 6.31 Hz, Tip-*i*Pr-CH₂), 3.181 (sept, 1H, ³J_{HH} = 6.31 Hz, Tip-*i*Pr-CH₂), 2.913 – 2.833 (m, 2 H, Tip-*i*Pr-CH₂), 2.751 – 2.616 (m, 3H, Tip-*i*Pr-CH₂), 2.364 (d, 3H, ³J_{HH} = 6.47 Hz, Tip-*i*Pr-CH₃), 2.079 (d, 3H, ³J_{HH} = 6.47 Hz, Tip-*i*Pr-CH₃), 1.822 (d, 3H, ³J_{HH} = 6.48 Hz, Tip-*i*Pr-CH₃), 1.679 – 1.646 (m, 10 H, Tip-*i*Pr-CH₃), 1.599 – 1.560 (m, 7H, Tip-*i*Pr-CH₃), 1.512 – 1.456 (m, 15 H, Tip-*i*Pr-CH₃), 1.359 – 1.309 (m, 28 H, Tip-*i*Pr-CH₃ overlapping with C(CH₃)₃), 1.259 – 1.245 (m, 16 H, Tip-*i*Pr-CH₃ overlapping with C(CH₃)₃), 1.209 – 1.089 (m, 27H, Tip-*i*Pr-CH₃), 0.889 (t, 3H, hexane), 0.752 (d, 3H, ³J_{HH} = 6.57 Hz, Tip-*i*Pr-CH₃), 0.691 (d, 3H, ³J_{HH} = 7.12 Hz, Tip-*i*Pr-CH₃), 0.587 (d, 3H, ³J_{HH} = 7.12 Hz, Tip-*i*Pr-CH₃), 0.446 – 0.403 (m, 6H, Tip-*i*Pr-CH₃), 0.342 (d, 3H, ³J_{HH} = 6.57 Hz, Tip-*i*Pr-CH₃) ppm.

¹³C-NMR (100.61 MHz, C₆D₆, 300 K) δ = 172.07 (s, 1C, C-Ph), 157.36, 155.70, 154.31, 154.19, 153.79, 153.61, 153.21, 151.15, 152.31, 152.04 (s, each 1C, Ar-C), 150.07, 149.58, 149.22, 149.11, 148.92 (s, each 1C, Ar-C), 139.94, 139.68, 139.28 (s, each 1C, Ar-C), 135.04, 133.43, 132.47 (s, each 1C, Ar-C), 129.55, 129.32 (s, each 1C, Ar-CH), 128.11, 127.88, 127.66, 127.63 (s, each 1C, Ar-CH overlapping with C₆D₆), 127.22 (s, 1C, Ar-CH), 123.81, 123.68, 122.76, 122.59, 122.45, 122.27, 122.00, 121.90, 121.60, 120.03 (s, each 1C, Ar-CH), 56.91, 56.47 (s, each 1C, C(CH₃)₃), 36.52, 35.87, 35.80, 35.56, 35.32, 35.04, 34.95, 34.63, 34.58, 34.54, 34.37 (s, each 1C, Tip-*i*Pr-CH), 43.69 (s, 2C, Tip-*i*Pr-CH), 31.92, 31.87 (s, each 1C, Tip-*i*Pr-CH), 31.63 (s, 2C, Tip-*i*Pr-CH), 29.74, 28.47, 28.11, 28.08, 28.02, 27.52, 26.90, 26.66 (s, each 1C, Tip-*i*Pr-CH₃), 25.38, 25.17, 25.03, 24.90, 24.67 (s, each 1C, Tip-*i*Pr-CH₃), 24.29, 24.25, 24.23, 24.20, 24.14, 24.05, 23.96, 23.88, 23.84 (s, each 1C, overlapping, Tip-*i*Pr-CH₃), 23.37, 23.08, 23.01, 22.48 (s, each 1C, Tip-*i*Pr-CH₃), 14.33 (s, 1C, Tip-*i*Pr-CH₃) ppm.

²⁹Si-NMR (79.49 MHz, C₆D₆, 300 K) δ = 26.6 (s, NHSi), -10.7 (s, SiTip), -10.9 (s, SiTip₂), -24.2 (s, SiTip₂), -100.4 (s, Si), -251.5 (s, unsubstituted Si), -309.3 (s, unsubstituted Si) ppm.

⁷⁷Se-NMR (76.31 MHz, C₆D₆, 300 K) δ = 53.86 ppm.

CP-MAS ²⁹Si-NMR (79.53 MHz, 15 KHz, 300K) δ = 26.8 (s, NHSi), -9.5 (s, SiTip), -12.1 (s, SiTip₂), -23.1 (s, SiTip₂), -99.1 (s, Si), -246.5 (s, unsubstituted Si), -306.7 (s, unsubstituted Si) ppm.

CP-MAS ²⁹Si-NMR (79.53 MHz, 13 KHz, 300K) δ = 26.8 (s, NHSi), -9.5 (s, SiTip), -12.1 (s, SiTip₂), -23.2 (s, SiTip₂), -99.1 (s, Si), -246.6 (s, unsubstituted Si), -306.9 (s, unsubstituted Si) ppm.

CP-MAS ²⁹Si-NMR (79.53 MHz, 7 KHz, 300K) δ = 26.6 (s, NHSi), -9.5 (s, SiTip), -12.3 (s, SiTip₂), -23.4 (s, SiTip₂), -99.5 (s, Si), -247.1 (s, unsubstituted Si), -307.6 (s, unsubstituted Si) ppm.

CP-MAS ²⁹Si-NMR (79.53 MHz, 5 KHz, 300K) δ = 26.5 (s, NHSi), -9.5 (s, SiTip), -12.3 (s, SiTip₂), -23.5 (s, SiTip₂), -99.5 (s, Si), -247.1 (s, unsubstituted Si), -307.7 (s, unsubstituted Si) ppm.

CP-MAS ⁷⁷Se-NMR (76.34 MHz, 15 KHz, 300K) δ = 39.94 (s) ppm.

CP-MAS ⁷⁷Se-NMR (76.34 MHz, 13 KHz, 300K) δ = 38.79 (s) ppm.

CP-MAS ⁷⁷Se-NMR (76.34 MHz, 10 KHz, 300K) δ = 37.51 (s) ppm.

CP-MAS ⁷⁷Se-NMR (76.34 MHz, 9 KHz, 300K) δ = 36.68 (s) ppm.

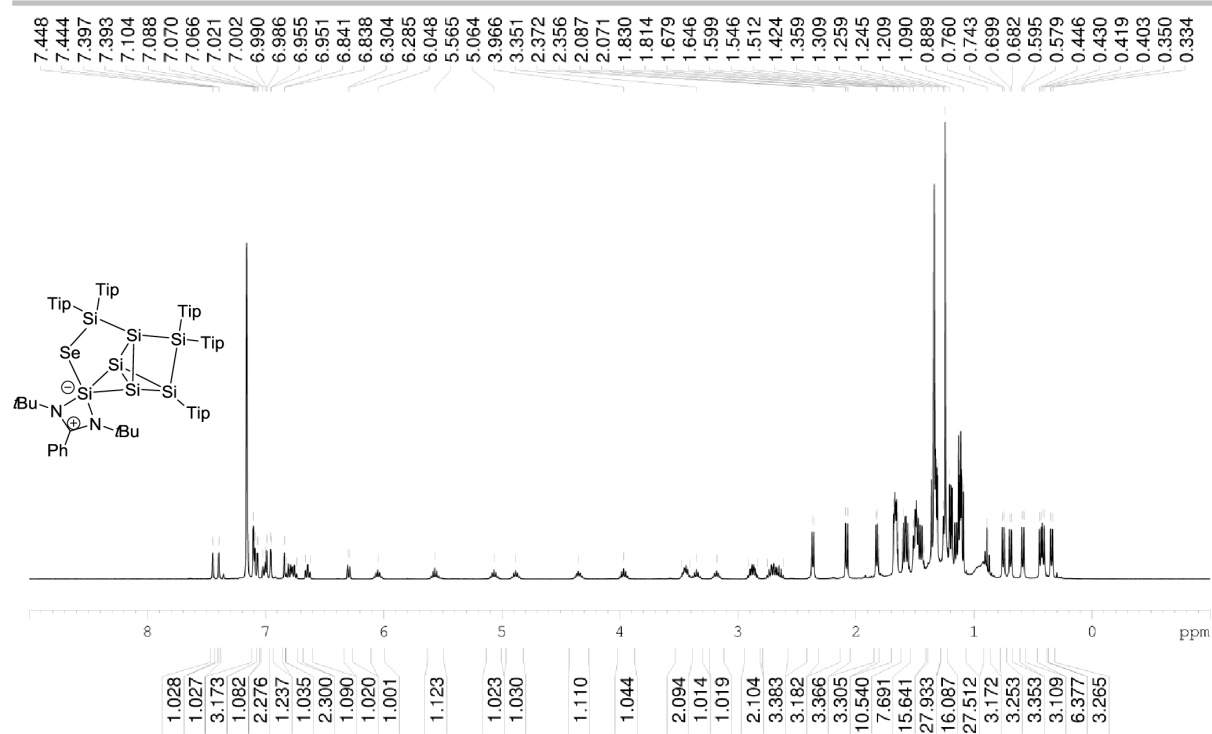
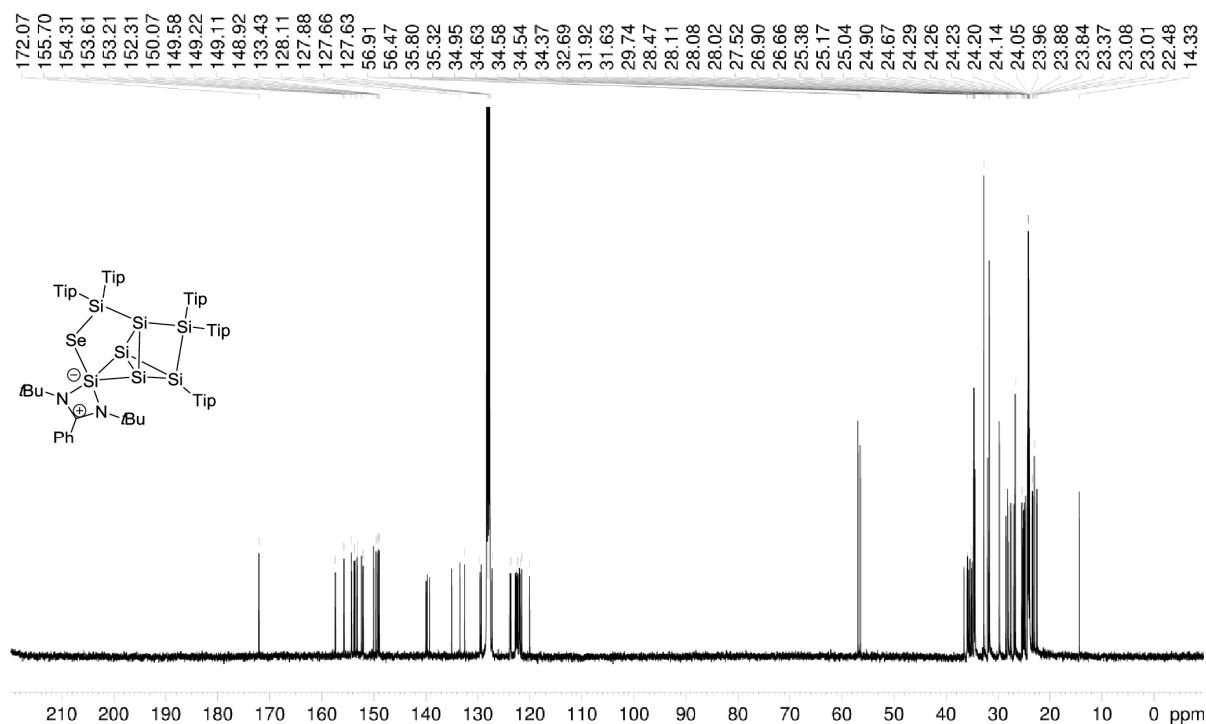
CP-MAS ⁷⁷Se-NMR (76.34 MHz, 5 KHz, 300K) δ = 36.72 (s) ppm.

Elemental analysis: calculated for C₉₀H₁₃₈N₂SeSi₇: C: 70.95 % ; H: 9.13 % ; N: 1.84 %. Found: C: 70.47 % ; H: 9.12 % ; N: 1.65 %.

UV/VIS (hexane): λ_{max} (ε) = 396 nm (2870 M⁻¹ cm⁻¹).

SUPPORTING INFORMATION

WILEY-VCH

Figure S7. ^1H NMR of **2b** in C_6D_6 (400.13 MHz, 300 K).Figure S8. ^{13}C NMR of **2b** in C_6D_6 (100.61 MHz, 300 K).

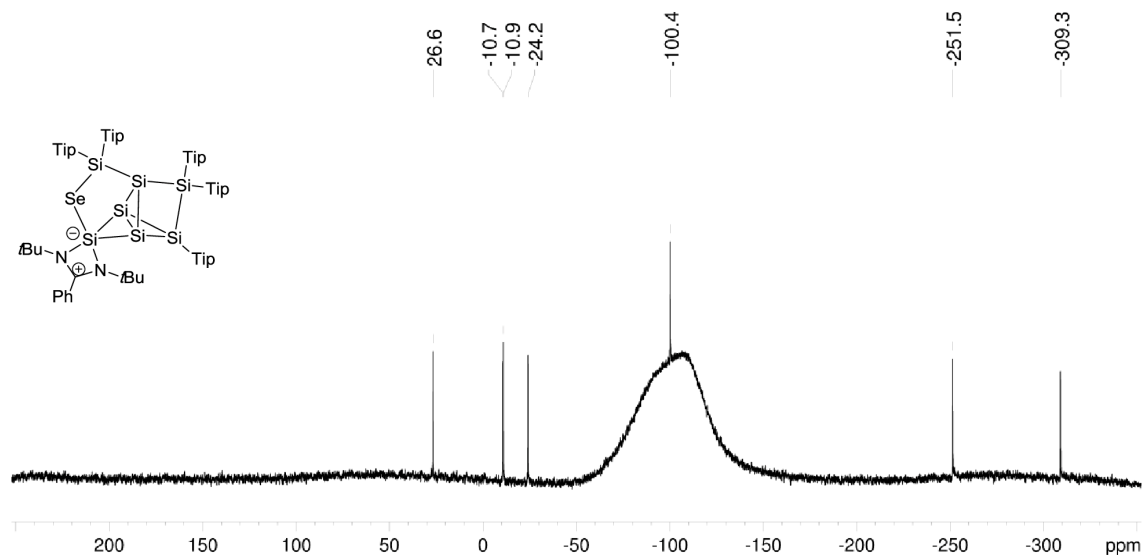


Figure S9. ^{29}Si NMR of **2b** in C_6D_6 (79.49 MHz, 300 K).

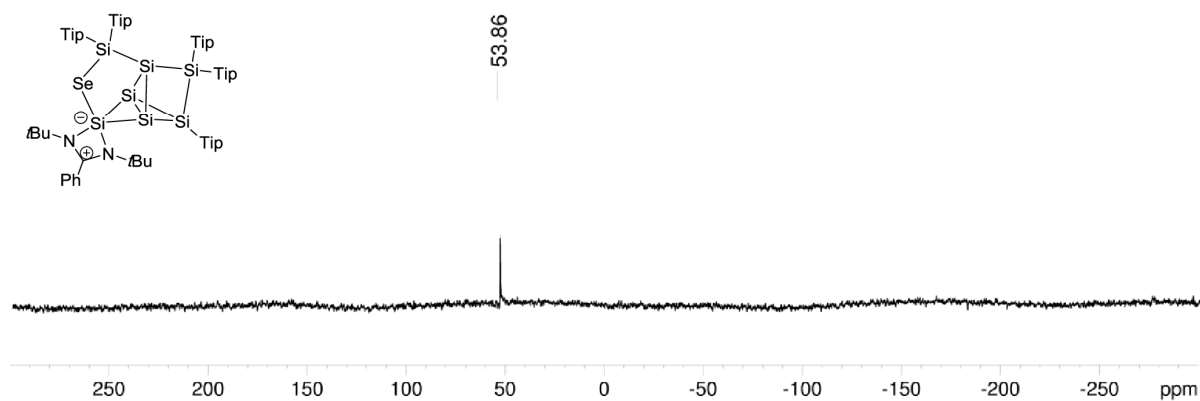


Figure S10. ^{77}Se NMR of **2b** in C_6D_6 (76.31 MHz, 300 K).

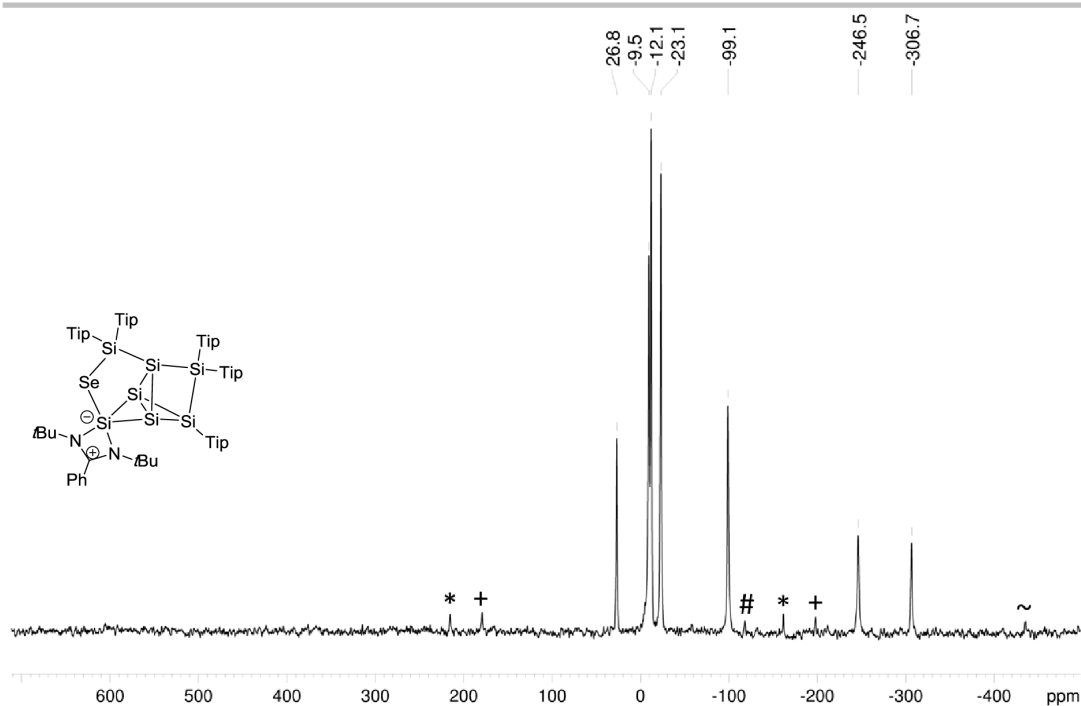


Figure S11. CP-MAS ^{29}Si NMR of **2b** (79.53 MHz, 15 KHz, 300 K), side spinning bands of: * NHSi (26.8 ppm), + SiTip (-9.5 ppm), # unsubstituted Si (-306.7 ppm), ~ unsubstituted Si (-246.5 ppm).

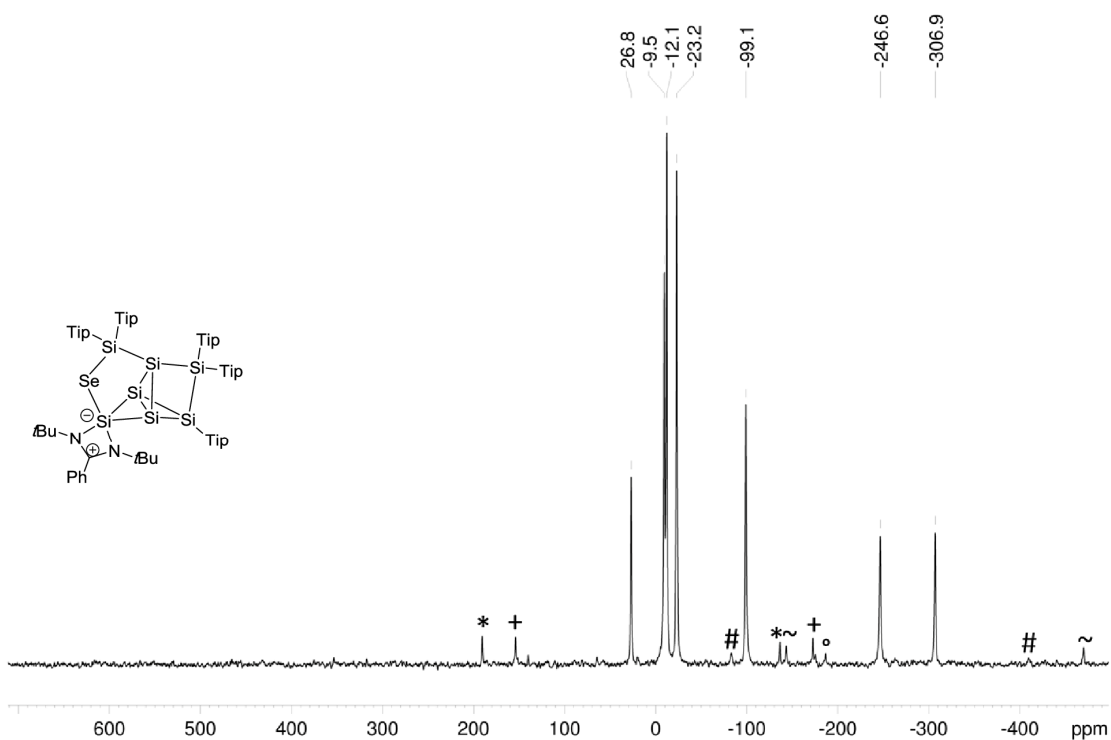


Figure S12. CP-MAS ^{29}Si NMR of **2b** (79.53 MHz, 13 KHz, 300 K), side spinning bands of: * NHSi (26.8 ppm), + SiTip (-9.5 ppm), ° Si(Tip) $_2$ (-23.2 ppm), # unsubstituted Si (-246.6 ppm), ~ unsubstituted Si (-306.9 ppm).

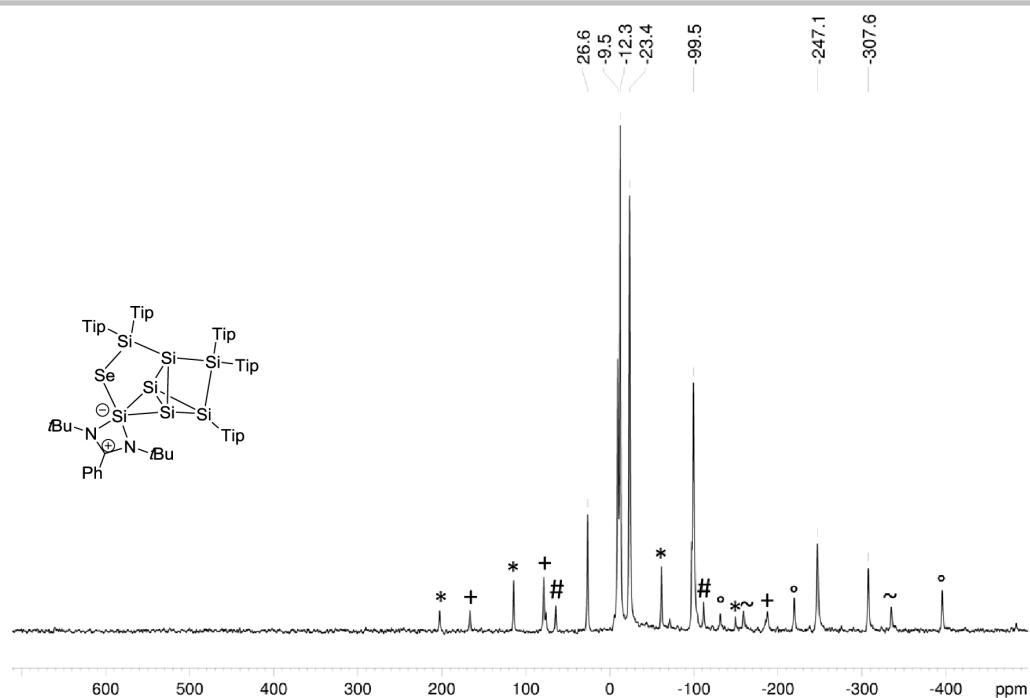


Figure S13. CP-MAS ^{29}Si NMR of **2b** (79.53 MHz, 7 KHz, 300 K), side spinning bands of * NHTip (26.6 ppm), + SiTip (-9.5 ppm), # Si(Tip) $_2$ (-23.4 ppm), ~ unsubstituted Si (-247.1 ppm), ° unsubstituted Si (-307.6 ppm).

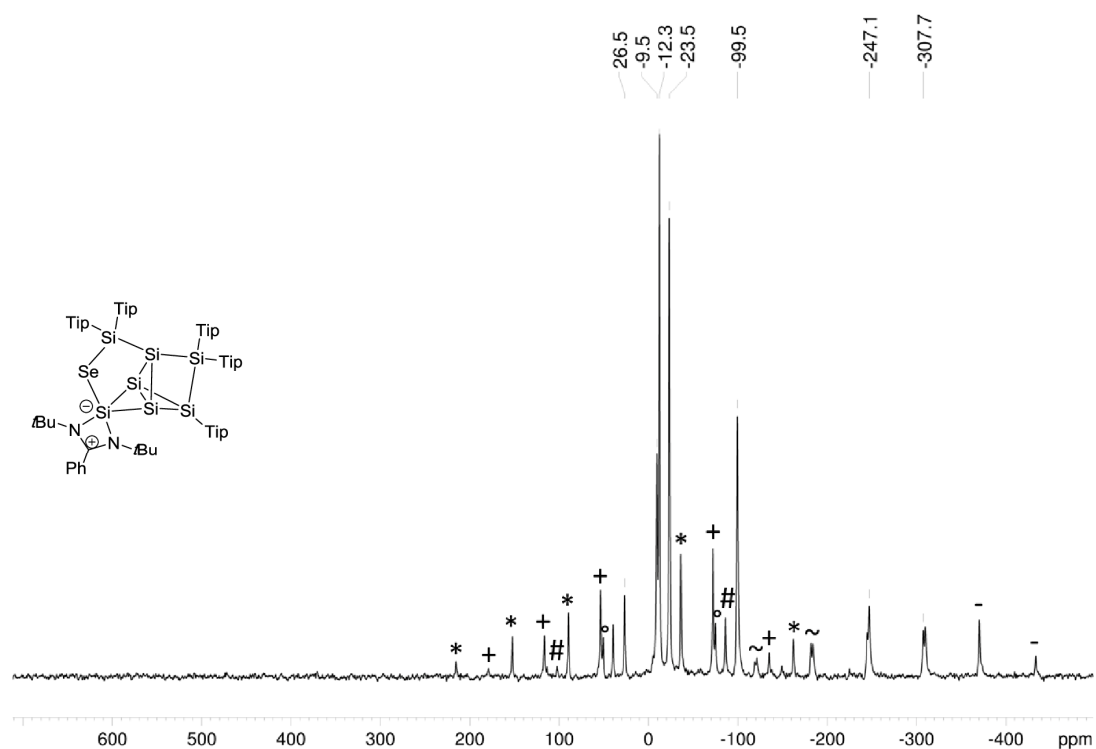


Figure S14. CP-MAS ^{29}Si NMR of **2b** (79.53 MHz, 5 KHz, 300 K), side spinning bands of * NHTip (26.5 ppm), + SiTip (-9.5 ppm), # Si(Tip) $_2$ (-23.5 ppm), ° Si(Tip) $_2$ (-12.3 ppm), ~ unsubstituted Si (-247.1 ppm), - unsubstituted Si (-307.7 ppm).

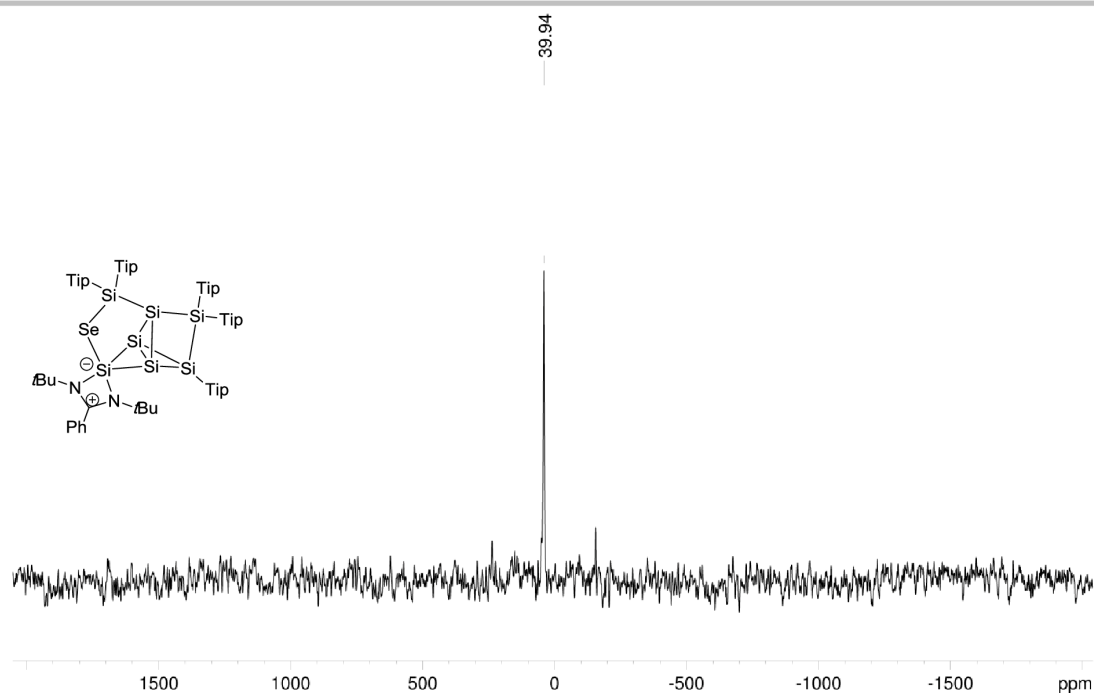


Figure S15. CP-MAS ^{77}Se NMR of **2b** (76.34 MHz, 15 KHz, 300 K).

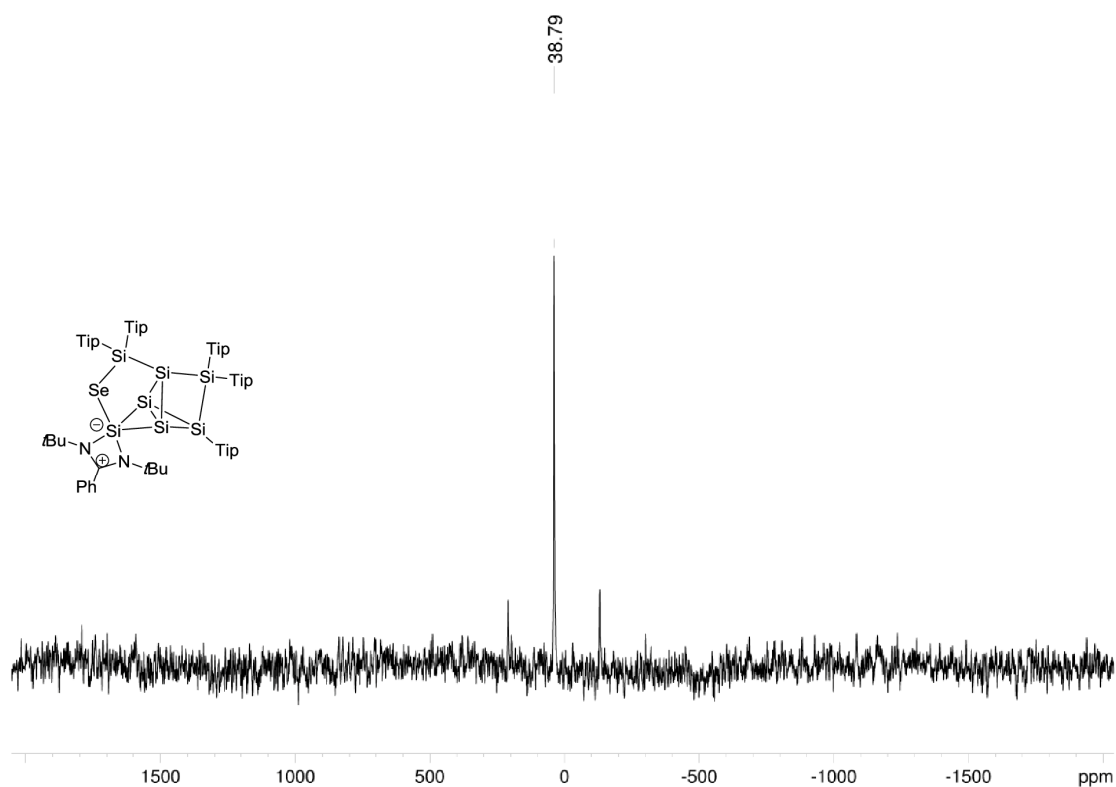


Figure S16. CP-MAS ^{77}Se NMR of **2b** (76.34 MHz, 13 KHz, 300 K).

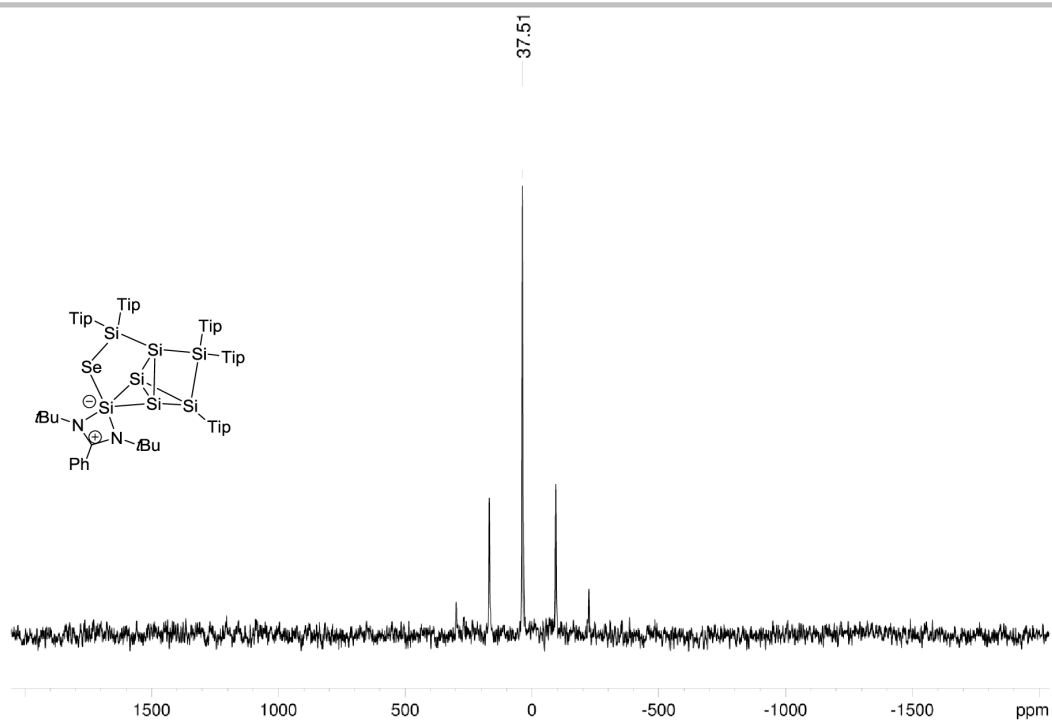


Figure S17. CP-MAS ^{77}Se NMR of **2b** (76.34 MHz, 10 KHz, 300 K).

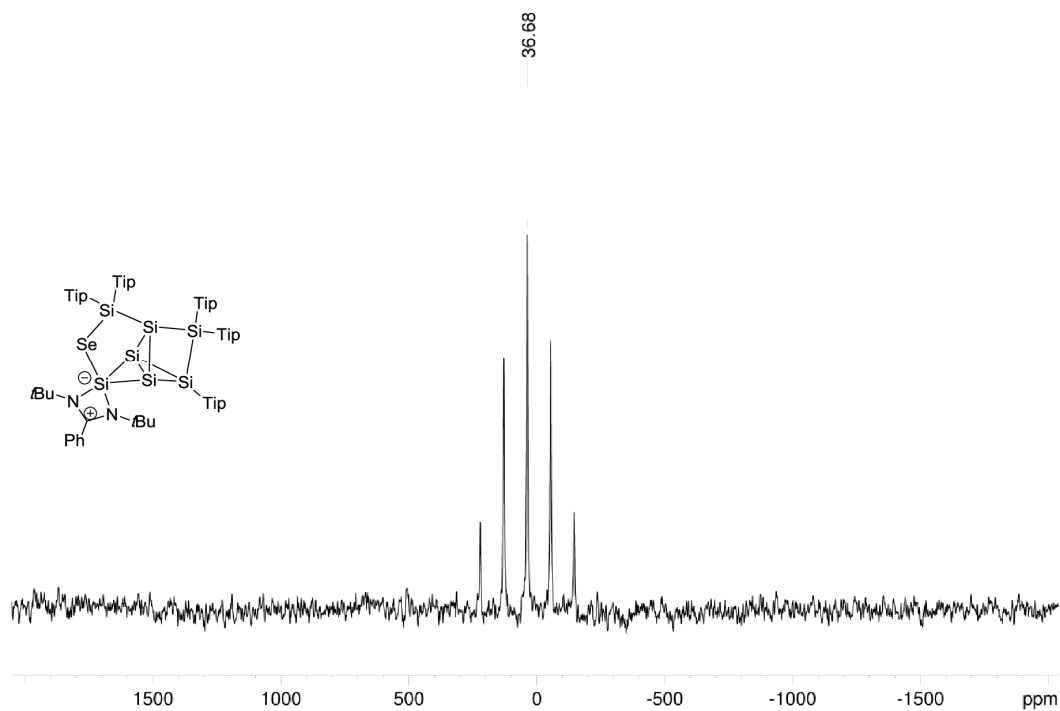


Figure S18. CP-MAS ^{77}Se NMR of **2b** (76.34 MHz, 7 KHz, 300 K).

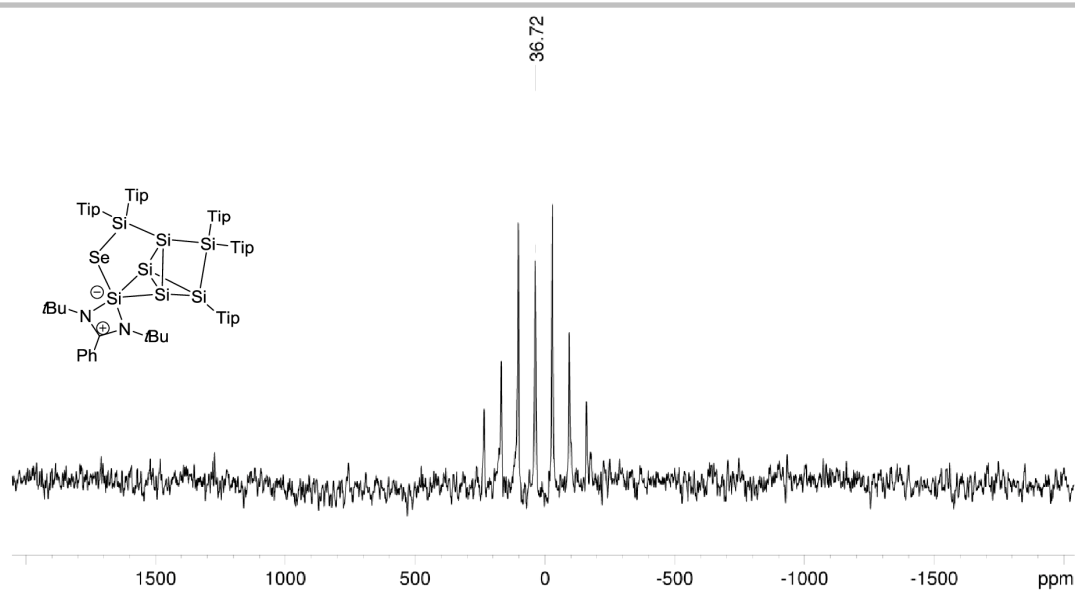


Figure S19. CP-MAS ^{77}Se NMR of **2b** (76.34 MHz, 5 KHz, 300 K).

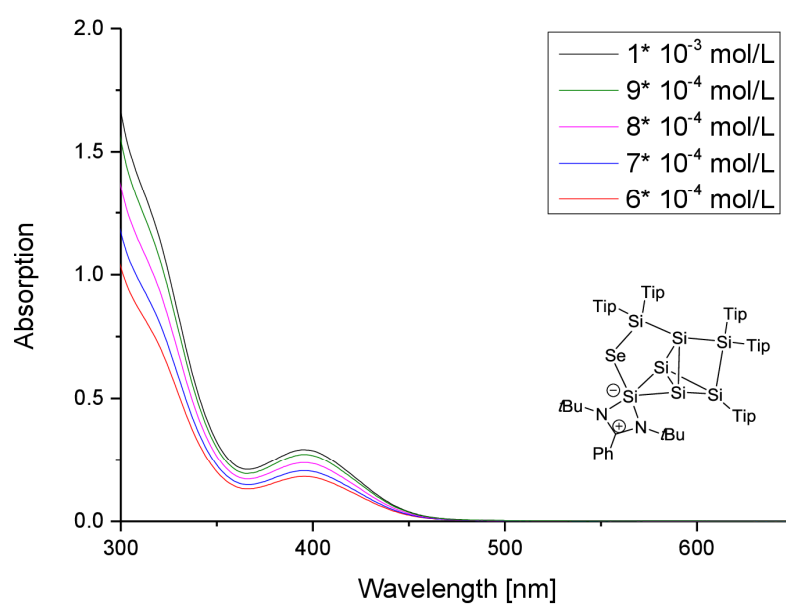


Figure S20. UV-Vis spectrum of **2b** in toluene at different concentrations.

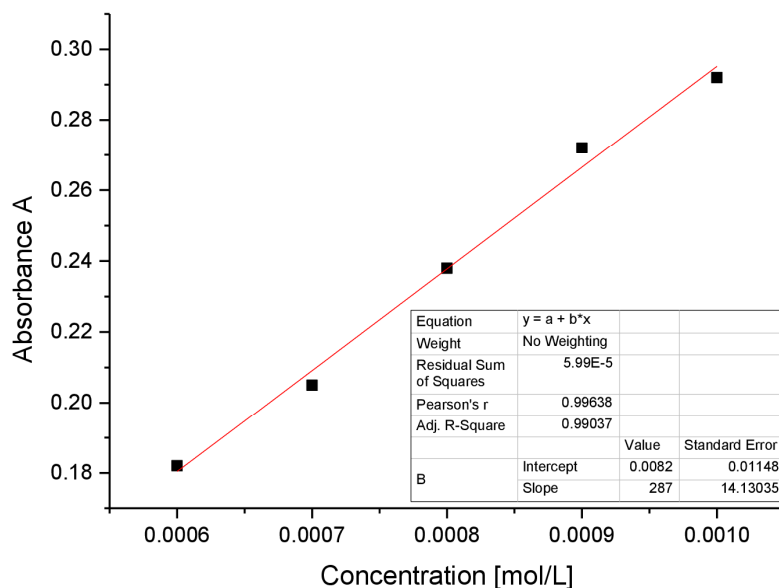


Figure S21. Determination of ϵ ($2870 \text{ M}^{-1} \text{ cm}^{-1}$) by linear regression of absorptions ($\lambda = 396 \text{ nm}$) of **2b** against concentration.

Preparation of tellurasiliconoid Si_7Te (**2c**)

Quantities: Si_6NHSi **1**, 250 mg (0.173 mmol), tellurium 154.60 mg (1.212 mmol), benzene 4 mL, stirred over three days at room temperature, filtered from hexane 10 mL, crystallization from hexane. Yield: 205 mg (0.13 mmol; 75 %) bright yellow crystals (mp. 380°C , dec.).

$^1\text{H-NMR}$ (400.13 MHz, C_6D_6 , 300 K) $\delta = 7.451 - 7.447$ (m, 1H, Ar-H), 7.399 – 7.394 (m, 1H, Ar-H), 7.385 – 7.380 (m, 0.2H, Ar-H), 7.350 – 7.346 (m, 0.2H, Ar-H), 7.224 – 7.217 (m, 0.2H, Ar-H), 7.140 – 7.136 (m, 1H, Ar-H), 7.110 – 7.077 (m, 4H, Ar-H), 7.019 – 6.976 (m, 3H, Ar-H), 6.922 – 6.918 (m, 1H, Ar-H), 6.903 – 6.899 (m, 0.2H, Ar-H), 6.851 (bs, 0.2H, Ar-H), 6.833 – 6.814 (m, 2H, Ar-H), 6.776 – 6.757 (m, 1H, Ar-H), 6.740 – 6.738 (m, 0.3H, Ar-H), 6.717 – 6.679 (m, 1H, Ar-H), 6.582 – 6.563 (m, 0.1H, Ar-H), 6.454 (d, 1H, $^3J_{\text{HH}} = 7.89 \text{ Hz}$, Ar-H), 6.144 (sept, 1H, $^3J_{\text{HH}} = 6.63 \text{ Hz}$, Tip-*i*Pr-CH₂), 5.848 (sept, 0.08H, $^3J_{\text{HH}} = 6.63 \text{ Hz}$, Tip-*i*Pr-CH₂), 5.657 (sept, 1H, $^3J_{\text{HH}} = 6.65 \text{ Hz}$, Tip-*i*Pr-CH₂), 5.456 – 5.388 (m, 0.2H, $^3J_{\text{HH}} = 6.17 \text{ Hz}$, Tip-*i*Pr-CH₂), 5.052 (sept, 1H, $^3J_{\text{HH}} = 6.18 \text{ Hz}$, Tip-*i*Pr-CH₂), 4.609 (sept, 1H, $^3J_{\text{HH}} = 6.74 \text{ Hz}$, Tip-*i*Pr-CH₂), 4.269 (sept, 1H, $^3J_{\text{HH}} = 6.74 \text{ Hz}$, Tip-*i*Pr-CH₂), 4.003 (sept, 0.1H, $^3J_{\text{HH}} = 6.44 \text{ Hz}$, Tip-*i*Pr-CH₂), 3.887 (sept, 1H, $^3J_{\text{HH}} = 6.44 \text{ Hz}$, Tip-*i*Pr-CH₂), 3.715 (sept, 0.1 H, $^3J_{\text{HH}} = 6.44 \text{ Hz}$, Tip-*i*Pr-CH₂), 3.632 (sept, 0.1 H, $^3J_{\text{HH}} = 6.44 \text{ Hz}$, Tip-*i*Pr-CH₂), 3.533 – 3.274 (m, 3H, Tip-*i*Pr-CH₂), 3.155 (sept, 1H, $^3J_{\text{HH}} = 5.90 \text{ Hz}$, Tip-*i*Pr-CH₂), 3.014 (sept, 0.14H, $^3J_{\text{HH}} = 5.39 \text{ Hz}$, Tip-*i*Pr-CH₂), 2.937 – 2.842 (m, 2H, Tip-*i*Pr-CH₂), 2.784 – 2.582 (m, 4H, Tip-*i*Pr-CH₂), 2.376 (d, 3H, $^3J_{\text{HH}} = 6.57 \text{ Hz}$, Tip-*i*Pr-CH₃), 2.233 (d, 0.44H, $^3J_{\text{HH}} = 6.57 \text{ Hz}$, Tip-*i*Pr-CH₃), 2.151 (d, 3H, $^3J_{\text{HH}} = 6.57 \text{ Hz}$, Tip-*i*Pr-CH₃), 1.936 – 1.862 (m, 1H, Tip-*i*Pr-CH₃), 1.802 (d, 4H, $^3J_{\text{HH}} = 6.52 \text{ Hz}$, Tip-*i*Pr-CH₃), 1.683 – 1.443 (m, 35H, Tip-*i*Pr-CH₃), 1.377 – 1.316 (m, 26 H, Tip-*i*Pr-CH₃ overlapping with $\text{C}(\text{CH}_3)_3$), 1.266 – 1.068 (m, 48H, Tip-*i*Pr-CH₃ overlapping with $\text{C}(\text{CH}_3)_3$), 0.711 (d, 3H, $^3J_{\text{HH}} = 6.48 \text{ Hz}$, Tip-*i*Pr-CH₃), 0.649 (d, 3H, $^3J_{\text{HH}} = 6.48 \text{ Hz}$, Tip-*i*Pr-CH₃), 0.574 (d, 3H, $^3J_{\text{HH}} = 6.48 \text{ Hz}$, Tip-*i*Pr-CH₃), 0.424 – 0.350 (m, 7H, Tip-*i*Pr-CH₃), 0.320 (d, 4H, $^3J_{\text{HH}} = 6.48 \text{ Hz}$, Tip-*i*Pr-CH₃), 0.260 (d, 0.6H, $^3J_{\text{HH}} = 6.48 \text{ Hz}$, Tip-*i*Pr-CH₃) ppm.

$^1\text{H-NMR}$ (300.13 MHz, C_6D_6 , 353 K) $\delta = 7.390 - 7.342$ (m, 2.5H, Ar-H), 7.152 (bs, 0.45H, Ar-H), 7.104 – 7.002 (m, 15H, Ar-H overlapping with toluene- d_8), 6.961 – 6.828 (m, 7.5H, Ar-H), 6.792 – 6.734 (m, 2.7H, Ar-H), 6.093 (d, 1H, $^3J_{\text{HH}} = 6.08 \text{ Hz}$, Tip-*i*Pr-CH₂), 5.755 (sept, 0.14H, $^3J_{\text{HH}} = 6.49 \text{ Hz}$, Tip-*i*Pr-CH₂), 5.587 (sept, 1H, $^3J_{\text{HH}} = 6.49 \text{ Hz}$, Tip-*i*Pr-CH₂), 5.356 (sept, 0.32H, $^3J_{\text{HH}} = 5.95 \text{ Hz}$, Tip-*i*Pr-CH₂), 5.004 (sept, 1H, $^3J_{\text{HH}} = 6.22 \text{ Hz}$, Tip-*i*Pr-CH₂), 4.221 (sept, 1H, $^3J_{\text{HH}} = 6.22 \text{ Hz}$, Tip-*i*Pr-CH₂), 3.911 (sept, 0.2H, $^3J_{\text{HH}} = 5.43 \text{ Hz}$, Tip-*i*Pr-CH₂), 3.807 (sept, 1H, $^3J_{\text{HH}} = 5.84 \text{ Hz}$, Tip-*i*Pr-CH₂), 3.661 (sept, 0.2H, $^3J_{\text{HH}} = 6.42 \text{ Hz}$, Tip-*i*Pr-CH₂), 3.570 – 3.420 (m,

SUPPORTING INFORMATION

WILEY-VCH

0.4H, Tip-*i*Pr-CH₂), 3.368 – 3.210 (m, 3H, Tip-*i*Pr-CH₂), 3.116 (sept, 1H, ³J_{HH} = 6.23 Hz, Tip-*i*Pr-CH₂), 3.017 – 2.645 (m, 7H, Tip-*i*Pr-CH₂), 2.336 – 2.275 (m, 3.7H, Tip-*i*Pr-CH₂), 2.154 – 2.038 (m, 13H, Tip-*i*Pr-CH₂), 1.886 (d, 0.6H, ³J_{HH} = 6.14 Hz, Tip-*i*Pr-CH₃), 1.795 – 1.073 (m, 127H, Tip-*i*Pr-CH₃), 0.669 – 0.590 (m, 8H, Tip-*i*Pr-CH₃), 0.540 (d, 3H, ³J_{HH} = 6.14 Hz Tip-*i*Pr-CH₃), 0.349 – 0.211 (m, 15H, Tip-*i*Pr-CH₃) ppm.

¹³C-NMR (100.61 MHz, C₆D₆, 300 K) δ = 171.81 (s, 1C, C-Ph), 157.48, 155.33, 154.10, 154.05, 153.61, 153.53, 153.47, 152.35, 151.44, 150.02, 149.64, 149.14, 148.85 (s, each 1C, Ar-C), 141.07, 138.76, 138.29 (s, each 1C, Ar-C), 133.70 (s, 1C, Ar-C), 131.89 (s, 1C, Ar-C), 129.59, 129.24, 129.05, 128.48 (s, each 1C, Ar-CH), 128.09, 127.85, 127.62 (s, each 1C, Ar-CH overlapping with C₆D₆), 123.87, 123.74 (s, each 1C, Ar-CH), 122.73 (s, 1C, Ar-CH), 122.53 (bs, 2C, Ar-CH), 121.92, 121.83, 121.63 (s, each 1C, Ar-CH), 119.88 (s, 1C, Ar-CH), 57.24, 56.90, 56.83, 56.06 (s, each 1C, C(CH₃)₃), 36.38, 35.97 (s, each 1C, Tip-*i*Pr-CH), 35.69 (bs, 2C, Tip-*i*Pr-CH), 35.54, 35.16 (s, each 1C, Tip-*i*Pr-CH), 34.62, 34.58, 34.52, 34.44, 34.34, 34.26 (bs, overlapping, each 1C, Tip-*i*Pr-CH), 32.94, 32.78 (s, each 1C, Tip-*i*Pr-CH), 32.64 (s, 2C, Tip-*i*Pr-CH), 31.92 (s, 2C, Tip-*i*Pr-CH), 31.83 (s, 1C, Tip-*i*Pr-CH), 30.02, 29.85, 28.74, 28.41, 28.27, 27.55, 26.73, 26.54, 26.30, 25.51, 25.41, 24.95, 24.60, 24.38 (s, each 1C, Tip-*i*Pr-CH₃), 24.25, 24.21, 24.19, 24.16, 24.01, 23.94, 23.84 (bs, each 1C, Tip-*i*Pr-CH₃), 23.52, 23.20, 22.53 (s, each 1C, Tip-*i*Pr-CH₃) ppm.

²⁹Si-NMR (79.49 MHz, C₆D₆, 300 K) δ = 2.3 (s, NHSi), -9.3 (s, SiTip), -30.9 (s, SiTip₂), -45.4 (s, SiTip₂), -86.7 (s, Si), -250.2 (s, Si), -299.3 (s, Si) ppm.

¹²⁵Te-NMR (126.24 MHz, C₆D₆, 300 K) δ = -93.71 (s), -22.84 (s) ppm.

CP-MAS ²⁹Si-NMR (79.53 MHz, 15 KHz, 300K) δ = 1.7 (s, NHSi), -9.6 (s, SiTip), -30.2 (s, SiTip₂), -45.5 (s, SiTip₂), -87.4 (s, Si), -247.2 (s, Si), -295.3 (s, Si) ppm

CP-MAS ²⁹Si-NMR (79.53 MHz, 13 KHz, 300K) δ = 1.6 (s, NHSi), -9.6 (s, SiTip), -32.2 (s, SiTip₂), -45.5 (s, SiTip₂), -87.6 (s, Si), -247.3 (s, Si), -295.5 (s, Si) ppm.

CP-MAS ²⁹Si-NMR (79.53 MHz, 7 KHz, 300K) δ = 1.3 (s, NHSi), -9.6 (s, SiTip), -30.2 (s, SiTip₂), -45.5 (s, SiTip₂), -87.9 (s, Si), -247.6 (s, Si), -296.1 (s, Si) ppm

CP-MAS ²⁹Si-NMR (79.53 MHz, 5 KHz, 300K) δ = 1.3 (s, NHSi), -9.6 (s, SiTip), -30.1 (s, SiTip₂), -45.5 (s, SiTip₂), -88.0 (s, Si), -247.7 (s, Si), -296.2 (s, Si) ppm

CP-MAS ¹²⁵Te-NMR (126.29 MHz, 15 KHz, 300K) δ = -136.86 (s) ppm.

CP-MAS ¹²⁵Te-NMR (126.29 MHz, 13 KHz, 300K) δ = -139.53 (s) ppm.

CP-MAS ¹²⁵Te-NMR (126.29 MHz, 11 KHz, 300K) δ = -141.70 (s) ppm.

CP-MAS ¹²⁵Te-NMR (126.29 MHz, 9 KHz, 300K) δ = -143.40 (s) ppm.

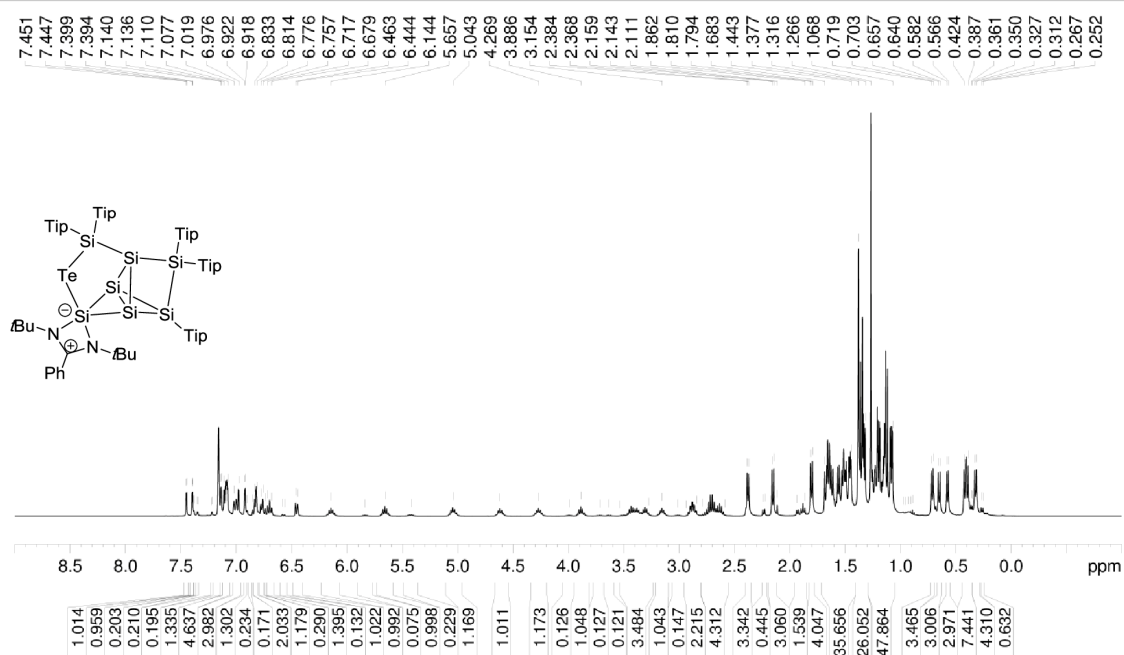
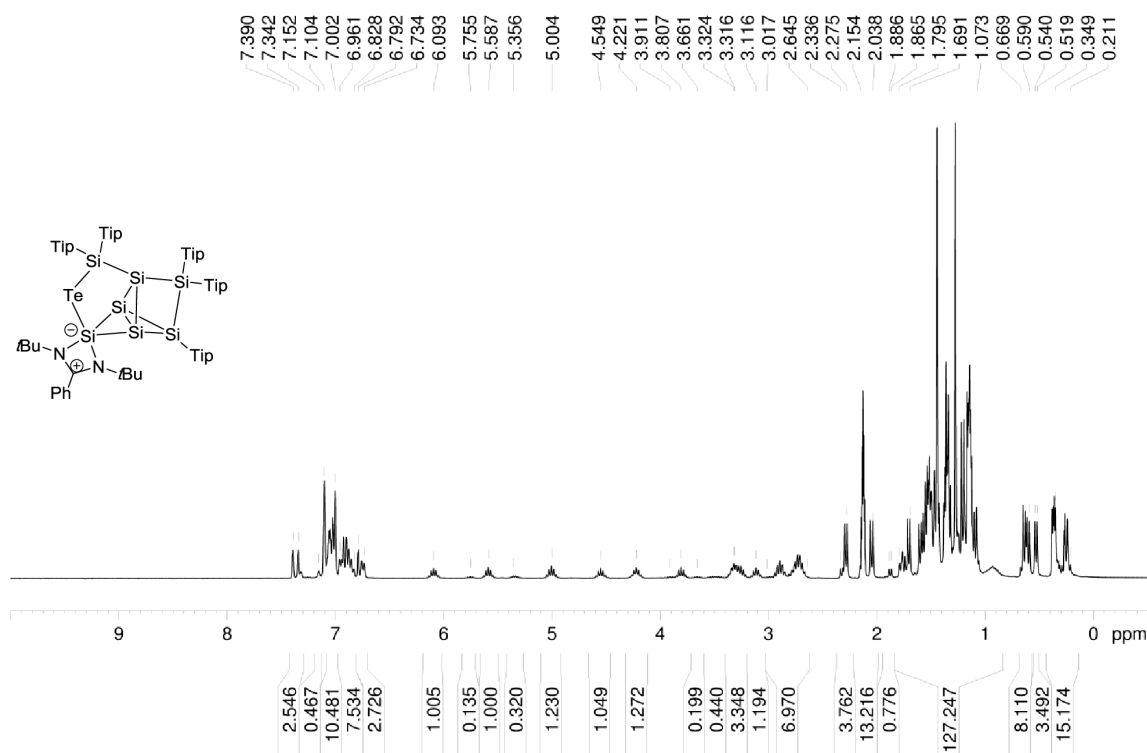
CP-MAS ¹²⁵Te-NMR (126.29 MHz, 5 KHz, 300K) δ = -145.42 (s) ppm.

Elemental analysis: calculated for C₉₀H₁₃₈N₂Si₇Te: C: 68.75 % ; H: 8.85 % ; N: 1.78 %. Found: C: 68.76 % ; H: 8.82 % ; N: 1.66 %.

UV/VIS (hexane): λ_{max} (ε) = 404 nm (2310 M⁻¹ cm⁻¹).

SUPPORTING INFORMATION

WILEY-VCH

Figure S22. ^1H NMR of **2c** in C_6D_6 (400.13 MHz, 300 K).Figure S23. ^1H NMR of **2c** in C_6D_6 (300.13 MHz, 353 K).

SUPPORTING INFORMATION

WILEY-VCH

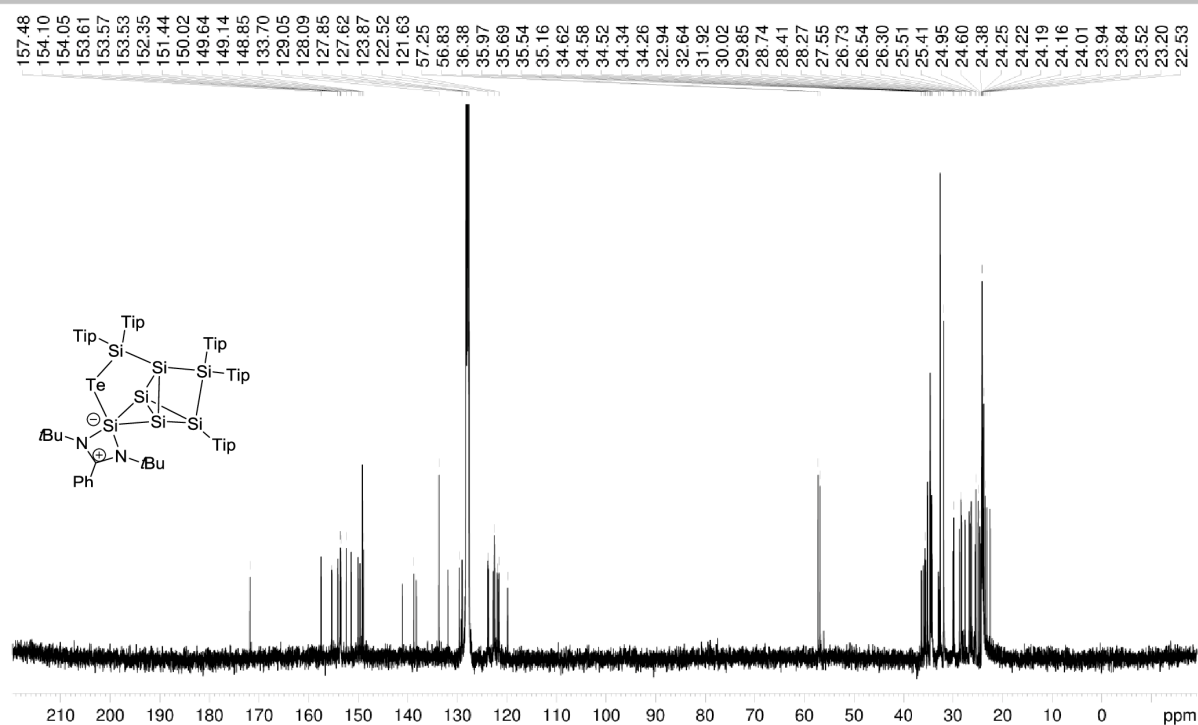


Figure S24. ¹³C NMR of **2c** in C₆D₆ (100.61 MHz, 300 K).

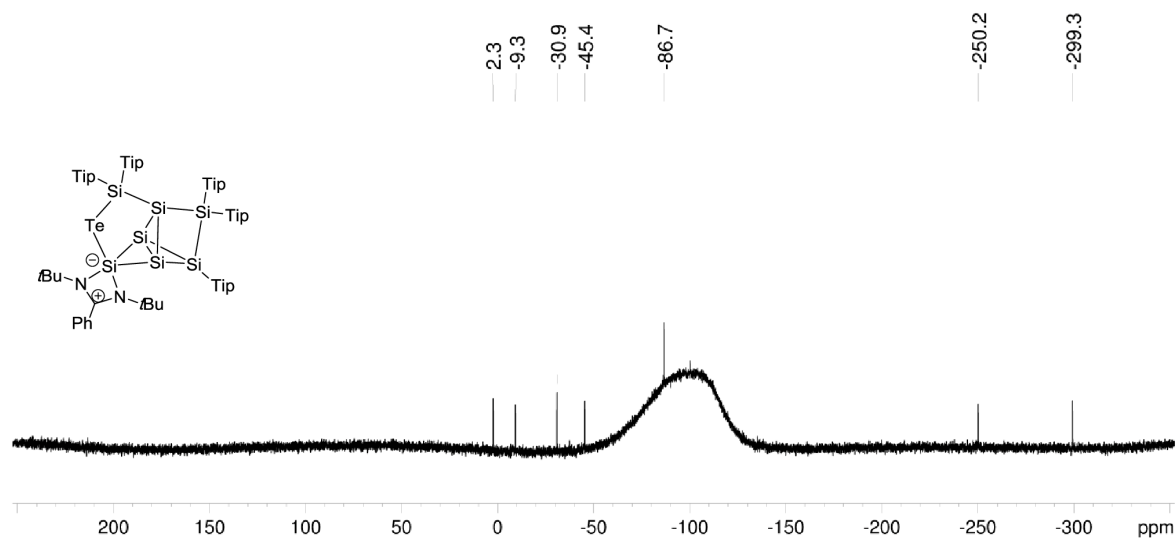


Figure S25. ²⁹Si NMR of **2c** in C₆D₆ (79.49 MHz, 300 K).

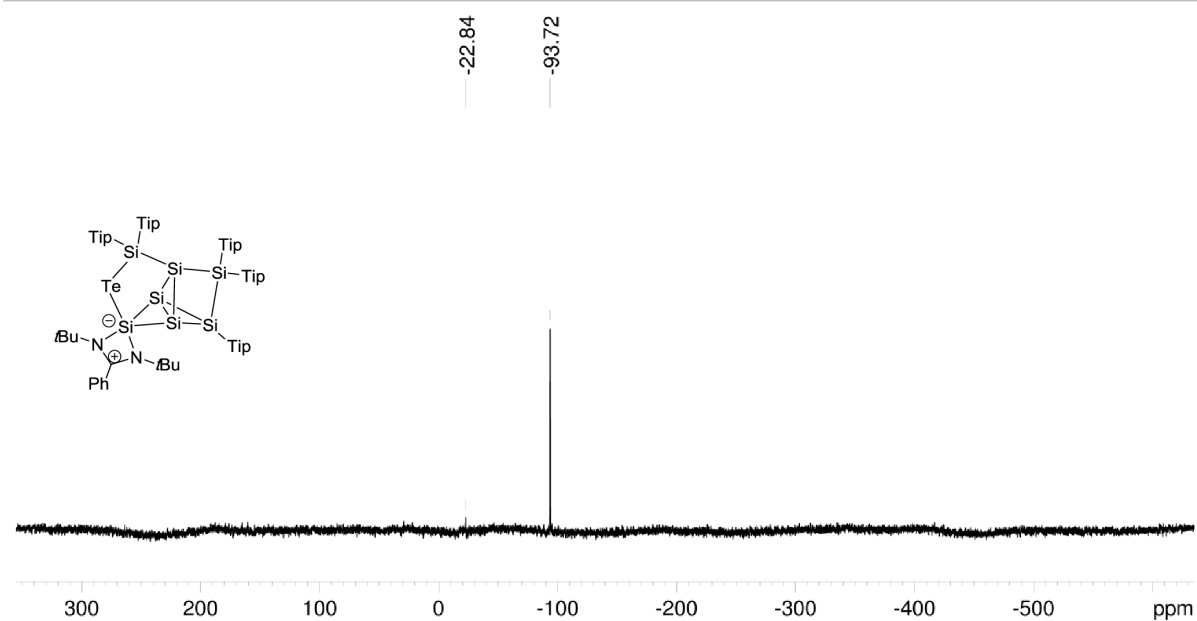


Figure S26. ^{125}Te NMR of **2c** in C_6D_6 (126.24 MHz, 300 K).

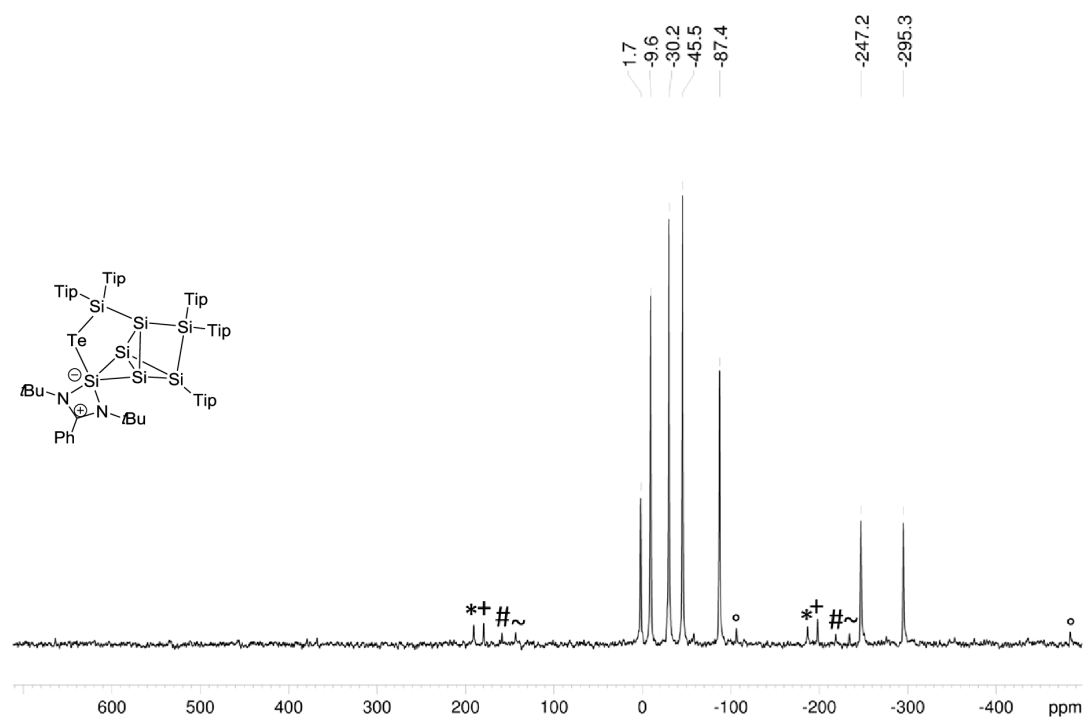


Figure S27. CP-MAS ^{29}Si NMR of **2c** (79.53 MHz, 15 KHz, 300 K), side spinning bands of: * N HSi (1.7 ppm), + SiTip (-9.6 ppm), # Si(Tip)_2 (-30.2 ppm), ~ Si(Tip)_2 (-45.5 ppm), ° unsubstituted Si (-295.3 ppm).

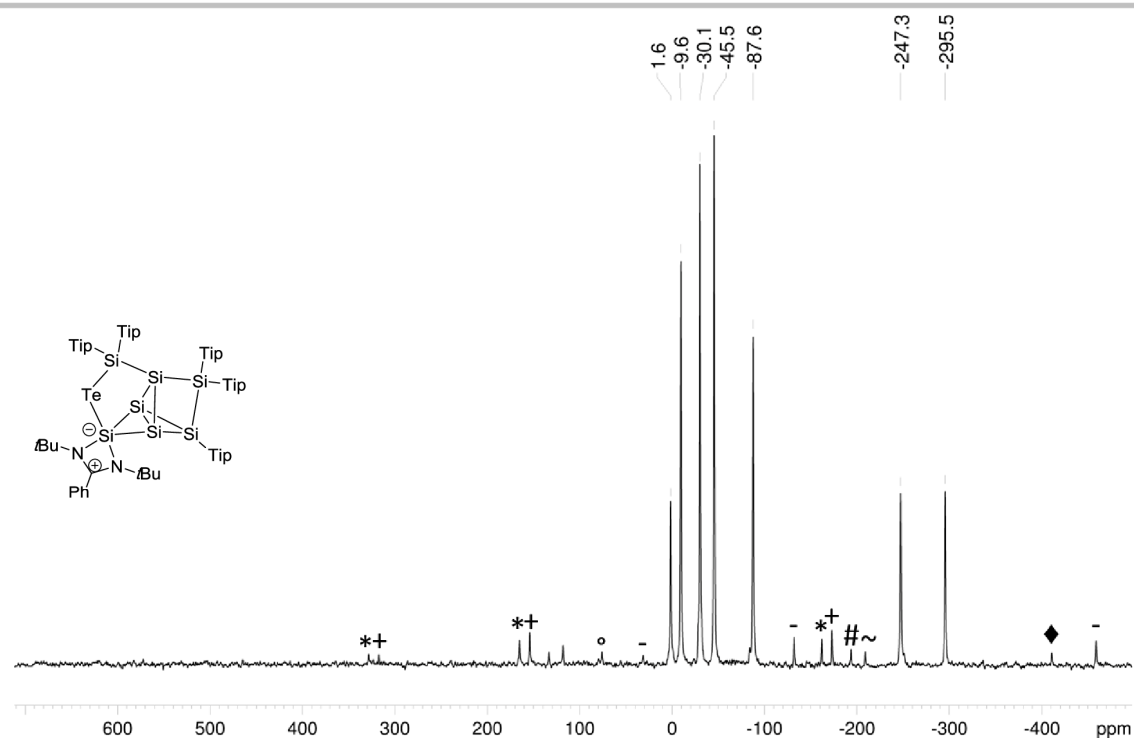


Figure S28. CP-MAS ^{29}Si NMR of **2c** (79.53 MHz, 13 KHz, 300 K), side spinning bands of: * NHSi (1.6 ppm), + SiTip (-9.6 ppm), # Si(Tip) $_2$ (-30.1 ppm), ~ Si(Tip) $_2$ (-45.5 ppm), ° unsubstituted Si (-87.6 ppm), ♦ unsubstituted Si (-247.3 ppm), - unsubstituted Si (-295.5 ppm).

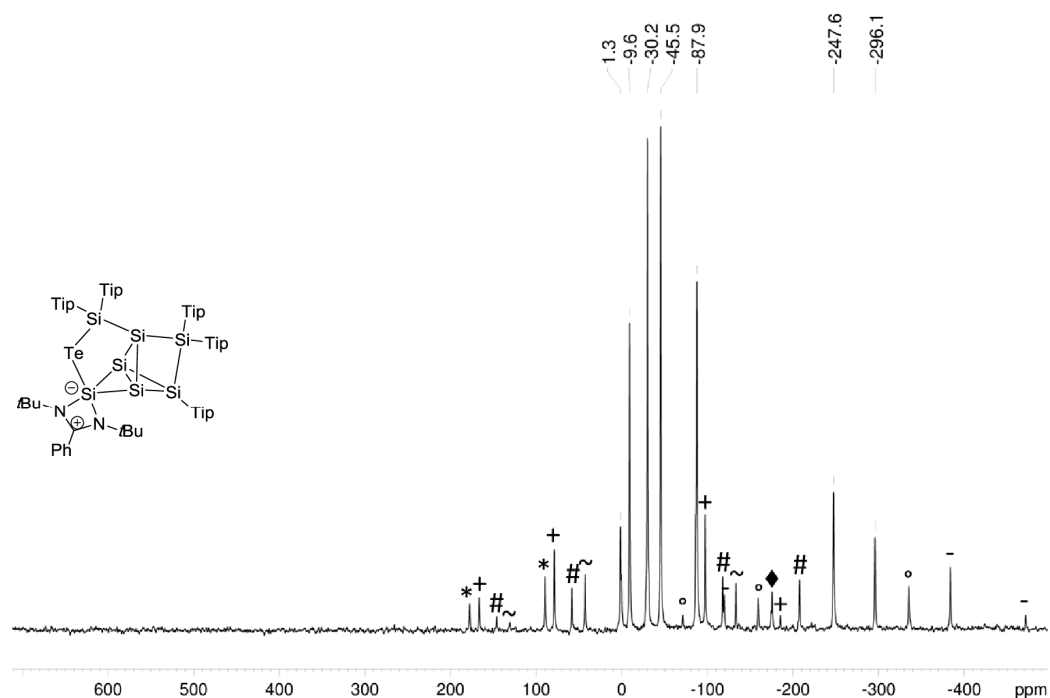


Figure S29. CP-MAS ^{29}Si NMR of **2c** (79.53 MHz, 7 KHz, 300 K), side spinning bands of: * NHSi (1.3 ppm), + SiTip (-9.6 ppm), # Si(Tip) $_2$ (-30.2 ppm), ~ Si(Tip) $_2$ (-45.5 ppm), ♦ unsubstituted Si (-87.9 ppm), ° unsubstituted Si (-247.6 ppm), - unsubstituted Si (-296.1 ppm).

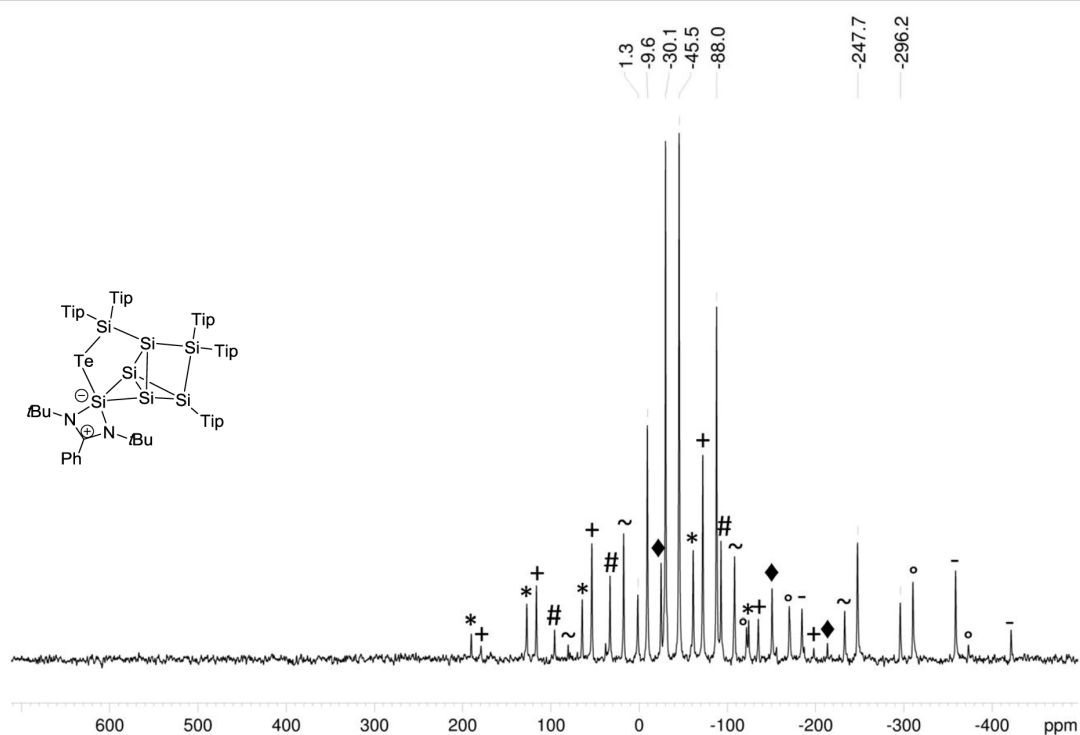


Figure S30. CP-MAS ^{29}Si NMR of **2c** (79.53 MHz, 5 KHz, 300 K), side spinning bands of: * NHSi (1.3 ppm), + SiTip (-9.6 ppm), # Si(Tip) $_2$ (-30.1 ppm), ~ Si(Tip) $_2$ (-45.5 ppm), ♦ unsubstituted Si (-88.0 ppm), ° unsubstituted Si (-247.7 ppm), - unsubstituted Si (-296.2 ppm).

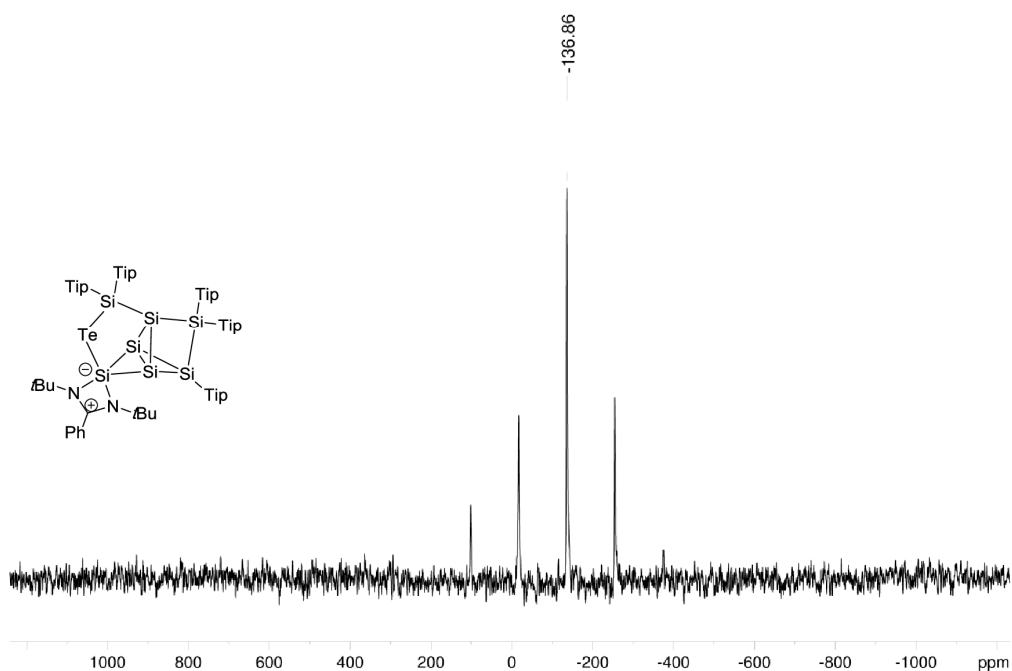


Figure S31. CP-MAS ^{125}Te NMR of **2c** (79.53 MHz, 15 KHz, 300 K).

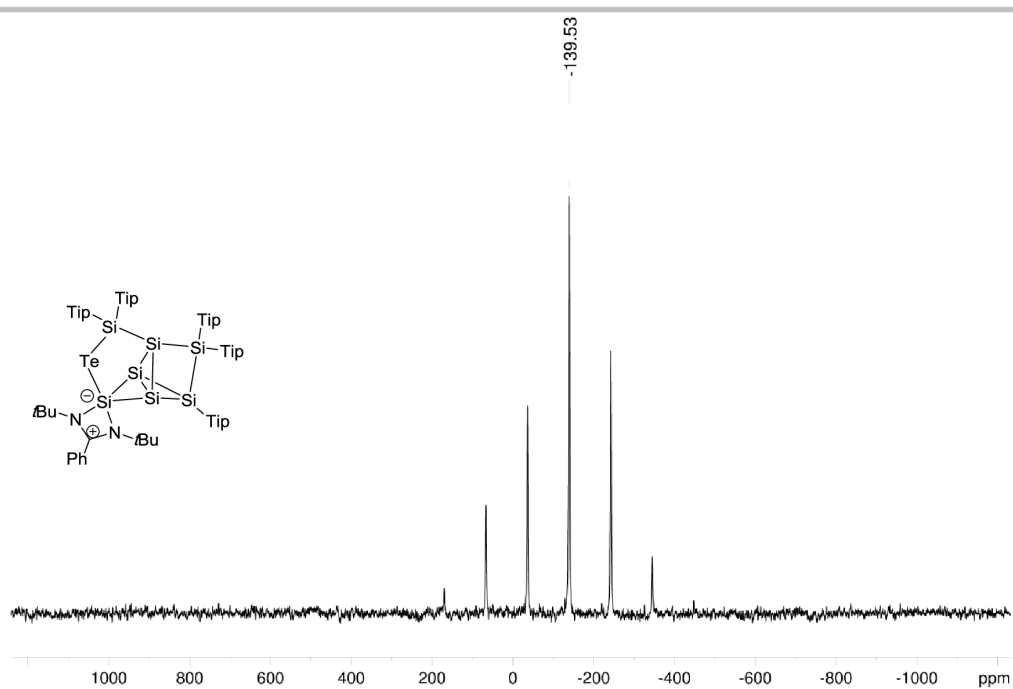


Figure S32. CP-MAS ^{125}Te NMR of **2c** (79.53 MHz, 13 KHz, 300 K).

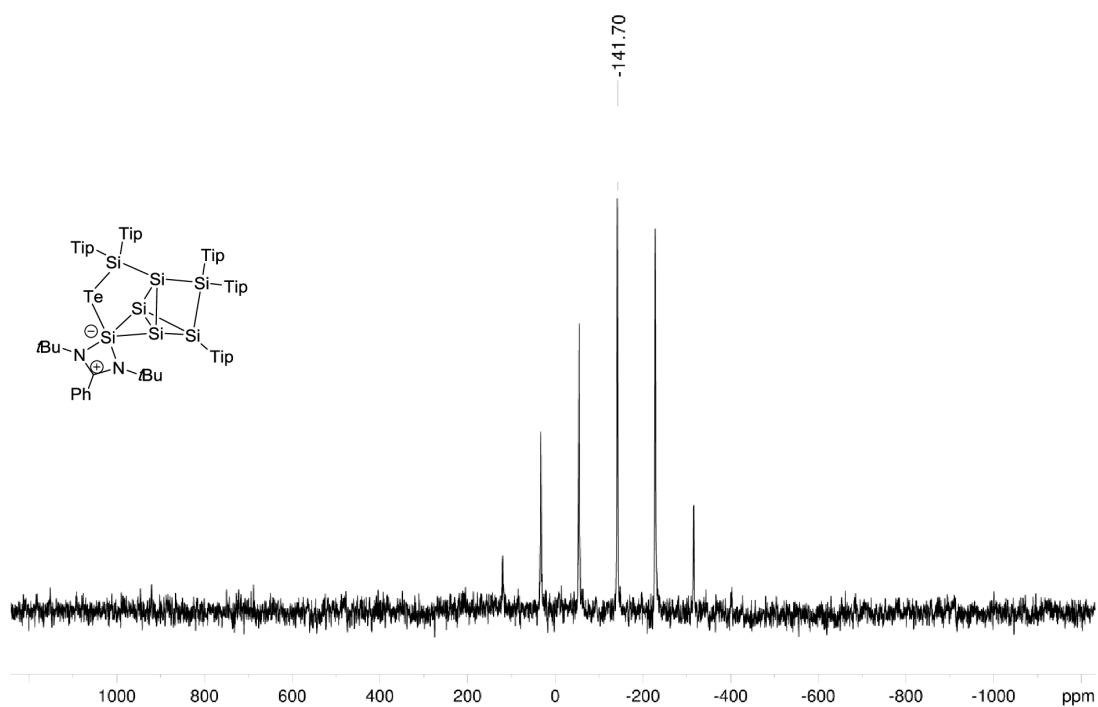


Figure S33. CP-MAS ^{125}Te NMR of **2a** (79.53 MHz, 11 KHz, 300 K).

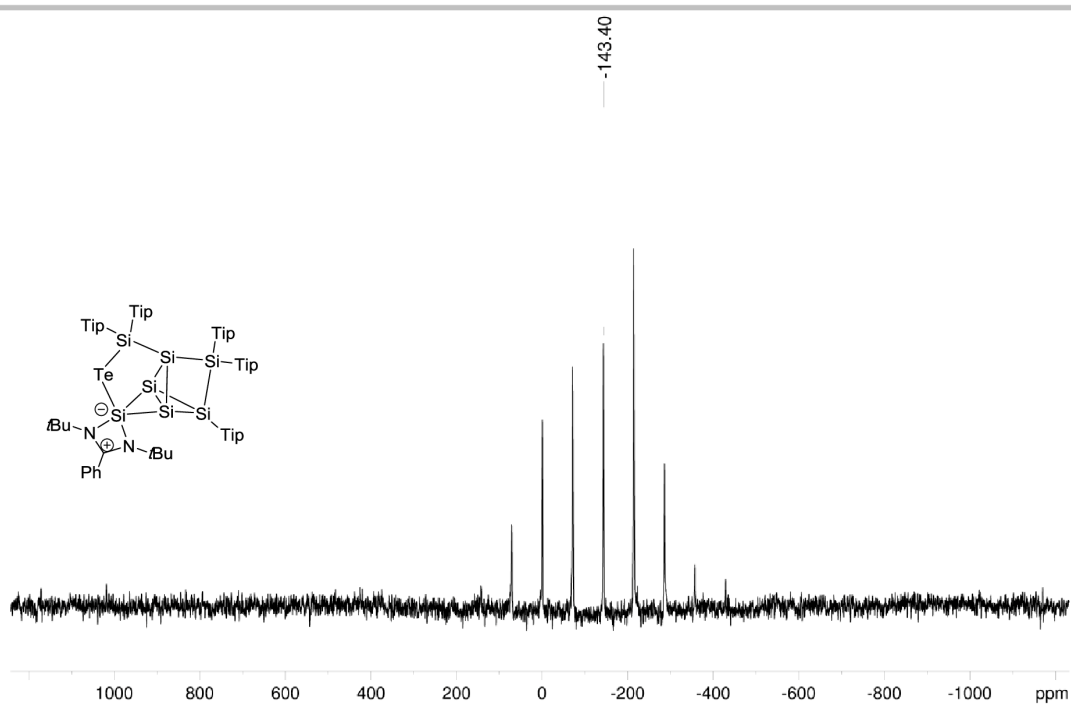


Figure S34. CP-MAS ^{125}Te NMR of 2c (79.53 MHz, 9 KHz, 300 K).

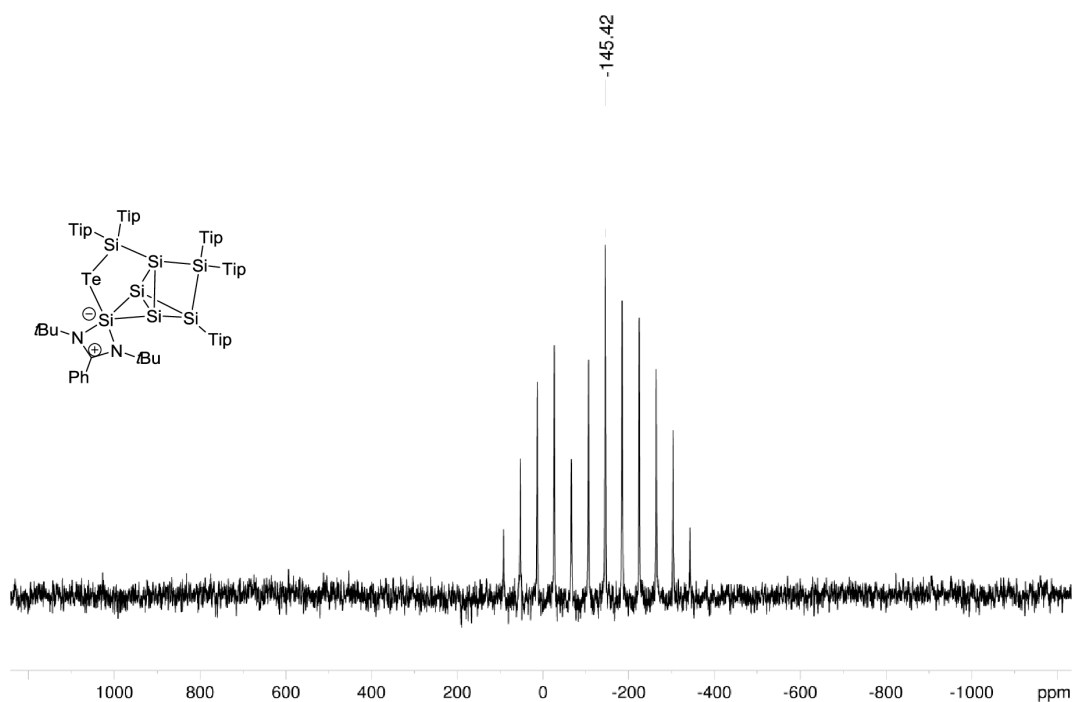


Figure S35. CP-MAS ^{125}Te NMR of 2c (79.53 MHz, 5 KHz, 300 K).

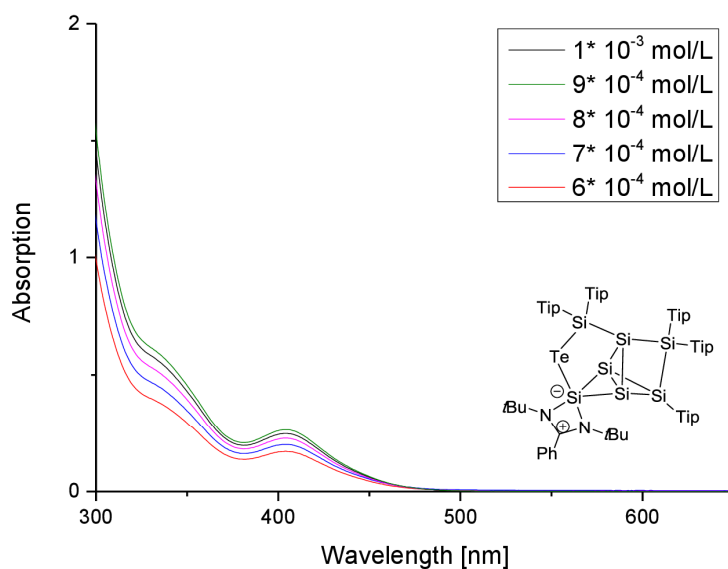


Figure S36. UV-Vis spectrum of **2c** in toluene at different concentrations.

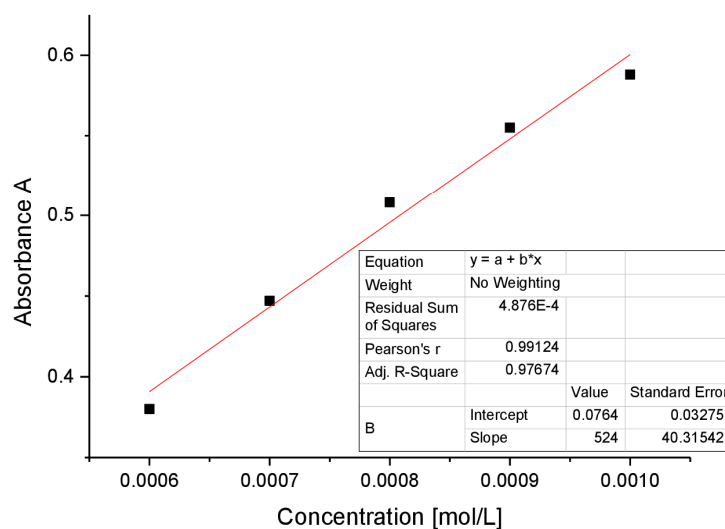


Figure S37. Determination of ε ($5240 \text{ M}^{-1} \text{ cm}^{-1}$) by linear regression of absorptions ($\lambda = 335 \text{ nm}$) of **2c** against concentration.

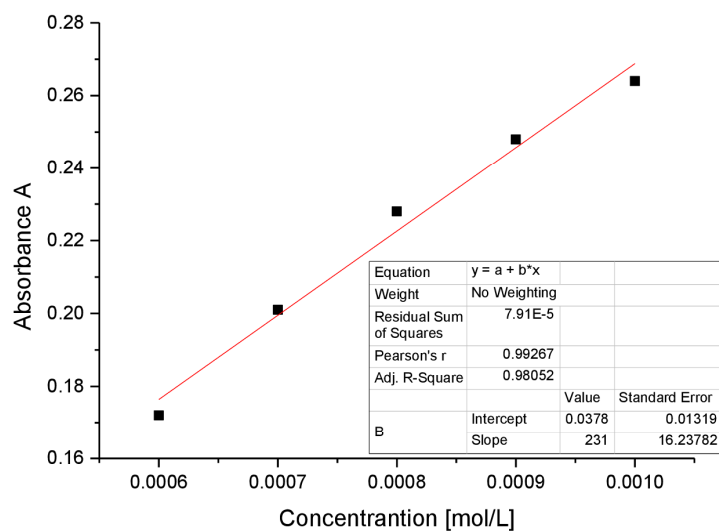


Figure S38. Determination of ϵ ($2310 \text{ M}^{-1} \text{ cm}^{-1}$) by linear regression of absorptions ($\lambda = 404 \text{ nm}$) of **2c** against concentration.

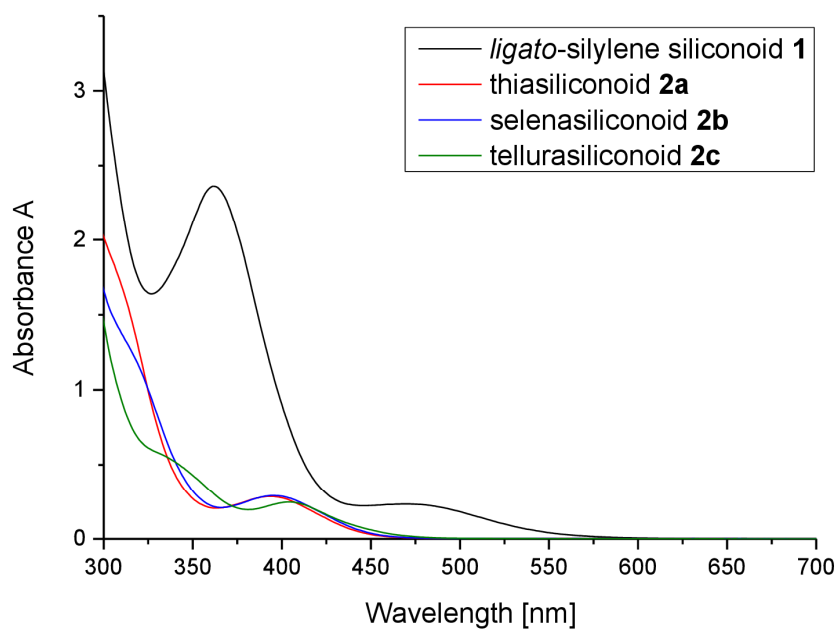


Figure S39. UV-Vis spectra of **1** and **2a-c** at $c = 10^{-3} \text{ mol L}^{-1}$ in toluene.

SUPPORTING INFORMATION

WILEY-VCH

4. Computational Details

Structural and geometry optimizations of **[1-Int]**, **[1-Int]⁺** and **2a** were performed using the Gaussian09 program package^[2] together with TurboMole V7.0.^[3] All geometry optimizations were computed using the BP86^[4,5] functional with Grimme dispersion correctors D3^[6] and the Becke-Johnson damping function^[7] in combination with the def2-SVP basis set.^[8] To ensure the presence of a local minimum on the potential energy surface, the subsequent analysis of the frequency and molecular orbitals was performed at the same level of theory. The optimized structures were plotted using ChemCraft 1.8.^[9]

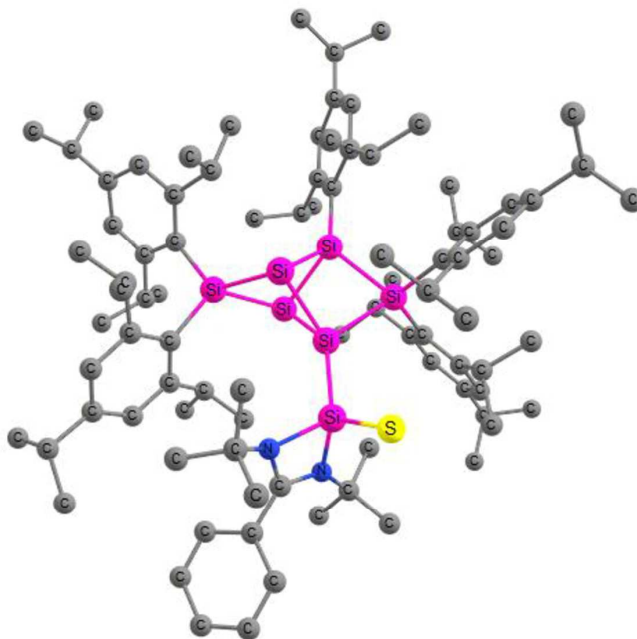


Figure S40. Optimized structure at the BP86-D3(BJ)/def2-SVP level of theory for **[1-Int]**. Bond distances are in [Å]. Hydrogen atoms omitted for clarity.

Table S1. Atomic coordinates of the optimized structure **[1-Int]** at the BP86-D3(BJ)/def2-SVP level of theory.

Si	0.176225000	0.948900000	-1.390277000
Si	0.448855000	0.452295000	1.372224000
Si	-0.057278000	-1.196516000	-0.377730000
Si	-1.537391000	1.239868000	0.323356000
Si	2.015953000	1.715268000	0.077342000
Si	-2.382493000	-0.986083000	0.090112000
Si	0.875562000	-3.168565000	-1.190334000
N	2.711708000	-3.076371000	-1.558349000
N	1.805992000	-4.273709000	0.005292000
C	2.957946000	-4.050133000	-0.651659000
C	3.389798000	-2.728940000	-2.829356000
C	2.531839000	-1.604951000	-3.440870000
H	2.476377000	-0.741150000	-2.746795000
H	1.499201000	-1.962199000	-3.634464000
H	2.970039000	-1.266363000	-4.400357000
C	4.812654000	-2.205083000	-2.581566000
H	4.806687000	-1.413509000	-1.809860000
H	5.218764000	-1.769604000	-3.517056000
H	5.498501000	-3.012611000	-2.261181000
C	3.400252000	-3.958372000	-3.761566000
H	4.031014000	-4.767212000	-3.338891000
H	3.816055000	-3.685434000	-4.753524000
H	2.367879000	-4.342477000	-3.892466000
C	1.382125000	-5.128407000	1.130422000
C	0.230267000	-4.366317000	1.818468000

SUPPORTING INFORMATION

WILEY-VCH

H	-0.199394000	-4.962035000	2.647617000
H	-0.593483000	-4.155510000	1.106863000
H	0.576839000	-3.394503000	2.222109000
C	0.852909000	-6.460701000	0.552339000
H	1.685212000	-7.076282000	0.155970000
H	0.146511000	-6.262309000	-0.278001000
H	0.334503000	-7.046529000	1.338618000
C	2.512750000	-5.391844000	2.140632000
H	2.930459000	-4.445362000	2.533260000
H	3.338120000	-5.983598000	1.701164000
H	2.102068000	-5.966988000	2.995114000
C	4.232583000	-4.791124000	-0.479253000
C	5.395857000	-4.155847000	0.002082000
H	5.372276000	-3.082979000	0.240206000
C	6.576942000	-4.894994000	0.169918000
H	7.478905000	-4.396911000	0.556373000
C	6.612602000	-6.260410000	-0.162195000
H	7.542983000	-6.834911000	-0.032666000
C	5.461352000	-6.889364000	-0.668264000
H	5.488157000	-7.954647000	-0.944923000
C	4.272821000	-6.159993000	-0.822090000
H	3.368395000	-6.640552000	-1.224032000
C	-2.523958000	2.850670000	0.526966000
C	-3.335864000	3.290871000	-0.563258000
C	-4.046888000	4.498512000	-0.448364000
H	-4.662182000	4.832237000	-1.298261000
C	-3.994982000	5.287970000	0.712672000
C	-3.223563000	4.823318000	1.790168000
H	-3.193097000	5.427151000	2.710802000
C	-2.492412000	3.621557000	1.725652000
C	-3.460865000	2.502790000	-1.865943000
H	-3.154897000	1.456043000	-1.647175000
C	-2.518639000	3.043543000	-2.953094000
H	-1.458317000	2.927900000	-2.656073000
H	-2.712981000	4.119497000	-3.148100000
H	-2.664409000	2.493027000	-3.904304000
C	-4.900576000	2.444891000	-2.402038000
H	-5.621446000	2.156589000	-1.614456000
H	-4.967453000	1.688711000	-3.208944000
H	-5.219797000	3.419670000	-2.828536000
C	-4.738936000	6.613210000	0.796379000
H	-4.589421000	7.003728000	1.827871000
C	-4.138171000	7.640027000	-0.184528000
H	-4.637161000	8.627075000	-0.084907000
H	-4.260974000	7.304075000	-1.236026000
H	-3.052708000	7.778616000	-0.003569000
C	-6.253296000	6.438259000	0.575958000
H	-6.681552000	5.708768000	1.293315000
H	-6.471437000	6.068624000	-0.448255000
H	-6.786528000	7.403882000	0.702501000
C	-1.651841000	3.203324000	2.928035000
H	-1.566572000	2.095283000	2.887525000
C	-2.277783000	3.574970000	4.281596000
H	-1.714044000	3.095065000	5.108368000
H	-3.335945000	3.250800000	4.348680000
H	-2.245888000	4.669550000	4.465706000
C	-0.226496000	3.768683000	2.811993000
H	0.406758000	3.423092000	3.656239000
H	-0.235318000	4.879130000	2.818230000
H	0.266442000	3.449309000	1.874465000
C	2.306892000	3.597081000	0.406161000
C	1.668980000	4.641970000	-0.333611000
C	2.151592000	5.960466000	-0.234115000

SUPPORTING INFORMATION

WILEY-VCH

H	1.669530000	6.740725000	-0.843311000
C	3.206085000	6.322084000	0.617535000
C	3.758581000	5.310917000	1.414348000
H	4.556727000	5.576215000	2.127332000
C	3.336366000	3.970762000	1.325585000
C	0.456291000	4.443730000	-1.239026000
H	0.043461000	3.431118000	-1.036550000
C	0.841609000	4.512022000	-2.728886000
H	1.362697000	5.465406000	-2.958141000
H	-0.057154000	4.453945000	-3.374749000
H	1.513913000	3.679532000	-3.016143000
C	-0.659785000	5.450716000	-0.907580000
H	-0.928673000	5.415624000	0.166188000
H	-1.573411000	5.217604000	-1.484636000
H	-0.366787000	6.491735000	-1.157557000
C	3.717990000	7.753555000	0.682645000
H	4.524322000	7.774295000	1.449681000
C	2.617016000	8.733107000	1.132452000
H	2.186901000	8.432458000	2.109588000
H	1.785706000	8.768077000	0.396910000
H	3.018900000	9.763310000	1.232268000
C	4.338695000	8.179377000	-0.662452000
H	5.146364000	7.483804000	-0.969097000
H	4.765880000	9.202296000	-0.598365000
H	3.575972000	8.183169000	-1.469781000
C	4.012521000	2.984508000	2.269155000
H	3.581705000	1.986788000	2.068012000
C	3.689968000	3.300076000	3.741772000
H	4.131824000	2.532578000	4.411438000
H	2.594676000	3.316724000	3.911783000
H	4.094382000	4.287818000	4.047500000
C	5.528390000	2.909093000	2.013466000
H	6.006173000	2.141109000	2.655180000
H	6.019465000	3.879581000	2.235900000
H	5.742592000	2.649686000	0.958124000
C	3.763737000	0.954453000	-0.191861000
C	4.416555000	0.067695000	0.724892000
C	5.756327000	-0.296752000	0.495874000
H	6.254354000	-0.956927000	1.222259000
C	6.497255000	0.191973000	-0.595541000
C	5.851160000	1.065539000	-1.481811000
H	6.417740000	1.468141000	-2.337937000
C	4.508888000	1.452743000	-1.299974000
C	3.739683000	-0.467799000	1.986802000
H	2.914763000	0.233674000	2.235795000
C	3.080888000	-1.825397000	1.732051000
H	3.845776000	-2.610858000	1.576034000
H	2.432650000	-1.792012000	0.838550000
H	2.451123000	-2.124958000	2.594982000
C	4.654633000	-0.543298000	3.220075000
H	4.053270000	-0.789237000	4.119451000
H	5.178870000	0.413761000	3.409298000
H	5.424117000	-1.337881000	3.120850000
C	7.970845000	-0.146714000	-0.772072000
H	8.249088000	0.154837000	-1.806569000
C	8.261260000	-1.650184000	-0.628123000
H	9.327210000	-1.868857000	-0.846064000
H	7.636177000	-2.252747000	-1.317304000
H	8.060893000	-2.000341000	0.406916000
C	8.826453000	0.685802000	0.205590000
H	8.577021000	0.432565000	1.258014000
H	8.643858000	1.771450000	0.072509000
H	9.909766000	0.493341000	0.054994000

SUPPORTING INFORMATION

WILEY-VCH

C	3.915543000	2.462099000	-2.276807000
H	2.845387000	2.590947000	-2.000840000
C	3.927819000	1.959995000	-3.729715000
H	4.963917000	1.816142000	-4.102738000
H	3.432823000	2.694818000	-4.398548000
H	3.395308000	0.994486000	-3.823468000
C	4.589937000	3.839465000	-2.142641000
H	4.552559000	4.205276000	-1.098037000
H	4.079464000	4.587112000	-2.783840000
H	5.654802000	3.792578000	-2.455313000
C	-3.907479000	-0.871931000	-1.058087000
C	-5.120340000	-0.455009000	-0.431715000
C	-6.316057000	-0.438917000	-1.176445000
H	-7.255583000	-0.142586000	-0.680724000
C	-6.353845000	-0.791893000	-2.532747000
C	-5.142740000	-1.154996000	-3.148201000
H	-5.145259000	-1.427717000	-4.214729000
C	-3.926910000	-1.209788000	-2.441829000
C	-5.204757000	-0.071293000	1.046483000
H	-4.168065000	-0.033690000	1.444678000
C	-5.797930000	1.332253000	1.266535000
H	-5.785263000	1.589753000	2.346440000
H	-6.852903000	1.390376000	0.925054000
H	-5.216955000	2.107727000	0.731446000
C	-5.972261000	-1.140012000	1.848482000
H	-5.504090000	-2.137785000	1.742754000
H	-7.023880000	-1.212684000	1.499223000
H	-5.991707000	-0.887024000	2.928904000
C	-7.661163000	-0.776353000	-3.312946000
H	-8.461912000	-0.488893000	-2.595145000
C	-7.637395000	0.281202000	-4.433704000
H	-7.429653000	1.292027000	-4.027589000
H	-8.609523000	0.316096000	-4.969455000
H	-6.849515000	0.051853000	-5.182231000
C	-8.004471000	-2.174374000	-3.862322000
H	-7.245840000	-2.512747000	-4.599383000
H	-8.990398000	-2.170736000	-4.373367000
H	-8.037267000	-2.926746000	-3.048061000
C	-2.667742000	-1.634822000	-3.184897000
H	-1.945864000	-2.028407000	-2.434442000
C	-1.991066000	-0.433613000	-3.864934000
H	-1.769110000	0.370504000	-3.134481000
H	-2.641226000	-0.000779000	-4.655799000
H	-1.029971000	-0.738948000	-4.328772000
C	-2.903018000	-2.767453000	-4.194634000
H	-1.928042000	-3.141142000	-4.565138000
H	-3.497745000	-2.430404000	-5.070476000
H	-3.431027000	-3.622463000	-3.725682000
C	-2.805547000	-2.248613000	1.488498000
C	-3.239118000	-3.557510000	1.092046000
C	-3.555474000	-4.512921000	2.075713000
H	-3.890697000	-5.509049000	1.748404000
C	-3.444508000	-4.249408000	3.450263000
C	-3.014212000	-2.970820000	3.826594000
H	-2.921374000	-2.741183000	4.901491000
C	-2.702164000	-1.971882000	2.882553000
C	-3.408870000	-3.996337000	-0.364403000
H	-2.837224000	-3.292982000	-1.006512000
C	-4.891750000	-3.965113000	-0.787041000
H	-5.470973000	-4.710075000	-0.200143000
H	-4.994343000	-4.221371000	-1.861643000
H	-5.353641000	-2.973666000	-0.631720000
C	-2.830251000	-5.395579000	-0.638241000

SUPPORTING INFORMATION

WILEY-VCH

H	-1.789675000	-5.487229000	-0.276971000
H	-2.810058000	-5.589040000	-1.728816000
H	-3.440350000	-6.192965000	-0.163099000
C	-3.743626000	-5.321429000	4.488947000
H	-3.670267000	-4.834861000	5.487525000
C	-5.169866000	-5.884052000	4.344731000
H	-5.391156000	-6.616533000	5.149310000
H	-5.300844000	-6.406535000	3.373657000
H	-5.926766000	-5.074869000	4.394156000
C	-2.686666000	-6.443231000	4.436673000
H	-1.665298000	-6.036490000	4.586758000
H	-2.701815000	-6.956315000	3.451696000
H	-2.872685000	-7.207804000	5.220453000
C	-2.261944000	-0.624529000	3.441927000
H	-2.091828000	0.049611000	2.575157000
C	-3.336496000	0.026258000	4.329909000
H	-3.583085000	-0.610724000	5.204859000
H	-4.274369000	0.201574000	3.767921000
H	-2.983625000	1.002265000	4.716944000
C	-0.924450000	-0.743036000	4.194489000
H	-1.036765000	-1.337574000	5.126221000
H	-0.536870000	0.259459000	4.476319000
H	-0.156488000	-1.241536000	3.566845000
S	-0.234321000	-4.154533000	-2.550975000

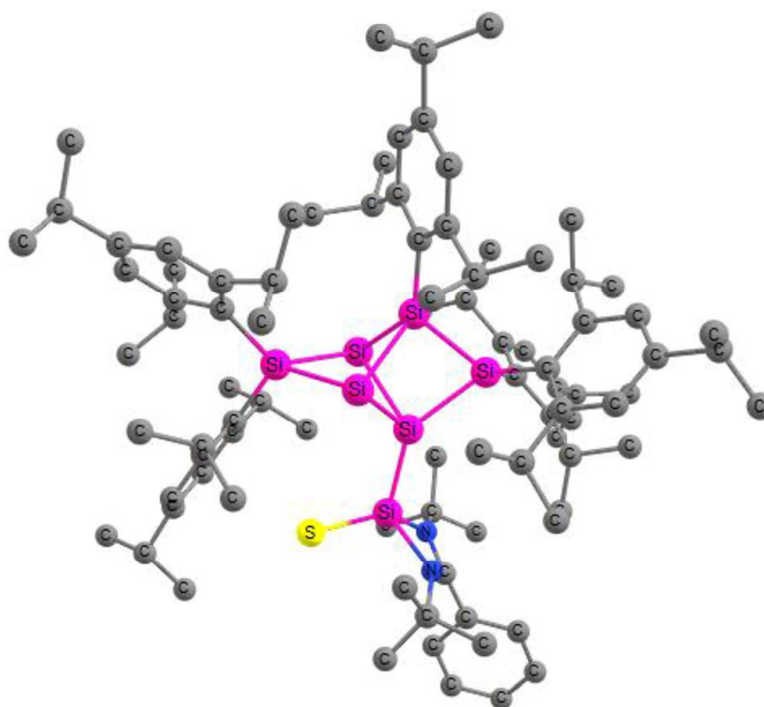


Figure S41. Optimized structure at the BP86-D3(BJ)/def2-SVP level of theory for **[1-Int]'**. Bond distances are in [Å]. Hydrogen atoms omitted for clarity.

Table S2. Atomic coordinates of the optimized structure **[1-Int]'** at the BP86-D3(BJ)/def2-SVP level of theory.

Si	1.204638000	-0.035297000	-1.336379000
Si	0.934215000	-0.399230000	1.434175000
Si	-0.862411000	-0.506376000	-0.267451000
Si	0.979402000	1.714144000	0.356538000
Si	2.632392000	-1.487142000	0.136337000

SUPPORTING INFORMATION

WILEY-VCH

Si	-1.386420000	1.764028000	0.253892000
Si	-1.976047000	-2.513923000	-0.669274000
N	-3.596786000	-2.756739000	0.276068000
N	-3.440216000	-2.471892000	-1.871321000
C	-4.275999000	-2.852023000	-0.880353000
C	-3.983994000	-2.901286000	1.694967000
C	-3.185909000	-1.832375000	2.467991000
H	-3.480867000	-0.812879000	2.152861000
H	-2.098352000	-1.939277000	2.293428000
H	-3.369178000	-1.925201000	3.556986000
C	-5.485718000	-2.660683000	1.936326000
H	-5.800712000	-1.672736000	1.547535000
H	-5.669945000	-2.665681000	3.029207000
H	-6.123011000	-3.442220000	1.482707000
C	-3.585459000	-4.321247000	2.151306000
H	-4.237465000	-5.080524000	1.674128000
H	-3.685096000	-4.420194000	3.251654000
H	-2.539824000	-4.539199000	1.860863000
C	-3.482652000	-2.772491000	-3.322761000
C	-2.185770000	-2.169863000	-3.897422000
H	-2.158845000	-2.285440000	-4.999158000
H	-1.300729000	-2.680187000	-3.465542000
H	-2.113528000	-1.092198000	-3.652080000
C	-3.489576000	-4.297631000	-3.560985000
H	-4.436488000	-4.753835000	-3.209395000
H	-2.641374000	-4.762220000	-3.017723000
H	-3.390317000	-4.513811000	-4.644866000
C	-4.711984000	-2.112594000	-3.976217000
H	-4.775475000	-1.041549000	-3.700852000
H	-5.652382000	-2.610870000	-3.672116000
H	-4.634110000	-2.184593000	-5.080363000
C	-5.629626000	-3.448373000	-1.035054000
C	-6.768650000	-2.686829000	-1.360586000
H	-6.673868000	-1.604028000	-1.514492000
C	-8.020717000	-3.312652000	-1.467386000
H	-8.910312000	-2.711266000	-1.710553000
C	-8.140086000	-4.698710000	-1.266277000
H	-9.123761000	-5.185746000	-1.353615000
C	-7.001085000	-5.463056000	-0.956133000
H	-7.087540000	-6.550286000	-0.805737000
C	-5.749513000	-4.841308000	-0.834971000
H	-4.849490000	-5.427942000	-0.595694000
C	2.164812000	3.188726000	0.529332000
C	2.242971000	4.139346000	-0.534197000
C	3.170137000	5.192874000	-0.450727000
H	3.229107000	5.912704000	-1.281973000
C	4.024597000	5.349267000	0.654167000
C	3.907051000	4.432409000	1.711229000
H	4.557893000	4.559757000	2.590944000
C	2.992329000	3.362204000	1.677604000
C	1.366664000	4.045390000	-1.782064000
H	0.498189000	3.399479000	-1.525734000
C	2.114807000	3.374488000	-2.944475000
H	2.366164000	2.325240000	-2.699286000
H	3.056624000	3.915528000	-3.175662000
H	1.492176000	3.370239000	-3.861780000
C	0.802681000	5.401756000	-2.235950000
H	0.337802000	5.957561000	-1.400637000
H	0.023410000	5.241294000	-3.007152000
H	1.590438000	6.043615000	-2.684755000
C	5.058943000	6.465267000	0.696713000
H	5.547118000	6.416149000	1.695745000
C	6.149907000	6.237507000	-0.369004000
H	6.940522000	7.014617000	-0.303906000
H	5.719789000	6.277422000	-1.392244000
H	6.627131000	5.243834000	-0.246975000
C	4.413852000	7.856918000	0.557725000
H	3.639453000	8.020147000	1.334864000
H	3.926064000	7.978255000	-0.432556000
H	5.176212000	8.658386000	0.653623000
C	2.946065000	2.394548000	2.856132000
H	1.934137000	1.933893000	2.850074000

SUPPORTING INFORMATION

WILEY-VCH

C	3.137747000	3.072359000	4.222162000
H	2.917447000	2.354730000	5.039676000
H	2.469945000	3.949717000	4.341157000
H	4.181944000	3.419234000	4.371891000
C	3.959164000	1.254041000	2.656736000
H	3.870851000	0.495967000	3.463526000
H	5.000180000	1.641057000	2.654887000
H	3.802281000	0.732561000	1.693207000
C	4.546280000	-1.175255000	0.147455000
C	5.195030000	-0.247985000	-0.728729000
C	6.584662000	-0.332030000	-0.938404000
H	7.049601000	0.372328000	-1.646019000
C	7.396708000	-1.266296000	-0.280324000
C	6.771925000	-2.104918000	0.651055000
H	7.393102000	-2.813912000	1.222778000
C	5.383512000	-2.073946000	0.882729000
C	4.488518000	0.869390000	-1.487107000
H	3.442119000	0.929557000	-1.117296000
C	4.442845000	0.555467000	-2.994461000
H	5.465683000	0.401659000	-3.397332000
H	3.974448000	1.380051000	-3.567246000
H	3.860517000	-0.367459000	-3.192565000
C	5.131298000	2.237916000	-1.196887000
H	5.149144000	2.446417000	-0.108674000
H	4.553292000	3.048879000	-1.677627000
H	6.172664000	2.297593000	-1.576529000
C	8.890383000	-1.357384000	-0.556130000
H	9.297380000	-2.140450000	0.122157000
C	9.613997000	-0.035784000	-0.234612000
H	9.436646000	0.274307000	0.815450000
H	9.259538000	0.786555000	-0.891527000
H	10.709331000	-0.136095000	-0.386541000
C	9.156008000	-1.808431000	-2.006112000
H	8.652941000	-2.772452000	-2.224357000
H	10.243667000	-1.933440000	-2.191933000
H	8.773729000	-1.059875000	-2.732164000
C	4.869947000	-2.999109000	1.976802000
H	3.773694000	-2.873081000	2.030392000
C	5.422673000	-2.579924000	3.353533000
H	4.983606000	-3.205654000	4.158702000
H	5.182721000	-1.519146000	3.571107000
H	6.526118000	-2.692198000	3.403759000
C	5.167916000	-4.474464000	1.655049000
H	4.743091000	-5.148589000	2.425857000
H	6.261435000	-4.662219000	1.616213000
H	4.731379000	-4.762189000	0.678433000
C	2.386506000	-3.372828000	0.039320000
C	1.915909000	-4.210043000	1.097608000
C	1.780181000	-5.587431000	0.862793000
H	1.394750000	-6.225592000	1.673410000
C	2.084096000	-6.177140000	-0.376737000
C	2.581862000	-5.349455000	-1.393322000
H	2.831557000	-5.796248000	-2.370406000
C	2.738621000	-3.964747000	-1.202568000
C	1.518765000	-3.692884000	2.483257000
H	1.908240000	-2.656244000	2.581488000
C	-0.007724000	-3.608870000	2.612493000
H	-0.458486000	-4.622029000	2.578057000
H	-0.434424000	-3.037856000	1.767395000
H	-0.302965000	-3.125073000	3.567525000
C	2.095547000	-4.511960000	3.651791000
H	1.840946000	-4.026968000	4.617291000
H	3.196381000	-4.606485000	3.596352000
H	1.672528000	-5.537706000	3.681491000
C	1.828789000	-7.656941000	-0.622638000
H	2.197062000	-7.882349000	-1.648655000
C	0.315369000	-7.952300000	-0.591718000
H	0.109511000	-9.010516000	-0.859813000
H	-0.234867000	-7.291507000	-1.291643000
H	-0.102048000	-7.770069000	0.421188000
C	2.603747000	-8.552835000	0.361243000
H	2.270678000	-8.383354000	1.407215000

SUPPORTING INFORMATION

WILEY-VCH

H	3.693326000	-8.348231000	0.319522000
H	2.443306000	-9.627457000	0.131456000
C	3.240718000	-3.115063000	-2.362573000
H	3.303015000	-2.064575000	-1.996824000
C	2.219186000	-3.093759000	-3.511322000
H	2.104075000	-4.098525000	-3.969674000
H	2.530603000	-2.386135000	-4.308956000
H	1.222882000	-2.787316000	-3.129407000
C	4.663506000	-3.492631000	-2.802596000
H	5.369966000	-3.401241000	-1.951719000
H	5.015772000	-2.820583000	-3.613022000
H	4.711665000	-4.535522000	-3.181782000
C	-1.907511000	3.213614000	-0.885464000
C	-1.957139000	4.499257000	-0.269687000
C	-2.410366000	5.608274000	-1.010940000
H	-2.469196000	6.595327000	-0.522434000
C	-2.786309000	5.501628000	-2.357407000
C	-2.691238000	4.236269000	-2.964316000
H	-2.968983000	4.132816000	-4.024843000
C	-2.272971000	3.094564000	-2.256708000
C	-1.574817000	4.730557000	1.192948000
H	-1.164416000	3.777204000	1.588229000
C	-0.456068000	5.774048000	1.362923000
H	-0.193732000	5.883410000	2.436084000
H	-0.764702000	6.774770000	0.993622000
H	0.463503000	5.472320000	0.825164000
C	-2.816025000	5.083139000	2.034568000
H	-3.589377000	4.293630000	1.960265000
H	-3.264566000	6.040719000	1.695281000
H	-2.549719000	5.196168000	3.105870000
C	-3.269580000	6.716147000	-3.138366000
H	-3.293333000	7.569553000	-2.424315000
C	-2.291412000	7.083318000	-4.271408000
H	-1.272520000	7.271971000	-3.876605000
H	-2.628542000	7.994387000	-4.809347000
H	-2.216091000	6.262327000	-5.015841000
C	-4.700635000	6.512431000	-3.671755000
H	-4.740458000	5.681405000	-4.407576000
H	-5.069638000	7.427465000	-4.181172000
H	-5.403065000	6.265385000	-2.849632000
C	-2.218997000	1.760214000	-2.997042000
H	-2.204180000	0.952863000	-2.227562000
C	-0.910311000	1.634700000	-3.794853000
H	-0.031211000	1.723096000	-3.127191000
H	-0.837831000	2.432441000	-4.564354000
H	-0.843232000	0.651651000	-4.305382000
C	-3.442242000	1.524681000	-3.897292000
H	-3.400227000	0.515256000	-4.350783000
H	-3.486479000	2.250744000	-4.735262000
H	-4.390122000	1.609844000	-3.327485000
C	-2.654998000	1.722382000	1.699506000
C	-4.033820000	1.627357000	1.330087000
C	-5.025975000	1.557610000	2.324484000
H	-6.081567000	1.486999000	2.015504000
C	-4.711638000	1.566897000	3.694342000
C	-3.357403000	1.661015000	4.045875000
H	-3.092013000	1.671155000	5.116442000
C	-2.329434000	1.741647000	3.084798000
C	-4.498518000	1.605247000	-0.125052000
H	-3.599182000	1.507050000	-0.762387000
C	-5.203878000	2.915171000	-0.517587000
H	-6.130692000	3.057511000	0.078118000
H	-5.484773000	2.904889000	-1.591312000
H	-4.548321000	3.791367000	-0.350800000
C	-5.363805000	0.379622000	-0.442279000
H	-4.833653000	-0.546457000	-0.154610000
H	-5.576876000	0.333648000	-1.530964000
H	-6.337640000	0.401505000	0.090950000
C	-5.795401000	1.446633000	4.756717000
H	-5.296356000	1.576024000	5.743125000
C	-6.861610000	2.549636000	4.622570000
H	-7.604386000	2.485547000	5.445268000

SUPPORTING INFORMATION

WILEY-VCH

H	-7.417618000	2.459269000	3.665420000
H	-6.401101000	3.558276000	4.648701000
C	-6.430038000	0.041744000	4.735282000
H	-5.660058000	-0.745346000	4.868648000
H	-6.937926000	-0.150318000	3.766460000
H	-7.184920000	-0.070053000	5.541992000
C	-0.898584000	1.837310000	3.601053000
H	-0.237420000	1.920238000	2.711579000
C	-0.662385000	3.084077000	4.470927000
H	-1.304487000	3.078664000	5.376680000
H	-0.877731000	4.015583000	3.912189000
H	0.392250000	3.125951000	4.809002000
C	-0.493177000	0.556174000	4.352040000
H	-1.063450000	0.445838000	5.299073000
H	0.587925000	0.571720000	4.606658000
H	-0.684899000	-0.346350000	3.735562000
S	-0.813323000	-4.135040000	-0.919169000

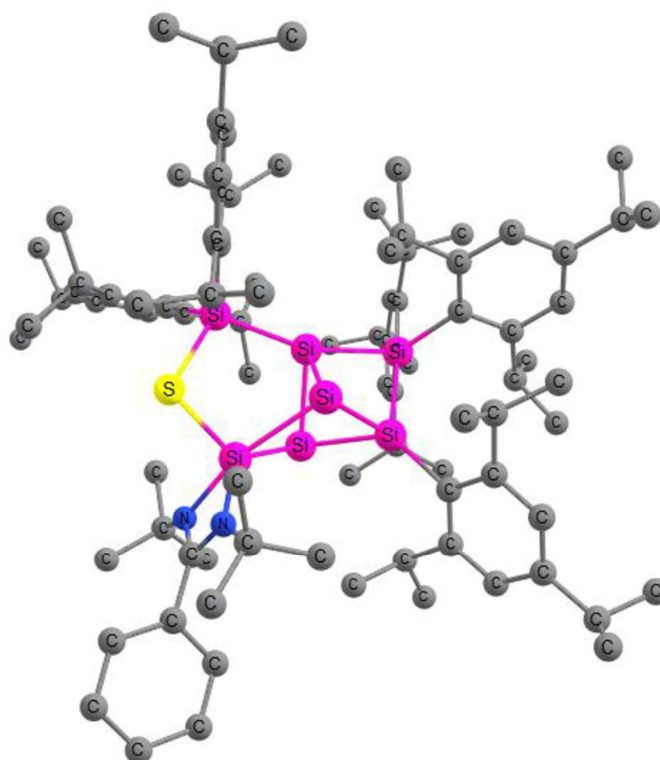


Figure S42. Optimized structure at the BP86-D3(BJ)/def2-SVP level of theory for **2a**. Bond distances are in [Å]. Hydrogen atoms omitted for clarity.

Table S3. Atomic coordinates of the optimized structure **2a** at the BP86-D3(BJ)/def2-SVP level of theory.

Si	0.534123000	0.891280000	-1.554294000
Si	0.181179000	1.493922000	1.239868000
Si	2.150910000	0.708139000	0.126774000
Si	1.558501000	-1.511808000	0.763942000
Si	-0.479196000	-0.502981000	0.062383000
Si	-2.711579000	-0.282196000	-0.607693000
Si	-0.934574000	2.717237000	-0.481779000
S	-2.867890000	1.906175000	-1.032193000
N	-0.480915000	4.324091000	-1.370918000
N	-1.601519000	4.272570000	0.483038000
C	-0.984543000	5.090281000	-0.371869000
C	0.295759000	4.649925000	-2.589362000
C	-0.255668000	3.750893000	-3.714547000
H	0.301281000	3.926991000	-4.657022000

SUPPORTING INFORMATION

WILEY-VCH

H	-1.329975000	3.962318000	-3.888208000
H	-0.152992000	2.682499000	-3.442579000
C	0.145936000	6.118170000	-3.028616000
H	0.651205000	6.238640000	-4.008243000
H	0.610954000	6.829282000	-2.321060000
H	-0.918686000	6.397066000	-3.158653000
C	1.783921000	4.336977000	-2.322822000
H	1.908962000	3.291696000	-1.973158000
H	2.190966000	5.011301000	-1.543199000
H	2.385173000	4.467577000	-3.245561000
C	-0.802768000	6.559211000	-0.217498000
C	-1.783227000	7.462562000	-0.674569000
H	-2.699452000	7.075732000	-1.145386000
C	-1.584580000	8.843664000	-0.530485000
H	-2.351098000	9.546283000	-0.892394000
C	-0.411328000	9.329770000	0.074046000
H	-0.258084000	10.414350000	0.186079000
C	0.564940000	8.429562000	0.535076000
H	1.484833000	8.805346000	1.009179000
C	0.373180000	7.046378000	0.389146000
H	1.137364000	6.335780000	0.736156000
C	-2.195447000	4.508636000	1.815377000
C	-3.008680000	3.248863000	2.173799000
H	-3.834102000	3.081993000	1.455983000
H	-3.427753000	3.349184000	3.194792000
H	-2.370483000	2.343183000	2.151093000
C	-1.069907000	4.715300000	2.853330000
H	-0.393773000	3.835556000	2.863180000
H	-1.498304000	4.840369000	3.869092000
H	-0.473026000	5.619408000	2.617381000
C	-3.145284000	5.723118000	1.807240000
H	-2.604533000	6.681491000	1.693902000
H	-3.699418000	5.759073000	2.767424000
H	-3.886068000	5.632097000	0.986957000
C	3.875374000	1.477007000	-0.102933000
C	4.396026000	2.486988000	0.756240000
C	5.674688000	3.019192000	0.501101000
H	6.085252000	3.792807000	1.169353000
C	6.455187000	2.595287000	-0.587756000
C	5.916413000	1.620821000	-1.446269000
H	6.506677000	1.281437000	-2.312070000
C	4.648270000	1.052928000	-1.228226000
C	3.560636000	3.051854000	1.901115000
H	2.908054000	2.227096000	2.257931000
C	4.380412000	3.556067000	3.097695000
H	5.124760000	2.804438000	3.430610000
H	3.711952000	3.781713000	3.954423000
H	4.929537000	4.491936000	2.860819000
C	2.621213000	4.157411000	1.380216000
H	3.209741000	5.005604000	0.968712000
H	1.970420000	4.538069000	2.194952000
H	1.962141000	3.772801000	0.575942000
C	7.847839000	3.165532000	-0.821639000
H	8.019399000	3.933335000	-0.034127000
C	7.956681000	3.865818000	-2.189687000
H	8.958030000	4.327371000	-2.321148000
H	7.191468000	4.661837000	-2.295633000
H	7.809065000	3.145912000	-3.022355000
C	8.927946000	2.077843000	-0.657793000
H	8.810860000	1.281695000	-1.423254000
H	8.862069000	1.594953000	0.338498000
H	9.946255000	2.506488000	-0.770058000
C	4.120883000	0.036949000	-2.241756000
H	3.302087000	-0.531539000	-1.747541000
C	5.165303000	-0.994158000	-2.698143000
H	4.669109000	-1.794626000	-3.283231000
H	5.667620000	-1.476211000	-1.838594000
H	5.942757000	-0.538424000	-3.347756000
C	3.519557000	0.764147000	-3.459771000
H	4.298784000	1.356654000	-3.984917000
H	2.709232000	1.457989000	-3.156325000
H	3.090979000	0.036796000	-4.180901000

SUPPORTING INFORMATION

WILEY-VCH

C	1.422190000	-2.203803000	2.561982000
C	0.949472000	-3.544514000	2.752361000
C	0.725613000	-4.026151000	4.057245000
H	0.355759000	-5.053769000	4.195025000
C	0.940445000	-3.243691000	5.201290000
C	1.444784000	-1.950575000	5.008749000
H	1.650788000	-1.319339000	5.887786000
C	1.702418000	-1.424362000	3.727913000
C	0.706298000	-4.528159000	1.602536000
H	0.491863000	-3.932156000	0.688288000
C	1.948999000	-5.401200000	1.330836000
H	1.766665000	-6.075650000	0.468402000
H	2.171175000	-6.029570000	2.219576000
H	2.844892000	-4.800878000	1.100030000
C	-0.495905000	-5.456617000	1.842936000
H	-0.717011000	-6.038006000	0.926058000
H	-1.404129000	-4.895263000	2.128277000
H	-0.283141000	-6.195165000	2.643344000
C	0.582795000	-3.766410000	6.585192000
H	0.384741000	-4.856520000	6.477244000
C	1.726581000	-3.595033000	7.600346000
H	2.660703000	-4.071983000	7.239412000
H	1.459370000	-4.050828000	8.576687000
H	1.946456000	-2.522602000	7.787180000
C	-0.718472000	-3.102061000	7.081608000
H	-1.545855000	-3.255163000	6.358996000
H	-0.579678000	-2.006352000	7.200303000
H	-1.031630000	-3.515213000	8.063843000
C	2.326011000	-0.030459000	3.698732000
H	2.429414000	0.262919000	2.633099000
C	1.436953000	1.024033000	4.379847000
H	1.874808000	2.038050000	4.268757000
H	1.327111000	0.824919000	5.466730000
H	0.421829000	1.044492000	3.934863000
C	3.736255000	-0.027516000	4.317533000
H	4.405577000	-0.746386000	3.808905000
H	3.706118000	-0.301447000	5.393140000
H	4.192229000	0.979862000	4.239114000
C	2.629565000	-2.684163000	-0.297012000
C	2.188310000	-3.385020000	-1.457041000
C	3.085511000	-4.230406000	-2.136748000
H	2.732181000	-4.765734000	-3.032343000
C	4.408130000	-4.427330000	-1.703293000
C	4.833564000	-3.723861000	-0.566653000
H	5.869390000	-3.864806000	-0.215430000
C	3.980758000	-2.850602000	0.134839000
C	0.775994000	-3.243288000	-2.017863000
H	0.144290000	-2.780486000	-1.226665000
C	0.759529000	-2.279418000	-3.214317000
H	1.378861000	-2.669771000	-4.050030000
H	1.161129000	-1.283772000	-2.928995000
H	-0.277802000	-2.135586000	-3.577795000
C	0.128030000	-4.583458000	-2.403974000
H	0.641663000	-5.056058000	-3.267549000
H	-0.928690000	-4.420759000	-2.699021000
H	0.150191000	-5.307055000	-1.563503000
C	5.349117000	-5.368652000	-2.442954000
H	6.311934000	-5.366334000	-1.884457000
C	5.637672000	-4.870503000	-3.872478000
H	6.358722000	-5.538437000	-4.389326000
H	6.061243000	-3.845762000	-3.862195000
H	4.709000000	-4.843662000	-4.481236000
C	4.813382000	-6.813407000	-2.445906000
H	3.855730000	-6.884827000	-3.003879000
H	4.626276000	-7.173016000	-1.413457000
H	5.535067000	-7.504958000	-2.929689000
C	4.538744000	-2.162119000	1.382818000
H	3.791377000	-1.407204000	1.711872000
C	5.840681000	-1.386317000	1.115615000
H	6.671053000	-2.062959000	0.823141000
H	6.160000000	-0.848740000	2.032655000
H	5.708516000	-0.631383000	0.317833000

SUPPORTING INFORMATION

WILEY-VCH

C	4.718326000	-3.170116000	2.535160000
H	5.405800000	-3.989227000	2.236377000
H	3.752820000	-3.620435000	2.835243000
H	5.152792000	-2.676019000	3.428959000
C	-3.004658000	-1.384480000	-2.155818000
C	-2.768282000	-0.989962000	-3.513105000
C	-3.053699000	-1.892030000	-4.555407000
H	-2.867963000	-1.570324000	-5.591722000
C	-3.558313000	-3.182355000	-4.327134000
C	-3.754803000	-3.570211000	-2.995534000
H	-4.126744000	-4.588176000	-2.793255000
C	-3.470485000	-2.714405000	-1.912879000
C	-2.254102000	0.390298000	-3.926206000
H	-1.798209000	0.861914000	-3.033357000
C	-3.425928000	1.284447000	-4.374325000
H	-3.068288000	2.306571000	-4.618835000
H	-4.187675000	1.381139000	-3.576616000
H	-3.920800000	0.864571000	-5.276356000
C	-1.162584000	0.347783000	-5.009756000
H	-1.532031000	-0.057875000	-5.975005000
H	-0.296007000	-0.262151000	-4.689534000
H	-0.795438000	1.374137000	-5.212124000
C	-3.816289000	-4.148697000	-5.474489000
H	-4.304332000	-5.047890000	-5.035817000
C	-2.485710000	-4.602019000	-6.109495000
H	-1.950828000	-3.741459000	-6.564519000
H	-2.658055000	-5.355039000	-6.907433000
H	-1.811941000	-5.047963000	-5.349503000
C	-4.773825000	-3.561349000	-6.527414000
H	-4.331774000	-2.671439000	-7.023374000
H	-5.733087000	-3.247264000	-6.067577000
H	-4.996429000	-4.306415000	-7.319898000
C	-3.646362000	-3.303495000	-0.511288000
H	-3.211398000	-2.589591000	0.216425000
C	-2.861574000	-4.612153000	-0.346752000
H	-3.197850000	-5.393558000	-1.058934000
H	-3.005234000	-5.015932000	0.673987000
H	-1.779218000	-4.452559000	-0.505408000
C	-5.121643000	-3.508838000	-0.125391000
H	-5.620204000	-4.212728000	-0.825157000
H	-5.682991000	-2.556894000	-0.131338000
H	-5.197192000	-3.934600000	0.896929000
C	-4.160371000	-0.413804000	0.635846000
C	-5.458687000	-0.026217000	0.177475000
C	-6.543699000	-0.029680000	1.071701000
H	-7.538978000	0.262445000	0.698626000
C	-6.396367000	-0.391369000	2.422078000
C	-5.122097000	-0.786120000	2.854588000
H	-4.996746000	-1.090434000	3.907166000
C	-4.006770000	-0.826262000	1.992564000
C	-5.745081000	0.384668000	-1.269608000
H	-4.782034000	0.415414000	-1.817297000
C	-6.612005000	-0.646846000	-2.015063000
H	-6.815320000	-0.300359000	-3.049952000
H	-7.588554000	-0.803363000	-1.509405000
H	-6.097087000	-1.624803000	-2.084867000
C	-6.346490000	1.798985000	-1.353522000
H	-6.446045000	2.115932000	-2.413118000
H	-5.696616000	2.531674000	-0.834677000
H	-7.357275000	1.842613000	-0.895810000
C	-7.581487000	-0.374194000	3.378230000
H	-7.198046000	-0.693120000	4.373362000
C	-8.664715000	-1.382947000	2.949157000
H	-9.093937000	-1.112883000	1.961008000
H	-9.499018000	-1.408053000	3.681671000
H	-8.247032000	-2.406857000	2.863398000
C	-8.161910000	1.044853000	3.533039000
H	-7.383692000	1.762134000	3.864907000
H	-8.987084000	1.058905000	4.276104000
H	-8.571391000	1.417150000	2.570067000
C	-2.699156000	-1.360990000	2.581132000
H	-1.966468000	-1.467394000	1.750530000

SUPPORTING INFORMATION

WILEY-VCH

C	-2.867031000	-2.757764000	3.205801000
H	-3.311771000	-3.476032000	2.487892000
H	-3.524001000	-2.731390000	4.100431000
H	-1.879123000	-3.146909000	3.526903000
C	-2.071829000	-0.393270000	3.596681000
H	-1.107156000	-0.798454000	3.965938000
H	-2.740939000	-0.234357000	4.469111000
H	-1.871834000	0.593234000	3.132936000

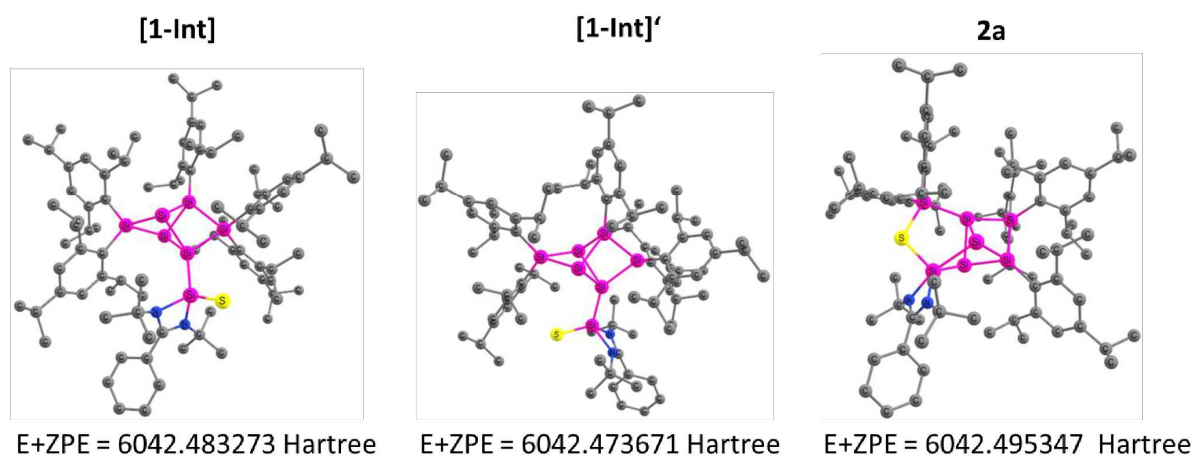


Figure S43: Free Gibbs energies in Hartree of [Int-1], [Int-1]' and 2a

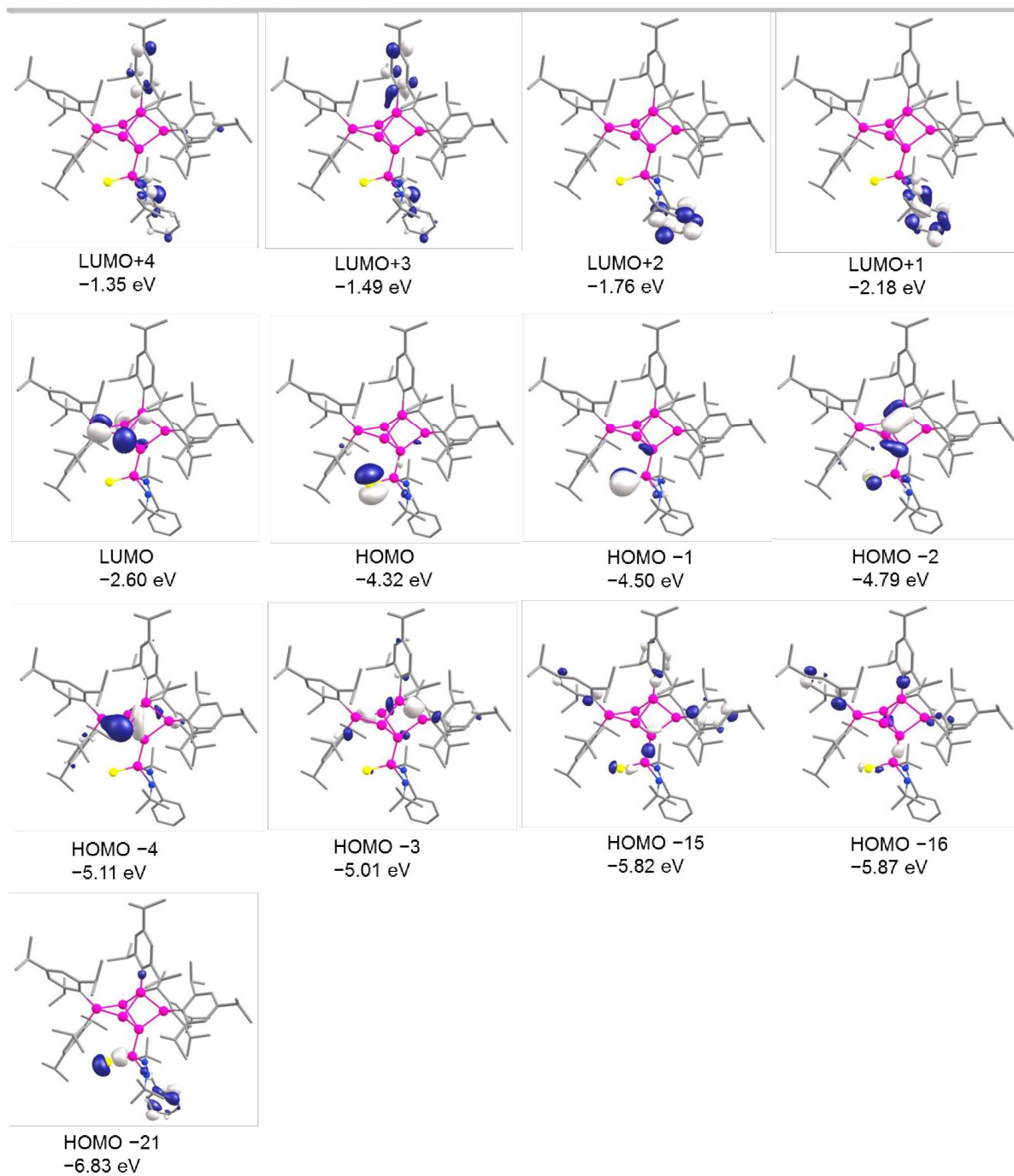


Figure S44: Selected molecular orbitals of $[1\text{-Int}]^*$ at the BP86-D3(BJ)/def2-SVP level of theory (isocontour value 0.051840).

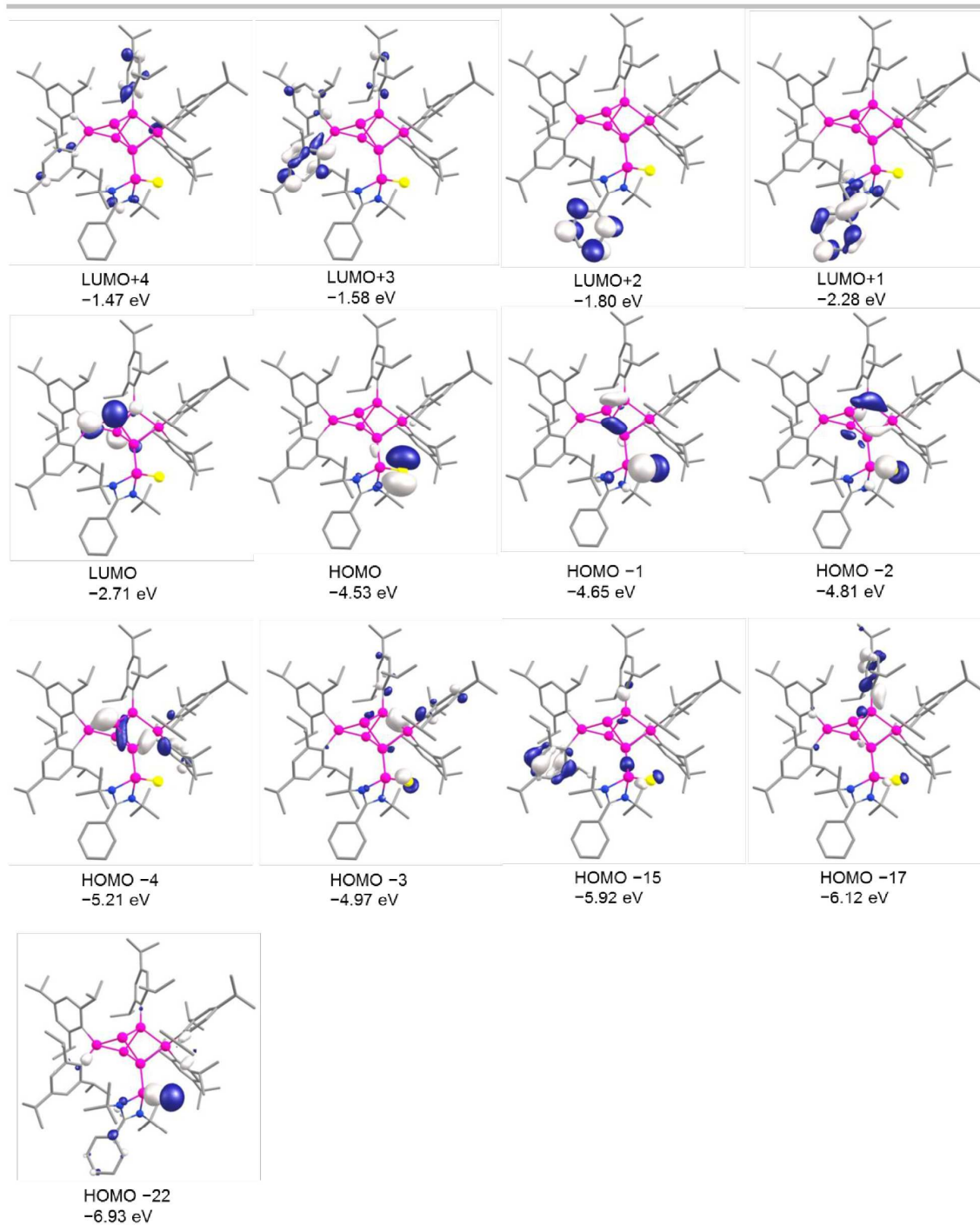


Figure S45: Selected molecular orbitals of [1-Int] at the BP86-D3(BJ)/def2-SVP level of theory (isocontour value 0.051840).

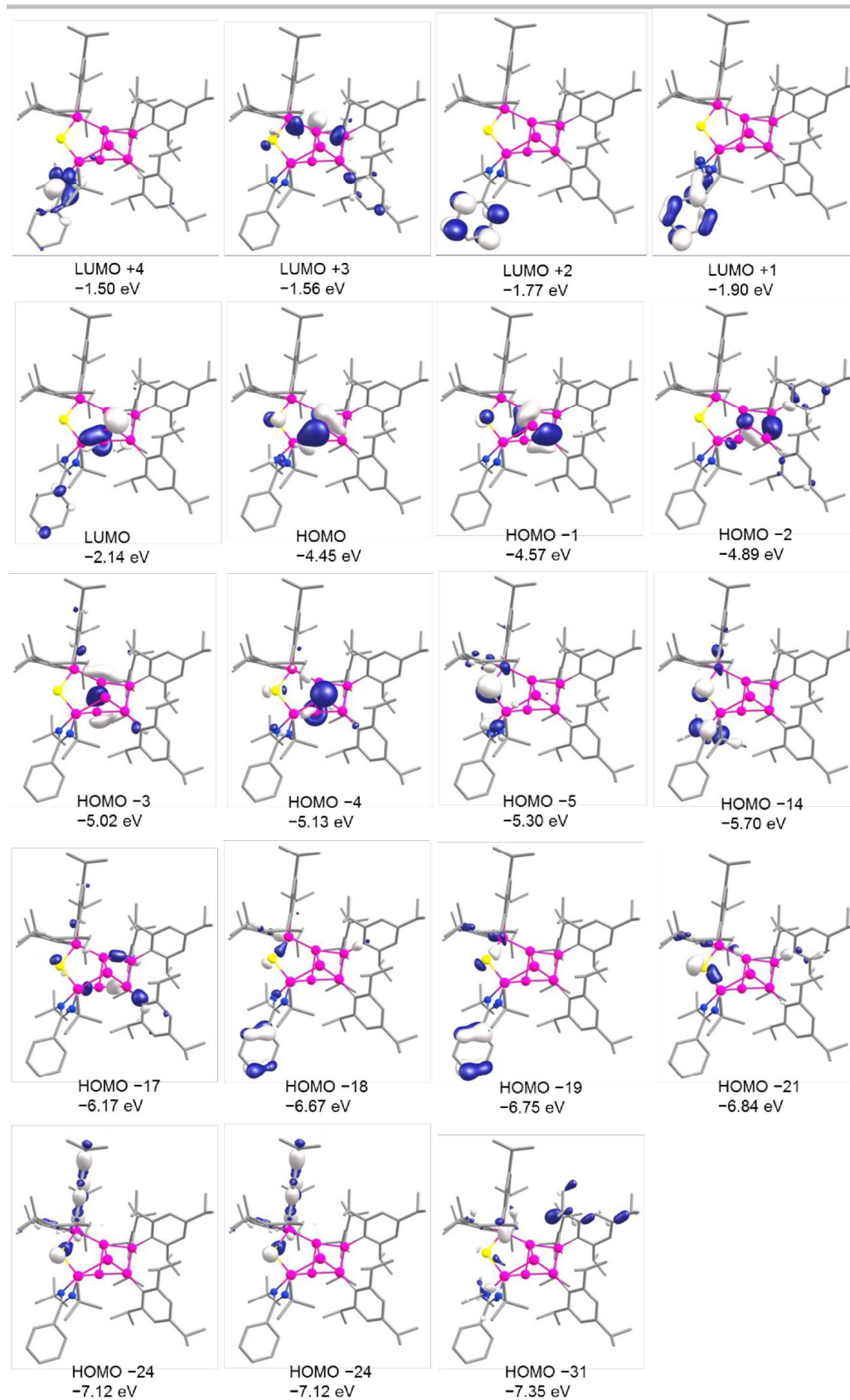


Figure S46: Selected molecular orbitals of **2a** at the BP86-D3(BJ)/def2-SVP level of theory (isocontour value 0.051840).

4. Details on X-Ray Diffraction Studies

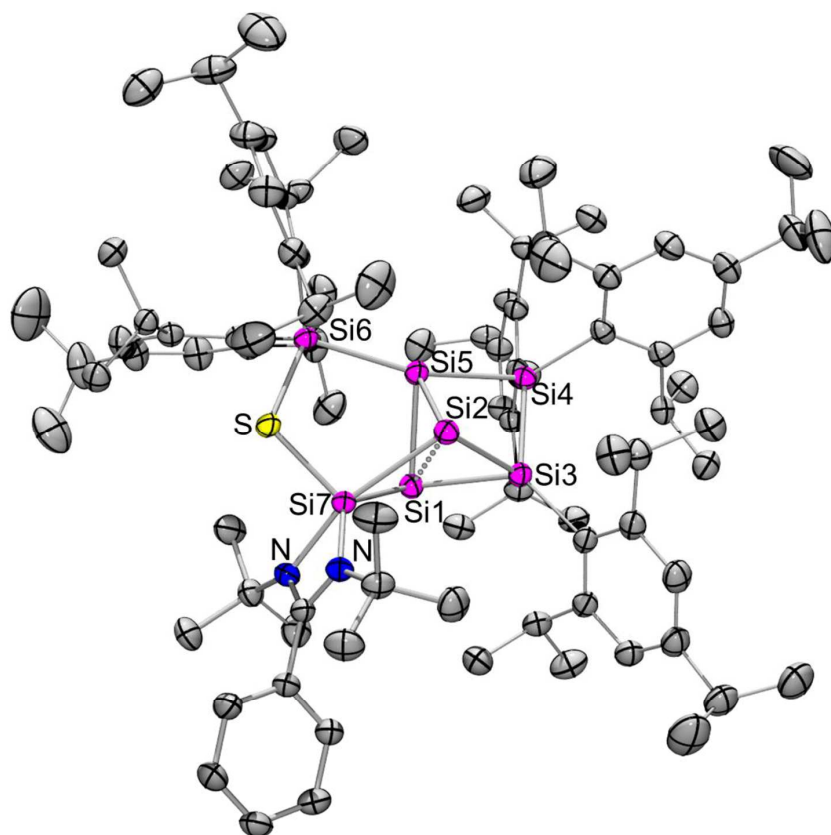


Figure S47. Molecular structure of siliconoid **2a** in the solid state. Hydrogen atoms omitted for clarity. Thermal ellipsoids represent 50% probability

Table S4. Crystal data and structure refinement for **2a** (CCDC: 2002645).

Identification code	sh4186a	
Empirical formula	C ₉₀ H ₁₃₈ N ₂ S Si ₇	
Formula weight	1476.71	
Temperature	173(2) K	
Wavelength	1.54178 Å	
Crystal system	Triclinic	
Space group	P-1	
Unit cell dimensions	$a = 14.4660(8)$ Å	$\alpha = 93.095(2)^\circ$
	$b = 15.1754(8)$ Å	$\beta = 103.849(2)^\circ$
	$c = 21.5361(12)$ Å	$\gamma = 96.291(2)^\circ$
Volume	$4546.9(4)$ Å ³	
Z	2	
Density (calculated)	1.079 Mg/m ³	
Absorption coefficient	1.508 mm ⁻³	
F(000)	1612	

SUPPORTING INFORMATION

WILEY-VCH

Crystal size	0.157 x 0.076 x 0.030 mm ³
Theta range for data collection	2.120 to 74.698°.
Index ranges	-18<=h<=17, -18<=k<=18, -26<=l<=25
Reflections collected	72856
Independent reflections	18426 [R(int) = 0.0365]
Completeness to theta = 67.679°	99.5 %
Absorption correction	Semi-empirical from equivalents
Max. and min. transmission	0.7538 and 0.6733
Refinement method	Full-matrix least-squares on F ²
Data / restraints / parameters	18426 / 0 / 937
Goodness-of-fit on F ²	1.035
Final R indices [I>2sigma(I)]	R1 = 0.0398, wR2 = 0.1088
R indices (all data)	R1 = 0.0448, wR2 = 0.1143
Extinction coefficient	n/a
Largest diff. peak and hole	0.535 and -0.312 e.Å ⁻³

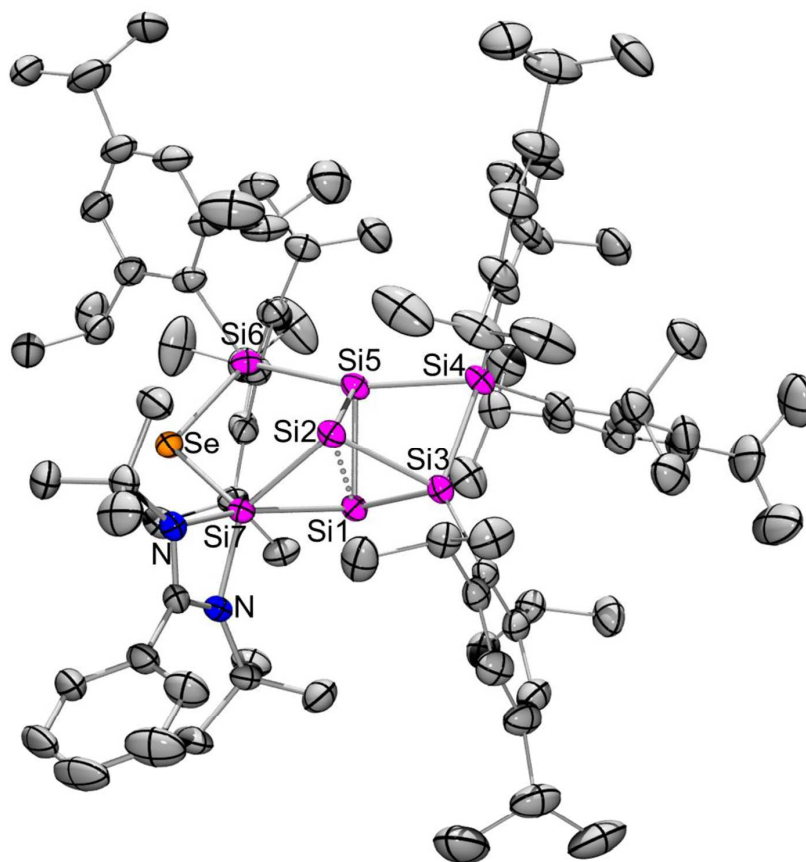


Figure S48. Molecular structure of siliconoid **2b** in the solid state. Hydrogen atoms omitted for clarity. Thermal ellipsoids represent 50% probability

Table S5. Crystal data and structure refinement for **2b** (CCDC: 2002646).

Identification code	sh4179a	
Empirical formula	C ₉₀ H ₁₃₇ N ₂ Se Si ₇	
Formula weight	1522.60	
Temperature	173(2) K	
Wavelength	0.71073 Å	
Crystal system	Monoclinic	
Space group	C2/c	
Unit cell dimensions	a = 42.0779(15) Å	$\alpha = 90^\circ$.
	b = 15.8350(5) Å	$\beta = 96.648(2)^\circ$.
	c = 27.2654(8) Å	$\gamma = 90^\circ$.
Volume	18044.9(10) Å ³	
Z	8	
Density (calculated)	1.121 Mg/m ³	
Absorption coefficient	0.551 mm ⁻¹	
F(000)	6584	

SUPPORTING INFORMATION

WILEY-VCH

Crystal size	0.192 x 0.131 x 0.101 mm ³
Theta range for data collection	2.320 to 27.896°
Index ranges	-55<= <i>h</i> <=55, -20<= <i>k</i> <=20, -35<= <i>l</i> <=31
Reflections collected	183269
Independent reflections	21532 [R(int) = 0.0639]
Completeness to theta = 25.242°	99.9 %
Absorption correction	Semi-empirical from equivalents
Max. and min. transmission	0.7456 and 0.7185
Refinement method	Full-matrix least-squares on F ²
Data / restraints / parameters	21532 / 57 / 988
Goodness-of-fit on F ²	1.016
Final R indices [I>2sigma(I)]	R1 = 0.0423, wR2 = 0.1005
R indices (all data)	R1 = 0.0621, wR2 = 0.1107
Extinction coefficient	n/a
Largest diff. peak and hole	0.469 and -0.410 e.Å ⁻³

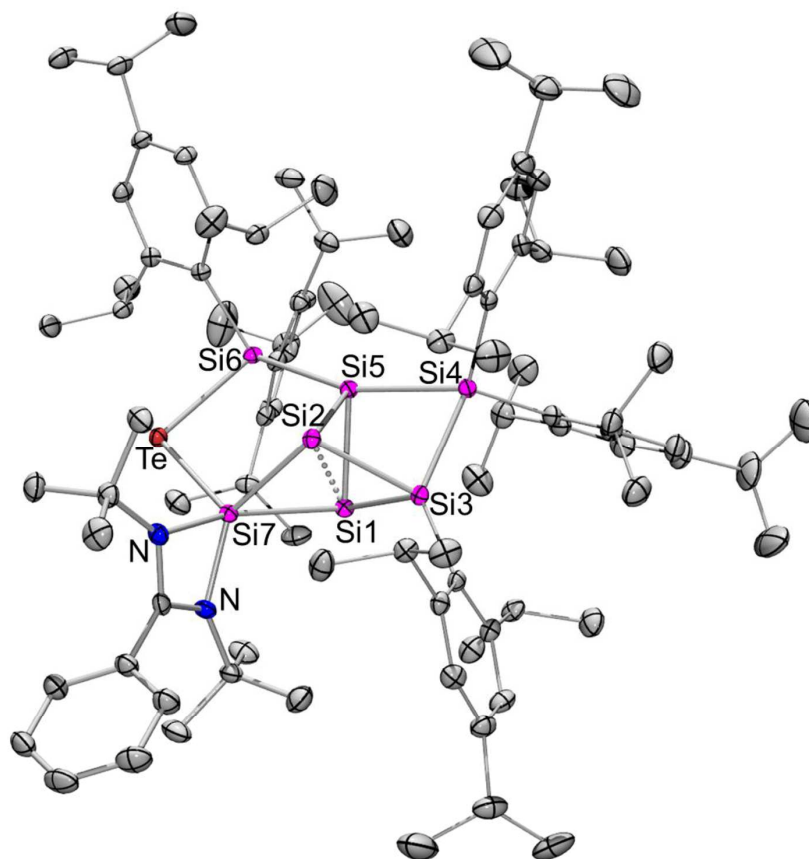


Figure S49. Molecular structure of siliconoid **2c** in the solid state. Hydrogen atoms omitted for clarity. Thermal ellipsoids represent 50% probability

Table S6. Crystal data and structure refinement for **2c** (CCDC: 2002647).

Identification code	sh4204	
Empirical formula	C ₉₀ H ₁₃₈ N ₂ Si ₇ Te	
Formula weight	1572.25	
Temperature	132(2) K	
Wavelength	0.71073 Å	
Crystal system	Monoclinic	
Space group	C2/c	
Unit cell dimensions	a = 41.4479(19) Å	$\alpha = 90^\circ$.
	b = 15.9849(8) Å	$\beta = 96.791(2)^\circ$.
	c = 27.2210(12) Å	$\gamma = 90^\circ$.
Volume	17908.5(15) Å ³	
Z	8	
Density (calculated)	1.166 Mg/m ³	
Absorption coefficient	0.469 mm ⁻¹	
F(000)	6736	

SUPPORTING INFORMATION

WILEY-VCH

Crystal size	0.301 x 0.217 x 0.092 mm ³
Theta range for data collection	1.367 to 28.723°
Index ranges	-55<=h<=56, -21<=k<=21, -36<=l<=36
Reflections collected	154815
Independent reflections	23155 [R(int) = 0.0543]
Completeness to theta = 25.242°	100.0 %
Absorption correction	Semi-empirical from equivalents
Max. and min. transmission	0.7458 and 0.7074
Refinement method	Full-matrix least-squares on F ²
Data / restraints / parameters	23155 / 6 / 948
Goodness-of-fit on F ²	1.012
Final R indices [I>2sigma(I)]	R1 = 0.0334, wR2 = 0.0709
R indices (all data)	R1 = 0.0521, wR2 = 0.0786
Extinction coefficient	n/a
Largest diff. peak and hole	0.804 and -0.711 e.Å ⁻³

4. References

- [1] N. E. Poitiers, L. Giarrana, K. I. Leszczyńska, V. Huch, M. Zimmer, D. Scheschke, *Angew. Chem.* **2020**, *132*, 8610-8614; *Angew. Chem. Int. Ed.* **2020**, *59*, 8532-8536.
- [2] M. J. Frisch, G. W. Trucks, H. B. Schlegel, G. E. Scuseria, M. A. Robb, J. R. Cheeseman, G. Scalmani, V. Barone, B. Mennucci, G. A. Petersson, H. P. Hratchian, A. F. Izmaylov, J. Bloino, G. Zheng, J. L. Sonnenberg, M. Hada, M. Ehara, K. Toyota, R. Fukuda, J. Hasegawa, M. Ishida, T. Najajima, Y. Honda, O. Kitao, H. Nikai, T. Vreven, J. A. Montgomery, J. E. Peralta, F. Ogliaro, M. Bearpark, J. J. Heyd, E. Brothers, K. N. Kudin, V. N. Staroverov, R. Kobayashi, J. Normand, K. Raghavachari, A. Rendell, J. C. Burant, S. S. Iyengar, J. Tomasi, M. Cossi, N. Rega, J. M. Millam, M. Klene, J. E. Knox, J. B. Cross, V. Bakken, C. Adamo, J. Jaramillo, R. Gomperts, R. E. Stratman, O. Yazyev, A. J. Austin, R. Cammi, C. Pomelli, J. W. Ochterski, R. L. Martin, K. Morokuma, V. G. Zakrzewski, G. A. Voth, P. Salvador, J. J. Dannenberg, S. Dapprich, A. D. Daniels, O. Farkas, J. B. Foresman, J. V. Ortiz, J. Cioslowski, D. J. Fox, *Gaussian09, Revision C.01*. Gaussian, Inc.: Wallingford CT, **2009**.
- [3] TURBOMOLE V7.0 2015 a development of University of Karlsruhe and Forschungszentrum Karlsruhe GmbH, 1989-2007; TURBOMOLE GmbH, since **2007**, available from <http://www.turbomole.com>; Karlsruhe.
- [4] A. D. Becke, *Phys. Rev. A* **1988**, *38* (6), 3098-3100.
- [5] J. P. Perdew, *Phys. Rev. B* **1986**, *33* (12), 8822-8824.
- [6] S. Grimme, J. Antony, S. Ehrlich, H. Krieg, *J. Chem. Phys.* **2010**, *132* (15), 154104.
- [7] S. Grimme, S. Ehrlich, L. Goerigk, *J. Comp. Chem.* **2011**, *32* (7), 1456-1465.
- [8] F. Weigend, R. Ahlrichs, *Phys. Chem. Chem. Phys.* **2005**, *7* (18), 3297-3305.
- [9] <https://www.chemcraftprog.com/>

Author Contributions

N. P. Conceptualization: Equal, Data curation: Lead; Formal analysis: Lead; Investigation: Lead; Methodology: Lead; Validation: Lead; Visualization: Lead; Writing original draft: Lead; Writing review & editing: Lead. V.H. Data curation (X-ray): Lead; Formal analysis (X-ray): Lead; X-ray structures: Lead. M. Z. VT NMR studies: Lead; CP/MAS NMR studies: Lead. D. S. Conceptualization: Lead; Funding acquisition: Lead; Methodology: Supporting; Project administration: Lead; Resources: Lead; Supervision: Lead; Writing original draft: Supporting; Writing review & edition: Supporting.

6.5 Nickel-Assisted Complete Cleavage of CO by a Silylene/Siliconoid Hybrid under Formation of an Si=C Enol Ether bridge

Electronic Supplementary Material (ESI) for ChemComm.
This journal is © The Royal Society of Chemistry 2020

**Nickel-Assisted Complete Cleavage of CO by a
Silylene/Siliconoid Hybrid under Formation of an Si=C Enol
Ether bridge**

Nadine E. Poitiers, Volker Huch, Michael Zimmer and David Scheschkewitz*

Krupp-Chair of General and Inorganic Chemistry, Saarland University, 66123 Saarbrücken, Germany

Electronic Supplementary Information

Table of Contents

<u>1. General</u>	S3
<u>2. Preparation, data and spectra (NMR, UV-vis, IR):</u>	S3
• Si=C Enol ether bridged siliconoid 2	S3
<u>3. Computational Details</u>	S10
• <i>Ligato</i> -silylene-functionalized siliconoid 1	S10
• [Int-a]	S14
• [Int-b]	S18
• [Int-c]	S23
• Si=C Enol ether bridged siliconoid 2	S27
<u>4. Details on X-ray Diffraction Studies</u>	S39
<u>5. References</u>	S40

1. General

All manipulations were carried out under a protective atmosphere of argon, by using a glovebox or standard Schlenk techniques. Ethereal solvents were dried by heating to reflux over Na/benzophenone and distilled and stored under an atmosphere of argon. Hydrocarbons were dried over sodium or potassium. Solution NMR spectra were recorded on a Bruker Avance IV 400 NMR spectrometer (^1H = 400.13 MHz, ^{13}C = 100.6 MHz, ^{29}Si = 79.49 MHz) and solid state NMR spectra on a Bruker Avance III 400 WB spectrometer (^{29}Si = 79.53 MHz). UV/Vis spectra were recorded on a Shimadzu UV-2600 spectrometer in quartz cells with a path length of 0.1 cm. Elemental analyses were performed on an elemental analyzer Leco CHN-900 and/or an elemental vario Micro Cube. Compound **1** was prepared according to our published procedure.¹

2. Preparation, data and spectra (NMR, UV-vis, IR)

Ligato-privo Si=C Enol ether bridged Si₆ siliconoid

Route A: Compound **2** is prepared by treating 1 equivalent of the *ligato*-siylene-functionalized siliconoid **1** (350 mg ; 0.237 mmol) with 1 equivalent of Bis(cycloocta-1,5-dien)nickel (74.41 mg ; 0.259 mmol) under CO atmosphere in 8 mL benzene. The suspension was slightly heated to 50°C until the color changed from bright red to brown. The mixture was stirred over night at room temperature until the color changed to green. All volatiles (caution, Ni(CO)₄!) were removed in vacuo and the crude product is extracted with 6 mL hexane. The hexane solution is concentrated and compound **2** is crystallized at -26°C as green crystals in 66 % yield (230 mg ; 0.156 mmol).

Route B: Compound **2** is prepared by treating 1 equivalent of the *ligato*-siylene-functionalized siliconoid **1** (250 mg ; 0.173 mmol) with 10 mol% of Bis(cycloocta-1,5-dien)nickel (4.76 mg ; 0.0173 mmol) under CO atmosphere in 8 mL benzene at 45°C over two days. The color changed from a bright red suspension to a green solution. All volatiles were removed in vacuo and the crude product is filtered from 6 mL hexane. Compound **2** is crystallized as green crystals at -26°C in 44 % yield (112 mg ; 0.076 mmol).

^1H -NMR (400.13 MHz, C₆D₆, 300 K) δ = 7.631 (0.074H, C₁₀H₈), 7.340 – 7.337 (m, 1H, Ar-H), 7.251 – 7.235 (m, 2H, Ar-H), 7.1838 (bs, 1H, Ar-H), 7.037 – 6.972 (m, 5H, Ar-H), 6.889 – 6.813 (m, 4H, Ar-H), 6.705 – 6.664 (m, 1H, Ar-H), 6.549 – 6.529 (m, 1H, Ar-H), 5.371 – 5.249 (m, 2H, Tip-*i*Pr-CH₂), 4.815 (bs, 1H, Tip-*i*Pr-CH₂), 4.584 (bs, 1H, Tip-*i*Pr-CH₂), 4.453 (sept, 1H, $^3J_{\text{HH}}$ = 6.25 Hz, Tip-*i*Pr-CH₂), 4.335 (sept, 1H, $^3J_{\text{HH}}$ = 6.25 Hz, Tip-*i*Pr-CH₂), 4.115 (sept, 1H, $^3J_{\text{HH}}$ = 6.25 Hz, Tip-*i*Pr-CH₂), 3.865 (sept, 1H, $^3J_{\text{HH}}$ = 6.25 Hz, Tip-*i*Pr-CH₂), 3.362 (sept, 1H, $^3J_{\text{HH}}$ = 6.25 Hz, Tip-*i*Pr-CH₂), 3.207 (sept, 1H, $^3J_{\text{HH}}$ = 6.25 Hz, Tip-*i*Pr-CH₂), 2.9358 – 2.617 (m, 5H, Tip-*i*Pr-CH₂), 2.222 (d, 3H, $^3J_{\text{HH}}$ = 6.32 Hz, Tip-*i*Pr-CH₂), 2.089 (d, 3H, $^3J_{\text{HH}}$ = 6.32 Hz, Tip-*i*Pr-CH₂), 1.850 (bs, 3H, Tip-*i*Pr-CH₃), 1.706 – 1.666 (m, 10H, Tip-*i*Pr-CH₃), 1.585 – 1.453 (m, 30H, Tip-*i*Pr-CH₃ overlapping with C(CH₃)₂), 1.315 – 1.216 (m, 26H, Tip-*i*Pr-CH₃), 1.126 – 1.046 (m, 14H, Tip-*i*Pr-CH₃), 0.8925 (t, 3H, hexane), 0.835 – 0.745 (m, 16H, Tip-*i*Pr-CH₃), 0.621 (s, 9H, C(CH₃)₂), 0.560 (d, 3H, $^3J_{\text{HH}}$ = 6.32 Hz, Tip-*i*Pr-CH₃), 0.400 (d, 3H, $^3J_{\text{HH}}$ = 6.32 Hz, Tip-*i*Pr-CH₃), 0.252 (d, 3H, $^3J_{\text{HH}}$ = 6.32 Hz, Tip-*i*Pr-CH₃) ppm.

^{13}C -NMR (100.61 MHz, C₆D₆, 300 K) δ = 175.66 (Ph-C), 156.99, 155.36, 153.51, 152.63, 152.54, 151.61, 149.79, 149.38, 148.50, 148.33, 147.20 (s, each 1C, Ar-C), 141.67, 140.67, 140.19, 139.60 (s, each 1C, Ar-CH), 135.54 (s, 1C, Ar-CH), 130.60, 129.91, 128.25, 127.80, 127.60, 127.20, 125.70 (s, each 1C, Ar-CH), 122.90, 122.49, 122.36, 121.91, 121.53, 121.01, 120.78, 120.41, 118.65 (s, each 1C, Ar-CH), 54.46, 53.11 (s, each 1C, C(CH₃)₂), 36.80, 35.78, 35.38 (s, each 1C, Tip-*i*Pr-CH), 34.88, 34.41, 34.37, 34.32, 34.25, 34.18 (s, each 1C, Tip-*i*Pr-CH), 32.30, 31.61, 31.16, 30.10 (s, each 1C, Tip-*i*Pr-CH), 28.06, 27.87, 27.58, 27.20, 26.80 (s, each 1C, Tip-*i*Pr-CH₃),

25.54 (s, 1C, Tip-*i*Pr-CH₃), 25.32 (bs, 1C, Tip-*i*Pr-CH₃), 24.76, 24.64, 24.50, 24.45, 24.15, 24.05, 23.98, 23.85, 23.83, 23.69, 23.62, 23.54, 23.54, 23.36 (s, each 1C, Tip-*i*Pr-CH₃), 22.89, 22.87 (bs, each 1C, Tip-*i*Pr-CH₃), 22.70, 21.78 (s, each 1C, Tip-*i*Pr-CH₃), 14.02, 12.11 (s, each 1C, NHC-*i*pr-CH₃) ppm.

²⁹Si-NMR (79.49 MHz, C₆D₆, 300 K) δ = 160.9 (s, *privo*-Si(Tip)₂), 30.4 (s, *ligato*-SiTip), -22.7 (s, *remoto*-Si(Tip)₂), -33.6 (s, *ligato*-Si-NHSi), -35.1 (NHSi), -268.2 (s, *nudo*-Si), -300.5 (s, *nudo*-Si) ppm.

CP-MAS ²⁹Si-NMR (79.53 MHz, 13KHz, 300K) δ = 160.9 (s, *privo*-Si(Tip)₂), 28.6 (s, *ligato*-SiTip), -22.5 (s, *remoto*-Si(Tip)₂), -34.4 (s, *ligato*-Si-NHSi), -37.9 (NHSi), -267.5 (s, *nudo*-Si), -303.4 (s, *nudo*-Si) ppm.

Elemental analysis: calculated for C₉₁H₁₃₈N₂Os₇: C: 74.22 % ; H: 9.45 % ; N: 1.90 %. Found: C: 73.89 % ; H: 9.00 % ; N: 1.85 %.

UV/VIS (hexane): λ_{max} (ϵ) = 638 nm (3640 M⁻¹ cm⁻¹).

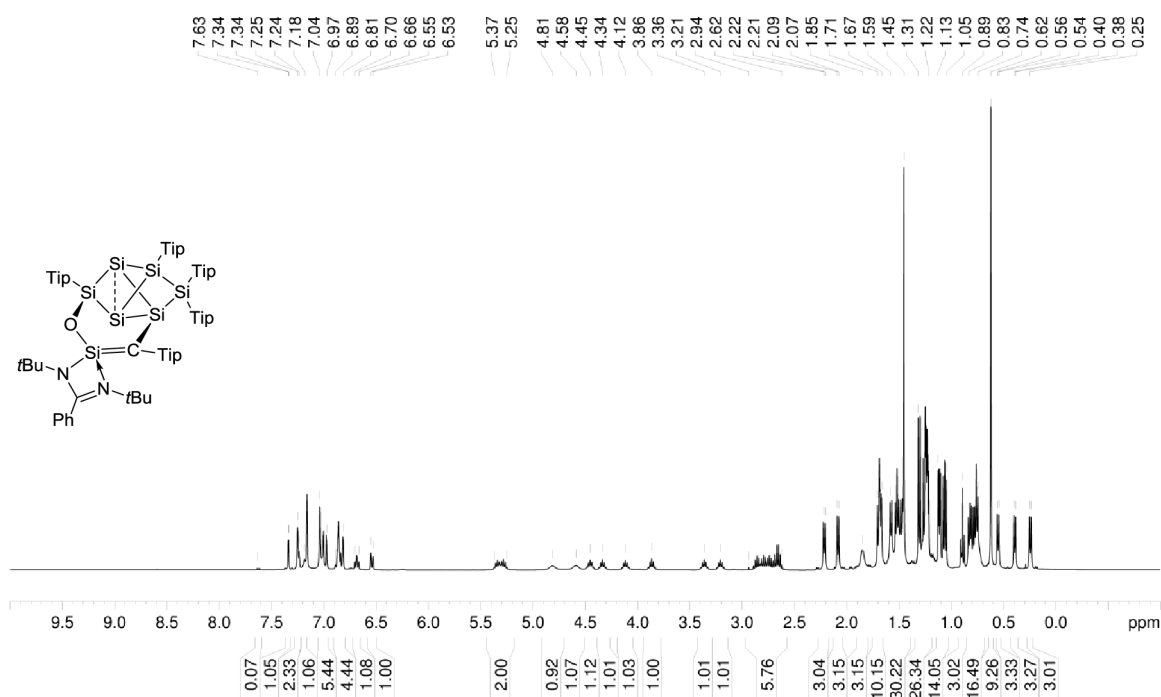


Figure S1. ¹H NMR of **2** in C₆D₆ (400.13 MHz, 300 K).

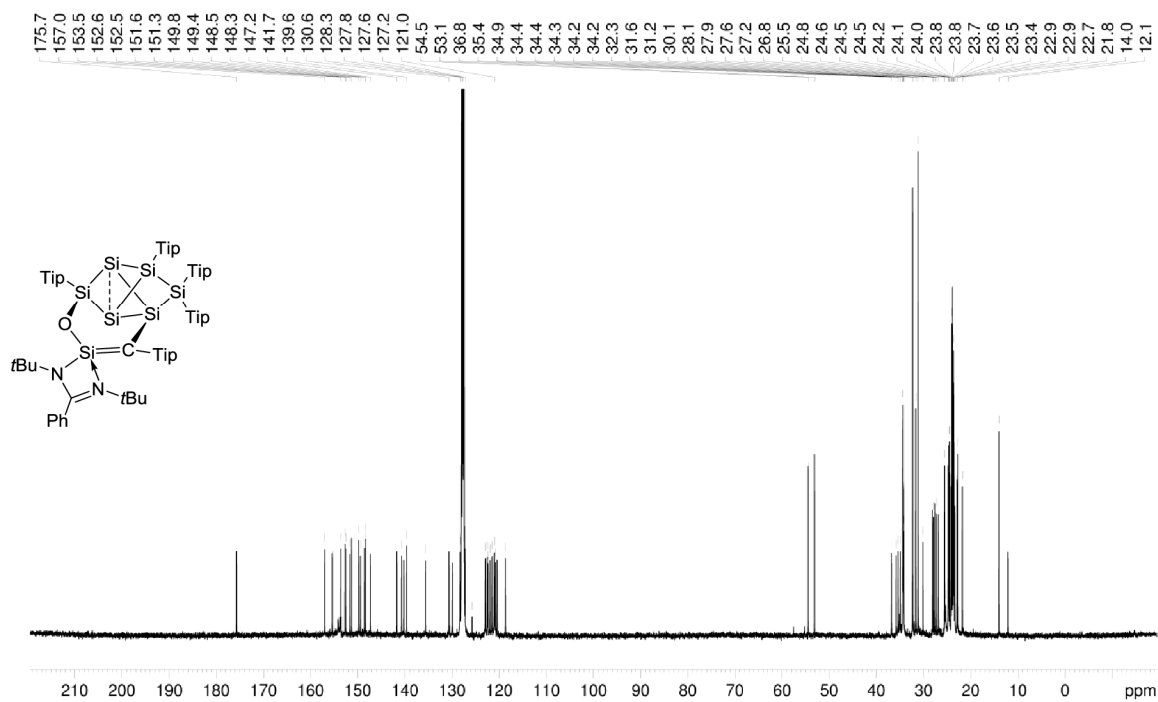


Figure S2. ¹³C NMR of **2** in C₆D₆ (100.61 MHz, 300 K).

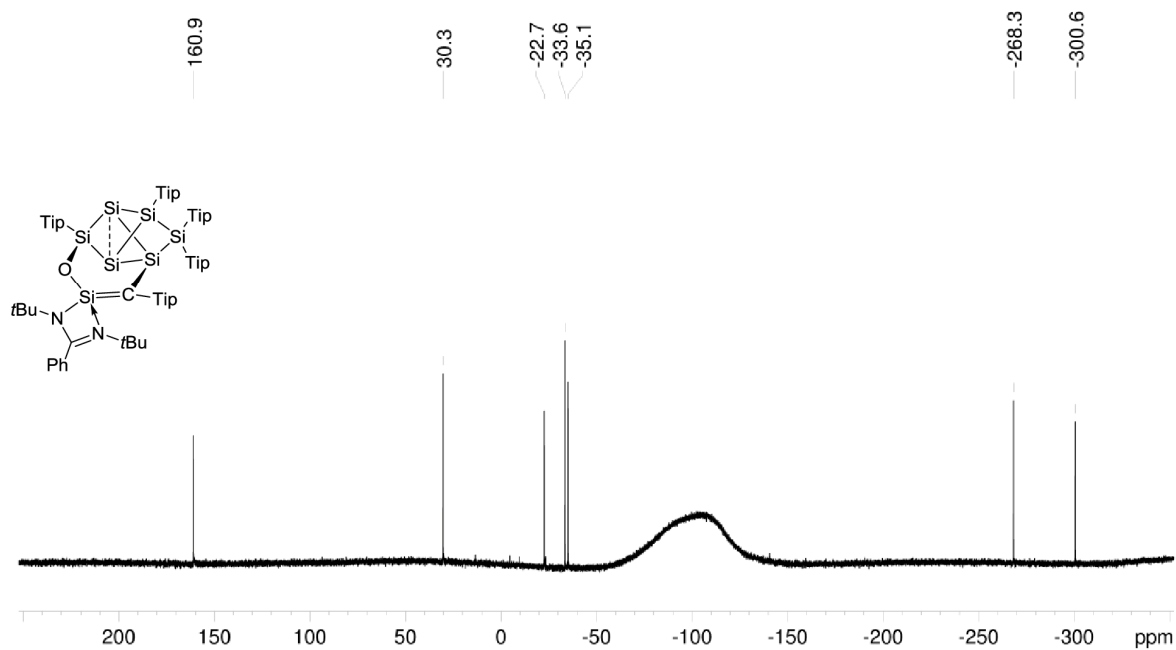


Figure S3. ²⁹Si NMR of **2** in C₆D₆ (79.49 MHz, 300 K).

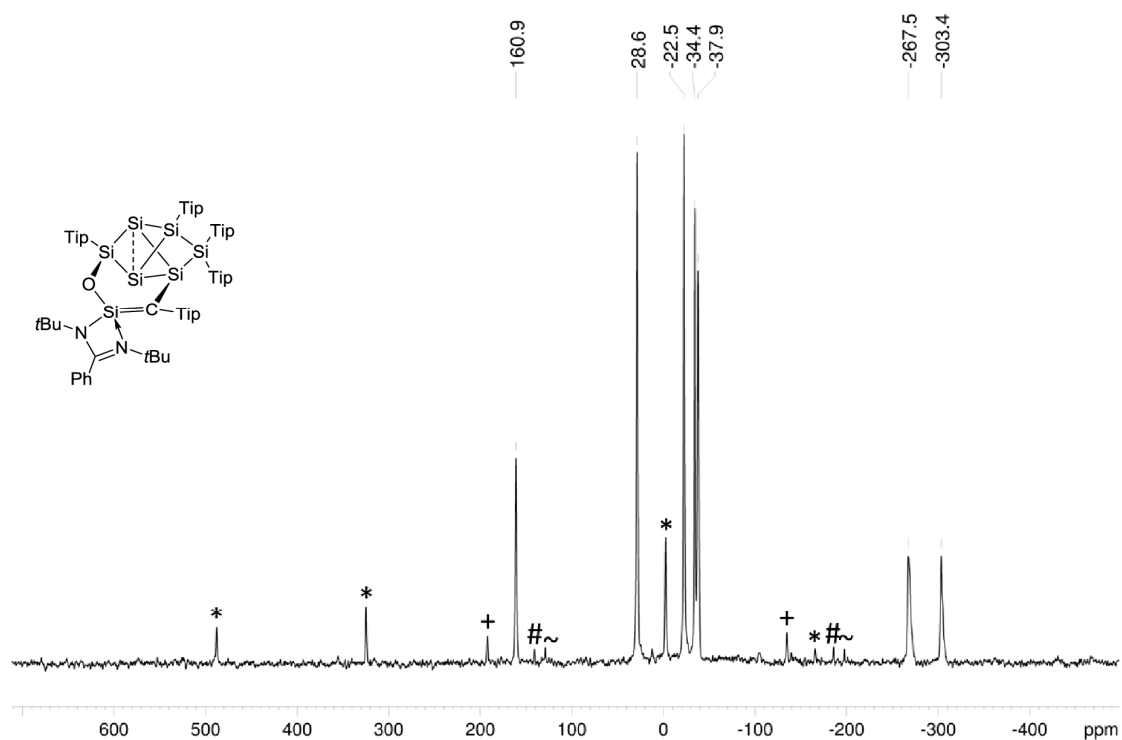


Figure S4. CP-MAS ^{29}Si NMR of **2** (79.53 MHz, 13 KHz, 300 K) with side spinning bands of: * *privo*-Si(Tip) $_2$ (160.9 ppm), + *ligato*-SiTip (28.6 ppm), # *remoto*-Si(Tip) $_2$ (-22.5 ppm), ~ *ligato*-Si-NHSi (-34.4 ppm).

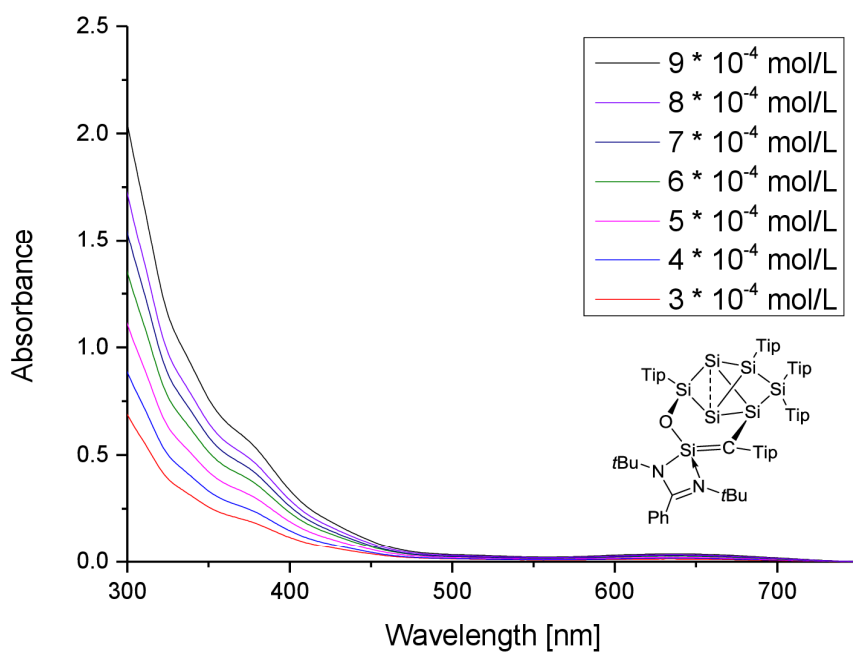


Figure S5. UV-Vis spectrum of **2** in hexane at different concentrations (9×10^{-4} mol/L to 3×10^{-4} mol/L).

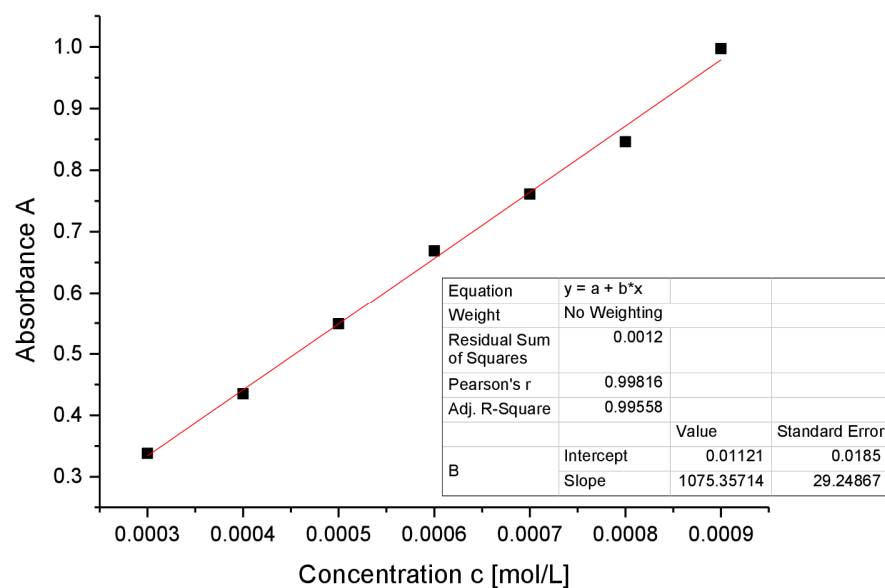


Figure S6. Determination of $\epsilon = 10750 \text{ (M}^{-1} \text{ cm}^{-1}\text{)}$ by linear regression of absorptions ($\lambda = 334 \text{ nm}$) of **2** against concentration.

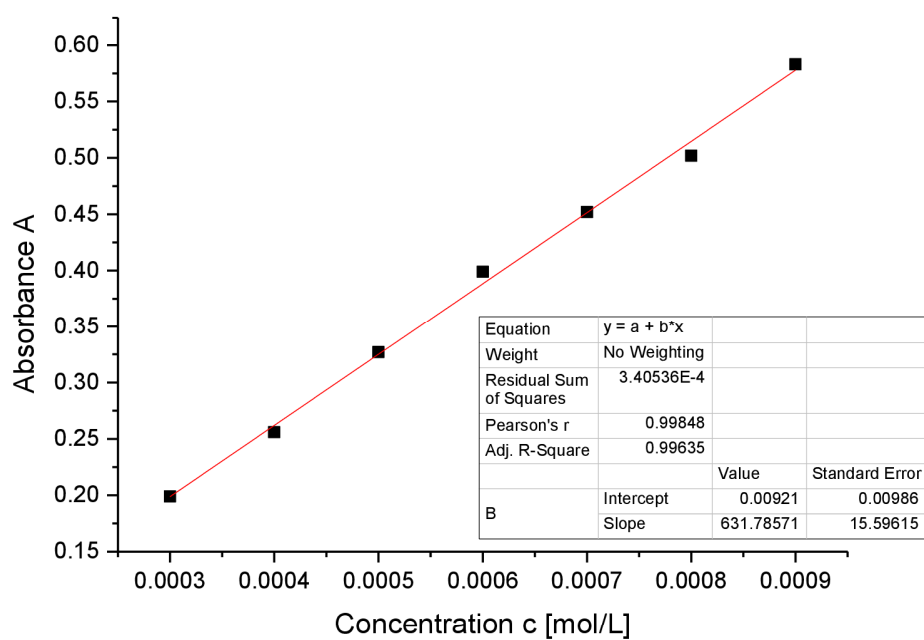


Figure S7. Determination of $\epsilon = 6310 \text{ (M}^{-1} \text{ cm}^{-1}\text{)}$ by linear regression of absorptions ($\lambda = 372 \text{ nm}$) of **2** against concentration.

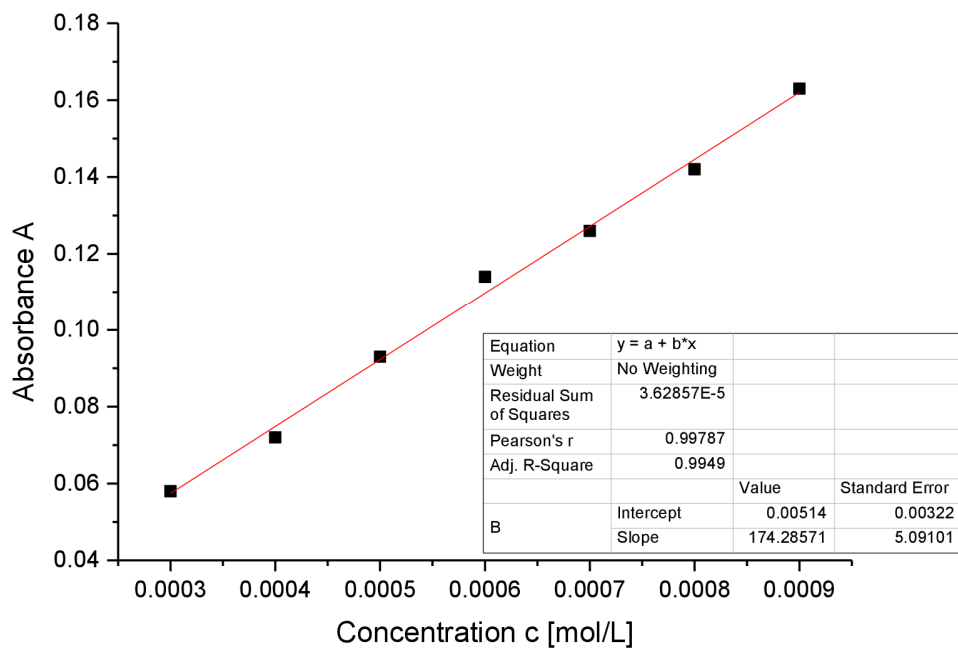


Figure S8. Determination of $\varepsilon = 1740 \text{ (M}^{-1} \text{ cm}^{-1}\text{)}$ by linear regression of absorptions ($\lambda = 432 \text{ nm}$) of **2** against concentration.

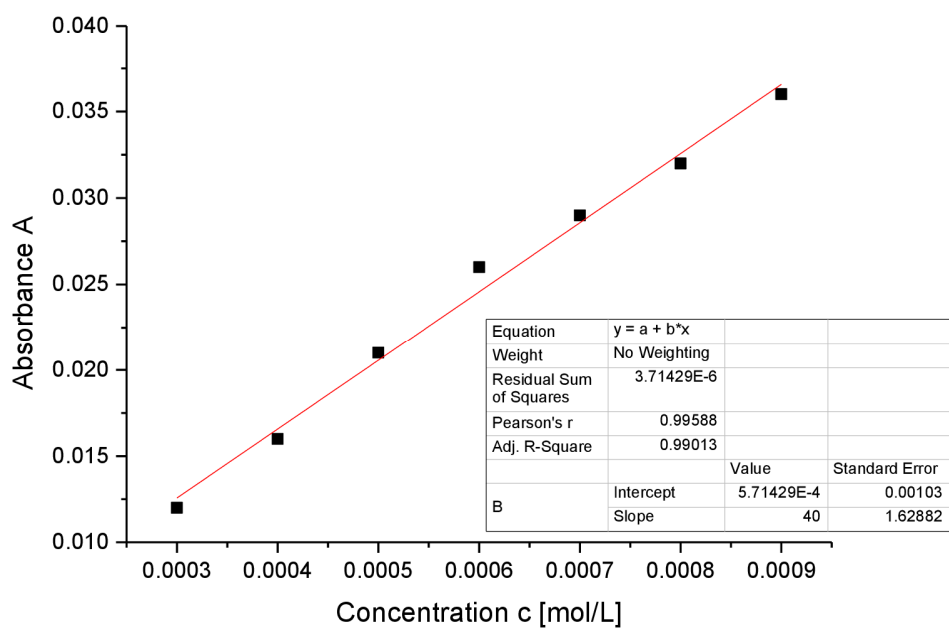


Figure S9. Determination of $\varepsilon = 400 \text{ (M}^{-1} \text{ cm}^{-1}\text{)}$ by linear regression of absorptions ($\lambda = 638 \text{ nm}$) of **2** against concentration.

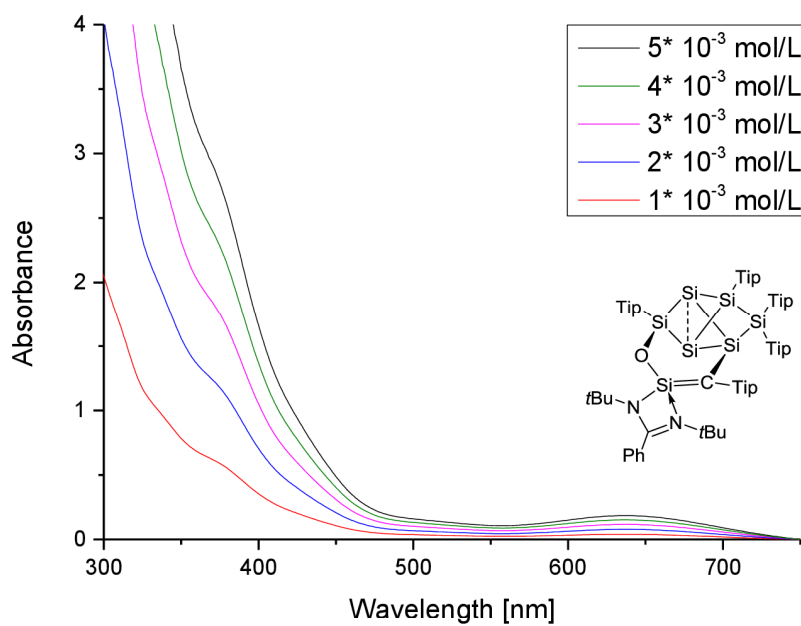


Figure S9. UV-Vis spectrum of **2** in hexane at different concentrations (5×10^{-3} mol/L to 1×10^{-3} mol/L).

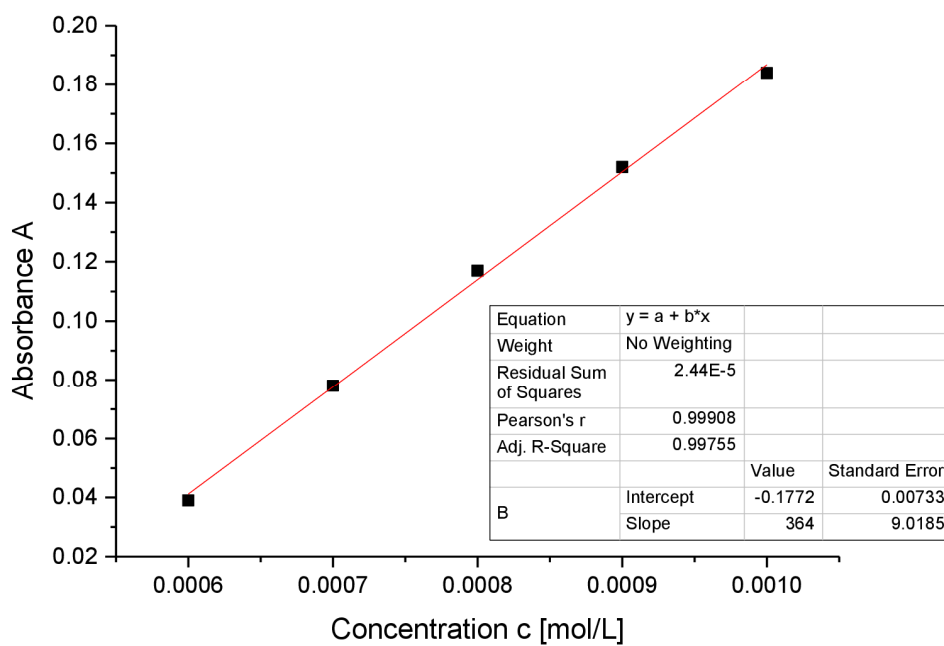


Figure S10. Determination of $\varepsilon = 3640$ ($\text{M}^{-1} \text{cm}^{-1}$) by linear regression of absorptions ($\lambda = 638$ nm) of **2** against concentration.

3. Computational Details

Structural and geometry optimizations of **1**, **[Int-a]**, **[Int-b]**, **[Int-c]**, and **2** were performed using the Gaussian09 program package^[2] together with TurboMole V7.0.^[3] All geometry optimizations were computed using the BP86^[4,5] functional with Grimme dispersion correctors D3^[6] and the Becke-Johnson damping function^[7] in combination with the def2-SVP basis set.^[8] To ensure the presence of a local minimum on the potential energy surface, the subsequent analysis of the frequency and molecular orbitals was performed at the same level of theory. The UV-Vis absorption spectrum was computed to determine the transition states using the CAM-B3LYP^[9] functional with Grimme dispersion correctors D3 and the Becke-Johnson damping function with the def2-SVPP basis set. The optimized structures were plotted using ChemCraft 1.8.^[10] The data from TD-DFT calculations were analysed with the GaussSum^[11] and OriginPro 9.0 programmes.^[12]

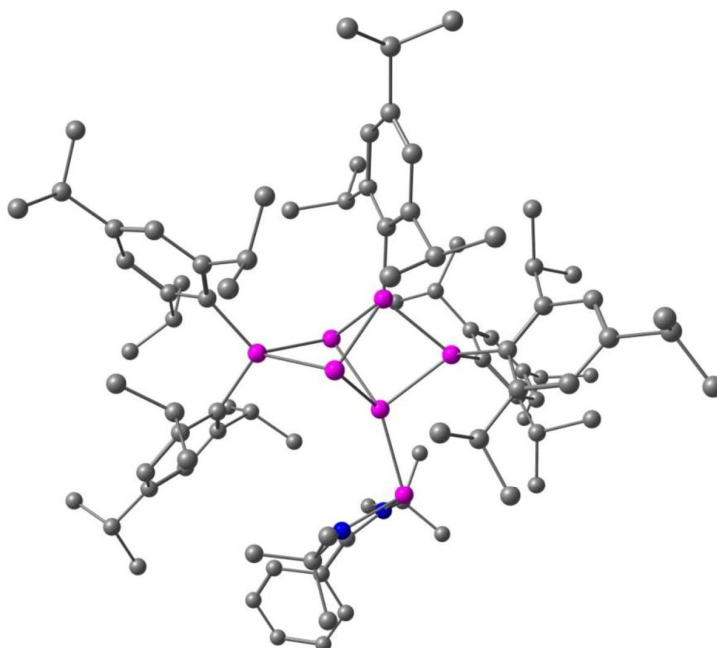


Figure S11. Optimized structure at the BP86-D3(BJ)/def2-SVP level of theory for **1**. Bond distances are in [Å]. Hydrogen atoms omitted for clarity.

Table S1. Atomic coordinates of the optimized structure **1** at the BP86-D3(BJ)/def2-SVP level of theory.

Si	0.195667586	0.874853889	-1.286999097
Si	0.442345407	0.434597390	1.483541342
Si	-0.005494444	-1.282998236	-0.226109021
Si	-1.525057674	1.235562893	0.384707451
Si	2.024725025	1.652778196	0.151599169
Si	-2.348830326	-0.971624427	0.104663537
Si	0.504210056	-3.411499333	-1.226091160
N	2.378764497	-3.298549370	-1.636938201
N	1.579065461	-4.427863796	0.015058554
C	2.706537885	-4.235416806	-0.709409114
C	3.058723066	-2.889972670	-2.883626866
C	2.079714850	-1.937034614	-3.596185924
H	1.847284887	-1.063046983	-2.953122809
H	1.123547410	-2.454789572	-3.825094492
H	2.512369152	-1.573625054	-4.549189434
C	4.353710358	-2.121705059	-2.566722408
H	4.153818976	-1.326366947	-1.824714859

H	4.755177340	-1.646248154	-3.484376835
H	5.136503889	-2.791171970	-2.163807099
C	3.342265592	-4.112838918	-3.780176747
H	4.064251763	-4.804592256	-3.302472897
H	3.771585380	-3.789168347	-4.750990066
H	2.403515672	-4.669566225	-3.981672764
C	1.265733304	-5.236511050	1.210348836
C	0.184709798	-4.451524084	1.982989493
H	-0.164883193	-5.021830275	2.866413630
H	-0.704295828	-4.253558007	1.350378418
H	0.572244503	-3.470418574	2.320358283
C	0.701265188	-6.608808301	0.777204584
H	1.474241619	-7.207070963	0.254981461
H	-0.161985975	-6.484830962	0.095470642
H	0.362125984	-7.184588391	1.662975457
C	2.490596287	-5.461022160	2.118911977
H	2.966011752	-4.503840780	2.400128790
H	3.254326716	-6.103293371	1.641110250
H	2.157984033	-5.966018760	3.048467436
C	3.974549795	-5.004695912	-0.620698708
C	5.185195647	-4.392897965	-0.230768745
H	5.199392107	-3.320439073	0.010308445
C	6.362536988	-5.152649018	-0.142061354
H	7.299132617	-4.667370758	0.171654538
C	6.348330907	-6.523204938	-0.451775402
H	7.274275362	-7.114968033	-0.381286218
C	5.148694540	-7.135513551	-0.856841198
H	5.132718034	-8.206326152	-1.113167350
C	3.968745329	-6.381826240	-0.938621377
H	3.029747818	-6.852689267	-1.266023495
C	-2.503872084	2.855432620	0.572470843
C	-3.297050725	3.309409331	-0.526554474
C	-3.998322887	4.522964383	-0.413075780
H	-4.599174913	4.868886503	-1.268475469
C	-3.952517865	5.306116845	0.753218492
C	-3.197977038	4.829663880	1.837399544
H	-3.170906860	5.429384875	2.761082872
C	-2.478133935	3.620824581	1.774535308
C	-3.399284679	2.534182817	-1.840341447
H	-3.129581080	1.478146587	-1.620797168
C	-2.401307532	3.058844983	-2.885115267
H	-1.357173651	2.911153550	-2.548539984
H	-2.558960087	4.141572840	-3.075558951
H	-2.526763954	2.522839665	-3.847953150
C	-4.815479659	2.523816055	-2.439665538
H	-5.580804288	2.245491656	-1.691779136
H	-4.864395005	1.781930846	-3.261142963
H	-5.088303404	3.513056803	-2.865403907
C	-4.682849711	6.639314523	0.833504143
H	-4.545887066	7.021368008	1.869910993
C	-4.053874597	7.665519439	-0.130274846
H	-4.543125803	8.657719743	-0.032918145
H	-4.162380487	7.337332229	-1.185817459
H	-2.970149225	7.790235034	0.070048759
C	-6.195309992	6.484445086	0.586842884
H	-6.644313343	5.755306307	1.291805455
H	-6.400900910	6.124593179	-0.443462837
H	-6.718977130	7.455609324	0.711280809
C	-1.651606476	3.187231179	2.981652448
H	-1.566779733	2.079541174	2.927741637
C	-2.294235019	3.539158651	4.332636424
H	-1.746746100	3.039549001	5.158690344
H	-3.355506739	3.220626809	4.377572992
H	-2.259731964	4.630095190	4.537443546
C	-0.222808491	3.751002904	2.889356527
H	0.401651867	3.388720734	3.733281408
H	-0.230215002	4.861246543	2.916312811
H	0.279275212	3.446481770	1.950963919

C	2.382306714	3.523930766	0.463277372
C	1.768391529	4.589047948	-0.265741687
C	2.297108076	5.890536812	-0.174331514
H	1.829734824	6.688467575	-0.772534176
C	3.382284796	6.212600965	0.654726001
C	3.917534243	5.181294981	1.438325306
H	4.740397203	5.417630684	2.133327024
C	3.443074366	3.858074887	1.360837098
C	0.534614498	4.428836440	-1.149858521
H	0.117040017	3.413839752	-0.969873866
C	0.888677433	4.541209552	-2.645074376
H	1.424053369	5.491285807	-2.853812046
H	-0.024478763	4.524024521	-3.272425229
H	1.537494958	3.706300333	-2.975030631
C	-0.560650071	5.439123059	-0.762863875
H	-0.807663507	5.373328758	0.314414407
H	-1.490374455	5.238026841	-1.326899151
H	-0.255555774	6.483242213	-0.984352796
C	3.945351027	7.625407010	0.710733756
H	4.768630724	7.616054014	1.459811870
C	2.889704811	8.641810346	1.186670091
H	2.470612448	8.353421446	2.172265114
H	2.044256920	8.707920725	0.469581971
H	3.329475992	9.657117598	1.279870301
C	4.550908524	8.033383089	-0.646723640
H	5.327053848	7.311072020	-0.972411265
H	5.014640825	9.040794011	-0.590205547
H	3.771298010	8.065538704	-1.437127566
C	4.089843716	2.843926496	2.296028226
H	3.624028664	1.861102240	2.093359553
C	3.779881926	3.165663819	3.770096957
H	4.197187337	2.382681170	4.437724438
H	2.685463544	3.216645189	3.940409665
H	4.215815376	4.139623870	4.077025514
C	5.600786391	2.716276276	2.033690992
H	6.053362588	1.927513096	2.668482950
H	6.127706064	3.667039646	2.259642756
H	5.799922034	2.455597197	0.975482885
C	3.743085787	0.851314471	-0.175004388
C	4.395412399	-0.074505973	0.698730651
C	5.709596241	-0.488116544	0.413565544
H	6.204174293	-1.186650712	1.106299163
C	6.426119804	-0.008754716	-0.698074355
C	5.779787687	0.902668895	-1.545651458
H	6.325567713	1.292971793	-2.421006796
C	4.460030560	1.333526265	-1.306902511
C	3.725459216	-0.632266354	1.950462301
H	2.897507720	0.060437390	2.214435741
C	3.079564781	-1.988486004	1.654604905
H	3.857291610	-2.763165550	1.504467789
H	2.449081686	-1.951531684	0.745380906
H	2.433398460	-2.307099138	2.497726622
C	4.642229933	-0.731152743	3.180271858
H	4.047780163	-1.023335686	4.070521476
H	5.143703960	0.230706932	3.404234963
H	5.430524141	-1.502870489	3.051858674
C	7.876625336	-0.403766802	-0.939075443
H	8.136161800	-0.067230527	-1.967693678
C	8.098150416	-1.924516984	-0.873959934
H	9.146405725	-2.183642536	-1.130577847
H	7.427660140	-2.462736147	-1.574055365
H	7.904915787	-2.314019322	0.148220986
C	8.802454589	0.340491313	0.045418746
H	8.576465264	0.049221431	1.093255521
H	8.667055488	1.438461569	-0.031061081
H	9.870006029	0.106200217	-0.151760039
C	3.842973677	2.334451162	-2.275637286
H	2.806771586	2.531371299	-1.924638150

C	3.705542985	1.749219855	-3.690858364
H	4.696093600	1.511988604	-4.133485271
H	3.199534206	2.470388108	-4.366697511
H	3.108020060	0.815994334	-3.673521437
C	4.584923207	3.681623448	-2.259349861
H	4.627210121	4.096612555	-1.232423486
H	4.067044940	4.421113611	-2.904151699
H	5.625347359	3.574313382	-2.633323635
C	-3.763999587	-0.881378576	-1.181003417
C	-5.046449463	-0.500570654	-0.685209564
C	-6.153146472	-0.498360588	-1.556412854
H	-7.147837878	-0.226485629	-1.164769429
C	-6.034907372	-0.834474823	-2.913820677
C	-4.755893761	-1.162840630	-3.399147696
H	-4.634850075	-1.417382015	-4.464756526
C	-3.625343050	-1.198408782	-2.562231381
C	-5.284389679	-0.136081062	0.781930761
H	-4.291454665	-0.093178230	1.278460134
C	-5.911394756	1.257436975	0.964925958
H	-6.035525451	1.481919684	2.045071806
H	-6.915860860	1.323712975	0.495767874
H	-5.271862704	2.050781925	0.532811628
C	-6.110241680	-1.222263785	1.497261559
H	-5.614551456	-2.210548664	1.438855626
H	-7.120480843	-1.313226460	1.044664921
H	-6.241907701	-0.973581356	2.570988958
C	-7.251087821	-0.840214121	-3.830219600
H	-8.128318652	-0.563924922	-3.203335884
C	-7.125875540	0.213620184	-4.947494021
H	-6.979805368	1.229207146	-4.526675815
H	-8.036022043	0.230310446	-5.583559026
H	-6.259481730	-0.003930336	-5.607696652
C	-7.511934791	-2.245592798	-4.406139192
H	-6.672829435	-2.574373941	-5.055294671
H	-8.436778028	-2.259747554	-5.020730041
H	-7.621062676	-2.995511076	-3.596232211
C	-2.280966328	-1.582582643	-3.172582235
H	-1.576143625	-1.744804924	-2.326624472
C	-1.703016866	-0.432505472	-4.012808156
H	-1.587349562	0.484689936	-3.401622838
H	-2.364983578	-0.187895388	-4.871242432
H	-0.701593426	-0.697476427	-4.411675883
C	-2.330294152	-2.891554809	-3.976965314
H	-1.305745857	-3.197695579	-4.274025588
H	-2.933566836	-2.786772448	-4.903632789
H	-2.763093635	-3.717972014	-3.379415015
C	-2.881892826	-2.252914664	1.442141145
C	-3.259180922	-3.563118198	0.998715238
C	-3.609848492	-4.544440592	1.943664326
H	-3.903224031	-5.542858469	1.582470468
C	-3.586645874	-4.300284856	3.327155946
C	-3.213362914	-3.017218006	3.750024973
H	-3.191684486	-2.804374699	4.832327594
C	-2.868784704	-1.995551690	2.842062766
C	-3.339621748	-3.961636266	-0.477751129
H	-2.801662835	-3.188976649	-1.063994342
C	-4.800108950	-3.999241152	-0.967601446
H	-5.367341647	-4.791359967	-0.433598384
H	-4.842827905	-4.219285721	-2.054508528
H	-5.314590772	-3.035360049	-0.800506798
C	-2.645440249	-5.296748079	-0.788451092
H	-1.574878214	-5.266464588	-0.507892393
H	-2.687492325	-5.504901273	-1.877491679
H	-3.122925914	-6.152626767	-0.267430976
C	-3.919899083	-5.396979066	4.329390197
H	-3.918643869	-4.925356632	5.337699836
C	-5.320452362	-5.991823930	4.092207535
H	-5.570848400	-6.741751385	4.871829146

H	-5.380459210	-6.502812299	3.108003158
H	-6.099144569	-5.202172706	4.107404797
C	-2.833964370	-6.491932150	4.324647890
H	-1.834257459	-6.063239363	4.542904004
H	-2.775621033	-6.988371161	3.332696543
H	-3.048267101	-7.274056812	5.083510201
C	-2.494123459	-0.640575791	3.431109076
H	-2.282619711	0.037970777	2.576254451
C	-3.642757639	-0.014776226	4.241051972
H	-3.918638281	-0.645052578	5.112509061
H	-4.550772896	0.114529436	3.619768459
H	-3.349103583	0.981397531	4.627976015
C	-1.205347888	-0.729751106	4.266700145
H	-1.357282059	-1.341341700	5.181691991
H	-0.868852283	0.279870997	4.585447225
H	-0.384031674	-1.193217638	3.681193836

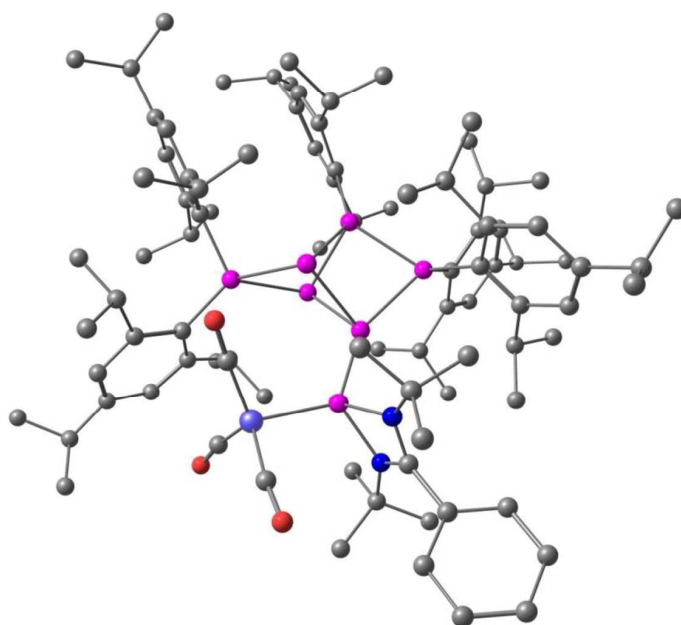


Figure S12. Optimized structure at the BP86-D3(BJ)/def2-SVP level of theory for **[Int-a]**. Bond distances are in [Å]. Hydrogen atoms omitted for clarity.

Table S2. Atomic coordinates of the optimized structure **[Int-a]** at the BP86-D3(BJ)/def2-SVP level of theory.

Si	-0.999583591	0.106429827	-1.306512127
Si	-0.508008891	-0.384384659	1.376911730
Si	1.157734292	-0.362849993	-0.401577706
Si	-0.796302903	1.811629930	0.334519654
Si	-2.377380603	-1.355010502	0.037105785
Si	1.536129162	1.979486927	-0.109659327
Si	2.043140346	-2.502210817	-0.042035773
N	3.572842778	-2.408584148	1.069701556
N	3.603699897	-2.840234226	-1.044913989
C	4.372647082	-2.820762704	0.066078931
C	3.851429045	-2.139770990	2.494755540
C	4.421279763	-0.715123340	2.617988412
H	5.399777567	-0.633676108	2.104131358
H	4.568363928	-0.439814276	3.681500981
H	3.734751267	0.023899041	2.162527099

C	4.819448409	-3.170585967	3.110484364
H	4.475758269	-4.204197391	2.906911602
H	4.846642532	-3.023288961	4.209448263
H	5.852698151	-3.061419251	2.731559290
C	2.502551195	-2.236695312	3.227402108
H	1.736888734	-1.600104321	2.737839116
H	2.611023376	-1.895805372	4.275744467
H	2.128402665	-3.277895789	3.230572235
C	5.786032984	-3.279799515	0.183317692
C	6.851764636	-2.356726005	0.194255231
H	6.640112205	-1.284673728	0.094309841
C	8.174536781	-2.807925108	0.325222008
H	8.999861833	-2.079083123	0.329782414
C	8.443617486	-4.181495665	0.450984710
H	9.481644169	-4.533887210	0.555504341
C	7.382443849	-5.103626186	0.449860926
H	7.584511451	-6.180152557	0.561708981
C	6.058164130	-4.658876331	0.317632748
H	5.223813764	-5.373112113	0.355001797
C	3.855663119	-3.338284221	-2.408413589
C	2.690079202	-2.802783860	-3.257093503
H	2.797840953	-3.111621100	-4.315649348
H	2.644179400	-1.696343893	-3.210561503
H	1.727327946	-3.202017777	-2.883000198
C	5.190281612	-2.799127589	-2.955962718
H	5.302917704	-3.094703156	-4.018860542
H	6.058887092	-3.198404164	-2.398043895
H	5.214533175	-1.692910781	-2.897170459
C	3.835785947	-4.881780266	-2.431668399
H	2.889853192	-5.259690209	-1.995722879
H	4.682877615	-5.301005839	-1.855129305
H	3.914254863	-5.252682087	-3.474303603
O	-0.687018609	-3.507293830	2.872502756
O	3.078384996	-5.946470741	1.171278187
O	-0.357824725	-5.380834503	-2.079299488
C	-0.199557186	-3.805799525	1.856193930
C	2.108390933	-5.356959242	0.893406886
C	-0.011594268	-4.895991634	-1.079947491
C	-2.228945750	3.074893532	0.167148820
C	-2.629068288	3.521038246	-1.129462839
C	-3.857910646	4.197975250	-1.279220318
H	-4.153431136	4.525751930	-2.287259193
C	-4.708699676	4.460259266	-0.195449047
C	-4.258054707	4.093785155	1.084846815
H	-4.879462332	4.355188456	1.955844997
C	-3.030327039	3.442520222	1.288197540
C	-1.776240180	3.358228848	-2.387919993
H	-0.831951515	2.854383991	-2.094398973
C	-2.466448865	2.489924824	-3.452736931
H	-3.454530302	2.905766832	-3.738491846
H	-2.633487596	1.456505470	-3.082039103
H	-1.848137101	2.429628384	-4.370843244
C	-1.382413676	4.724318067	-2.979896548
H	-0.657656384	4.582302626	-3.807299452
H	-0.898420485	5.368855464	-2.222548827
H	-2.263769475	5.267798051	-3.381746014
C	-6.083352597	5.098771329	-0.354861449
H	-6.236148982	5.748003449	0.537655314
C	-7.176391806	4.009204750	-0.321387922
H	-7.095143148	3.388456834	0.592809845
H	-7.071533217	3.329588849	-1.192336129
H	-8.191531044	4.458306490	-0.351226029
C	-6.221630528	5.979790281	-1.604698342
H	-6.174064902	5.375437953	-2.535319358
H	-5.421394457	6.746332260	-1.656506768
H	-7.200436615	6.502160829	-1.606252355
C	-2.503664816	3.309763208	2.709965583
H	-1.784850153	2.457204472	2.719817794

C	-1.725872005	4.596602345	3.048539584
H	-0.843254784	4.718495001	2.392801410
H	-1.382471435	4.591205234	4.102021921
H	-2.376025618	5.485087924	2.904999843
C	-3.583435562	3.047146547	3.765003346
H	-4.245355363	3.928533827	3.896898495
H	-3.118317246	2.844792744	4.750948420
H	-4.213360248	2.181491986	3.488026322
C	-2.834056351	-3.006486287	-0.871691923
C	-3.378581735	-4.092487507	-0.115107604
C	-3.743047068	-5.297066168	-0.741020364
H	-4.132506648	-6.117051398	-0.118465636
C	-3.645262547	-5.477123754	-2.126865072
C	-3.188577003	-4.388441462	-2.877273373
H	-3.119773335	-4.505565268	-3.969614566
C	-2.775025026	-3.172390022	-2.299090252
C	-3.710381062	-3.983686818	1.366229615
H	-3.152590448	-3.115177817	1.773553716
C	-5.224104441	-3.713274825	1.511397460
H	-5.513539827	-2.758273015	1.032405995
H	-5.532263335	-3.665589409	2.575659661
H	-5.801468978	-4.530275374	1.030066852
C	-3.292141420	-5.221432181	2.181382600
H	-3.970660924	-6.079618458	1.992820823
H	-3.334557596	-5.002690346	3.267350995
H	-2.261870634	-5.543173435	1.933899609
C	-3.990137843	-6.803106153	-2.787013833
H	-3.909837487	-6.646752638	-3.886201901
C	-2.965361790	-7.885309452	-2.390905045
H	-3.165747985	-8.838624648	-2.924232208
H	-3.010215716	-8.091081666	-1.300238185
H	-1.932819241	-7.558178745	-2.624795542
C	-5.432269103	-7.247003683	-2.479429012
H	-6.165684639	-6.470397070	-2.778791376
H	-5.571733079	-7.440956353	-1.394802519
H	-5.680987860	-8.185257912	-3.018539214
C	-2.245907314	-2.140600920	-3.292647943
H	-2.323145094	-1.140626463	-2.818007019
C	-0.756752994	-2.402644160	-3.559903420
H	-0.608420902	-3.407379074	-4.006042450
H	-0.183266070	-2.363404862	-2.612619824
H	-0.329330958	-1.641302426	-4.243479625
C	-3.041507337	-2.039978702	-4.604832247
H	-2.703391101	-1.150875330	-5.176937069
H	-4.128601071	-1.932741642	-4.414561519
H	-2.896814561	-2.921949824	-5.263275792
C	-3.923622263	-0.627028023	0.925926373
C	-4.087334707	-0.569395112	2.351224282
C	-5.258238607	0.007311821	2.880914224
H	-5.380644211	0.031423891	3.975838384
C	-6.284541924	0.526420891	2.072944466
C	-6.122698248	0.440627258	0.682898567
H	-6.928051675	0.817389505	0.032753055
C	-4.977527920	-0.134289975	0.101613904
C	-3.097774140	-1.151789716	3.370373096
H	-2.333922265	-1.727206875	2.811379635
C	-2.343627678	-0.070862955	4.162404665
H	-1.853807404	0.659673745	3.490029327
H	-1.554511790	-0.538127293	4.787613360
H	-3.028692882	0.485034911	4.833885450
C	-3.753539922	-2.122677131	4.371241688
H	-4.434687627	-1.593212121	5.070324691
H	-2.969445985	-2.615662112	4.981815627
H	-4.340499501	-2.911088329	3.867632199
C	-7.551482747	1.117189372	2.677785653
H	-8.188444618	1.446240157	1.826305084
C	-7.256261957	2.355892144	3.543329107
H	-6.709983975	3.127552156	2.964449271

H	-6.630445830	2.094319358	4.422277262
H	-8.196671789	2.807619989	3.923052419
C	-8.340470150	0.054394237	3.467293782
H	-9.295897398	0.470638045	3.850806378
H	-7.757760907	-0.308684469	4.340287856
H	-8.573975962	-0.824533795	2.832501343
C	-4.952192009	-0.301759600	-1.414525210
H	-3.895045438	-0.499260940	-1.705121335
C	-5.391682160	0.960267595	-2.171422431
H	-5.202893578	0.845829199	-3.258492425
H	-4.848460658	1.855196601	-1.811605339
H	-6.479291481	1.147496856	-2.048363780
C	-5.793811095	-1.523554599	-1.832549121
H	-5.753144512	-1.674295432	-2.931468765
H	-6.856891358	-1.375385572	-1.546565040
H	-5.432189885	-2.452136065	-1.350771522
C	2.987289805	2.295042184	1.107212661
C	4.301235316	2.234749035	0.552950161
C	5.425105154	2.471670765	1.366484298
H	6.432800985	2.433599558	0.919541230
C	5.308007225	2.743819750	2.736263385
C	4.013201028	2.781972403	3.277973345
H	3.896267133	2.980586114	4.354504510
C	2.858282324	2.575555048	2.499840823
C	4.564912671	1.910729752	-0.913643470
H	3.593361932	1.677447143	-1.387392937
C	5.160516122	3.118745885	-1.657209870
H	5.316385423	2.889920313	-2.731626004
H	6.141804510	3.410546036	-1.227137894
H	4.482154376	3.992830683	-1.594804468
C	5.414657343	0.642037469	-1.063991315
H	4.905381995	-0.216936145	-0.583296307
H	6.418478591	0.760418213	-0.604401674
H	5.568574261	0.391260958	-2.133957476
C	6.537966337	2.970536085	3.604561995
H	7.419899544	2.951032675	2.925587997
C	6.505507928	4.349518613	4.290336646
H	6.395124411	5.164954046	3.546701384
H	7.437564380	4.528466943	4.866522732
H	5.654737335	4.425828073	5.000062198
C	6.713684617	1.833567375	4.630421184
H	5.854729875	1.795524738	5.333660203
H	7.635342736	1.978144219	5.232596874
H	6.778785219	0.846983414	4.128460384
C	1.516634601	2.615854537	3.225219935
H	0.716038171	2.692009683	2.455526895
C	1.391144735	3.822629283	4.169372268
H	1.496783580	4.782419766	3.624331200
H	2.159713400	3.801209754	4.969038827
H	0.405509300	3.817871265	4.672695636
C	1.284045785	1.301736974	3.989908418
H	0.294350911	1.302470848	4.490532152
H	2.065777104	1.149530722	4.764318554
H	1.313579088	0.430832087	3.305609913
C	1.756633396	3.197019069	-1.580059754
C	1.740296657	4.581791536	-1.229947211
C	1.984978173	5.558008337	-2.212199099
H	1.987857786	6.619801747	-1.916572409
C	2.212268305	5.220413420	-3.556325383
C	2.190811189	3.859210962	-3.896058558
H	2.360447995	3.581066113	-4.949582689
C	1.981803141	2.842001858	-2.942938243
C	1.490450074	5.066630838	0.199452485
H	1.214911963	4.182870452	0.816434784
C	0.298395870	6.037015932	0.282756155
H	0.449264995	6.928899364	-0.360603038
H	0.164404728	6.399895791	1.322325599
H	-0.643170120	5.541422970	-0.027923141

C	2.766265592	5.671713605	0.813861051
H	3.077314804	6.585344158	0.264075959
H	3.605533866	4.949209169	0.786523951
H	2.596628146	5.954970227	1.873581700
C	2.466825195	6.291537330	-4.607805599
H	2.610241781	5.764535317	-5.577720402
C	3.757974200	7.076899921	-4.306394366
H	4.629861341	6.396703370	-4.220020875
H	3.672533606	7.634786677	-3.349823032
H	3.971202537	7.815734021	-5.107423694
C	1.256125070	7.232613026	-4.760821735
H	1.430240700	7.977134617	-5.565981821
H	1.063154982	7.792997021	-3.821591931
H	0.334682603	6.666290973	-5.005545490
C	2.027482552	1.399545144	-3.448906450
H	2.010610667	0.729797536	-2.559307254
C	3.304534974	1.081612505	-4.248668187
H	3.346943731	-0.000196517	-4.491823667
H	4.220485667	1.340995142	-3.684197737
H	3.336662785	1.634688547	-5.210432660
C	0.780321295	1.062761222	-4.279974647
H	0.661009039	1.765713437	-5.131114642
H	-0.136688572	1.115378908	-3.659745906
H	0.847495039	0.033947068	-4.689678130
Ni	0.757629444	-4.296672422	0.426724476

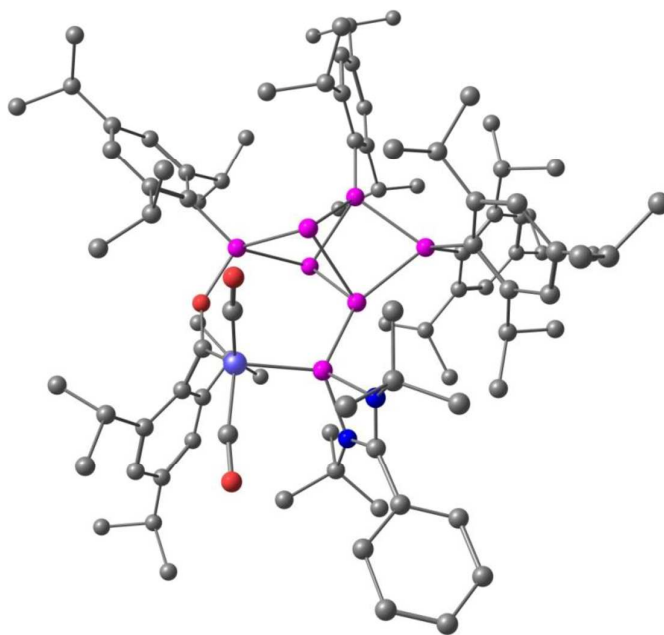


Figure S13. Optimized structure at the BP86-D3(BJ)/def2-SVP level of theory for **[Int-b]**. Bond distances are in [Å]. Hydrogen atoms omitted for clarity.

Table S3. Atomic coordinates of the optimized structure **[Int-b]** at the BP86-D3(BJ)/def2-SVP level of theory.

Si	-0.525697556	1.099388087	1.355307534
Si	-0.405382530	0.791797276	-1.484921966
Si	0.161345197	-0.884224919	0.195456507
Si	-2.368903374	0.632919909	-0.124929889
Si	0.518955696	2.587102543	-0.202232053

Si	-2.064284110	-1.705186545	0.093265745
Si	2.369395488	-1.229801619	-0.449911486
N	2.560464480	-2.875736886	-1.361110857
N	3.317148009	-2.448858527	0.614187568
C	3.389528783	-3.337566625	-0.395770468
C	2.390747768	-3.272757748	-2.775384088
C	2.176959086	-4.791573929	-2.916309737
H	3.076380346	-5.370306627	-2.634284425
H	1.945947488	-5.024411659	-3.975606101
H	1.319102285	-5.126702500	-2.301560388
C	3.620772229	-2.827692990	-3.593032361
H	3.774182650	-1.735763846	-3.500242570
H	3.479494741	-3.073397887	-4.665603274
H	4.536863774	-3.341186922	-3.238212168
C	1.124416996	-2.544699554	-3.259855570
H	0.240314038	-2.861350298	-2.672774551
H	0.931991839	-2.769166880	-4.327448386
H	1.236096219	-1.447085830	-3.158889636
C	4.296128454	-4.515942762	-0.462949885
C	3.833115014	-5.813564435	-0.161491128
H	2.779088483	-5.963499136	0.107846344
C	4.717906180	-6.901355741	-0.199311495
H	4.350611798	-7.911065091	0.041488738
C	6.067439655	-6.703512402	-0.541862411
H	6.759939260	-7.559243449	-0.571533517
C	6.529827380	-5.411861382	-0.846671999
H	7.584693541	-5.250975850	-1.118130339
C	5.651187931	-4.316805960	-0.806174747
H	6.004376438	-3.302371565	-1.043113193
C	3.932459603	-2.380672107	1.948381290
C	2.948343783	-1.560772291	2.797568638
H	3.348863067	-1.415682838	3.819797708
H	1.963907848	-2.065559591	2.863081850
H	2.793215827	-0.561323238	2.343521773
C	4.110193249	-3.778476723	2.568214630
H	4.407698206	-3.669643838	3.630975507
H	4.893643600	-4.367894536	2.055703225
H	3.160153486	-4.350059501	2.530971087
C	5.282342858	-1.637218300	1.872213332
H	5.144460609	-0.613735625	1.471173332
H	5.997278584	-2.175632877	1.220150071
H	5.725729214	-1.548854796	2.884842487
O	2.197760228	2.702278198	0.230590673
O	2.402533054	0.781065979	-3.933037194
O	5.952664338	-1.037423315	-1.385230015
C	3.264697304	1.908388789	0.096671119
C	2.782891071	0.760452425	-2.824245416
C	5.037542806	-0.309863570	-1.276212670
C	-3.995489090	1.598969490	0.004423166
C	-4.659273150	1.664647118	1.267230379
C	-5.834557955	2.426895951	1.385697416
H	-6.334811540	2.480416610	2.365635704
C	-6.383984330	3.125435574	0.296182030
C	-5.731434539	3.033105971	-0.944435167
H	-6.158709342	3.574140812	-1.803605581
C	-4.550573312	2.285278218	-1.114063448
C	-4.114164168	0.973917108	2.516619440
H	-3.383431544	0.207029831	2.178409444
C	-3.360363290	1.976208404	3.409465557
H	-4.032415369	2.798479543	3.734287380
H	-2.502291083	2.428570649	2.871487471
H	-2.967852061	1.477078051	4.319567588
C	-5.188425962	0.232976247	3.329258955
H	-4.704875502	-0.392134332	4.107058784
H	-5.790792721	-0.440571455	2.691448994
H	-5.879041971	0.934853969	3.843140828
C	-7.637675244	3.973522873	0.459536057
H	-7.888506582	4.377066231	-0.546912884

C	-7.372518812	5.172563895	1.391676267
H	-6.521870406	5.783140871	1.026022064
H	-7.121484110	4.831139348	2.418316416
H	-8.266340355	5.827535350	1.463461733
C	-8.837571320	3.136302880	0.941572863
H	-8.655379562	2.717562880	1.953920374
H	-9.034162573	2.285447036	0.257733398
H	-9.756960962	3.756281161	0.997394787
C	-3.855001092	2.284726699	-2.472000173
H	-3.269885331	1.340827620	-2.528639770
C	-4.824050574	2.306637315	-3.664389643
H	-5.618439850	1.539424635	-3.562823526
H	-4.274958464	2.115282101	-4.609563414
H	-5.320353353	3.293728470	-3.775578641
C	-2.843865197	3.441872821	-2.564745831
H	-3.351588838	4.424690029	-2.470296397
H	-2.305645182	3.423450415	-3.535291561
H	-2.082802170	3.385317596	-1.763060735
C	4.272020594	2.125445691	1.179684559
C	5.650083697	2.286095850	0.824636137
C	6.637258299	2.153842051	1.811391488
H	7.692989030	2.276097988	1.523833470
C	6.314651951	1.885047410	3.155012317
C	4.955664883	1.846212541	3.507799078
H	4.696623883	1.694287060	4.566837781
C	3.920535810	2.003981288	2.565726957
C	6.028137978	2.794745975	-0.562773898
H	5.218402266	2.474541684	-1.251758506
C	6.032148612	4.338798159	-0.531391755
H	5.062302359	4.733884010	-0.165967076
H	6.216897990	4.754798243	-1.544266178
H	6.824214504	4.719488462	0.148803401
C	7.356893266	2.248888614	-1.102725243
H	8.228726278	2.634577632	-0.531765931
H	7.498829876	2.563378283	-2.157529401
H	7.387651217	1.142459591	-1.069017383
C	7.401563499	1.687239446	4.202410512
H	6.886758651	1.481840276	5.167806486
C	8.286266683	0.469138501	3.873359172
H	9.044429882	0.301374580	4.667168745
H	8.828251239	0.615154640	2.915187272
H	7.678891219	-0.453431119	3.773725007
C	8.248283187	2.962101243	4.387021537
H	7.611512138	3.832309167	4.646637710
H	8.798965988	3.215044084	3.456355059
H	8.998790461	2.827538173	5.194377222
C	2.477482163	2.095991336	3.054025327
H	1.831713132	1.570465633	2.314833979
C	2.198690977	1.461586667	4.425096782
H	2.670148323	2.035996056	5.250073852
H	2.551571413	0.415733862	4.492809789
H	1.105092242	1.464727557	4.613054391
C	2.024182661	3.570885721	3.095762336
H	0.944917735	3.627998414	3.347496208
H	2.184339404	4.076179312	2.126171241
H	2.588953197	4.124615239	3.875618838
C	0.086080633	4.362822044	-0.662738586
C	0.704794043	4.838894488	-1.857262022
C	0.441303025	6.144271641	-2.302364378
H	0.924288701	6.499409636	-3.227307507
C	-0.433197159	6.999532514	-1.606509112
C	-1.054910396	6.505921215	-0.448431064
H	-1.753914790	7.164282325	0.093495686
C	-0.823176545	5.203169697	0.036332844
C	1.603204241	3.941701159	-2.702980290
H	1.690640410	2.953634793	-2.193838898
C	0.959790896	3.664135770	-4.072337713
H	-0.034414418	3.188030305	-3.944520298

H	1.590272356	2.978996423	-4.671627301
H	0.815133993	4.603202868	-4.646862801
C	3.036454526	4.481627771	-2.818861990
H	3.066784907	5.452431602	-3.357696094
H	3.676324029	3.762836492	-3.370594302
H	3.479641345	4.631852005	-1.815512366
C	-0.724786492	8.406340229	-2.111238885
H	-1.401826178	8.882447774	-1.367169217
C	-1.467693828	8.367407654	-3.461582277
H	-2.401216932	7.772902574	-3.388378542
H	-0.837485598	7.905182492	-4.250674287
H	-1.733237988	9.391309432	-3.799475471
C	0.554660171	9.260186348	-2.194952218
H	0.317306628	10.299347216	-2.505639108
H	1.268153756	8.844459515	-2.937501539
H	1.075370547	9.301250026	-1.216567176
C	-1.572383196	4.762157183	1.289123161
H	-1.324668801	3.690743717	1.461457146
C	-3.096965896	4.864015733	1.105454247
H	-3.627408784	4.492045001	2.003819206
H	-3.445420172	4.265700297	0.242953412
H	-3.412948496	5.915969547	0.943350915
C	-1.109597927	5.552625599	2.527092975
H	-1.570365623	5.140884519	3.449680975
H	-1.406610882	6.620285785	2.450934812
H	-0.008774877	5.517614862	2.642214438
C	-2.101006132	-2.995923612	-1.318264095
C	-1.589330664	-4.286425629	-0.989257337
C	-1.521161072	-5.286883411	-1.977125728
H	-1.129223545	-6.283466795	-1.712271959
C	-1.936060324	-5.056611566	-3.298670192
C	-2.438142079	-3.782019898	-3.610829031
H	-2.766981479	-3.574778910	-4.642154351
C	-2.527378148	-2.752608437	-2.655218196
C	-1.116201287	-4.633168106	0.420478821
H	-1.124514619	-3.697396428	1.013294256
C	-2.081846317	-5.610965010	1.111418339
H	-1.753585694	-5.826445880	2.149642342
H	-2.135106198	-6.575192052	0.562799182
H	-3.103862976	-5.185391649	1.163813787
C	0.340078187	-5.117380297	0.442482203
H	0.997429459	-4.364765289	-0.035753570
H	0.464728147	-6.079808803	-0.098024689
H	0.686245545	-5.271923279	1.486025184
C	-1.846065345	-6.149887640	-4.354344418
H	-1.368761802	-7.029914062	-3.867832339
C	-3.246557044	-6.580414132	-4.832855639
H	-3.876879730	-6.910964859	-3.982206233
H	-3.179756741	-7.415734866	-5.561415974
H	-3.772553398	-5.739335737	-5.332373456
C	-0.952094770	-5.725923317	-5.535125814
H	-1.385012349	-4.858597842	-6.076774712
H	-0.838332774	-6.553797363	-6.265997278
H	0.057676834	-5.430897105	-5.184790086
C	-3.060048496	-1.403169484	-3.124741881
H	-3.109449701	-0.742976611	-2.230713720
C	-4.479584459	-1.497206207	-3.709842444
H	-5.191616530	-1.927576475	-2.978912426
H	-4.505142640	-2.133957819	-4.618965619
H	-4.848049239	-0.492323561	-3.996823744
C	-2.091316489	-0.745974961	-4.123561229
H	-2.433569522	0.273039813	-4.400479371
H	-2.009327126	-1.342186431	-5.056774140
H	-1.070878922	-0.657211870	-3.696174415
C	-3.080224474	-2.352808585	1.578571988
C	-4.454607700	-2.631570566	1.314881716
C	-5.268878986	-3.161193457	2.331241549
H	-6.324518513	-3.383638326	2.104774615

C	-4.778594143	-3.399838690	3.626664808
C	-3.432608912	-3.092731880	3.882424973
H	-3.039142577	-3.266442499	4.897872197
C	-2.572391315	-2.583252471	2.889063257
C	-5.079289346	-2.399063450	-0.060541655
H	-4.321801086	-1.883127830	-0.689847903
C	-6.296376232	-1.458391389	-0.014684199
H	-7.121495382	-1.879387907	0.597717514
H	-6.693075227	-1.291897711	-1.037882440
H	-6.023734271	-0.468857106	0.402232880
C	-5.404995889	-3.740378702	-0.742968906
H	-6.155032142	-4.311234575	-0.155756388
H	-4.495788385	-4.365811536	-0.843976206
H	-5.821094628	-3.581186114	-1.759317002
C	-5.680791588	-3.954733334	4.720577811
H	-5.051975920	-4.067546992	5.632067434
C	-6.224917036	-5.348296505	4.351950457
H	-5.399654903	-6.055556821	4.130609214
H	-6.875007159	-5.299983522	3.452771756
H	-6.831462804	-5.770432785	5.180678479
C	-6.821336997	-2.974213999	5.057304534
H	-7.446719252	-3.361194564	5.889237205
H	-7.485932609	-2.818257553	4.181258975
H	-6.424239638	-1.982395920	5.354341614
C	-1.125976736	-2.289501222	3.281170655
H	-0.565931445	-2.070618102	2.344026683
C	-0.433087684	-3.481609519	3.963770110
H	0.641147302	-3.260959365	4.133788273
H	-0.501497122	-4.399166996	3.346304484
H	-0.881159491	-3.709243722	4.953478047
C	-1.034736767	-1.024065474	4.149748174
H	-1.576146514	-1.154853123	5.110909290
H	-1.479981033	-0.152685076	3.627607209
H	0.022200048	-0.773519933	4.376356662
Ni	3.468600035	0.531491870	-1.203361082

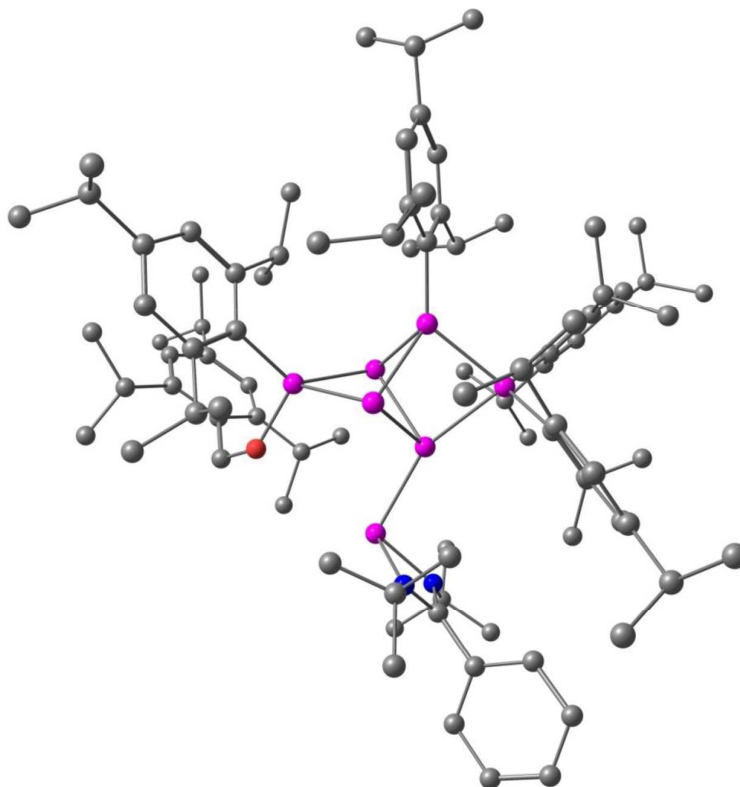


Figure S14. Optimized structure at the BP86-D3(BJ)/def2-SVP level of theory for **[Int-c]**. Bond distances are in [Å]. Hydrogen atoms omitted for clarity.

Table S4. Atomic coordinates of the optimized structure **[Int-c]** at the BP86-D3(BJ)/def2-SVP level of theory.

Si	0.951428118	0.001146030	-1.272718793
Si	0.174149641	0.634396668	1.396216412
Si	-1.205511092	0.862508110	-0.618995123
Si	0.289063589	-1.550658401	0.456933950
Si	2.137757757	1.353673287	0.299886646
Si	-1.985345861	-1.379609597	-0.151103621
Si	-1.378949544	3.274692944	-0.796021259
N	-2.650041504	3.673398340	0.625116507
N	-3.204521543	3.554722272	-1.457767526
C	-3.668992453	3.886891647	-0.229928960
C	-2.600064750	3.686293527	2.098870214
C	-3.102817358	2.326289180	2.617979638
H	-4.164751026	2.165388837	2.351036535
H	-3.012113446	2.257954119	3.720801652
H	-2.520343234	1.502197592	2.163753668
C	-3.429813666	4.834497676	2.711268941
H	-3.164329827	5.806894262	2.248756198
H	-3.210316081	4.897595094	3.796732967
H	-4.518736569	4.678115364	2.598280184
C	-1.120473054	3.895960311	2.477748440
H	-0.479972475	3.107209821	2.029784859
H	-0.993551272	3.849908349	3.577843286
H	-0.751736457	4.876310775	2.114082811
C	-5.034800880	4.360146656	0.126280030
C	-5.983629991	3.424410766	0.589036065
H	-5.706905215	2.362727415	0.664011099
C	-7.268706883	3.850312254	0.959725664
H	-8.003105843	3.113577908	1.320945050
C	-7.613430353	5.210512608	0.874464891
H	-8.620892076	5.544258037	1.168117544

C	-6.668212522	6.146141383	0.416325723
H	-6.933244438	7.213091465	0.354025977
C	-5.382655349	5.723982294	0.043644179
H	-4.635110393	6.454466930	-0.301771185
C	-3.643763118	3.955019392	-2.807789056
C	-3.020543272	2.912483065	-3.755789804
H	-3.224304130	3.162044151	-4.816454441
H	-3.423147249	1.904481365	-3.539976309
H	-1.918444453	2.873926772	-3.617090563
C	-5.176045580	3.965086296	-2.977071165
H	-5.419359665	4.111830544	-4.049185552
H	-5.652709951	4.784899649	-2.408010917
H	-5.627662087	3.011179216	-2.648831873
C	-3.079149361	5.358298325	-3.126467131
H	-1.975348385	5.368972465	-3.016380345
H	-3.500230584	6.115003746	-2.433132792
H	-3.333924462	5.661758988	-4.163212766
O	2.056040423	3.151133083	0.033641612
C	2.791781550	3.940162270	-0.695526853
C	1.326350156	-3.101935352	0.817471146
C	1.623683994	-3.987405166	-0.263255711
C	2.456249201	-5.096851357	-0.035797820
H	2.685307500	-5.768838692	-0.878270739
C	3.008555968	-5.368695865	1.228345942
C	2.682488620	-4.506286007	2.287225157
H	3.097988484	-4.719556345	3.285473152
C	1.845647444	-3.386478700	2.112129094
C	1.089201171	-3.762850230	-1.676550118
H	0.273753624	-3.008988300	-1.606677459
C	2.183865436	-3.184071816	-2.589522798
H	3.063256221	-3.860884046	-2.632230413
H	2.530035899	-2.196299948	-2.222680116
H	1.807866559	-3.050118454	-3.624647574
C	0.469379984	-5.025147586	-2.297446437
H	-0.045322733	-4.764317533	-3.244299378
H	-0.283402340	-5.480196898	-1.626380051
H	1.236955407	-5.793103956	-2.531033890
C	3.946865363	-6.548880353	1.439394990
H	4.183919652	-6.583008264	2.526377845
C	5.271336892	-6.339096288	0.678237071
H	5.758318119	-5.388211339	0.975600421
H	5.097488746	-6.295607444	-0.417873504
H	5.980796141	-7.170426973	0.875010732
C	3.283860161	-7.886910954	1.062102274
H	3.040462054	-7.924993936	-0.020766462
H	2.339361440	-8.039495774	1.623272527
H	3.959837424	-8.739919861	1.281579374
C	1.540435025	-2.502823409	3.316821173
H	0.637475130	-1.909477528	3.055759853
C	1.219225620	-3.313514281	4.583568857
H	0.457289492	-4.094852591	4.386388445
H	0.835857918	-2.646533947	5.383753815
H	2.121172050	-3.817123633	4.990523021
C	2.676644620	-1.498749267	3.572321427
H	3.636987130	-2.021834770	3.765187902
H	2.452403697	-0.858658864	4.450645068
H	2.831530683	-0.834825313	2.701433288
C	3.672752866	3.275459880	-1.676663315
C	5.078849647	3.248718765	-1.440929927
C	5.923672939	2.756901049	-2.445614442
H	7.006646403	2.712608347	-2.252728631
C	5.424656306	2.306910545	-3.684620708
C	4.034531523	2.346188229	-3.894702054
H	3.641858630	1.987458802	-4.858605970
C	3.137020053	2.822802931	-2.921338931
C	5.622498110	3.776414328	-0.116914526
H	4.854295456	3.557704900	0.653769720
C	6.906932634	3.079476382	0.349315453

H	6.780667767	1.978380724	0.371738805
H	7.165965903	3.409795218	1.375828462
H	7.773132501	3.322166376	-0.302717834
C	5.789746326	5.308079299	-0.184816664
H	6.546703107	5.585595406	-0.948759688
H	6.123826666	5.711449208	0.794833764
H	4.827612223	5.791070169	-0.451022381
C	6.362518573	1.797210839	-4.771759448
H	5.724224552	1.504035695	-5.635327748
C	7.317364519	2.907341198	-5.253603295
H	7.955792263	2.549775665	-6.089160952
H	7.990873328	3.238023156	-4.434599080
H	6.754293891	3.796968340	-5.602448008
C	7.140962013	0.545424462	-4.323485939
H	6.452511885	-0.269520289	-4.022905229
H	7.794389657	0.769518739	-3.453590981
H	7.790729550	0.167622914	-5.141090364
C	1.641072372	2.945165417	-3.199185071
H	1.100113732	2.588670045	-2.293498230
C	1.250950510	4.423753412	-3.388170649
H	1.767255920	4.859409446	-4.269917437
H	1.527996893	5.018044249	-2.490553339
H	0.154791837	4.521614208	-3.533880282
C	1.150142721	2.077810907	-4.362172003
H	0.042336830	2.108441840	-4.413762710
H	1.450714425	1.017359327	-4.232607954
H	1.537071214	2.430679330	-5.341562301
C	3.727477234	1.041827927	1.266020589
C	3.963356468	1.837758776	2.427639022
C	5.108468063	1.589462799	3.205920412
H	5.283221451	2.204771848	4.103483085
C	6.014147696	0.562493196	2.890484109
C	5.735223554	-0.246798919	1.775188197
H	6.418586649	-1.079266080	1.549012427
C	4.605015459	-0.041214841	0.964079608
C	2.956141464	2.871201895	2.941087853
H	2.160743999	2.998309847	2.181329756
C	2.260174653	2.346122759	4.211743336
H	1.743618689	1.385863731	4.004888331
H	1.500436485	3.072506673	4.569117953
H	2.984747743	2.172555336	5.035090525
C	3.570985805	4.265454240	3.149049585
H	4.397119715	4.249836346	3.891094145
H	2.801838066	4.974481357	3.519103569
H	3.969591864	4.671673260	2.197919304
C	7.231116089	0.290350694	3.764022601
H	7.798197828	-0.535139833	3.278672436
C	6.805970166	-0.195938151	5.164121221
H	6.150655106	-1.088286737	5.095646236
H	6.241575324	0.592429456	5.705844321
H	7.691101931	-0.460421411	5.780325860
C	8.164240315	1.512583325	3.849165913
H	9.066682156	1.280785180	4.452978263
H	7.654748830	2.375563456	4.327869061
H	8.495267778	1.835651576	2.841599021
C	4.317442841	-0.995819924	-0.191709110
H	3.210057298	-1.119790289	-0.227180103
C	4.899750565	-2.401683036	0.003182591
H	4.524080381	-3.077775395	-0.789037442
H	4.598770908	-2.835977529	0.977552842
H	6.008758026	-2.406415119	-0.059815488
C	4.757604422	-0.383297234	-1.531008732
H	4.510971692	-1.059090372	-2.376153324
H	5.852147807	-0.204476612	-1.537669269
H	4.261959352	0.587927470	-1.720504232
C	-3.451966015	-1.100190357	1.058786360
C	-4.669716040	-0.678731328	0.442837998
C	-5.765639815	-0.293515850	1.237468820

H	-6.705137082	0.015515186	0.748519827
C	-5.705421085	-0.297309502	2.640614449
C	-4.513151632	-0.740322194	3.236524733
H	-4.445664441	-0.769004818	4.336276243
C	-3.394719842	-1.148919141	2.482790578
C	-4.844628071	-0.675302593	-1.073902101
H	-3.839870438	-0.801138731	-1.524184579
C	-5.693200160	-1.873149865	-1.535946453
H	-5.766868300	-1.899664211	-2.643273660
H	-6.722697088	-1.814740661	-1.122820352
H	-5.241778200	-2.830179302	-1.207956118
C	-5.369966948	0.658266351	-1.614643731
H	-4.679626027	1.482342740	-1.346366487
H	-6.381861430	0.907169839	-1.231797845
H	-5.441798897	0.622677778	-2.721667078
C	-6.885215729	0.182133207	3.476590865
H	-7.726488172	0.362592978	2.769514438
C	-7.347212074	-0.881639116	4.489619824
H	-7.585665587	-1.840240300	3.985316065
H	-8.251781790	-0.542010157	5.036408499
H	-6.560135371	-1.086483439	5.245739483
C	-6.566180481	1.520923810	4.172201323
H	-5.712518939	1.410151872	4.873770513
H	-7.438714599	1.885179270	4.754664800
H	-6.292614946	2.304732843	3.437012524
C	-2.183573870	-1.659602672	3.263284808
H	-1.406492426	-1.941107511	2.518617968
C	-2.531206418	-2.919257169	4.079151087
H	-2.953038210	-3.715382829	3.437575500
H	-3.280266932	-2.694077962	4.8671170831
H	-1.627529837	-3.320283797	4.579678341
C	-1.575952566	-0.584974709	4.180894975
H	-0.705463304	-0.988743374	4.737079769
H	-2.314294208	-0.222897620	4.926664340
H	-1.225095974	0.293754525	3.601216770
C	-2.407428552	-2.754972605	-1.416838032
C	-2.702184725	-4.041467989	-0.875087404
C	-3.041608638	-5.103926769	-1.731236814
H	-3.276404705	-6.086890517	-1.290868536
C	-3.077273052	-4.950551253	-3.127312322
C	-2.758848543	-3.687975030	-3.650964924
H	-2.771019683	-3.557541268	-4.745901683
C	-2.430547941	-2.589481581	-2.830904349
C	-2.684652590	-4.315267430	0.627642826
H	-2.333612067	-3.390713314	1.133696178
C	-1.683258250	-5.417755570	1.015716052
H	-1.951112882	-6.396496144	0.564592558
H	-1.663461395	-5.551644081	2.117529676
H	-0.656262203	-5.156682794	0.691392576
C	-4.107670481	-4.603667628	1.140347227
H	-4.551414561	-5.475682381	0.615828600
H	-4.770039717	-3.729465104	0.978162988
H	-4.106923616	-4.832923368	2.226089007
C	-3.429745439	-6.116611281	-4.040721081
H	-3.404066869	-5.729178445	-5.083915270
C	-4.854544757	-6.636547296	-3.769434824
H	-5.603322738	-5.824070668	-3.866800343
H	-4.941260927	-7.050790316	-2.742576078
H	-5.125062061	-7.445562788	-4.480275268
C	-2.387060202	-7.246860488	-3.935626633
H	-2.621541065	-8.071939843	-4.640816750
H	-2.364745110	-7.676016146	-2.911484439
H	-1.367278397	-6.875464527	-4.162928857
C	-2.091474904	-1.269321867	-3.519199514
H	-2.026270651	-0.483850626	-2.733001404
C	-3.166166643	-0.829145733	-4.528083506
H	-2.913988310	0.163150106	-4.954217414
H	-4.164965163	-0.756709284	-4.052679953

H	-3.250641742	-1.538681601	-5.377505925
C	-0.707682679	-1.343115994	-4.185684659
H	-0.674052110	-2.142803668	-4.955883846
H	0.081047813	-1.560683781	-3.437515153
H	-0.450823463	-0.380778410	-4.672458972

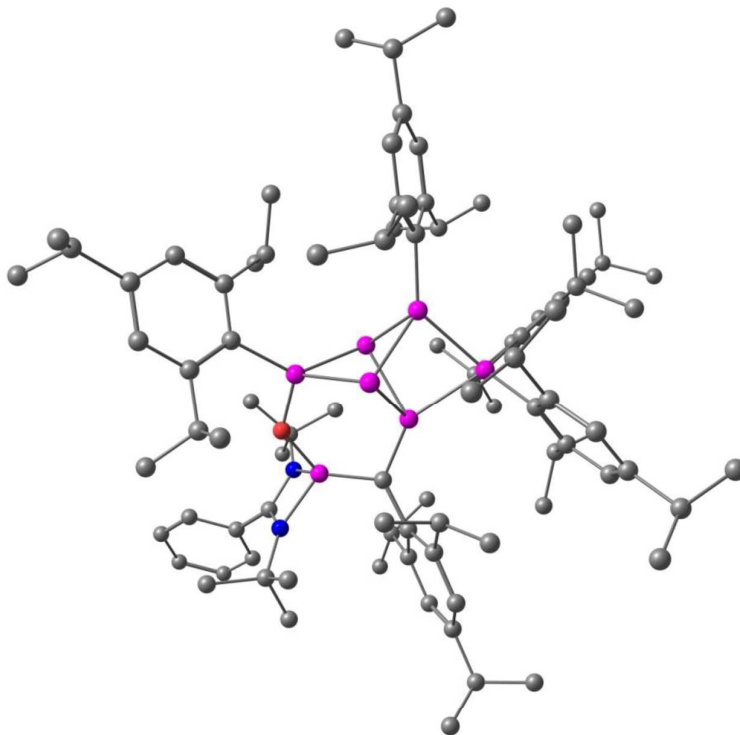


Figure S15. Optimized structure at the BP86-D3(BJ)/def2-SVP level of theory for **2**. Bond distances are in [Å]. Hydrogen atoms omitted for clarity.

Table S5. Atomic coordinates of the optimized structure **2** at the BP86-D3(BJ)/def2-SVP level of theory.

Si	-0.294305372	1.261767703	1.295707973
Si	1.131875771	2.354461370	-0.245938360
Si	-0.196145250	0.911266358	-1.577540235
Si	0.329461783	-0.734942488	0.114545351
Si	-1.964683924	-1.410728717	0.099931412
Si	-2.114939792	0.958765700	-0.219253802
Si	3.140670196	0.111823616	0.480115129
N	4.061722269	0.516315373	2.093590935
N	4.973114847	0.023666896	0.185738421
O	2.678617033	1.676843172	0.068535785
C	2.095040733	-1.273118666	0.138497604
C	1.313665825	4.159311100	-0.760924266
C	2.239149181	4.506121005	-1.789913993
C	2.273453334	5.829037578	-2.266488420
H	2.987039139	6.090113048	-3.064489844
C	1.404778310	6.819648339	-1.773410960
C	0.471512137	6.452835000	-0.787878242
H	-0.227881298	7.217705203	-0.414940899
C	0.398795272	5.143347522	-0.279020569
C	3.109103481	3.449852910	-2.474829170
H	3.154001313	2.566019804	-1.808674724
C	4.563151479	3.900095752	-2.691994226

H	5.164987797	3.067782263	-3.113349473
H	5.031742304	4.216445447	-1.737235948
H	4.640551436	4.748145083	-3.404879225
C	2.447265026	3.002454808	-3.794449091
H	3.026868400	2.183548829	-4.271038600
H	2.380769158	3.845514241	-4.514761009
H	1.419133708	2.627049715	-3.610371922
C	1.443742387	8.241354511	-2.318884493
C	1.017563013	8.281340943	-3.800019259
H	0.012848522	7.832896033	-3.939748003
H	1.729229528	7.712930598	-4.435688740
H	0.988019105	9.325070622	-4.178183116
C	-0.635891689	4.807215689	0.795340176
H	-0.916853962	3.739098760	0.654176911
C	-0.002742747	4.925601800	2.194666145
H	-0.729795245	4.646178045	2.985288166
H	0.335957669	5.966235141	2.384327240
H	0.877487054	4.257263216	2.291841905
C	-1.945400271	5.602988827	0.698460506
H	-2.372413269	5.556027945	-0.322668281
H	-1.813908017	6.670949056	0.974721219
H	-2.699269471	5.170820473	1.387463895
C	-3.546605651	2.202225024	-0.142295579
C	-3.903357881	2.994704594	-1.272832492
C	-4.884721566	3.994513435	-1.128031917
H	-5.153317740	4.617559256	-1.996461769
C	-5.534840640	4.233966685	0.093437777
C	-5.189344005	3.428311945	1.193129572
H	-5.690495588	3.594018419	2.160463313
C	-4.213166717	2.420243669	1.101343836
C	-3.214013263	2.827307902	-2.623879240
H	-2.794677907	1.798236829	-2.639901166
C	-2.021781387	3.793430684	-2.754883815
H	-1.471421723	3.621381921	-3.703870827
H	-1.299265679	3.660223335	-1.925848817
H	-2.361544212	4.850787890	-2.739809391
C	-4.168466290	2.957950858	-3.821731179
H	-3.654978982	2.653969745	-4.757700436
H	-4.513956093	4.003150285	-3.968347319
H	-5.067883078	2.320752176	-3.697770794
C	-6.562074489	5.349933674	0.227105397
H	-6.701348384	5.784121754	-0.788274104
C	-6.037364713	6.471055631	1.146497367
H	-6.758412477	7.313981436	1.200735066
H	-5.067126180	6.865938225	0.782092663
H	-5.878265456	6.095824934	2.179741796
C	-7.928771044	4.822411548	0.702625131
H	-8.308611404	4.027136535	0.029221518
H	-8.680268726	5.639226038	0.733771736
H	-7.861473510	4.392435660	1.724361674
C	-3.860251621	1.636786105	2.364111288
H	-3.246140788	0.762012847	2.054910354
C	-3.002614868	2.504436336	3.302751250
H	-3.544657130	3.429721483	3.591961073
H	-2.054577348	2.804323284	2.809677314
H	-2.745498629	1.952501962	4.230456631
C	-5.084237005	1.078658288	3.108521423
H	-5.739505444	0.494675964	2.435617485
H	-5.691924472	1.885040112	3.571516823
H	-4.751276034	0.398142475	3.918256813
C	-3.103237245	-1.880270241	1.572577230
C	-4.498743512	-1.992717496	1.281462617
C	-5.401342291	-2.359587552	2.294239798
H	-6.470076230	-2.456283915	2.042060750
C	-4.983634901	-2.593450818	3.615141275
C	-3.618627024	-2.442799087	3.898126022
H	-3.278930918	-2.608027052	4.934175281
C	-2.671911283	-2.099108714	2.910345427

C	-5.069636650	-1.752785314	-0.115382677
H	-4.244734463	-1.381942131	-0.755625227
C	-5.568878908	-3.073157175	-0.731009643
H	-6.408835870	-3.494062790	-0.138726082
H	-4.757582477	-3.827266034	-0.764274381
H	-5.929131667	-2.919544131	-1.769189512
C	-6.146424281	-0.653458749	-0.140900736
H	-6.522267924	-0.505206665	-1.174774551
H	-5.737071758	0.316180524	0.205276603
H	-7.019450270	-0.910312919	0.495318877
C	-5.976441965	-2.986751076	4.700510520
C	-7.032005159	-1.887609464	4.929330705
H	-7.646846838	-1.726774194	4.018551634
H	-6.555836812	-0.919143220	5.184207266
H	-7.721463105	-2.163388044	5.755007057
C	-6.635478993	-4.344982431	4.390968865
H	-7.238875203	-4.293210878	3.459929746
H	-7.313613076	-4.656043312	5.213568618
H	-5.872451915	-5.137667883	4.250873375
C	-1.219682755	-1.955073208	3.360018568
H	-0.593192154	-1.803212339	2.452397262
C	-0.702409221	-3.206322783	4.091161421
H	-1.302058894	-3.428305193	4.998191821
H	0.346406253	-3.061786505	4.416218336
H	-0.736756243	-4.100674885	3.438123876
C	-1.053463117	-0.699182579	4.232909320
H	-1.308746630	0.215876237	3.659893224
H	-0.007411301	-0.598312193	4.584362554
H	-1.713770626	-0.737428394	5.125102554
C	-2.224477017	-2.721182738	-1.277566184
C	-1.911635910	-4.064577302	-0.915609104
C	-2.141397501	-5.109194454	-1.831950871
H	-1.905065095	-6.145840704	-1.538821600
C	-2.660876143	-4.873609701	-3.113763194
C	-2.940256954	-3.543143662	-3.469837876
H	-3.333463681	-3.330965779	-4.477289216
C	-2.732521319	-2.468365863	-2.585981010
C	-1.359218572	-4.431794022	0.460967755
H	-1.148905568	-3.483511313	1.002869681
C	-0.017212657	-5.179634259	0.378682169
H	-0.122953075	-6.161235158	-0.129178564
H	0.379961549	-5.372718511	1.396865083
H	0.742407692	-4.592293604	-0.173332972
C	-2.407266724	-5.207336667	1.280787545
H	-3.344035166	-4.625146880	1.387765023
H	-2.028350339	-5.431112850	2.299575270
H	-2.653565713	-6.173713581	0.791990071
C	-2.876100717	-6.016193336	-4.096633537
C	-1.889030114	-5.921550673	-5.277318818
H	-2.057782273	-4.993015933	-5.863093680
H	-2.007775626	-6.783217238	-5.967869928
H	-0.839150882	-5.903052753	-4.920902483
C	-4.335327264	-6.087967605	-4.583996041
H	-4.612686640	-5.179642614	-5.159783614
H	-5.039525819	-6.171439071	-3.731106881
H	-4.489601266	-6.963593018	-5.249166562
C	-3.051827008	-1.065782522	-3.098875607
H	-2.981763147	-0.374900623	-2.229086003
C	-4.469030490	-0.934246198	-3.681258258
H	-4.594454345	-1.544053708	-4.600415723
H	-4.675921712	0.120130512	-3.953992783
H	-5.240452415	-1.257781300	-2.956300497
C	-1.999526271	-0.604918198	-4.121005647
H	-1.999263122	-1.258923111	-5.018840920
H	-0.981434304	-0.633271383	-3.681336406
H	-2.195764283	0.435516714	-4.455411341
C	2.638075943	-2.586046765	-0.290406030
C	2.293564509	-3.155689061	-1.565464331

C	2.887351702	-4.364767559	-1.970672411
H	2.616443400	-4.780270126	-2.952201766
C	3.810024905	-5.062477686	-1.173442527
C	4.107316599	-4.526631084	0.089383606
H	4.796396485	-5.085459986	0.742378688
C	3.538644375	-3.324260378	0.548085742
C	1.292166962	-2.480884138	-2.502286558
H	0.461045767	-2.090243699	-1.866822408
C	0.641220467	-3.435768143	-3.511281456
H	0.212739889	-4.326802600	-3.012264929
H	1.359926368	-3.777453431	-4.286615249
H	-0.187724008	-2.923261914	-4.036164452
C	1.894620486	-1.265926893	-3.226647115
H	2.764773079	-1.566932507	-3.847285175
H	2.223611997	-0.497696582	-2.500418832
H	1.143890804	-0.799815893	-3.898053255
C	4.440396201	-6.364242685	-1.648739801
H	5.106704865	-6.718761385	-0.829976150
C	3.376287609	-7.452936608	-1.889381700
H	2.765298563	-7.621403466	-0.979094642
H	3.845817602	-8.417444802	-2.177856808
H	2.682940998	-7.159698486	-2.706045512
C	5.313740490	-6.146133127	-2.899724644
H	5.813276828	-7.088088581	-3.211478588
H	6.097167510	-5.383362488	-2.711940996
H	4.700931439	-5.791725396	-3.755747179
C	3.786221443	-2.884599891	1.989024035
H	3.873903732	-1.781672655	2.004564827
C	2.546021058	-3.224496470	2.834024458
H	1.653468439	-2.722664741	2.411303727
H	2.670531919	-2.891211669	3.887097656
H	2.359439298	-4.318658160	2.840152965
C	5.063027660	-3.443957388	2.629588940
H	5.004539254	-4.540098714	2.798320800
H	5.228068969	-2.975776787	3.623192924
H	5.957194042	-3.252571191	2.000550579
C	5.235065676	0.416807158	1.454704823
C	3.687571051	1.116719526	3.387108474
C	4.707410706	0.800234367	4.497843630
H	4.290208035	1.127721348	5.471545961
H	5.671987031	1.321333334	4.352005555
H	4.901194436	-0.290074962	4.556242276
C	3.537805074	2.642453493	3.202870568
H	2.822673008	2.863493995	2.386700758
H	4.512129701	3.103770555	2.943261813
H	3.168623312	3.113074110	4.136712966
C	2.332968741	0.493641363	3.762054813
H	1.572915469	0.676381760	2.971144655
H	1.952002297	0.937074158	4.703090556
H	2.422530482	-0.602623056	3.890459455
C	6.572190294	0.708330339	2.031785467
C	7.089062584	2.018450581	1.954568177
H	6.511534251	2.799854684	1.437955956
C	8.334131136	2.313375609	2.530854943
H	8.734808697	3.336982128	2.470076709
C	9.066571822	1.305159841	3.182684414
H	10.042864899	1.538900501	3.634831823
C	8.551497782	-0.000848803	3.256943979
H	9.121431998	-0.792014096	3.767992753
C	7.306127546	-0.302397864	2.684315451
H	6.888042382	-1.316802777	2.752630461
C	5.894313603	-0.357206680	-0.909836051
C	6.879210043	0.789225496	-1.216543289
H	7.452992913	0.548965377	-2.134676500
H	7.606237352	0.946250605	-0.397185105
H	6.329632271	1.736517347	-1.389965591
C	6.647613504	-1.652979733	-0.549938894
H	5.926416723	-2.466608899	-0.333101465

H	7.308432589	-1.506597918	0.327095929
H	7.282563707	-1.970300473	-1.402174583
C	5.007740459	-0.613880810	-2.136020997
H	4.303707204	-1.444547700	-1.937690735
H	5.632865222	-0.890647205	-3.007881727
H	4.424183639	0.291354370	-2.400833971
C	2.822705806	8.895979312	-2.111493393
H	3.611522385	8.360995983	-2.681653483
H	3.116241045	8.884597980	-1.041901367
H	2.817360269	9.950754244	-2.458454579
H	0.698853727	8.830132305	-1.738204777
H	-5.396113173	-3.099804742	5.643715419
H	-2.655447547	-6.959196031	-3.548003388

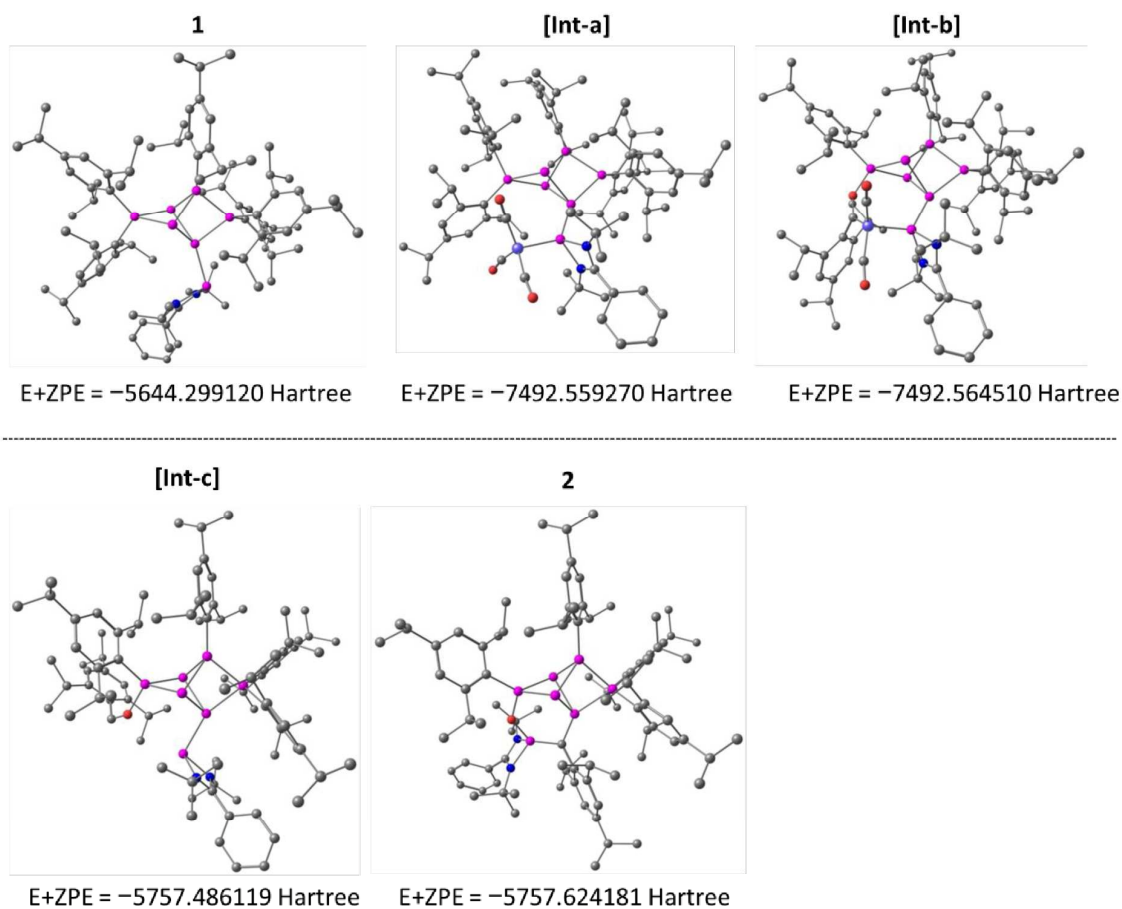


Figure S16:: Free Gibbs energies in Hartree of 1, [Int-a], [Int-b], [Int-c] and 2.

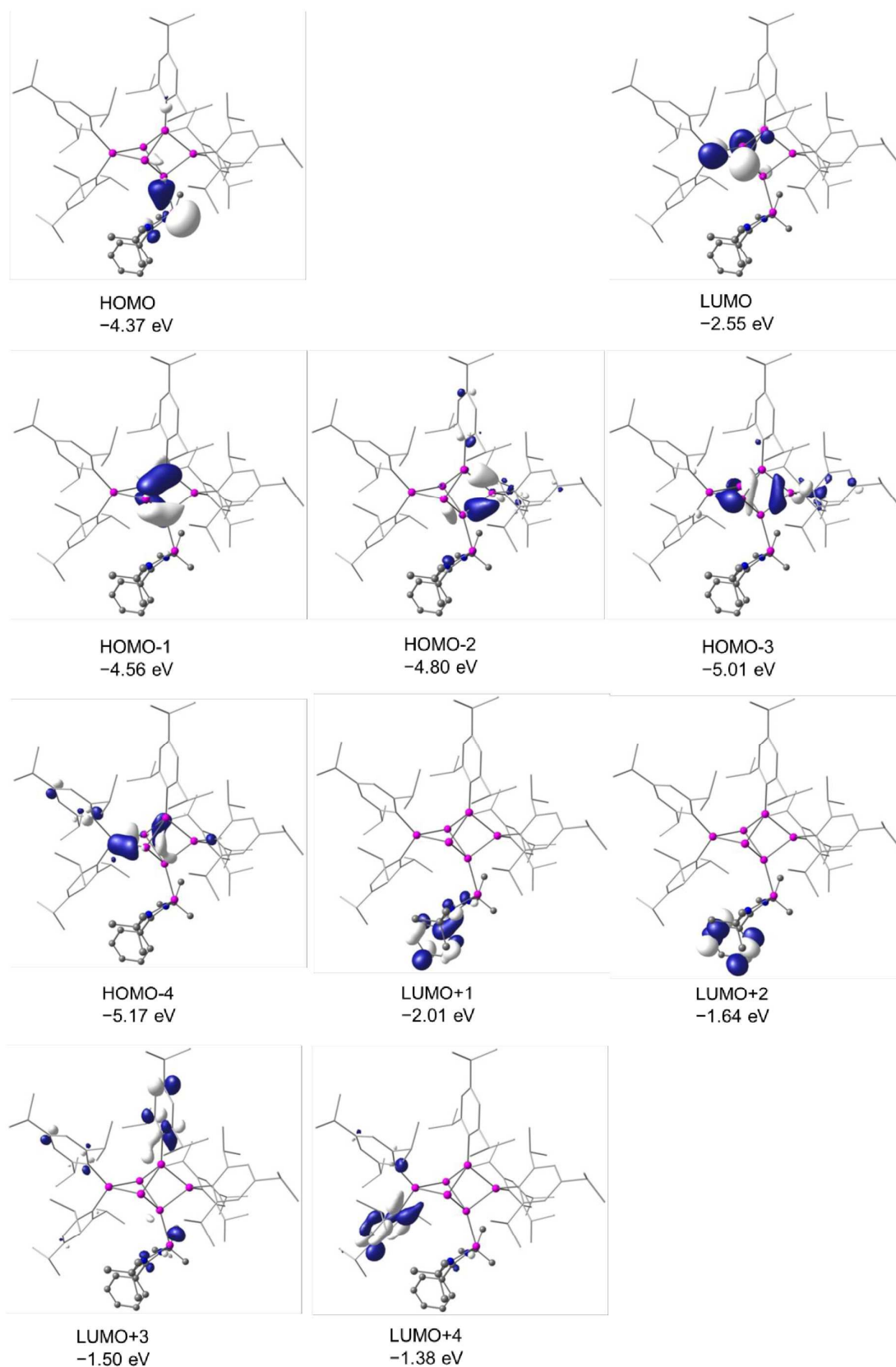


Figure S17: Selected molecular orbitals of **1** at the BP86-D3(BJ)/def2-SVP level of theory (isocontour value 0.051840)

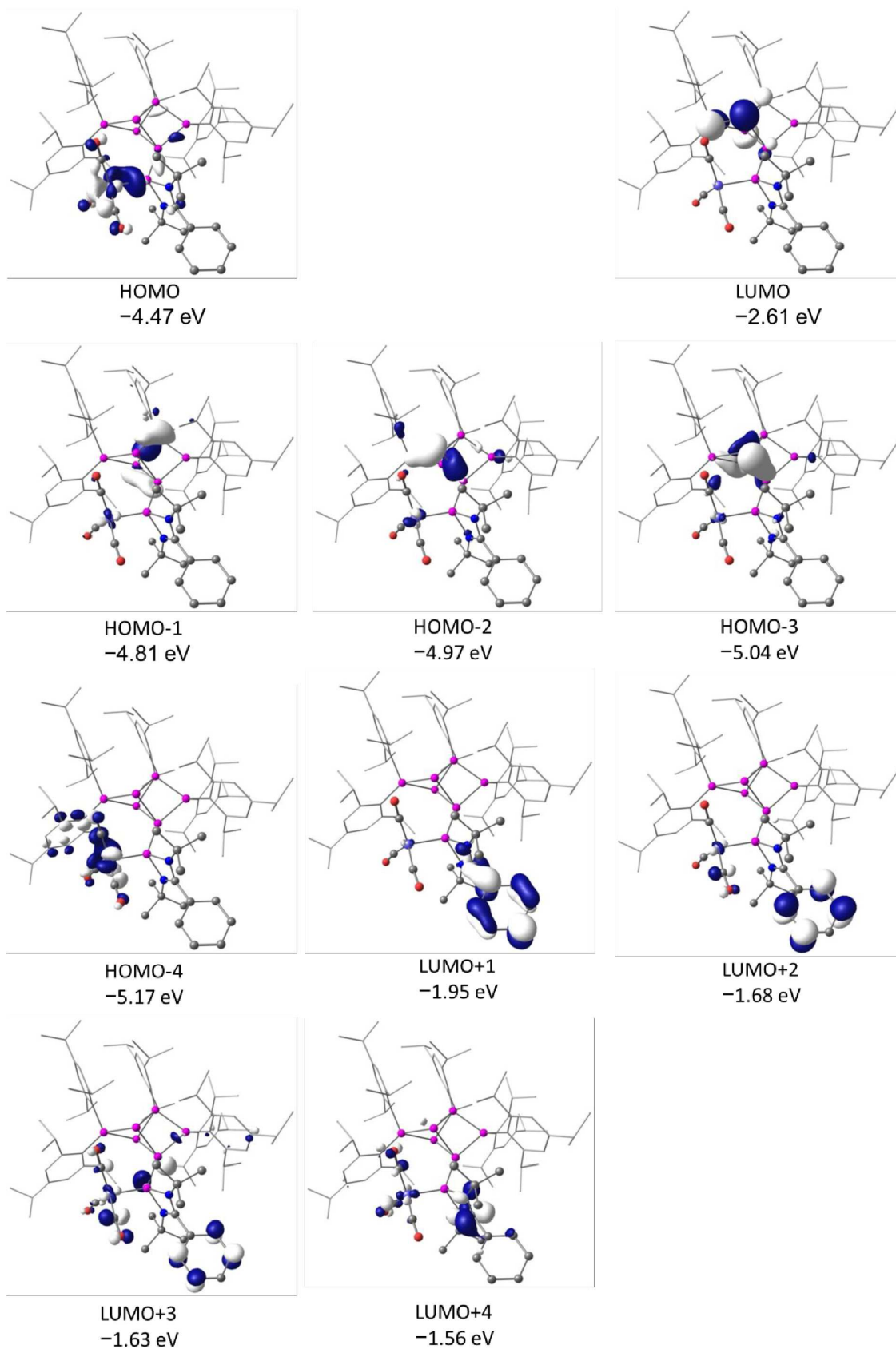


Figure S18: Selected molecular orbitals of **[Int-a]** at the BP86-D3(BJ)/def2-SVP level of theory (isocontour value 0.051840).

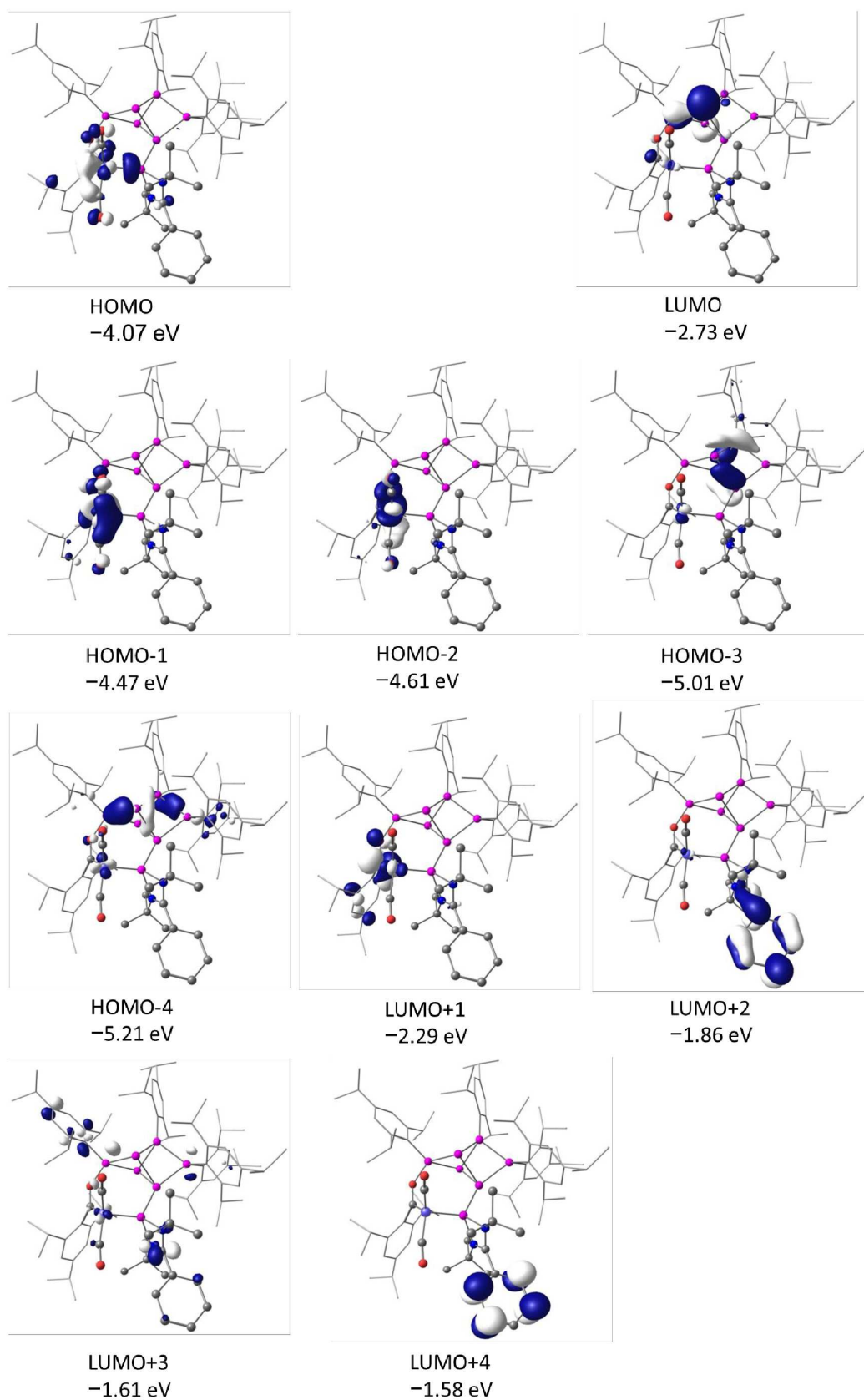


Figure S19: Selected molecular orbitals of **[Int-b]** at the BP86-D3(BJ)/def2-SVP level of theory (isocontour value 0.051840).

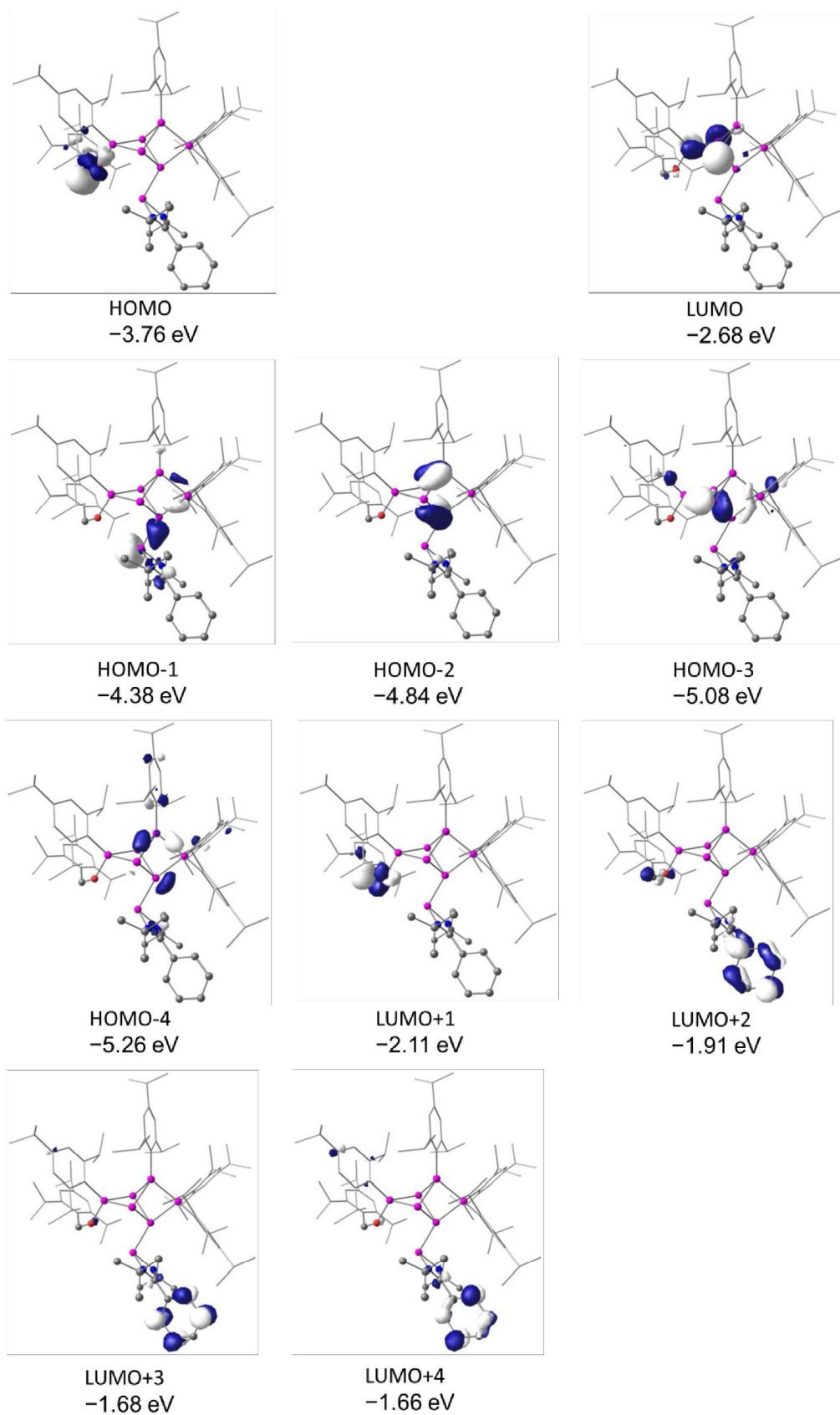


Figure S20: Selected molecular orbitals of **[Int-c]** at the BP86-D3(BJ)/def2-SVP level of theory (isocontour value 0.051840).

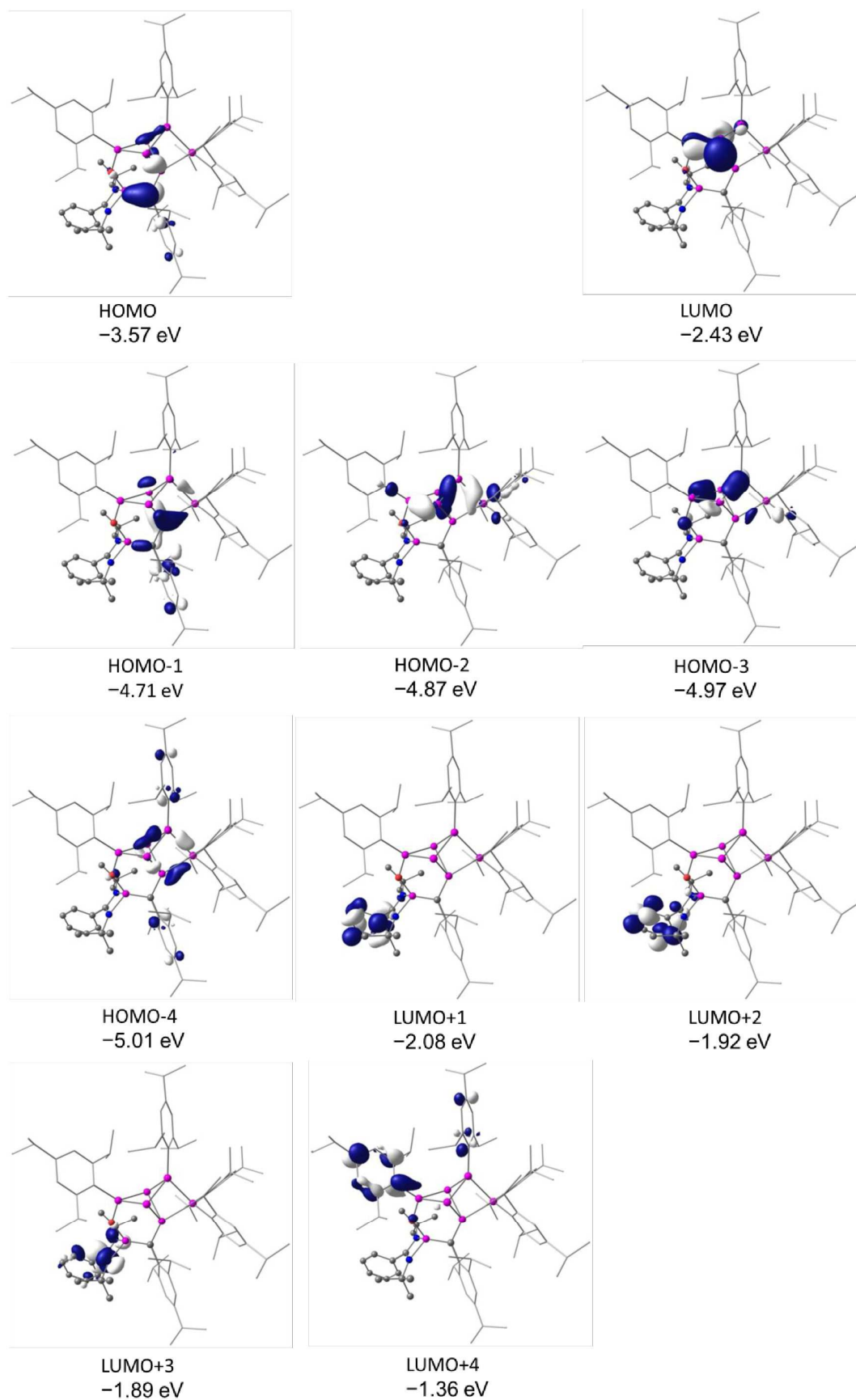


Figure S21: Selected molecular orbitals of **2** at the BP86-D3(BJ)/def2-SVP level of theory (isocontour value 0.051840).

S36

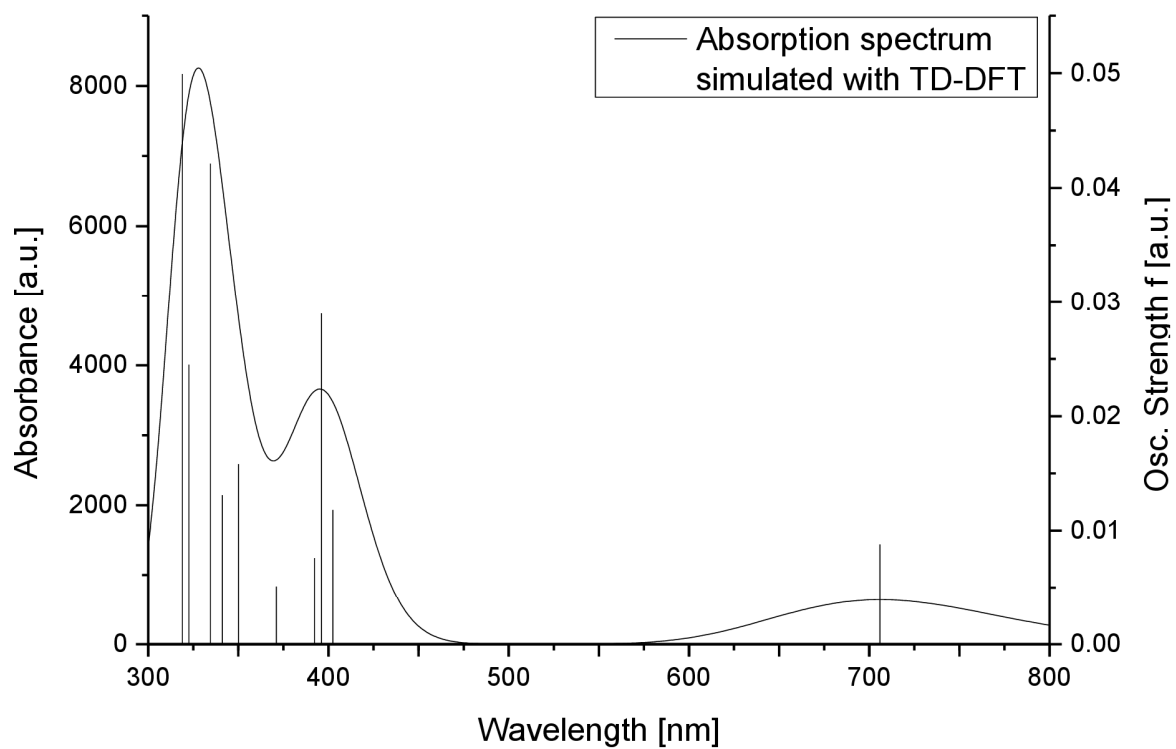


Figure S22. Calculated transitions (vertical bars) and simulated UV-Vis absorption spectrum of siliconoid 2.

Table S6: Selected electronic transitions and optical parameters of the TD-DFT calculations of siliconoid **2**.

Transition No.	$\lambda_{\text{calc. max}}$ [nm]	Transitions	f	Contribution [%]
1	705	HOMO \rightarrow LUMO	0.0088	91
		HOMO-1 \rightarrow LUMO		4
2	402	HOMO-3 \rightarrow LUMO	0.0118	57
		HOMO-2 \rightarrow LUMO		19
		HOMO-1 \rightarrow LUMO		11
		HOMO \rightarrow LUMO+3		3
3	396	HOMO-4 \rightarrow LUMO	0.029	22
		HOMO-3 \rightarrow LUMO		13
		HOMO-1 \rightarrow LUMO		51
		HOMO-2 \rightarrow LUMO		3
4	392	HOMO \rightarrow LUMO+3	0.0076	78
		HOMO-4 \rightarrow LUMO		3
		HOMO \rightarrow LUMO+7		2
5	371	HOMO-3 \rightarrow LUMO	0.0051	17
		HOMO-2 \rightarrow LUMO		59
		HOMO-15 \rightarrow LUMO		2
		HOMO-5 \rightarrow LUMO		9
		HOMO-4 \rightarrow LUMO		3
		HOMO-1 \rightarrow LUMO		2

4. Details on X-ray Diffraction Studies

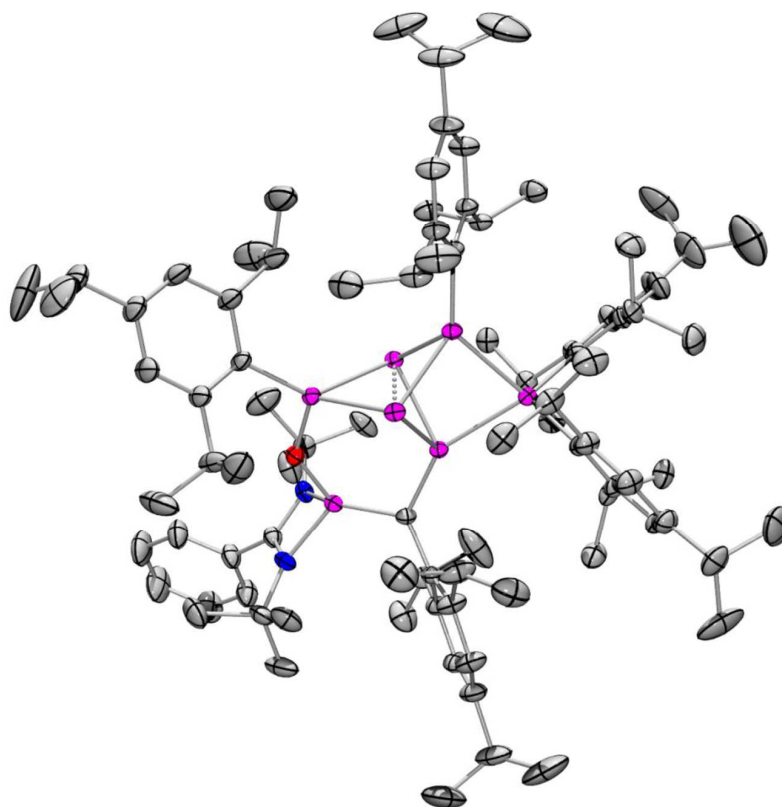


Figure S23. Molecular structure of siliconoid **2** in the solid state. Hydrogen atoms omitted for clarity. Thermal ellipsoids represent 50% probability.

Table S7. Crystal data and structure refinement for **2** (CCDC: 2016837).

Identification code	sh3999b	
Empirical formula	C ₉₁ H ₁₃₈ N ₂ O Si ₇ , C ₇ H ₁₄	
Formula weight	1558.83	
Temperature	133(2) K	
Wavelength	0.71073 Å	
Crystal system	Monoclinic	
Space group	P2 ₁ /c	
Unit cell dimensions	$a = 13.0001(3)$ Å	$\alpha = 90^\circ$.
	$b = 28.8076(8)$ Å	$\beta = 93.4546(9)^\circ$.
	$c = 26.4244(6)$ Å	$\gamma = 90^\circ$.
Volume	$9878.0(4)$ Å ³	
Z	4	
Density (calculated)	1.048 Mg/m ³	
Absorption coefficient	0.140 mm ⁻¹	
F(000)	3416	
Crystal size	$0.343 \times 0.083 \times 0.028$ mm ³	
	S39	

Theta range for data collection	1.925 to 29.594°
Index ranges	-18<=h<=18, -40<=k<=33, -36<=l<=35
Reflections collected	159316
Independent reflections	27713 [R(int) = 0.0382]
Completeness to theta = 25.242°	99.9 %
Absorption correction	Semi-empirical from equivalents
Max. and min. transmission	0.7459 and 0.7132
Refinement method	Full-matrix least-squares on F ²
Data / restraints / parameters	27713 / 311 / 1110
Goodness-of-fit on F ²	1.039
Final R indices [I>2sigma(I)]	R1 = 0.0492, wR2 = 0.1436
R indices (all data)	R1 = 0.0613, wR2 = 0.1541
Extinction coefficient	n/a
Largest diff. peak and hole	1.489 and -0.380 e.Å ⁻³

PLAT097 B LEVEL ALERT: The largest peaks of residual electron density are located near the co-crystallized hexane molecule indicating some unresolved disorder.

5. References

- [1] N. E. Poitiers, L. Giarrana, K. I. Leszczyńska, V. Huch, M. Zimmer, D. Scheschke, *Angew. Chem. Int. Ed.* 2020, **59**, 8532-8536.
- [2] M. J. Frisch, G. W. Trucks, H. B. Schlegel, G. E. Scuseria, M. A. Robb, J. R. Cheeseman, G. Scalmani, V. Barone, B. Mennucci, G. A. Petersson, H. P. Hratchian, A. F. Izmaylov, J. Bloino, G. Zheng, J. L. Sonnenberg, M. Hada, M. Ehara, K. Toyota, R. Fukuda, J. Hasegawa, M. Ishida, T. Najajima, Y. Honda, O. Kitao, H. Nikai, T. Vreven, J. A. Montgomery, J. E. Peralta, F. Ogliaro, M. Bearpark, J. J. Heyd, E. Brothers, K. N. Kudin, V. N. Staroverov, R. Kobayashi, J. Normand, K. Raghavachari, A. Rendell, J. C. Burant, S. S. Iyengar, J. Tomasi, M. Cossi, N. Rega, J. M. Millam, M. Klene, J. E. Knox, J. B. Cross, V. Bakken, C. Adamo, J. Jaramillo, R. Gomperts, R. E. Stratman, O. Yazyev, A. J. Austin, R. Cammi, C. Pomelli, J. W. Ochterski, R. L. Martin, K. Morokuma, V. G. Zakrzewski, G. A. Voth, P. Salvador, J. J. Dannenberg, S. Dapprich, A. D. Daniels, O. Farkas, J. B. Foresman, J. V. Ortiz, J. Cioslowski, D. J. Fox, *Gaussian09, Revision C.01*, Gaussian, Inc.: Wallingford CT, 2009.
- [3] TURBOMOLE V7.0 2015 a development of University of Karlsruhe and Forschungszentrum Karlsruhe GmbH, 1989-2007; TURBOMOLE GmbH, since 2007, available from <http://www.turbomole.com>; Karlsruhe.
- [4] A. D. Becke, *Phys. Rev. A* 1988, **38** (6), 3098-3100.
- [5] J. P. Perdew, *Phys. Rev. B* 1986, **33** (12), 8822-8824.
- [6] S. Grimme, J. Antony, S. Ehrlich, H. Krieg, *J. Chem. Phys.* 2010, **132** (15), 154104.
- [7] S. Grimme, S. Ehrlich, L. Goerigk, *J. Comp. Chem.* 2011, **32** (7), 1456-1465.
- [8] F. Weigend, R. Ahlrichs, *Phys. Chem. Chem. Phys.* 2005, **7** (18), 3297-3305.
- [9] T. Yanai, D. Tew, N. Handy, *Chem. Phys. Lett.*, 2004, **393**, 51-57.
- [10] <https://www.chemcraftprog.com/>
- [11] N. M. O'Boyle, A. L. Tenderholt, K. M. Langner, *J. Comput. Chem.* 2008, **29**, 839-845.
- [12] <http://www.OriginLab.com>.

Author Contributions

N. P. Conceptualization: Equal, Data curation: Lead; Formal analysis: Lead; Investigation: Lead; Methodology: Lead; Validation: Lead; Visualization: Lead; Writing original draft: Lead; Writing review & editing: Lead. V.H. Data curation (X-ray): Lead; Formal analysis (X-ray): Lead, X-ray structures: Lead. M. Z. CP/MAS NMR studies: Lead. D. S. Conceptualization: Lead, Funding acquisition: Lead; Methodology: Supporting; Project administration: Lead; Resources: Lead; Supervision: Lead; Writing original draft: Supporting; Writing review & edition: Supporting.

7 Permission of Redistribution/Licensing

- Yannic Heider*, Nadine E. Poitiers*, Philipp Willmes, Kinga I. Leszczyńska, Volker Huch, David Scheschkewitz, Site-selective functionalization of Si₆R₆ siliconoids, *Chem. Sci.*, **2019**, *10*, 4523-4530.
(<https://doi.org/10.1039/C8SC05591B>)

This article was published by the Royal Society of Chemistry (RSC) as an “Open Access” article and is licensed under a “Creative Commons Attribution-NonCommercial 3.0 Unported (CC BY-NC 3.0)” Licence (<https://creativecommons.org/licenses/by-nc/3.0/>).

- Nadine E. Poitiers, Luisa Giarrana, Kinga I. Leszczyńska, Volker Huch, Michael Zimmer, David Scheschkewitz, Indirect and Direct Grafting of Transition Metals to Siliconoids. *Angew. Chem. Int. Ed.* **2020**, *59*, 8532-8536 (<https://doi.org/10.1002/anie.202001178>); *Angew. Chem.* **2020**, *132*, 8610-8614 (<https://doi.org/10.1002/ange.202001178>).

Copyright © 2020 Wiley-VCH Verlag GmbH & Co. KGaA.

This article was reproduced with the permission from Wiley-VCH:

JOHN WILEY AND SONS LICENSE
TERMS AND CONDITIONS

Oct 06, 2020

This Agreement between Saarland University – Nadine Poitiers ("You") and John Wiley and Sons ("John Wiley and Sons") consists of your license details and the terms and conditions provided by John Wiley and Sons and Copyright Clearance Center.

License Number	4922540119490
License date	Oct 05, 2020
Licensed Content Publisher	John Wiley and Sons
Licensed Content Publication	Angewandte Chemie International Edition
Licensed Content Title	Indirect and Direct Grafting of Transition Metals to Siliconoids
Licensed Content Author	Nadine E. Poitiers, Luisa Giarrana, Kinga I. Leszczyńska, et al
Licensed Content Date	Mar 20, 2020
Licensed Content Volume	59
Licensed Content Issue	22
Licensed Content Pages	5
Type of Use	Dissertation/Thesis
Requestor type	Author of this Wiley article
Format	Print and electronic
Portion	Full article
Will you be translating?	No
Title	Stable Functionalized Unsaturated Siliconoids: From a tetraylene/siliconoid hybrid to application in homogeneous catalysis
Institution name	Saarland University
Expected presentation date	Oct 2020
Requestor Location	Saarland University Campus C4.1
	Saarbrücken, Saarland 66123 Germany Attn: Saarland University
Publisher Tax ID	EU826007151
Total	0.00 EUR
Terms and Conditions	

- Nadine E. Poitiers, Luisa Giarrana, Volker Huch, Michael Zimmer, David Scheschkewitz, Exohedral functionalization vs. core expansion of siliconoids with Group 9 metals: catalytic activity in alkene isomerization, *Chem. Sci.*, **2020**, *11*, 7782-7788.
(<https://doi.org/10.1039/D0SC02861D>)

This article was published by the Royal Society of Chemistry (RSC) as an “Open Access” article and is licensed under a “Creative Commons Attribution-NonCommercial 3.0 Unported (CC BY-NC 3.0)” Licence (<https://creativecommons.org/licenses/by-nc/3.0/>).

- Nadine E. Poitiers, Volker Huch, Michael Zimmer, David Scheschkewitz, Chalcogen-expanded unsaturated silicon clusters: thia-, selen- and tellurasiliconoids, *Chem. Eur. J.* **2020**, *published as early view*.
<https://doi.org/10.1002/chem.202003180>

Copyright © 2020 Wiley-VCH Verlag GmbH & Co. KGaA.

This article was reproduced with the permission from Wiley-VCH:

JOHN WILEY AND SONS LICENSE
TERMS AND CONDITIONS

Oct 14, 2020

This Agreement between Saarland University – Nadine Poitiers ("You") and John Wiley and Sons ("John Wiley and Sons") consists of your license details and the terms and conditions provided by John Wiley and Sons and Copyright Clearance Center.

License Number	4927500254200
License date	Oct 14, 2020
Licensed Content Publisher	John Wiley and Sons
Licensed Content Publication	Chemistry - A European Journal
Licensed Content Title	Chalcogen-Expanded Unsaturated Silicon Clusters: Thia-, Seleno-, and Tellurasiliconoids
Licensed Content Author	David Scheschkewitz, Michael Zimmer, Volker Huch, et al
Licensed Content Date	Oct 12, 2020
Licensed Content Volume	0
Licensed Content Issue	0
Licensed Content Pages	5
Type of Use	Dissertation/Thesis
Requestor type	Author of this Wiley article
Format	Print and electronic
Portion	Full article
Will you be translating?	No
Title	Stable Functionalized Unsaturated Siliconoids: From a tetrylene/siliconoid hybrid to application in homogeneous catalysis
Institution name	Saarland University
Expected presentation date	Oct 2020
Requestor Location	Saarland University Campus C4.1
	Saarbrücken, Saarland 66123 Germany Attn: Saarland University
Publisher Tax ID	EU826007151
Total	0.00 EUR
Terms and Conditions	

- Nadine E. Poitiers, Volker Huch, Michael Zimmer, David Scheschkewitz, Nickel-Assisted Complete Cleavage of CO by a Silylene/Siliconoid Hybrid under Formation of an Si=C Enol Ether bridge, *Chem. Comm.* **2020**, 56, 10898-10901. <https://doi.org/10.1039/D0CC04922K>

This communication was reproduced with the permission from The Royal Society of Chemistry:

RE: Permission Request Form: Nadine Elisabeth Poitiers

https://webmail.uni-saarland.de/imp/view.php?view_token=swphu24...

Datum: 06.10.2020 [13:58:04 CEST]
Von: "CONTRACTS-COPYRIGHT (shared)" <Contracts-Copyright@rsc.org>
An: "'nadine.poitiers@uni-saarland.de'" <nadine.poitiers@uni-saarland.de>
Betreff: RE: Permission Request Form: Nadine Elisabeth Poitiers

Many thanks for sending the permissions request below. The Royal Society of Chemistry (RSC) hereby grants permission for the use of your paper(s) specified below in the printed and microfilm version of your thesis. You may also make available the PDF version of your paper(s) that the RSC sent to the corresponding author(s) of your paper(s) upon publication of the paper(s) in the following ways: in your thesis via any website that your university may have for the deposition of theses, via your university's Intranet or via your own personal website. We are however unable to grant you permission to include the PDF version of the paper(s) on its own in your institutional repository. The Royal Society of Chemistry is a signatory to the STM Guidelines on Permissions (available on request).

Please note that if the material specified below or any part of it appears with credit or acknowledgement to a third party then you must also secure permission from that third party before reproducing that material.

Please ensure that the thesis states the following:

Reproduced by permission of The Royal Society of Chemistry

and include a link to the paper on the Royal Society of Chemistry's website.

Please ensure that your co-authors are aware that you are including the paper in your thesis.

Best wishes,

Chloe Szebrat
Contracts and Copyright Executive
Royal Society of Chemistry
Thomas Graham House
Science Park, Milton Road
Cambridge, CB4 0WF, UK
www.rsc.org

From: nadine.poitiers@uni-saarland.de <nadine.poitiers@uni-saarland.de>
Sent: 05 October 2020 16:07
To: CONTRACTS-COPYRIGHT (shared) <Contracts-Copyright@rsc.org>
Subject: Permission Request Form: Nadine Elisabeth Poitiers

Name: Nadine Elisabeth Poitiers

Institution: Saarland University

Email: nadine.poitiers@uni-saarland.de

Address:

Campus C4.1

Saarbrücken
66123
Germany

I am preparing the following work for publication:

RE: Permission Request Form: Nadine Elisabeth Poitiers

https://webmail.uni-saarland.de/imp/view.php?view_token=swphu24...

Article/chapter title: Nickel-assisted complete cleavage of CO by a silylene/siliconoid hybrid under formation of an Si[double bond, length as m-dash]C enol ether bridge
Journal/book title: Stable Functionalized Unsaturated Siliconoids: From a tetrylene/siliconoid hybrid to application in homogeneous catalysis
Editor/author(s): Nadine Elisabeth Poitiers
Publisher: Nadine Elisabeth Poitiers, Saarland University
Is this request for a thesis?: Yes

I would very much appreciate your permission to use the following material:

Journal/book title: Chemical Communications
Editor/author(s): Nadine E. Poitiers, Volker Huch , Michael Zimmer and David Scheschkewitz*
ISBN/DOI: DOI: 10.1039/D0CC04922K
Year of publication: 2020
Page(s): 10898-10901
Type of material: full paper, Supporting information
Figure/image number (if relevant):

Any additional comments:

Agree to terms: I agree

This communication is from The Royal Society of Chemistry, a company incorporated in England by Royal Charter (registered number RC000524) and a charity registered in England and Wales (charity number 207890). Registered office: Burlington House, Piccadilly, London W1J 0BA. Telephone: +44 (0) 20 7437 8656.

The content of this communication (including any attachments) is confidential, and may be privileged or contain copyright material. It may not be relied upon or disclosed to any person other than the intended recipient(s) without the consent of The Royal Society of Chemistry. If you are not the intended recipient(s), please (1) notify us immediately by replying to this email, (2) delete all copies from your system, and (3) note that disclosure, distribution, copying or use of this communication is strictly prohibited.

Any advice given by The Royal Society of Chemistry has been carefully formulated but is based on the information available to it. The Royal Society of Chemistry cannot be held responsible for accuracy or completeness of this communication or any attachment. Any views or opinions presented in this email are solely those of the author and do not represent those of The Royal Society of Chemistry. The views expressed in this communication are personal to the sender and unless specifically stated, this e-mail does not constitute any part of an offer or contract. The Royal Society of Chemistry shall not be liable for any resulting damage or loss as a result of the use of this email and/or attachments, or for the consequences of any actions taken on the basis of the information provided. The Royal Society of Chemistry does not warrant that its emails or attachments are Virus-free; The Royal Society of Chemistry has taken reasonable precautions to ensure that no viruses are contained in this email, but does not accept any responsibility once this email has been transmitted. Please rely on your own screening of electronic communication.

More information on The Royal Society of Chemistry can be found on our website: www.rsc.org

8 Curriculum Vitae